



# Bulletin of the Mineral Research and Exploration

<http://bulletin.mta.gov.tr>



## THE GEOLOGICAL EVOLUTION OF SORGUN (YOZGAT)-YILDIZELİ (SİVAS) FORELAND BASIN, PETROGRAPHIC, GEOCHEMICAL ASPECTS AND GEOCHRONOLOGY OF VOLCANISM AFFECTING THE BASIN

Ali Ekber AKÇAY<sup>a\*</sup> and Metin BEYAZPİRİNÇ<sup>b</sup>

<sup>a</sup>General Directorate of Mineral Research and Exploration, Department of Geology, Ankara [orcid.org/0000-0002-0771-444X](https://orcid.org/0000-0002-0771-444X)

<sup>b</sup>General Directorate of Mineral Research and Exploration, Department of Geology Ankara [orcid.org/0000-0001-7907-5977](https://orcid.org/0000-0001-7907-5977)

Research Article

### Keywords:

Sorgun-Yıldızeli foreland basin, Slab breakoff, Subduction and collision-related volcanism, Geochemistry, <sup>40</sup>Ar/<sup>39</sup>Ar Geochronologic dating.

### ABSTRACT

Sorgun-Yıldızeli basin is an east-west trending asymmetric marginal foreland (peripheral foreland basin) formed as a result of the consumption of oceanic crust of the northern branch of Neotethys due to the collision of Sakarya continent in the north and Kırşehir Block in the south. It provides much information about the geodynamic evolution of the region. The basement of the study area consists of Late Palaeozoic-Mesozoic Akdağmadeni Massif. Akdağmadeni Massif was intruded by Cenomanian-Maastrichtian granitoids and is overlain tectonically by Late Cretaceous Artova ophiolitic melange within the İzmir-Ankara-Erzincan suture zone and by Cenomanian-Maastrichtian Darmik Formation. The volcano-sedimentary sequence deposited in Sorgun-Yıldızeli foreland basin developed on the relicts of the İzmir-Ankara-Erzincan Suture Zone along the northern margin of Kırşehir Block and was named the Boğazköy Formation. The pelitic, clastic and coarse clastic levels of Upper Palaeocene-Middle Eocene Boğazköy Formation including İzmir-Ankara-Erzincan Suture Zone slices and olistostromes are differentiated as the Dolak member. Toward the inner part of the basin, a turbiditic sequence of conglomerate, sandstone, claystone including rare limestone beds was deposited, consisting of conglomerate, sandstone, claystone, rarely limestone and alternations of three different volcanic rocks (acidic, basic and intermediate) related to subduction and/or collision. Calc-alkaline lava and pyroclastics of basaltic and basalt-andesite composition were differentiated as the Pazarcık volcanic member, with lava and pyroclastics of dacitic and rhyolitic composition called the Sarayözü volcanic member and calc-alkaline lava and pyroclastics of andesitic, trachyandesitic and dacitic composition called Kiremitlik volcanic member in Sorgun-Yıldızeli basin. According to the <sup>40</sup>Ar/<sup>39</sup>Ar geochronologic method, the ages of 57.2±2.0 Ma and 56.7±1.8 Ma were obtained for Pazarcık volcanics, 48.8±1.5 Ma for Sarayözü volcanics and 45.1±1.3 Ma and 47.3±0.6 Ma for Kiremitlik volcanics. The reefal limestones which are not thick and occur in higher parts of the Boğazköy Formation were called the Limestone member. The uppermost section of the sequence which consists of generally clastic and coarse clastics is named the Konacı member. When the sedimentation and volcanism continued in the basin, gabbroic intrusions occurred as sills and laccoliths cutting the Boğazköy Formation. These gabbroic rocks were named the Yaycılar Gabbro. The age of 51.0 ± 0.7 Ma was found for the Yaycılar Gabbro with the <sup>40</sup>Ar/<sup>39</sup>Ar geochronologic method. As a result of slab breakoff, the relicts of the consumed oceanic crust and the released massifs were uplifted rapidly and the units of Middle-Late Eocene Tokuş Formation were deposited progressively on the Boğazköy Formation and on outcropping basement rocks in the basin which was controlled by an extensional tectonic regime. Upper Miocene-Pliocene (İncesu Formation), Pliocene and Quaternary terrestrial sediments were deposited unconformably on all older units.

Received Date: 15.12.2016

Accepted Date: 14.09.2017

## 1. Introduction

Significant portions of the Tertiary basins in Turkey are related to arcs, foreland basins and post-collisional basins. Arc-related basins and foreland basins have

been linked to the closure of the Neo-Tethys Ocean (Görür et al., 1997).

The majority of basins forming during and after the continental collision along the İzmir-Ankara-

\* Corresponding author: Ali Ekber AKÇAY, [aliekber.akcay@mta.gov.tr](mailto:aliekber.akcay@mta.gov.tr)

<http://dx.doi.org/DOI: 10.19111/bulletinofmre.336625>

Erzincan Suture Zone between the Anatolide-Tauride and Pontide tectonic units (Figure 1) (Ketin, 1966) are filled with volcano-sedimentary rocks. While post-collisional basins are widespread on the Anatolide-Tauride and Pontide tectonic units, foreland basins generally have east-west trends between the southern margin of İzmir-Ankara-Erzincan Suture Zone and Anatolide-Tauride and Kırşehir Blocks.

The volcanic rocks in these basins have been studied by many researchers (for example; Armutlu Peninsula: Genç and Yılmaz, 1997; Ercan et al., 1998; Biga Peninsula: Ercan et al., 1990, 1995; Genç, 1998; Genç et al., 2004; Dönmez et al., 2005; around Gümüşhane: Tokel, 1972; Arslan and Aliyazıcıoğlu, 2001; around Ordu: Terzioğlu, 1984; around Kastamonu: Peccerillo and Taylor, 1976; around Kargı: Yılmaz and Tüysüz, 1984; around Taşova-Amasya: Alpaslan and Terzioğlu, 1998; around Çankırı and Çorum: Tüysüz and Dellaloğlu, 1992; around Amasya-Çorum: Keskin et al., 2008; Atakay Gündoğdu, 2009; around Yozgat: Büyükönel, 1985; Tiryaki and Ekici, 2012; around Tokat-Sivas: Yılmaz et al., 1994; around Yıldızeli-Akdağmadeni: Alpaslan, 2000; Koçbulut et al., 2001). Yılmaz et al. (1997), Akçay et al. (2008) and Dalkılıç et al. (2008) produced a 1/100.000 scale geologic map covering the region of the study area.

There are two different opinions relating to tectonic environment and origin of Middle Eocene magmatic rocks cropping out in broad areas of the Anatolide-Tauride and Pontide tectonic units. According to the first view, Eocene magmatism formed in a magmatic arc environment (e.g.; Peccerillo and Taylor, 1976; Yılmaz et al., 1981; Yılmaz and Tüysüz 1984; Okay and Satır, 2006; Ustaömer et al., 2009). According to the second view, these magmatic rocks formed linked to post-collisional events following the collision of the Anatolide and Pontide tectonic units (Genç and Yılmaz, 1997; Genç et al., 2005; Tüysüz and Dellaloğlu, 1992; Yılmaz et al., 1993; Terzioğlu, 1984; Alpaslan and Terzioğlu, 1998; Alpaslan, 2000; Tüysüz et al., 1995; Koçbulut et al., 2001; Tiryaki and Ekici, 2012; Aldanmaz et al., 2000; Köprübaşı and Aldanmaz, 2004; Altunkaynak, 2007; Keskin et al., 2004, 2008; Yılmaz et al., 2001; Altunkaynak and Dilek, 2013; Gülmez et al., 2013). Keskin et al. (2004) proposed slab-breakoff as an alternative model for formation of Middle Eocene volcano-sedimentary units. This model was later adapted by other researchers for Eocene magmatism in western and north-western Turkey (e.g., Köprübaşı and Aldanmaz, 2004; Altunkaynak and Dilek, 2006;

Altunkaynak, 2007; Genç and Altunkaynak, 2007; Gülmez et al., 2013).

It is difficult to distinguish volcanic rocks retaining subduction signatures (subduction, collision, post-collision) from each other using only geochemical data. Thus, determining the geodynamic processes leading to the formation of studied basins will help to reveal the origin and the source characteristics of the volcanism. The study area that is located between Sorgun (Yozgat) and Yıldızeli (Sivas) is bounded to the north by ophiolitic rocks and to the south by metamorphic rocks of the Akdağmadeni Massif (Figure 1). It includes volcano-sedimentary units representing both a foreland basin developing linked to subduction and collision in the Late Palaeocene-Early Lutetian period and to post-collisional basins which began opening in the Middle Eocene. In previous studies, these basins in the study area have not been distinguished, although the tectonic setting and the origin of Lower Tertiary volcanic rocks cropping out in the region were interpreted through post-collisional basin model. This study mapped these basins developing due to different geodynamic processes in detail, and aimed to determine the geodynamic evolution of the basin by determining stratigraphic, sedimentologic, petrography, geochemical and geochronological properties of units comprising the basin fill.

## 2. Regional Geology

The study area located south of the Central Pontides encompasses the İzmir-Ankara-Erzincan Suture (IAESZ) (Şengör and Yılmaz, 1981) and the northern edge of the Kırşehir Block (Figure 1).

The İzmir-Ankara-Erzincan Suture Zone comprising accretionary wedge and ensimatic island arc units separates the Sakarya continent to the north from the Kırşehir Block to the south (Figure 1).

Tüysüz and Dellaloğlu (1992) and Tüysüz et al. (1995) proposed that consumption of the oceanic crust belonging to the northern branch of Neotethys occurred in two different subduction events. The first was an ensialic arc on the Sakarya continent, whereas the other produced an ensimatic island arc with intra-oceanic subduction.

The metamorphic, ophiolitic and plutonic rocks forming the Kırşehir Block in the south have been named by different names such as the Kırşehir

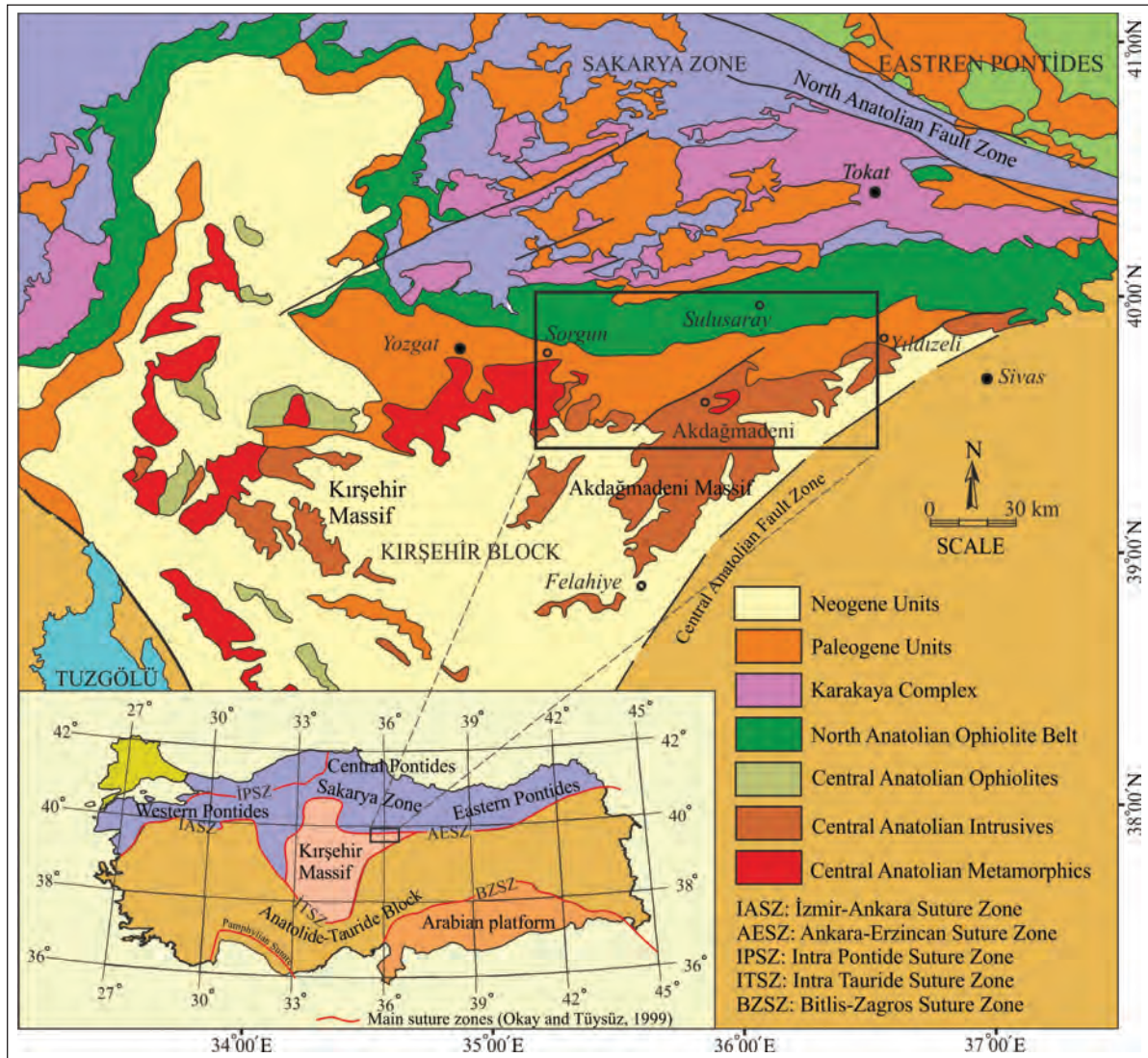


Figure 1- Location map of the study area.

crystalline massif (Bailey and McCallien, 1950, Egeran and Lahn, 1951), Central Anatolian massif, Kızılırmak Massif (Ketin, 1955, 1963; Erkan and Ataman, 1981), Central Anatolian Crystalline Melange, (Göncüoğlu et al., 1991, 1992) and the Central Anatolian Crystalline Complex (Erler and Bayhan, 1995). The same rock units are locally known as the Kırşehir Massif (Egeran and Lahn 1951), Akdağ Massif (Vache, 1963) and Niğde Massif (Göncüoğlu, 1977; Whitney et al., 2003). In this study, the name Akdağmadeni Massif (Şahin, 1999) has been adopted. This tectonic unit comprises Late Palaeozoic-Mesozoic-aged calcschist, quartzite, quartzschist, amphibole schist, amphibolite, gneiss, marble and dolomitic marble. The units generally have undergone greenschist to amphibolite facies metamorphism but the lower levels experienced higher degrees of metamorphism (Yılmaz et al., 1995).

The metamorphic rocks of the Akdağmadeni Massif (Figure 2) are commonly cut by Cenomanian-Maastrichtian-age granitoid rocks (Central Anatolian Granitoids; Erler and Bayhan, 1995). The Central Anatolian granitoids consist mainly of granite, granodiorite, syenite, microgranite, granite porphyry, monzonite and tonalite. There are skarn zones and Pb-Zn mineralizations along intrusive contacts with metamorphic rocks.

The Akdağmadeni Massif is tectonically overlain by the Late Cretaceous Artova ophiolitic melange (Özcan et al., 1980) of IAESZ and the Cenomanian-Maastrichtian Darmik Formation (Akçay et al., 2008; Dalkılıç et al., 2008) (Figure 2). The Artova ophiolitic melange comprises serpentinized peridotite, dunite, harzburgite, gabbro, diabase, pyroxenite dikes, pillow

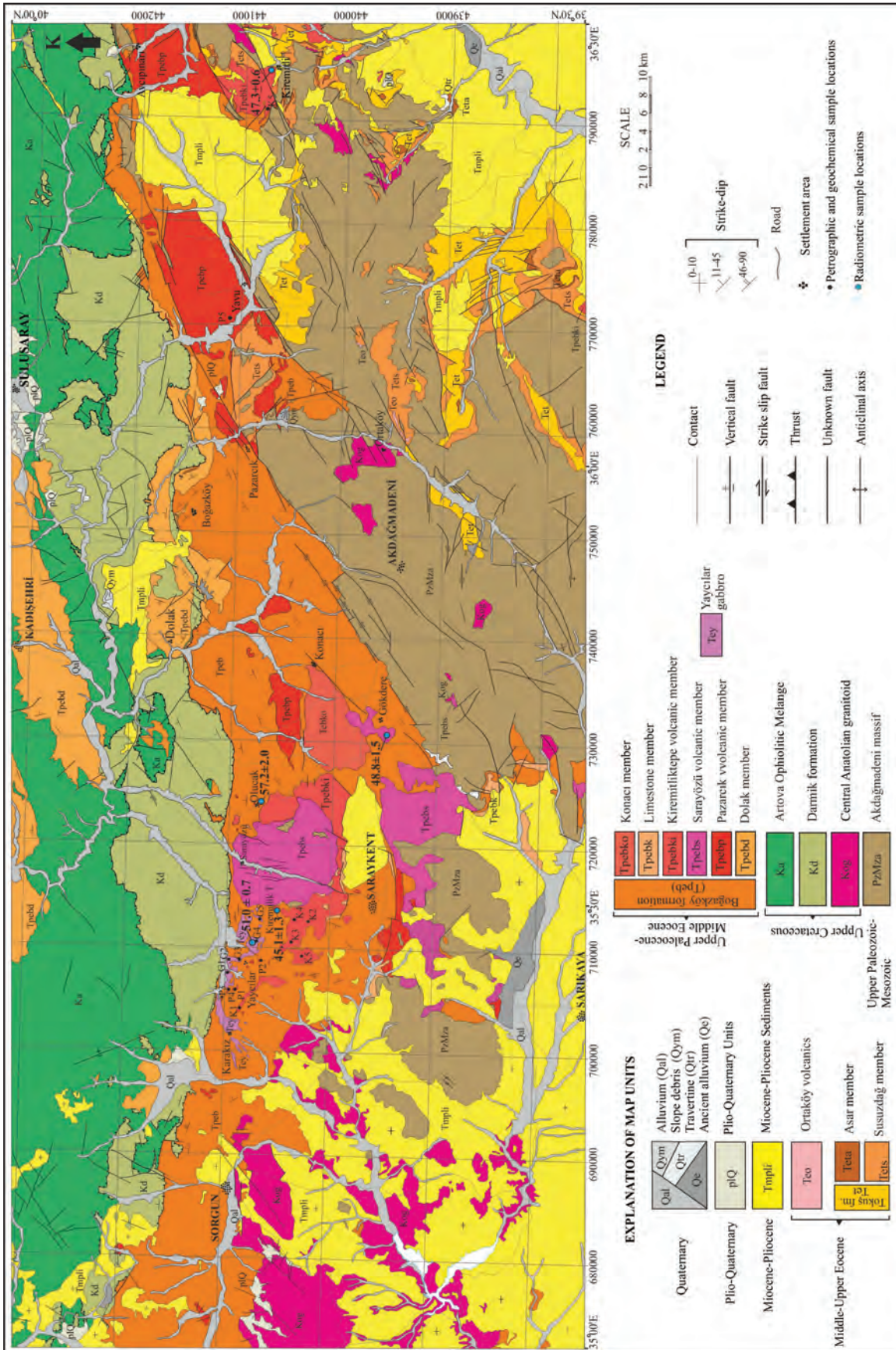


Figure 2- Geologic Map of the study.

lavas, deep sea sedimentary rocks (radiolarian chert, mudstone, calciturbidites) lacking primary textures, along with metamorphic rocks of the Sakarya continent and Triassic to Cretaceous-aged limestone slices and blocks. Late Tithonian-Berriasian and late Albian-early Cenomanian ages have been obtained from ephiophiolitic sediments within the Artova ophiolitic melange (Beyazpıriñç et al., 2014). Previous studies have obtained ages of  $179\pm 15$  Ma (Dilek and Thy, 2006) and 180 My (Sarifakıođlu et al., 2011) from plagiogranites of the ophiolitic series. According to these data, the age of oceanic crust consumed by subduction was Jurassic-Cretaceous. The Darmik Formation (Figure 3), following the Artova ophiolitic melange with a tectonic contact, consists of basaltic and andesitic lava and pyroclastic deposits in the lower levels with conglomerate, sandstone, claystone, mudstone, clayey limestone, micritic limestones and calciturbidites with volcanic interlayers in the upper sections. Beyazpıriñç et al. (2014) determined the following fossils in claystone, mudstone, clayey limestone and micritic limestones in the upper sections of the Darmik Formation and identified the age as Santonian-Maastrichtian according to these fossil assemblages. Santonian: *Marginotruncana coronata* Bolli, *Marginotruncana cf. tarfayaensis* (Lehmann), *Marginotruncana pseudolinneiana* Pessagno, *Dicarinella cf. asymetrica* (Sigal), *Dicarinella concovata* (Brotzen), *Globigerinelloides* sp., *Heterohelix* sp., *Marginotruncana* sp. fossil assemblages.

Santonian-Early Maastrichtian: *Globotruncana bulloides* Vogler, *Globotruncana cf. arca* (Cushman), *Globotruncana cf. linneiana* (d'Orbigny), *Globotruncana* sp., *Globotruncanita* sp., *Heterohelix* sp. fossil assemblage.

Campanian-Maastrichtian: *Reinhardtites levis* Prins ve Sissingh, *Micula swastica* Stradner ve Steinmetz, *Arkhangelskiella cymbiformis* Vekshina, *Lucianorhabus cayeuxii* Deflandre, *Quadrum gothicum* (Deflandre), *Prediscosphaera cretacea* (Arkhangelsky), *Tranolithus phacelosus* Stover, *Micula decussata* Vekshina, *Microrhabdulus decoratus* Deflandre, *Cretarhabdus crenulatus* Bramlette ve Martini, *Watznaueria barnesae* (Black, Black ve Barnes), *Biscutum* sp. nanno fossil assemblage.

An age of  $98.7\pm 2.4$  Ma ( $^{40}\text{Ar}/^{39}\text{Ar}$ ; plagioclase) has been obtained from the volcanic rocks of the Darmik Formation. When the palaeontologic and geochronologic data are assessed together, it is

observed that the Darmik Formation formed during the Cenomani-Maastrichtian period (Beyazpıriñç et al., 2014).

The Late Palaeocene-Middle Eocene Bođazkđy Formation that is composed of volcano-sedimentary rocks unconformably overlies the units mentioned above. The basal sections of the Bođazkđy Formation comprise gabbroic rocks emplaced as sills and laccoliths, called the Yaycılar gabbro (Figure 3). The Middle-Late Eocene-aged Tokuř Formation (Yılmaz, 1982) overlies the Bođazkđy Formation and basement rocks with an unconformity. In this study, basal conglomerates (Yılmaz et al., 1995) and the sandstone, claystone, fossiliferous limestone (Yılmaz et al., 1995) of Tokuř Formation are distinguished as Susuzdađ member and Asar member, respectively (Figure 3).

The Susuzdađ member is represented by reddish-brown, grey, poorly sorted conglomerate, sandstone and mudstone representing alluvial fan, fan-delta and fluvial sediments. The Asar member is yellowish-grey, cream, and yellow colour, has massive-thick bedded layers with dissolution cavities with pebble, and consists of sand and clay in the basal sections and fossiliferous limestone in the upper sections. Samples obtained from different levels in the Asar member have obtained *Discocyclus* sp., *Sphaerogypsina* sp., *Lockhartia* sp., *Asterigerina* sp., *Nummulites* sp., *Nummulites* spp., *Assilina* spp., *Nummulites* gr. *perforatus* (Montfort), *Nummulites* sp., *Orbitolites* sp., *Alveolina* sp., *Rotalia* sp., *Gypsina* sp., *Haymanaella* sp., *Nummulites* gr. *perforatus* (De Montfort), *Nummulites* cf. *perforatus* (De Montfort), *Gyroidinella magna* Le Calvez, *Linderina brugesii* Schlumberger, *Assilina* cf. *exponens* (Sowerby), *Alveolina* gr. *fusiformis* (Sowerby), *Alveolina* cf. *fusiformis* (Sowerby), *Glomalveolina* sp., *Assilina* sp., Rotaliidae, Textulariidae, Miliolidae algae, bryozoans, gastropods and macro shell fragments for a Late Lutetian-Bartonian age. However, according to a fossil assemblage including *Orbitolites complantus* Lamack, *Assilina exponens* (Sowerby), *Assilina* cf. *spira* (de Roissy), *Nummulites* cf. *millecaput* (Boubee), *Nummulites* cf. *helveticus* Kaufmann, and *Locharia cushmani* Applin et Jordan (Yılmaz et al., 1995) within the unit, however, the age of the unit is Lutetian-Priabonian. As a result, the age of the Tokuř Formation can be said to be Middle-Upper Eocene.

The acidic lava and pyroclastic rocks interfingering with the basal conglomerates (Susuzdađ member) of the Tokuř Formation around Ortakđy are named as the

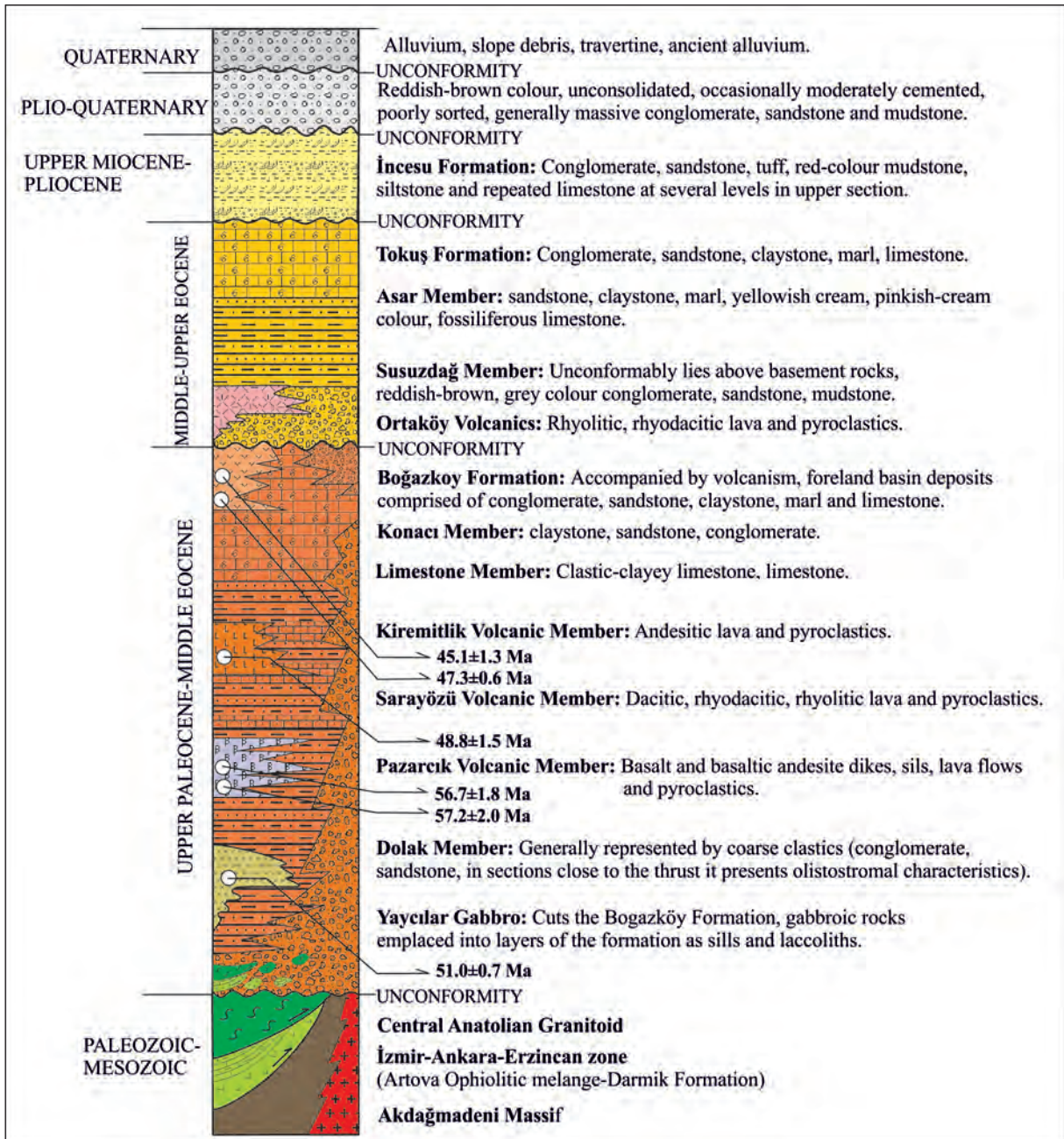


Figure 3- Generalized stratigraphic section of the study area (no scale).

Ortaköy volcanics in this study (Figures 2, 3). The unit is represented by yellowish, light grey colour rhyolite and rhyodacite lava and pyroclastic rocks. Yılmaz et al. (1995) called the unit the Ortaköy tuff and stated that even though it appears to interfinger with the Eocene-age Susuzdağ member, it may be younger.

Above this whole sequence, an angular unconformity is overlain by alluvial fan, loosely consolidated conglomerate, sandstone, tuff, red coloured mudstone, and siltstone deposited in a

braided fluvial and lacustrine environment with several repeated levels of carbonate sediments in upper levels called the the Late Miocene-Pliocene İncesu Formation (Yılmaz, 1981). Based upon the presence of fossils e.g. o *Cyprideis* cf. *vetroundulate* Kırtıcı, *Cyprideis torosa* Jones, *Cyprideis tuberculata* (Mehes), *Jlyocypris gibba*, *Hypraion gracile* Kaup, lower molar teeth belonging to *Choerolophodon Pentelici*, bone and tooth pieces belonging to *Proboscidae* (elephants) order, and pollen such as *Monoporollenites solaris*, *Pityosporites microalatus*,

*Periporopollenites multiparatus* obtained from various locations of the unit, the age is Late Miocene-Pliocene (Kara, 1997).

The İncesu Formation is unconformably overlain by Plio-Quaternary units. The Plio-Quaternary sedimentary rocks are reddish-brown colour, poorly to moderately consolidated, poorly sorted, and comprise generally massive conglomerate, sandstones and mudstone. They generally contain the rock fragments derived from the underlying sedimentary rocks. The youngest sediments in the study area are represented by alluvium (Qal), ancient alluvium (Qe), slope debris (Qym) and travertine sediments.

### 3. Material and Methods

A detailed geological map was produced for the study area between Sorgun-Yıldızeli covering the 1/100.000 scale Yozgat I34, I35 and Sivas I36 sheets. Where necessary, areas outside the study area were visited in order to make correlations and observations. Thin sections were prepared from 58 hand samples collected from the study area and investigated in detail with a polarising microscope and petrographic identification performed. The great majority of volcanic rocks cropping out in the study area have been affected by alteration. A total of 17 samples chosen during field studies and petrographic investigations were sent to Canada ACME Labs for analysis (major, trace and rare earth elements). At the laboratory, these samples were ground to powder and then 0.2 g fractions were mixed with 1.5 g Li-BO<sub>2</sub> and heated to 105°C. The hot mixture and 100 ml 5% HNO<sub>3</sub> were mixed and the solution was evaporated in an ICP-ES (inductively coupled plasma emission spectrometer) to identify major element oxides and trace elements. The detection limit for major element oxides was 0.002-0.04%. For rare earth element (REE) analysis, samples prepared with the methods above were placed in an ICP-MS (inductively coupled plasma mass spectrometer). The trace element detection limit was between 0.01 and 5 ppm.

In order to determine the radiometric ages, a total of 6 samples - 2 samples from the Pazarçık volcanic member, 1 sample from the Sarayözü volcanic member, 2 samples from the Kiremitlik volcanic member and 1 sample from the Yaycılar gabbro – were sent to Actlabs Canada for analysis by Dr. Yakov Kapusta. Geochronologic ages were determined for plagioclase minerals from 5 samples and whole rock sludge for 1 sample with the <sup>40</sup>Ar/<sup>39</sup>Ar method.

During the sample preparation process, samples were wrapped in aluminium foil for fluid scanning and isotope measurements and bottled in insulated quartz vials. Within the quartz vials, K and Ca salts and LP-6 biotite packets were placed together mixed with samples for fluid monitoring. After studying fluid monitoring, the fluid gradient measured for each sample was used to calculate J values. The age of LP-6 biotite is accepted as 128.1 Ma. In an externally-heated oven, <sup>40</sup>Ar/<sup>39</sup>Ar step heating experiments were completed with the temperature value monitored with a thermocouple. Argon isotope analyses were completed with a Micromass 5400 mass spectrometer. Isotope values measured in the mass spectrometer were recorded with the aid of a computer linked to the spectrometer and the process was observed. To check the accuracy of the obtained ages, plateau age calculations were supported by isochron calculations.

### 4. Sorgun-Yıldızeli Basin Geology

#### 4.1. Stratigraphic, Petrographic and Geochronologic Characteristics

The rock assemblages apparently deposited in two separate E-W oriented basins between Sorgun (Yozgat) and Yıldızeli (Sivas) were determined to be the products of a single large basin (“Sorgun-Yıldızeli basin”) developing due to the same geodynamic processes (Figure 2).

The basin fill is represented mainly by the Boğazköy Formation and its differentiated sub-units. The gabbroic, shallowly emplaced sills and laccoliths into the basal sections of the Boğazköy Formation are distinguished as the Yaycılar gabbro (Figure 3).

##### 4.1.1. Boğazköy Formation

The volcano-sedimentary sequence deposited during the late Palaeocene-middle Eocene period was named as Boğazköy Formation by Özcan et al. (1980) and this is accepted as the formal term by the Turkish Stratigraphy Committee (Turkish Stratigraphy Committee Bulletin (TSKB), 1987).

The section located at the base of Boğazköy Formation and containing slices and olistostromes from IAESZ with generally pelitic, clastic and occasionally poorly sorted coarse clastics are distinguished as the Dolak member.

Toward the interior, and in relatively deeper sections of the basin, three different types of basic, intermediate

and acidic composition subduction- and/or collision-related volcanic rocks are interlayered with sparse limestone and with turbiditic conglomerate, sandstone and claystone. These volcanic levels are distinguished as the Pazarcık, Sarayözü and Kiremitlik volcanic members. Reefal limestones in the upper section of the Boğazköy Formation, called the Limestone Member, is generally differentiated from the Konacı member of coarse clastic sediments forming the upper portion of the sequence (Figures 2, 3).

**Dolak Member:** The Dolak member (Akçay et al., 2008; Dalkılıç et al., 2008) forms the base of the Boğazköy Formation and is generally represented by clastics and coarse-grained clastic rocks. The Dolak member has an olistostromal character in sections close to the thrust line and contains large blocks and slices from the Artova ophiolitic melange and Darmik Formation (Figure 4 a,b,c,d). This unit is equivalent to the Kılıçlı Olistostrome defined in previous studies (Yılmaz, 1982). The Dolak member varies in thickness between 150 and 450 m.

The fossil assemblages identified in the samples from the pelitic levels of Dolak member are given

below and according to these fossil assemblages, the late Palaeocene-Lutetian age assigned to the unit: Late Palaeocene-early Eocene: (near Çiçekli village) *Chiasmolithus consuetus* (Bramlette and Sullivan), *Neochiastozygus perfectus* Perch-Nielsen, *Reticulofenestra dictyoda* (Deflandre and Fert), *Coccolithus eopelagicus* (Bramlette and Riedel), *Ericsonia robusta* (Bramlette and Sullivan), *Ericsonia formosa* (Kamptner), *Ericsonia cava* (Hay and Mohler), *Ericsonia ovalis* Black, *Sphenolithus moriformis* (Brönnimann and Stradner), *Toweius tovae* Perch-Nielsen, *Toweius eminens* (Bramlette and Sullivan), *Cruciplacolithus tenuis* (Stradner), *Ellipsolithus macellus* (Bramlette and Sullivan), *Fasciculithus tympaniformis* Hay and Mohler nano fossil assemblage.

**Late Ypresian-Lutetian:** *Ericsonia formosa* (Kamptner), *Discoaster multiradiatus* Bramlette and Riedel, *Toweius eminens* (Bramlette and Sullivan), *Chiasmolithus consuetus* (Bramlette and Sullivan), *Reticulofenestra dictyoda* (Deflandre, Deflandre and Fert), *Zygrhablithus bijugatus* (Deflandre and Fert), *Tribrachiatum bramlettei* (Brönnimann and Stradner), *Ericsonia cava* (Hay and Mohler), *Ericsonia*

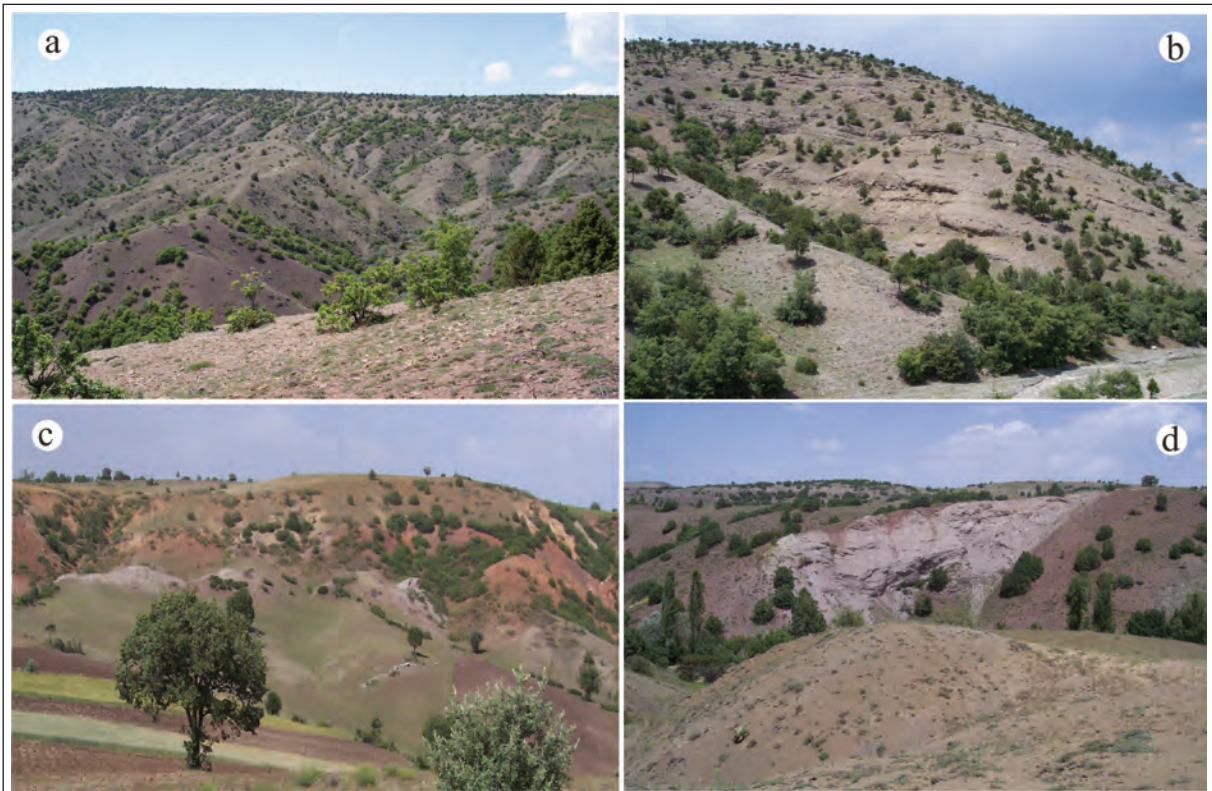


Figure 4- Photographs of the Dolak Member which consists of coarse grained clastic sediments (a,b) (west of Kayakışla village) and olistostromal sections (c,d) (northeast of Alicik village).

*robusta* (Bramlette and Sullivan), *Chiasmolithus consuetus* (Bramlette and Sullivan), *Rhabdosphaera tenuis* Bramlette and Sullivan, *Ericsonia formosa* (Kamptner), *Ericsonia obruta* Perch-Nielsen, *Pontosphaera plana* (Bramlette and Sullivan), *Nannotetrina* sp., *Toweius eminens* (Bramlette and Sullivan), *Toweius tovae* Perch-Nielsen, *Sphenolithus primus* Perch-Nielsen, *Coccolithus eopelagicus* (Bramlette and Riedel), *Tribrachiatius orthostylus* Shamrai nano fossil assemblage.

**Pazarcık Volcanic Member:** This unit described as the Pazarcık Volcanics (Özcan et al., 1980; TSKB, 1987) in previous studies comprises basalt and basaltic andesitic volcanic rocks forming dikes, sills, lava flows and pyroclastic interlayers within the Boğazköy Formation (Figure 5 a,b,c).

The dominant rock type in the Pazarcık volcanic member is basaltic andesite. Basaltic andesite samples have porphyritic and rare amygdoloidal textures. Plagioclase, altered mafic minerals and pyroxene minerals in the form of phenocrysts are distributed in a microlithic texture groundmass. Plagioclase (andesine according to optical properties) minerals display polysynthetic twinning-zoning and sieve texture. Pyroxenes are rarely found and represented by anhedral augite. The iddingsitised mafic minerals are all pseudomorphs and were probably originally olivine. Besides, in some samples, amphibole minerals with partially preserved outer rim and altered to clay and chlorite at the center are found.

Basalts have microcrystalline porphyritic texture, with subhedral-euhedral phenocrysts (mainly

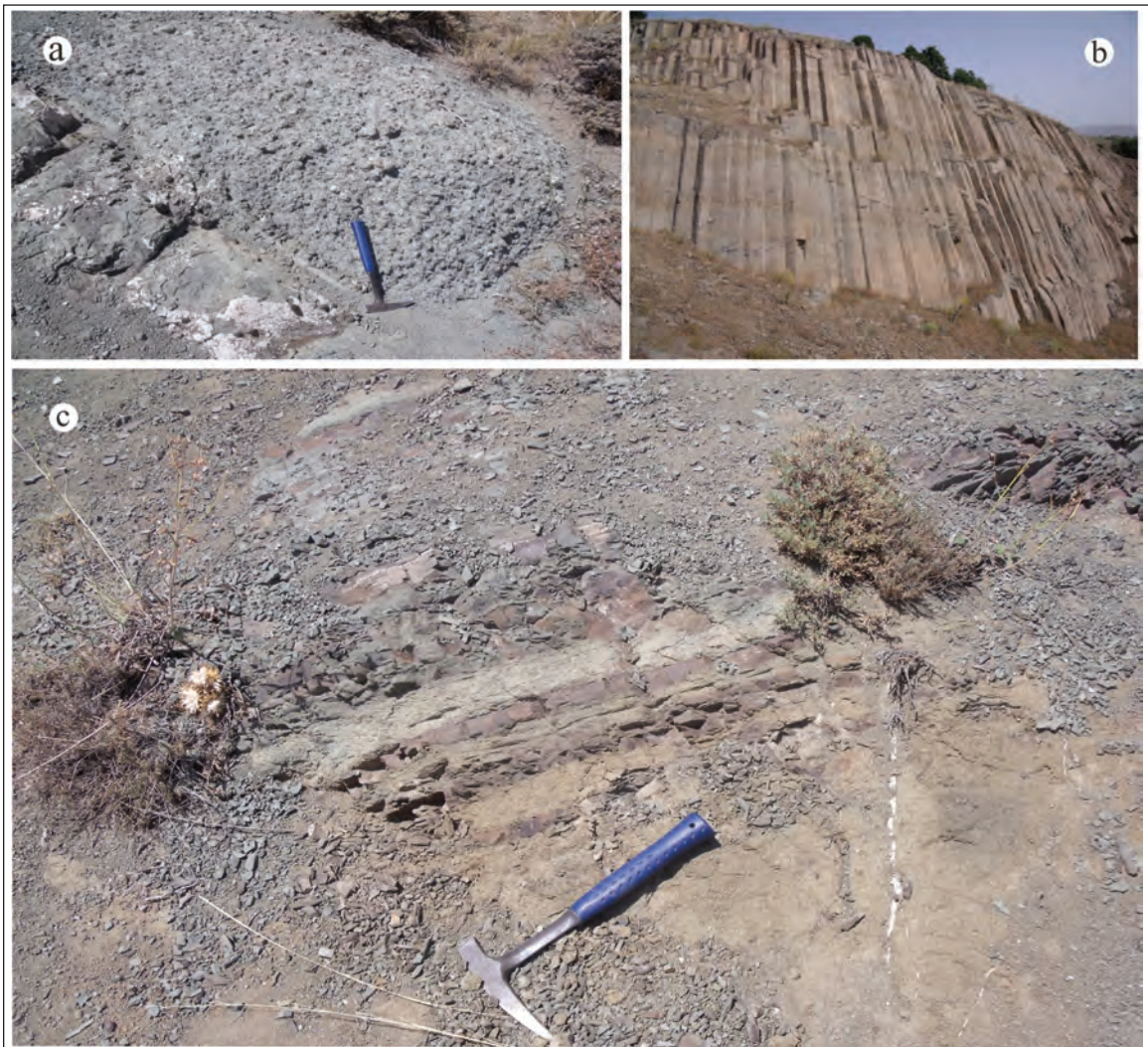


Figure 5- Photographs of the Pazarcık Volcanic Member showing (a) pyroclastic levels (Avcıpnarı village), (b) columnar basalt levels (Pazarcık village) and (c) interlayering within turbiditic sedimentary layers (Avcıpnarı village).

plagioclase, pyroxene, olivine and a few mafic mineral pseudomorphs) in a groundmass of devitrified glass. The majority of plagioclase minerals (andesine-labradorite), comprising the main component, are microlithic, locally forming microphenocrysts, with anhedral and rounded crystal form. Olivines form microphenocrysts which are partially iddingsitised and serpentinized around the rims, with partial or full carbonitisation in the centres. Auxilliary components include opaque minerals with different crystal sizes.

Plagioclase from the Pazarcık volcanic member was dated with the  $^{40}\text{Ar}/^{39}\text{Ar}$  geochronological age methods and yielded age of  $57.2 \pm 2.0$  Ma (Figure 6 a,b), whereas whole rock sludge from a basalt sample from Alimpınar village outside the study area was dated as  $56.7 \pm 1.8$  My (Figure 6 c,d).

*Sarayözü Volcanic Member:* Dacite, rhyodacite, rhyolitic lava and pyroclastic rocks in the Boğazköy Formation were named as the Sarayözü volcanic member in this study (Figure 7 a,b).

The unit is fragmented by N-S oriented faults and altered near Sarayözü and its northern sections. Hot springs along the valley where the Saray stream

flows have locally caused hydrothermal alteration and limonitisation, hematitisation and kaolinisation developed in these sections. Locations where limonitisation and hematitisation dominate are yellowish-brown or dark brown in colour; whereas in sections where kaolinisation was effective the unit is yellowish-cream and white colour with locally silicification.

In rhyolite samples with porphyritic texture, phenocrysts of quartz, feldspar and rare biotite minerals are distributed within a fine-grained felsic groundmass. The quartz grains are subhedral-anhedral, with partial undulose extinction and grains have experienced magmatic corrosion. Feldspars are euhedral comprising albite-oligoclase composition plagioclases. In samples, quartz and feldspars rarely form glomeroporphyric texture. Samples with spherulitic textures are found within rhyolitic lava.

Plagioclase in dacite from the Sarayözü volcanic member yielded  $^{40}\text{Ar}/^{39}\text{Ar}$  age of  $48.8 \pm 1.5$  Ma (Figure 8 a,b).

*Kiremitlik Volcanic Member:* This unit is composed dominantly of andesitic lava and pyroclastic rocks.

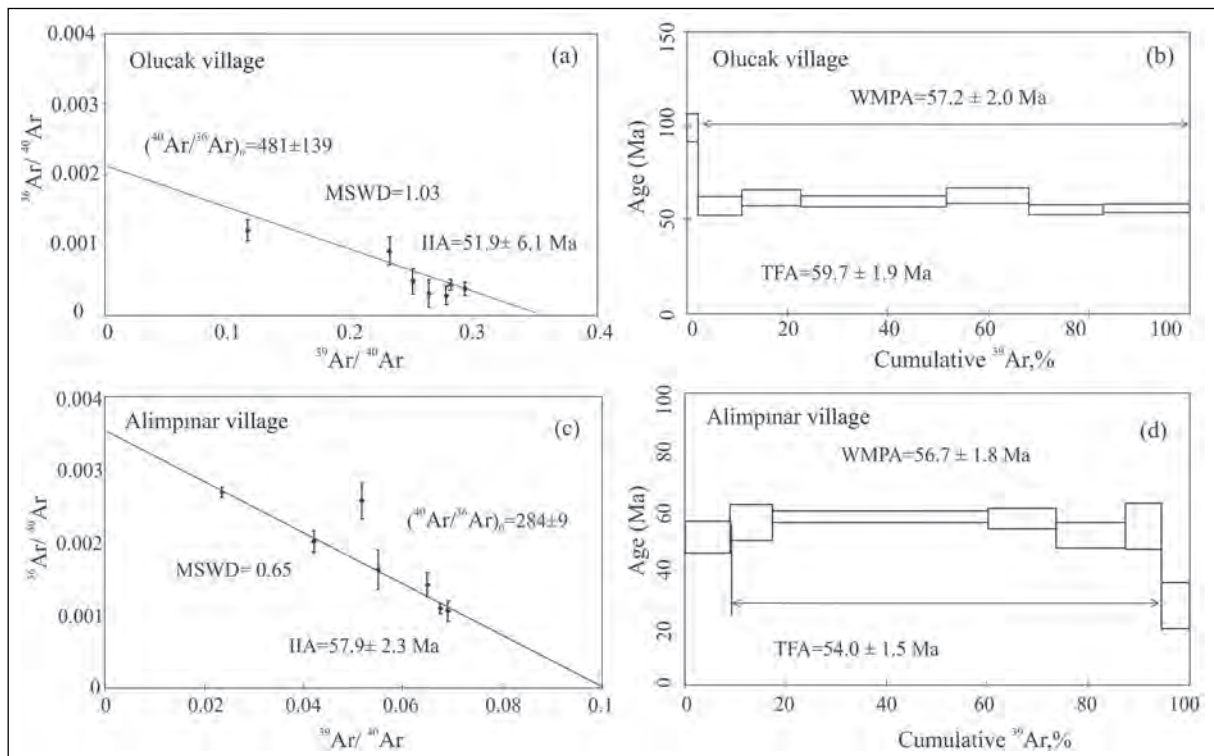


Figure 6- Age dates of two basalt samples from the Pazarcık volcanic member; plagioclase (a, b) and whole rock (c, d) isochron and plateau age diagrams (IIA = inverse isochron age; TFA= total fission age; WMPA= weighted mean plateau age; MSWD: mean square weighted deviation).

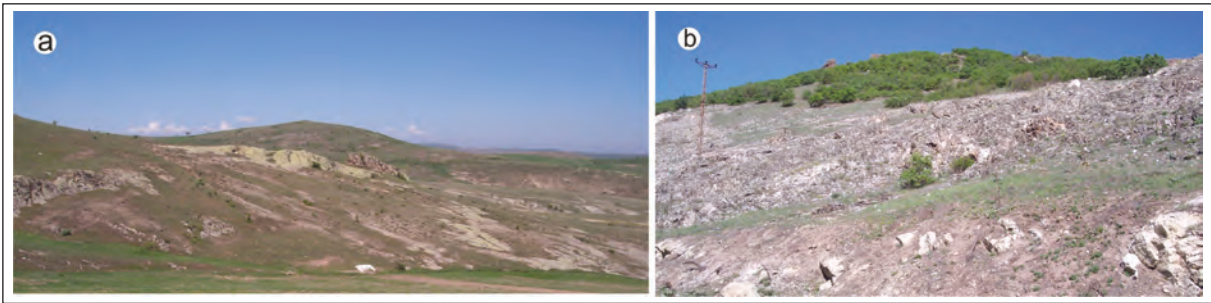


Figure 7- Photographs showing the Sarayözü volcanic member; a view from rhyolite dome(a) and rhyolite with advanced degree of alteration (b) (Sarayözü village).

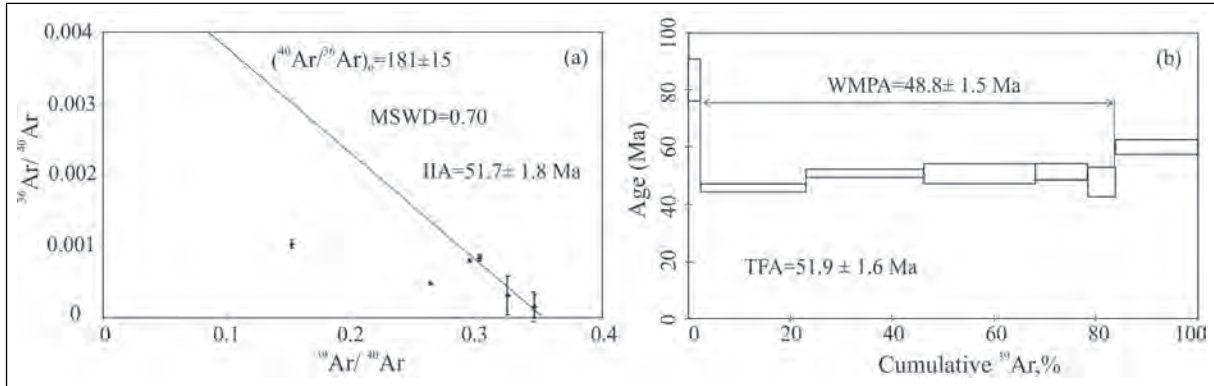


Figure 8- Radiometric age dates on plagioclase from dacites in the Sarayözü volcanic member showing isochron (a) and plateau age (b) diagrams (Gökdere village-Çarşak Tepe).

It is located in the upper sections of the Boğazköy Formation and was named as the Kiremitlik volcanic member in this study (Figure 9).

The unit has been defined as andesite, hyaloandesite and pyroxene andesite by petrographic investigations.

Andesites have porphyritic texture with phenocrysts of plagioclase, mica and rare amphibole in a microlithic groundmass. Plagioclase is mainly represented by polysynthetic twinned-zoned oligoclase-andesine types. In some samples, plagioclase is intensely carbonitised, partially argillised and the grains



Figure 9- Photographs showing the andesites terrains of the Kiremitlik volcanic member (south of Kiremitlik Tepe).

locally combine to form glomeroporphyric texture. Amphiboles have opacity and occasionally the interior is in the form of chloritised pseudomorphs. Micas are fine to coarse grained, partially euhedral with partial opacity of prismatic forms and biotite minerals display opaque mineral exsolutions. Altered mafic minerals with preserved outer rims are possibly amphibole minerals in the form of chlorite-carbonate pseudomorphs. Mafic minerals rarely have opacity. Flow textures observed in the groundmass consist of plagioclase microliths in a glassy matrix. Samples with more volcanic glass in groundmass are described as hyaloandesite.

Pyroxene andesite has similar mineral paragenesis as does the hyaloandesites; however it is distinguished by containing a much lower amount of volcanic glass material. Pyroxene andesite has porphyritic texture. Phenocrysts of plagioclase, pyroxene and altered mafic minerals are distributed in a groundmass with microgranular texture. Plagioclase is partially chloritised-sericitised with polysynthetic twinning-zoning and an oligoclase-andesine character. Pyroxene is fine to coarse grained and partially euhedral augite.

Altered mafic minerals are chloritised and carbonitised amphibole minerals. In addition, mafic mineral relicts from which iron oxide is completely removed were identified. Feldspar and pyroxene minerals rarely occur together to form a glomeroporphyric texture.

Plagioclase in andesite from the Kiremitlik volcanic member yielded  $^{40}\text{Ar}/^{39}\text{Ar}$  geochronologic ages of  $45.1 \pm 1.3$  and  $47.3 \pm 0.6$  Ma (Figure 10 a,b,c,d).

**Limestone Member:** Levels of clastic-clayey limestone and limestone in the upper sections of the Boğazköy Formation were named as the Limestone member (Akçay et al., 2008; Dalkılıç et al., 2008). The unit represents neritic limestone with yellowish-grey, yellowish-cream, locally beige colour, thick to very thick bedded and generally fossiliferous limestone. The maximum thickness measured is 34 m. The unit was formed in a calm shallow marine environment. Samples obtained from different levels of the Limestone member of the Boğazköy Formation contain *Assilina* gr. *exponens* Sowerby, *Nummulites* sp., *Asterigerina* sp., *Discocyclina* sp., *Lockhartia* sp., *Acarinina* sp., *Globigerina* sp., *Morozovella*

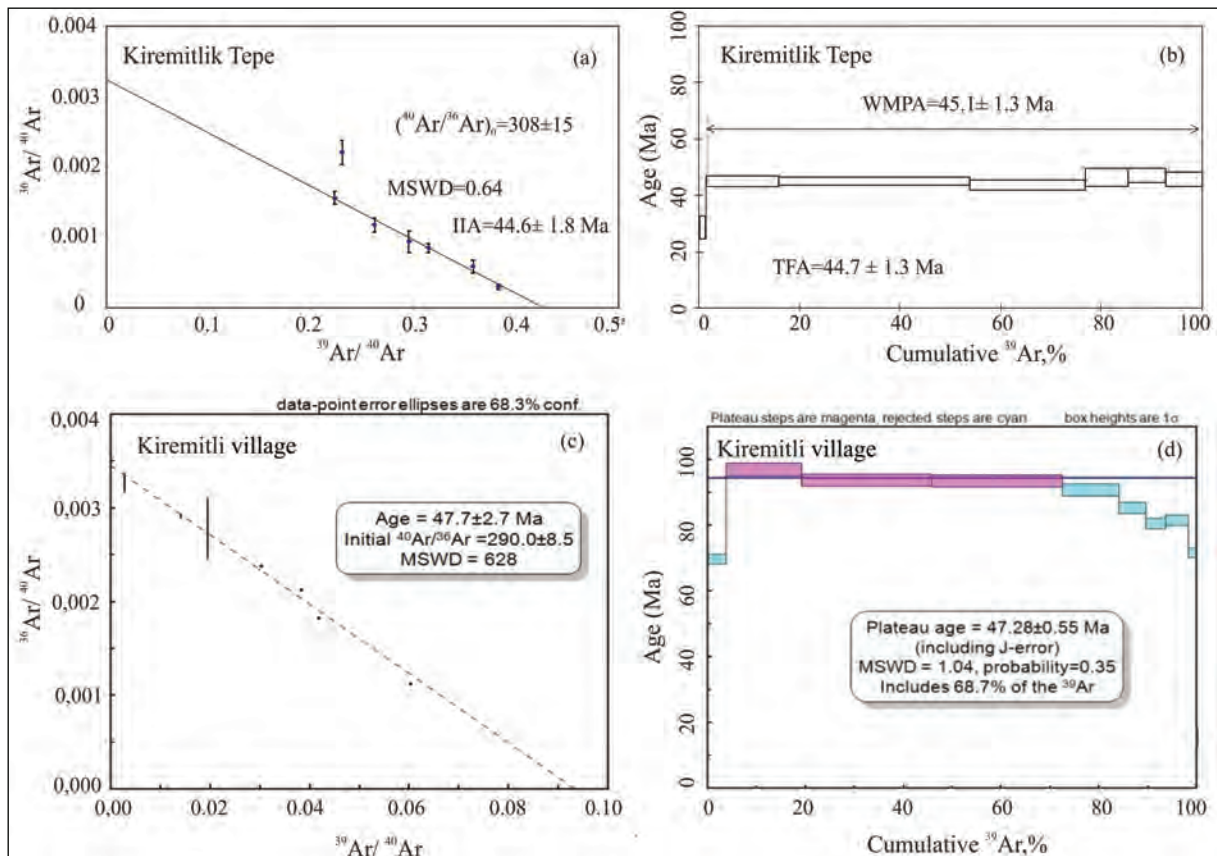


Figure 10- Plagioclase isochron and plateau age diagrams from two andesite samples belonging to the Kiremitlik volcanic member (Kiremitlik Tepe and Kiremitli village).

sp., Miliolidae, Rotaliidae, Textulariidae algae, bryozoans and macro shell fragments. According to this palaeontological data, it is dated to the Lutetian.

**Konacı Member:** The uppermost levels of the Boğazköy Formation, generally represented by clastic rocks, are named as the Konacı member (Özcan et al., 1980). The unit contains siltstone, sandstone and conglomerate with claystone and clayey limestone interlayers (Figure 11). The dominant rock type is observed to be intercalations of conglomerate and sandstone. The conglomerate is greyish yellow, yellow and pale colours, massive, medium to thick layered with locally thin layers. Clasts vary from very small to very large in size and are subangular to rounded, matrix-supported, and locally well sorted and polygenic. The unit does not show lateral continuity, but has apparent thickness of nearly 300 m.

Samples obtained from clayey limestone levels in the Konacı member which form the uppermost levels of the Boğazköy Formation include *Acarinina spinuloinflata* (Bandy), *Acarinina bullbrooki* (Bolli), *Acarinina cf. pentacamerata* (Subbotina), *Turborotalia frontosa* (Subbotina), *Turborotalia* sp., and *Morozovella* sp. with an early-middle Eocene (late Ypresian-Lutetian) age. However, when the stratigraphic location of the member and the middle Eocene radiometric age for the underlying volcanic rocks are considered together, Konacı member is assigned to the middle Eocene.

#### 4.1.2. Yaycılar Gabbro

Gabbroic rocks emplaced as sills and laccoliths in the basal sections of the Boğazköy Formation are named the Yaycılar gabbro (Figure 12 a,b).

The Yaycılar gabbro mainly consists of plagioclase and pyroxene with lesser biotite and opaque minerals. The majority of the pyroxene group minerals are anhedral clinopyroxenes, accompanied by a small amount of orthopyroxene. Plagioclase is the other significant component and is characterised by twinning and prismatic shape. The Yaycılar gabbro generally displays granular texture. Ophitic texture can also be observed in some samples.

The Yaycılar gabbro is cut by a micro-monzonite dike-vein systems with a thickness ranging between 5-10 cm (Figure 12 a). Veins cutting the gabbro have holocrystalline granular texture and monzonitic composition. They contain potassium-feldspar, plagioclase and secondary calcite minerals. The majority of the feldspars are argillised. Chloritisation is observed within the rocks and opaque minerals are common. At the boundary zone between the monzonitic dike-vein systems and gabbro, the gabbro displays an advanced degree of alteration and weathering.

Plagioclase from the Yaycılar gabbro yielded  $^{40}\text{Ar}/^{39}\text{Ar}$  geochronologic age of  $51.0 \pm 0.7$  Ma (Figure 13 a,b).



Figure 11- Photographs showing the general appearance of clastic rocks forming the Konacı member (Konacı village).

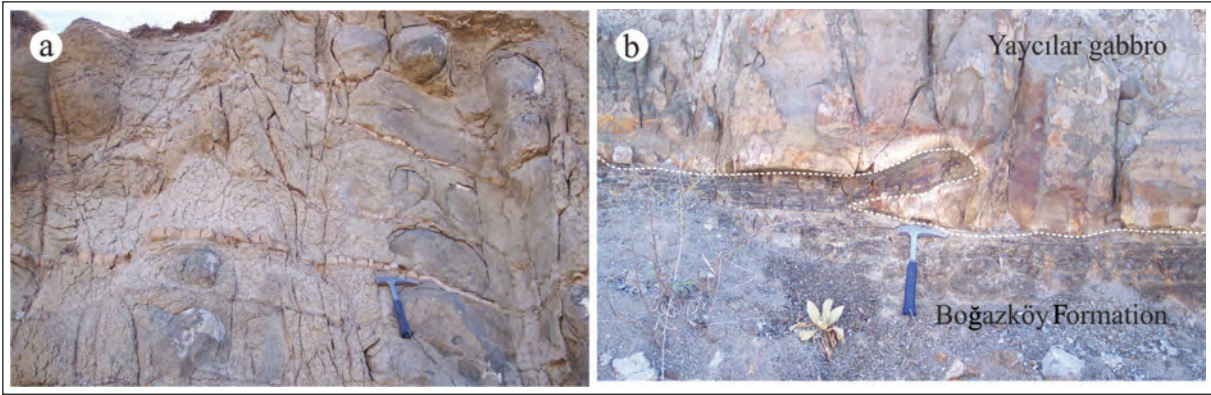


Figure 12- Photographs showing the Yaycılar gabbro; dike-vein systems with micro-monzonitic composition (a) and intrusive contact of the gabbro with the Boğazköy Formation (b) (Karakız village).

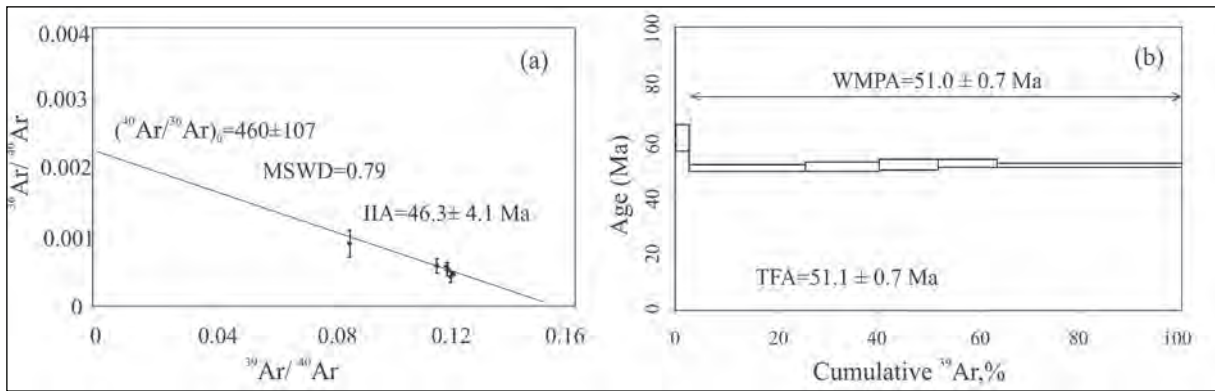


Figure 13- Plagioclase isochron (a) and plateau (b) age diagrams from Yaycılar gabbro (Yaycılar village).

## 4.2. Geochemical Characteristics

To characterise the volcanism affecting the Sorgun-Yıldızeli foreland basin geochemically, a total of 17 samples were collected from members of the Boğazköy Formation including 5 samples from the basaltic Pazarçık volcanic member, 6 samples from the andesite-dacite Kiremitlik volcanic member and 6 samples from the Yaycılar gabbroic sills and laccoliths in the basal sections of the Boğazköy Formation. As the Sarayözü member had undergone an advanced degree of alteration, fresh samples appropriate for analysis could not be obtained. The results of the chemical analyses are given in table 1.

### 4.2.1. Classification

The Pazarçık and Kiremitlik volcanic members and the Yaycılar gabbro were classified on the total alkali versus silica (TAS) diagram (Le Bas et al. 1986) (Figure 14 a) and the Pazarçık volcanics generally have basaltic composition. Samples mainly plot in the basaltic andesite, trachybasalt and basaltic

trachyandesite fields. One of the samples from the Kiremitlik volcanic member is trachyandesite and another is rhyolite, the rest are dacite in composition.

As seen in table 1, some of the samples has very high loss on ignition values (LOI), ranging between 3.95-9.06 in the Pazarçık volcanic member, 0.80-3.68 in the Kiremitlik volcanic member and 3.09-4.53 in the Yaycılar gabbro. In petrographic investigations, some of the samples from Kiremitlik member have thin to thick carbonate and silica veinlets and filling cavities and iron oxide on fractures, indicating the role of alteration processes which also affect the chemical results.

As hydrothermal alteration processes may cause changes in the major oxide values of rocks (especially  $\text{SiO}_2$ ,  $\text{CaO}$ ,  $\text{K}_2\text{O}$  and  $\text{Na}_2\text{O}$ ), the samples are plotted on the  $\text{SiO}_2$ -Zr/TiO<sub>2</sub> diagram of Winchester and Floyd (1977) and the Zr/Ti-Nb/Y diagram modified by Pearce (1996), utilising less mobile elements to classify altered rocks. due to low alteration and metamorphism conditions (Figure 14 c,d). In figure

Table 1- Whole rock (major, trace and rare earth elements) chemical analysis results for rock samples from the Pazarcık volcanic member, Kiremitlik volcanic member and Yaycılar gabbro.

SAMPLE NO	KİREMİTLİK VOLCANIC MEMBER						PAZARCIK VOLCANIC MEMBER					YAYCILAR GABBRO					
	K1	K2	K3	K4	K5	K6	P1	P2	P3	P4	P5	G1	G2	G3	G4	G5	G6
Major Oxides Wt. %																	
SiO <sub>2</sub>	59	62,2	65,7	67,6	68,9	66	49,9	49	48,7	48,3	49,3	46,8	50,5	48,9	47,9	49,3	50,6
Al <sub>2</sub> O <sub>3</sub>	16,7	15,75	16,8	15,55	15,4	15,5	15,3	16,35	16,5	15,95	16,3	16,05	17,4	16,9	16,85	16,9	19
Fe <sub>2</sub> O <sub>3</sub>	6,08	5,11	2,77	3,84	2,85	3,47	9,85	9,92	10,45	9	10,1	11,65	10,45	10,65	11,25	10,7	8,5
CaO	3,72	4,43	3,78	3,74	3	3,84	8,46	8,68	7,97	10,05	9,08	8,7	8,08	8,06	9,24	8,84	7,75
MgO	1,84	0,44	0,33	0,6	0,49	0,5	5,42	4,64	5,01	3,18	4,76	5,93	4,02	4,95	5,4	4,17	4,29
Na <sub>2</sub> O	5,37	3,91	4,42	4,09	4,51	4,28	4,55	3,42	4,41	2,96	3,47	3,81	4,06	3,84	3,25	4,02	4,36
K <sub>2</sub> O	2,14	2,72	2,7	2,63	3,18	2,86	1,67	1,56	2,04	1,1	2,07	1,44	2,1	1,65	1,39	1,6	1,98
Cr <sub>2</sub> O <sub>3</sub>	<0,01	<0,01	<0,01	0,01	<0,01	<0,01	0,01	<0,01	<0,01	<0,01	<0,01	0,01	<0,01	<0,01	0,01	<0,01	0,01
TiO <sub>2</sub>	0,66	0,69	0,67	0,59	0,47	0,58	0,94	1,01	1,14	0,97	1,05	1,15	1,22	1,12	1,15	1,14	0,9
MnO	0,08	0,06	0,01	0,03	0,04	0,03	0,18	0,17	0,18	0,15	0,17	0,19	0,17	0,18	0,17	0,17	0,08
P <sub>2</sub> O <sub>5</sub>	0,31	0,27	0,27	0,22	0,17	0,24	0,28	0,25	0,29	0,25	0,34	0,24	0,31	0,28	0,24	0,26	0,24
SrO	0,03	0,05	0,05	0,04	0,04	0,05	0,06	0,06	0,07	0,05	0,08	0,08	0,07	0,07	0,06	0,05	0,09
BaO	0,06	0,1	0,1	0,13	0,1	0,12	0,06	0,06	0,06	0,04	0,06	0,06	0,05	0,04	0,04	0,05	0,05
Loss on Ignition	3,68	2,84	2,8	2,16	0,8	1,54	4,86	6,15	5,03	9,06	3,95	4,53	3,19	4,3	3,26	4,23	3,81
Total	99,67	98,57	100,4	101,23	99,95	99,01	101,54	101,27	101,85	101,06	100,73	100,64	101,62	100,94	100,21	101,43	101,66
Trace Elements ppm																	
Ba	492	777	811	1005	805	933	535	467	488	339	513	469	385	349	364	375	370
Cr	10	30	20	40	20	20	50	10	20	10	20	50	20	40	40	30	60
Cs	1,13	2,75	1,91	2,1	2,43	2,15	3,32	1,03	6,02	0,66	1,29	1,8	0,67	0,71	0,66	2,5	1,25
Ga	19	17,7	19,1	17,1	16,8	17,2	18	18,7	18,7	18,3	18,6	18,7	19,6	19,3	18,7	19,6	18,8
Hf	4,4	4,4	5	4,6	4,9	4,6	2,8	2,9	2,7	2,7	3,1	2,1	2,7	2,6	2,2	3	2,3
Nb	9,3	11,1	13,3	10,5	12,5	11,8	6,5	4,8	5,2	6,2	7,8	3,6	5,4	4,7	3,8	5,3	4,7
Rb	56,2	81,7	58,1	82,1	108	91,9	46,6	32,1	45,9	24,1	61	28,1	50,8	31,8	32,1	33,9	49,1
Sn	1	1	1	1	1	1	1	1	1	1	1	1	1	1	1	1	1
Sr	336	463	497	431	388	468	491	550	571	501	710	713	614	626	574	447	762
Ta	0,6	0,8	1	0,8	1	0,9	0,3	0,2	0,3	0,3	0,4	0,1	0,3	0,2	0,2	0,3	0,2
Th	7,19	15,55	18,65	15,05	20	18	5,29	7,06	4,21	5,38	5,9	5,8	3,8	3,7	3,03	4,46	3,23
Tl	<0,5	<0,5	<0,5	<0,5	<0,5	<0,5	<0,5	<0,5	<0,5	<0,5	<0,5	<0,5	<0,5	<0,5	<0,5	<0,5	<0,5
U	1,65	3,24	2,39	3,2	4,45	4,13	1,43	2,24	1,19	1,1	1,55	1,22	0,92	0,87	0,72	1,08	0,8
V	98	101	107	102	79	98	280	267	300	249	277	385	295	290	375	287	225
W	<1	1	1	<1	1	1	<1	<1	<1	<1	<1	<1	<1	<1	<1	<1	<1
Y	27	20	18,8	18,7	15,8	17,6	24,3	23,4	24,9	22,3	25,1	22,7	26,2	25,5	21,8	26,7	19,9
Zr	159	156	181	160	172	168	93	91	87	87	99	62	86	83	68	98	75
As	0,8	2	1,3	1,7	1,3	0,9	0,6	3,5	0,2	0,2	1,1	0,3	<0,2	1,7	0,8	1,2	<0,2
Be	1,55	1,31	1,4	1,58	1,6	1,76	1,27	1,04	1,11	0,88	1,37	0,88	1,05	0,9	0,8	1,22	1,02
Bi	<0,01	0,1	0,07	0,04	0,06	0,04	0,02	0,17	0,04	0,03	0,07	0,04	0,02	0,07	0,04	0,05	0,02
Cd	0,05	0,06	0,02	0,02	0,02	0,03	0,11	0,08	0,16	0,08	0,1	0,1	0,09	0,15	0,12	0,07	0,04
Co	10,8	7,5	3,8	5	3,1	5,6	30,2	28,6	32,6	26,7	32,2	37,8	30	32,9	37,4	34,2	26,5
Cu	11,8	15,5	17,4	20,6	8,2	45,6	111,5	49,2	96,4	28,4	109	105	113	142,5	89,3	102	14,6
Ge	0,2	0,12	0,12	0,13	0,14	0,16	0,17	0,11	0,12	0,11	0,11	0,1	0,11	0,1	0,08	0,1	0,08
Mo	0,84	0,62	0,66	1,09	1,52	1,27	0,76	0,82	0,86	0,41	1,1	0,74	1,05	0,92	0,5	0,81	1,06
Ni	2,4	8,3	4,6	11,3	5,7	8,3	26,3	9,9	20	10,4	23,5	32,5	16,3	23,3	25	23,5	23,5
Pb	8,3	15,9	17,3	14,1	18,2	16	10	13,2	4,9	5,8	8,8	6,6	4,5	3,3	3,6	3,9	1,8
Sb	0,23	0,36	0,37	0,26	0,41	0,26	0,16	0,52	0,15	0,18	0,21	0,1	0,11	0,15	0,15	0,21	0,1
Zn	45	24	37	36	29	15	89	78	86	71	77	89	74	75	70	82	28
Rare Earth Elements ppm																	
Ce	45,6	58,5	68,8	59,5	61	73,5	37,4	37,3	34,2	41,1	42,3	36,8	31	30,4	24,5	33,2	25,6
Dy	4,52	3,55	3,4	3,24	2,77	3,09	4,44	4,28	4,47	4,03	4,51	4,17	4,71	4,47	3,97	4,71	3,58
Er	2,88	2	2,08	2,02	1,68	1,89	2,52	2,63	2,63	2,43	2,55	2,39	2,8	2,75	2,3	2,92	2,16
Eu	1,34	1,18	1,26	1,1	0,97	1,15	1,37	1,41	1,4	1,33	1,38	1,41	1,41	1,35	1,19	1,37	1
Gd	4,75	3,88	4	3,8	3,21	3,75	4,84	4,62	4,88	4,25	5,06	4,66	4,85	4,83	3,97	4,84	3,59
Ho	1,03	0,77	0,73	0,72	0,6	0,69	0,94	0,94	0,97	0,88	0,97	0,91	1,06	0,98	0,86	1,07	0,77
La	25	33,7	38,9	33,4	36,5	42,6	19	19,1	16,7	20,6	21,3	19,1	15,3	14,8	12	16,5	12,8
Lu	0,47	0,34	0,36	0,32	0,29	0,32	0,37	0,38	0,39	0,34	0,39	0,34	0,42	0,41	0,35	0,44	0,34
Nd	21,8	23,1	26,3	23,2	20,9	27,1	19,4	19,3	19,2	20	21,7	19,7	17,7	17,4	14,3	18,3	13,7
Pr	5,78	6,57	7,66	6,83	6,57	8,11	4,83	4,82	4,51	5,21	5,48	4,79	4,14	4,15	3,4	4,38	3,37
Sm	4,47	4,28	4,51	4,05	3,4	4,37	4,24	4,38	4,45	4,18	4,87	4,36	4,26	4,12	3,55	4,42	3,15
Tb	0,74	0,58	0,62	0,59	0,48	0,55	0,72	0,72	0,74	0,66	0,74	0,7	0,77	0,75	0,65	0,79	0,57
Tm	0,43	0,31	0,31	0,29	0,25	0,28	0,36	0,37	0,36	0,33	0,37	0,34	0,41	0,39	0,34	0,43	0,3
Yb	2,88	2,15	2,17	1,92	1,71	1,97	2,29	2,39	2,49	2,25	2,49	2,17	2,63	2,51	2,21	2,76	2,1
Mg#	37,50	14,60	19,10	23,60	25,40	22,20	52,20	48,10	48,70	41,20	48,30	50,20	43,30	47,90	48,70	43,60	50,00
Eu/Eu*	0,89	0,89	0,91	0,86	0,90	0,87	0,93	0,96	0,92	0,97	0,85	0,96	0,95	0,93	0,97	0,91	0,91

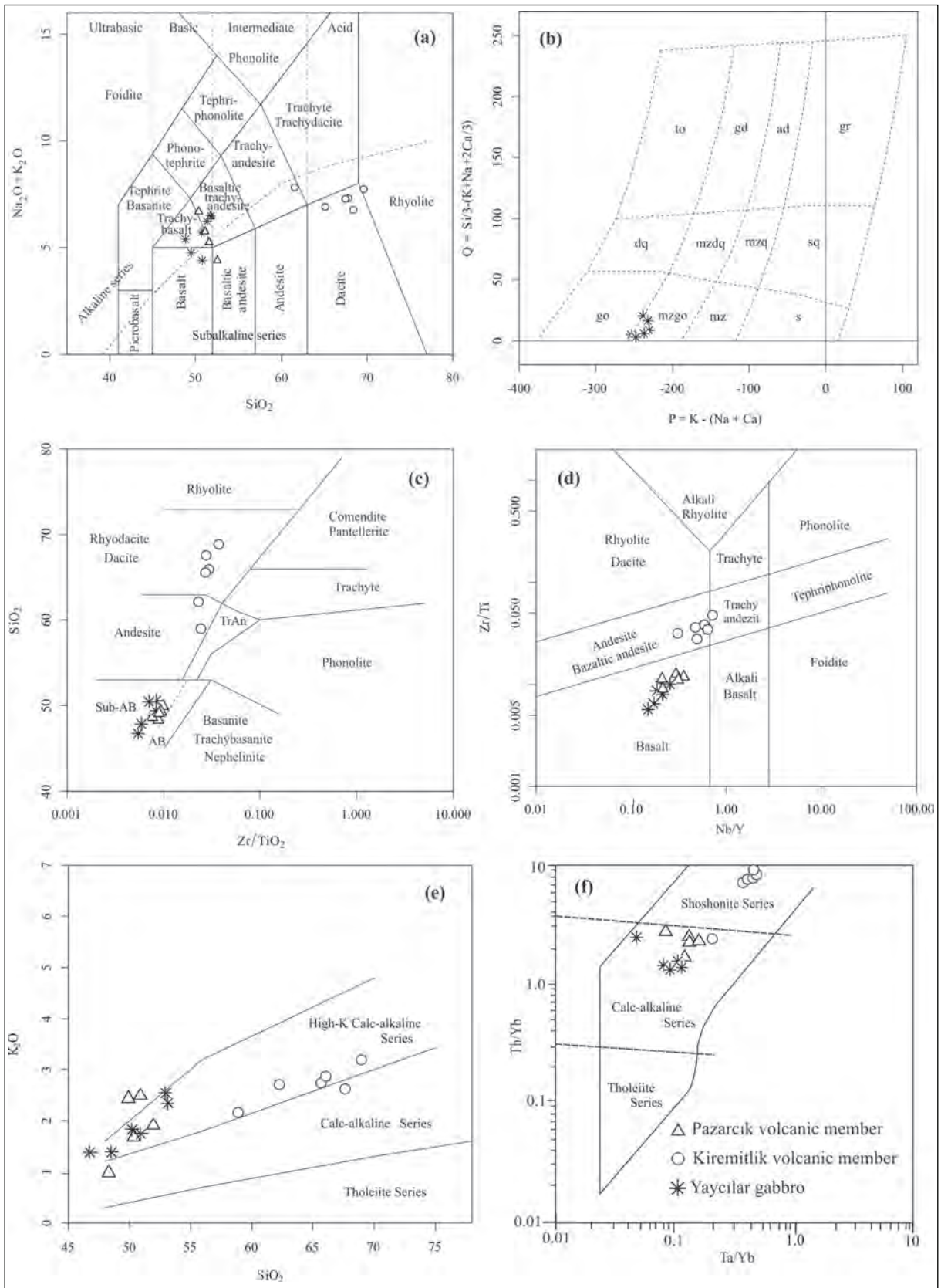


Figure 14- Classification diagrams of Pazarçık and Kiremitlik volcanic rocks (a) Le Bas et al. (1986), (b) Debon and Le Fort (1983), (c) Winchester and Floyd (1977), (d) Pearce (1996), (e) Peccerillo and Taylor (1976), and (f) Pearce (1983).

14c, d, samples from the Pazarcık volcanic member and the Yaycılar gabbro exhibit sub-alkaline trend and are basalt in composition. Two samples from the Kiremitlik volcanic members are andesite and four samples are rhyodacite/dacite in composition (Figure 14 c). On Pearce's (1996) Zr/Ti-Nb/Y diagram, samples from the Pazarcık volcanic member and the Yaycılar gabbro plot in the field of basalt, samples from the Kiremitlik volcanic member range in composition from andesite/basaltic andesite to trachyandesite (Figure 14 d). It is apparent from the classification diagrams that samples of the Kiremitlik volcanic member have partially experienced alteration (silicification). Thus, the most plausible classification diagram for altered samples is the Zr/Ti-Nb/Y diagram of Winchester and Floyd (1977) modified by Pearce (1996). Consequently, based on petrographic data and Zr/Ti-Nb/Y classification diagram, the Pazarcık and Kiremitlik volcanic member are the products of basaltic and andesitic volcanism, respectively.

Samples from the Yaycılar gabbro is similar to that of the Pazarcık volcanic member on the TAS diagram, but on the P-Q diagram of Debon and Le Fort (1983) they are classified as gabbro-monzogabbro (Figure 14 b).

Samples are plotted on the  $\text{SiO}_2$  versus  $\text{K}_2\text{O}$  diagram of Peccerillo and Taylor (1976) and Ta/Yb-Th/Yb diagram of Pearce (1983) utilising less-mobile elements (such as Th, Ta and Yb) during alteration (Figure 14 e,f). It is clear from the figure 14e that they generally exhibit calcalkaline trend (or high-K calcalkaline), except 2 samples from the Pazarcık volcanic having shoshonitic affinities (Figure 14 e). On the Ta/Yb versus Ta/Yb diagram (Pearce, 1983), samples from the Pazarcık volcanic member and Yaycılar gabbro have calc-alkaline trends, the great majority of the samples from the Kiremitlik volcanic member are clearly plotted in the field of shoshonite (Figure 14 f).

Samples from the Kiremitlik volcanic member have geochemical features similar to shoshonites with their low  $\text{TiO}_2$  and  $\text{Fe}_2\text{O}_3$  contents, enrichment in Ba, Rb, Ce and Pb elements and high total alkali ( $\text{Na}_2\text{O} + \text{K}_2\text{O} > 5\%$ ) contents, despite having low  $\text{K}_2\text{O}$  values relative to  $\text{Na}_2\text{O}$  ( $\text{K}_2\text{O} / \text{Na}_2\text{O} < 1$ )

According to Morrison (1980), in subduction belts during consumption of the subduction phase shoshonitic rocks may be formed related to arc deformation.

Though the magma source generating the Kiremitlik volcanic member may not be typical, the similar characteristics to shoshonitic magma may be due to hot asthenospheric mantle rising during slab breakoff and pushed deep under the continent by subduction and collision events causing crustal material to melt or due to crustal contamination during ascent of magma through continental crust.

#### 4.2.2. Major Oxides and Trace Element Characteristics

In order to determine the role of fractional crystallisation processes, variation diagrams of major-oxides are plotted against  $\text{SiO}_2$  in figure 15. It is clear from the figure there is a negative correlation between  $\text{SiO}_2$  and CaO, MgO,  $\text{TiO}_2$ , and  $\text{FeO}_t$ , a positive correlation between  $\text{SiO}_2$  and  $\text{Na}_2\text{O}$ ,  $\text{K}_2\text{O}$ . The plots of  $\text{SiO}_2$  against  $\text{Al}_2\text{O}_3$ ,  $\text{P}_2\text{O}_5$  in Pazarcık volcanic member and Yaycılar gabbro exhibit roughly vertical trends with increasing  $\text{Al}_2\text{O}_3$  and  $\text{P}_2\text{O}_5$ , but in Kiremitlik volcanic member, there is a clear negative correlation between  $\text{SiO}_2$  and  $\text{Al}_2\text{O}_3$ ,  $\text{P}_2\text{O}_5$ .

The negative correlations between  $\text{SiO}_2$  and  $\text{FeO}_t$ , MgO, CaO,  $\text{TiO}_2$  are qualitatively related with the removal of olivine, pyroxene, Ca-plagioclase and titanohematites from the melt at the beginning of crystallisation. The positive correlation between  $\text{SiO}_2$  and  $\text{K}_2\text{O}$ ,  $\text{Na}_2\text{O}$  may also indicate a fractionation trend, since Na-plagioclase and mica minerals are the last minerals to crystallise from a melt and thus, they become enriched within a melt during fractional crystallisation.

The variation diagrams of  $\text{SiO}_2$  versus trace elements (Rb, Ba, Sr, Zr, Nb, Sm, Ni, Co, Th, La, Y, V) are given in figure 16. On these diagrams, there is a positive correlation between  $\text{SiO}_2$  and Rb, Ba, Th, Zr, Hf, Nb, and La elements. These elements occur within minerals forming during slightly later stages of crystallisation and thus show positive correlation. Sr, Sm, Ni, Co, Y, and V elements occur within minerals crystallising in the early stages so they show negative correlation with  $\text{SiO}_2$ . The positive correlation between  $\text{SiO}_2$  and Rb, Ba and Th elements can be explained by fractionation of feldspars and amphiboles, the negative trend of Sr is due to substitution of Sr for Ca in Ca-plagioclase and removal of Ca-plagioclase from the melt at the early stages of fractional crystallisation.

The magnesium number ( $\text{Mg\#} = \text{molar } 100 \times \text{MgO} / [\text{MgO} + \text{tFe}_2\text{O}_3]$ ) of the Pazarcık volcanic member

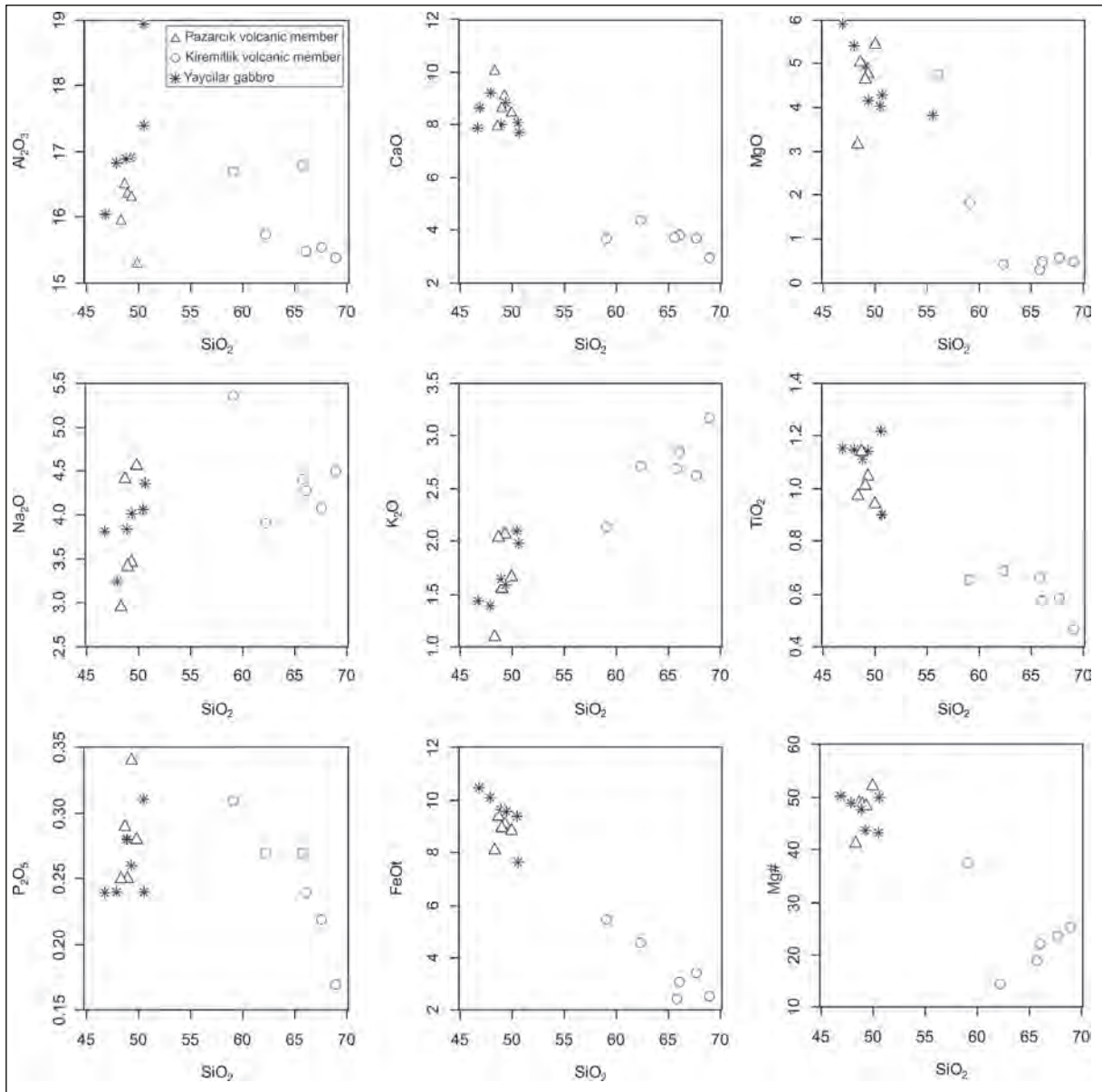


Figure 15-  $\text{SiO}_2$  (%) versus major oxide (%) variation diagrams for Pazarçık and Kiremitlik volcanic members and Yaycılar gabbro.

ranges from 41.18 to 51.26, from 43.25 to 50.21 in the Yaycılar gabbro and from 14.37 to 37.48 in the Kiremitlik volcanic member.

The observed variations on Harker diagrams and the moderate-low Mg number of the units indicate that they have experienced variable amounts of fractional crystallisation and as a result, the volcanism in the Sorgun-Yıldızeli basin was derived from evolved magma.

The variation diagrams of  $\text{SiO}_2$  versus major oxides and trace elements display that samples from the Pazarçık and Kiremitlik volcanics form separate

groups, with fractional crystallisation trends within each group. This may be due to different reasons such as crustal contamination, residence time within the crust, variable degree of partial melting of the magma source, evolution of the magma as a result of a single fractional crystallisation process, or developments of magmatic processes in separate stages.

#### 4.2.3. Trace and Rare Earth Element (REE)

##### Characteristics

Mid-Ocean Ridge Basalts (MORB) and chondrite-normalised multi-element distribution diagrams of

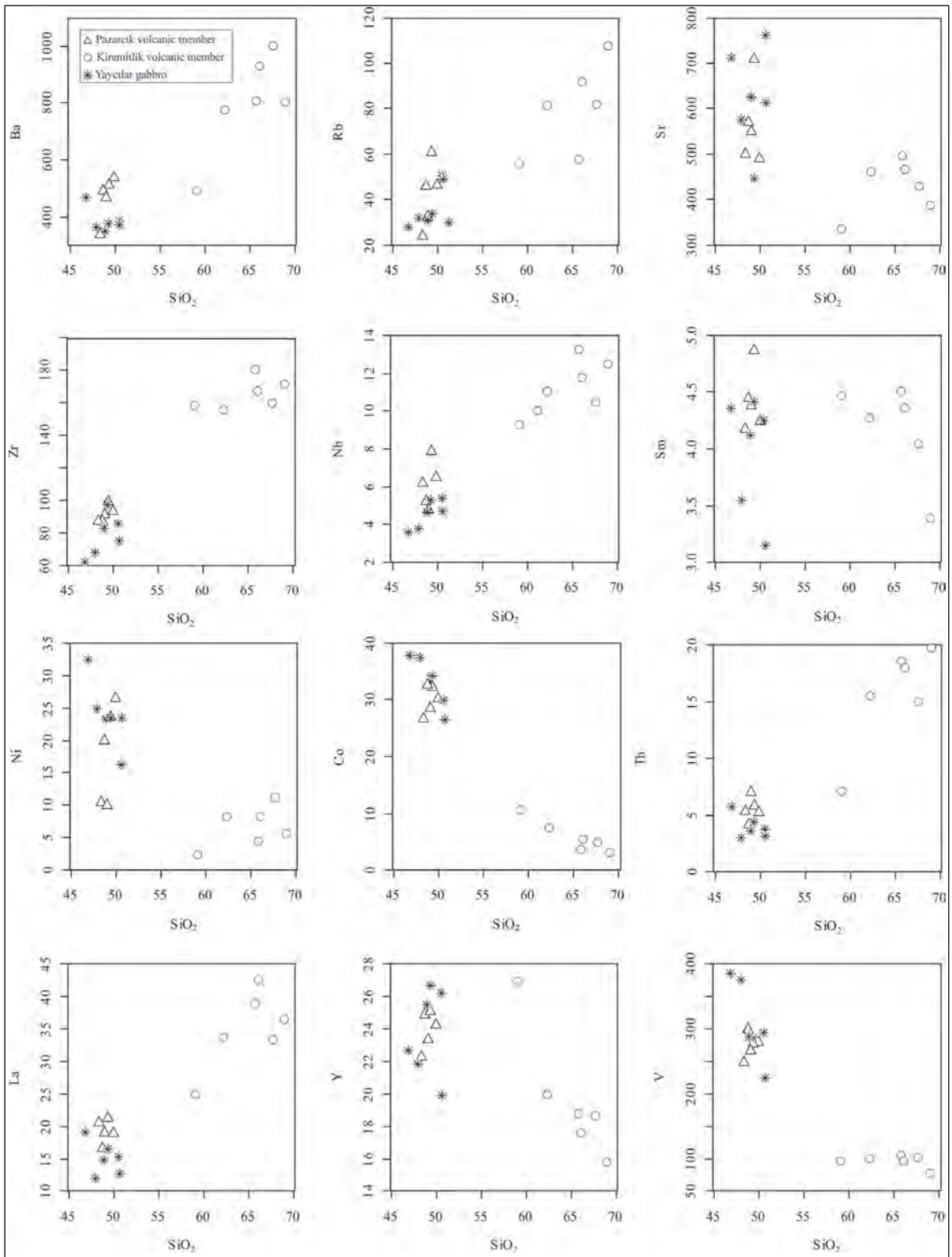


Figure 16- SiO<sub>2</sub> (%) versus trace element (ppm) variation diagrams for Pazarcık and Kiremitlik volcanic members and Yaycılar gabbro.

Pazarcık and Kiremitlik volcanic samples are illustrated in figure 17 to determine the source characteristics of the volcanic rocks. Features common for all samples are the enrichment in large ion lithophile elements (Sr, K, Rb, Ba and Th) and the depletion in Nb, Ta, Ti, Y and Yb elements. Clear enrichment in large ion lithophile elements combined with the Nb-Ta negative anomaly are similar to characteristic geochemical properties of active continental margin or arc magmatism and indicate the presence of subduction components in magma source (Gill, 1981; Fitton et al., 1988; Pearce, 1983; Wilson, 1989). Depletion of Y and Yb elements is considered to be due to the presence of amphibole and/or some garnet (Figure 17 a).

On chondrite - normalised multi - element distribution diagrams, light rare earth elements (LREE) appear to be enriched relative to heavy rare earth elements (HREE). The concave distribution of rare earth elements may correspond to the fractional crystallisation process and the removal of amphibole and pyroxene minerals during fractionation (Figure 17 b).

The  $Eu/Eu^*$  ratios ( $Eu/Eu^* = Eu_n / (Sm_n + Gd_n)^{0.5}$ ) are 0.85-0.97 for the Pazarcık volcanic member, 0.9-0.97 for the Yaycılar gabbro and 0.86-0.91 for the Kiremitlik volcanic member. If this ratio is larger than 1, a positive anomaly is present, if it is smaller than 1, a negative anomaly exists. According to these values, the Yaycılar gabbro has a weak negative Eu anomaly, while the Pazarcık and Kiremitlik volcanic member have a moderate degree of negative anomaly. This negative anomaly indicates fractional crystallisation and plagioclase fractionation.

#### 4.2.4. *Effects of Subduction Components and/or Crustal Contamination*

With the aim of determining whether subduction zone enrichment and/or crustal contamination with intraplate enrichment was effective on the genesis of the Yaycılar gabbro and Pazarcık and Kiremitlik volcanics, samples are assessed on diagrams using trace element ratios such as Th/Y, Nb/Y and Rb/Y (Figure 18 a,b).

The Th/Nb ratio of samples from the Yaycılar gabbro is 0.70-1.61, while this ratio is 0.76-1.47 for Pazarcık volcanic samples and 0.77-1.60 for samples from the Kiremitlik volcanic member. When the Th/Y against Nb/Y diagram is examined, samples appear to plot close to the Th/Nb=1 line. Th is enriched

in continental crust, while Nb is found at smaller amounts. High Th/Nb ratios indicate that rocks have experienced crustal contamination (Pearce, 1983). This contamination may be due to subduction effects, but may also be due to assimilation of wall rocks during the rising of magma to the surface. With the increase in Nb/Y ratio, increasing Th/Y shows intraplate enrichment, while low Nb/Y ratios with increasing Th/Y ratio shows subduction zone enrichment (Figure 18 a).

On the Rb/Y-Nb/Y diagram, Rb/Nb=1 line indicates intraplate enrichment, while vertical trend shows subduction zone enrichment and/or crustal contamination (Edwards et al., 1991). The Rb/Nb ratios vary from 6.40 to 10.45 in samples from the Yaycılar gabbro, 3.89-8.83 in the Pazarcık volcanic member and 4.37-8.64 in the Kiremitlik volcanic member. The vertical trend shows that subduction zone enrichment and/or crustal contamination has played a significant role in the evolution of magma. The magma generating the Kiremitlik volcanic member experienced greater crustal contamination and/or intraplate enrichment relative to the Pazarcık volcanic member (Figure 18b).

#### 4.2.5. *Tectonic Environment*

The Pazarcık and Kiremitlik volcanic members and Yaycılar gabbro were evaluated on tectonic discrimination diagrams (Figure 19 a,b,c,d). As seen in the ternary plot of Th-Hf/3-Nb/16 (Wood, 1980), samples plot in the field of calcalkaline volcanic arc basalts (Figure 19a). Agrawal et al. (2008) used trace elements that are easily mobilised in low alteration and metamorphism conditions (La, Sm, Yb, Nb and Th) to determine the tectonic environment of basic and ultrabasic rocks (island arc, continental rift, oceanic island and mid-ocean ridge). On this tectonic discrimination diagram, the Pazarcık volcanics and Yaycılar gabbro cluster in the island arc basalt field (Figure 19b).

Figure 19c shows the Th/Yb versus Ta/Yb diagram of Pearce (1983). Accordingly, samples from the Pazarcık and Kiremitlik volcanic members and Yaycılar gabbro are plotted within the volcanic arc field (Figure 19c). Although the Pazarcık volcanic member and Yaycılar gabbro fall in the calc-alkali series, the Kiremitlik volcanic member samples cluster in the shoshonitic field. In the tectonic discrimination diagram (Figure 19d) of Thieblemont and Tegyey

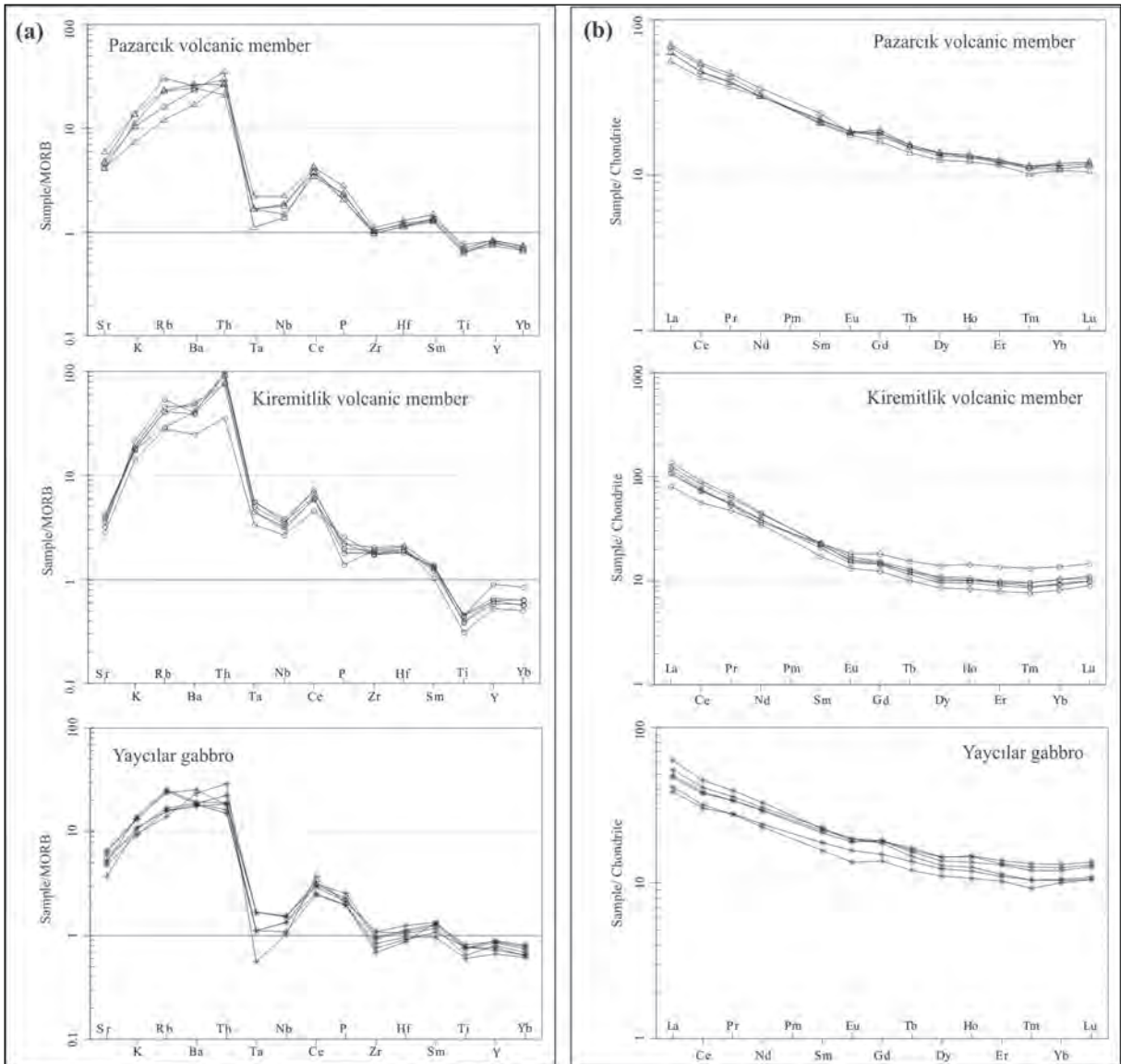


Figure 17- (a) MORB (Pearce, 1983) and (b) Chondrite-normalised (Boynton, 1984) multi-element distribution diagrams of Pazarlık and Kiremitlik volcanic members and Yaycılar Gabbro.

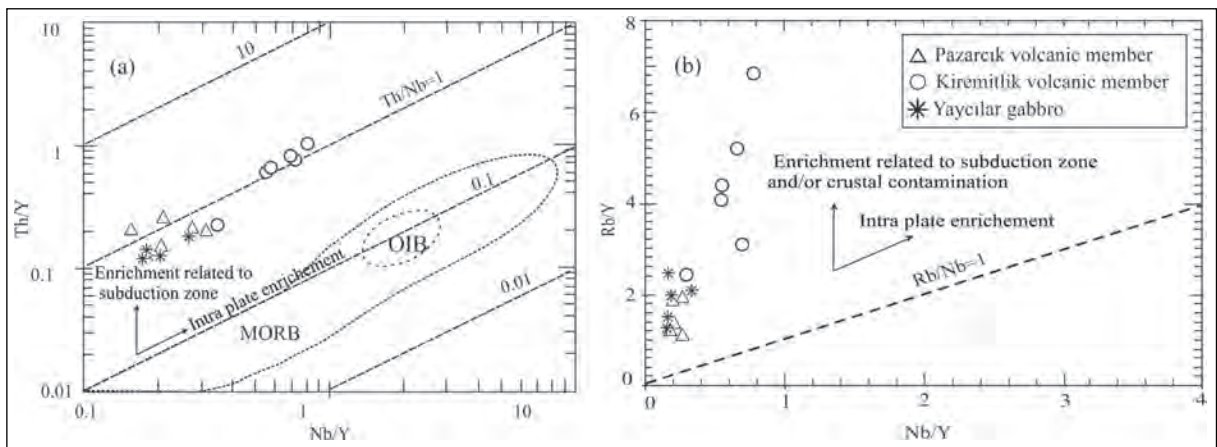


Figure 18- (a) Nb/Y vs. Th/Y (Pearce, 1983) and (b) Nb/Y vs. Rb/Y (Edwards et al., 1991) diagrams of Pazarlık and Kiremitlik volcanic members and Yaycılar Gabbro.

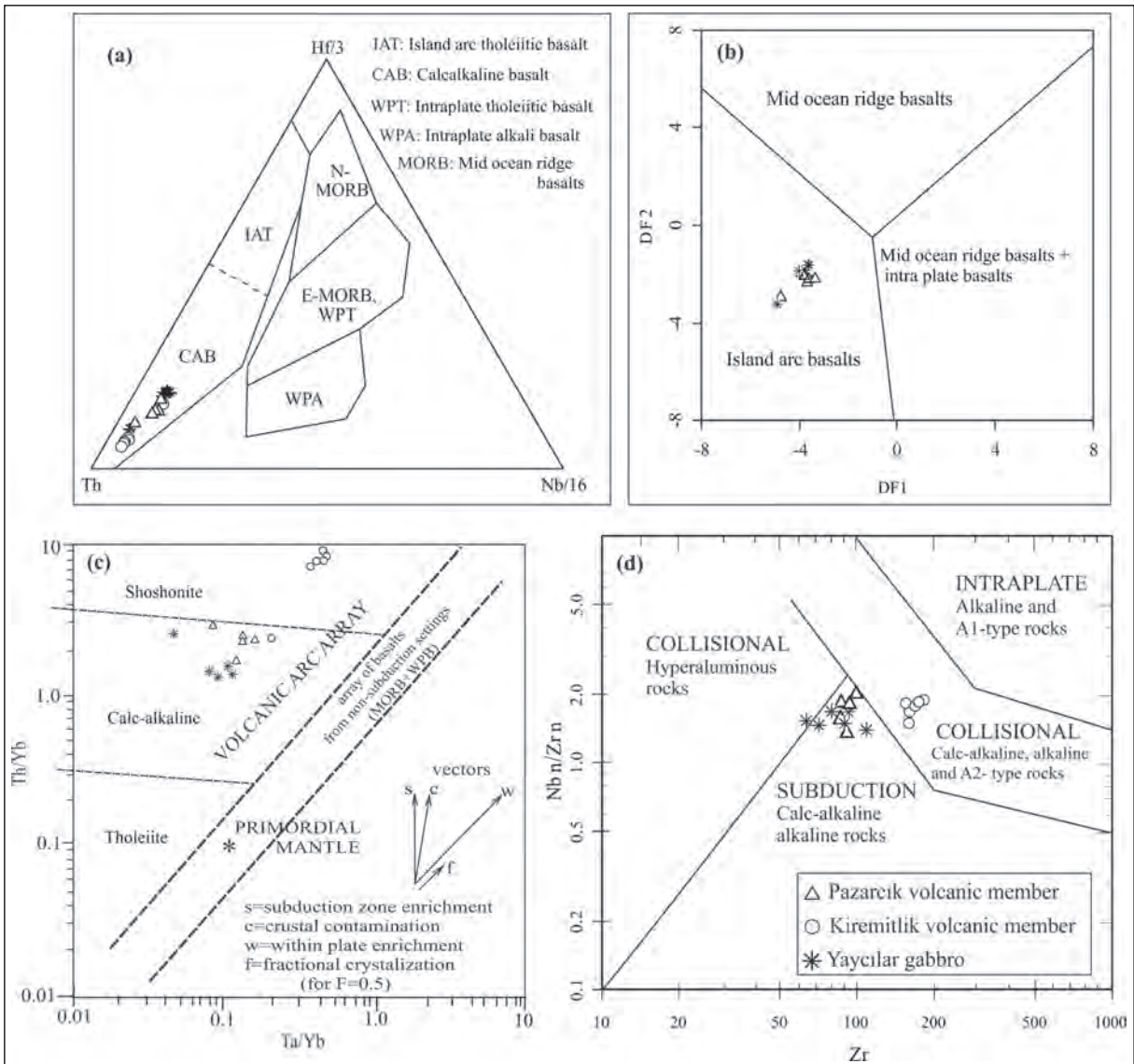


Figure 19- Tectonic discrimination diagrams for Pazarçık and Kiremitlik volcanics (a) Th-Hf/3-Nb/16 ternary diagram of Wood (1980), (b) DF1 vs. DF2 diagram of Agrawal et al. (2008), (c) Th/Yb vs. Ta/Yb discrimination diagram of Pearce (1983 and (d) Zr vs. Nb<sub>n</sub>/Zr<sub>n</sub> diagram of Thieblemont and Tegyey (1994). [DF1= 0.3518\*ln(La/Th)+0.6013\*ln(Sm/Th)-1.3450\*ln(Yb/Th)+2.1056\*ln(Nb/Th)-5.4763; DF2= 0.3050\*ln(La/Th)-1.1801\*ln(Sm/Th)+1.6189\* ln(Yb/Th)+1.226\* ln(Nb/Th)-0.9944].

(1994), Pazarçık volcanic member and Yaycılar Gabbro are located in the field related to subduction, whereas samples from the Kiremitlik volcanic member fall in the field related to collision (Figure 19d).

In this study, it is considered that the Pazarçık volcanic member was derived from a mantle source metasomatized by subduction zone components. The Kiremitlik volcanic member was derived from a mantle source at the base of continental lithosphere metasomatized by subduction events which evolved with partial melting during the slab breakoff process occurring in the late stage of collision.

### 5. Geologic Evolution of Sorgun-Yıldızeli Basin and Discussion

The geologic, sedimentologic, petrographic and geochemical data obtained in this study indicate the Sorgun-Yıldızeli basin is an east-west oriented asymmetric foreland basin. It developed along the northern edge of the Kırşehir Block, above the remnants of the İzmir-Ankara-Erzincan Suture Zone during the subduction of oceanic crust belonging to the northern branch of Neotethys and the collision of the Sakarya continent to the north with the Kırşehir Block to the south.

In light of data obtained from the Sorgun-Yıldızeli foreland basin, an attempt is made to explain the evolution of the basin under the following headings; pre-collisional period (pre-Maastrichtian), collision period (late Maastrichtian-early Palaeocene (early stage) and late Palaeocene-early Lutetian (late stage) periods) and post-collisional period (Lutetian-late Eocene).

### 5.1. Pre-Collision Period (Pre-Maastrichtian)

During this period, the floor of the Neotethys ocean began to descend under the Sakarya continent to the north beginning in the Cenomanian (Tüysüz and Dellaloğlu, 1992; Tüysüz et al., 1995). Consumption of the oceanic crust of the northern branch of Neotethys occurred in two different subduction events according to Tüysüz and Dellaloğlu (1992) and Tüysüz et al. (1995). The first of these produced an ensialic arc on the Sakarya continent (Andes-type active continental margin volcanic belt), while the second was intraoceanic subduction producing an ensimatic island arc (Figure 20).

### 5.2. Collisional Period

#### 5.2.1. Late Maastrichtian-Early Palaeocene (Early Stage)

According to Keskin et al. (2008), toward the end of the Maastrichtian the Kırşehir Block to the south and the Sakarya continent to the north were close enough to initiate collision. Due to the irregularity of the partly colliding continental margins, deposition continued in remnant basins along the collision zone. For example, the remnant basin where the Hıdırnalı group was deposited located south of Tokat (Yılmaz et al., 1993; 1997) continued to experience marine sedimentation until the beginning of the Lutetian.

Our observations in areas where the Hıdırnalı group outcrops (for correlation of sedimentologic and structural characteristics with the Sorgun-Yıldızeli basin) indicate that this remnant basin transformed into a foreland basin from the late Palaeocene in similar to that of the Sorgun-Yıldızeli basin (Figure 21 a,b).

#### 5.2.2. Late Palaeocene-Early Lutetian Period (Late Stage)

Due to continuing N-S oriented compression, the accretionary complex was sliced, overthrust and formed an imbricated structure, causing thickening of the accretionary complex in this period. As a result of continued subduction of oceanic crust and dragging under of the Kırşehir Block, remnant basins along the collision zone were severely narrowed and experienced deformation. From the late Palaeocene period they were transformed into east-west oriented asymmetric margin foreland basins.

Deposition of the Dolak member represented by olistoliths and slices belonging to the accretionary complex along the northern margin of the Sorgun-Yıldızeli foreland basin, alluvial fan and fan delta sediments, continued during the late Palaeocene-middle Eocene period. Olistoliths of varying sizes belonging to the accretionary complex are present within the unit and, slices and thrust plates of ophiolite show that intense compression and shortening was effective during basin development (Figure 22a).

While basin deposition continued in the late Palaeocene-early Eocene period, basaltic lava and pyroclastics of Pazarcık volcanic member carrying subduction signatures, formed in the basin (Figure 22b).

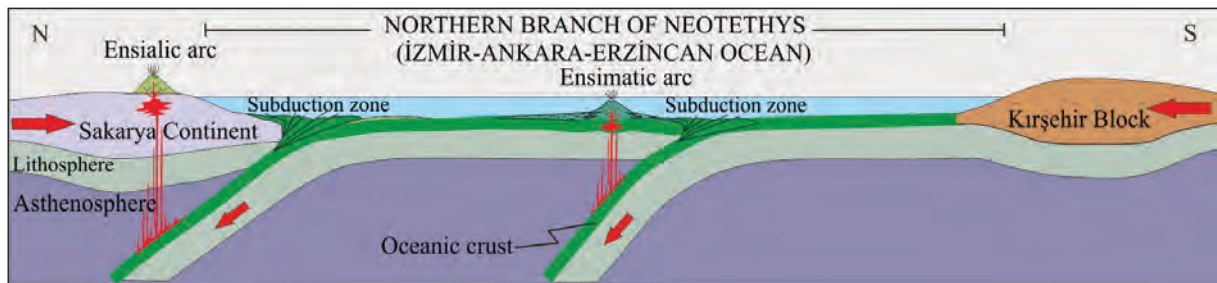


Figure 20- Model section showing tectonic evolution of the northern branch of the Neotethys ocean in the pre-Maastrichtian period (adapted from Tüysüz and Dellaloğlu, 1992).

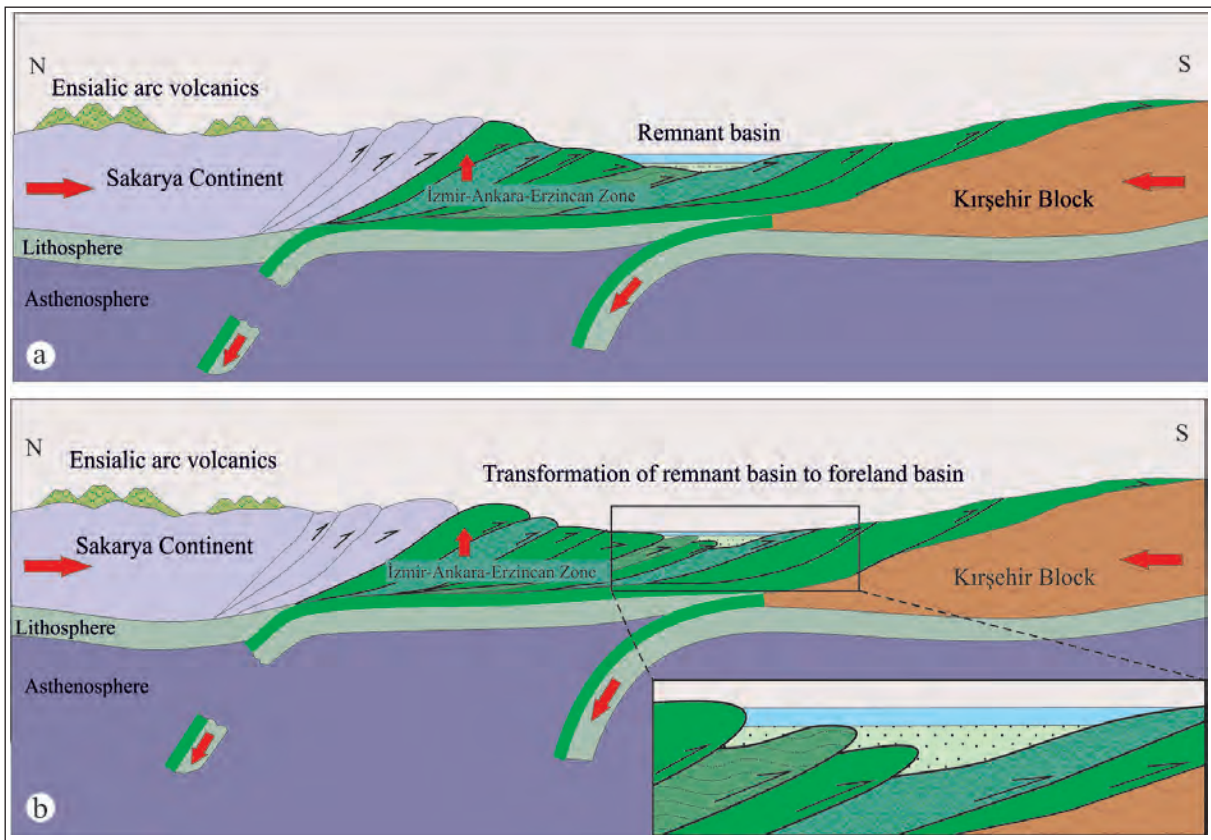


Figure 21- Model section showing tectonic evolution of the northern branch of the Neotethys ocean in (a) Late Maastrichtian-Early Palaeocene and (b) Late Palaeocene.

These volcanics were interpreted by Alpaslan (2000) as due to low-degree partial melting of the upper mantle in an extensional tectonic regime formed in the region in the stage following collision between the Pontides and Anatolides or as products of intraplate magmatism after collision by Koçbulut et al. (2001). In this study, the Pazarcık volcanics are interpreted as products of subduction-related magmatism formed in a compressional tectonic regime.

The Yaycılar gabbro exhibiting similar geochemical characteristics to the Pazarcık volcanics, was emplaced in basal sections of the Boğazköy Formation as sills and laccoliths (Figure 22c).

In the early-middle Eocene period, the composition of volcanism changed from basic to acidic and as a result, Sarayözü dacite and rhyolite volcanic member was formed (Figure 22d). This compositional change in volcanism may have developed as a result of different mechanisms such as differentiation and fractional crystallisation processes in the evolution of magmas, variable degrees of partial melting or partial melting due to dehydration reactions of crustal rocks

as a result of emplacement of basic magma into the lower sections of the continental crust.

In the late stage of collision in the middle Eocene, slab breakoff related to collision was accompanied by emplacement of the Kiremitlik volcanics comprising andesitic lava and pyroclastic rocks (Figure 22e).

The Kiremitlik volcanic member is considered to have derived from a mantle source that evolved as a result of partial melting of the base of the continental lithosphere. This lithosphere had been metasomatised by subduction events due to heat transfer to the continental lithosphere linked to the slab breakoff mechanism.

A study by Keskin et al. (2008) of the western continuation of the study area in the Amasya-Çorum area proposed that volcanism in the middle Eocene developed as a result of slab breakoff. According to this model, with the final closure of remnant basins along the collision zone, sedimentation continued in the Çankırı basin during the Eocene, the suture zone elevated above sea level and experienced significant

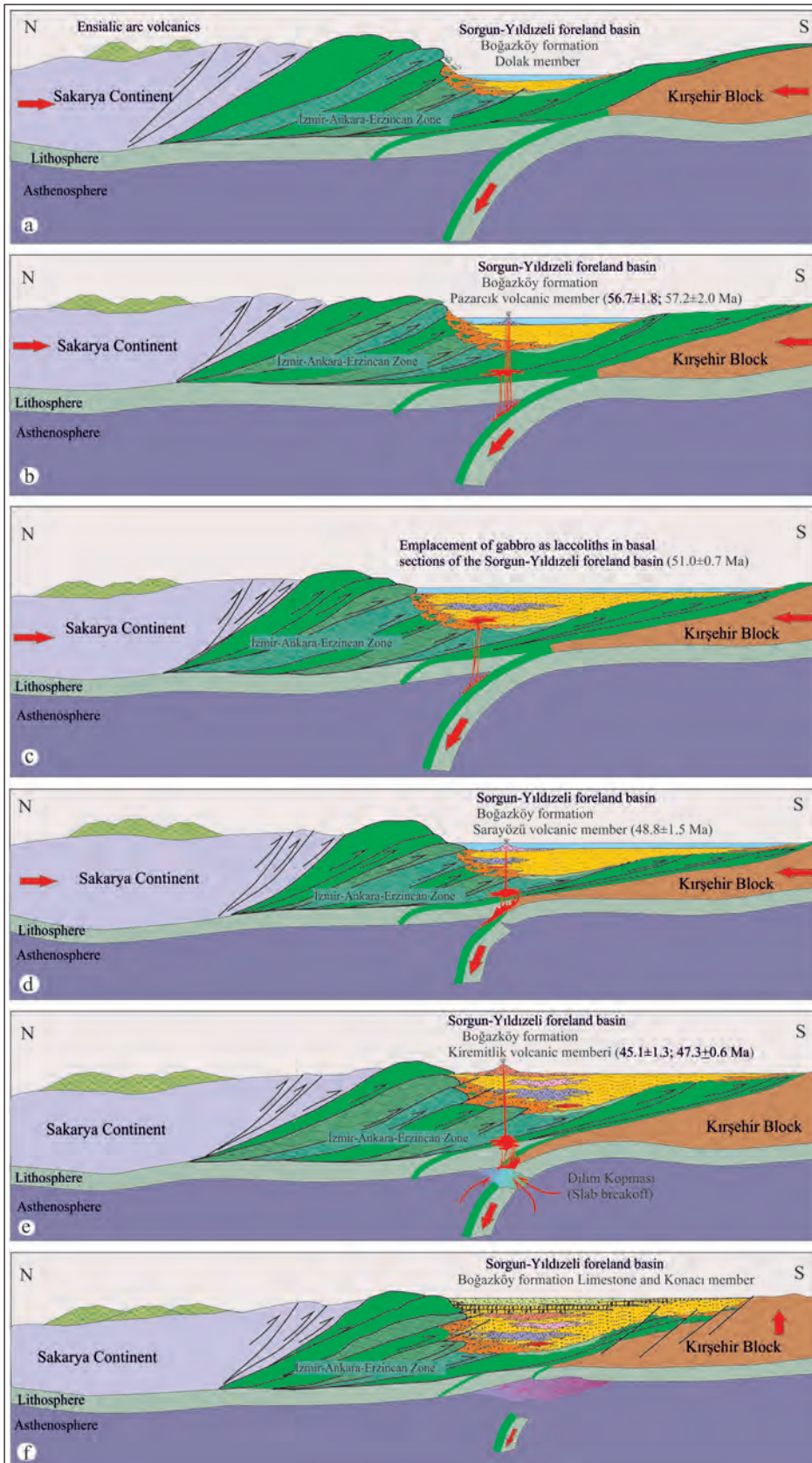


Figure 22- Model section showing tectonic evolution of the Sorgun-Yıldızeli foreland basin in the Late Palaeocene-Early Lutetian period.

erosion until the end of the early Eocene. Beneath the collision zone, with the slab pull of the oceanic lithosphere representing the northern Neotethys ocean controlling the basin, the region became a shallow marine environment with a new transgression in the Lutetian.

Kaymakçı et al. (2009) interpreted the Çankırı basin as a part of a fore-arc basin in terms of location in the Late Cretaceous and stated that a series of piggy-back basins developed above in the Paleocene and later periods with forearc sequences deposited in southward depositional environments.

According to the model recommended in this study, with the remnant basins along the collision zone between the Sakarya continent to the north and the Kırşehir Block to the south experiencing deformation in the late Palaeocene and transformation into foreland basins, though some sections were covered by younger units, not only the Çankırı basin but the eastern extension of this basin of the Çorum, Yozgat, Sorgun and Yıldızeli basins continued sedimenting into the early Lutetian period. Due to relaxation after slab breakoff in the Lutetian, the Kırşehir Block began to be uplifted, the Sorgun-Yıldızeli foreland basin shallowed significantly and the Limestone member comprising reefal limestones and the Konacı member consisting clastic rocks with claystone and clayey limestone layers were deposited (Figure 22f).

### 5.3. Post-Collisional Period (Lutetian-Early Eocene)

During the rapid uplift and relaxation of the Kırşehir Block as a result of slab breakoff in the Lutetian under control of an extensional tectonic regime above the regressive foreland basin and basement rocks, after collision transgressive basins developed (Figure 23a).

The slab breakoff event was effective in transforming the compressional tectonic regime characterised by thrust faulting that dominated until the Lutetian period into an extensional tectonic regime with normal faulting effective in the Lutetian.

The middle-late Eocene Tokuş Formation, comprising the basal conglomerate Susuzdağ member was deposited unconformably above the Akdağmadeni Massif and Boğazköy Formation in a post-collisional basin. The alluvial fan and fan delta sediments of Susuzdağ member pass laterally and vertically into sandstone, sandy limestone, claystone, shale and Nummulites limestone of the Tokuş Formation (Figure 23c).

These post-collisional basins representing the Lutetian-late Eocene period contain volcanic products with characteristics partly similar to the volcanics in the foreland basins as they evolved during the late Palaeocene-early Lutetian period. According to the model proposed in this study, the foreland basins contain volcanic rocks related to subduction processes before slab breakoff and to collision developing during the slab breakoff process. In contrast, post-collisional basins formed in the middle-upper Eocene period contain volcanic rocks related to partial melting of continental lithosphere metasomatised by previous subduction events which hot asthenosphere filled the broken slab volume and magma chambers were emplaced in different sections of the continental crust. Near Ortaköy in the study area, the basal conglomerates of the Tokuş Formation (Susuzdağ member) and the interleaved acidic composition lava and pyroclastic rocks (Ortaköy volcanics) may have developed as a result of this type of mechanism (Figure 23b).

## 6. Conclusions

The rock assemblages that were apparently deposited in two separate E-W oriented basins between Sorgun (Yozgat) and Yıldızeli (Sivas) were determined to be products of a single large basin developed as a result of the same geodynamic processes (“Sorgun-Yıldızeli basin”).

The Sorgun-Yıldızeli basin developed as an east-west oriented asymmetric margin foreland basin accompanied by volcanism related to subduction and/or collision in the late Palaeocene-middle Eocene period during the process of consumption of oceanic crust of the northern branch of Neotethys and the collision of the Sakarya continent to the north with the Kırşehir Block to the south.

The basin fill consists mainly of the Boğazköy Formation and its differentiated subunits. In the basal section of this formation, gabbroic sills and laccoliths, emplaced at shallow depths are called the Yaycılar gabbro.

Interspersed with sedimentary rocks within the basin are also basalt, basaltic andesitic composition lava and pyroclastics of the Pazarcık volcanic member, dacite and rhyolite composition lava and pyroclastics of the Sarayözü volcanic member and andesite and trachyandesite composition lava and pyroclastics of the Kiremitlik volcanic member.

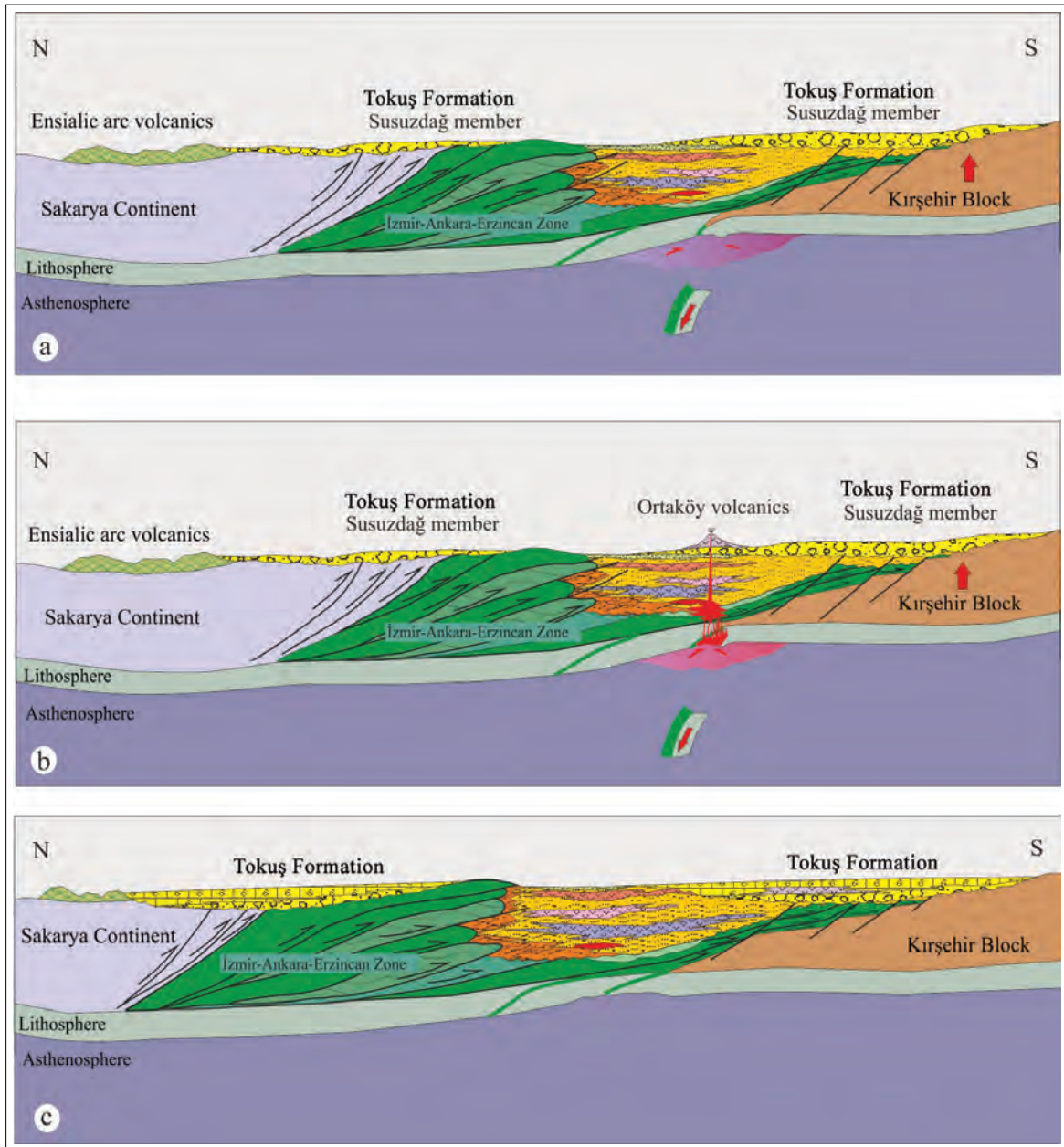


Figure 23- Model section showing tectonic evolution of post-collisional basin (Lutetian-Late Eocene period).

Based on geochemical data, together with multi-element distribution and tectonic discrimination diagrams, the Pazarcık volcanic member may be interpreted as a product of calcalkaline character volcanism related to active subduction in the late Palaeocene-early Eocene period ( $57.2 \pm 2.0$  My and  $56.7 \pm 1.8$  My). Yaycılar gabbro ( $51.0 \pm 0.7$  My) exhibiting similar geochemical features to that of Pazarcık volcanics is the product of subduction-related magmatism. The Kiremitlik volcanic member ( $45.1 \pm 1.3$  Ma and  $47.3 \pm 0.6$  Ma) is interpreted as the product of calcalkaline character volcanism related

to collision and developed during the slab breakoff process in the middle Eocene.

Rapid uplift of the Kırşehir Block due to slab breakoff occurring in the Lutetian led to development of transgressive post-collisional basins over the regressive foreland basin and basement rocks under control of an extensional tectonic regime, with volcanic activity continuing in these basins.

The basal conglomerate (Susuzdağ member) of the Tokuş Formation comprising post-collisional basin

fill around Ortaköy and the interfingering with the acidic composition lava and pyroclastic rocks of the Ortaköy volcanics are interpreted as a product of post-collisional volcanism effective after slab breakoff.

### Acknowledgements

This study includes a portion of the findings obtained during the “Geology and Geodynamic evolution process of the Akdağmadeni Massif” organised by the Directorate of Geological Studies of the General Directorate of Mineral Research and Exploration (MTA). Whole rock geochemical analyses and  $^{40}\text{Ar}/^{39}\text{Ar}$  geochronologic age dating was performed in ActLabs Canada. Petrographic identification of samples was completed by Geo. Eng. (MS) Asuman Besbelli, Dr. Nihal Görmüş, Geo. Eng. Sema Çobankaya, and Geo. Eng. (MS) Ezgi Ulusoy, and palaeontologic dating was performed by Dr. Erkan Ekmekçi, Dr. Aynur Hakyemez, Dr. Fatma Gedik, Geo. Eng. (MS) Ayşegül Aydın and Geo. Eng. (MS) Dilek Tokatlı. Firstly, we would like to thank the department of Geological Research of the General Directorate of Mineral Research and Exploration and Prof. Dr. Ali Yılmaz, Geo. Eng. Mustafa Dönmez, Geo. Eng. (MS) Sibel Karacadoğan and Geo. Eng. Halil Keskin for their constructive reviews and contributions to the preparation of the publication. Additionally, we thank the reviewers Prof. Dr. Ş. Can Genç, Prof. Dr. Orhan Tatar and Prof. Dr. Faruk Aydın for detailed reviews and beneficial and important criticism which improved the first draft.

### References

Agrawal, S., Guevara, M., Verma S. 2008. Tectonic discrimination of basic and ultrabasic volcanic rocks through log-transformed ratios of immobile trace elements. *International Geology Review* 50, 1057–1079.

Akçay, A. E., Dönmez, M., Kara, H., Yergök, A. F., Esentürk, K. 2008. 1/100.000 Ölçekli Türkiye jeoloji haritaları, Kırşehir sheet İ-34, No: 81. General Directorate of the Mineral Research and Exploration, Ankara.

Aldanmaz, E., Pearce, J., Thirrhvall, M.F., Mitchell, J. 2000. Petrogenetic evolution of late Cenozoic, post-collision volcanism in western Anatolia, Turkey. *Journal of Volcanology and Geothermal Research* 102, 67-95.

Alpaslan, M. 2000. Pazarcık volkanitinin (Yıldızeli-Sivas) mineralojik-petrografik ve jeokimyasal özellikleri. *Türkiye Jeoloji Bülteni* 43/2, 49-60.

Alpaslan, M., Terzioğlu, N. 1998. Pontidlerde çarpışma sonrası volkanizmaya bir örnek: Sürmeli Volkaniti (Taşova-Amasya), CÜ Mühendislik Fakültesi Dergisi, Seri A: Yerbilimleri, 15, 1, 13-20.

Altunkaynak, Ş. 2007. Collision-driven slab breakoff magmatism in northwestern Anatolia, Turkey. *Journal of Geology* 115, 63-82.

Altunkaynak, Ş., Dilek, Y. 2006. Timing and nature of postcollisional volcanism in western Anatolia and geodynamic implications. In: *Postcollisional Tectonics and Magmatism in the Mediterranean Region and Asia*, Y. Dilek and S. Pavlides (eds.), Geological Society of America, Special Paper, 409, 321-351.

Altunkaynak, Ş., Dilek, Y. 2013. Eocene mafic volcanism in northern Anatolia: its causes and mantle sources in the absence of active subduction. *International Geology Review* 55 (13), 1641-1659.

Arslan, M., Aliyazıcıoğlu, İ. 2001. Geochemical and petrological characteristics of the Kale (Gümüşhane) volcanic rocks: Implications for the Eocene evolution of Eastern Pontide arc volcanism, Northeast Turkey, *International Geology Review* 43, 595-610.

Atakay Gündoğdu, E. 2009. Çorum Güneybatısındaki Volkanik Kayaçların Jeolojik Ve Petrolojik Özellikleri ve Alaca Höyük Kazısında Jeoarkeolojik Çalışmalar, PhD Thesis, Institute of science, Ankara Universty, 194p. (unpublished).

Bailey, E.B., Mc Callien, W.J. 1950. Ankara melanji ve Anadolu şarriyajı. *Maden Tetkik ve Arama Dergisi* 40, 12-16.

Beyazpırınç, M., Akçay, A.E., Tarhan, N., Sönmez, M.K., Havzoğlu, T., Bilgiç, T., Bademler, F., Ünal, M. 2014. Akdağmadeni masifinin jeolojisi ve jeodinamik evrimi projesi 2011-2012 yıllarına ait ara rapor. General Directorate of Mineral Research and Exploration Report No: 11763, Ankara (unpublished).

Boynton, W. V. 1984. Cosmochemistry of the rare earth elements: meteorite studies. In: Henderson P (eds) *Rare Earth Element Geochemistry*. Elsevier, Amsterdam, 63-114.

Büyükönal, G. 1985. Distribution of the major and trace elements in the volcanic rocks of Yozgat area, Turkey. *Bulletin of the Mineral Research and Exploration* 105-106; 68-82.

Dalkılıç, H., Dönmez, M., Akçay, A. E. 2008. 1/100 000 Ölçekli açınısma nitelikli Türkiye Jeoloji Haritaları Serisi, Yozgat-Sheet İ35, No: 82. General Directorate Mineral Research and Exploration, Ankara.

- Debon, F., Le Fort, P. 1983. A chemical–mineralogical classification of common plutonic rocks and associations. *Transactions of the Royal Society of Edinburgh, Earth Sciences* 73, 135–149.
- Dilek, Y., Thy, P. 2006. Age and petrogenesis of plagiogranite intrusions in the Ankara melange, Central Turkey. *Island* 15, 44-57.
- Dönmez, M., Bilgin, Z.R., Akçay, A.E., Kara, H., Yergök, A.F., Esentürk, K. 2005. 1/100.000 Ölçekli açınama nitelikli Türkiye Jeoloji Haritaları Serisi, Kırşehir Sheet 131 , No: 46. General Directorate of Mineral Research and Exploration, Ankara.
- Dönmez, M., Akçay, A.E., Genç, Ş.C., Acar Ş. 2005. Biga yarımadasında Orta-Üst Eosen volkanizması ve denizel ignimbritler, *Maden Tetkik ve Arama Dergisi* 131, 49-61.
- Edwards, A., Menzies, M., Thirlwall, M. 1991. Evidence from Muriah, Indonesia, for the interplay of supra-subduction zone and intraplate processes in the genesis of potassic alkaline magmas. *J.Petrol.*, vol. 32(3), p.555-592.
- Egeran, E.N., Lahn, E. 1951. Kuzey ve Orta Anadolu'nun tektonik durumu hakkında not. *Maden Tetkik ve Arama Dergisi* 41, 23-27.
- Ercan, T., Ergül, E., Akçören, F., Çetin, A., Granit, S., Asutay, J. 1990. Balıkesir-Bandırma arasının jeolojisi, Tersiyer volkanizmasının petrolojisi. *Maden Tetkik ve Arama Dergisi* 110, 113-30.
- Ercan, T., Satır, M., Steinitz, G., Dora, A., Sarıfakioğlu, E., Adis, C., Walter, H.-J., Yıldırım, T. 1995. Biga yarımadası ile Gökceada, Bozcaada ve Tavşan adalarındaki (KB Anadolu) Tersiyer volkanizmasının özellikleri. *Maden Tetkik ve Arama Dergisi* 117, 55-86.
- Ercan, T., Türkecan, A., Guillou, H., Satır, M., Sevin, D., Şaroğlu, F. 1998. Marmara denizi çevresindeki Tersiyer volkanizmasının özellikleri. *Maden Tetkik ve Arama Dergisi* 120, 199–221.
- Erkan, Y., Ataman, G. 1981. Orta Anadolu masifi (Kırşehir yöresi) metamorfizma yaşı üzerine K-Ar yöntemi ile bir inceleme. *Yerbilimleri* 8, 27-30.
- Erlor, A., Bayhan, H. 1995. Orta Anadolu granitoyitlerinin genel değerlendirilmesi ve sorunları. *Yerbilimleri* 17, 49-67.
- Fitton, J.G., James, D., Kempton, P.D., Ormerod, D.S., Leeman, W.P. 1988. The role of lithospheric mantle in the generation of late Cenozoic basic magmas in the Western United States, *Journal of Petrology, Special Issue*, 331-349.
- Genç, Ş.C. 1998. Evolution of the Bayramiç magmatic complex. *Journal of Volcanology and Geothermal Research* 85 (1-4), 233-249.
- Genç, Ş.C., Yılmaz, Y. 1997. An example of post-collisional magmatism in northwestern Anatolia: the Kızderbent volcanics (Armutlu peninsula, Turkey). *Turkish Journal of Earth Sciences* 6, 33–42.
- Genç, Ş.C., Dönmez, M., Akçay, A., Altunkaynak, Ş. 2004. The Middle Eocene to Late Miocene magmatic evolution of the Biga peninsula, NW Turkey. 32<sup>nd</sup> International Geological Congress, Florence, Italy, Abstracts Part 2, 1298.
- Genç, Ş.C., İşseven, T., Keskin, M., Tüysüz, O. 2005. Armutlu yarımadası (KB Anadolu) Eosen magmatik kayalarının petrolojik evrimi ve paleomanyetizma özelliklerinin araştırılması. TÜBİTAK Projesi (Proje No: 102Y032).
- Genç, Ş.C., Altunkaynak, Ş. 2007. Eybek graniti (Biga yarımadası, KB Anadolu) üzerine: yeni jeokimya verileri ve yeni bir değerlendirme. *Hacettepe Üniversitesi Yerbilimleri Uygulama ve Araştırma Merkezi Dergisi* 28 (2), 75-98.
- Gill, J.B. 1981, *Orogenic andesites and Plate tectonics*, Springer - Verlag, New York, 138 p.
- Göncüoğlu, M.C. 1977. *Geologie des westlichen Niğde Massivs*. Univ. Bonn, Ph.D. Thesis, 181 p. (unpublished).
- Göncüoğlu, M.C., Toprak, V., Kuşçu, I., Erler, A., Olgun, E. 1991. Orta Anadolu Masifi'nin batı bölümünün jeolojisi, Bölüm 1: Güney Kesim. TPAO Rapor No: 2909, 140 p. (unpublished).
- Göncüoğlu, M.C., Erler, A., Toprak, V., Yalınz, K., Olgun, E., Rojaj, B. 1992. Orta Anadolu Masifi'nin batı bölümünün jeolojisi, Bölüm 2: Orta Kesim. TPAO Rapor No: 3155, 76 p. (unpublished).
- Görür, N., Akkök, R., Sakıncı, M., Ünal, G., Yalıtırak, C. 1997. Türkiye'nin Tersiyer Havzaları ve Kömür Potansiyeli. *Türkiye Kömür Arama Hedeflerinin Belirlenmesi ve Arama Yöntemlerinin Saptanması, Yurt Madenciliğini Geliştirme Vakfı Yayınları*, s. 8-37.
- Gülmez, F., Genç, S.C., Keskin, M., Tüysüz, O. 2013. A postcollision slab-breakoff model for the origin of the Middle Eocene magmatic rocks of the Armutlu-Almacık belt, NW Turkey and its regional implications, in Robertson, A.H.F., Parlak, O., and Ünlügenç, U.C., eds., *Geological development of Anatolia and the Easternmost Mediterranean region: Geological Society, London, Special Publications*, 372.

- Kara, H. 1997. 1/100.000 ölçekli açınsama nitelikli Türkiye jeoloji haritaları serisi, Yozgat G 19 paftası, No. 54. Maden Tetkik ve Arama Genel Müdürlüğü, Ankara.
- Kaymakçı, N., Özçelik, Y., White, S.H., Van Dijk, P.M. 2009. Tectono-stratigraphy of the Çankırı Basin: Late Cretaceous to Early Miocene evolution of the Neotethyan Suture Zone in Turkey. Geological Society, London, Special Publications 311, 67–106.
- Keskin, M., Genç, S.C., Tüysüz, O. 2004. Tectonic setting and petrology of collision-related Eocene volcanism around the Çankırı Basin, North Central Turkey. 32nd IGC, Florence 2004 Abstracts Part 2, 1299.
- Keskin, M., Genç, S.C., Tüysüz, O. 2008. Petrology and geochemistry of postcollisional Middle Eocene volcanic units in North-Central Turkey: Evidence for magma generation by slab breakoff following the closure of the Northern Neotethys Ocean. *Lithos* 104 (1-4), 267-305.
- Ketin, İ. 1955. Yozgat bölgesinin jeolojisi ve Orta Anadolu Masifinin tektonik konumu. *Türkiye Jeoloji Kurumu Bülteni* 6, 1-40.
- Ketin, İ. 1963. 1:500.000 ölçekli Türkiye Jeoloji Haritası (Kayseri). Maden Tetkik ve Arama Genel Müdürlüğü yayınları, 82 s. Ankara.
- Ketin, İ. 1966. Anadolunun tektonik birlikleri, *Maden Tetkik ve Arama Dergisi* 66, 20-34
- Koçbulut, F., Yılmaz Şahin, S., Tatar, O. 2001. Akdağmadeni (Yozgat)- Yıldızeli (Sivas) arasındaki Kaletepe volkanitinin mineralojik - petrografik ve jeokimyasal incelenmesi. *İÜ Yerbilimleri Dergisi*, Cilt 14, Sayı 1-2, 77-91.
- Köprübaşı, N., Aldanmaz, E. 2004. Geochemical constraints on the petrogenesis of Cenozoic I-Type granitoids in Northwest Anatolia, Turkey: Evidence for magma generation by lithospheric delamination in a post-collisional setting. *International Geology Review* 46, 705-729.
- Le Bas, M.J., Le Maitre, R.W., Streckeisen, A., Zanettin, B. 1986. A chemical classification of volcanic rocks based on the total alkali-silica diagram. *Journal of Petrology* 27, 745–750.
- Morrison, G.W. 1980. Characteristics and Tectonic Setting of the Shoshonite Rock Association. *Lithos* 13, 97-108.
- Okay, A.İ., Tüysüz, O. 1999. Tethyan sutures of northern Turkey. In "The Mediterranean Basins: Tertiary extension within the Alpine orogen" (eds. B. Durand, L. Jolivet, F. Horváth and M. Séranne), Geological Society, London, Special Publication 156, 475-515.
- Okay, A.İ., Satır, M. 2006. Geochronology of Eocene plutonism and metamorphism in northeast Turkey: evidence for a possible magmatic arc. *Geodinamica Acta* 19 (5), 251–266.
- Özcan, A., Erkan, A., Keskin, E., Oral, A., Sümengen, M., Tekeli, O. 1980. Kuzey Anadolu fayı-Kırşehir masifi arasının temel jeolojisi. Maden Tetkik ve Arama Genel Müdürlüğü Rapor No:1604. Ankara (unpublished).
- Pearce, J.A. 1983. Role of the sub-continental lithosphere in magma genesis at destructive plate margins. In: Hawkeswoeth, C.J. and Norry, M.J., (Eds), *Continental basalts and Mantle Xenolithes*. Nantwich: Shiva, 230-249.
- Pearce, J. A. 1996. A user's guide to basalt discrimination diagrams. In: Wyman, D. A. (ed.) *Trace Element Geochemistry of Volcanic Rocks: Applications for Massive Sulphide Exploration*. Geological Association of Canada, Short Course Notes 12, 79–113.
- Peccerillo, A., Taylor, S.R. 1976. Geochemistry of eocene calc-alkaline volcanic rocks from the Kastamonu area, northern Turkey. *Contributions to Mineralogy and Petrology* 58, 63-81.
- Sarıfakıoğlu, E., Sevin, M., Esirtgen, E., Duran, S., Parlak, O., Bilgiç, T., Dönmez, M., Dilek, Y. 2011. Çankırı-Çorum havzasını çevreleyen ofiyolitik kayaların jeolojisi: Petrojenezi, tektoniği ve cevher içerikleri. Maden Tetkik ve Arama Genel Müdürlüğü Rapor No: 11449, Ankara (unpublished).
- Şahin, M.B. 1999. Akdağmadeni masifi metamorfiteri, Evciler-Çatköy kesiminin mineralojik ve petrolojik özelliklerinin incelenmesi. Doktora Tezi, HÜ Fen Bilimleri Enstitüsü, 105 s. Ankara (unpublished).
- Şengör, A.M.C., Yılmaz, Y. 1981. Tethyan evolution of Turkey. *A Plate Tectonic Approach*. *Tectonophysics* 75, 181-241.
- Terzioğlu, N. 1984. Ordu güneyindeki Eosen yaşlı Bayırköy volkanitlerinin jeokimyası ve petrolojisi, C.Ü. Mühendislik Fak. Dergisi, Seri-A Yerbilimleri, 1,43-60
- Thieblemont, D., Tegyey, Y. 1994. Geochemical discrimination of differentiated magmatic rocks attesting for the variable origin and tectonic setting of calc-alkaline magmas. *Comptes Rendus De L Academie Des Sciences Serie II* 319 (1), 87–94.
- Tiryaki, C., Ekici, T. 2012. Çarpışma sonrası kalk-alkalin Yozgat Volkaniklerinin Petrolojisi *Türkiye Jeoloji Bülteni* 55, 1

- Tokel, S. 1972. Stratigraphical and Volcanic History of the Gümüşhane Region (NE Turkey), Doktora Tezi, Univ. Col. of London, UK.
- Türkiye Stratigrafi Komitesi Bülteni, 1987, Sayı: 1, 15 s. Ankara.
- Tüysüz, O., Dellaloğlu, A.A. 1992. Çankırı havzasının tektonik birlikleri ve jeolojik evrimi. Türkiye 9. Petrol Kongresi Kitabı, 333-349.
- Tüysüz, O., Dellaloğlu, A.A., Terzioğlu, N. 1995. A magmatic belt within the Neo-Tethyan suture zone and its role in the tectonic evolution of Northern Turkey. *Tectonophysics* 243, 173-191.
- Ustaömer P.A., Ustaömer T., Collins A.S., Reischpeitsch J. 2009. Lutetian Arc-Type Magmatism Along The Southern Eurasian Margin: New U-Pb La-Icpms And Whole-Rock Geochemical Data From Marmara Island, NW Turkey, *Mineralogy And Petrology* 96, 177-196.
- Vache, R. 1963. Akdağmadeni kontakt yatakları ve bunların Orta Anadolu Kristaline karşı olan jeolojik çerçevesi. *Maden Tetkik ve Arama Dergisi* 19, 22-36.
- Whitney, D.L., Teyssier, C., Fayon, A.K., Hamilton, M.A., Heizler, M. 2003. Tectonic controls on metamorphism, partial melting and intrusion: timing and duration of regional metamorphism and magmatism in the Niğde Massif, Turkey, *Tectonophysics*, 376, 37-60
- Wilson, M. 1989. *Igneous Petrogenesis*, Unwin Hyman Ltd., London, UK, 466p.
- Winchester, J.A., Floyd, P.A. 1977. Geochemical classification of different magma series and their differentiation products using immobile elements. *Chemical Geology* 20, 325-343.
- Wood, D.A. 1980. The application of a Th-Hf-Ta diagram to problems of tectonomagmatic classification and to establishing the nature of crustal contamination of basaltic lavas on the British Tertiary Volcanic Province: *Earth and Planetary Science Letters*, 50, 11-30.
- Yılmaz, A. 1981. Tokat ile Sivas Arasındaki bölgede ofiyolitli karışığın iç yapısı ve yerleşme yaşı. *Türkiye Jeoloji Kurumu Bülteni* 24, 31-38
- Yılmaz, A. 1982. Dumanlı dağı (Tokat) ile Çeltek dağı (Sivas) dolaylarının temel jeoloji özellikleri ve ofiyolitli karışığın konumu. *Maden Tetkik ve Arama Genel Müdürlüğü Rapor No:7230*, Ankara (unpublished).
- Yılmaz, A., Uysal, Ş., Yusufoglu, H., Ağan, A., İnal, A., Aydın, N., Bedi, Y., Havzoğlu, T., Göç, D., İnal, E., Erkan, E.N. 1994. Akdağmasifi (Sivas) dolayının jeolojik incelemesi. *Maden Tetkik ve Arama Genel Müdürlüğü Rapor No:9721*, Ankara (unpublished).
- Yılmaz, A., Uysal, S., Bedi, Y., Yusufoglu, H., Havzoğlu, T., Ağan, A., Göç, D., Aydın, N. 1995. Akdağ masifi ve dolayının jeolojisi. *Maden Tetkik ve Arama Dergisi* 117, 125-138.
- Yılmaz, A., Uysal, S., Bedi, Y., Atabey, E., Yusufoglu, H., Havzoğlu, T., Ağan, A., Aydın, N. 1997. 1/100.000 Ölçekli Türkiye jeoloji haritaları, Sivas-F22 paftası, No: 46. *Maden Tetkik ve Arama Genel Müdürlüğü*, Ankara.
- Yılmaz, Y., Gürpınar, O., Yiğitbaş, E., Yıldırım, M., Genç, Ş.C., Güner, Ö.F., Elmas, A., Bozcu, M., Çalışkan, B.A. 1993. Tokat masifi ve yakın çevresinin jeolojisi. *Türkiye Petrolleri Anonim Ortaklığı Rapor No: 3390*.
- Yılmaz, Y., Tüysüz, O., Yiğitbaş, E., Genç, Ş.C., Şengör, A.M.C. 1997. Geology and tectonic evolution of the Pontides. In: Robinson, A.G. (Ed.), *Regional and Petroleum Geology of the Black Sea and Surrounding Region*. *Memoir*, vol. 68. American Association of Petroleum Geologists, pp. 183–226.
- Yılmaz, Y., Tüysüz, O. 1984. Kastamonu-Boyabat-Vezir-köprü-Tosya arasındaki bölgenin jeolojisi (İlgaz-Kargı masiflerinin etüdü). *Maden Tetkik Arama Enstitüsü Rapor No: 275, 275p*
- Yılmaz, Y., Genç, S.C., Karacık, Z., Altunkaynak, Ş. 2001. Two contrasting magmatic associations of NW Anatolia and their tectonic significance. *Journal of Geodynamics* 31, 243-271.





# Bulletin of the Mineral Research and Exploration

<http://bulletin.mta.gov.tr>



## TECTONIC GEOMORPHOLOGY OF BAŞKALE FAULT ZONE

Azad SAĞLAM SELÇUK<sup>a\*</sup> and Meryem DÜZGÜN<sup>b</sup>

<sup>a</sup>*Yüzüncü Yıl University, Faculty of Engineering-Architecture, Department of Geological Engineering, 65080 Tuşba/Van. orcid.org/0000-0003-4943-3870*

<sup>b</sup>*Yüzüncü Yıl University, Institute of Science, 65080 Tuşba/Van. orcid.org/0000-0001-6017-2312*

Research Article

Key words:

Başkale Fault Zone, Morphotectonic, geomorphic indices, uplift rates, the Eastern Anatolia.

### ABSTRACT

Başkale Fault Zone is located between Şemdinli-Yüksekova fault zone in southeast Turkey and Guilato-Siahcheshmeh-Khoy fault system in southeast Iran. The fault zone started from Yavuzlar town to Işıklar village in southwest. BFZ is composed of three different segments which have directions with varying N75°E to N 80°E. The offset streams, fault controlled drainage system such as Çığılsuyu stream, alluvial fans which line up parallel to the fault and have deformation structure, fault straight, Plio-Quaternary volcanic rocks and volcanic structures, ridge travertines which continues their formations today indicate that BFZ is active as morphotectonic. The objective of the investigation is to determine the effect of Başkale Fault Zone on morphotectonic evolution of the region. With this aim, morphometric indices such hypsometric integral, drainage basin asymmetry, the ratio between the width and the height of valley and crimp in front of the mountain were produced with Digital Elevation Model of study area and were explained with their meaning. Depending on the results of morphometric models, it appears that the region has young topography and actively rises. It was concluded that the rate of topographies rise in the region increased from east to west and typically rates were greater than of 0.5 mm in year.

Accepted Date: 10.07.2016

Received Date: 28.07.2016

## 1. Introduction

Başkale Fault Zone is located with the western section of the East Anatolia-Iran plateau forming the East Anatolia Compressional Tectonic Block (EACT). This block, defined by modeling of long-term GPS measurements (Reilinger et al., 2006; Djomour et al., 2011), is bounded by the left-lateral strike-slip Northeast Anatolian Fault in the northwest, by the Lesser Caucasus in the north/northeast and by the Bitlis-Zagros thrust belt in the south (Figure 1). It is proposed that the EACT developed under a N-S oriented compressional tectonic regime related to the continent-continent collision between the Arabian and Eurasian plate 13 million years ago (Şengör and Kidd, 1979; Şengör and Yılmaz, 1981; Dewey et al., 1986; Şaroğlu and Yılmaz, 1986; Yılmaz et al., 1987; Koçyiğit et al., 2001) (Figure 1). However, some studies published in recent years have stated that the tectonic regime represented by compression-shortening is only active along the Bitlis-Zagros

thrust zone and between the end of the Late Miocene and end of the Early Pliocene (Koçyiğit et al., 2001; Koçyiğit, 2013). Koçyiğit et al. (2001) stated that instead of a compressional-shortening tectonic regime in the EACT block, a compressional type of neotectonic regime ended in the Late Pliocene. Linked to this regime, NW-SE and NE-SW oriented strike-slip faults, E-W oriented reverse/thrust faults and folds, N-S oriented normal faults and N-S oriented extensional fractures determining the location of significant volcanic centers developed in the region. Among the main neotectonic structures in the region are NW-SE oriented right-lateral strike-slip faults (Çaldıran (CF), Bitlis (BF) and Erciş (KEF) faults, etc.), NE-SW oriented left-lateral strike-slip faults (Ahlat fault (AhF), Başkale (BFZ) fault zone, etc.) and almost E-W oriented thrust faults (Muş-Gevaş thrust zone, Bitlis Zagros suture zone (BZSZ), Gürpınar fault (GF) and Van fault zone (TF) etc.) (Arpat et al., 1977; Şaroğlu et al., 1984; Koçyiğit, 1985a, 1985b;

\* Corresponding author: Azad Sağlam SELÇUK, [azadsaglam@gmail.com](mailto:azadsaglam@gmail.com)  
<http://dx.doi.org/10.19111/bulletinofmre.315757>



# Bulletin of the Mineral Research and Exploration

<http://bulletin.mta.gov.tr>



## TECTONIC GEOMORPHOLOGY OF BAŞKALE FAULT ZONE

Azad SAĞLAM SELÇUK<sup>a\*</sup> and Meryem DÜZGÜN<sup>b</sup>

<sup>a</sup>*Yüzüncü Yıl University, Faculty of Engineering-Architecture, Department of Geological Engineering, 65080 Tuşba/Van. orcid.org/0000-0003-4943-3870*

<sup>b</sup>*Yüzüncü Yıl University, Institute of Science, 65080 Tuşba/Van. orcid.org/0000-0001-6017-2312*

Research Article

### Key words:

Başkale Fault Zone, Morphotectonic, geomorphic indices, uplift rates, the Eastern Anatolia.

### ABSTRACT

Başkale Fault Zone is located between Şemdinli-Yüksekova fault zone in southeast Turkey and Guilato-Siahcheshmeh-Khoy fault system in southeast Iran. The fault zone started from Yavuzlar town to Işıklar village in southwest. BFZ is composed of three different segments which have directions with varying N75°E to N 80°E. The offset streams, fault controlled drainage system such as Çığılsuyu stream, alluvial fans which line up parallel to the fault and have deformation structure, fault straight, Plio-Quaternary volcanic rocks and volcanic structures, ridge travertines which continues their formations today indicate that BFZ is active as morphotectonic. The objective of the investigation is to determine the effect of Başkale Fault Zone on morphotectonic evolution of the region. With this aim, morphometric indices such hypsometric integral, drainage basin asymmetry, the ratio between the width and the height of valley and crimp in front of the mountain were produced with Digital Elevation Model of study area and were explained with their meaning. Depending on the results of morphometric models, it appears that the region has young topography and actively rises. It was concluded that the rate of topographies rise in the region increased from east to west and typically rates were greater than of 0.5 mm in year.

Accepted Date: 10.07.2016

Received Date: 28.07.2016

## 1. Introduction

Başkale Fault Zone is located with the western section of the East Anatolia-Iran plateau forming the East Anatolia Compressional Tectonic Block (EACT). This block, defined by modeling of long-term GPS measurements (Reilinger et al., 2006; Djomour et al., 2011), is bounded by the left-lateral strike-slip Northeast Anatolian Fault in the northwest, by the Lesser Caucasus in the north/northeast and by the Bitlis-Zagros thrust belt in the south (Figure 1). It is proposed that the EACT developed under a N-S oriented compressional tectonic regime related to the continent-continent collision between the Arabian and Eurasian plate 13 million years ago (Şengör and Kidd, 1979; Şengör and Yılmaz, 1981; Dewey et al., 1986; Şaroğlu and Yılmaz, 1986; Yılmaz et al., 1987; Koçyiğit et al., 2001) (Figure 1). However, some studies published in recent years have stated that the tectonic regime represented by compression-shortening is only active along the Bitlis-Zagros

thrust zone and between the end of the Late Miocene and end of the Early Pliocene (Koçyiğit et al., 2001; Koçyiğit, 2013). Koçyiğit et al. (2001) stated that instead of a compressional-shortening tectonic regime in the EACT block, a compressional type of neotectonic regime ended in the Late Pliocene. Linked to this regime, NW-SE and NE-SW oriented strike-slip faults, E-W oriented reverse/thrust faults and folds, N-S oriented normal faults and N-S oriented extensional fractures determining the location of significant volcanic centers developed in the region. Among the main neotectonic structures in the region are NW-SE oriented right-lateral strike-slip faults (Çaldıran (CF), Bitlis (BF) and Erciş (KEF) faults, etc.), NE-SW oriented left-lateral strike-slip faults (Ahlat fault (AhF), Başkale (BFZ) fault zone, etc.) and almost E-W oriented thrust faults (Muş-Gevaş thrust zone, Bitlis Zagros suture zone (BZSZ), Gürpınar fault (GF) and Van fault zone (TF) etc.) (Arpat et al., 1977; Şaroğlu et al., 1984; Koçyiğit, 1985a, 1985b;

\* Corresponding author: Azad Sağlam SELÇUK, [azadsaglam@gmail.com](mailto:azadsaglam@gmail.com)  
<http://dx.doi.org/10.19111/bulletinofmre.315757>



Figure 1- Location of the study area within Turkey's neotectonic framework (block boundaries taken from Reilinger et al., 2006; Djmour et al., 2011) (NAFZ: North Anatolia Fault Zone, EAFZ: East Anatolia Fault Zone, BZSZ: Bitlis-Zagros Suture Zone, CF: Çaldıran Fault, KTF: Karllova triple junction, VFZ: Varto Fault Zone, NEAF: Northeast Anatolia Fault, EACT: East Anatolia Compressional Tectonic block).

Koçyiğit et al., 1985; Şaroğlu and Yılmaz, 1986; Saroğlu et al., 1987; Cisternas et al., 1989; Rebai et al., 1993; Koçyiğit et al., 2001; Dhont and Chorowicz, 2006; Horasan and Boztepe-Güney, 2006) (Figure 2). These faults or fault zones are the source of many destructive earthquakes occurring in the region from the historical period to the present day.

After the 23 October 2011 Van earthquake more detailed studies of the young tectonics of the Lake Van Basin have been completed by different researchers. The majority of these studies have focused on the basic properties of the main fault that produced the 2011 Van earthquake and the place of this mechanism in the geodynamic structure of the region (Özkaymak et al., 2011; Emre et al., 2012; Bayraktar et al., 2013; Görgün 2013; Doğan and Karakaş 2013; Altıner et al., 2013, Elliott et al., 2013; Koçyiğit, 2013). Some of these studies have drawn attention to the Başkale Fault Zone (BFZ), located southeast of Lake Van Basin and one of the NE-SW oriented strike-slip fault zones, as being a neotectonic structure that is active and has potential to produce earthquakes (Emre et al., 2012; Koçyiğit, 2013). Due to its active tectonic properties, the Başkale basin and Başkale Fault Zone have an important place in understanding the tectonic evolution of the region. With the active property of producing more than one earthquake proven, the BFZ has only been studied in limited fashion to date. The BFZ was only mapped after the 25 January 2005

Sütlüce earthquake (Mw 4.8, 4.9 and 5.5) (KOERİ, 2011) and is included on Turkey's Active Fault Map.

This study aimed to research the BFZ, controlling the western and eastern boundaries of the Başkale Basin, using morphometric indices such as mountain-front sinuosity ( $S_{mf}$ ), valley floor width to height ratio ( $V_f$ ), asymmetry factor (AF) and hypsometric integral (HI) and its effect on regional geomorphologic evolution.

### 1.1. Başkale Fault Zone

The Başkale basin is southeast of Lake Van; located between the BZSZ bounding the south of the lake and the Guilato-Siahcheshmeh-Khoy Fault system located in northwest Iran (Figure 2). This NE-SW striking basin has width of 9-15 km and length of 82 km (Figure 3a). The east and west sides of the Başkale basin is controlled by faults. While basement rocks are located in the footwall of these faults bounding the basin, the sediments filling the basin are generally fluvial and current alluvium. Three basic geologic units separated by unconformities may be distinguished in Başkale basin: (1) Pre-Neogene basic metamorphic rocks comprised of dominantly marble and schists (Yılmaz, 1971; Ricou, 1971; Yılmaz, 1975; Boray, 1975; Erdoğan, 1975, Göncüoğlu and Turhan, 1984); (2) Neogene continental sediments and volcanic rocks (lacustrine limestone, sandstone and basalt-

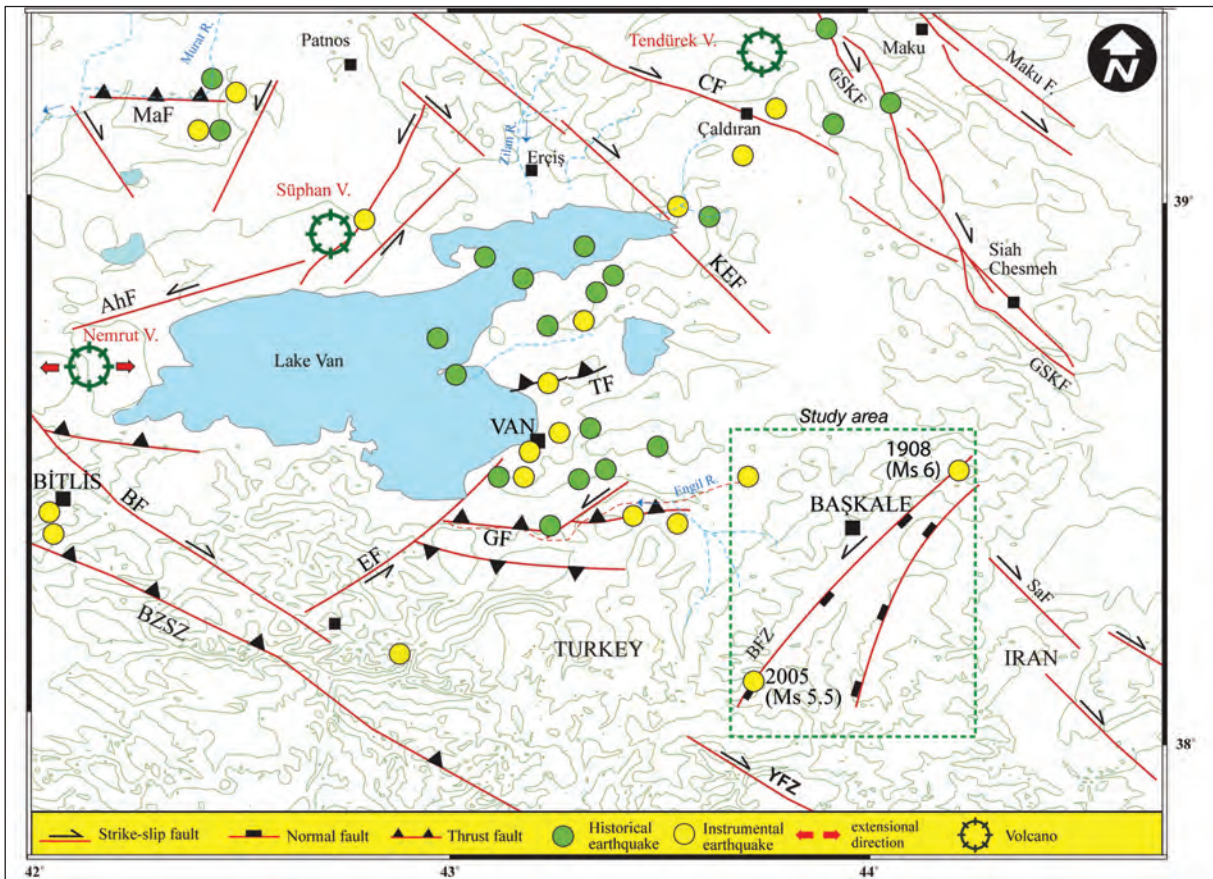


Figure 2- Seismotectonic map of the study area and surroundings (faults: Koçyiğit et al., 2001, Karakhanian et al., 2004; earthquakes Ergin et al., 1967; Soysal et al., 1981; Ambraseys and Finkel, 1995; Tan et al., 2008) (BZSZ: Bitlis-Zagros Suture Zone, MaF: Malazgirt Fault, CF: Çaldıran Fault, GSKF: Guilato-Siahcheshmeh-Khoy Fault, KEF: Karayazı-Erçiş Fault, TF: Van Fault, SaF: Salamas Fault, BFZ: Başkale Fault Zone, YFZ: Yüksekova Fault Zone, GF: Gürpınar Fault, EF: Edremit Fault, BF: Bitlis Fault, AhF: Ahlat Fault).

tuff); and (3) Quaternary alluvial, fluvial and colluvial sediments and travertine formations (Figure 3b). The contacts between units in the basin are generally fault-controlled (Figure 4a). While Quaternary sediments form the basin fill, metamorphic rocks are located in the west of the basin, while volcanic rocks are generally located along the eastern edge (Figure 3b). Travertine deposits dominantly developed along the Çamlık Fault bounding the southeast of Başkale basin (Figure 4b-c). The BFZ begins in the northeast, north of Yavuzlar, and continues until Işıklı village in the southwest (Figure 3). With strike varying from dominantly N10°E and N40°E, the BFZ is generally comprised of left lateral strike-slip faults with normal component. While the west section of the basin is controlled by two faults (Işıklı and Ziraniş faults), the east section is controlled by a single fault (Çamlık fault). One of the faults bounding the NW of the Başkale basin is the Ziraniş fault, which is nearly 20 km long with strike N5°E to N-S. This

edge of the basin is represented by a structural contact between pre-Miocene basement rocks and Quaternary alluvium (Figure 3b). The more southern Işıklı Fault may be followed for 14 km between Ortayol and Işıklı and has a right-curving geometry. South of Başkale it presents a linear strike between pre-Miocene basement rocks of marble-schist intercalations and Miocene-aged sedimentary rocks (Figure 3b). The central sections of the basin are controlled by younger normal faults compared to the faults controlling the edges and in this area they appear to have formed a stepped morphology. The Ereğ and Alabayır Faults begin in the north near Yavuzlar village and may be followed to Ilıcak village in the south. Cutting the fluvial sediments of the Çığılsu river, they form 2-3 m steps within these sediments. Çamlık Fault bounds the southeast of the basin and also controls it. With nearly 30 km length, it has strike varying from N10°-25°E. Ancient and new travertine deposits outcrop along the Çamlık Fault (Figure 4b-c). The fissure ridge

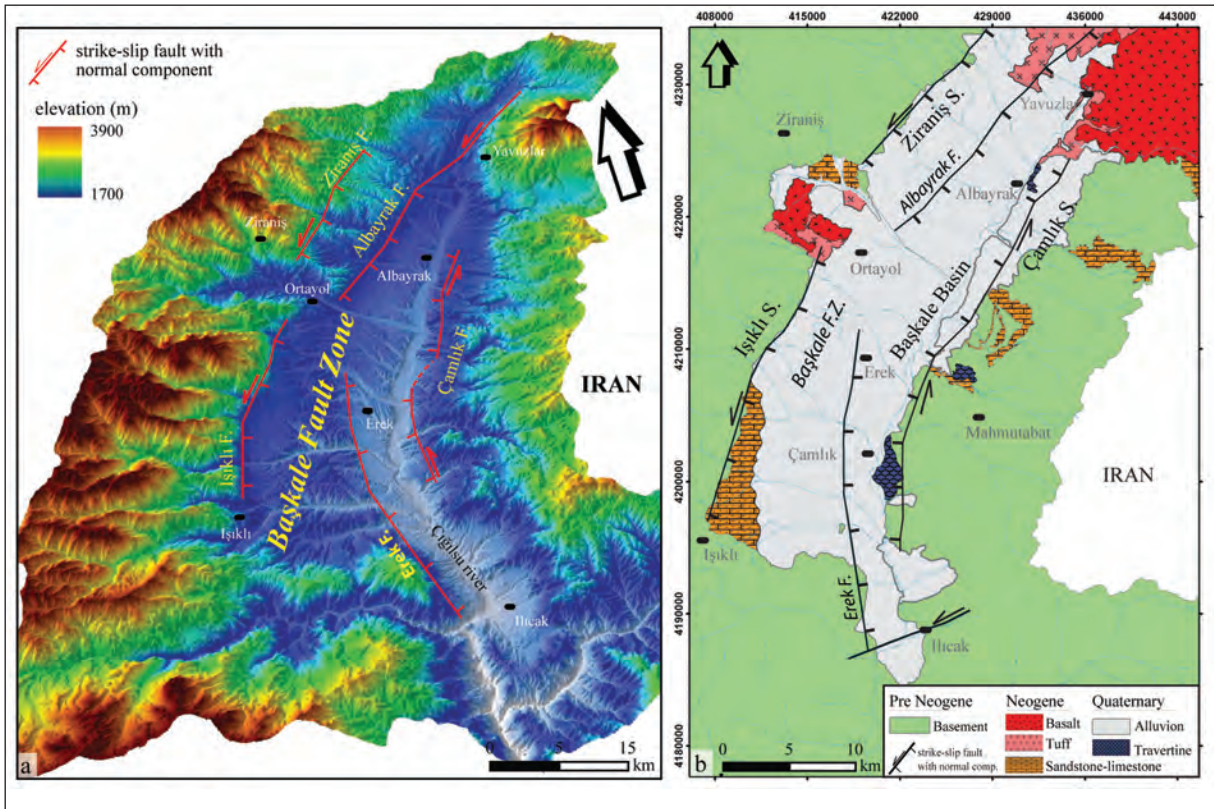


Figure 3- a) Extension of the Başkale Fault Zone on digital elevation model b) Geologic map of the Başkale basin (adapted from Ateş et al., 2007).

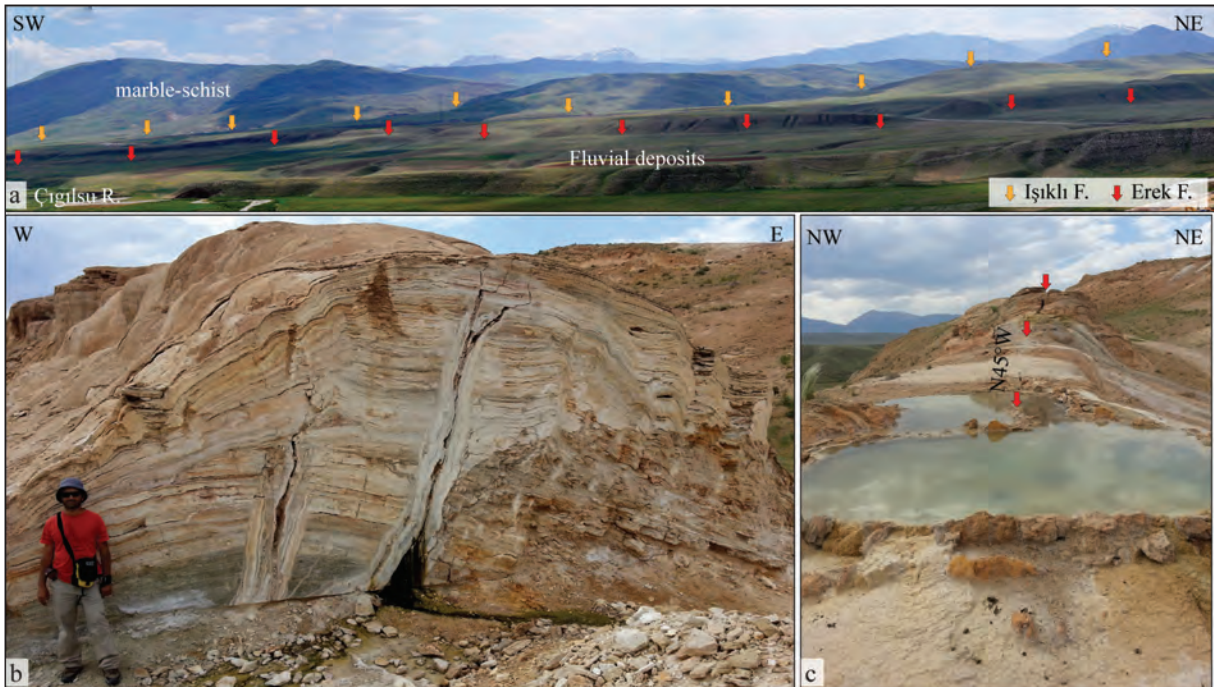


Figure 4- a) Extension of Işıklı and Ereğ Fault in the field b) Cross section of fissure ridge travertines along Çamlık Fault c) Longitudinal appearance of fissure ridge travertines

travertines and terrace-type travertines with formation continuing currently are noteworthy.

Başkale Fault Zone is a tectonically active fault zone and is the source of more than one earthquake in the instrumental period. In previous years though the Başkale Fault was described, it was named the Başkale Fault zone due to the occurrence of more than one active fault almost parallel to each other and the deformation zone occurring along these faults (Başkale basin). As proven by the 1908 Başkale earthquake (Mw 6.0) (Ambraseys and Finkel, 1995; Ambraseys, 2001) and 25 January 2005 Sütluce earthquakes (Mw 4.8, 4.9 and 5.5) (KOERİ, 2011), the BFZ is a seismically active fault zone (Koçyiğit, 2005; Emre et al., 2005, 2012).

## 2. Method

Research to date has shown that activity occurring along the fault has left different geomorphological evidence at the surface (Bull, 1977; Keller, 1986; Keller and Pinter, 2002; Gordon, 1998; Giamboni et al., 2005). One of the most commonly used methods for interpretation of this evidence is morphometric analysis. Morphometric analysis is one of the most important tools used to research the effect of tectonic activity on development of geomorphic processes and surface morphology (Keller and Pinter, 2002). This analysis is completed using morphometric indices and generally is used to describe regional tectonic activity. The obtained numerical data may be used with the aim of understanding the geomorphological evolution of large areas or determining which active fault segment is more active (Strahler, 1952; Bull and McFadden, 1977; Keller et al., 2000; Azor et al., 2002; Keller and Pinter, 2002; Font et al., 2010; Gürbüz and Gürer, 2008; Özkaymak and Sözbilir, 2012; Yıldırım, 2014; Özsayın, 2016).

For determination of the morphological characteristics of Başkale Fault Zone and to be able to complete morphometric analyses, a digital elevation model (DEM) of the study area with 10 m resolution was created using the ArcMap program. The drainage basins and fluvial network in the region were drawn on the created DEM base. Morphometric indices (mountain-front sinuosity ( $S_{mf}$ ), valley floor width to height ratio ( $V_p$ ), asymmetry factor, (AF) and hypsometric curve and integral (HE and HI) were calculated using different tools within the ArcMap program.

## 3. Morphometric Analyses

### 3.1. Mountain-front sinuosity ( $S_{mf}$ )

Mountain-front sinuosity is an effective method to distinguish tectonically active mountain fronts from inactive mountain fronts and is described by the following equation (Bull and McFadden, 1977; Keller and Pinter, 2002).

$$S_{mf} = \frac{L_{mf}}{L_s}$$

In this formula,  $L_{mf}$  is the sinuous length of the mountain front while  $L_s$  is the length of a straight line along the front.  $S_{mf}$  is a function of erosion and tectonic activity and values change linked to uplift rate (Rockwell et al., 1984). If mountain fronts are controlled by active faults, they give low  $S_{mf}$  values, while with the reduction in uplift rate and/or tectonism erosion becomes dominant and  $S_{mf}$  values increase (Keller and Pinter, 2002; Silva et al., 2003; Bull, 2007; Pérez-Peña et al., 2010).

In this study the  $S_{mf}$  values for the mountain fronts long the segments of the BFZ controlling the basin were calculated. These values generally varied between 1.0 and 2.0. The S2 and S4-S7 segments controlling the west edge and the northeast of the basin gave low  $S_{mf}$  values (in the interval 1.07-1.08; Table 1, Figure 5a and 5b) and these values show that these segments are more active in the region. The S7-8-9 segments controlling the east edge of the basin and the S3 segment located in the south gave low  $S_{mf}$  values (in the interval 1.53-1.95, Table 1, Figure 5a) and as a result the west and central segments may be described as being less active segments.

Table 1- Mountain-front sinuosity ( $S_{mf}$ ) values (for points see figure 5).

Mountain-front	Smf
S1	1,33
S2	1,08
S3	1,56
S4	1,08
S5	1,06
S6	1,07
S7	1,04
S8	1,75
S9	1,95
S10	1,53

### 3.2. Valley floor width to height ratio ( $V_p$ )

One of the most commonly used indices to understand the tectonic uplift rate occurring in a

region is the valley floor width to height ratio. This ratio is described by the following formula:

$$V_f = \frac{2V_{fw}}{(E_{ld} - E_{sc}) + (E_{rd} - E_{sc})}$$

In this formula,  $V_{fw}$  is the width of the valley floor,  $E_{ld}$  and  $E_{rd}$  are the height of the right and left slopes (from water level), and  $E_{sc}$  represents the height of the valley floor (Bull and McFadden, 1977; Bull 1977). The  $V_f$  values vary linked to the shape of the valley. If “V”-shaped valleys have low  $V_f$  values, this indicates the regional uplift rate is high and there is excavation occurring (Bull and McFadden 1977; Rockwell et al., 1984; Silva et al., 2003; El Hamdouni et al., 2008). Contrarily if there are high  $V_f$  values, the uplift rate is low indicating that tectonism is less effective compared to erosional processes.

In this study the  $V_f$  values in fluvial channels were calculated for mountain fronts. Thus, the aim was to distinguish tectonic classes based on relative activities and uplift rates according to segment and to allow discussion (Rockwell et al., 1984; Silva et al., 2003; Bull, 2007).

The  $V_f$  values calculated for 37 different drainage basins within the Başkale basin varied from 0.2 to 2.6 (Table 2, Figure 5a). The valleys of the SE-flowing streams in the footwall perpendicular to the Ziraniş fault controlling the west edge of Başkale basin and valleys of streams flowing along the Erek and Albayrak faults controlling the central section of the basin offer low  $V_f$  values (valleys forming controlled by S2 and S4-S7, Table 2, Figure 5a). The valleys in these areas are V-shaped. The valleys developing linked to segments controlling the east edge of the basin appear to have higher  $V_f$  values (S8-S10, Table 1, Figure 5a). From the  $V_f$  values it may be said that the segments controlling the west edge and the northeast of the Başkale basin are more active compared to other segments.

Studies in recent years have stated there is a correlation between the  $V_f$  index and  $S_{mf}$  index and that the degree of activity of faults may be determined linked to this ratio (Rockwell et al., 1984; Silva et al., 2003). Linked to this classification, the Ziraniş and Işıklı faults (S1,S2) controlling the basin have active mountain fronts and appear to be faults with high activity controlling the basin (Figure 5b). At the same time, segments located in the northeast of the basin and those controlling the central section of the basin (S4-7) are younger and may be said to have high activity

Table 2- Valley floor width to height ratio ( $V_f$ ) values (for points see figure 5).

Valley	$V_f$	Valley	$V_f$
1a	0,30	4c	1,05
1b	0,28	5a	0,45
1c	0,62	5b	0,35
1d	0,57	6a	0,52
1e	0,34	6b	0,31
1f	0,24	6c	0,35
1g	0,41	7a	0,48
2a	0,31	7b	0,69
2b	1,01	7c	0,52
2c	0,20	8a	0,55
2d	0,32	9a	2,60
2e	2,16	9b	0,67
3a	0,92	9c	1,74
3b	1,97	10a	0,87
3c	2,63	10b	0,61
3d	1,26	10c	1,29
3e	2,70	10d	0,82
3f	2,58	10e	1,44
4a	2,17	10f	0,69
4b	0,81	10g	1,02

(Figure 5b). The Çamlık Fault controlling the east edge of the basin provided higher  $V_f$  and  $S_{mf}$  values. This fault appears to be moderately active compared to other faults. The uplift rate linked to these values in the west and north of Başkale basin (S1, S2, S4-7) is  $>0.5 \text{ mm yr}^{-1}$ , while moving toward the east this rate appears to be 0.05 and  $0.5 \text{ mm yr}^{-1}$  (Figure 5b).

### 3.3. Asymmetry Factor, (AF)

The drainage basin asymmetry index is one of the easiest ways to understand whether a drainage network developed under tectonic control. This index is described by this formula.

$$AF = 100 \frac{(Ar)}{(At)}$$

Here,  $Ar$  is the area to the right of the drainage basin while  $At$  is the total area of the drainage basin. If a region is under tectonic control, the best results are understood from the texture and geometry developing within the fluvial network. To define this and determine the tendency toward tectonic control, this index is used (Keller and Pinter, 2002). If the AF value is around 50,

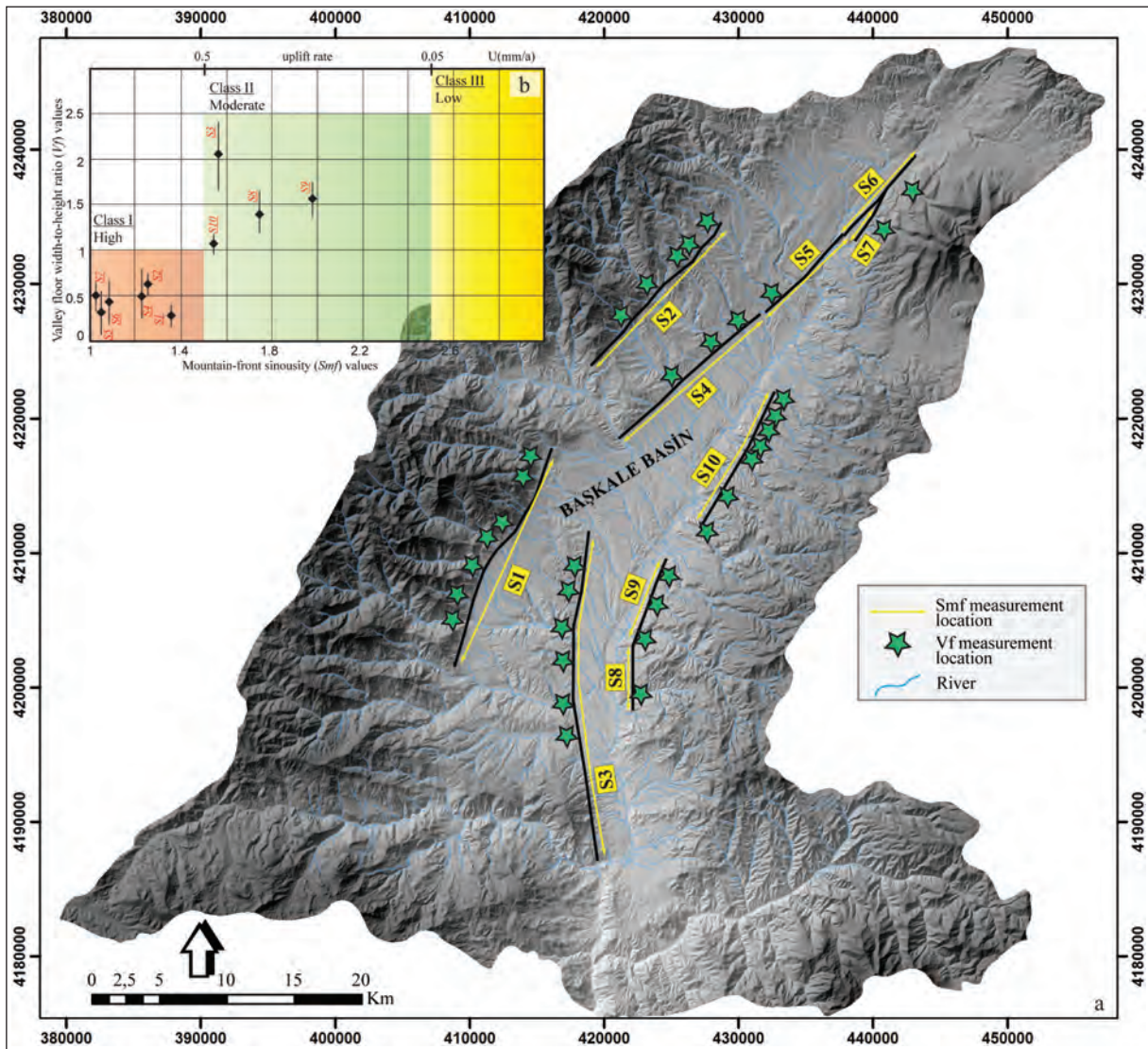


Figure 5- a) Location of  $S_{mf}$  and  $V_f$  measurements in Başkale basin b) Graphic appearance of  $S_{mf}$  and  $V_f$  values calculated for each segment and representative tectonic classes (uplift rates taken from Rockwell et al., 1984).

it indicates there is no tendency in the basin; in other words there is no tectonism affecting the basin. If this value is “ $AF > 50 < AF$ ”, it shows the basin was affected by tectonism. The drainage basin asymmetry value was calculated for 89 different basins and sub-basins controlled by the Başkale Fault Zone.

Some researchers in recent years have stated that when the AF value is taken as an absolute function, this value shows the direction of asymmetry and that basin asymmetry may be collected in four classes linked to this value. These are symmetric basin ( $AF < 5$ ), basin with low symmetry ( $5 < AF < 10$ ), basin with moderate asymmetry ( $10 < AF < 15$ ) and basin with dominant asymmetry ( $AF > 15$ ) (Perez-Peña et al., 2010; Giaconia et al., 2012).

The asymmetry factor was calculated for 20 sub-basins located within Başkale basin (Figure 6). Of these basins, 12 were symmetric-low symmetric basins while 8 were within the asymmetric basin classification. The sub-basins at the southwest edge of the basin were symmetric-low symmetric, while those toward the northwest were dominantly asymmetric. It is thought that this basin symmetry difference in the north and south sections of the west edge of the basin is due to lithology. In the south section the basement rocks are dominantly marble-schist intercalations, while the volcanic and fluvial deposits that outcrop in the central and northern sections are more easily eroded and this may have caused them to gain asymmetric character. The sub-basins in the east of the basin are in the asymmetric class in the central

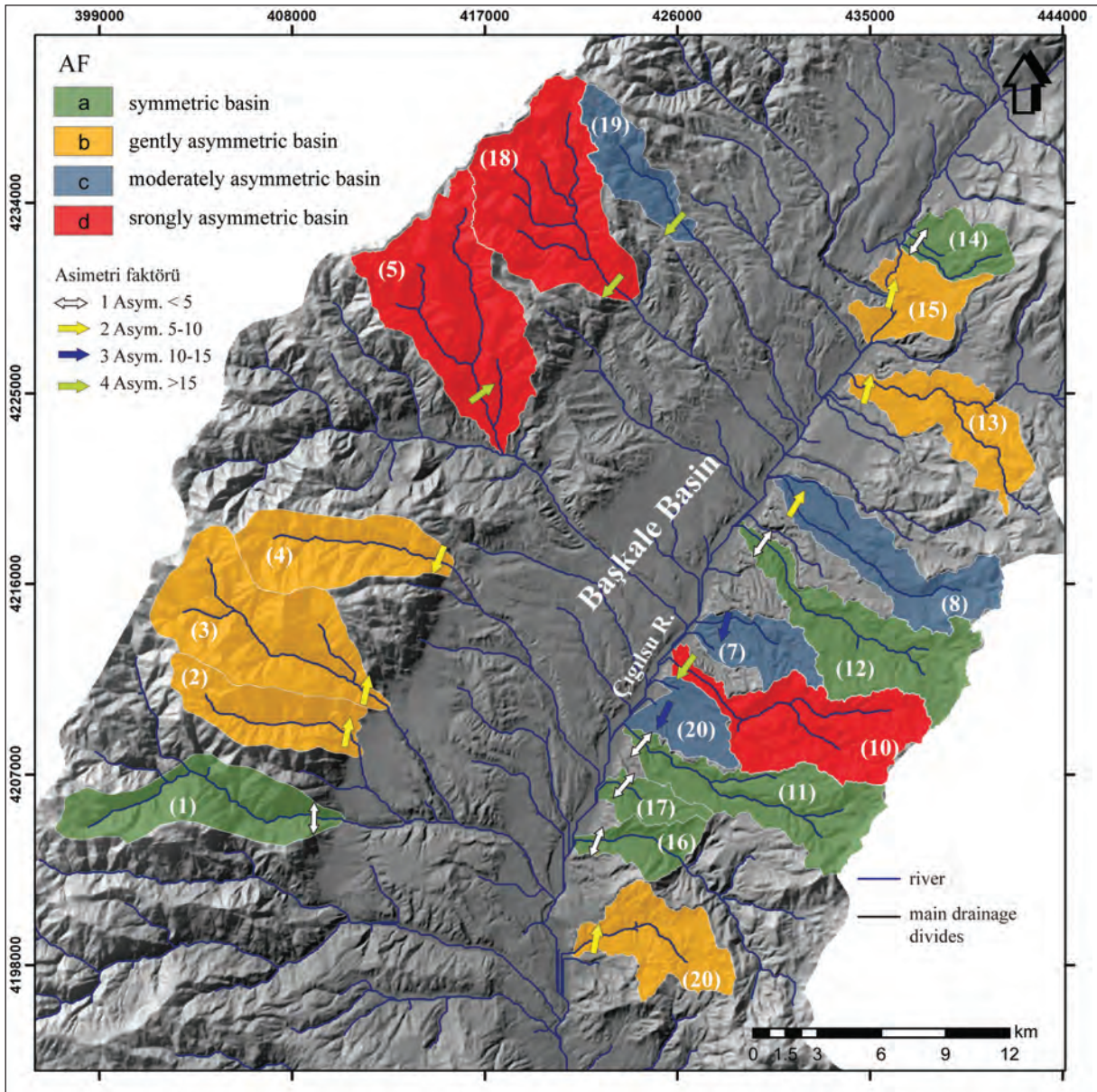


Figure 6- Asymmetry of drainage basins in sub-basins of the Başkale basin.

section, while toward the southeast and northeast the sub-basins are symmetric-low symmetric (Figure 6).

The sub-basins controlled by the Işıklı Fault in the west section of the basin have an asymmetry toward the northwest, while the sub-basins controlled by the Ziranış Fault have an asymmetry toward the south-southwest (Figure 6). The sub-basins controlled by the Çamlık Fault in the south do not show any tendency, while those in the central section have a tendency toward the south-southwest. Sub-basins controlled by Çamlık Fault in the north have an asymmetry toward the north-northeast (Figure 6).

The asymmetry directions for sub-basins located within the Başkale basin display differences in orientation. The Başkale basin and the BFZ controlling development of this basin are located in the area between the right-lateral strike-slip Guilato–Siahcheshmeh–Khoy and Yüksekova fault zones (Figure 2). At the same time, according to block models linked to GPS data, the Hakkari block located within the Başkale basin is moving in an anti-clockwise direction (Reilinger et al., 2006; Djamour et al., 2011). The effect of these two right-lateral strike-slip fault zones controlling the main tectonic evolution of the region on the Başkale basin and BFZ has led

to the different directions of asymmetry in the sub-basins.

#### 3.4. Hypsometric curve and integral (HE and HI)

Hypsometric analysis shows the sensitivity of drainage evolution in an area to current tectonism and this analysis has been commonly used in geomorphology, hydrology and active tectonic areas in recent years (Ciccacci et al., 1992; Lifton and Chase, 1992; Ohmori, 1993; Willgoose, 1994; Willgoose and Hancock, 1998; D'Alessandro et al., 1999; Chen et al., 2003; Yıldırım, 2014; Özkaymak, 2015; Özsayın, 2016). This analysis comprises two stages; hypsometric curve and integral. The shape of the hypsometric curve (HE) is linked to the degree of excavation within a basin. While convex-shaped HE characterize immature, weakly eroded basins, S-shaped HE indicate moderately eroded basins and concave-shaped HE indicate very eroded basins (Keller and Pinter, 2002; Pérez-Peña et al., 2009a; Giaconia et al., 2012). Hypsometric integral values represent young basins if larger than 0.5 ( $HI > 0.5$ ), while values lower than 0.3 ( $HI < 0.3$ ) indicate old basins. If the value is  $0.3 < HI < 0.5$ , it shows the basin has completed formation. In this study the hypsometric curve and integral values were calculated using the CalHypso program (Pérez-Peña et al., 2009a, b) working within the ArcGIS program.

The hypsometric curves and hypsometric integrals were calculated for 20 sub-basins within the Başkale basin. The sub-basins located on the west slope of the basin are generally convex and S-shaped, with HI values larger than 0.35. The basins in the west edge of the basin, especially, controlled by the Işıklı and Ziraniş segments dominantly display convex HE, while moving toward the north along their extensions S-shaped basins are observed (Figure 7a). It may be said that basins in this area are younger linked to the hypsometric curves of the sub-basins. On the east slope, the sub-basins in the south section of the Çamlık segment display dominantly convex and S-shaped hypsometric curves (Figure 7a-c). Moving toward the north, the presence of concave basins is noted (Figure 7a, d). The sub-basins in this area are younger than those in the south, while those in the north appear to have completed their basin development. However, the volcanic units outcropping in the northeast of Başkale basin are more easily abraded and eroded, which may lead to concave hypsometric curves in these basins.

#### 4. Discussion and Conclusions

Başkale basin, located in the southeast of Van province, is one of the basins formed in the neotectonic period controlled by NE-striking left-lateral strike-slip faults with normal component (Figure 2). With the aim of analyzing tectonic activity of the basin in the Quaternary period, geomorphic indices like the mountain-front sinuosity, hypsometric integral, drainage basin asymmetry and valley floor width to height ratio were used for morphometric calculations along the BFZ controlling the basin and these results are correlated with segments of the BFZ.

Shown as an active fault on Turkey's Active Fault Map updated in 2012 (Emre et al., 2012) and controlling Başkale basin, the BFZ is a left-lateral strike-slip fault with normal component. It comprises three main fault segments. The clearest morphological lineations are the Işıklı and Ziraniş faults bounding the northwest of the basin and dipping southeast, the Çamlık Fault located on the eastern edge of the basin dipping west, and the Ereğ and Albayrak faults located in the central section of the basin forming stepped geometry toward the basin. The current morphotectonic activity of the BFZ is visible in offset stream beds, fault-controlled drainage systems (like Çığlısuyu stream), alluvial fans parallel to faults with deformation, fault terraces, hot springs and fissure ridge travertine formation that continues today.

Some researchers have proposed that geomorphological analyses provide important information to use in comparing the uplift rates in a region (Rockwell et al., 1984; Mayer, 1986; Silva et al., 2003; Bull, 2007). The researchers divided uplift rate into three different classes linked to  $V_f$  and  $S_{mf}$  values;  $>0.5 \text{ mm yr}^{-1}$  (class 1) for tectonically active mountain fronts,  $0.05\text{--}0.5 \text{ mm yr}^{-1}$  (class 2) for moderate mountain fronts and  $<0.05 \text{ mm yr}^{-1}$  (class 3) for inactive mountain fronts (Figure 5b).  $S_{mf}$  and  $V_f$  values were calculated for each segment controlling the Başkale basin. The degree of activity and uplift rates of segments linked to these values were analyzed. According to the findings, the uplift rate of segments controlling the west edge of Başkale basin is  $>0.5 \text{ mm yr}^{-1}$  and these are within class 1 (active) (Figure 5b). On the eastern edge, this uplift rate is between  $0.05$  and  $0.5 \text{ mm yr}^{-1}$  with the segments controlling this area located within class 2 (moderately active) (Figure 5b). According to block modeling linked to GPS data, the Hakkari block located within Başkale basin is

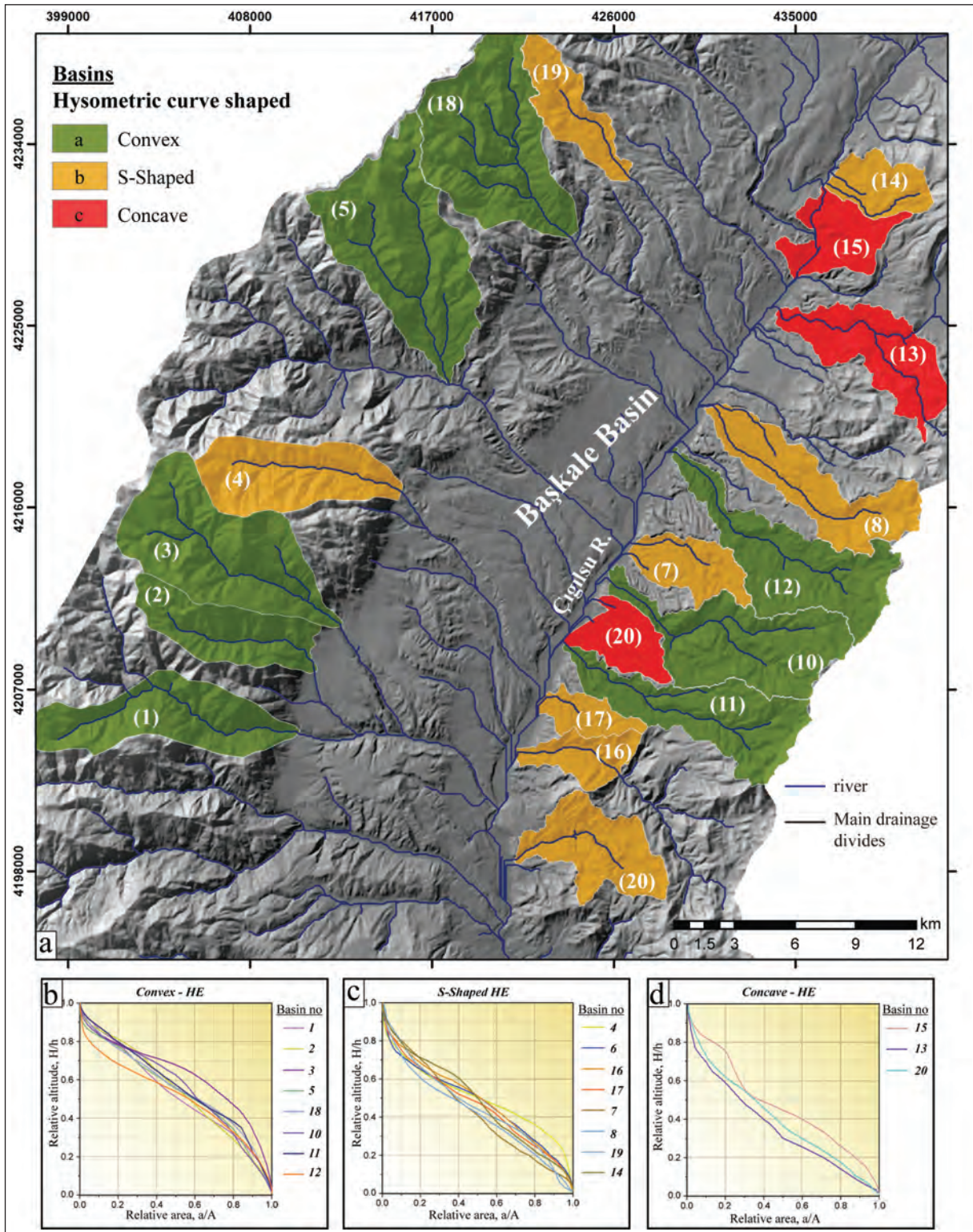


Figure 7- a) Classification linked to hypsometric curve and integral values of sub-basins within the Başkale Basin, b), c), and d) graphs of the hypsometric curves for the sub-basins.

moving in an anticlockwise direction (Reilinger et al., 2006; Djamour et al., 2011). Due to this motion, the west sections of the basin appear to have greater uplift rates, while moving to the east these uplift rates may be said to reduce. In short, the results of analyses show the uplift rates increase in the Hakkâri block from east to west.

Drainage basin asymmetry, hypsometric curves and integral values for 20 sub-basins located within the Başkale basin show the sub-basins on the west edge of the basin are generally young and asymmetric. The Ziraniş and Işıklı faults controlling these basins actively control the region and this shows the basins have a tendency toward asymmetry. However, when the direction of asymmetry is examined, the sub-basins on the Işıklı Fault tend toward the northeast, while the sub-basins on the Ziraniş Fault tend toward the southwest (Figure 6). Similarly, basins in the northern section of the Çamlık Fault tend toward the northeast, while moving to the south there is no asymmetry observed. The difference in asymmetry directions in these sub-basins is thought to be due to the tectonics of the region not just being controlled by the BFZ but also by the Guilato–Siahcheshmeh–Khoy and Yüksekova fault zones.

When HE and HI values are considered, it appears that the west and southeast edges of the basin are formed of young sub-basins. The sub-basins southeast of the Işıklı, Ziraniş and Çamlık faults especially provide high HI integral values. However, though the sub-basins on both slopes of the basin generally have different types of HE and HI values, the sub-basins controlled by the Işıklı, Ziraniş and Çamlık (southeast section) faults, especially are young, while the sub-basins in the northeast section of the Çamlık Fault appear older (Figure 7). This data shows the development of the Başkale basin was controlled by the Işıklı and Ziraniş faults along the west edge of the basin.

In conclusion, in light of findings obtained from digital elevation models, the Başkale Fault Zone is a left-lateral strike-slip fault with normal component. The morphological elements developed within Başkale basin appear to be controlled by the BFZ. The fault plains developing in front of the Işıklı and Ziraniş Faults controlling the west edge of Başkale basin and the secondary stepped faults cutting these fault plains show they advance toward the east of the basin. Morphometric analysis results show the area has a very young topography and is actively uplifting.

The uplift rate in the region increases from east to west and in western sections is determined to be more than 0.5 mm per year.

### Acknowledgements

The authors wish to thank Prof. Dr. Hasan Sözbilir and Prof. Dr. Ercan Aksoy for contributions to the review process of this study.

### References

- Altner, Y., Söhne, W., Güney, C., Perl, J., Wang, R., Muzli M. 2013. A geodetic study of the 23 October 2011 Van, Turkey earthquake. *Tectonophysics*, 588, 118-134.
- Ambraseys, N.N. 2001. Reassessment of earthquakes, 1900-1999, in the Eastern Mediterranean and the Middle East. *Geophysical Journal International* 145, 471-487, doi:10.1046/j.0956-540x.2001.01396.x/epdf
- Ambraseys, N.N., Finkel, A.C. 1995. The seismicity of Turkey and adjacent areas: A historical review, 1500-1800. M.S. Eren Beyoğlu, Istanbul.
- Arpat, E., Şaroğlu, F., İz, H.B. 1977. 1976 Çaldıran Depremi. *Yeryuvarı and İnsan* 17, 29-41.
- Ateş, Ş., Mutlu, G., Özerk, O.Ç., Çiçek, İ., Karakaya Gülmez, F., Bulut Üstün, A., Karabıyıkçıoğlu, M., Osmañcelebioğlu, R., Özata, A., Aksoy, A. 2007. Van İlinin Yerbilim Verileri, Maden Tetkik ve Arama Genel Müdürlüğü, Rapor no: 10961. 152s Ankara (unpublished).
- Azor, A., Keller, E.A., Yeats, R.S. 2002. Geomorphic indicators of actiand fold growth: South Mountain-Oak Ridge anticline, Andntura basin, southern California. *Bulletin of the Geological Society of America* 114, 745-753.
- Bayraktar, A., Altunışık, A.C., Pehlivan M. 2013. Performance and damages of reinforced concrete buildings during the October 23 and November 9, 2011 Van, Turkey, earthquakes. *Soil Dynamics and Earthquake Engineering*, 53, 49-72.
- Boray, A. 1975. Bitlis dolayının yapısı ve metamorfizması. *Türkiye Jeoloji Bülteni*, 18, 81-84.
- Bull, W.B. 1977. Tectonic geomorphology of the Mojaand Desert, California, U.S. Geological Surandy Contract Report 14-0-001-G-394.
- Bull, W.B. 2007. Tectonic Geomorphology of Mountains: A New Approach to Paleoseismology. Wiley-Blackwell, USA.

- Bull, W.B., McFadden, L.D. 1977. Tectonic geomorphology north and south of the Garlock fault, California. *Geomorphology in Arid Regions*, 115-138.
- Chen, Y.C., Sung, Q., Cheng, K.Y. 2003. Along-strike variations of morphotectonic features in the Western Foothills of Taiwan: Tectonic implications based on stream-gradient and hypsometric analysis. *Geomorphology* 56, 109-137, doi:10.1016/S0169-555X(03)00059-X.
- Ciccacci, S., D'Alessandro, L., Fredi, P., Palmieri, E.L. 1992. Relations between morphometric characteristics and denudational processes in some drainage basins of Italy. *Zeitschrift fur Geomorphologie* 36, 53-67.
- Cisternas, A., Philip, H., Bousquet, J. C., Cara, M., Deschamps, A., Dorbath, L., Tatevossian, R. 1989. The Spitak (Armenia) earthquake of 7 December 1988: Field observations, seismology and tectonics. *Nature*, 339(6227), 675-679, doi:10.1038/339675a0.
- D'Alessandro, L., Del Monte, M., Fredi, P., Lupia-Palmeri, E., Peppoloni, S. 1999. Hypsometric analysis in the study of Italian drainage basin morphoevolution. *Transactions, Japanese Geomorphological Union* 20, 187-202.
- Dewey, J.F., Hempton, M.R., Kidd, W.S.F., Saroğlu, F., Şengör, A.M.C. 1986. Shortening of continental lithosphere: The neotectonics of Eastern Anatolia - A young collision zone. *Geological Society Special Publication*, pp. 1-36.
- Dhont, D., Chorowicz, J. 2006. Review of the neotectonics of the Eastern Turkish-Armenian Plateau by geomorphic analysis of digital elevation model imagery. *International Journal of Earth Sciences* 95, 34-49.
- Djamour, Y., Andriant, P., Nankali, H.R., Tavakoli, F. 2011. NW Iran-eastern Turkey present-day kinematics: Results from the Iranian permanent GPS network. *Earth and Planetary Science Letters*, 307, 27-34, doi:10.1016/j.epsl.2011.04.029.
- Doğan, B., Karakaş, A. 2013. Geometry of co-seismic surface ruptures and tectonic meaning of the 23 October 2011 M w 7.1 Van earthquake (East Anatolian Region, Turkey). *Journal of Structural Geology*, 46, 99-114, doi:10.1016/j.jsg.2012.10.001.
- El Hamdouni, R., Irigaray, C., Fernández, T., Chacón, J., Keller, E.A. 2008. Assessment of tectonic and geomorphic processes, southwest border of the Sierra Nevada (southern Spain). *Geomorphology* 96, 150-173, doi:10.1016/j.geomorph.2007.08.004.
- Elliott, J.R., Copley, C., Holley, R., Scharer, K., Parsons, B. 2013. The 2011 Mw 7.1 Van (Eastern Turkey) earthquake. *Journal of Geophysical Research: Solid Earth*, 118, 1619-1637.
- Emre, Ö., Doğan, A., Özalp, Ö., Yıldırım, Y. 2005. 25 Ocak 2005 Hakkari Depremi Hakkında Ön Değerlendirme. *Maden Tetkik ve Arama Genel Müdürlüğü. Rapor No: 123. Ankara (unpublished)*
- Emre, Ö., Duman, T.Y., Özalp, S., Olgun, Ş., Elmacı, H. 2012. 1:250.000 ölçekli Türkiye diri fay haritaları serisi, Van (NJ38-5) Paftası, Seri No:52, Maden Tetkik ve Arama Genel Müdürlüğü, Ankara-Türkiye.
- Erdoğan, T. 1975. Gölbaşı Civarının Jeolojisi. TPAO. Rapor, 929, 18.
- Ergin, K., Güçlü, U., Uz, Z. 1967. Türkiye ve civarının deprem kataloğu (MS. 11-1964). İstanbul, İTÜ, Maden Fakültesi, Arz Fiziği Enstitüsü yayınları.
- Font, M., Amorese, D., Lagarde, J.L. 2010. DEM and GIS analysis of the stream gradient index to evaluate effects of tectonics: The Normandy intraplate area (NW France). *Geomorphology* 119, 172-180, doi:10.1016/j.geomorph.2010.03.017.
- Giaconia, F., Booth-Rea, G., Martínez-Martínez, J.M., Azañón, J.M., Pérez-Peña, J.V. 2012. Geomorphic analysis of the Sierra Cabrera, an actiand pop-up in the constrictional domain of conjugate strike-slip faults: The Palomares and Polopos fault zones (eastern Betics, SE Spain). *Tectonophysics* 580, 27-42, doi:10.1016/j.tecto.2012.08.028.
- Giamboni, M., Wetzel, A., Schneider, B. 2005. Geomorphic response of alluvial riandrs to actiand tectonics: Example from the southern Rhine Graben. *Aust. J. Earth Sci.* 97, 24-37.
- Gordon, R.G. 1998. The plate tectonic approximation: plate nonrigidity, diffuse plate boundaries, and global plate reconstructions. *Annual Review of Earth and Planetary Sciences*, pp. 615-642, doi:10.1146/annurev.earth.26.1.615.
- Göncüoğlu, M. C., Turhan, N. 1984. Geology of the Bitlis metamorphic belt. *Maden Tetkik Arama yayınları* (In: Tekeli, O. ve Göncüoğlu, M.C. (eds), 237-244.
- Görgün, E. 2013. The 2011 October 23 M-W 7.2 Van-Ercis, Turkey, Earthquake And Its Aftershocks", *Geophysical Journal International*, 1052-1067.
- Gürbüz, A., Gürer, Ö. F. 2008. Tectonic geomorphology of the north Anatolian Faultzone in the Lake Sapanca Basin (eastern Marmara region, Turkey). *Geosciences Journal*, 12(3), 215-225.

- Horasan, G., Boztepe-Güney, A. 2006. Observation and analysis of low frequency crustal earthquakes in Lake Van and its vicinity, eastern Turkey Journal Seismology. 11, 1-13. doi:10.1007/s10950-006-9022-2
- Karakhanian, A.S., Trifonov, V.G., Philip, H., Avagyan, A., Hessami, K., Jamali, F., Bayraktutan, M.S., Bagdassarian, H., Arakelian, S., Davtian, V., Adilkhanyan, A., 2004. "Active faulting and natural hazards in Armenia, eastern Turkey and northwestern Iran", Tectonophysics, 380, 189–219.
- Keller, E. A. 1986. Investigation of active tectonics: Use of surficial Earth processes. In R. E. Wallace (Ed.), Active tectonics (pp. 136–147). Washington, DC: National Academy Press. Studies in Geophysics.
- Keller, E. A. Seaandr, D.B., Laduzinsky, D.L., Johnson, D.L., Ku, T.L., 2000. Tectonic geomorphology of actiand folding oandr buried reandrse faults: San Emigdio Mountain front, Southern San Joaquin Valley, California. Bulletin of the Geological Society of America 112, 86-97, doi:10.1130/0016-7606(2000)112%3C86:TGOAFO%3E2.0.CO;2.
- Keller, E. A. Pinter, N., 2002. Actiand Tectonics, Prentice Hall, New Jersey.
- Koçyiğit, A. 1985a. Karayazi Fayı. Yerbilimleri, 28, 67-72.
- Koçyiğit, A. 1985b. Muratbast - Balabantas (Horasan) arasında Çobandede Fay kuşağının jeotektonik özellikleri ve Horasan-Narman depremi yüzey kırıkları. Cumhuriyet Üniversitesi, Mühendislik Fakültesi Dergisi, 2, 17-33.
- Koçyiğit, A. 2005. Sütlice (Hakkari) Depreminin Kaynağı: Başkale Fay Kuşağı, GD Türkiye) Deprem Sempozyumu, Denizli, Turkey.
- Koçyiğit, A. 2013. New field and seismic data about the intraplate strike-slip deformation in Van region, East Anatolian plateau, E. Turkey. Journal of Asian Earth Sciences 62, 586-605, doi:10.1016/j.jseaes.2012.11.008.
- Koçyiğit, A., Yılmaz, A., Adamia, S., Kuloshvili, S. 2001. Neotectonic of East Anatolian Plateau (Turkey) and Lesser Caucasus: Implication for transition from thrusting to strike-slip faulting. Geodinamica Acta 14, 177-195, doi:10.1016/S0985-3111(00)01064-0.
- KOERI, 2011. KOERI (Boğaziçi Üniversitesi Kandilli Rasathanesi ve Deprem Araştırma Enstitüsü), 2011 - 2012 (<http://www.koeri.boun.edu.tr/scripts/Ist5.asp>)
- Lifton, N.A., Chase, C.G. 1992. Tectonic, climatic and lithologic influences on landscape fractal dimension and hypsometry: implications for landscape evolution in the San Gabriel Mountains, California. Geomorphology 5, 77-114, doi:10.1016/0169-555X(92)90059-W.
- Mayer, L. 1986. Tectonic geomorphology of escarpments and mountain fronts. Actiand Tectonics, 125-135.
- Ohmori, H. 1993. Changes in the hypsometric curand through mountain building resulting from concurrent tectonics and denudation. Geomorphology 8, 263-277, doi:10.1016/0169-555X(93)90023-U.
- Özkaymak, Ç., Sözbilir, H., Bozkurt, E., Dirik, K., Topal, T., Alan, H., Çağlan, D. 2011. 23 Ekim 2011 Tabanlı-Van Depreminin Sismik Jeomorfolojisi ve Doğu Anadolu'daki Aktif Tektonik Yapılarla Olan İlişkisi. JMO Jeoloji Mühendisliği Dergisi 35 (2) 175-199.
- Özkaymak, Ç., Sözbilir, H. 2012. Tectonic geomorphology of the Spildağı high ranges, western Anatolia. Geomorphology, 173–174, 128–140.
- Özkaymak, Ç. 2015. Tectonic analysis of the Honaz Fault (western Anatolia) using geomorphic indices and the regional implications. Geodinamica Acta, 27:2-3, 110-129.
- Özsayın, E. 2016. Relative tectonic activity assessment of the Çameli Basin, Western Anatolia, using geomorphic indices, Geodinamica Acta, doi: 10.1080/09853111.2015.1128180.
- Pérez-Peña, J.V., Azañón, J.M., Azor, A. 2009a. CalHypso: An ArcGIS extension to calculate hypsometric curands and their statistical moments. Applications to drainage basin analysis in SE Spain. Computers and Geosciences 35, 1214-1223, doi:10.1016/j.cageo.2008.06.006.
- Pérez-Peña, J.V., Azañón, J.M., Booth-Rea, G., Azor, A., Delgado, J. 2009b. Differentiating geology and tectonics using a spatial autocorrelation technique for the hypsometric integral. Journal of Geophysical Research: Earth Surface 114.
- Pérez-Peña, J.V., Azor, A., Azañón, J.M., Keller, E.A. 2010. Actiand tectonics in the Sierra Nevada (Betic Cordillera, SE Spain): Insights from geomorphic indexes and drainage pattern analysis. Geomorphology 119, 74-87, doi:10.1029/2008JF001092.
- Rebai, S., Philip, H., Dorbath, L., Borissoff, B., Haessler, H., Cisternas, A. 1993. Active tectonics in the lesser Caucasus: coexistence of compressive and extensional structures. Tectonics, 12(5), 1089-1114, doi:10.1029/93TC00514.

- Reilinger, R., McClusky, S., Andrnant, P., Lawrence, S., Ergintav, S., Cakmak, R., Ozener, H., Kadirov, F., Guliev, I., Stepanyan, R. 2006. GPS constraints on continental deformation in the Africa-Arabia-Eurasia continental collision zone and implications for the dynamics of plate interactions. *Journal of Geophysical Research: Solid Earth* (1978–2012) 111, doi:10.1029/2005JB004051.
- Ricou, L. 1971. Le croissant ophiolitique péri-arabe: Une ceinture de nappes mises en place au Crétacé supérieur.
- Rockwell, T.K., Keller, E.A., Johnson, D.L. 1984. Tectonic geomorphology of alluvial fans and mountain fronts near Andntura, California. *Tectonic Geomorphology*, 183-207.
- Silva, P.G., Goy, J.L., Zazo, C., Bardají, T., 2003. Fault-generated mountain fronts in southeast Spain: Geomorphologic assessment of tectonic and seismic activity. *Geomorphology* 50, 203-225, doi:10.1016/S0169-555X(02)00215-5.
- Soysal, H., Sipahioğlu, S., Koçak, D., Altınok, Y. 1981. Türkiye ve Çevresinin Tarihsel Deprem Kataloğu (MÖ 2100-MS 1900). TUBİTAK Projesi (TBAG), Ankara:.
- Strahler, A.N. 1952. Hypsometric (area-altitude) analysis of erosional topography. *Bulletin of the Geological Society of America* 63, 1117-1142.
- Şaroğlu, F., Yılmaz, G., Erdoğan, R. 1984. "Horasan–Narman depreminin jeolojik özelliği ve Doğu Anadolu'da depreme yönelik çalışmaların gerekliliği", *Kuzeydoğu Anadolu I. Ulusal Deprem Sempozyumu. Atatürk Üniversitesi, Erzurum*, 349-360.
- Şaroğlu, F., Yılmaz, Y. 1986. Doğu Anadolu'da neotektonik dönemdeki jeolojik evrim and havza modelleri. *Maden Tektik ve Arama Dergisi*, 107, 73-94.
- Şaroğlu, F., Emre, Ö., Boray, A. 1987. Türkiye'nin diri faylari ve depremsellikleri. *Maden Tetkik ve Arama Genel Müdürlüğü. Report No: 5216.*
- Şengör, A.M.C., Kidd, W.S.F. 1979. Post-collisional tectonics of the Turkish-Iranian plateau and a comparison with Tibet. *Tectonophysics* 55, 361-376, doi:10.1016/0040-1951(79)90184-7.
- Şengör, A. M. C., Yılmaz, Y. 1981. Tethyan evolution of Turkey: A plate tectonic approach. *Tectonophysics*, 75(3-4), 181-190,193-199,203-241, doi:10.1016/0040-1951(81)90275-4.
- Şengör, A.M.C., Görür, N., and Şaroğlu, F., 1985. Strike-slip faulting and related basin formation in zones of tectonic escape: Turkey as a case study.
- Tan, O., Tapirdamaz, M.C., Yörük, A. 2008. "The earthquake catalogues for Turkey", *Turkish Journal of Earth Sciences*, 17(2), 405-418.
- Willgoose, G. 1994. A statistic for testing the elevation characteristics of landscape simulation models. *Journal of Geophysical Research* 99, 13987-13996, doi:10.1029/94JB00123.
- Willgoose, C., Hancock, G. 1998. Revisiting the hypsometric curand as an indicator of form and process in transport-limited catchment. *Earth Surface Processes and Landforms* 23, 611-623.
- Yıldırım, C. 2014. Relative tectonic activity assessment of theTuz Gölü fault zone; Central Anatolia, Turkey. *Tectonophysics*,630, 183–192.
- Yılmaz, O. 1975. Casas Bölgesi (Bitlis Masifi) kayaçlarının petrografik ve stratigrafik incelenmesi. *Türkiye Jeoloji Bülteni*, 18-1, 33-40.
- Yılmaz, Y. 1971. Etüde petrographique et geochronologique de la region de Casa (Partie Meridionale du Masif de Bitlis, Turquie, These de doct 3 cycle). *Univ. Sci.Med. Greonable*, 230.
- Yılmaz, Y., Şaroğlu, F., Güner, Y. 1987. Initiation of the neomagmatism in East Anatolia. *Tectonophysics* 134, 177-199, doi:10.1016/0040-1951(87)90256-3.



# Bulletin of the Mineral Research and Exploration

<http://bulletin.mta.gov.tr>



## MOLLUSCAN BIOSTRATIGRAPHY OF EARLY MIOCENE DEPOSITS OF THE KALE-TAVAS AND ACIPAYAM BASINS (DENİZLİ, SW TURKEY)

Yeşim BÜYÜKMERİÇ<sup>a\*</sup>

<sup>a</sup>Bülent Ecevit Üniversitesi, Mühendislik Fakültesi, Jeoloji Mühendisliği Bölümü, 67100 İncivez-Zonguldak/Türkiye, [orcid.org/0000-0003-2678-3907](http://orcid.org/0000-0003-2678-3907)

Research Article

### Key words:

Aquitanian, Late Burdigalian, Mollusca, Paleobiogeography, Paleocology, Stratigraphy.

### ABSTRACT

In the present work, a stratigraphic framework of the early Miocene units of the Kale-Tavas and Acıpayam deposits is proposed. Two stratigraphic sections from the brackish-marine deposits of Aquitanian (Yenidere formation) and three sections from the shallow marine units of late Burdigalian (Kale formation) age have been logged. In total 23 mollusc species are identified similar to those of the areas in the Mediterranean province. The fauna indicates that the Mediterranean Tethys occupied the southwestern part of the Denizli region only during the early Miocene. A tectonic pulse in the basin during the early Miocene may have been very important to understand the limits of marine Tethyan influence in the area.

Received Date: 24.09.2016

Accepted Date: 09.01.2017

## 1. Introduction

The continuous northward drift of the African Plate has been driving regional differentiations in basin developments in the convergent boundary zone during the Cenozoic period (Meulenkamp et al., 2000; Meulenkamp and Sissingh, 2003). In Oligo-Miocene time, development of the basins in SW Anatolia was mainly influenced by these complex and successive regional geotectonic events as for example the emplacement of the ophiolitic Lycian nappes and later N-S extensional regimes (Şengör and Yılmaz, 1981; Koçyiğit, 1984; Şenel, 1997; Seyitoğlu and Scott, 1991; Collins and Robertson, 1998, 2003; Bozkurt, 2003; Sözbilir, 2005; Westaway, 2006; Westaway et al., 2005). Also global sea level fluctuations caused alternating marine-nonmarine phases in the region. These phases are represented by detritic and carbonated sediments, known as intramontane "Oligo-Miocene Lycian molasse" which are found in NE-SW directed intramontane Denizli, Kale-Tavas and Çardak-Dazkırı subbasins (Sözbilir, 2005) and Acıpayam piggy-back basin (Alçiçek and ten Veen, 2008).

Oligocene units are found in the middle and

northeastern part of the Lycian molasse (Çardak-Dazkırı, Denizli and northeastern part of Kale-Tavas subbasins). Their invertebrate fossils represent late Rupelian – early Chattian (SBZ22 and P19) assemblages (İslamoğlu, 2008; İslamoğlu and Gedik, 2005; İslamoğlu et al., 2006; 2007; Özcan et al., 2008; İslamoğlu and Hakyemez, 2010).

Marine early Miocene units are only found in the south- southwestern part of the Kale-Tavas and Acıpayam basins (Figure 1). Although a few paleontological studies for early Miocene deposits are available in the region, the stratigraphical framework of the marine units is still controversial. In earlier works, two different early Miocene sedimentary cycles have been distinguished: the Aquitanian flysch and the Burdigalian-Helvetian marine-lagoonal unit (Altunlu, 1955 and Nebert, 1956; 1961). An early Aquitanian age was proposed based on the ostracod and foraminifer fauna for the base of early Miocene sections in the Yenişehir - Kale region (Gökçen, 1982). In subsequent work, however, these deposits were considered to belong to the middle part of the Oligocene Mortuma Formation (Akgün and Sözbilir, 2001). Some authors considered these deposits to be of late Oligocene age (Benda and Meulenkamp, 1990;

\* Corresponding author: Yeşim BÜYÜKMERİÇ [yesim.buyukmeric@yahoo.com](mailto:yesim.buyukmeric@yahoo.com)  
<http://dx.doi.org/10.19111/bulletinmre.302166>

Seyitoğlu and Scott, 1996). The Yenidere formation rests unconformably on the Mortuma formation, and was considered to be of Aquitanian age based on both its stratigraphical position (Hakyemez, 1989) and palynomorph associations (Becker-Platen, 1970; Akgün and Sözbilir, 2001). The upper units consist of carbonates (Kale formation) that have been dated as Burdigalian (Hakyemez, 1989; Gökçen, 1982; Özcan et al., 2008).

Some levels of the Yenidere and Kale formations are rich in molluscs, but these were not previously studied. Detailed information on the mollusc content of the stratigraphical units will be helpful to understand the regional stratigraphy. This study aims to document the mollusc species in the Miocene Kale-Tavas and Acıpayam basins in order to assess palaeoenvironmental evolution as well as paleobiogeographic signature.

## 2. Material and Methods

This study is based on the MTA (General Directorate of Mineral Research and Exploration)

project (16 B45). Initial paleontological results of Miocene faunas are reported in İslamoğlu et al. (2006, 2007). Here the mollusc faunas are studied within a stratigraphical context. They were collected as handpicking samples from outcropping surfaces and cleaned from sediment remains in the paleontology-sedimentology laboratory of MTA. Photographs were taken in the Natural History Museum, Vienna, Austria. Molluscs are in repositories of Bülent Ecevit University, Geological Engineering Department.

## 3. Geological Setting

Oligo-Miocene deposits in the Denizli region developed on an imbricated basement, comprising Mesozoic- Paleozoic rocks of the Menderese massive, the allochthonous Mesozoic rocks of Lycian nappes and Paleocene - Eocene supra-allochthonous sediments (Konak et al., 1986; Sözbilir, 2005). The Kale-Tavas subbasin is located in the southwestern part of the Denizli region (Figure 1). Its Oligo-Miocene sediments are described as Akçay group (Hakyemez, 1989). Oligocene marine-brackish deposits bearing

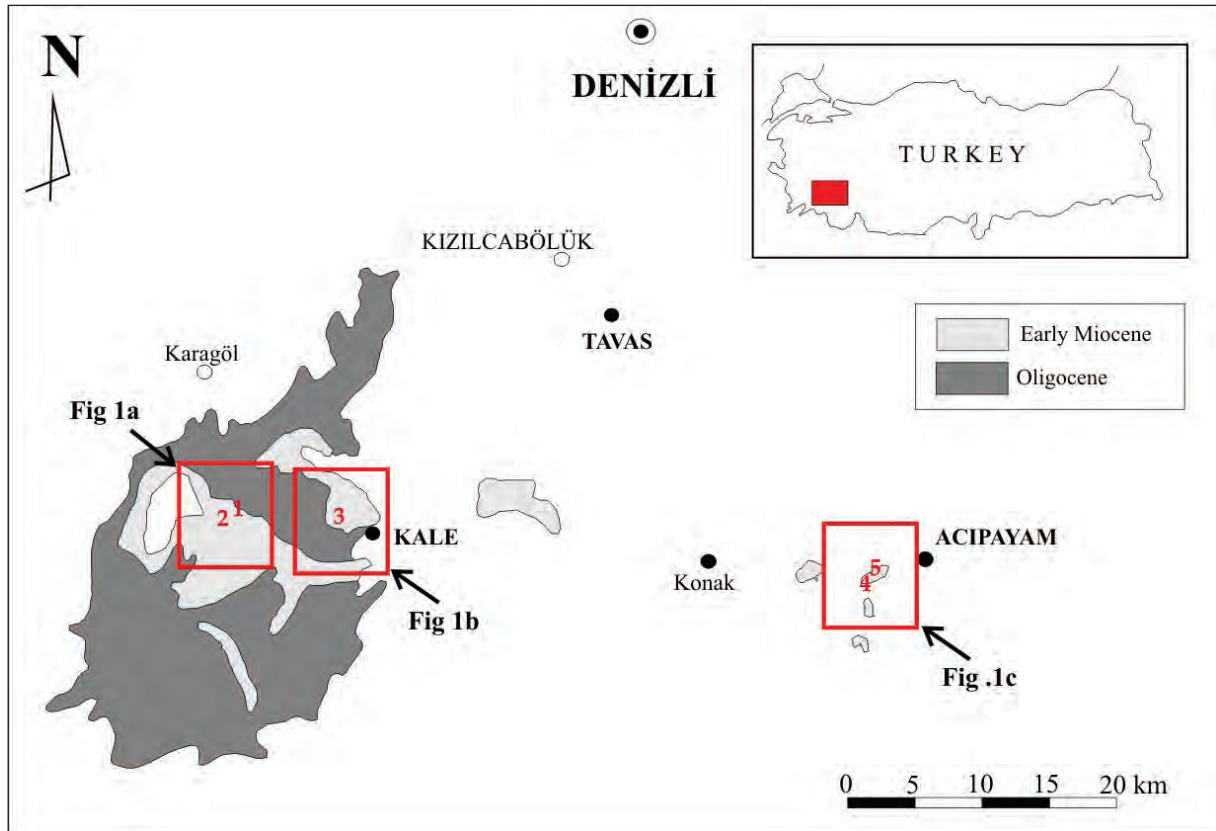


Figure 1- Oligo-Miocene units and measured stratigraphical sections in the studied region. Yenidere formation (Aquitanian): 1) Kurbağlık, 2) Sulugüme, Kale formation (Burdigalian): 3) Kale-Delibağ, 4) Kuleburnu, 5) Alacain (modified from the 1:500.000 geological map of the archive of MTA Geological Research Department).

molluscs are widely distributed in the middle, north and northeastern part of the Lycian molasse region (Çardak-Dazkırı/Acıgöl, Denizli and Kale-Tavas sub-molasse basins) (İslamoğlu, 2008; İslamoğlu and Hakyemez, 2010; İslamoğlu et al., 2005, 2006, 2007).

The early Miocene succession in the Kale-Tavas subbasin includes the Yenidere, Künar and Kale formations (Hakyemez, 1989). Early Miocene deposits are only exposed in the southwestern part of the region (Kale-Tavas sub-molasse basin) overlying clastic Oligocene units. The Yenidere formation consists of brackish – lagoonal sediments and includes shallow marine intervals, the latter are mostly restricted to the lower part of the formation. In overlying intervals terrestrial facies, including coal-bearing fine detritics representing swamp depositional environments are found. A number of the coal layers are exploited. The Yenidere formation represents a very short transgressive basal interval overlain by regressive deposits. It is rich in brackish molluscs and ostracods but lacks benthic and planktic foraminifers. The formation is overlain by the terrestrial Künar formation that consists of cross-bedded conglomerates (fluvial sediments: Hakyemez, 1989). This unit lacks any fossils. The Kale formation consists of shallow marine reefal carbonates and detritics representing a transgressive succession. Shallow marine molluscs, benthic foraminifers, corals and ostracods are common. The Yenidere and Kale formations overlay the Oligocene Mortuma formation with an angular unconformity. A conformable contact between Aquitanian and Burdigalian rocks was proposed based on observations of Akgün and Sözbilir (2001). However, in our work, the contact between the Yenidere and Kale formations could not be observed.

#### 4. Results

##### 4.1. Facies, Fossil Contents and Paleoecology

Five stratigraphic sections have been logged in the early Miocene Yenidere and Kale formations and five facies types are distinguished.

The localities, detailed lithological explanations and fossil contents of the sections are shown in the maps and tables (Figures 1a, 1b, 1c, 2-7). Correlation of the sections and facies are shown in the correlation table (Figure 8).

Coordinates and thickness of the sections are listed below:

*Kurbağalık section*: (9,5 m) (Yenidere formation), measured in an open coal pit, 12 km E of Kurbağalık, south of Gediktepe, geological map sheet (1:25.000) Denizli M21-d3, X: 52612, Y: 52000, Z: 800

*Sulugüme section* (98.6 m) (Yenidere formation), measured in the Sulugüme river valley, south of Arıkayası tepe, geological map sheet (1:25.000) Denizli M21-d3, X: 51800, Y: 50600; Z: 740.

*Kale-Delibag section* (27.8 m) (Kale formation): measured from the outcrop W of Kale town, N of Delibağ, near Kavakpınarı, geological map sheet (1:25.000) Denizli N21-b1, X: 62000, Y: 44800, Z: 1060.

*Kuleburnu section* (275 m): measured from the outcropsouth of Acıpayam - Mevlütler, geological map sheet (1:25.000) Denizli N22-b1, X: 02774, Y: 37448, Z: 1504.

*Alacain section* (173.8 m): measured from the outcrop, W of Acıpayam, geological map sheet (1:25.000) Denizli N22-b1, X: 02750, Y: 43050, Z: 1370

##### *Unit 1: Brackish sediments with shallow marine intercalations*

This facies is identified in the lower and middle part of the Yenidere formation (Figure 8). Shallow marine molluscs are found together with brackish molluscs indicating short-term proximal marine incursions from the shore towards the near shore or estuarine environments. Shallow marine species such as *Turritella turris* de Basterot, 1825, *Mytilus (Crenomytilus) aquitanicus* (Mayer, 1858), *Anadara cardiiformis* (de Basterot, 1825), *Euspira helicina helicina* (Brocchi, 1814) and *Melongena lainei* (de Basterot, 1825) representing shallow marine environment (Lozouet et al., 2001, Landau et al., 2013). *Melanopsis hantkeni* Hofmann, 1870 is confined to the estuarine –fluvial and river mouth nearshore paleoenvironments.

##### *Unit 2: Brackish - Lagoonal sediments:*

This facies is observed in the lower and middle levels of the Yenidere formation. Brackish – lagoonal facies include coal-bearing detritics (Kurbağalık and Sulugüme sections, Figure 8). *Mesohalina margaritacea* (Brocchi, 1814), *Granulolabium plicatum* (Bruguière, 1792), *Terebralia lignitarum*

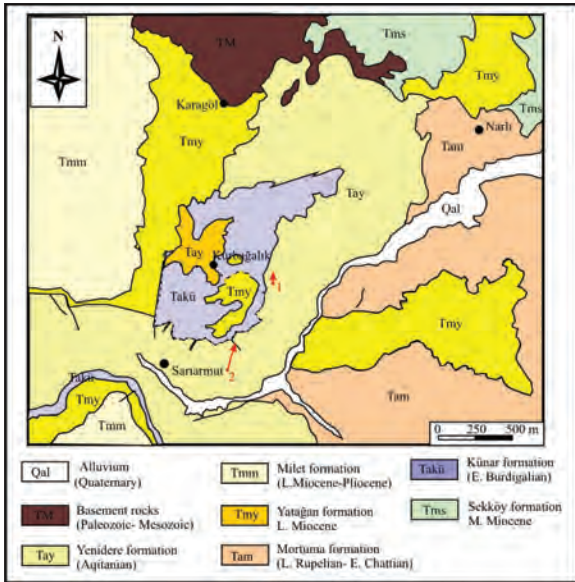


Figure 1a- Kurbagalık (1) and Sulugüme (2) sections and geological map of the surrounding area (Denizli N21, Hakyemez, 1982; Archive of MTA Geological Research Department).

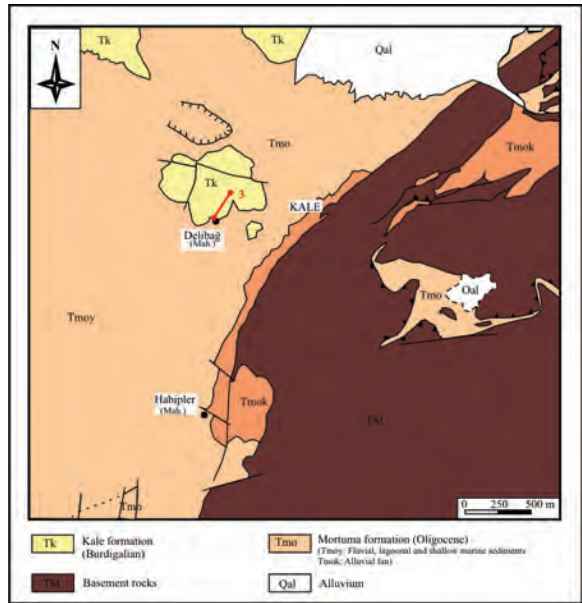


Figure 1b- Kale-Delibag section (3) and geological map of the surrounding area (Denizli N21, archive of MTA Geological Research Department).

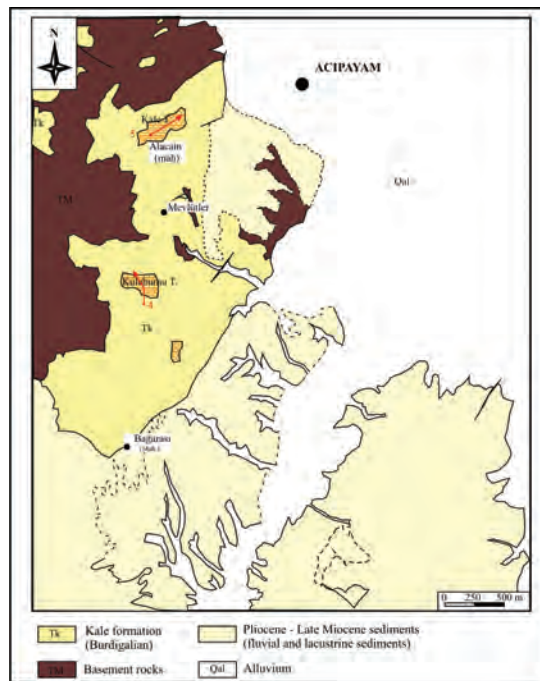


Figure 1c- Kuleburnu (4) and Alacain (5) sections and geological map of the surrounding area (Denizli N22; archive of MTA Geological Research Department).

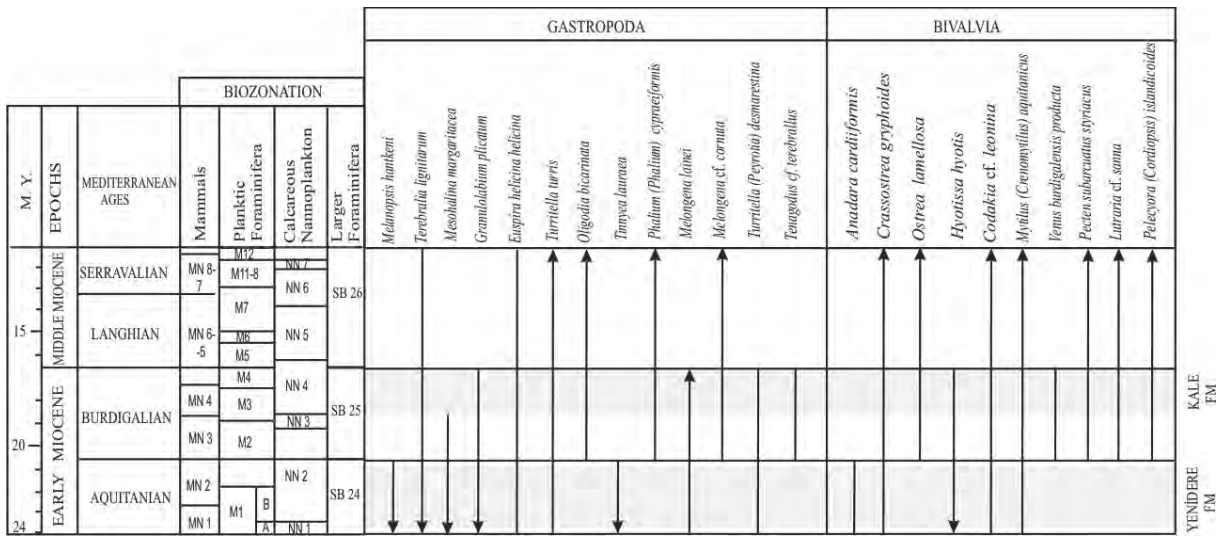


Figure 2- Stratigraphical ranges of the mollusc species in the Kale-Tavas subbasin.

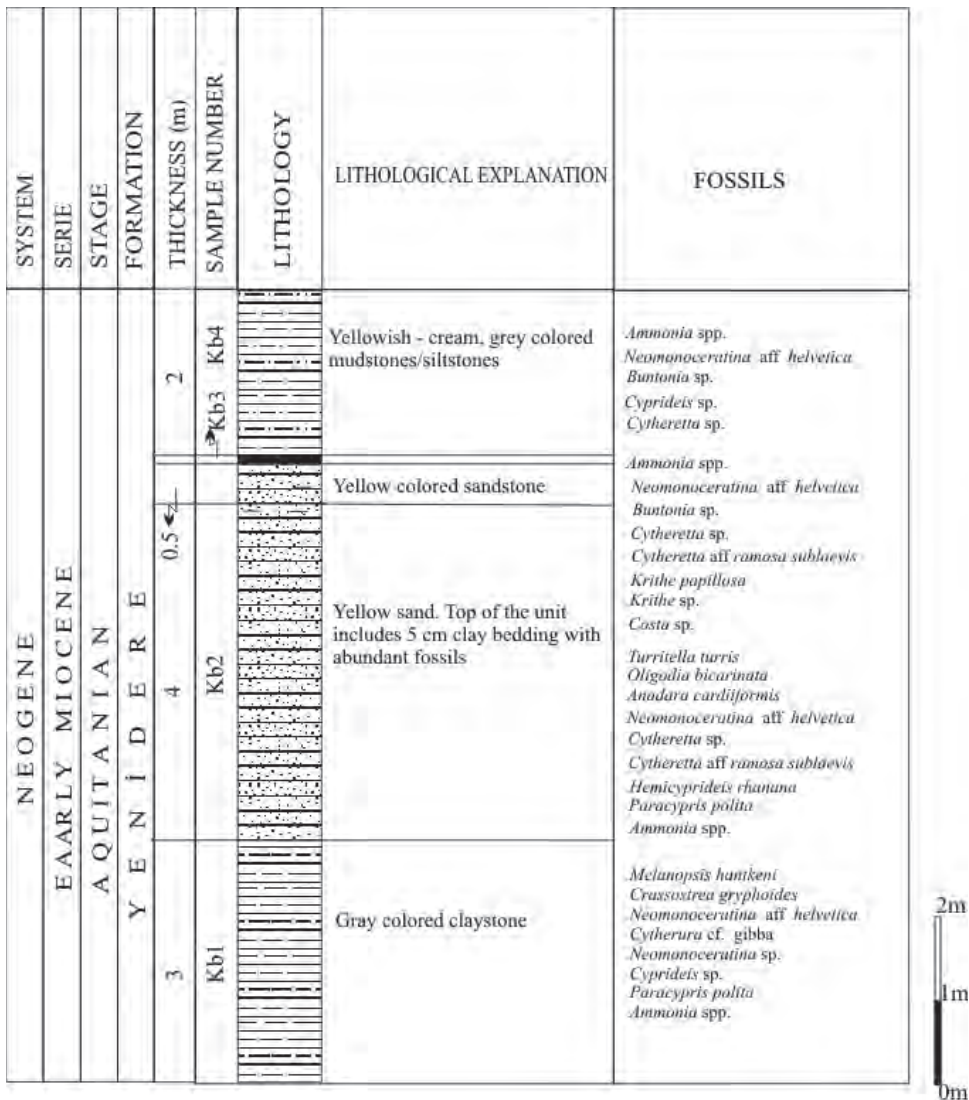


Figure 3- Kurbağalık measured stratigraphical section.

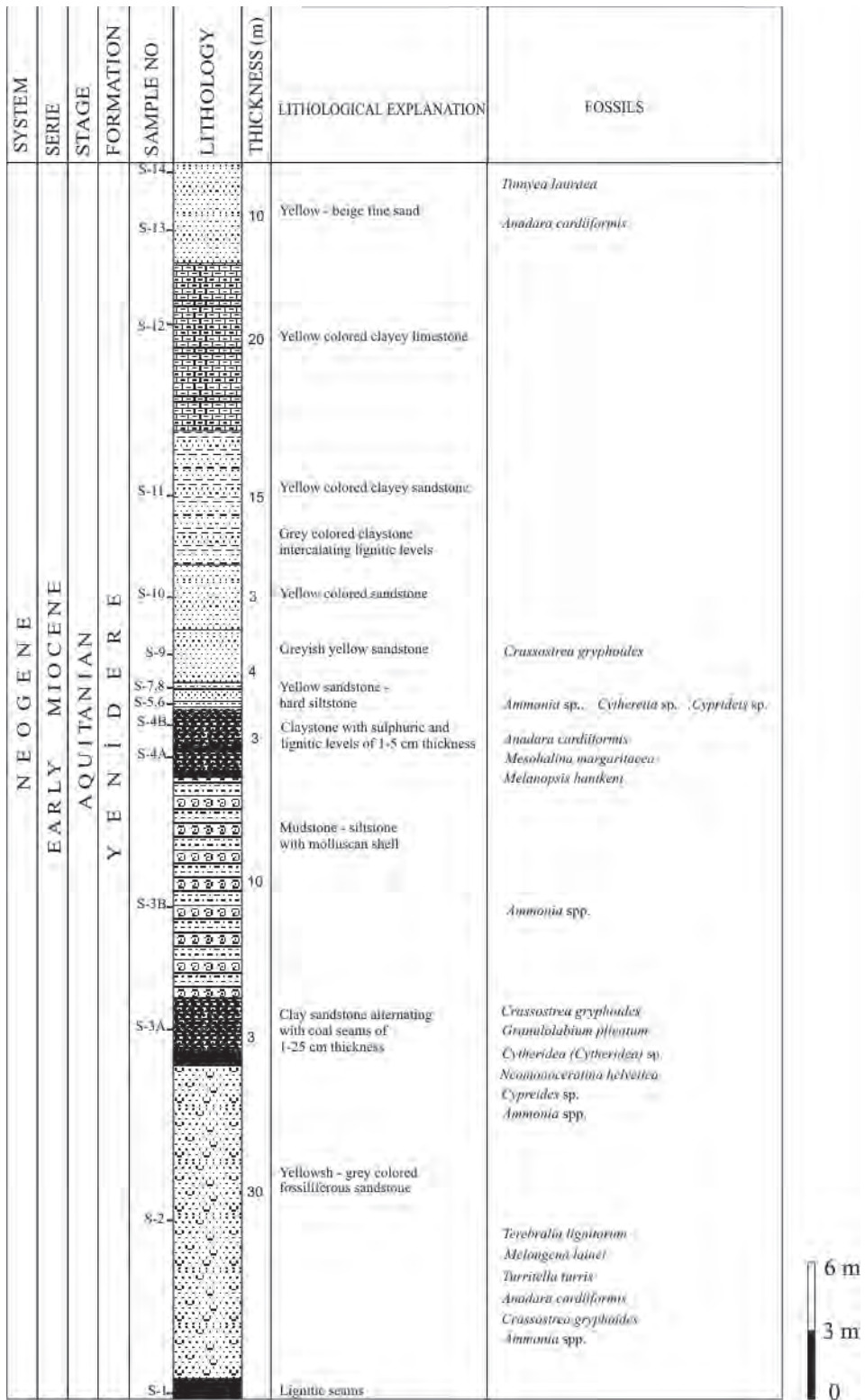


Figure 4- Sulugöme measured stratigraphical section.

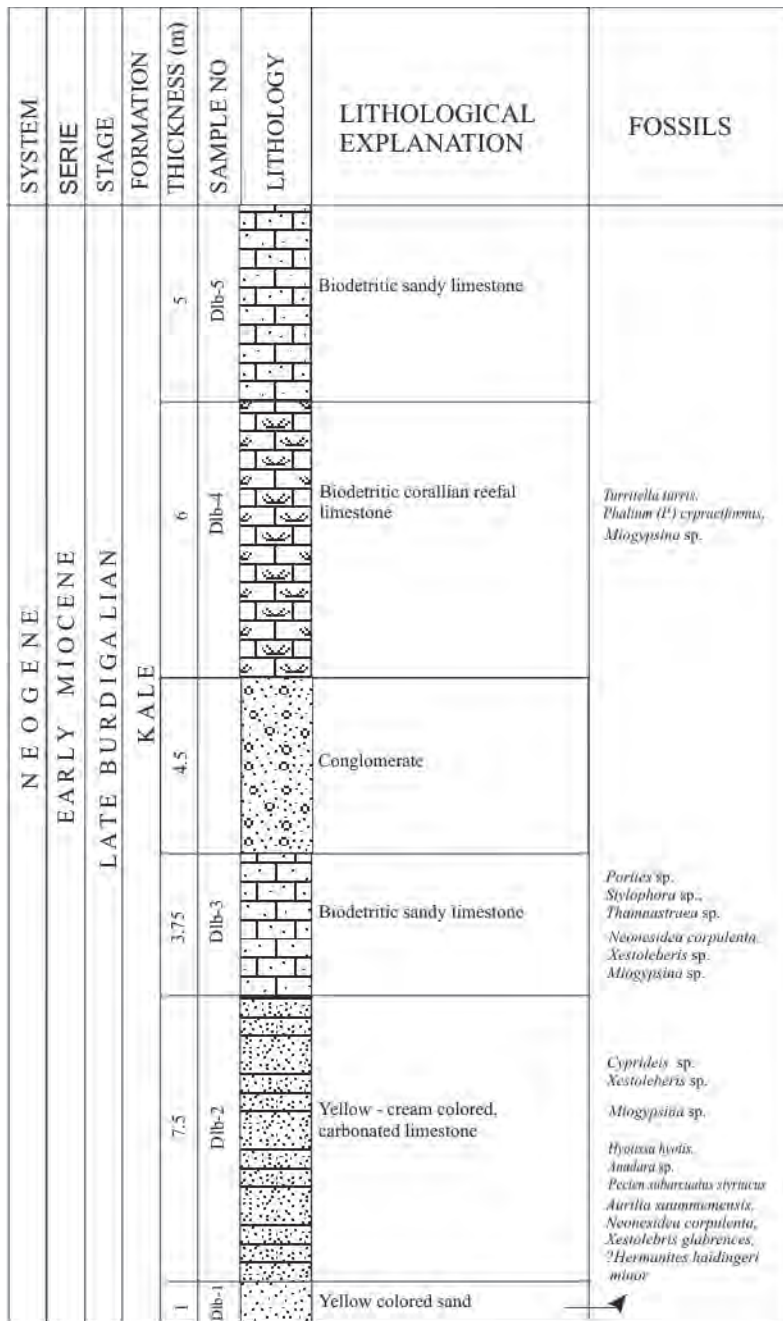


Figure 5- Kale-Delibag measured stratigraphical section.

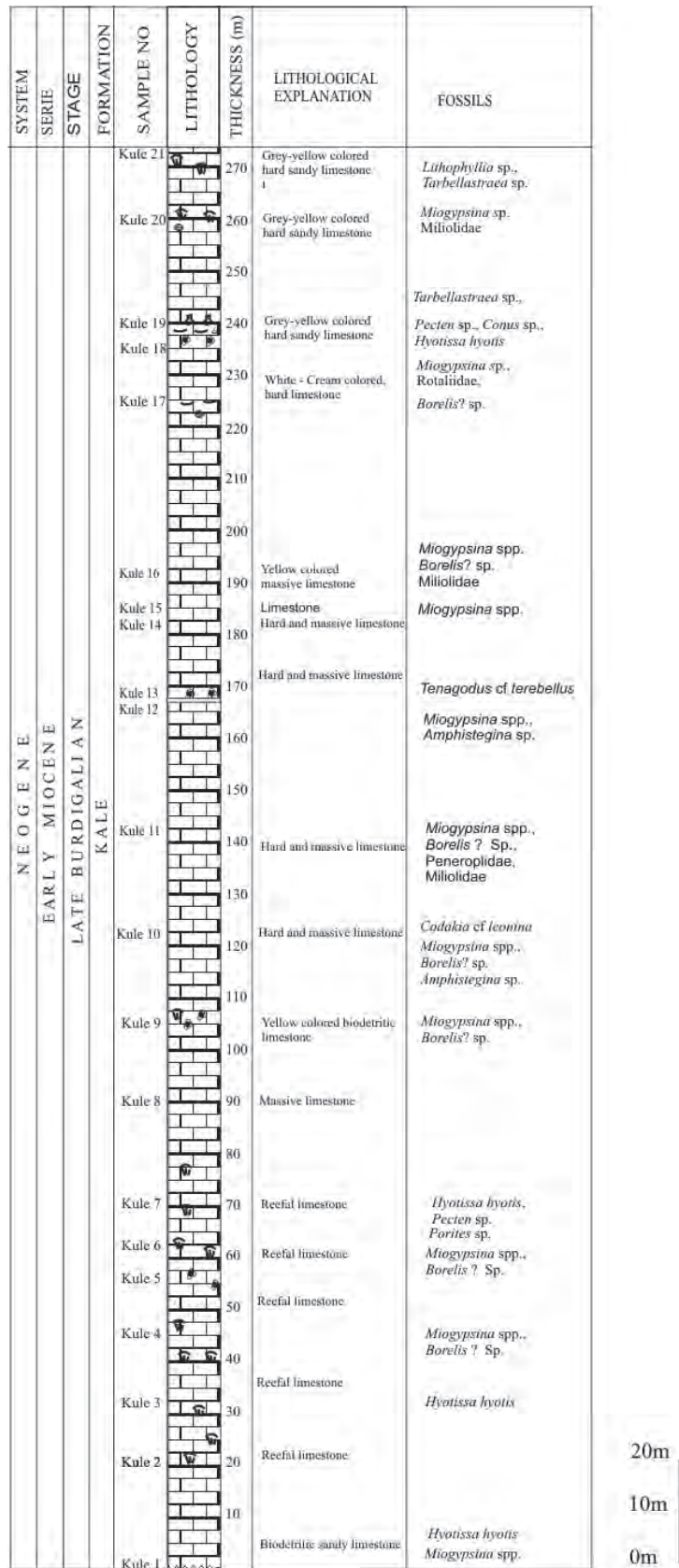


Figure 6- Kuleburnu measured stratigraphical section.

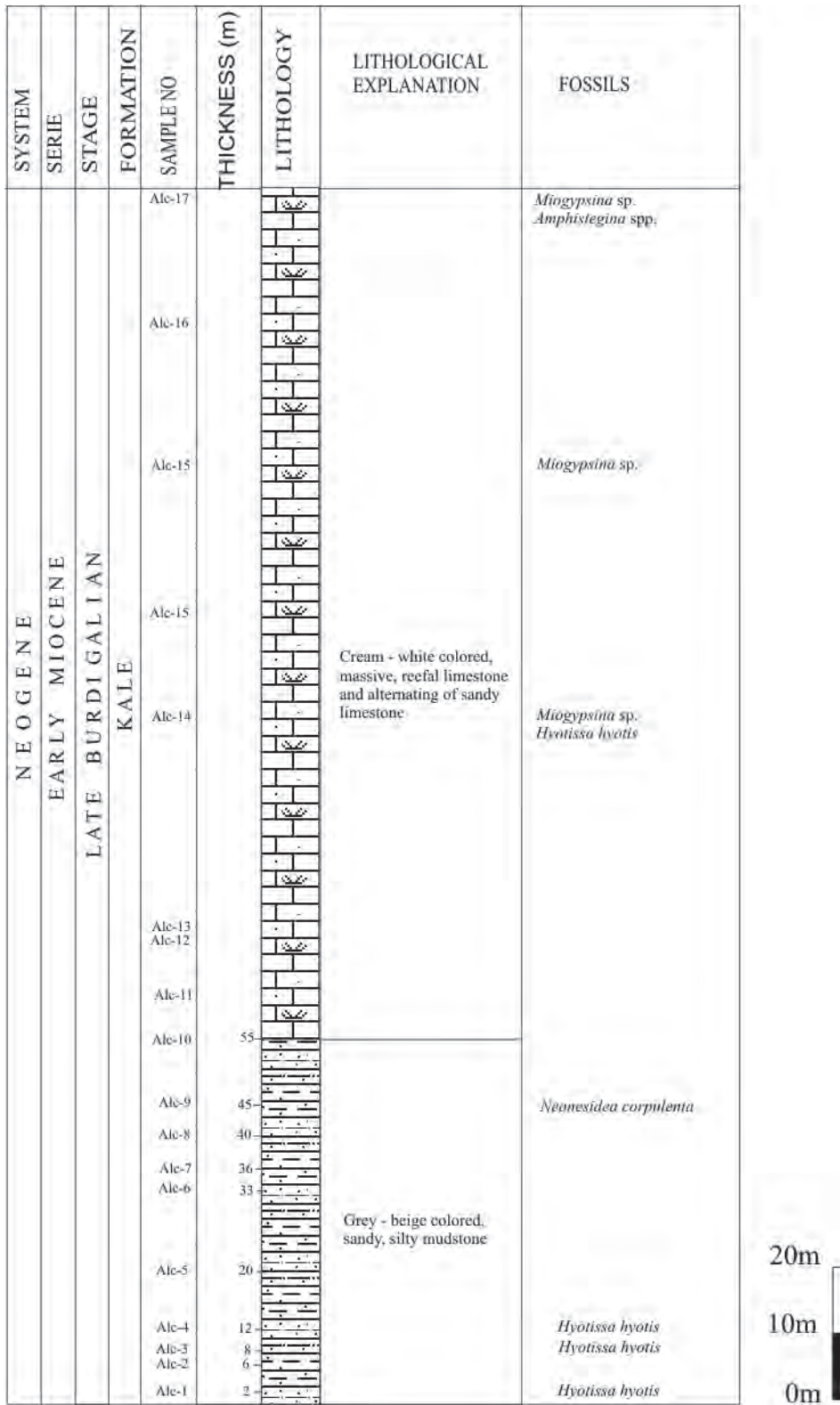


Figure 7- Alacain measured stratigraphical section.



(Eichwald, 1830), *Granulolabium plicatum* (Bruguière, 1792), and *Crassostrea gryphoides* (Schlotheim, 1813) are common species. *Mesohalina margaritacea* and *Granulolabium plicatum* are reported from lagoonal to littoral environments indicating oligo/mesohaline salinities (Báldi, 1973; Barthelt, 1989; Harzhauser and Mandic, 2001). *Terebralia lignitarum* (Eichwald, 1830) is common in the brackish units of the Oligocene in the Denizli (İslamoğlu, 2008) and Serravalian Karaman basins (Landau et al., 2013). The low diversity bivalve assemblage is predominated by the brackish ostreid *Crassostrea gryphoides* (Schlotheim, 1813).

#### *Unit 3: Swamp - marsh sediments:*

This facies forms the uppermost fine detritics of the Yenidere formation (Sulugüme section, Figure 8) and is dominated by *Tinnyea lauraea* (Mathéron, 1842) and *Melanopsis hantkeni* Hofmann, 1870, representing a swamp environment (İslamoğlu et al. 2008; Neubauer et al. 2013; Harzhauser et al. 2016). *Melanopsis* - *Mesohalina* (synonym of *Tympanotonos*: Harzhauser et al., 2016) communities are also considered to represent, low salinity assemblages with freshwater influences from the mainland, brackish water lagoons or mangrove swamps possibly under influence of rivers (Báldi, 1973). *Melanopsis hantkeni* Hofmann, 1870 is confined to oligohaline estuarine-fluvial and river mouth nearshore paleoenvironments (Barthelt, 1989; Harzhauser and Mandic, 2001; Neubauer et al. 2013, 2016; Harzhauser et al., 2016). This unit includes also a few thick coal seams exploited economically.

#### *Unit 4: Shallow marine detritics:*

The facies is observed in the Kale formation (Delibağ section, Figure 8). Grey - beige colored, sandy-silty mudstones, sandy limestones. Mollusc contents and coral fauna are poor. Only ostreid bivalves [*Ostrea lamellosa* Brocchi, 1814, *Hyotissa hyotis* (Linnaeus, 1758)] and *Porites* colonies were observed. *Hyotissa hyotis* is a stenohaline ostreid living in the sublittoral environments under fully marine conditions (Harzhauser and Mandic 2001). A single balanid species, *Creussia miocaenica* Prochazka, 1893 is also found (plate 2, Figure 6).

#### *Unit 5: Carbonates - Reefal carbonates:*

This facies is defined in the Kale formation (Figure 8). Light grey - yellow - beige coloured hard

limestone - reefal limestone - detritic limestones. The ostreid bivalve *Hyotissa hyotis* is a commonly occurring species. Benthic foraminifers (*Miogypsina*, *Amphistegina*, *Borelis*), red algae and corals (*Porites*, *Tarbellastraea*) are also abundant.

#### 4.2. Biostratigraphy

Molluscan findings from the Yenidere and Kale formations are recorded herein for the first time. Two stratigraphical sections from the Yenidere formation (Kurbağalık, Sulugüme; Figure 1a) and three sections from Kale formation (Delibağ, Kuleburnu, Alacain) have been logged and sampled for molluscs. The distribution of benthic foraminifers, ostracods and corals collected from the same sections supports Aquitanian and late Burdigalian ages of the formations (İslamoğlu et al. (2006, 2007).

In total, 23 molluscan taxa are identified and all biostratigraphical data are interpreted together. Figure 2 gives the stratigraphic ranges of molluscs, correlated with geochronologic and biostratigraphic data modified from previous works (Rögl 1996, 1998; Rögl et al. 1993; Cahuzac and Poignant 1997; Steininger 1999; Harzhauser et al. 2002, Gradstein et al. 2004). Occurrence of each mollusc species in the sections is given (Table 1). Characteristic mollusc species are illustrated in Plates 1-3.

##### 4.2.1. Aquitanian (Yenidere Formation)

The stratigraphical range of molluscan species in the Kurbağalık and Sulugüme sections from the Yenidere formation indicates an Aquitanian age (Figures 2-4). *Mesohalina margaritacea* (Brocchi, 1814) became extinct during the mid-Burdigalian (Harzhauser et al., 2016). *Tinnyea lauraea* (Mathéron, 1842) originated in the Oligocene and was common during the early Miocene (Harzhauser et al. 2016). *Granulolabium plicatum* (Bruguière, 1792) is specific for Oligocene, but also abundant in the Aquitanian stratotype deposits (Lozouet et al. 2001) and Eggenburgian - Karpatian settings in Austria, Central Paratethys (Harzhauser et al. 2003). *Turritella (Peyrotia) desmarestina* de Basterot, 1825 is known from early Miocene deposits (Lozouet et al. 2001). The taxonomic position of *Melanopsis hantkeni* Hofmann, 1870 is discussed by Harzhauser et al. (2016). It is a geographically widespread species known from the Oligocene deposits of the Central Paratethys, also extending to Greece and Iran (Harzhauser, 2004), Turkey (Thrace and Denizli basins: İslamoğlu, 2008; İslamoğlu and Hakyemez,

Table 1- Occurrence of the mollusc species in the sections

	Yemidere formation (Aquitamian)											Kale formation (Late Burdigalian)														
	Kurbagalk		Sulugtime						Delibag			Kuleburnu				Alacain										
	Kb1	Kb2	S2	S3	S4b	S3a	S6	S9	S13	S14	D1b1	D1b4	Kule1	Kule3	Kule7	Kule10	Kule13	Kule17	Kule18	Kule19	Alc1	Alc1	Alc3	Alc4	Alc14	
<i>Melanopsis hantkeni</i> Hofmann, 1870	X				X		X																			
<i>Terebralia lignitarum</i>			X																							
<i>Mesohalina margaritacea</i>					X																					
<i>Granulolabium plicatum</i>				X																						
<i>Euspira helicina helicina</i>			X																							
<i>Turritella turris</i>		X	X									X														
<i>Oligodita bicarinata</i>		X																								
<i>Tinysea lauracea</i>									X																	
<i>Phalium (Phalium) cypraeiformis</i>											X															
<i>Melongena lainei</i>			X																							
<i>Melongena cf. cornuta</i>			X																							
<i>Turritella (Peyroita) desmarestina</i>			X																							
<i>Tenagodus cf. terebellus</i>																X										
<i>Modiolus</i> sp.												X														
<i>Conus</i> sp.																				X						
<i>Crommium</i> sp.												X														
<i>Anadara cardifformis</i>		X	X		X				X																	
<i>Anadara</i> sp.											X															
<i>Crassostrea gryphoides</i>	X	X	X		X			X																		
<i>Ostrea lamellosa</i>																		X	X							
<i>Hyotissa hyotis</i>												X	X	X	X			X	X	X	X	X	X	X	X	X
<i>Codakia cf. leonina</i>																X										
<i>Mytilus (Crenomytilus) aquitanicus</i>			X																							
<i>Venus (Antigona) burdigalensis producta</i>														X												
<i>Pecten subarcuatus styriacus</i>											X															
<i>Pecten</i> sp.													X													
<i>Lutaria cf. sama</i>																X										
<i>Pelecycora (Corditopsis) islandicoides</i>																X										

2010; İslamoğlu et al. 2008), misidentified as *M. impressa* Krauss, 1852 (Harzhauser et al. 2016). The present study shows that the stratigraphical range of *M.hantkeni* extends to Aquitanian. *Terebralia lignitarum* (Eichwald, 1830) is known from late Oligocene - middle Miocene deposits (Landau et al. 2013).

This Aquitanian mollusc assemblage is associated with early Miocene ostracods, *Neomonoceratina helvetica* Oertli, 1958, *Paracypris polita* Sars, 1866, *Cytheretta* aff. *ramosa sublaevis* Triebel, 1952, *Cytherura* cf. *gibba* (Mueller, 1785) and *Krithe papillosa* (Bosquet, 1852). The age of the formation is also supported by palynomorph assemblages (Akgün and Sözbilir, 2001).

#### 4.2.2. Late Burdigalian (Kale Formation)

The molluscan assemblage of the Kale formation represents a late Burdigalian age (Figure 2). The mollusc-bearing levels of three sections (Kale-Delibâğ, Kuleburnu and Alacain) contains the gastropods *Turritella turris* de Basterot, 1825, *Tenagodus* cf. *terebellus* Lamarck, 1818, *Conus* sp. and bivalves *Hyotissa hyotis* (Linnaeus, 1758), *Codakia* cf. *leonina* (de Basterot, 1825), *Ostrea lamellosa* Brocchi, 1814, *Venus (Antigona) burdigalensis producta* Schaffer, 1910 and *Pecten subarcuatus styriacus* Hilber, 1879 (Figure 2). The first occurrences of *Oligodia bicarinata* (Eichwald, 1830), *Phalium (Phalium) cypraeiformis* (Borson, 1820), *Melongena* cf. *cornuta* (Agassiz, 1843), *Pecten subarcuatus styriacus* Hilber, 1879, *Lutraria* cf. *sanna* de Basterot, 1825, *Pelecypora (Cordiopsis) islandicoides* (Lamarck, 1818) and *Ostrea lamellosa* Brocchi, 1814 have been reported from Burdigalian deposits (Figures 4-6). *Venus (Antigona) burdigalensis producta* Schaffer, 1910 and *Tenagodus* cf. *terebellus* Lamarck, 1818 are characteristic species for Burdigalian (Schultz and Piller, 2005). The stratigraphical range of *Hyotissa hyotis* is between Oligocene - Burdigalian. The absence of *Mesohalina margaritacea* (Brocchi, 1814), that became extinct during the mid-Burdigalian (Harzhauser et al., 2016) restricts the age of the association to late Burdigalian.

The ostracod species *Aurila soummamensis* Coutelle and Yassini, 1974, *Neonesidea corpulenta* (Mueller, 1894), *Xestoleberis glabrenses* (Reuss, 1850), *Hermanites* aff. *haidingeri minor* Ruggieri, 1962 support a Burdigalian age. The Kale-Delibâğ section was dated as Burdigalian by previous workers,

based mainly on the occurrence of the larger benthic foraminifer species *Miogypsina intermedia* Drooger (SBZ25 biozone) (Özcan et al. 2008).

## 5. Discussion

### 5.1. Correlation and Paleoenvironmental History of the Basin

Aquitanian and Late Burdigalian deposits of the Kale-Tavas molasse subbasin are extremely poor in molluscs, benthic foraminifers and coral fossils. Although it is not possible to observe the contact between Aquitanian and late Burdigalian, their fossil content show important faunal differences and facies changes. The correlation of the units is based on the analyses of lithology, paleoecology and biostratigraphy of measured stratigraphical sections, as presented above. Lateral facies relationships can only be observed in the sections within the same formation. The lowermost coarse detritic interval (grey colored, thick bedding, poorly sorted conglomerates) of the Aquitanian Yenidere formation overlies the terrestrial part of the late Rupelian - early Chattian Mortuma formation discordantly (Figures 9, 10). Shallow marine intervals are intercalated in the lower and middle parts of the Yenidere formation. However, the formation shows an overall regressive tendency, with increasing swamp deposits and thicker lignitic coal seams in the upper parts. The Yenidere formation is overlain by the terrestrial Künar formation that consists of cross-bedding conglomerates (fluvial sediments: Hakyemez, 1989). In previous works, an early Aquitanian age was proposed based on the ostracod and foraminifer fauna for the base of the early Miocene deposits in the Kale region (Gökçen, 1982). Considering the stratigraphical relationship between Yenidere and Kale formations, the age of the Künar formation should be considered as early Burdigalian.

The shallow marine - reefal facies of the Kale formation rests on the terrestrial units of the Mortuma formation (late Rupelian - early Chattian) with an angular discordancy. The mollusc assemblage of the Kale formation documents a late Burdigalian age and fully marine species representing tropic-subtropic conditions.

### 5.2. Early Miocene Paleobiogeography of the Region

The molluscan assemblages described here are quite similar to the early Miocene faunas of the area

of the Bay of Biscay through the Mediterranean basins to as far to the east as Central Iran (Harzhauser et al. 2002). During the early Miocene the closure time of the Tethian corridor took place, preventing further faunal exchanges between the western Indian - eastern African provinces and the eastern Mediterranean seaway between the Anatolian and Arabian/African plates (Rögl, 1998, 1999; Harzhauser et al., 2002).

In the Kale-Tavas molassic subbasin, *Melanopsis hantkeni*, *Granulolabium plicatum*, *Terebralia lignitarum*, *Mesohalina margaritacea* and *Mytilus (Crenomytilus) aquitanicus* are common species in the Aquitanian deposits, also abundantly occurring in the early Miocene sublittoral coastal mudflats and swamps in Greece, Iran and Turkey (Thrace, Denizli, Mut, Sivas basins). *Terebralia lignitarum*, *Pelecypora (Cordiopsis) islandicoides*, *Turritella turris*, *Oligodia bicarinata*, *Ostrea lamellosa*, *Crassostrea gryphoides*, *Codakia leonina* and *Pecten subarcuatus styriacus* are found in the upper Burdigalian deposits, but also reported from the western Taurids (*Antalya basin*: İslamoğlu, 2002; İslamoğlu and Taner, 2003a, b). *Turritella desmarestina*, *Venus (A.) burdigalensis producta*, *M. cornuta* are known from the upper Burdigalian settings (*Kasaba basin, W. Taurids*: İslamoğlu, 2004a,b; İslamoğlu and Taner, 2002; 2003a). *Crassostrea gryphoides* (Schlotheim, 1813) is a common species in the upper Burdigalian deposits of Kahramanmaraş (Hoşgör, 2008) and Antalya basins (İslamoğlu and Taner, 2003a). *V. burdigalensis producta*, found in the Kale formation, is characteristic species for Eggenburgian of the Central Paratethys (Hoernes, 1870; Schaffer, 1912; Papp, 1952; Schultz and Piller, 2001, 2003 and 2005). It was also reported from the upper Burdigalian units of the Kasaba basin (İslamoğlu and Taner, 2003a). *Terebralia bidentata*, *Mytilus (Crenomytilus) aquitanicus* and *Hyotissa hyotis* are reported from the late Burdigalian (Mut Basin: M.Taurids, S Turkey) (Atabey et al., 2000; Mandic et al., 2004).

### 5.3. Timing of Late Oligocene - Early Miocene Tectonics

The molasse sediments of SW Anatolia have been intensively studied, because of their importance for regional tectonics. It is suggested that these deposits developed during post-orogenic tectonic activities such as compression, extension and uplifting (Koçyiğit, 1984). The late Oligocene to early Miocene age is accepted either for a southeastward emplacement

of the Lycian nappes (Collins and Robertson, 1998, 2003; Akgün and Sözbilir, 2001) or for a NW-SE trending extensional collapse of the Lycian orogene (Seyitoğlu and Scott, 1996; Bozkurt, 2003), resulting in depositional sequences in the emerged areas and surrounding interconnected depressions of the Lycian orogene (Sözbilir, 2005). It was also suggested that the Acıpayam area is the youngest and non-folded piggy-back succession of the Lycian Nappes (Alçiçek and ten Veen, 2008).

Some previous works refer to a regional Aquitanian transgression in the foreland that left a marine sedimentary unit before the final emplacement of the Lycian Allochthon (Poisson, 1977; Şenel, 1997). However, we here demonstrate that the Aquitanian period is represented by rhythmic deposits with a regressive tendency, whereas the early Burdigalian is represented by thick coarse fluvial sedimentation and the late Burdigalian by transgressive sedimentation comprising mainly thick carbonates. Two stratigraphical gaps are demonstrated by the presence of unconformities between the Chattian - Aquitanian and Oligocene - late Burdigalian deposits. Thus, our findings support the idea that uplifting of the source area and subsidence of the basin affected the stratigraphical framework of the Kale-Tavas and Acıpayam subbasins (Sözbilir, 2005; Alçiçek and ten Veen, 2008).

## 6. Conclusions

Molluscan biostratigraphical data indicates that the Yenidere formation developed during the Aquitanian whereas the Kale formation is of late Burdigalian age. The Yenidere formation consists of brackish – lagoonal, and sometimes terrestrial facies such as swamps, coal-bearing detritics as well as very shallow marine incursions. The represented mollusc faunas can be correlated with coeval Aquitanian and late Burdigalian assemblages in the Mediterranean- Iranian province. The presence of angular disconformities could be determined between the Oligocene (late Rupelian - early Chattian) units (Mortuma formation), the Aquitanian (Yenidere formation) and between Oligocene - late Burdigalian (Kale formation) units. The stratigraphical relationship between Aquitanian and late Burdigalian units were not observed. These findings help the understanding of timing of Oligo-Miocene tectonic pulses in the basin, which probably occurred at the end of the Oligocene and in the latest Aquitanian – earliest Burdigalian. Mollusc faunas

lack Indo-Pacific species. Therefore during early Miocene times, the region was part of the Eastern Mediterranean-Iranian province.

### Acknowledgements

This study was carried out within the scope of MTA (General Directorate of Mineral Research and Exploration) project with the number of 2002-16 B45 in 2002. Mollusc specimens were studied in the Naturhistorisches Museum, Vienna (NHMW) thanks to E.U. Synthesis Foundation grant (AT-TAF-356). Special thanks go to Mathias Harzhauser (Director of the Paleontology-Geology Department, NHMW), who provided technical and laboratory facilities in 2005. Many thanks to Alice Schumacher of the same institute, for taking the photographs of the fossils. Many thanks to colleagues of MTA for their support during the field work (Neşat Konak and Hulusi Sarıkaya) and for fossil identifications (Fatma Gedik: benthic foraminifers; ostracods Gönül Atay, Sedef Babayiğit: scleractinian corals). The author thanks Frank P. Wesselingh, Arie W. Janssen (Naturalis Biodiversity Center, Leiden, the Netherlands), M. Cihat Alçiçek (Pamukkale University) and also two anonymous reviewers for their helpful critics on the manuscript.

### References

- Akgün, F., Sözbilir, H. 2001. A palynostratigraphic approach to the SW Anatolian molasse basin: Kale-Tavas molasse and Denizli molasse. *Geodynamica Acta* 14(1-3), 71-93.
- Alçiçek, M.C., ten Veen, J.H. 2008. The late Early Miocene Acıpayam piggy-back basin: Refining the last stages of Lycian nappe emplacement in SW Turkey. *Sedimentary Geology* 208, 101-113.
- Altınlı, E. 1955. The Geology of southern Denizli, *Rev. Fac. Sci, Univ. İstanbul Ser. B20* (1-2), 1-47.
- Atabey, E., Atabey, N., Hakyemez, A., İslamoğlu, Y., Sözeri, Ş., Özçelik, N., Saraç, G., Ünay, E., Babayiğit, S., 2000. Mut ve Karaman arasındaki Miyosen havzalarının litostratigrafisi ve sedimentolojisi (Orta Toroslar, G. Türkiye), *Maden ve Tetkik Arama Dergisi* 122, 53-72.
- Báldi, T. 1973. Mollusc fauna of Hungarian upper Oligocene (Egerian). *Akadémiai Kiado, Budapest*, p 511
- Barthelt, D. 1989. Faziesanalyse und Untersuchungen der Sedimentationsmechanismen in der Unteren Brackwasser Molasse Oberbayerns. *Münchner Geowissenschaftliche Abhandlungen A17*: 1-118.
- Becker - Platen, J. D. 1970. Lithostratigraphische Untersuchungen in Kanozoikum südwest-Anatoliens (Kanozoikum und Braunkohlen der Türkei). *Beihefte zum Geologischen Jahrbuch* 97, 1-244.
- Benda, L., Meulenkamp, J.E. 1990. Biostratigraphic correlations in the Eastern Mediterranean Neogene 9. sporomorph associations and event stratigraphy of the Eastern Mediterranean Neogene, *Newsl. Stratigr.* 23 (1), 1-10.
- Bozkurt, E. 2003. Origin of NE-trending basins in western Turkey, *Geodynamica Acta*, 16, 61-81.
- Cahuzac, B., Poignant, A. 1997. Essai de biozonation de l'Oligo-Miocène dans les bassins européens à l'aide des grands foraminifères néotiques. *Bulletin de la Société Géologique de France* 168, 155-169.
- Collins, AS., Robertson, AHF. 1998. Process of late Miocene episodic thrust-sheet translation in the Lycian Taurides, SW Turkey. *Journal of the Geological Society London* 155, 759-772.
- Collins, AS., Robertson, AHF. 2003. Kinematic evidence for late Mesozoic-Miocene emplacement of the Lycian Allochthon over the Western Anatolide belt, SW Turkey. *Geological Journal* 38, 295-310
- Gökçen, N. 1982. Denizli -Muğla çevresi Neojen istifinin stratigrafisi ve paleontolojisi, Doçentlik tezi, Hacettepe Üniversitesi, 154 s. 8 Levha, 2 Ek, Ankara (unpublished).
- Gradstein F. M., Ogg J. G., Smith A. G. 2004. *A Geologic Time Scale 2004*. Cambridge University Press, Cambridge, 589p.
- Hakyemez, Y. 1989. Kale-Kurbağalık (GB Denizli) bölgesindeki Senozoyik yaşlı çökel kayaların jeolojisi ve stratigrafisi [Stratigraphy and geology of Cainozoic sedimentary rocks in the Kale-Kurbağalık (SW Denizli)]. *Maden Tetkik ve Arama Dergisi* 109, 9-21.
- Harzhauser, M. 2004. Oligocene gastropod faunas of the eastern Mediterranean (Mesohellenic Trough/Greece and Esfahan- Sirjan Basin/central Iran). *Courier Forschungsinstitut Senckenberg* 248, 93-181.
- Harzhauser, M., Mandic, O. 2001. Late Oligocene gastropods and bivalves from the Lower and Upper Austrian Molasse Basin, in Piller W. E. and Rasser M. W. (eds), *Paleogene of the Eastern Alps*. Österreichische Akademie der Wissenschaften Schriftenreihe der Erdwissenschaftlichen Kommissionen, Band 14, Verlag der Österreichischen Akademie der Wissenschaften, Vienna 671-795.

- Harzhauser, M., Piller, W. E., Steininger F. F. 2002. Circum - Mediterranean Oligo - Miocene biogeographic evolution – the gastropods' point of view. *Palaeogeography, Palaeoclimatology, Palaeoecology* 183: 103-133.
- Harzhauser, M., Mandic, O., Zuschin, M. 2003. Changes in Paratethyan marine molluscs at the Early/Middle Miocene transition: diversity, palaeogeography and palaeoclimate. *Acta Geologica Polonica* 53/4: 323-339.
- Harzhauser, M., Mandic, O., Büyükmeriç, Y., Neubauer, T. A., Kadolsky, D., Landau, B. M. 2016. A Rupelian mangrove swamp mollusc fauna from the Thrace Basin in Turkey, *Archiv für Molluskenkunde* 145/1: 23-28.
- Hoernes M. 1870. Die fossilen Mollusken des Tertiären Becken von Wien, II, Bivalven. *Abhandlungen der kaiserlich - königlichen geologischen Reichsanstalt* 4, 1-479.
- Hoşgör, İ. 2008. Presence of *Crassostrea gryphoides* (Schlotheim) from the lower- middle Miocene sequence of Kahramanmaraş basin (SE Turkey); Its taxonomy, paleoecology and paleogeography. *Mineral Research and Exploration Bulletin* 136, 17-28.
- İslamoğlu, Y. 2002. Antalya Miyosen havzasının mollusk faunası ile stratigrafisi [The molluscan fauna and stratigraphy of Antalya Miocene basin (westerncentral Taurids, SW Turkey)] *Bulletin of Mineral Research and Exploration* 123/124, 27-58.
- İslamoğlu, Y. 2004a. Kasaba Miyosen havzasının *Bivalvia* ve *Scaphopoda* faunası (Batı Toroslar, GB. Türkiye) [*Bivalvia* and *Scaphopoda* fauna of Kasaba Miocene basin (Western Taurids, SW Turkey)]. *Bulletin of Mineral Research and Exploration* 129: 29-55.
- İslamoğlu, Y. 2004b. Kasaba Miyosen havzasının *Gastropoda* faunası (Batı Toroslar, GB. Türkiye), *Bulletin of Mineral Research and Exploration* 128, 137-170.
- İslamoğlu, Y. 2008. Molluscan biostratigraphy and paleoenvironmental reconstruction of Oligocene deposits in the Denizli and Kale-Tavas subbasins (SW Turkey). *Geodiversitas* 30 (2), 261-85.
- İslamoğlu, Y., Taner G. 2002. Kasaba Miyosen havzasında *Ucarsu* ve *Kasaba* Formasyonlarının mollusk faunası ve stratigrafisi [Mollusc content and stratigraphy of the *Ucarsu* and *Kasaba* formations in Kasaba Miocene basin]. *Bulletin of Mineral Research and Exploration* 125, 31-57.
- İslamoğlu, Y., Taner, G. 2003. Antalya Miyosen havzasının *Bivalvia* faunası (Batı- Orta Toroslar, GB. Türkiye), *Bulletin of Mineral Research and Exploration* 127, 1- 27.
- İslamoğlu, Y., Taner, G. 2003. Antalya Miyosen havzasının *Gastropoda* faunası (Batı- Orta Toroslar, GB. Türkiye), *Bulletin of Mineral Research and Exploration* 127, 29- 65.
- İslamoğlu, Y., Taner G. 2004. Antalya Miyosen havzasının *Gastropoda* faunası (Batı-Orta Toroslar, GB. Türkiye) [*Gastropoda* fauna of Antalya Miocene basin (Western Taurids, SW Turkey)]. *Bulletin of Mineral Research and Exploration* 127, 29- 65.
- İslamoğlu, Y., Gedik, F. 2005. Biostratigraphy of the Oligocene deposits of the Denizli basin based on mollusc and benthic foraminifer fauna (SW Turkey), 12<sup>th</sup> Congress R.C.M.N.S. – 6- 11 September, Vienna, Patterns and Process in the Neogene of the Mediterranean Region, Department of Paleontology /University of Vienna, Natural History Museum Vienna, Austria, Abstracts, 109-110.
- İslamoğlu, Y., Atay, G., Gedik, F., Aydın, A., Hakyemez, A., Babayiğit, S., Sarıkaya, H. 2005. Batı Toroslardaki denizel Oligosen - Miyosen biyostratigrafisi (Denizli). *Mineral Research and Exploration report*, No: 10763, 155 pp., Ankara (unpublished).
- İslamoğlu, Y., Gedik, F., Aydın, A., Atay, G., Hakyemez, A., Babayiğit, S. 2006. Foraminifera, Nannoplankton, Coral and Ostrocooda Biostratigraphy of the Oligocene Lagoonal and Marine Deposits in Denizli Region (SW Turkey), 59. Geological Congress of Turkey, March 20-24.2006, The Chamber of Geological Engineers, Congress Center of General Directorate of Mineral Research and Exploration, 245-249, Ankara.
- İslamoğlu, Y., Gedik, F., Çulha, G. 2007. Mollusc, benthic foraminifer and ostracod faunas of the early Miocene deposits in Denizli region and biostratigraphic pre-results (SW Anatolia, Turkey). 16th International Petroleum and Natural Gas Congress and Exhibition of Turkey, 29-31 May 2007, Ankara, 91-93.
- İslamoğlu, Y. Harzhauser, M., Gross, M., Jiménez-Moreno, G., Coric, S., Kroh, A., Rögl, F., Made, J.V.D. 2008. From Tethys to Eastern Paratethys: Oligocene depositional environments, paleoecology and paleobiogeography of the Thrace Basin (NW Turkey). *International Journal of Earth Sciences (IJES)* 99: 183-200.
- İslamoğlu, Y., Hakyemez, A. 2010. Oligocene history of the Çardak – Dazkırı subbasin (Denizli, SW Turkey): Integrated molluscan and planktonic foraminiferal biostratigraphy. *Turkish Journal of Earth Science* 19, 473-496.

- Koçyiğit, A. 1984. Intra plate tectonic development in southwestern Turkey and adjacent areas. Bulletin of the Geological Society of Turkey 27 (1), 1-16.
- Konak, N., Akdeniz, Çakır, M.H. 1986. Çal-Çivril-Karahallı dolayının jeolojisi. Mineral Research and Exploration report, No: 8945, 122 pp., Ankara (unpublished).
- Landau, B.M., Harzhauser, M., İslamoğlu, Y., da Silva, C. M. 2013. Systematics and palaeobiogeography of the gastropods of the middle Miocene (Serravalian) Karaman basin, Turkey, Cretaceous Research, 11-13, 584 pp., 82 plates.
- Lozouet, P., Lesport, J., Renard, P. 2001. Révision des Gastropoda (Mollusca) du stratotype de l'Aquitainien (Miocène inférieur): site de Saucats 'Larey', Gironde, France. Cossmanniana hors série 3: 1-189.
- Mandic O., Harzhauser M., Schlaf J., Piller W. E., Schuster F., Wielandt-Schuster U., Nebelsick J. H., Kroh A., Rögl F., Bassant P. 2004. Palaeoenvironmental reconstruction of an epicontinental flooding-Burdigalian (early Miocene) of the Mut Basin (southern Turkey). Courier Forschungsinstitut Senckenberg 248, 57-92.
- Meulenkamp, J.E., Sissingh, W. 2003. Tertiary palaeogeography and tectonostratigraphic evolution of the Northern and Southern Peri-Tethys platforms and the intermediate domains of the African-Eurasian convergent plate boundary zone. Palaeogeography, Palaeoclimatology, Palaeoecology 196, 209-228
- Meulenkamp, J.E., Sissingh, W., Londeix, L., Cahuzac, B., Calvo, J.P., Daams, R., Studencka, B., Kovac, M., Nagymarosy, A., Rusu, A., Badescu, D., Popov, S.V., Scherba, I.G., Roger, J., Platel, J.P., Hirsch, F., Sadek, A., Abdel-Gawad, G.I., Yaich, C., Ben Ismail-Lattrache, K., Bouaziz, S. 2000. Late Rupelian (32-29 Ma). In: Dercourt, J., Gaetani, M., Vrielynck, B., Barrier, E., Bijou-Duval, B., Brunet, M.F., Cadet, J.P., Crasquin, S. and Sandulescu, M. (eds), Peri-Tethys Atlas, Paleogeographic Maps with an Explanatory Notes, Paris, 171-178.
- Nebert, K. 1956. Denizli – Acıgöl mevkiinin jeolojisi. Maden ve Tetkik Arama Raporu, No: 2509, 225 s, Ankara (unpublished).
- Nebert, K. 1961. Tavas-Kale (Güneybatı Anadolu) bölgesine ait yeni müşahadelere [New findings belonging Tavas-Kale area (southwest Anatolia)]. Maden Tetkik ve Arama Dergisi 57, 57-64 .
- Neubauer, T.A., Harzhauser, M., Kroh, A. 2013. Phenotypic evolution in a fossil gastropod species lineage: evidence for adaptive radiation?. Palaeogeography, Palaeoclimatology, Palaeoecology, 370, 117-126.
- Neubauer, T.A., Harzhauser, M., Mandic, O., Georgopoulou, E., Kroh, A. 2016. Paleobiography and historical biogeography of the non-marine caenogastropod family Melanopsidae. Palaeogeography, Palaeoclimatology, Palaeoecology 444, 124-143.
- Özcan, E., Less, G., Bıldı-Beke, M., Kollányi, K., Acar, F. 2008. Oligo-Miocene foraminiferal record (Miogypsinidae, Lepidocyclinidae and Nummulitidae) from the Western Taurides (SW Turkey): Biometry and implications for the regional geology. Journal of Asian Earth Sciences 34, 740-760.
- Papp A. 1952. Über die Verbreitung und Entwicklung von Clithon (Vittoclythion) pictus (Neritidae) und einige Arten der Gattung Pirenella (Cerithidae) im Miozän Österreichs. Sitzungsberichte der österreichischen Akademie der Wissenschaften, mathematisch-naturwissenschaftliche Klasse, abteilung 1 (2/3), 103-127.
- Poisson, A. 1977. Recherches géologiques dans les Taurides occidentales. These Doct d'Etat, Orsay, no: 1902, 795p.
- Rögl, F. 1996. Stratigraphic correlation of the Paratethys Oligocene and Miocene. Mitteilungen der Geologischen Bergbaustud Österreichischen 41, 65-73.
- Rögl, F. 1998. Paleogeographic considerations for Mediterranean and Paratethys seaways (Oligocene to Miocene), Ann. Naturhist. Mus. Wien. 99A, 279-310.
- Rögl, F. 1999. Mediterranean and Paratethys. Facts and hypotheses of an Oligocene to Miocene paleogeography (short overview). Geologica Carpathica. 50, 339-349.
- Rögl F., Zapfe H., Bernor R. L., Brzobohaty L., Daxner-Höck G., Draxler I., Fejfar O., Gaudant J., Hermann P., Rabeder G., Schultz O., Zetter R. 1993. Die Primatenfundstelle Gotzendorf an der Leitha (Obermiozän des Wiener Beckens Niederösterreich). Jahrbuch der Geologischen Bundesanstalt Wien 136, 503-526.
- Schaffer F.X. 1912. Das Miozän von Eggenburg. Die Fauna der ersten Mediterranstufe des Wiener Beckens und die geologischen Verhältnisse der Umgebung des Manhartsberges in Niederösterreich. Die Gastropoden der Miozänbildungen von Eggenburg. Jahrbuch der Kaiserlich-Königlichen Geologischen Reichsanstalt 22, 127-193.
- Schultz, O., Piller, W. 2001. Bivalvia Neogenica

- (Nuculacea - Unionacea), *Catalogus Fossilium Austriae*, Ein systematisches Verzeichnis aller auf österreichischem Gebiet festgestellten Fossilien, Band 1/Teil 1, 1-379, 56 pls, Verlag der Österreichischen Akademie der Wissenschaften, Wien.
- Schultz, O., Piller, W. 2003. Bivalvia Neogenica (Lucinoidea - Mactroidea), *Catalogus Fossilium Austriae*, Ein systematisches Verzeichnis aller auf österreichischem Gebiet festgestellten Fossilien, Band 1/Teil 2, 380-690 pp, 39 pls, Verlag der Österreichischen Akademie der Wissenschaften, Wien.
- Schultz, O., Piller, W. 2005. Bivalvia Neogenica (Solenioidea - Clavelloidea), *Catalogus Fossilium Austriae*, Ein systematisches Verzeichnis aller auf österreichischem Gebiet festgestellten Fossilien, Band 1/Teil 3, 691-1212, 57 pls, Verlag der Österreichischen Akademie der Wissenschaften, Wien.
- Seyitoğlu, G., Scott, B. 1991. Late Cenozoic crustal extension and basin formation in west Turkey. *Geological Magazine* 128 (2), 155-166.
- Seyitoğlu, G., Scott, B. 1996. The cause of N-S-extensional tectonics in Western Turkey: Tectonic escape vs. back-arc spreading vs orogenic collapse, *J. Geodyn.* 22, 145-153.
- Sözbilir, H. 2005. Oligo-Miocene extension in the Lycian orogen: evidence from the Lycian molasse basin, SW Turkey. *Geodinamica Acta* 18, 255-282.
- Şenel, M. 1997. 1:100.000 ölçekli Türkiye Jeoloji Haritaları, Denizli J-9 paftası Maden Tetkik ve Arama Genel Müdürlüğü, Yayınları No:16, Ankara, 18 s.
- Şengör, A.M.C., Yılmaz, Y. 1981. Tethyan evolution of Turkey: A plate tectonic approach. *Tectonophysics* 75, 181-241.
- Steininger F.F. 1999. Chronostratigraphy, geochronology and biochronology of the "European Land Mammal Mega-Zones" (ELMMZ) and the Miocene "Mammal-Zones" (MN-Zones), in Rössner G. E. and Heissig K. (eds), *The Miocene Land Mammals of Europe*, Verlag Dr. Friedrich Pfeil, München: 9-24.
- Westaway, R. 2006. Cenozoic cooling histories in the Menderes Massif, western Turkey may be caused by erosion and flatsubduction, not low-angle normal faulting. *Tectonophysics* 412, 1-25.
- Westaway, R., Guillou, H., Yurtmen, S., Demir, T., Scallet, S., Rowbotham, M. G. 2005. Constraints on the timing and regional conditions at the start of the present phase of crustal extension in western Turkey, from observations in and around the Denizli region, *Geodinamica Acta* 18, 209-238.

## PLATES

**Plate 1**

Figure 1a-b. *Granulolabium plicatum* (Bruguière, 1792), BEUN-2016-DM001

Figure 2a-b. *Terebralia lignitarum* (Eichwald, 1830), BEUN-2016-DM002

Figure 3. *Melanopsis hantkeni* Hofmann, 1870, BEUN-2016-DM003

Figure 4. *Oligodia bicarinata* (Eichwald, 1830), BEUN-2016-DM004

Figure 5a-b. *Turritella turris* de Basterot, 1825, BEUN-2016-DM005

Figure 6. *Turritella turris* de Basterot , 1825, BEUN-2016-DM006

Figure 7a-b. *Tinnyea lauraea* (Mathéron, 1842), BEUN-2016-DM007

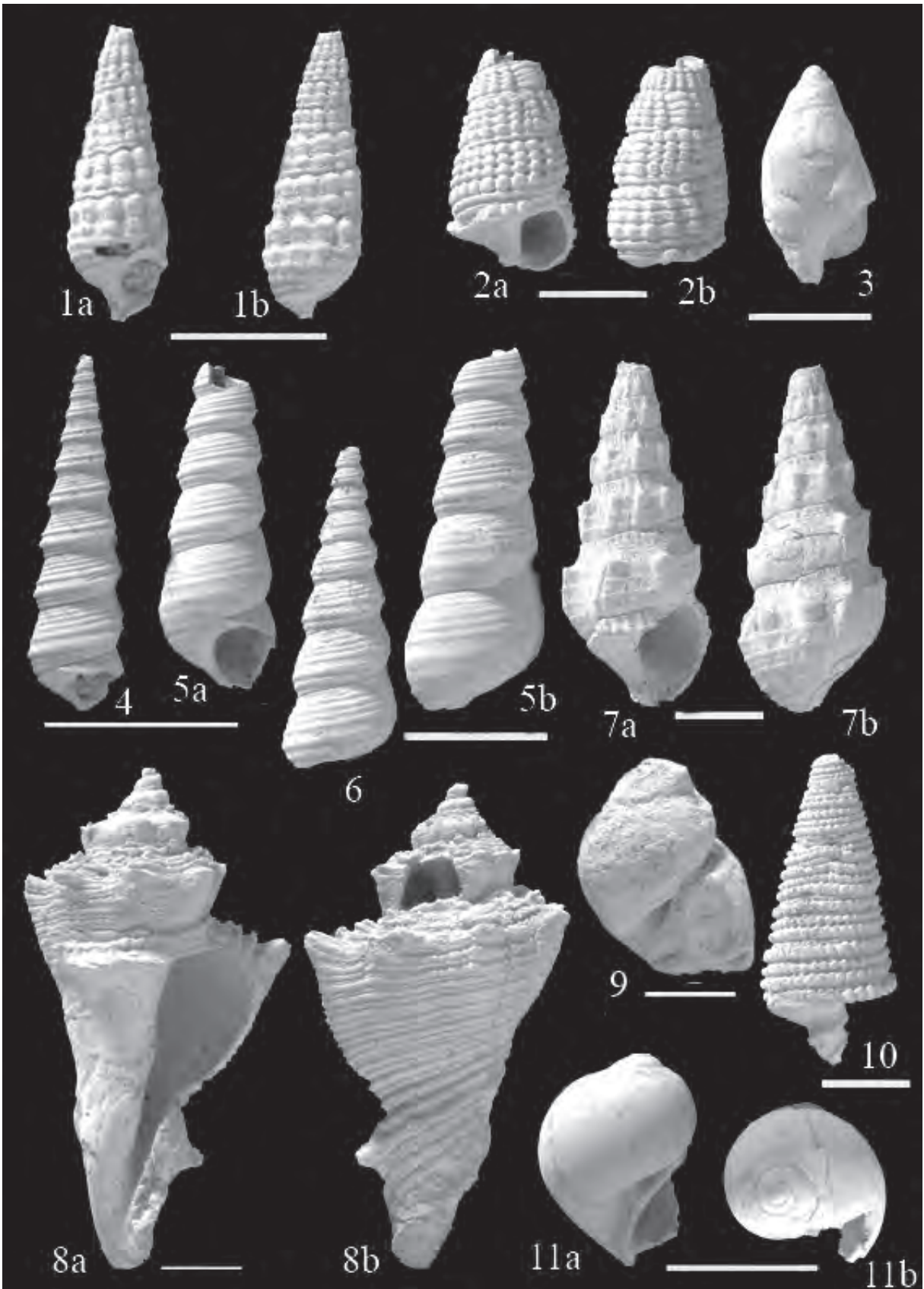
Figure . 8a-b. *Melongena lainei* (de Basterot, 1825), BEUN-2016-DM008

Figure 9. *Crommium* sp. BEUN-2016-DM027

Figure 10. *Mesohalina margaritacea* (Brocchi, 1814), BEUN-2016-DM009

Figure 11a-b. *Euspira helicina helicina* (Brocchi, 1814), BEUN-2016-DM010

scale bar is 1cm



**Plate 2**

Figure 1a-b. *Melongena lainei* (de de Basterot, 1825), BEUN-2016-DM011

Figure 2. *Melongena* cf. *cornuta* (Agassiz, 1843), BEUN-2016-DM012

Figure 3. *Modulus* sp., BEUN-2016-DM013,

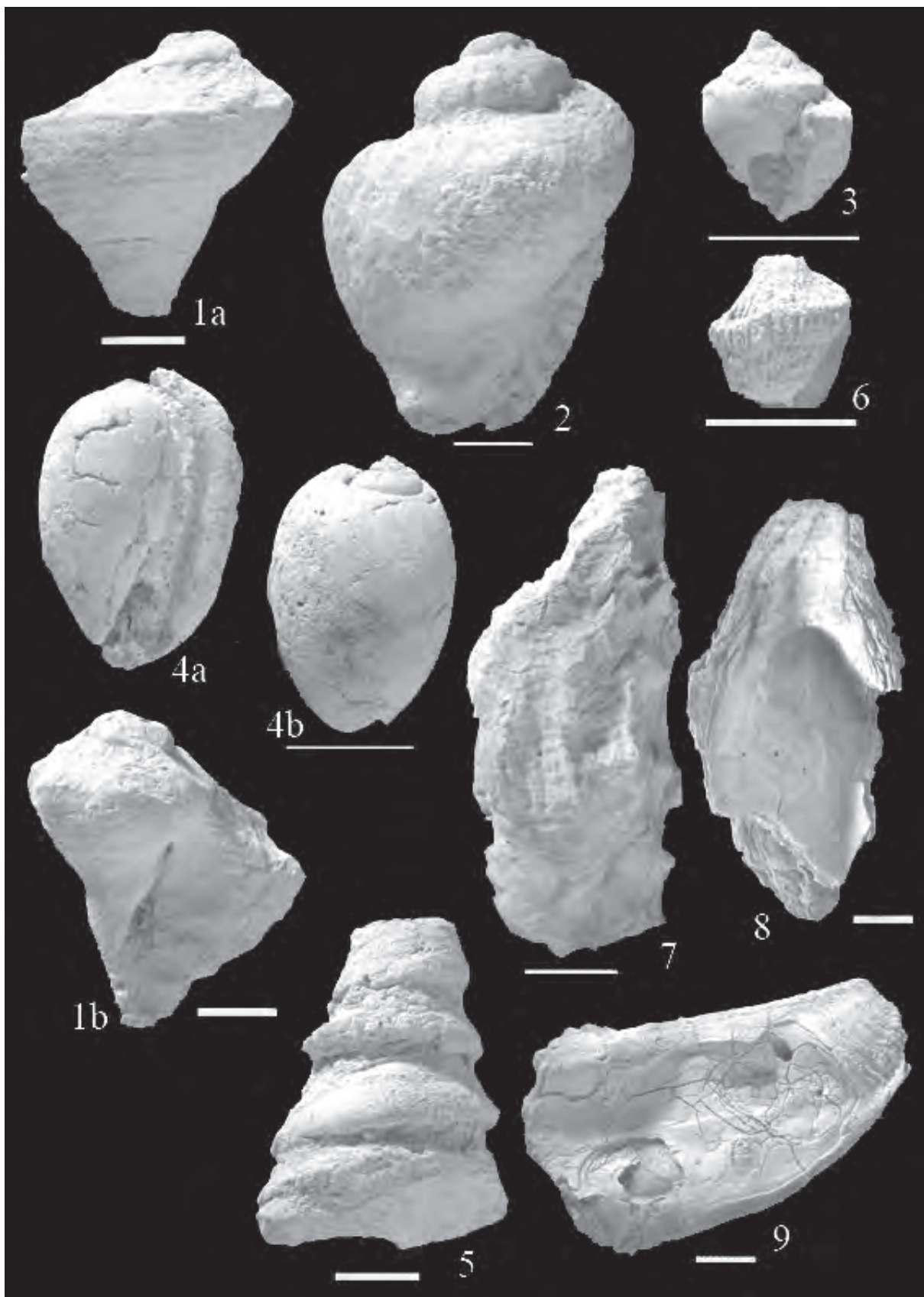
Figure 4a-b. *Phalium* (*Phalium*) *cypraeiformis* (Borson, 1820), BEUN-2016-DM014

Figure 5. *Turritella* (*Peyrotia*) *desmarestina* de Basterot, 1825, BEUN-2016-DM015

Figure 6. *Creussia miocaenica* Prochazka, 1893 (balanid species), dorsal view, BEUN-2016-DM016

Figure 7-8-9. *Crassostrea gryphoides* (Schlotheim, 1813), BEUN-2016-DM017

scale bar is 1cm



**Plate 3.**

Figure 1a-b. *Ostrea lamellosa* Brocchi, 1814, BEUN-2016-DM018

Figure 2a-b. *Hyotissa hyotis* (Linnaeus, 1758), BEUN-2016-DM019

Figure 3a-b. *Codakia* cf. *leonina* (de Basterot, 1825), BEUN-2016-DM020

Figure 4. *Lutraria* cf. *sanna* de Bastetot, 1825, BEUN-2016-DM021

Figure 5. *Pelecypora* (*Cordiopsis*) *islandicoides* (Lamarck, 1818), BEUN-2016-DM022

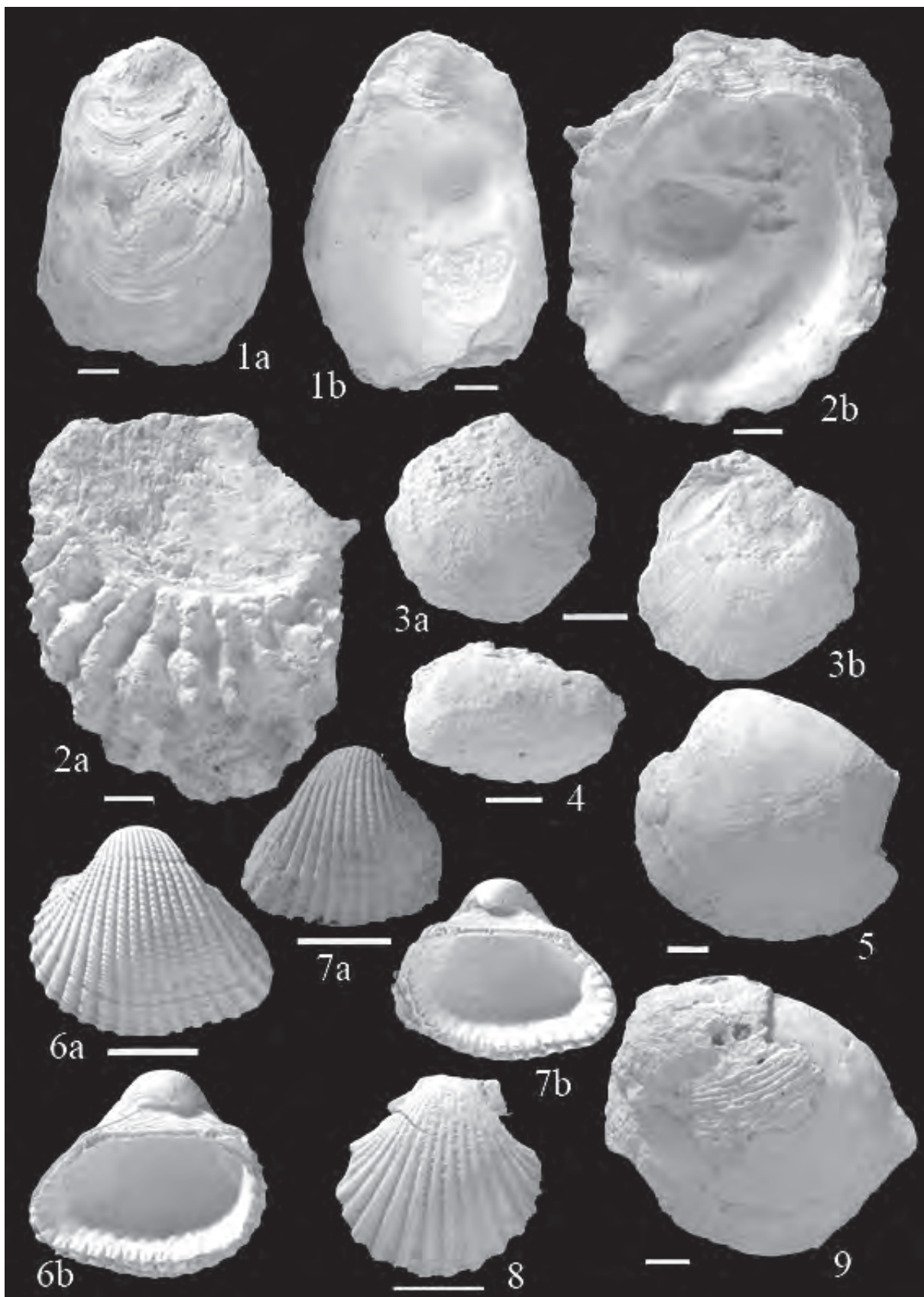
Figure 6a-b. *Anadara cardiiformis* (de Basterot, 1825), BEUN-2016-DM023

Figure 7a-b. *Anadara cardiiformis* (de Basterot, 1825), BEUN-2016-DM024

Figure 8. *Pecten subarcuatus styriacus* Hilber, 1879, BEUN-2016-DM025

Figure 9. *Venus* (*Antigona*) *burdigalensis producta* Schaffer, 1910, BEUN-2016-DM026

scale bar is 1cm







# Bulletin of the Mineral Research and Exploration

<http://bulletin.mta.gov.tr>



## MOLLUSCAN ASSEMBLAGE AND PALEOECOLOGY OF LOWER MIOCENE SEQUENCES OF MUNZUR MOUNTAINS (EASTERN ANATOLIA, TURKEY)

Müjde GÜRİSOY\*

\*General Directorate of Mineral Research and Exploration, Şehit Cuma Dağ Natural History Museum, 06800 Ankara.  
orcid.org 0000-0002-6320-2000

Research Article

### Keywords:

Bivalvia, Gastropoda,  
Paleoecological Diversity,  
Lower Miocene, Tunceli.

### ABSTRACT

The research subject is the Miocene aged units that located in the Munzur Mountains at the Ovacık district of the Tunceli province. There is a continuous sediment deposits from Paleozoic to Cenozoic at the Munzur Mountains. The neritic limestones of the Miocene Başpınar formation outcropping in the Ovacık district are rich in fossil groups of gastropods and bivalves. In this study, 336 samples from the Başpınar formation have been evaluated. Seven species of Gastropoda (*Globularia carlei*, *Granulolabium plicatum*, *Granulolabium (Tiaracerithium) thiarella*, *Tympanotonus margaritaceus*, *Terebralia subcorrugata*, *Nassarius erunala*, *Cerithium vulgatum*,) and four species of Bivalvia (*Cardita rusticana*, *Anadara aquitanica*, *Cubitostrea digitalina*, *Ostrea lamellosa*) were identified. One more species of Bivalvia was identified by using open nomenclature (*Chlamys* sp.). The studied fossil assemblage of the Başpınar formation indicates a lower Miocene age. Furthermore, for the first time in this study, paleoecological species diversity is calculated by using the Simpson, Shannon-Weaver, Epilou and Margalef indices for the locations where the fossils were collected. Numerical results are obtained by comparing bivalves and gastropods. According to these results, the Gastropoda specimens shows higher dominance (Simpson index  $D = 0,82$ ), higher species diversity (Shannon-Weaver index  $H = 2,53$ ) and higher species richness (Margalef index  $M = 1,23$ ) when correlated with Bivalvia specimens. The Epilou index value ( $Ep = 0,9$ ) gives the result that the species numbers in the gastropods are approximately equal to each other.

Received Date: 17.08.2016

Accepted Date: 17.05.2017

## 1. Introduction

The study area is located 20 km northeast of Ovacık district of Tunceli province (Figure 1). Munzur Mountains which are located at the northeastern end of the Taurus belt, are associated with both the Pontids and the Taurids (Özer, 1994). The oldest units in the study area are Permian and the youngest units are Miocene aged. The gastropod and bivalve fossils found in Miocene sediments in the region, provide important insights for the Miocene paleogeography, biostratigraphy and paleoecology.

Since 1940's Munzur Mountains have been the subject of many studies about the determination of its geological features, geological mapping (Ketin, 1945; Baykal, 1953; Nebert, 1955 and 1959); petroleum exploration (Kurtman, 1961); the determination of coal

potentials (Ağralı, 1967; Kurdoğlu, 1976); geological, tectonical and stratigraphical researchs (Özgül et al., 1981; Tüysüz, 1993; Özer, 1994). Nevertheless, no detailed studies were conducted about the bivalves and gastropods. With this study, detailed systematic studies and paleoecologic diversity applications have been made. The aim of this compilation and application study, is to put forward the systematics of the mollusk fossils and to make paleoecological species diversity (Simpson, Shannon-Wiener, Epilou and Margalef Indices).

## 2. Material and Method

The materials examined in this study are the samples from the archives of the Directorate of MTA Natural History Museum (MTA project number: 8034 and inventory numbers: 80/175, 80/176, 80/177,

\* Corresponding author: Müjde GÜRİSOY [mujde.gursoy@gmail.com](mailto:mujde.gursoy@gmail.com)  
<http://dx.doi.org/10.19111/bulletinofmre.334249>

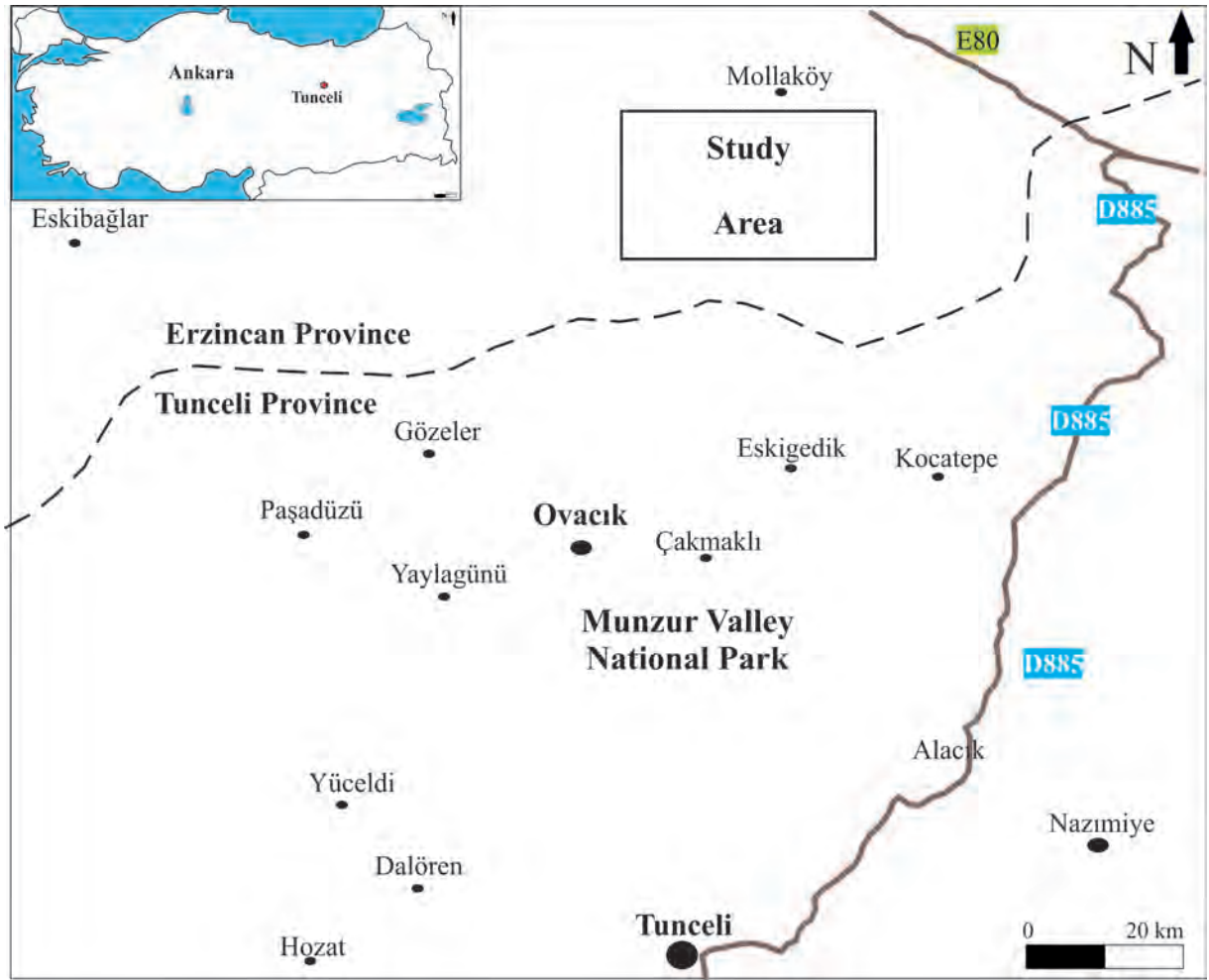


Figure 1- Location map of the study area.

80/178, 80/179, 80/180, 80/181, 80/182, 80/183, 80/184) which were collected for the project titled “Sedimentology and Biostratigraphy of the Lignite Bearing Lower Miocene Sediments from Munzur Mountains” carried out by Karabıyıköğlü and Örcen (1986). A total of 336 samples are redescribed. Systematic determinations are made according to Moore (1964-1969) and Wenz (1938-1943).

For the characterization of these archive samples, Alpha ( $\alpha$ ) Species Diversity Quantitative Indexes (Simpson-D, Shannon-Wiener-H, Margalef-M ve Pielou-Ep) have been used. From these indices, Alpha ( $\alpha$ ) Diversity is used to calculate the quantitative variability of the environment (Whittaker, 1972). The total number of individuals for the identified species are counted, the required calculations were made with the formulas and a table of species diversity was created for the restricted location.

### 3. Regional Geology and Stratigraphy

Samples that constitute the subject of this work were taken from the area located 20 km to the northeast of Ovacık district of Tunceli province which is located at the 1: 25.000 scaled geological map Erzincan I42c3 (Figure 2).

According to the stratigraphical and the structural relationships, the rock units of the region can be separated into three different groups; these are “Munzur Limestone Units”, “Ovacık Units” and Tertiary “Post-Tectonic Units” (Figure 3) (Özgül et al., 1981).

Munzur Mountains are characterized by a sequence of Mesozoic limestones, late Cretaceous ophiolitic melange and early Miocene conglomerate, mudstone, marl, limestone and lignite interbeds. Locally, Quaternary sediments cover these units (Karabıyıköğlü and Örcen, 1986).

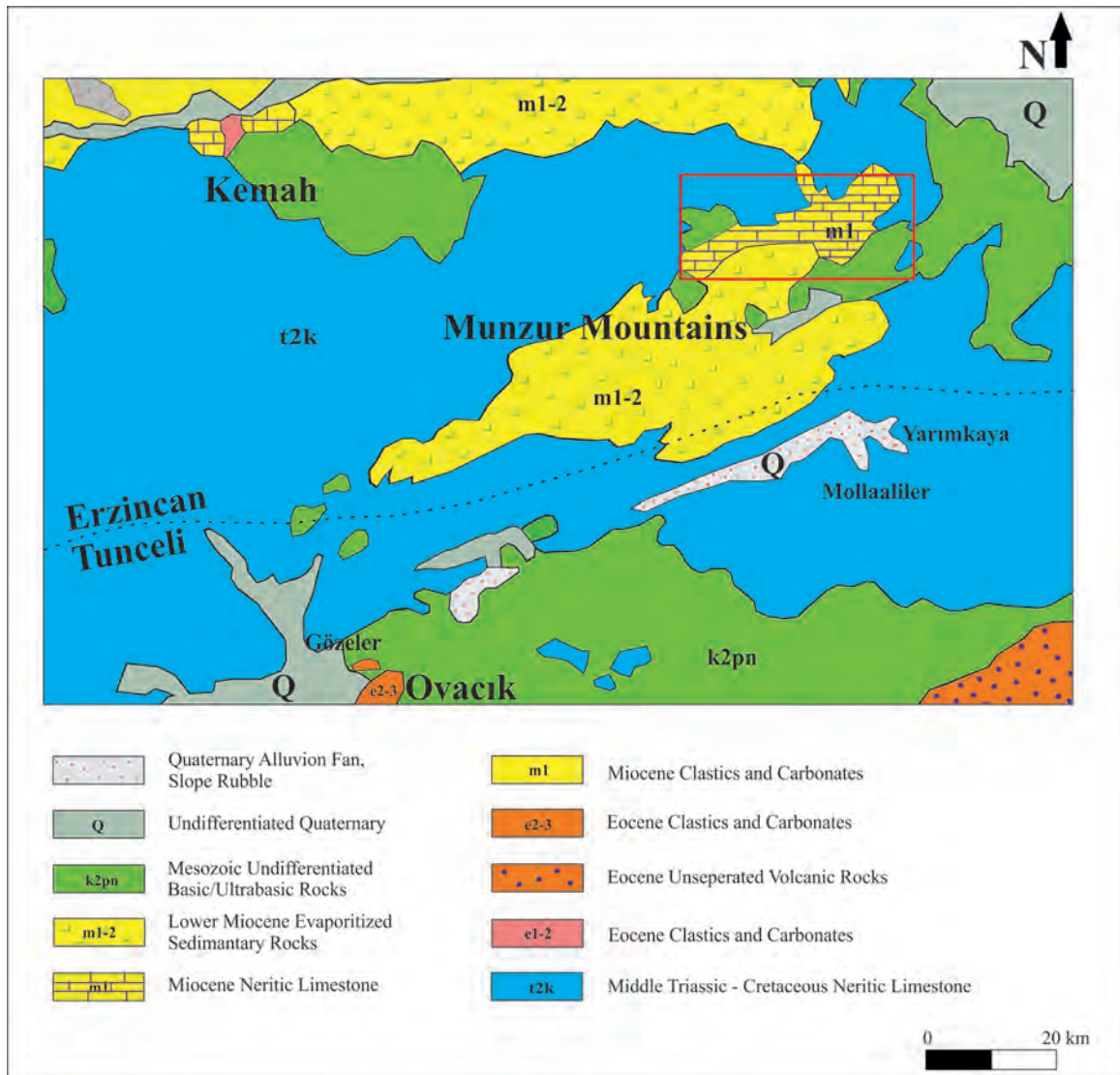


Figure 2- Geological map of the Munzur mountains (adapted from the Tarhan, 2008)

Mesozoic limestones are the most common units seen in the region. These units, defined as the “Munzur Limestone Units”, represent a large part of the Mesozoic (Upper Triassic - Upper Cretaceous) (Özgül, 1981). The unit with algal and reefal limestone facies is generally deposited on a shallow carbonate platform. At the last stages of sedimentation, the carbonate platform was replaced by deep sea sedimentation (Karabıyıköğlü and Örcen, 1986).

The Upper Cretaceous Ophiolitic Melange overlies the Munzur limestones resting over a tectonic contact. This unit defined within the scope of the “Ovacık Group”, is called the Eriç Ophiolitic Complex and consists of various sizes of neritic and pelagic limestone blocks and ophiolites. (Özgül, 1981).

The Early Miocene “Başpinar formation” includes clastics, fossiliferous limestones and volcanic rocks. This unit begins with a conglomerate that contains pebbles and blocks of the basement rocks and overlies the Eocene rock units with an angular unconformity. On the other hand, it is locally overlain by Quaternary sediments. The limestone layers of the formation are quite rich in fossils. The beds contain micro and macro fossils of benthic organisms such as bivalves, gastropods, echinids and corals. The determination of the age of the formation was based on the Burdigalian fossil assemblages (Özgül et al., 1981).

Karabıyıköğlü and Örcen (1986) stated that the sediments defined within the scope of the “Başpinar formation” are characterized by conglomerates,

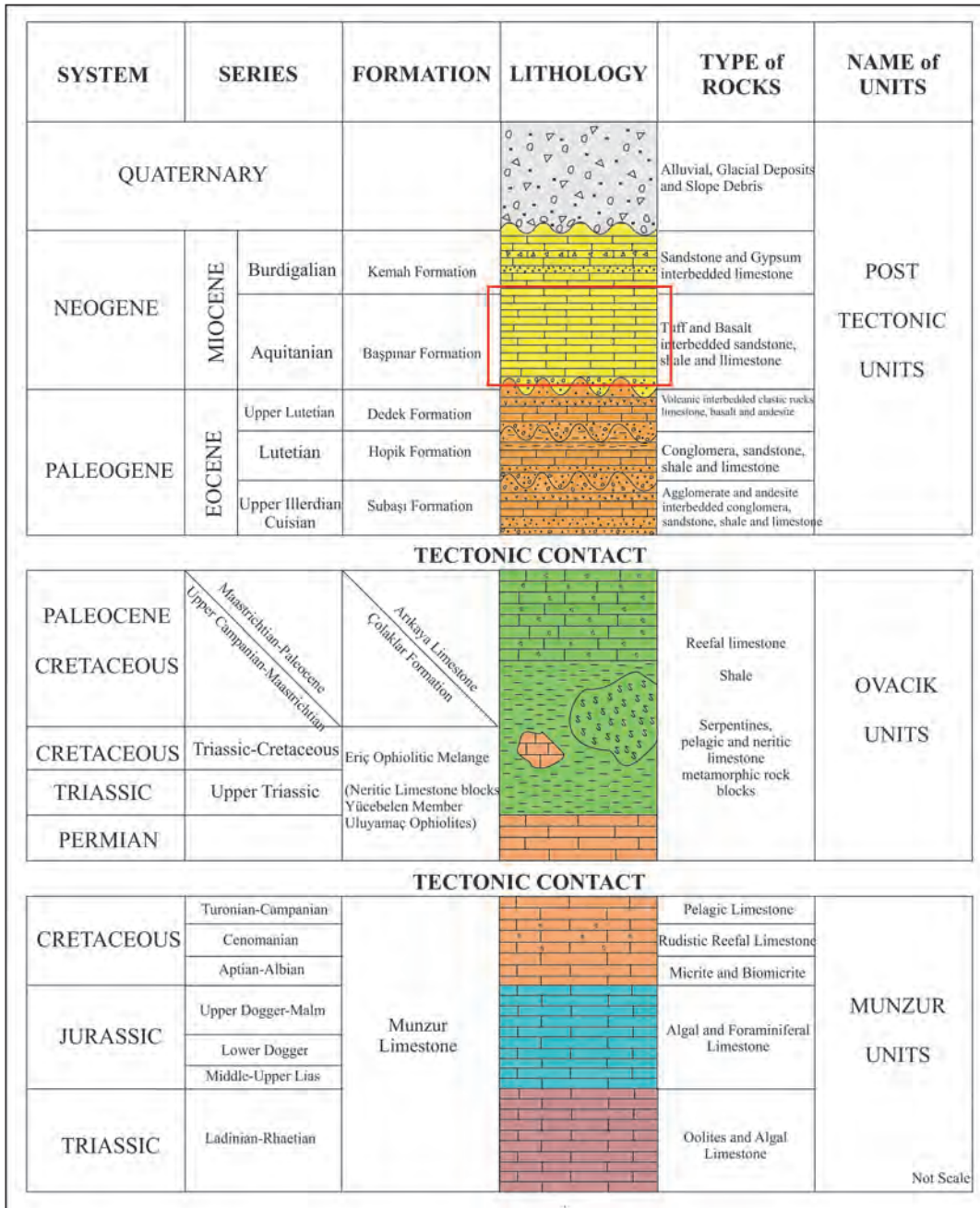


Figure 3- Litostratigraphy units of the Munzur mountains (modified from Özgül et al., 1981)

limestones, mudstones and marls, and a limited amount of marl layers interbedded with lignite. Based on the described micro and macro fossil samples, the authors suggested an early Early Miocene (Aquitanian) age for the formation.

The Başpınar formation contains limestones and clastic rocks that reflect the litoral and sublitoral environmental conditions. To the north, in the high

regions of the Munzur Mountains, clay-silt grade rocks and limestone layers are the dominant lithologies. The gypsum and coal beds found in the northeast of Ovacık district reflect a deltaic environment. The Başpınar Formation is interbedded with tuff, agglomerate and basalt in the South of the Ovacık. Volcanics are not present in the region of Munzur Mountains (Özgül et al., 1981).

CHRONOSTRATIGRAPHY	LITHOLOGY	SAMPLES NUMBER	Foraminifera	Algae	Bryozoa	Echinid Spine	Ostracoda	Annelida	Gastropoda	Bivalvia	BIOSTRATIGRAPHY	ENVIRONMENT
Aquitanian		83									Gastropoda - Bivalvia Assemblage Biozone	LAGOON - MARSCH COASTAL ENVIRONMENT
		81										
		79										
		78										
		77										
		76										
		75										
		74										
		73										
		72										
		71										
		69										
		68										
67												
66												
65												
64												
63												
62												
61												

Figure 4- Distribution of described fossils of Tırbi Musa yaylası section (modified from Karabıyıköğlü and Örcen, 1986)

#### 4. Tırbi Musa Yaylası Section

The specimens (81-83) of Tırbi Musa Yaylası Section measured for the project were titled "Sedimentology and Biostratigraphy of the Lignite Bearing Lower Miocene Sediments from Munzur Mountains" by Karabıyıköğlü and Örcen (1986) (Figure 4).

The section has total thickness of 140 m and alternated marl and limestone. The ecological characteristics of the described fossils are taken into consideration and tried to explain environmental interpretation.

#### 5. Systematic Paleontology

Genus: *Globularia* Swainson, 1840

*Globularia carlei* (Finlay, 1927)

Plate I, Figures 1a, b, c

1927 *Natica carlei* Finlay, page 498, plate 57.

1961 *Globularia (Cernina) carlei* (Finlay), Dey, page 54, plate 5, figures 3-6.

2009 *Globularia carlei* (Finlay), Harzhauser et al., page 338, figures 2c, d.

2010 *Globularia (Globularia) carlei* (Finlay), Kulkarni et al., page 327, figures 3b1, 3b2

2011 *Globularia carlei* (Finlay), Hasani and Vaziri, page 127, figures 7C<sub>1</sub>-C<sub>2</sub>

**Description:** The shells are trochiform, 5-6 whorls, the last whorl encloses all the previous whorls and constitute 5/6 of the total height. There is a small nucleus in the centre and this embryonic shell is followed by teleoconch. The sutures are slightly inclined and deep; thin oblique eadial ridges can be observed on the shell surface. The aperture is wide and elongated downward.

**Dimensions:** Ten partly damaged shells

Height: 30 mm, Width: 25 mm, The last whorl height: 25 mm.

**Similarities and Differences:** The mouth structure, the stepwise transition of the whorls and the pointed protoconch are the similar features with the specimens of Dey (1961), Harzhauser et al., (2009), Kulkarni et al., (2010) and Hasani and Vaziri (2011).

**Paleogeographical Distribution and Paleocological Features:** *Globularia carlei* is widespread in Burdigalian of Kutch basin and Kerala in India (Harzhauser et al., 2009), Miocene epoch in Kachchh, Gujarat in southwest India and Kenya (Dey, 1961; Kulkarni, 2010), in Early Miocene of Sirjan-Kerman in Iran (Hasani and Vaziri, 2011). The genus *Globularia* is living epifaunally and it is a sediment grazer in the lagoon or shallow subtidal environments.

**Stratigraphical Distribution:** Lower Miocene

Genus: *Granulolabium* Cossmann, 1889

*Granulolabium plicatum* (Bruguière, 1789)

Plate I, Figures 2a, b

1789 *Cerithium plicatum* Bruguière, page 488, plate 11.

1906 *Potamides (Pirenella) plicata* (Bruguière), Cossmann, Serie 78, page 116, plate 11, figures 17,18.

1924 *Pirenella plicata* (Bruguière), Cossmann and Peyrot, serie 73, page 267-269, plate 5, figures 99-101; plate6, figures 42, 44.

1939 *Pirenella plicata* (Bruguière), Stchépinsky, page 35, plate 10, figures 25-27.

1946 *Pirenella plicata* (Bruguière), Stchépinsky, page 138, plate 30, figures 13-14.

1958 *Pirenella plicata* (Bruguière), Hölzl, page 191.

1973 *Pirenella plicata* (Bruguière), Baldi, page 259, plate 29, figure 3.

1986 *Granulolabium plicatum* (Bruguière), Lozouet, page 27, figures 1-5.

2001 *Granulolabium plicatum* (Bruguière), Lozouet et al., page 27, plate 8, figures 1a-1b, 2a-2c, 3a-3c.

2002 *Granulolabium plicatum* (Bruguière), Harzhauser, page 73, plate 1, figures 17-20.

2004 *Pirenella plicata* (Bruguière), Özoğul, page 18, plate 1, figures 1-3,

2004 *Granulolabium plicatum* (Bruguière), harzhauser, page 120, plate 4, figures 13-14, plate 5, figures 1-4.

2007 *Granulolabium plicatum* (Bruguière), harzhauser, page 95, plate 2, figure 10.

**Description:** The shell is medium-sized conical, the number of whorls are 8-9, the suture is not deep; there are spiral bands on the whorls and there is four quadrangular granules side by side and from top to bottom. The aperture is narrow, the siphon is short, the columella edge is flat.

**Dimensions:** Seventy-eight partly damaged shells

Height: 30 mm, Width: 25 mm, The last whorl height: 25 mm.

**Similarities and Differences:** It shows similar characteristics with the samples of Cossmann (1906), Cossmann and Peyrot (1924), Özoğul (2004) and Harzhauser (2002, 2004, 2007) in terms of the numbers of the whorls, granules on the whorls and aperture morphology.

**Paleogeographical Distribution and Paleocological Features:** It is characteristic in Aquitaine Basin in France and in Aquitanian of Italy (Cossmann and Peyrot, 1924). It is widespread in Eggenburgian of the Vienna Basin (Hölzl, 1958), in Hungary (Egerian), in Germany (Burdigalian) (Baldi, 1973). It is one of the widespread form in the Late Oligocene and Miocene seas in Europe. It is found in a large part of the Western Tethys, and then slowly disappears after Early Miocene. Lastly it is observed at Carpathians, Korneuburg, Vienna Basin of Paratethys (Harzhauser, 2007). It is observed at Lower Miocene in Sivas, Turkey. (Stchépinsky, 1939) and Lower Miocene in Erzincan-Turkey (Özoğul, 2004). Lozouet (1986) has performed a study for the *Granulolabium* genus by using Nannoplankton biozone. According to this study, samples taken from 5 different regions of Oligocene-Early Miocene age, *Granulolabium* genus was determined as typical lagoonal and very shallow coastline form and inhabit the oligohaline salinity. The living representatives of this genus have an epifaunal lifestyle in muddy areas and lagoons in the mediolitoral zone (10- 150 cm) and are sediment grazers (Lozouet vd., 2001; Harzhauser and Mandic, 2001).

**Stratigraphic Distribution:** Lower Miocene

Genus: *Granulolabium* Cossmann, 1889

Subgenus: *Tiaracerithium* Sacco, 1895

*Granulolabium (Tiaracerithium) thiarella* (Grateloup, 1832)

Plate I, Figures 3a, b

1895 *Tiaracerithium pseudotiarella* var. *pseudopicta* Sacco, serie 17, page 35, plate 2, figure 92.

1922 *Pirenella pseudotiarella* d'Orbigny, Cossmann and Peyrot, serie 73, page 278, plate VI, figures 40-41.

1922 *Pirenella pseudotiarella* d'Orbigny var. *pictoides* Cossmann ve Peyrot, serie 73, pages 53-57, plate 6, figure 41.

1986 *Granulolabium (Tiaracerithium) pseudotiarella* (d'Orbigny), Lozouet, page 185, plate 2, figure 5.

2001 *Granulolabium (Tiaracerithium) thiarella* (Grateloup, 1832), Lozouet et al., page 28, plate 8, figure 4.

**Description:** The shell is quite small conic and the number of whorls are 9-10, beginning from protoconch the first eight whorls are striae and the last two whorls are with tubercules.

**Dimensions:** Fifty-five well preserved shells

Height: 9 mm, Width: 5 mm, The last whorl height: 2,5 mm.

**Similarities and Differences:** The samples are similar with the figures 40-41 of Cossmann and Peyrot (1922) and plate 8, figure 4 of Lozouet et al. (2001) in terms of whorl morphology, the first eight whorls are striae and tubercules on the last two whorls.

**Paleogeographical Distribution and Paleocological Features:** It is characteristic in Aquitaine basin in France (Cossmann and Peyrot, 1922; Lozouet et al., 2001). This genus is living epifaunally in the lagoon or shallow subtidal environments and it is a grazer (Lozouet 1986-2001).

**Stratigraphic Distribution:** Lower Miocene

Genus: *Tympanotonus* Schumacher, 1817

*Tympanotonus margaritaceus* Brocchi, 1814

Plate I, Figures 4a, b, c

1814 *Murex margaritaceus* Brocchi, page 447, plate 9, figure 24.

1921 *Tympanotonus margaritaceus* (Brocchi); Wenz, p. 131, pl. 15, fig. 1.

1921 *Tympanotonus margaritaceus* (Brocchi), Wenz, page 131, plate 15, figure 1.

1922 *Tympanotonus margaritaceus* (Brocchi), Cossmann and Peyrot, serie 73, page 248-253, plate 5, figures 60, 64, 67; plate 7, figures 1, 2, 6.

1938 *Tympanotonus (T.) margaritaceus* (Brocchi), Wenz, page 739-740, figure 2142.

1946 *Tympanotonus margaritaceus* (Brocchi), Stchépinsky, page 61, plate 30, figures 3-6.

1996 *Tympanotonus (T.) margaritaceus* Brocchi, Taner, plate 2, figures 3, 3a.

2001 *Tympanotonus margaritaceus* (Brocchi), Harzhauser and Mandic, page 696, plate 1, figures 4-6.

2001 *Tympanotonus margaritaceus* (Brocchi), Harzhauser and Kowalke, page 364, figures 5.7-5.9.

2004 *Tympanotonus margaritaceus* (Brocchi), Harzhauser, page 98, plate 5, figure 11.

2005 *Tympanotonus margaritaceus* (Brocchi), Esu et al., page 78.

2008 *Tympanotonus margaritaceus* (Brocchi), İslamoğlu, page 266.

2010 *Potamides (Mesohalina) margaritaceus* (Brocchi), Esu and Girotti, plate 6, figures 1-3.

**Description:** The shell is medium-sized, straight conical; number of whorls is 6-7 in the broken sample; suture is not deep; the whorls are decorated with two rows of thick and a thinner middle row of tight nodular granules; the mouth is narrow and siphon is short.

**Dimensions:** Fourty-five partly damaged shells

Height: 15 mm, Width: 5 mm, The last whorl height: 5 mm

**Similarities and Differences:** Although most of the samples have been broken, the tight nodular granules, the short siphon and the mouth structure constitute

the similarities with the *Tympanotonus margaritaceus* specimens of Cossmann (1922), Stchépinsky (1946) and Harzhauser (2004). Even if the fossils described by Esu and Girotti (2010) as *Potamides (Mesohalina) margaritaceus* (plate 6, figure 1-3) are similar to our specimens, they have more whorls.

**Paleogeographical Distribution and Paleocological Features:** *Tympanotonus margaritaceus* specimens is characteristic in Aquitaine basin in France. They are wide spreading from Hungary to the Pyrenees in Middle Miocene (Taner, 1996). Most *Potamides* live in shallow lagoons, low or variable salinity and salty inland lakes and muddy coastal plains (Esu and Girotti, 2010; Harzhauser, 2004). The genus *Tympanotonus* lives epifaunally in coastal, lagoonal or subtidal environments and herbivorous. (Lozouet et al., 2001, Esu et al., 2005; Esu and Girotti, 2010).

**Stratigraphic Distribution:** Lower-Middle Miocene

Genus: *Terebralia* Swainson, 1840

*Terebralia subcorrugata* (d'Orbigny, 1852)

Plate I, Figures 5a, b

1852 *Cerithium subcorrugatum* d'Orbigny, 3, page 80.

1906 *Terebralia subcorrugata* (d'Orbigny), Cossmann, serie 7, page 125, plate 10, figures 21-22.

1922 *Terebralia subcorrugata* (d'Orbigny), Cossmann and Peyrot, page 260, plate 6, figures 61-62.

1986 *Terebralia subcorrugata* (d'Orbigny), Lozouet, page 169, figure 1d.

2001 *Terebralia subcorrugata* (d'Orbigny), Lozouet et al., page 26, plate 8, figures 6a-6b, 7a-7b, plate 9, figure 10.

2003 *Terebralia subcorrugata* (d'Orbigny), İslamoğlu and Taner, serie 127, page 29-65, plate 2, figures 4a, 4b, 5, 6.

2005 *Terebralia subcorrugata* (d'Orbigny), Esu et al., page 78.

2010 *Terebralia subcorrugata* (d'Orbigny), Esu and Girotti, seri 53 (1), page 137-174.

**Description:** The shell is medium conical, number of whorls is 8-9, suture line is not deep, there are

four rows spiral strips on each whorl, side by side granulated; the last whorl is wide, mouth is nearly rounded.

**Dimensions:** Twenty-eight partly damaged shells

Height: 30 mm, Width: 25 mm, The last whorl height: 25 mm.

**Similarities and Differences:** Number of whorls, granules and mouth structure is similar to the specimens of Cossmann (1906), Cossmann and Peyrot (1922), İslamoğlu and Taner (2003) and Esu and Girotti (2010).

**Paleogeographical Distribution and Paleocological Features:** It is typical in Aquitaine basin in France (Cossmann and Peyrot, 1922). It is widespread in Aquitanian in Italy; Sarmatian in Austria, Hungary and Poland; Oligo-Miocene (Aquitanian) Mainz, Bavaria, Northern Alps, Vienna, Greece and Turkey (Lozouet, 1986; Esu and Girotti 2010); Early Miocene in Antalya, Turkey (İslamoğlu and Taner, 2003). The genus *Terebralia* lives epifaunally in lagoon or limited subtidal zone and it is a sediment grazer (Esu and Girotti, 2010).

**Stratigraphic Distribution:** Lower Miocene

Genus: *Cerithium* Bruguière, 1789

*Cerithium vulgatum* Bruguière, 1792

Plate I, Figures 6a, b, c

1757 *Cerithium goumier* Adanson, page 156, plate 10, figure 3.

1792 *Cerithium vulgatum* Bruguière, page 481.

1883 *Cerithium vulgatum* var. *mutica* Bruguière, Bucquoy, Doutzenberg and Dollfuss, page 5, plate 22, figures 1-15.

1895 *Cerithium vulgatum* var. *spinosa* Bucquoy, Sacco, serie 17, page 6, plate 1, figures 15-31.

1922 *Cerithium (Vulgocerithium) vulgatum* Bruguière, Cossmann and Peyrot, serie 73, page 188, plate 5, figures 33-34.

1997 *Cerithium (Thericium) vulgatum* Bruguière, Anistratenko, page 69, figure 1a.

2004 *Cerithium (Thericium) vulgatum* Bruguière, Landau et al., page 8, plate 1, figures 10-11.

2006 *Cerithium (Thericium) vulgatum* Bruguière, Chirli, page 87, plate 35, figures 7-15.

2013 *Thericium vulgatum* (Bruguière), Harzhauser et al., page 359, plate 1, figure 7.

**Description:** The shell is medium sized conical, the number of whorls is 8-9, the suture is not deep and it is like a chain. There are beaked granules on the whorls and the number of granules are 10-12 at the last whorl. And also there are four chain-like lines on the last whorl similar to the suture line.

**Dimensions:** Sixty-five partly damaged shells

Height: 40 mm, Width: 15 mm, The last whorl height: 15 mm.

**Similarities and Differences:** Number of whorls, chain-like suture line, and granules are the similar features to *C. vulgatum* var. *spinosa* and *C. vulgatum* var. *mutica* specimens of Sacco (1895) and Bucquoy et al. (1883). The species *Thericium vulgatum* described by Harzhauser et al. (2013) on a single eroded specimen is considered synonymous with *Cerithium vulgatum* Bruguière, 1792.

**Paleogeographical Distribution and Paleocological Features:** It was described in Aquitaine Basin in France (Cossmann and Peyrot, 1922); widespread from Miocene to Pliocene in Italy, in Tortonian at northern Italy (Sacco, 1895); Lower Miocene in Mediterranean and Atlantic region (Harzhauser et al., 2013). The genus *Cerithium* lives muddy and sandy grounds epifaunally in shallow subtidal environments that is the irregular sea water changes and rich in organic matters and it is a sediment grazer (Satyanarayana and Sundaram, 1972).

**Stratigraphic Distribution:** Miocene - Pliocene

Genus: *Nassarius* Duméril, 1805

*Nassarius erunala* Landau et al. 2013

Plate I, Figures 7a, b, c

2013 *Nassarius erunala* Landau et al., 11-13, page 175, plate 26, figures 7a-7b; 8a-8b.

**Description:** The specimens are very small and conical, 4-5 whorls, the final whorl height is approximately two times higher than the spir height; protoconch is rounded. The whorls are decorated with thick vertical lines, these lines constitute small granules towards the suture line. The mouth is extended downward, anterior is open; there are 2-3 lateral lines on the columella edge.

**Dimensions:** Twelve well preserved shells

Width: 5 mm, Height: 10 mm, The last whorl height: 5 mm.

**Similarities and Differences:** In terms of the number of whorls, granules and aperture structure of have similar features with the specimens of *Nassarius erunala* Landau et al. (2013).

**Paleogeographical Distribution and Paleocological Features:** Proto-Mediterranean Sea (Serravalian) in Karaman Basin, Turkey. The family of Nassariidae lives epifaunally in lagoons or limited shallow subtidal zones and it is carnivorous. (Carpentier et al., 1998).

**Stratigraphic Distribution:** Middle Miocene

Genus: *Cardita* Bruguière, 1792

*Cardita rusticana* Mayer, 1861

Plate II, Figures 1a, 1b

1861 *Cardita rusticana* Mayer, Mayer, serie 9, page 361.

1899 *Cardita rusticana* Mayer, Sacco, serie 27, page 11, plate 4, figure 1.

1914 *Cardita rusticana* Mayer, Cossmann and Peyrot, serie 2, page 40, plate 2, figures 15-20.

2012 *Cardita rusticana* Mayer, Cahuzac et al., page 388, plate 1.3.

**Description:** The shell is oval, the anterior side is short and rounded, the posterior side is straight from the umbo to the paleal edge, the paleal side has a long arc shape. The teeth are heterodontic; the hook is inflated and curved towards the front edge. The shell is decorated with radial lines and there are sequent granules along the lines.

**Dimensions:** Two well preserved valves

Height: 15 mm, Length: 25 mm.

**Similarities and Differences:** In terms of the anterior and the posterior sides features, teeth and sockets of the clamping system, swelling of the hook and sharp radial lines, *Cardita rusticana* Mayer is similar to the specimens Sacco (1899) and Cossman and Peyrot (1914).

**Paleogeographical Distribution and Paleocological Features:** It is characteristic in Aquitaine basin in France. The specimens are widespread in Tertiary (Tongriano) of Italy (Sacco, 1899); Miocene of Austria, Poland and Russia (Cossmann and Peyrot, 1914). The genus *Cardita* lives infaunally and facultatively mobile in lagoons or limited subtidal environments and it is a suspension feeder (Carpentier et al., 1998).

**Stratigraphic Distribution:** Miocene

Genus: *Anadara* Gray, 1847

*Anadara aquitanica* (Mayer, 1861)

Plate II, Figures 2a, 2b

1831 *Arca diluvii* Lamarck, du Bois de Montpéroux, page 63, plate 7, figures 10, 11, 12.

1861 *Arca aquitanica* Mayer, seri 9, page 362.

1882 *Arca diluvii* (Lamarck), Bucquoy, Dautzenberg and Dollfus, 2, plate 31, figures 13-17.

1898 *Anadara diluvii* (Lamarck), Sacco, seri 26, page 20, plate 4, figures 7-12.

1914 *Arca (Anadara) diluvii* (Lamarck), Cossmann and Peyrot, seri 2, page 149, plate 8, figures 3-6; plate 10, figure 53.

2005 *Anadara* cf. *A. diluvii* (Lamarck), Esu et al., page 78.

2010 *Anadara* cf. *A. aquitanica* (Mayer), Esu and Girotti, 53 (1), page 137-174.

**Description:** The shell is oval, the anterior side is short and round, the posterior side is straight from the hook and joins with the palial edge, approximately forming a right angle. The palial edge is long arc shaped. The umbo is inflated and curved towards the anterior side. The shell is decorated with radial lines and 2-3 growth lines which are parallel to the palial side.

**Dimensions:** Twenty-four well preserved valves

Height: 15 mm, Length: 25 mm.

**Similarities and Differences:** The shapes of the anterior and posterior sides and the radial growth lines on the shell are similar to *Arca (Anadara) diluvii* in Cossmann and Peyrot (1914), *Anadara* cf. *A. diluvii* in Esu et al. (2005) and *Anadara* cf. *A. aquitanica* in Esu and Girotti (2010).

**Paleogeographical Distribution and Paleocological Features:** The specimens are widespread in Tertiary (Tongriano) of Italy (Sacco, 1898); Aquitanian-Burdigalian of Aquitaine basin in France (Cossmann and Peyrot, 1914); Oligo-Miocene (Aquitanian) of Mainz, Bavaria, Northern Alps, Vienna, Greece and Turkey (Esu and Girotti, 2010). The genus *Anadara* lives semi-infaunally and facultatively mobile in sandy and pebbly substrates in litoral zone (infracircular zone) and it is a suspension feeder (Esu and Girotti, 2010).

**Stratigraphic Distribution:** Lower-Middle Miocene

Genus: *Ostrea* Linnaeus, 1815

*Ostrea lamellosa* Brocchi, 1814

Plate II, Figures 3a, 3b

1814 *Ostrea lamellosa* Brocchi, Brocchi, tome 2, page 564.

1831 *Ostrea lamellosa* Brocchi, du Bois de Montpéroux, page 74, plate 8, figures 13-14.

1870 *Ostrea lamellosa* Brocchi, Hörnes, seri 2, page 444, plate 71, figures 1-4.

1882 *Ostrea edulis* var. *lamellosa* Brocchi, Bucquoy, Dautzenberg and Dollfus, seri 2 (14), plate 5, figures 1, 2, 3, 4.

1914 *Ostrea lamellosa* Brocchi, Cossmann and Peyrot, page 378, plate 22, figures 7-9.

1999 *Ostrea lamellosa* Brocchi, Munteanu and Munteanu, seri 2, plate 3, figures 3a, b.

2001 *Ostrea lamellosa* Brocchi, Schultz, page 358, plate 55, figures 1a-1b.

2003 *Ostrea lamellosa* Brocchi, İslamoğlu and Taner, page 8, plate 2, figures 1a, 1b, 2.

2003 *Ostrea lamellosa* Brocchi, Videt, page 36, plate 8, figures 1-4.

2004 *Ostrea lamellosa* Brocchi, Özoğul, page 32, plate 7, figures 1a-b, 2a-b; plate 8, figures 1a-b, 2a-b.

2014 *Ostrea lamellosa* Brocchi, Mikuž and Gašparič, page 159, plate 3, figures 1a-1b.

**Description:** The shell is very close to oval and small. The right valve is slightly convex and ornamented with regular and marked lamellae. The ligament is preserved and the umbo is not too swollen; the muscle scar is close to the posterior side; thin

concentric growth lines are present over the shell surface.

**Dimensions:** Eight damaged valves

Height: 25 mm, Length: 20 mm, Thickness: 3 mm.

**Similarities and Differences:** In terms of the ligament, the umbo, the muscle scar pattern and the morphology of lamellae are similar to the specimens of *Ostrea lamellosa* Brocchi, 1814 from Munteanu and Munteanu, 1999; İslamoğlu and Taner, 2003; Videt, 2003; Özoğlu, 2004; Mikuž and Gašparič, 2014.

**Paleogeographical Distribution and Paleocological Features:** The specimens are widespread in Lower to Middle Miocene of Austria, France, Germany and Italy; in Lower Miocene of Aquitaine Basin in France (Cossmann and Peyrot, 1914); Middle Miocene of Loire Basin; Eggenburgian-Badenian of Vienna basin (Schultz, 2001). It appears in the Lower Miocene in Mediterranean Basin and spreads rapidly during the Middle and Upper Miocene (Videt, 2003), in the Lower Miocene at Erzincan province of Turkey (Özoğlu, 2004) and Miocene in Slovenia (Mikuž and Gašparič, 2014). The species *Ostrea lamellosa* lives stationary epifaunal in coastal shallow tidal zone and it is a suspension feeder (Dewiyanti and Sofyatuddin, 2012).

**Stratigraphic Distribution:** Miocene

Genus: *Cubitostrea* Sacco, 1897

*Cubitostrea digitalina* (Eichwald, 1830)

Plate II, Figures 4a, 4b

1830 *Ostrea digitalina* Eichwald, page 213.

1831 *Ostrea digitalina* Eichwald, du Bois de Montpéroux, page 74, plate 8, figures 13-14.

1999 *Cubitostrea digitalina* (Eichwald), Munteanu and Munteanu, seri 2, plate 4, figures 8a, b.

2005 *Cubitostrea digitalina* (Eichwald), El-Hedeny, 24 (2), page 719-733, plate II, figures A-B.

2013 *Cubitostrea digitalina* (Eichwald), Hosseinipour and Dastanpour, page 1984, plate 1, figures f-h.

**Description:** The shell is small and triangular shaped. The valve is quite flat and ornamented with concentric lamellae. The ligament is not good preserved.

**Dimensions:** Six damaged valves

Width: 20 mm, Height: 25 mm, Thick: 4 mm.

**Similarities and Differences:** In terms of the shape and the radial growth lines of the shell our samples are similar to the specimens of du Bois de Montpéroux (1831) and El-Hedeny (2005).

**Paleogeographic Distribution and Paleocological Features:** It is widespread in France, Germany, Austria and Bulgaria in Miocene (Munteanu and Munteanu, 1999) and in Egypt in Middle Miocene (El-Hedeny, 2005). The genus *Cubitostrea* lives stationary epifaunal in shallow subtidal zone and it is a suspension feeder (Dewiyanti and Sofyatuddin, 2012).

**Stratigraphic Distribution:** Miocene

Genus: *Chlamys* Röding, 1798

*Chlamys* sp.

Plate II, Figures 5

**Description:** The shell is small-sized and triangular with thick radial lines over the shell surface.

**Dimensions:** Three damaged valves

Height: 35 mm, Width: 40 mm.

**Similarities and Differences:** Our specimen shows similar characteristic features to *Chlamys (Aequipecten) liberata* (Cossmann and Peyrot, 1914; page 126, plate 17, figures 14-17) which is widespread in Lower Miocene (Aquitainian) but it is left open to nomenclature as there is only one broken shell. The genus *Chlamys* lives stationary epifaunal and it is a suspension feeder.

## 6. Paleocological Species Diversity

In this study, a total of 336 fossils specimens are identified and the paleocological species diversity is calculated for the interpretation of the paleoenvironment of the study area.

The determination of diversity for specific geographical areas is important for paleocological interpretations. In this regard, a new science branch "Ecometry Studies" has been developed (Simpson, 1949; Shannon-Weaver, 1948). Ecometry is based on

numerical expression of ecological concepts. It was developed to estimate the diversity of ecosystems in a specific area for different branches of science (biology, zoology, botany) quantitatively. Biological richness or diversity refer to the differences and variability of the organisms, the environment they live in and their interactions with this environment (Gaston and Spicer, 2004).

Various indices are being used to determine the ecological species diversity and distribution of a region. Alfa ( $\alpha$ ) diversity which is determined locally gives the number of species in a single habitat. Beta ( $\beta$ ) diversity is the ratio of species among local habitats. The gamma ( $\gamma$ ) diversity also shows the diversity but in a greater extent where the research area is formed by numerous smaller sampling areas. Gamma diversity is expressed by the formula “ $\gamma = \alpha \times \beta \times \text{total habitat area}$ ” (Gülsoy and Özkan, 2008).

Diversity studies on fossil molluscs have started in the 1990s (CoBabe et al., 1994; Strong et al., 2008; Dinapoli et al., 2010; Petrova et al., 2012; Sharma et al., 2013). This study is unique as it is conducted on archived fossil samples. Only the alfa ( $\alpha$ ) diversity index values are calculated because the fossil samples were gathered from a restricted area. Four different index values are used for calculations and according to these formulas an attempt is made to interpret the paleoecological diversity numerically.

6.1. Simpson (D) Index: This index, which is used to introduce the environmental diversity, shows the predominance of species. Dominancy is limited between 0 and 1; the greater the D values, the greater the diversity of the environment (Simpson, 1949).

$$D = 1 - C \quad C = \sum [ Ni (Ni-1) / N (N-1) ]$$

Ni: total number of individuals of a species

N: total number of individuals

6.2. Shannon – Weaver (H) Index: It indicates species diversity. Its value is limited between 0 and 5;  $H > 2,5$  indicates that species diversity is increased. (Shannon and Wiener, 1949).

$$H = - \sum [ pi \log_2 (pi) ] \quad pi = Ni / N$$

Ni: total number of individuals of a species

N: total number of individuals

6.3. Margalef (M) Index: It indicates species richness. It is not limited to any value. The highest M value indicates the highest species richness. (Margalef, 1958).

$$M = (S - 1) / \ln N$$

S: number of species

N: total number of individuals

6.4. Pielou (Ep) Index: Its value is limited between 0 and 1 and indicates the distribution of dominance according to species. If there are equal numbers of individuals in each species, Ep value is 1 (Pielou, 1960).

$$Ep = H / \log_2 S$$

H: Shannon-Weaver Index

S: number of species

## 7. Discussions and Conclusions

As a result of individual counts, the numbers and percentages of the species are determined (Table 1) and percentage (%) distribution graphics were prepared (Figure 5).

Table 1- Number of species and percentages of Gastropoda and Bivalvia

Species	Number	%
<i>Globularia carlei</i>	10	3
<i>Granulolabium plicatum</i>	78	27
<i>Granulolabium (Tiaracerithium) thiarella</i>	55	19
<i>Terebralia subcorrugata</i>	28	10
<i>Nassarius erunalae</i>	12	4
<i>Tympanotonus margaritaceus</i>	45	15
<i>Cerithium vulgatum</i>	65	22
Total Gastropoda	293	87
<i>Cardita rusticana</i>	2	5
<i>Anadara aquitanica</i>	24	56
<i>Ostrea lamellosa</i>	8	18
<i>Cubitostrea digitalina</i>	6	14
<i>Chlamys</i> sp.	3	7
Total Bivalvia	43	13

Accordingly, the fossils belongs to Gastropoda class (87%) is more dominant than bivalves. This dominancy is due to the gastropods are more mobile and are more adaptable to sea level changes and salinity.

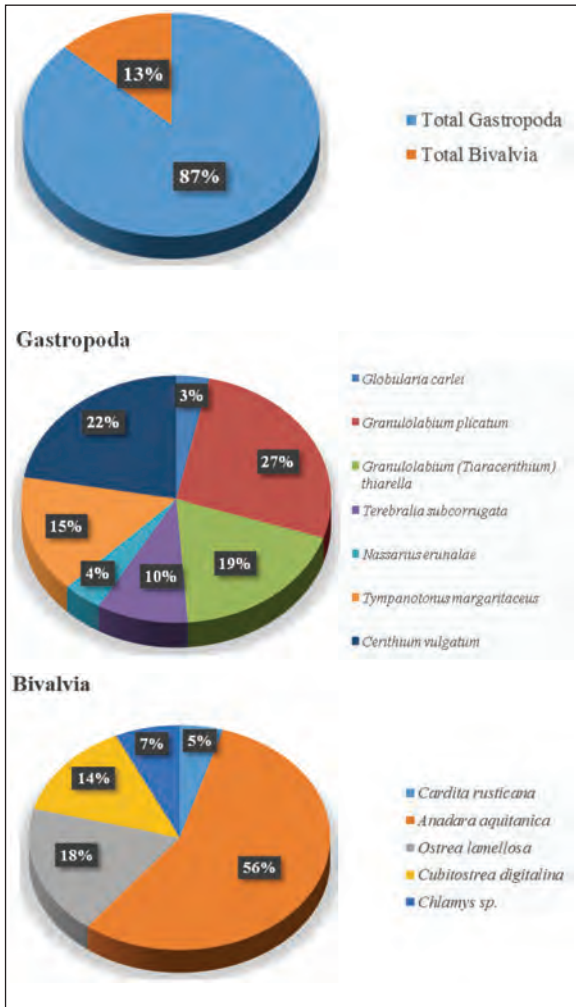


Figure 5- Graphics of Species Percentage Distribution (Gürsoy, 2016).

Result of the diversity index (Simpson, Shannon – Wiener, Margalef, Pielou) values of the specimens which were gathered from the Başpınar Formation of Tunceli-Ovacık district that are calculated by the appropriate formulas;

- The index values of the Gastropoda species are higher than the Bivalvia, this indicates the dominance of gastropods in the habitat (Table 2);

- Simpson Index value for gastropods is close to 1 ( $D = 0,82$ ) and this indicates a more or less equality in diversity among the species;

- The Shannon-Wiener Index value is greater than 2,5 for gastropods, and this shows a greater variety for this class (Table 2);

- The Epilou Index value, which indicates the distribution of dominance by species, is ( $Ep = 0,9$ ) for gastropods indicating that the defined gastropod species are approximately equal in number (Table 2).

- According to the Margalef index value, the class with the highest M value has the highest species richness; Gastropods have a higher species diversity than bivalves with a value of 1,23 (Table 2).

Table 2- Diversity index values of Gastropoda and Bivalvia.

Diversity Indexes	Gastropoda	Bivalvia
Simpson (D) (0-1)	0,82	0,64
Shannon-Weaver (H) (0-5)	2,53	1,8
Margalef (M) (limitsiz)	1,23	1,06
Epilou (Ep) (0-1)	0,9	0,33

The Başpınar Formation was characterized by a sequence of conglomerate, mudstone, limestone and marls. The age of the formation was assigned to Burdigalian (Özgül et al. 1981) and to Aquitanian (Karabıyıköğlü and Örcen, 1986) by previous workers. As described fossils of this study, table 3 and table 4 are made.

These tables show the distribution of species identified from various locations in Europe, Balkans and Asia until today. Among the collected samples, the most commonly found species (*Cerithium vulgatum*, *Tympanotonus margaritaceus*, *Terebralia subcorrugata*, *Granulolabium plicatum*, *Granulolabium (Tiaracerithium) thiarella* and *Anadara aquitanica*) are the ones that have a distribution in the Aquitanian basin in France (Eames and Clarke, 1967). Besides these species *Ostrea lamellosa*, *Cubitostrea digitalina* and *Cardita rusticana* (Table 4) can be found up to Middle Miocene.

The Başpınar formation is characterized by a sequence of conglomerates, mudstones, limestones and marls and assigned to Burdigalian (Özgül et al., 1981) and to Aquitanian (Karabıyıköğlü and Örcen, 1986) by the previous workers. In this study, the age of the formation is assigned as Aquitanian-Burdigalian (Table 5) and according to the environmental features of the fauna we can conclude that the paleoenvironmental conditions were that of a brackish water lagoon.

Table 3- Paleogeographic distribution of described species belongs to Gastropoda class.

<b>Gastropoda</b>	<i>Globularia carlei</i>	<i>Granulolobium plicatum</i>	<i>Granulolobium (Turacerithium) thiarella</i>	<i>Tympanotomus margaritaceus</i>	<i>Terebralia subcorrugata</i>	<i>Cerithium vulgatum</i>	<i>Nassarius ornatae</i>
France	Aquitanian (Cossmann and Peyrot, 1917)	Aquitanian (Cossmann and Peyrot, 1917)	Aquitanian (Cossmann and Peyrot, 1922; Lozouet, 2001)	Aquitanian (Cossmann and Peyrot, 1922; Lozouet, 2001)	Aquitanian (Cossmann and Peyrot, 1922; Lozouet, 2001)	Aquitanian (Cossmann and Peyrot, 1922)	
Italy		Aquitanian (Cossmann, 1906)	Aquitanian (Sacco, 1895)	Late Oligocene (Edu and Girotti, 2010)		Tortonian (Sacco, 1895) Middle Miocene (Harzhauser, 2013)	
Austria		Eggenburgian (Högl, 1958)		Early Miocene (Harzhauser and Kowalik, 2001)			
Germany		Burdigalian (Balch, 1973)					
Hungary		Egerian (Högl, 1958)					
Poland							
Russia							
India	Burdigalian (Dey, 1961; Kulkarni, 2010)						
Kenya	Miocene (Dey, 1961; Kulkarni, 2010)						
Iran	Early Miocene (Hasani and Vaziri, 2011)						
Turkey		Early Miocene (Özgül, 2004)		Egerian- Eggenburgian	Early Miocene (Isinoglu and Dincer, 2011)		Middle Miocene (Londat et al., 2013)

Table 4- Paleogeographic distribution of described species belongs to Bivalvia class.

<b>Bivalvia</b>	<i>Anadara aquitanica</i>	<i>Cardita rusticana</i>	<i>Cubitostrea digitalina</i>	<i>Ostrea lamellosa</i>
France	Aquitanian-Burdigalian (Cossmann and Peyrot, 1914)	Aquitanian (Cossmann and Peyrot, 1914)	Aquitanian (Montpéroux, 1831) Miocene (Munt. and Munt., 1999)	E.-M.Miocene (Munt. and Munt., 1999)
Italy	Tongriano (Sacco, 1898)	Tongriano (Sacco, 1899)		E.-M.Miocene (Munt. and Munt., 1999)
Austria		Miocene (Cossmann and Peyrot, 1914)	Miocene (Munt. and Munt., 1999)	Eggenburgian-Badenian (Munt. and Munt., 1999)
Germany	Oligo-Miocene (Esu and Girotti, 2010)	Miocene (Cossmann and Peyrot, 1914)	Miocene (Munt. and Munt., 1999)	E.-M.Miocene (Munt. and Munt., 1999)
Poland		Miocene (Cossmann and Peyrot, 1914)		
Hungary				Eggenburgian-Badenian (Munteanu and Munteanu, 1999)
Bulgaria			Miocene (Munteanu and Munteanu, 1999)	Miocene (Munteanu and Munteanu, 1999)
Russia		Miocene (Cossmann and Peyrot, 1914)		
Greece	Oligo-Miocene (Esu and Girotti, 2010)			
Egypt			Middle Miocene (El-Hedeny, 2005)	
Turkey	Oligo-Miocene (Esu and Girotti, 2010)			E.-M.Miocene (Özoğul, 2004)



- Ağralı, B. 1967. Tunceli İli Ovacık-Yarımkaya Linyit Zuhurunun 1/25.000 Ölçekli Jeolojik Etüdü Hakkında Rapor, Maden Tetkik ve Arama Rapor No: 155, Ankara, (unpublished).
- Anistratenko, V.V. 1997. Molluscs of the genus *Cerithium* Bruguière, 1789 (Gastropoda, Cerithidae) of the Black Sea. *Ruthenica* 7: 69-72.
- Baldi, T. 1973. Mollusc Fauna of the Hungarian Upper Oligocene (Egerian), Akademiai Kiado, Budapest.
- Baykal, F. 1953. Çimen Munzur Dağları Mıntığında Jeolojik Etüdler. Maden Tetkik ve Arama Rapor no: 2058, Ankara (unpublished).
- Brocchi, G. B. 1814. Conchiologia fossile subapennina con osservazioni geologiche sugli Apennini e sul suolo adiacente. Milano Vol. I: pp. LXXX + 56 + 240; Vol. II, p. 241-712, pl. 1-16.
- Bruguière, J.G. 1789-1792. Encyclopedie méthodique ou par ordre de matières. Histoire naturelle des vers. Pancoucke, Paris. Vol. 1, part 1, p. 1-344 [June 1789]; Vol. 1, part 2, p. 345-758 [13 Feb. 1792; dates after N. Evenhuis, 2003, *Zootaxa*, 166: 37; *Zootaxa*, 207]; Atlas pl. 1-189 [1791]; pl. 190-286 [1797] pl. 287-390 [1798] pl. 391-488.
- Bucquoy, E., Dautzenberg, P., Dollfuss, G. 1882-1886. Les Molusques marins du Roussillon. Tome Ier. Gastropodes. J.B.Bailliére. 570 p., 66 pls., Paris.
- Carpentier, K.E., Niem, V.H., Poutiers, J.M. 1998. The living marine resources of the Western Central Pacific. Volume 1. Seaweeds, corals, bivalves and gastropods. Food and Agriculture Organization of The United Nations, Rome.
- CoBabe, E.A., Allmon, W.D. 1994. Effects of sampling on paleoecologic and taphonomic analyses in high diversity fossil accumulations: an example from the Eocene Gosport Sand, Alabama. *Lethaia*, Vol. 27, 167-178.
- Cossmann, M. 1906. Essais de Paléoconchologie Comparée, 7, 261 p., Paris.
- Cossmann, M., Peyrot, A. 1909-1924. Conchologie Néogénique de l'Aquitaine. Actes de la Société Linnéenne de Bordeaux, (1889), 548p.; (1909-1912), 718 p.; (1913-1914), 496 p.; (1915-1916), 568p.; (1916-1919), 709 p.; (1917-1918), 834p.; (1922-1924), 621 p.
- Dewiyanti, I., Karina, S. 2012. Diversity of Gastropods and Bivalves in mangrove ecosystem rehabilitation areas in Aceh Besar and Banda Aceh districts, Indonesia. *Aquaculture, Aquarium, Conservation & Legislation International Journal of the Bioflux Society*. vol.5, issue 2, 55-59.
- Dey, A.K. 1961. The Miocene Mollusca from Quilon, Kerala (India); *Memoirs of the Geological Survey of India, Palaeontologia Indica* 36 1-129.
- Dinapoli, A., Klussmann-Kolb, A. 2010. The long way to diversity-Phyogeny and evolution of the Heterobranchia (Mollusca: Gastropoda). *Molecular Phylogenetics and Evolution* (55): 60-76.
- du Bois de Montpereux, 1831. *Conchologie Fossile et Aperçu Géognostique des Formations du Plateau Wolhyni- Podolien*. 76 sayfa, 8 levha., Simon Schropp, Berlin.
- Eames, F.E., Clarke, W.J. 1967. Mayer's Stratotype area Aquitanian faunas. *Eclogae Geologicae Helvetiae*. B.60, H.2, 553-566.
- Eichwald, E. 1830. *Naturhisto rische Skizze vo n Lith auen, Volh yn ien und Podolien in geognostisch- rminera logischcr: botanischer und zoologi scher Hinsicht*. – Ibidem 1-256.
- El-Hedeny, M.M. 2005. Taphonomy and Paleoecology of the Middle Miocene oysters from Wadi Sudr, Gulf of Suez, Egypt. *Revue de Palobiologie Genève*. 24(2): 719-733.
- Esu, D., Girotti, O., Pignatti, J. 2005. Late Oligocene-?Miocene mollusc and foraminiferal assemblages from the vicinity of Otranto (Southern Apulia, Italy): a non-marine to marine transition, *Rendiconti della Società Paleontologica Italiana*, (2): 75-85.
- Esu, D., Girotti, O. 2010, Late Oligocene Molluscan Fauna from Otranto (Apulia, Southern Italy): an example of alternating freshwater, lagoonal and emerged environments, *Paleontology*, 53(1): 137-174.
- Finlay, H.J. 1927. New specific names for Austral mollusca. *Transactions Proceedings New Zealand Institute* 57: 488-533.
- Gaston, K.J., Spicer, J.I. 2004. *Biodiversity: an introduction*. 2nd Edition., 190p., Blackwell.
- Gülsoy, S., Özkan, K. 2008. Tür Çeşitliliğinin Ekolojik Açıdan Önemi ve Kullanılan Bazı İndisler. *Süleyman Demirel Üniversitesi Orman Fakültesi Dergisi*, (1): 168-178.
- Gürsoy, M. 2016. Munzur Dağları Alt Miyosen Çökelleri Mollusk Faunası Taksonomisi ve Paleoekolojik Özellikleri. 69. Türkiye Jeoloji Kurultayı, 11-15 Nisan 2016, Maden Tetkik ve Arama Ankara (Oral Presentation).
- Harzhauser, M. 2002. *Marine und brachyhaline Gastropoden aus dem Karpatium des Korneuburger Beckens*

- und der Kreuzstettener Bucht (Österreich, Untermiozan). Beitr. Palaont., 27: 61-159, Wien.
- Harzhauser, M. 2004. Oligocene Gastropod faunas of the Eastern Mediterranean (Mesohellenic Trough, Greece and Esfahan-Sirjan Basin, Central Iran). Courier Forschungsinstitut Senckenberg, 248: 93–181.
- Harzhauser, M. 2007. Oligocene and Aquitanian Gastropod Faunas from the Sultanate of Oman and their biogeographic implications fort he early western Indo-Pacific. Paleontographica Abt.A, 280 (4-6), 75-121.
- Harzhauser, M., Kowalke, T. 2001. Early Miocene brackish-water mollusca from the eastern Mediterranean and from the central Paratethys, a faunistic and ecological comparison by selected faunas. Journal of the Czech Geological Society, 46 (3-4): 353–374.
- Harzhauser, M., Mandic, O. 2001. Late Oligocene gastropods and bivalves from the Lower and Upper Austrian Molasse Basin. In PILLER, W. E. and RAS SER, M. W. (eds). Paleogene of the Eastern Alps. Österreichische Akademie der Wissenschaften, Schriftenreihe der Erdwissenschaftlichen Kommissionen, 14: 671-795.
- Harzhauser, M., Reuter, M., Piller, W.E., Berning, B., Kroh, A., Mandic, O. 2009. Oligocene and Early Miocene gastropods from Kutch (NW India) document an early biogeographic switch from western Tethys to Indo-Pacific. Palaontol Z, 83:333–372.
- Harzhauser, M., Reuter, M., Mandic, O., Schneider, S., Piller, W.E., Brandano, M. 2013. “Pseudo-Sarmatien” Mollusc Assemblages from the Early Messinian Oolite Shoals of Sicily (Italy). Rivista Italiana di Paleontologia e Stratigrafia. V.119, no.3, 4 pls., pp. 351-386.
- Hasani, M.J., Vaziri, M.R. 2011. Early-Miocene Gastropods from Khavich Area, South of Sirjan, (Kerman, Iran): Biostratigraphy, Paleogeography and Paleoecology. Journal of Sciences, Islamic Republic of Iran 22(2): 125-133.
- Hosseinipour, F., Dastanpour, M. 2013. Lower Miocene Oyster Shells from the Southeast Zagros Basin (Zade Mahmud area, Iran) and their Paleoecology. Arab Journal Geosciences (6), 1977-1989.
- Hözl, O. 1958. Die Mollusken Fauna des Oberbayerischen Burdigals-Geologica Bavarica, nr. 38, 348 p., Bavarica, München.
- Hörnes, M. 1870. Die Fossilen Mollusken des Tertiärbeckens von Wien. Abh.D. Kgl. Geol. Reichsanst, II, Univalven, Wien.
- İslamoğlu, Y. 2008. Molluscan biostratigraphy and paleo-environmental reconstruction of Oligocene deposits in the Denizli and Kale-Tavas subbasins (SW Turkey). Geodiversitas, 30, 261–285.
- İslamoğlu, Y., Taner, G. 2003. Antalya Miyosen Havzasının Gastropoda Faunası (Batı-Orta Toroslar, GB Türkiye), Maden Tetkik ve Arama Dergisi, 127, sayfa 29-65.
- Karabıykoğlu, M., Örçen, S. 1986. Munzur Dağları Linyit İçeren Alt Miyosen Çökellerinin Sedimentolojisi ve Biyostratigrafisi. Maden Tetkik ve Arama Rapor No:2033, Ankara (unpublished).
- Ketin, İ. 1945. 64/3 paftası ile 63/1 paftası üzerindeki Ovacık Bölgesine ait Jeolojik Rapor. Maden Tetkik ve Arama Rapor No: 1628, Ankara (unpublished).
- Kulkarni, K.G., Kapoor S.B., Borkar, V.D. 2010. Molluscan fauna from the Miocene sediments of Kachchh, Gujarat, India – Part 3. Gastropods, J. Earth Syst. Sci. 119, No. 3, 307–34.
- Kurdoğlu, Y. 1976. Tunceli İli Ovacık – Yarımkaya Linyit Sahasına Ait Rapor, Maden Tetkik ve Arama Rapor No: 174.
- Kurtman, F. 1961. Munzurlarda Kemah ve Ovacık Bölgelerine Ait Petrol İstikşaf Etüdü. Maden Tetkik ve Arama Rapor No: 22, Ankara, (unpublished).
- Landau, B.M., Marquet, R., Grigis, M. 2004. The Early Pliocene Gastropoda (Mollusca) of Estepona, southern Spain. Part 2 Orthogastropoda, Neotaenioglossa. Palaentol, 4, 108 pp.
- Landau, B.M., Harzhauser, M., İslamoğlu, Y., Da Silva, C. M. 2013. Systematics and palaeobiogeography of the gastropods of the middle Miocene (Serravalian) Karaman Basin, Turkey, Cainozoic Research, volumes 11-13, 50 Years of WTKG 1963-2013, printed in Hungary for the Tertiary Research Group (London) & the Werkgroep voor Tertiaire en Kwartaire Geologie (Rotterdam) 584 pp., 82 plates. Eever, K.A., Matenco, L., Gariia-Castellanos, D., Cloetingh, S.A.P.L. 2010. The evolution of the Danube gateway between Central and Eastern Paratethys (SE Europe): Insight from numerical modelling of the causes and effects of connectivity between basins and its expression in the sedimentary record. Tectonophysics, 502, 175-195.
- Lozouet P. 1986. Redéfinition des genres *Potamides* et *Pirenella* (Gastropoda: Prosobranchia) à partir des espèces actuelles et fossiles. Implications Phylétiques et Biogéographiques. Annales de Paléontologie, 72(3) : 163-210, 15 figs, 3 pls.

- Lozouet, P., Lesport, J.F., Renard, P. 2001. Révision des Gastropoda (Mollusca) du Stratotype de l'Aquitainien (Miocène Inf.) : Site de Saucats "Larrey", Gironde, France. *Cossmanniana*, S.3 (1-189).
- Margalef, R. 1958. Information Theory in Ecology. *International Journal of General Systems*. 3: 36-71.
- Mayer, C. 1861. Description des coquilles fossiles des terrains tertiaires superieures (suite). *Journal de Conchyliologie*, 9: 358-373.
- Mikuž, V., Gašparič, R., 2014. Nekaj redkih fosilov iz Slovenskih goric/ Some rare fossils from Slovenske gorice, Slovenia. *Geologija*. 57(2): 155-166.
- Moore, R.C. 1964-1969. *Tretise on Invertebrate Paleontology, Mollusca 6 Bivalvia*, 489p., The University of Kansas, USA.
- Munteanu, E., Munteanu, M.T. 1999. Upper Badenian Bivalves in the Cernavoda Area, *Acta Paleontologica Romaniae*, (2): 275-286.
- Nebert, K. 1955. Munzur Dağın Jeolojisi (Kemaliye'nin Doğusu) 1/100.000 Mikyasındaki "Divrik 62-4" Harita Paftası Üzerinde Yapılan Jeolojik Harita Çalışmaları Hakkında Rapor, Maden Tetkik ve Arama Rapor No: 2513, Ankara.
- Nebert, K. 1959. Munzur Dağı Bölgesinin Jeolojisi Hakkında Rapor. *Maden Tetkik ve Arama Dergisi*, (52): 35-44, Ankara, (unpublished).
- Orbigny, d'. 1852. *Prodrome de Paléontologie Stratigraphique Universelle des Animaux Mollusques et Rayonnés faisant suite aux Cours élémentaire de Paléontologie et de Géologie Stratigraphiques*. Masson, Paris, vol.3, 196 p.
- Özer, E. 1994. Munzur Dağlarının (Kemah-İliç-Erzincan) Stratigrafisi. *Türkiye Jeoloji Bülteni*, 37(2): 53-64.
- Özgül, N., Turşucu, A., Özyardımcı, N., Şenol, M., Bingöl, İ., Uysal, Ş. 1981. Munzur Dağlarının Jeolojisi. Maden Tetkik ve Arama Rapor No: 6995, Ankara, (unpublished).
- Özoğul, M.A. 2004. Tercan (Erzincan) – Aşkale (Erzurum) çevresi Tersiyer istifinin Paleontolojik İncelemesi ve faunanın Maden Tetkik ve Arama Müzesindeki Tanzimi. Ankara Üniversitesi Yüksek Lisans Tezi (unpublished).
- Petrova, S., Mehmed, E., Mollov, I., Georgiev, D., Velcheva, I. 2012. Molluscs (Mollusca: Gastropoda, Bivalvia) from The Upper Eocene of Perunika Village (East Rhodopes, Bulgaria)-Preliminary Results. *Acta Zoologica Bulgarica*, (4): 233-236.
- Pielou, E. C. 1960. A Single Mechanism to Account for Regular, Random and Aggregated Populations. *Journal of Ecology*. 48(3): 574-584.
- Sacco, F. 1895. I molluschi dei terreni terziarii del Piemonte e della Liguria. P.XVII, 83 pp., 370 fig.
- Sacco, F. 1898. I molluschi dei terreni terziarii del Piemonte e della Liguria. P.XXVI, 99 pp., 431 fig.
- Sacco, F. 1899. I molluschi dei terreni terziarii del Piemonte e della Liguria. P.XXVII, 110 pp., 441 fig.
- Satyanarayana, R.K., Sundaram, K.S. 1972. Ecology of Intertidal Molluscs of Gulf of Mannar and Palk Bay. *Indian National Science Academy*, 38 (5-6): 462-474.
- Schultz, O. 2001. *Bivalvia Neogenica (Nuculacea-Unionacea)*. In *Catalogus Fossilium Austriae 1 (1)*, ed. W.E. Piller, 1-379. Wien: Osterreichische Akademie der Wissenschaften.
- Shannon, C. E., Weaver, W. 1948. A Mathematical Theory of Communication. *The Bell System Technical Journal*, (27): 379-423; 623-656.
- Sharma, K.K., Bongotra, K., Saini, M. 2013. Diversity and distribution of Mollusca in relation to the physico-chemical profile of Gho-Manhasan stream, Jammu (J&K). *International Journal of Biodiversity and Conservation* , 5(4), 240-249.
- Simpson, E.H. 1949. Measurement of Diversity. *Nature*. (163), pp. 688.
- Stchépinsky, V. 1939. Faune Miocene du vilayet de Sivas (Turquie). *Maden Tetkik ve Arama Ens. Monogr. Ser.C*, No:1, Ankara.
- Stchépinsky, V. 1946. Türkiye'nin Karakteristik Fosilleri. *Maden Tetkik ve Arama Ens. Monogr.Ser. D*, No:9, Ankara.
- Strong, E.E., Gargominy, O., Ponder, W.F., Bouchet, P. 2008. Global diversity of gastropods (Gastropoda; Mollusca) in freshwater. *Hydrobiologia* 595: 149-166.
- Taner, G. 1996. Batı Trakya Havzasının Egeriyen Mollusk Faunası, *TPJD Bülteni*, 8 (1): 66-81.
- Tarhan, N. 2008. Erzincan I42 Paftası. *Türkiye Jeoloji Haritaları N: 84*. Maden Tetkik ve Arama Genel Müdürlüğü Jeoloji Etüdleri Dairesi, Ankara.
- Tüysüz, O. 1993. Erzincan Çevresinin Jeolojisi ve Tektonik Evrimi. 2.Ulusal Deprem Mühendisliği Konferansı, 10-13.
- Videt, B. 2003. Dynamique des Paleoenvironnements A Huitres du Cretace Superieur Nord\_Aquitain

- (So France) et du Mio-Pliocene Andalou (Se Espagne): Biodiversite, Analyse Sequentielle, Biogeochimie. 10 pl., 304 p. Universite Rennes.
- Wenz, W. 1921. Das Mainzer Becken und seine Randgebiete. 352 p., Willy Ehlig, Heidelberg.
- Wenz, W. 1938-43. Gastropoda, Handbuch der Palaozoologie, 1-2 , 1639 pp., Berlin.
- Whittaker, R.H. 1972. Evolution and Measurement of Species Diversity. Taxon, Vol. 21, No. 2/3 (May, 1972),pp 213-225.

## PLATES

**PLATE I**

1a, b, c *Globularia carlei* (Finlay, 1927)

2a, b *Granulolabium plicatum* (Bruguière, 1789)

3a, b *Granulolabium (Tiaracerithium) thiarella* (Grateloup, 1832)

4a, b, c *Tympanotonus margaritaceus* (Brocchi, 1814)

5a, b *Terebralia subcorrugata* (d'Orbigny, 1852)

6a, b, c *Cerithium vulgatum* (Bruguière, 1792)

7a, b, c *Nassarius erunalae* Landau et al., 2013

(The bars shows that 1 cm for each sample.)

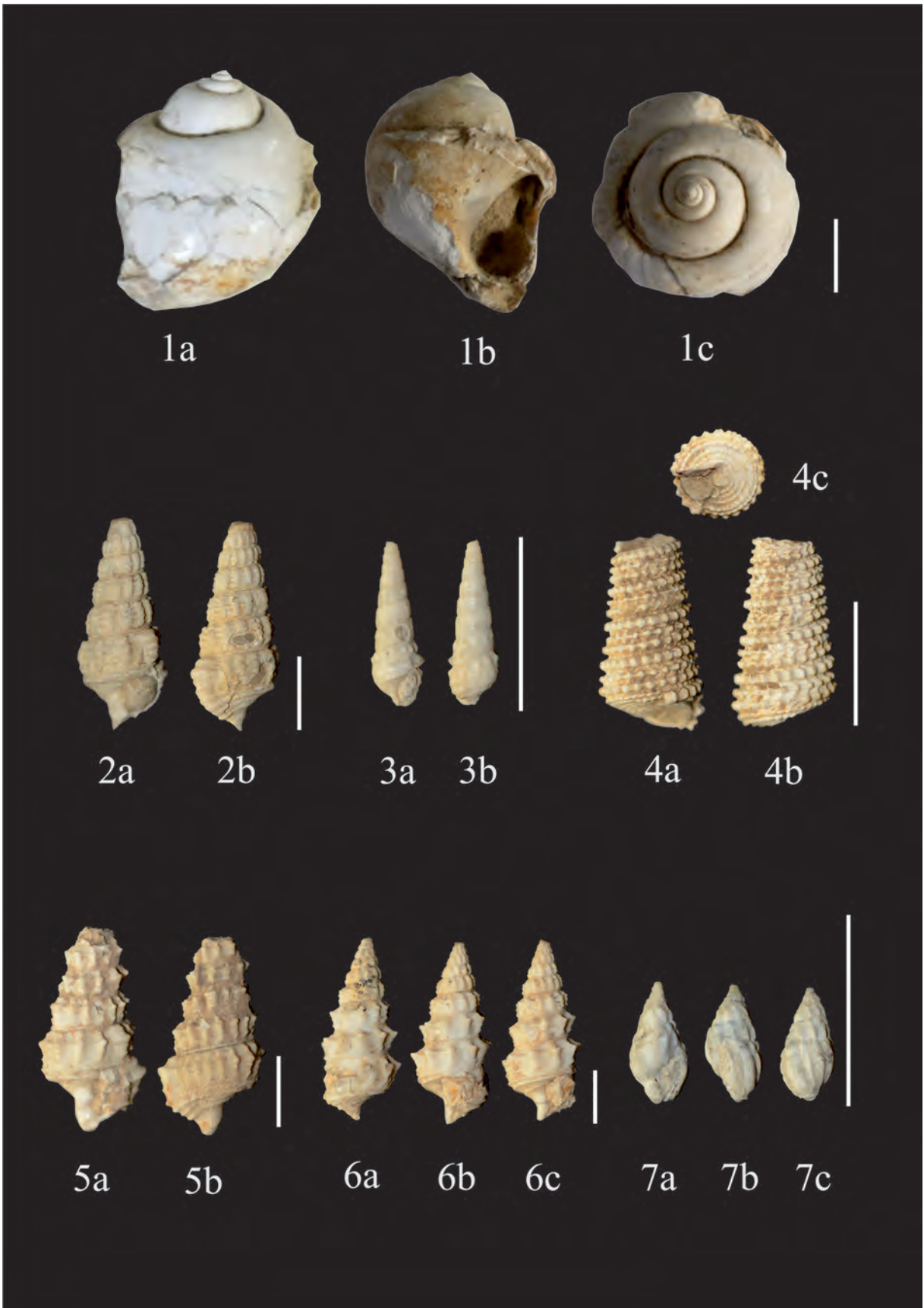


**PLATE II**

1a, b *Cardita rusticana* Mayer, 1899

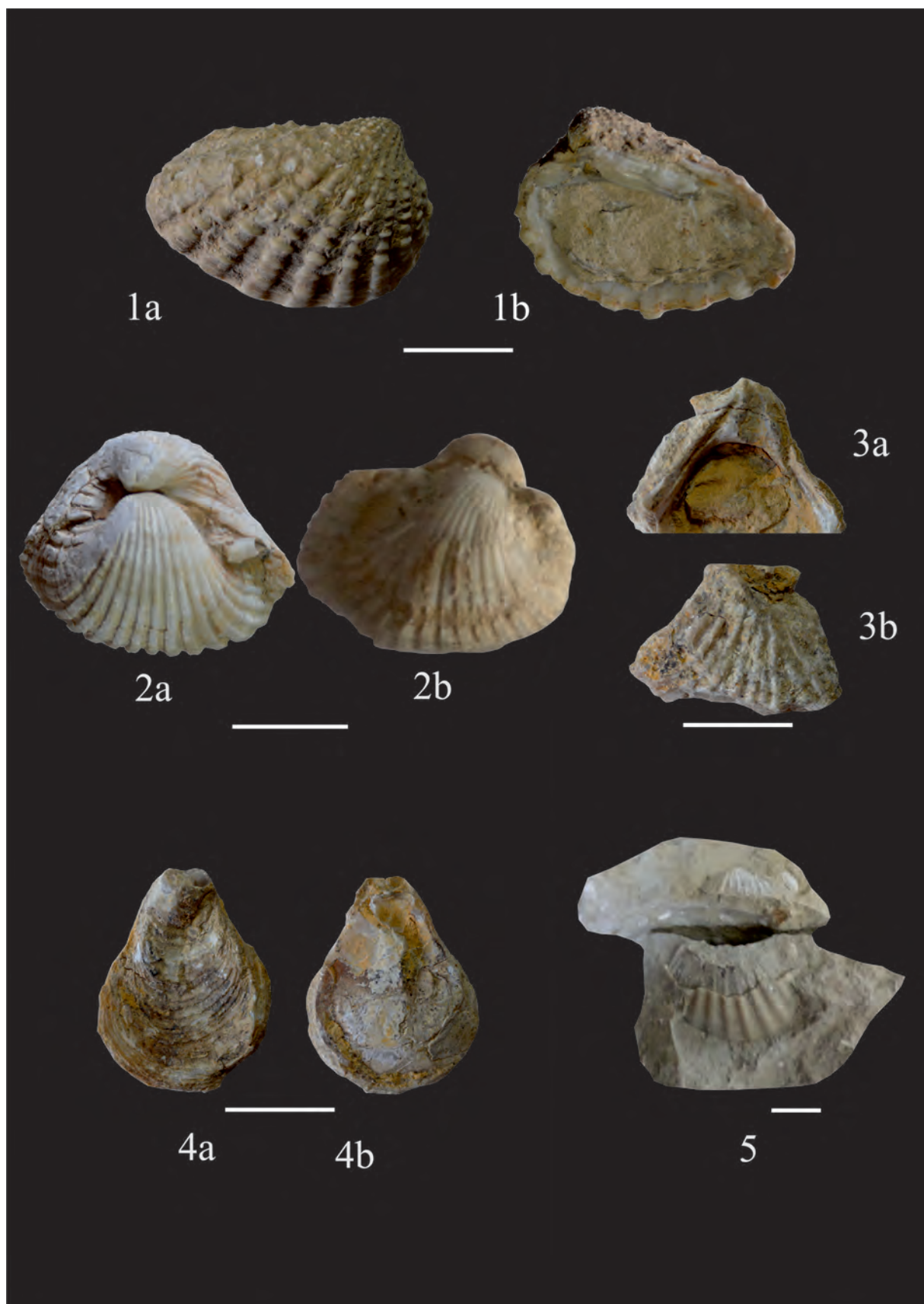
2a, b *Anadara aqutanica* Mayer, 1861

3a, b *Ostrea lamellosa* Brocchi, 1814

4a, b *Cubitostrea digitalina* Eichwald, 1830

5 *Chlamys* sp.

(The bars shows that 1 cm for each sample.)







# Bulletin of the Mineral Research and Exploration

<http://bulletin.mta.gov.tr>



## WHOLE ROCK GEOCHEMISTRY AND TECTONIC SETTING OF JURASSIC AGED LISAR GRANITE, TALESH MOUNTAINS, NORTH IRAN

Roghieh BOZORG SEGHINSARA<sup>a</sup>, Hossein SHEIKHI KARIZAKI<sup>a</sup>, Mohssen MOAZZEN<sup>b\*</sup>,  
Mohsen POURKERMANI<sup>a</sup> and Afshin ASHJA ARDALAN<sup>a</sup>

<sup>a</sup>Department of Geology, Azad Islamic University, North Tehran Branch, Tehran, Iran

<sup>b</sup>Department of Earth Sciences, University of Tabriz, 51664, Tabriz, Iran

<sup>b</sup>Tabriz Üniversitesi, Yer Bilimleri Bölümü, 51664, Tebriz, İran

Research Article

### Keywords:

A-type granite, Palaeotethys, Post-collision, Cimmerian, Talesh, North Iran.

### ABSTRACT

The Late Jurassic aged Lisar granite in North Iran is in tectonic contact of the form of thrust and strike slip faults with Upper Cretaceous sandy limestone and is covered by Paleogene polygenetic conglomerate in the Talesh Mountain at the western continuation of the Alborz range. The rock samples of the granite are pink coloured and coarse-grained with K-feldspar, quartz, plagioclase, biotite and amphibole. The Lisar granite is more likely emplaced in an extensional environment indicated with numerous space filling silica-rich aplitic veins in the rocks. The granite samples are moderately altered and feldspars are changed to sericite and clay minerals and biotite is partially converted to chlorite. The Lisar granite has derived from a high K magma and is A-type in nature, belonging to A<sub>2</sub> subgroup. The rock samples of granite are characterized by distinct negative Eu anomaly and a decrease from LREE to HREE contents. The parental melts of the granite were generated from partial melting of a lower continental crustal source with possible contribution from the mantle materials. The Lisar granite represents Cimmerian post-collision magmatism in north Iran following closure of Palaeotethys Ocean and subsequent collision.

Received Date: 02.08.2016

Accepted Date: 19.04.2017

## 1. Introduction

Palaeomagnetic studies show that Iran was a part of Gondwana up to Early Carboniferous (Muttoni et al., 2009). It separated from Gondwana and moved northward from Early Permian to Upper Triassic, when it collided with Turan plate. The Alborz range is taken to represent Palaeotethys suture in north Iran (Figure 1) formed by collision of the Turan and the Iranian plates in Upper Triassic. The Jurassic aged Lisar granite is located in North Iran within the Talesh mountain range. The Talesh Mountain range is a continuation of the Alborz range towards the west. Rock units considered by different researchers to mark the Palaeotethys suture in North Iran are accretionary units of the Mashhad area (Alavi, 1991; Majidi, 1991; Mirnejad et al., 2013; Shafaii Moghdam et al., 2015), Gorgan schists (Ghavidel et al., 2007; Delaloy et al., 1981), metamorphic rocks of the Gasht and Masuleh area (Clark et al., 1975) and Shanderman

eclogites (Zanchetta et al., 2009; Omrani et al., 2013). The Palaeotethys suture can be traced to the east to Afghanistan and China and towards the west into Turkey (Zhang et al., 2008). The Palaeotethys ocean closed 225 Ma ago which followed by uplifting of the Turan plate and emplacement of allochthonous nappes on the Iranian plate (Stampfli, 1993). Magmatic activities, especially granitoid magmatism, related to the Palaeotethys subduction are well documented along the suture in China. The magmatic arc at Yunnan area (southwestern Yunnan, China), with basaltic-andesitic to granodiorite composition has an age of 292- 282 Ma (Hennig et al., 2009). I-type and S-type granitoids of Hindu Kush in Afghanistan have ages of 210, 112 and 193 Ma, respectively (Debon et al., 1987). These granites with roughly Triassic age are traced westward into east of Iran, where the Binalud granites and granodiorites, dated 256 to 211 Ma (Majidi, 1978; Berberian and Berberian, 1981), are intruded into

\* Corresponding author: Mohssen MOAZZEN moazzen@tabrizu.ac.ir  
<http://dx.doi.org/10.19111/bulletinofmre.336499>

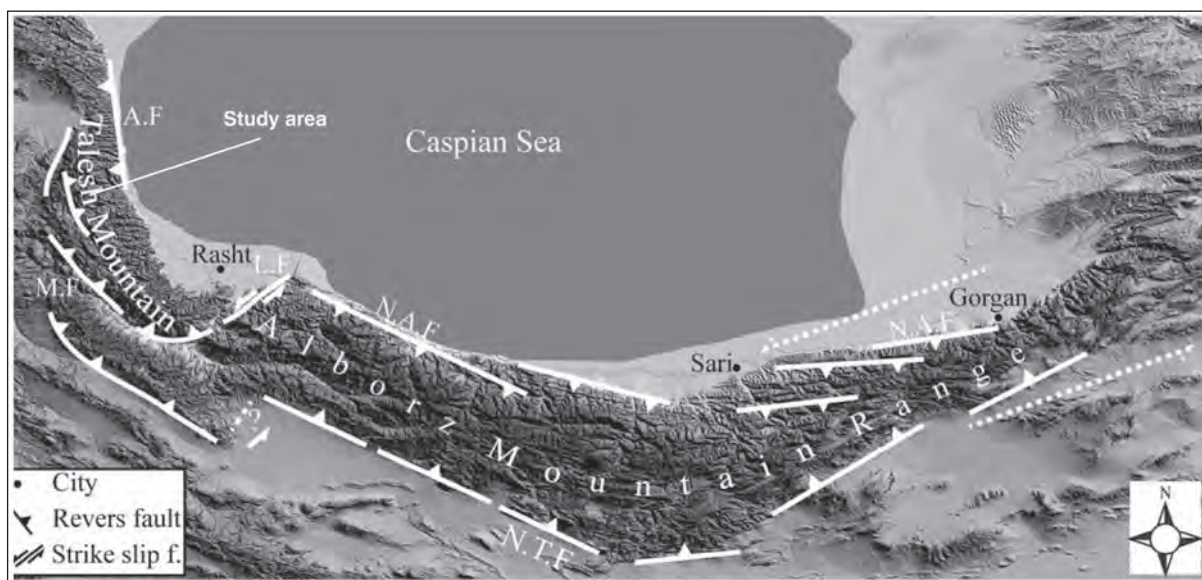


Figure 1- The location of the study area in Talesh Mountains at the west of Alborz range. AF: Astara Fault, MF: Masuleh Fault, LF: Lahijan Fault, NAF: North Alborz Fault, NTF: North Tehran Fault.

the Hercynian sediments. Boulin (1981) considered that they are a result of Palaeotethys subduction and collision. There are some traces of Palaeotethys along Baiburt-Sevanian terranes (Caucasus) (Gamkrelidze and Shengelia, 2007). Western Turkey is known as marking site of Palaeo- and Neotethys sutures. At the Karaburun Peninsula (west of Turkey), there are some granitoid intrusions with I-type affinity. They are 222-239 Ma old and are a result of Palaeotethys subduction (Erkül et al., 2008). The Palaeotethys suture is traceable towards the east at the Sakarya, Mersin and Karakaya areas (Moix et al., 2008). Stampfli and Kozur (2006) believe that Karakaya fore arc basin had formed due to northward subduction of Palaeotethys. Also, some researchers believe that Palaeotethys subduction is southward (Şengör, 1979, 1990; Jassim and Goff, 2006; Ruban et al., 2007).

Despite a wealth of knowledge on Palaeotethys-related magmatism towards the east and west of Iran, there are limited publications on possible Palaeotethys-related granitoid magmatism in Iran. The Jurassic aged Lisar granite is located to the north of the suture in north Iran. Geochemical data and age dating of this spatially important granitoid will furnish more information on Palaeotethys evolution in Iran. This paper presents the petrography and whole rock geochemistry of this granite to describe geochemical features of the granite in relation with petrological processes and tectonic setting.

## 2. Geological Background and Local Geology

The study area is located within the West Alborz-Azerbaijan geological unit of Iran. It comprises a part of the Talesh Mountain range which is bounded to the west by Astara fault and Caspian Sea depression. The Alborz range represents late Precambrian to Eocene sedimentary and volcanic strata, which are intruded by Palaeozoic to Tertiary plutons and dikes (Annells et al., 1975, 1977; Stöcklin, 1974; Axon et al., 2001). This range marks a collision belt and is bounded by reverse faults characterized by southward dipping faults in the north and northward dipping faults in the south. Therefore the Alborz belt is V-shaped in N-S sections (Figure 1). The evolution of the Alborz belt mainly occurred in the Cenozoic (Rezaeian et al., 2012). Opening and subsequent closure of the Neotethys along the Zagros Mountains and opening of the Red Sea had important effects on the structural evolution of the Alborz belt (Axen et al., 2001; Guest et al., 2006; Omrani et al., 2013). Collision of the Gondwana-derived blocks with Eurasia occurred in the Late Triassic, resulting in the Eo-Cimmerian deformation in North Iran, followed by a strong but poorly known Neo-Cimmerian compression event in Middle-Late Jurassic times that mainly affected Central Iran (Zanchi et al., 2009). Structural and seismological data for the Alborz Range show that deformation is partitioned along parallel thrusts and left lateral strike-slip faults (Jackson et al., 2002; Allen et al., 2003; Ritz et al., 2006). Talesh Mountain, west of the Alborz Range (Figure 1), consists of

metamorphic rocks, granitoids, mafic, ultramafic rocks and sedimentary rocks that have a wide range of ages from Palaeozoic to Tertiary.

The Lisar area is a part of the Talesh Mountain range. The oldest rock units in the Talesh Mountains are pelitic schists and ultramafic rocks with Carboniferous to Permian age, which are exposed to the south of the Lisar area (not shown on the map of figure 2 but are indicated in the cross section, figure 2). Upper Cretaceous strata are andesite, dacite and tuffs, occasionally interlayered with shale and grey limestone. The finely laminated shales are dark and contain carbonaceous materials. Calcareous sandstone is other rock type in the Upper Cretaceous unit. The lowermost strata of the Paleogene units are made of a polygenetic conglomerate with Upper Cretaceous andesite, dacite, shale, limestone and some mafic volcanic rock fragments. It also contains pink-colour fragments of the Lisar granite (Figure 3a). This conglomerate is overlaying by andesitic tuffs, lava and brecciated lava. The dark limestone is cut by late light calcite veins. Veins also are found in Paleogene andesitic lavas. The andesitic lavas show megaporphyritic texture (with large plagioclase crystals) occasionally (Figure 3b). These rocks contain fragments of Lisar granite as xenoliths. The Neogene unit is mainly made of a polygenetic conglomerate

and intercalated marl but the variation of fragment types is limited to limestone and volcanic fragments. In some parts it is consisted only from volcanic rock fragments (Figure 3c).

The Lisar granite appears as three separated outcrops (Asadian, 1999, Figure 2). It is emplaced and/or displaced along a north-south trending faults. Owing to very dense vegetation and soil coverage, it is not easy to determine the contacts of the granite, but it is in tectonic contact (strike slip fault) with Upper Cretaceous sandy limestone to the west and is covered by Palaogene polygenetic conglomerate to the east. This granite appears as medium- to coarse-grained and pink coloured. K-feldspar, plagioclase, amphibole and quartz are visible in hand specimens. The granite samples appear as fresh rocks in the field which are hard to break by hammer. The Lisar granite appears as two distinct types in the field, the lighter granite and the darker one. The only difference is in the modal percentage of ferromagnetic minerals (mainly amphibole, see petrography section below). Microgranular mafic enclaves, which are similar to the main granite in mineralogy, can be seen in the field (Figure 3d). These are taken to represent rapidly cooled, fine-grained walls of the pluton, which are entered the solidifying magma. In some parts the Lisar granite is very fine-grained and appears with aplitic

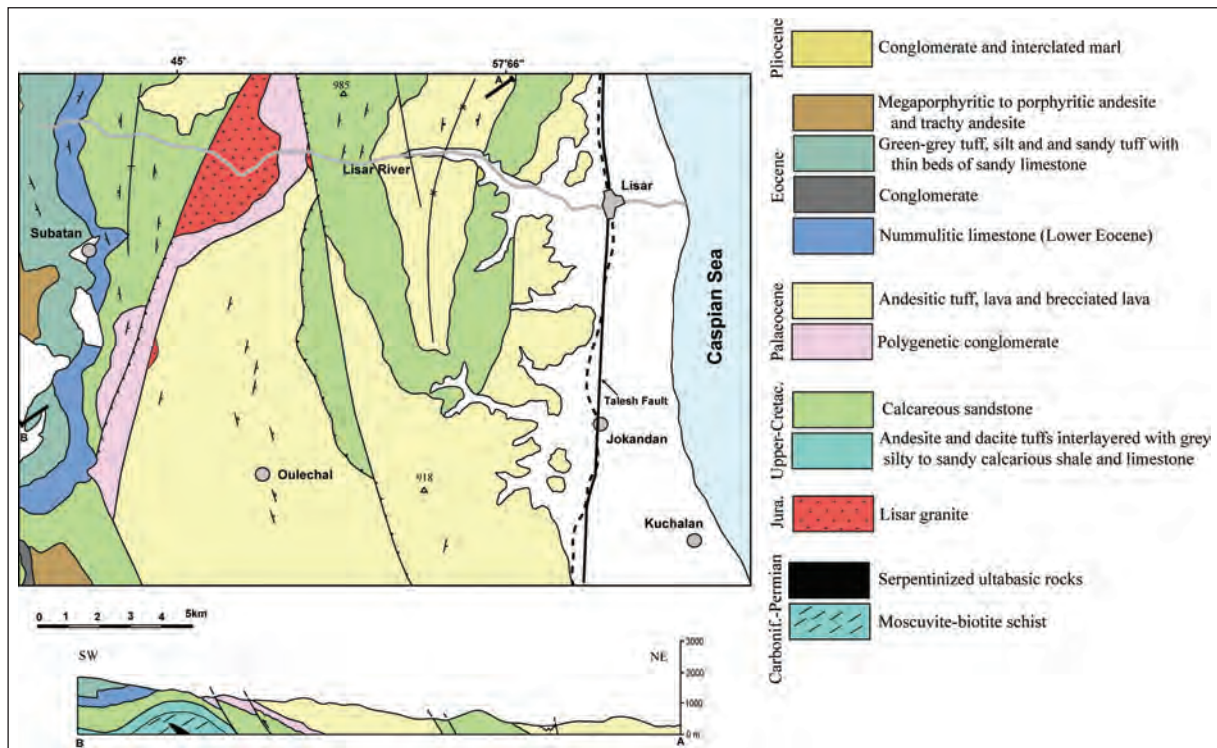


Figure 2- Simplified geological map of the Lisar area adapted from the 1:100000 scale geological map of Khalkhal (Asadian, 1999).

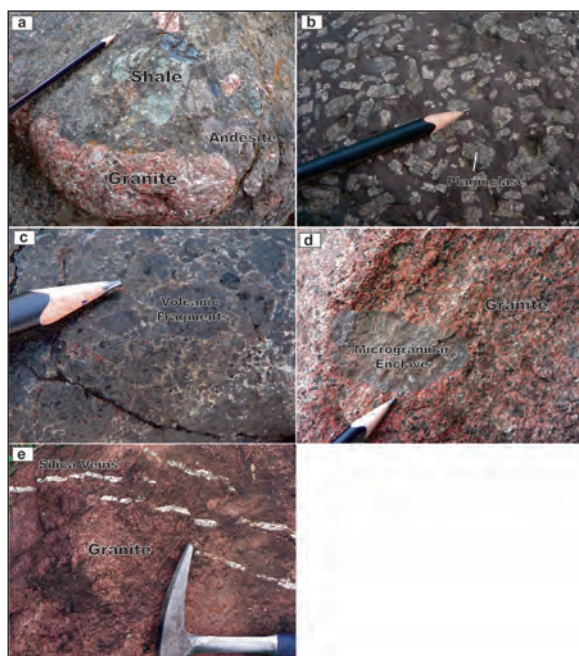


Figure 3- a) Paleogene conglomerate with Upper Cretaceous andesite, dacite, shale, limestone and some mafic volcanic rock, and Lisar granite fragments. b) Relatively large plagioclase in andesitic lavas. c) Neogene conglomerate consisted only from volcanic rock fragments. d) Microgranular dark enclaves, similar to the main granite in mineralogy within the main granite. e) Parallel silica veins in the Lisar granite showing an extensional regime during its emplacement.

texture. Parallel silica-rich aplitic veins in the Lisar granite (Figure 3e) point to extensional regime during emplacement of the granite and the later veins.

### 3. Study Methods

To study the Lisar granite, several rock samples were collected from the granite and the associated rocks. 60 thin sections were made from these rocks. Petrography studies were carried out by mineral composition and textural description of the samples. In order to study the geochemical features of the Lisar granite, 11 optically well-defined representative samples among 60 investigated samples under the microscope were chosen for chemical analysis. These samples had the lowest alteration effects. The samples were crashed and pulverized by ZPS Ltd. in Tabriz, Iran. About 1 kg of each sample was crashed using a steel jaw crusher and then was pulverized to 200 mesh or 75 micron. ~ 50 gr of each sample was packed in suitable plastic bags and were sent to Activation Laboratories in Ancaster, Canada for analysis. To analyse the samples for major, minor and trace

elements, known amount of sample was mixed with lithium metaborate and were fused on gas heater. The resulted beads were used for XRF analysis of major oxides. They used for ICP-MS analyses after digestion in acid and needed dilution. International standards were used for calibrations. The uncertainties for major oxides is better than  $\pm 2\%$  and for the minor and trace elements is better than 5%.

### 4. Petrography

The Lisar granite is red to pink in colour and appears as very hard rock in the field. However microscopic studies show that minerals, mainly feldspar, are altered. The rocks have different amphibole contents and are as relatively darker (with relatively more amphibole) and lighter (with relatively lower amphibole) granites. Except for amphibole content, there is no difference in mineralogy of these two types of granites under the microscope. The major minerals in the Lisar granite are K-feldspar (perthite and orthoclase), quartz, plagioclase (albite to oligoclase, based on optical properties), amphibole and biotite. The minor phases are zircon, apatite, titanite and opaque minerals. Chlorite (after biotite), sericite (after K-feldspar) and clay minerals (after plagioclase) are alteration products. The main textures are granular, perthite, poikilitic and intergrowth micrographic textures (Figure 4). Quartz appears as xenomorphic crystals and micrographic texture appears at the margin of large plagioclase crystals. Amphiboles are dark green to brown pleochroic hornblende, which occurs as crystals among other minerals and as inclusions in large perthitic K-feldspar. Amphibole crystals show accumulation in some parts of the rock resembling cumulate texture. Biotite, which is less abundant than hornblende, is altered to chlorite along cleavage. The granophyre texture in some samples points to eutectic crystallization of quartz and feldspar in these rocks. Some samples from the Lisar granite show slight deformation and also cataclastic textures. Small crushed crystals of quartz can be seen along with larger quartz crystals in the samples with cataclastic texture. Estimation of mineral modal percentages was made by investigation of thin sections under the microscope and plagioclase, K-feldspar and quartz contents were plotted on Streckeisen diagram (Figure 5). All samples are granite according to this diagram.

The Lisar granite samples are very similar to some A-type granites in the world such as Krajaa granite in Finland (Juravanen et al., 2005), Gebel Musa A-type

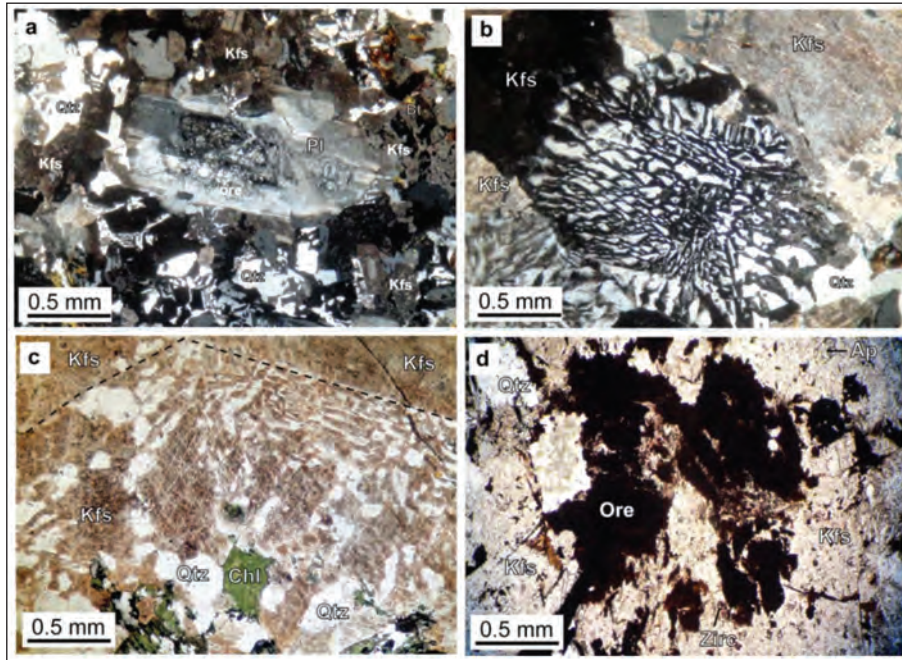


Figure 4- Petrographical features of the Lisar granite a) K-feldspar, plagioclase and quartz are the main mineral phases in the Lisar granite. b) Graphic texture in the Lisar sample. c) K-feldspar as the main mineral and d) Apatite and opaque minerals in the rock.

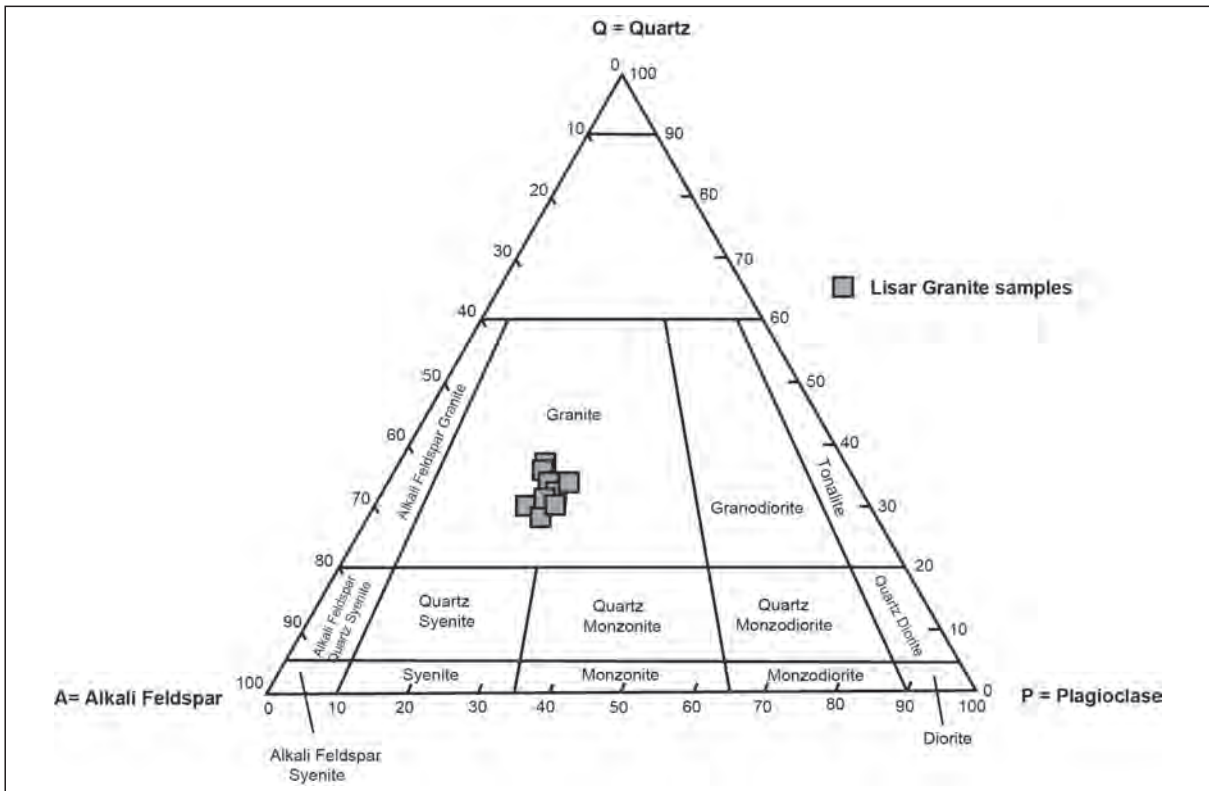


Figure 5- Streckeisen diagram for the studied samples indicating granite mineral composition for the rocks.

granite from Egypt (Katzir et al., 2006), pink A-type granites from Rajasthan, India (Kaur et al., 2007) and Mianning A-type granite from south China (Huang et al., 2008). All these A-type granites are formed from predominant K-feldspar (mainly as perthite), quartz and subordinate amounts of plagioclase. They may contain biotite and hornblende. The Lisar granite is K-rich, therefore Na-rich phases such as Na-amphibole (e.g. riebeckite) are not present in the samples.

## 5. Whole Rock Geochemistry

Table 1 includes the major oxide contents and normative mineralogical composition and table 2 contains the minor and trace element contents of the analysed samples.

All samples from Lisar granite plot in the granite and alkali granite fields on the plot of De La Roche et al. (1980) (Figure 6a). On diagram of Th versus Co

(after Hastie et al., 2007), the analysed samples show high K calc-alkaline and shoshonitic nature for the original magma (Figure 6b).

The parental magma had high K content (Figure 6b, Hastie et al., 2007), was either I or A-type (Figure 6c) and mainly of metaluminous to peraluminous nature (Figure 6d). The samples are ferroan and mainly alkaline on the diagrams of Frost et al. (2001) (Figure 7). The Lisar granite has A-Type geochemical feature, such as high Ga/Al ratios, elevated concentration of HFSE (e.g. Zr, Nb and Y), low CaO, MgO, Cr, Co, Ni, Sr and Eu contents as compared to S- and I-type granitoids (Whalen et al., 1987; Eby, 1990; Frost et al., 2001). Using Whalen et al. (1987) diagrams (Figure 8), an A-type affinity is evident for the studied samples. On REE diagram normalized to chondrite values (Figure 9a), Lisar granite samples show a distinct negative Eu anomaly. A decrease from LREE content to HREE content is visible. These features

Table 1- Major oxides and CIPW norm mineral composition of Lisar granite samples.

Sample	RB4	RB39	RB12	RB5B	RB8	RB6	RB13	RB20	RB9	RB38	RB7
Major Oxides wt%											
SiO <sub>2</sub>	72.08	71.78	72.13	65.95	67.93	66.72	65.87	64.41	64.85	67.77	68.11
TiO <sub>2</sub>	0.33	0.31	0.42	0.60	0.71	0.67	0.62	0.65	0.71	0.52	0.64
Al <sub>2</sub> O <sub>3</sub>	12.9	12.21	12.46	13.92	14.05	13.96	13.85	13.96	13.73	14.32	13.98
Fe <sub>2</sub> O <sub>3</sub> <sup>T</sup>	2.54	2.33	2.74	5.17	5.38	5.27	5.19	5.39	5.28	3.68	3.49
MnO	0.04	0.04	0.05	0.11	0.11	0.10	0.10	0.12	0.11	0.06	0.05
MgO	0.13	0.11	0.13	0.42	0.54	0.63	0.48	0.64	0.71	0.49	0.53
CaO	0.64	0.69	0.66	1.78	1.63	1.53	1.86	2.58	2.62	1.34	1.22
Na <sub>2</sub> O	3.48	3.75	3.46	4.65	4.13	4.39	4.58	3.79	4.01	4.04	4.12
K <sub>2</sub> O	5.25	5.86	5.38	3.8	3.58	3.73	3.66	3.92	3.88	4.69	4.87
P <sub>2</sub> O <sub>5</sub>	0.03	0.04	0.04	0.14	0.14	0.11	0.12	0.18	0.17	0.14	0.15
LOI	1.29	1.64	1.71	1.8	1.84	1.69	1.74	3.03	3.16	1.78	1.86
Total	98.71	98.76	99.18	98.34	100.04	98.80	98.07	98.67	99.23	98.83	99.02
CIPW Norm, wt%											
Quartz	30.264	27.049	30.013	20.752	26.303	23.002	21.296	21.846	21.321	23.114	22.526
Corundum	0.400	0.00	0.00	0.00	0.752	0.182	0.00	0.00	0.00	0.496	0.072
Orthoclase	31.026	34.631	31.794	22.451	21.157	22.043	21.629	23.166	22.930	27.716	28.780
Albite	29.447	30.177	29.278	39.347	34.947	37.147	38.755	32.070	33.932	34.185	34.862
Anorthite	2.979	0.00	2.577	5.886	7.172	6.872	6.422	9.501	8.004	5.733	5.073
Hypersthene	0.324	0.00	0.324	0.916	1.345	1.569	1.102	1.479	1.101	1.230	1.320
Ilmenite	0.077	0.094	0.105	0.231	0.242	0.218	0.220	0.259	0.242	0.139	0.111
Hematite	2.540	2.857	2.740	5.170	5.380	5.270	5.190	5.390	5.280	3.680	3.490
Titanite	0.00	0.630	0.307	1.177	0.00	0.00	1.242	1.271	1.433	0.00	0.00
Rutile	0.286	0.00	0.235	0.00	0.584	0.550	0.00	0.00	0.00	0.443	0.580
Apatite	0.071	0.095	0.095	0.332	0.332	0.261	0.284	0.426	0.403	0.332	0.355
Total	97.414	97.123	97.467	96.548	98.213	97.114	96.343	95.656	96.085	97.059	97.169

Table 2- Rare earth and trace elements contents of the studied samples (all in ppm).

Sample	RB4	RB39	RB12	RB5B	RB8	RB6	RB13	RB20	RB9	RB38	RB7
Sc	3	4	4	11	9	11	8	11	11	8	10
Be	4	3	4	3	2	3	2	3	2	3	2
V	17	15	15	25	27	25	26	32	30	30	28
Ba	558	633	537	592	612	588	603	685	703	730	741
Sr	47	42	44	106	98	95	111	102	106	110	112
Y	62	69	65	63	65	64	63	56	58	49	46
Zr	430	455	415	416	427	420	423	302	312	416	420
Co	2	1	1	4	3	3	1	6	4	4	4
Cu	70	112	86	70	68	75	91	170	166	60	57
Zn	40	61	52	90	94	98	87	100	98	60	69
Ga	20	18	21	21	17	19	22	21	20	20	21
Ge	2	1	1	2	1	1	1	2	2	1	1
Rb	209	212	227	126	119	123	115	141	139	151	158
Nb	15	13	15	22	25	23	25	18	17	19	18
Mo	4	5	4	4	5	4	5	5	4	2	2
Ag	1	0.7	0.8	0.5	0.4	0.7	0.6	<0.5	<0.5	<0.5	<0.5
Sn	9	8	11	6	7	12	8	8	7	7	9
Sb	<0.5	<0.5	<0.5	0.6	0.7	0.6	<0.5	1.2	1.1	0.7	0.6
Cs	3.4	4.1	3.7	2	2	2	1	2.6	2.5	3.6	3.4
La	65.9	64.6	65.4	51.5	55.4	52.7	51.9	56.3	55.8	51.2	52.3
Pr	13.1	14.3	12.5	11.9	12.1	11.8	12.2	11.7	11.8	11.1	11.2
Nd	44.8	45.69	44.6	45.6	45.7	46.1	45.4	44.9	50.6	41.8	40.9
Sm	9	8	8	9.9	9.6	9.8	9.6	9.3	9.1	8.8	8.9
Eu	0.61	0.77	0.69	1.92	1.89	1.97	1.93	1.61	1.48	1.44	1.28
Gd	8.2	8.1	7.8	10.1	10.8	10.4	10.2	8.7	8.6	8.4	8.3
Tb	1.5	1.6	1.4	1.8	1.7	1.8	1.8	1.5	1.3	1.4	1.3
Dy	10.3	10.2	10.7	11.1	11.4	11.3	11.1	9.7	9.8	9	8
Ho	2.2	3.1	2.8	2.3	2.4	2.4	2.5	2	2	1.8	1.8
Er	6.6	6.4	6.3	6.9	6.3	6.8	6.9	5.9	5.3	5.3	5.7
Tm	1.07	1.12	1.23	1.06	1.07	1.12	1.08	0.9	0.7	0.81	0.82
Yb	7.4	8.1	7.3	7	8	7	7	6	6	5.6	5.9
Lu	1.11	1.09	1.16	1.06	1.07	1.06	1.06	0.95	0.91	0.84	0.79
Hf	11.6	10.8	11.2	8	9.1	8.3	8.1	5.8	5.7	7.7	7.5
Ta	1.7	1.6	1.4	1.7	1.8	1.8	1.8	1.4	1.2	1.4	1.3
W	2	4	2	1	4	3	3	3	3	<1	<1
Tl	0.6	0.5	0.6	0.5	0.5	0.4	0.5	0.5	0.4	0.5	0.4
Pb	18	17	18	19	17	19	18	24	25	14	15
Th	24.9	25.2	24.6	13.1	13.3	13.3	13.1	15.4	15.1	15.6	15.4
U	6.3	6.5	6.3	3.5	3.7	3.4	3.7	3.2	3.3	1.8	1.9

are characteristic of A-type granites (e.g. Obnäs rapakivi A-type granite from Finland, Jurvanen et al., 2005). Lisar samples have low Nb (13–25 ppm), high Sr (42–112 ppm) and moderate Rb (115–227 ppm) concentrations. The chondrite-normalized REE diagram (Figure 9a) shows that the Lisar samples are LREE enriched with a flat HREE and negative Eu anomaly. This indicates the removal of plagioclase by fractional crystallization. Negative anomalies in Ba, Sr, and Eu, as shown in the primitive mantle-normalized trace element and REE diagrams (Figure 9b), testifies for fractional crystallization of feldspar while Nb, Ta, Zr and Hf are not depleted, implying

little contribution of subduction-related components in the magma source of Lisar granite. The depletion of Ti coupled with high Nb and Ta concentrations suggests crystallization of Fe-Ti oxides as the main Ti-bearing phase, with little influence of rutile or titanite. Rutile and titanite usually have high concentrations of Nb and Ta (Manning and Bohlen 1991; McDonough 1991; Green 1995; Rudnick et al. 2000; Foley et al. 2002). Ilmenite usually has much lower Nb and Ta (Ding et al. 2009). Therefore, crystallization of Fe-Ti oxide (more likely ilmenite) consumed Ti, leading to depletion of Ti in the resulted granite without significant decrease of Nb and Ta. The decrease in Sr

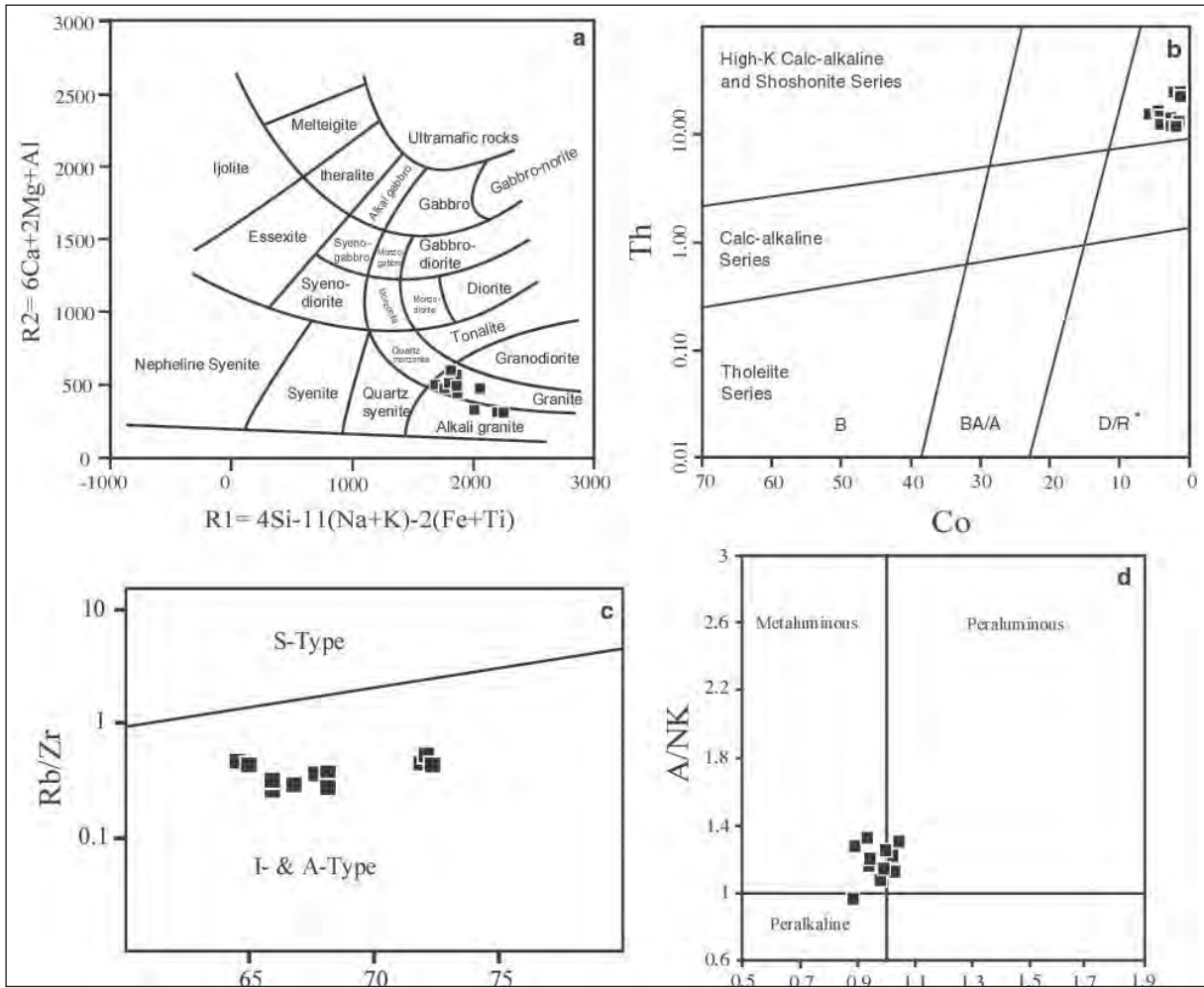


Figure 6- a) Classification of granites according to De La Roche et al. (1980). The samples plot in the granite and alkali granite fields. b) Th vs. Co diagram of Hastie et al. (2007) indicates high K calc-alkaline magma for the Lisar granite. c) The studied rocks have either I or A-type nature. d) The original magma had metaluminous to peraluminous characteristic on A/NK versus ASI diagram.

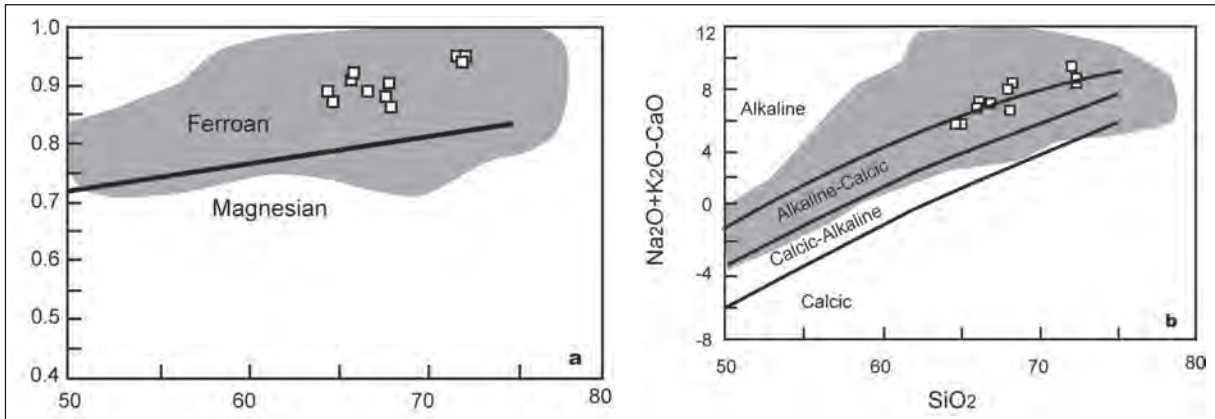


Figure 7- Ferroan (a) and mainly alkaline nature (b) for the Lisar samples on the diagrams from Frost et al. (2001).

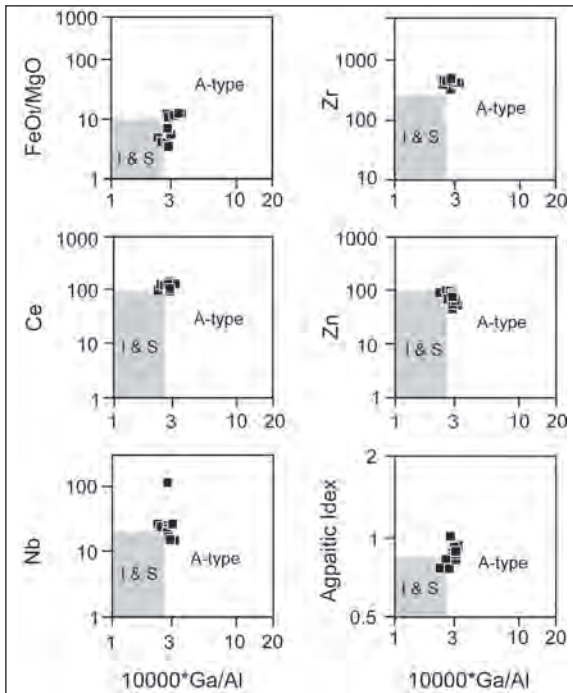


Figure 8- Determination of granite type according to trace elements and apatitic index (Whalen et al., 1987). The Lisar granite is A-type according to these diagrams.

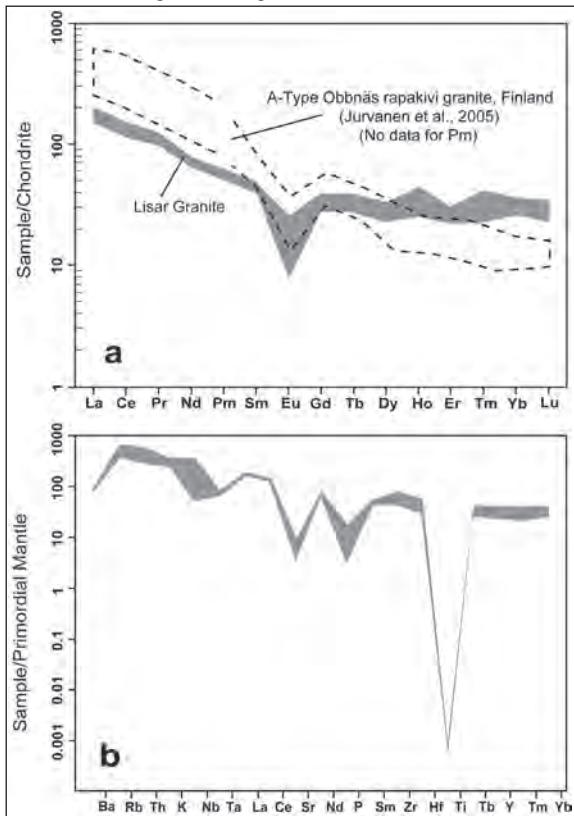


Figure 9- a) Trace elements contents of the studied samples normalized to chondrite (normalizing values from Sun and McDonough, 1989). Trace element pattern for Obbnäs rapakivi granite (Jurvanen et al., 2005) is provided for comparison. b) Element content normalized to primordial mantle. Distinct Eu, Ti, P and Sr is obvious.

and Ba and slight increase in Rb with increasing  $\text{SiO}_2$  may also be due to plagioclase fractionation (Figure 10).

Based on the trace element contents of the rocks, amphibole and plagioclase crystallization was the main factor controlling the rock composition and fractional crystallization. According to Watson and Harrison (1984) the amount of dissolved phosphorus (and Zr) can be used to estimate the granitic magma crystallization temperature. Apatite was found as small needle-like inclusions in other minerals in the

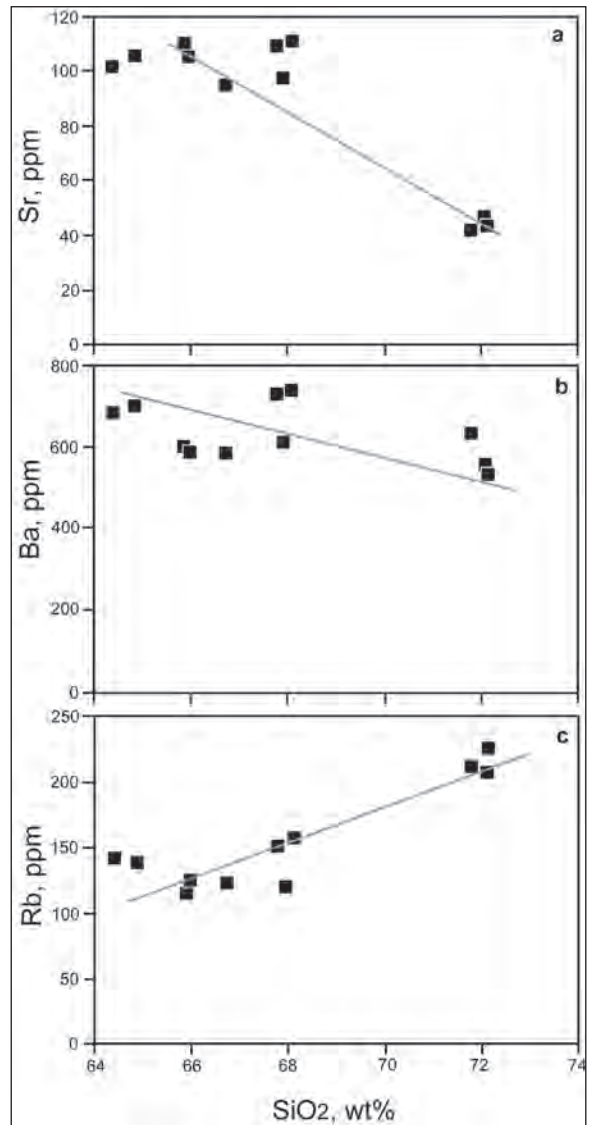


Figure 10- Variation diagrams for Sr, Ba and Rb versus  $\text{SiO}_2$  for the Lisar samples. Decreasing of Sr and Ba and slight increasing of Rb contents are in agreement with plagioclase fractionation as a controlling factor in the Lisar granite generation.

Lisar granite. According to  $P_2O_5$  versus  $SiO_2$  diagram of Watson and Harrison (1984), The Lisar granite was crystallized at temperatures about 800 to 900°C (Figure 11). These temperatures are close to liquidus temperatures estimated for A-type melts at 5 kbar (Shkodzinsky, 1985). Some samples with lower temperatures on this diagram may show samples with low modal apatite content. Nb-Y-3Ga triangular diagram of Eby (1992) shows that the studied samples are of  $A_2$  subgroup (Figure 12). On the discrimination diagrams of Pearce (1996) Lisar samples fall in the within plate granites (Figure 13a). On  $SiO_2$  versus  $Al_2O_3$  diagram of Maniar and Piccolli (1989) the samples plot mainly in the post orogenic field (Figure 13b).

## 6. Discussion

A-type granites occur in diverse tectonic settings including oceanic islands, continental rifts, extensional parts of the continental crust, stable continental crust and post orogenic environment. These type of granite may form as non-orogenic (during continental rifting) and post-orogenic intrusions during extensional régime (Sylvester, 1989). Therefore two main types of A-type granites are non-orogenic and post-orogenic granites. Post orogenic granites tend to have more crustal components.  $A_1$  subgroup of A-type granites (Eby, 1992) are similar to oceanic island rocks in overall composition, while  $A_2$  subgroup are similar to average of composition of oceanic rocks and mean crustal composition.  $A_1$  subgroup occurs mainly during rifting within the plates and is usually accompanied by mafic rocks as a result of plume or hot spot activities,

while  $A_2$  subgroup represents post-collision events (Eby, 1992).

Different possibilities for generation of A-type granitic melts are proposed. Some are summarized below. Re-melting of granitic melts containing quartz, plagioclase and K-feldspar, which have experienced at least one melting event already (Collins et al., 1982; Clemens et al., 1986; Whalen et al., 1987) is a possible source for A-type granitic melts. This possibility is argued by Creaser et al. (1991) and Landenberger and Collins (1996). Partial melting of dehydrated lower crust, resulted as residua from fractionation of I-type magma at temperatures exceeding 900°C in a subduction-related environment (Landenberger and Collins, 1996) is proposed instead. However Creaser et al. (1991) stated that partial melting of such a residua cannot provide chemical features of A-type granites. They proposed partial melting of tonalitic to granodioritic crust for generation of A-type granitic magma. Taylor et al. (1981) and Harris et al. (1986) consider the per-alkaline nature of non-orogenic A-type granites as a result of  $CO_2$  and halogen-rich fluid metasomatism during emplacement or later events. Whalen et al. (1987) believe that highly dehydrated alkaline phase and low  $CO_2$  content of these types of rocks is in contradiction with this hypothesis. As it is evident there is not a consensus for the origin of A-type granite magmas but some observations on Yb/Ta and Y/Nb ratios for A-type granites (White Mountain, Eby, 1992) show that they are related to silica under saturated mafic rocks. These mafic rocks can be directly related to silica-rich highly fractionated rocks (A-type granites). This may

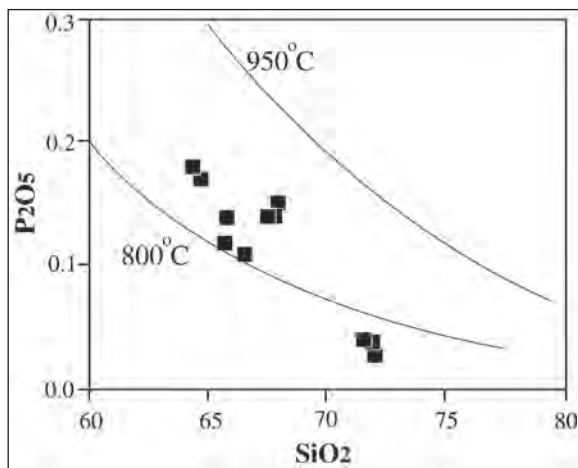


Figure 11- According to  $P_2O_5$  versus  $SiO_2$  diagram of Watson and Harrison (1984), The Lisar granite was crystallized at temperatures about 800 to 900°C.

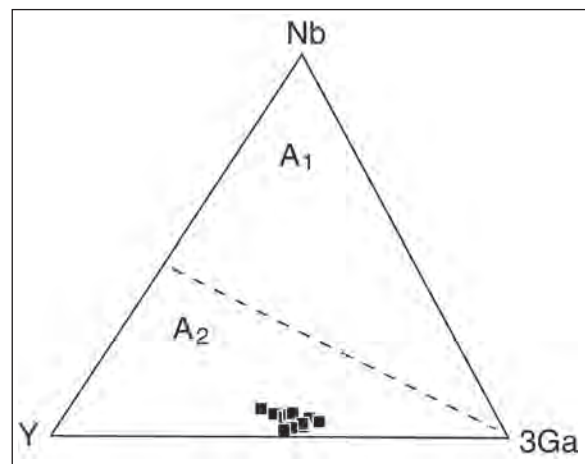


Figure 12- Nb-Y-3Ga triangular diagram to distinguish  $A_1$  from  $A_2$  granites (Eby, 1992). The studied samples are of  $A_2$  subgroup.

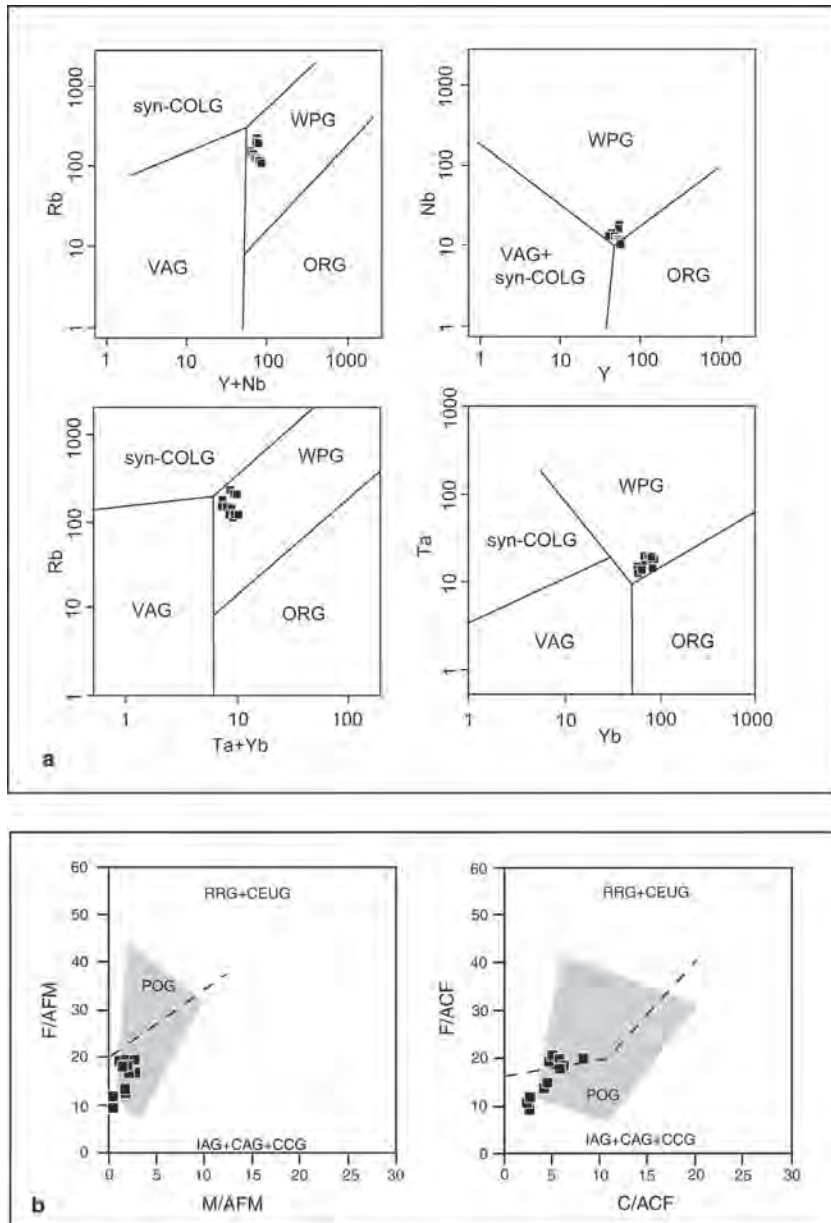


Figure 13- a) Within plate nature for the studied samples on discrimination diagrams of Pearce et al. (1984). b) Diagrams of Maniar and Piccolli indicate a post-collision setting for the Lisar granite.

testify to mantle origin for at least some of the A-type granites.

It is difficult to consider a single source as origin for the Lisar granite magma unequivocally. Some chemical features of Lisar granites show that they could have been originated from a crustal source, which may have been affected by the mantle materials (e.g. Ce/Pb versus MgO content, Figure 14). The studied samples show high SiO<sub>2</sub> (>64 wt%) and low MgO (<0.71 wt%) and TiO<sub>2</sub> (<0.31 wt%) concentrations. This suggests

that the original magma was not directly derived from a mantle source. There are not mafic or intermediate igneous rocks contemporarily associated with the Lisar granite. This, rules out its formation from a directly mantle-derived magma. Since extensive fractional crystallization (Peccerillo et al., 2003; Shellnutt et al., 2009) generates considerable amounts of mafic rocks, which is not the case for the Lisar granite. Mafic volcanic rocks of the area are much younger than Lisar granite. Major and trace element contents of the studied samples are more compatible with a lower

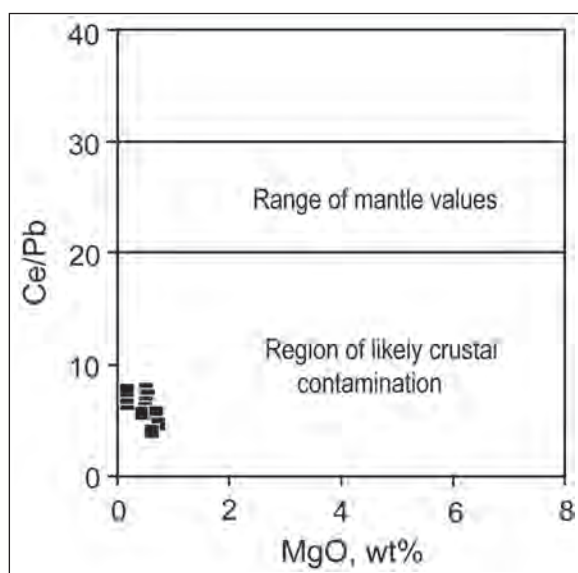


Figure 14- Ce/Pb versus MgO diagram for the studied rocks which shows crustal materials contribution in genesis of Lisar granite magma.

continental crust origin with possible some limited mantle source contribution for this granite.

Bonin (2007) considers some geochemical characteristics for A-type granites. This granites have  $Zr+Nb+Ce+Y>350$ . The sum of these trace elements is above 376 ppm for all samples from the Lisar granite. According to Bonin (2007) Y/Nb ratio for  $A_1$  subgroup is  $<1.2$  while it is  $>1.2$  for  $A_2$  subgroup. This ratio for the Lisar granite is 2.52 to 5.31, compatible with  $A_2$  subgroup. In terms of tectonic environment, considering the studied granite of  $A_2$  subgroup, it is formed more likely in an extensional post-orogenic setting. This is verified by the field observations (parallel veins within the granite) and chemical properties. Recently Madanipour et al. (2015) dated one sample of Lisar granite (U/Pb on zircon) and reported a  $179\pm 18$  Ma concordia age. This age is corresponding to Late Jurassic. Therefore Lisar granite represents Cimmerian post-collision magmatism in north Iran following closure of Palaeotethys ocean and subsequent collision.

## Conclusions

Most researchers believe that the continuation of the Palaeotethys suture from China into west Turkey can be traced in North Iran along the Alborz Mountains (Alavi, 1991; Omrani et al., 2013, Shafaii Moghadam et al., 2015). This opinion is debated and other researchers consider the continuation of Palaeotethys to the north and outside of the Iranian crust (Zanchetta

et al., 2009). Study of Palaeotethys ophiolites and high pressure rocks (eclogites and blueschists) helps to work out the location of this suture in northern Iran (Zanchetta et al., 2009; Omrani et al., 2013; Shafaii Moghadam et al., 2015). Granitoids play an important role in this regard and study of granitoid plutons at different tectonic settings can help to reconstruct the geodynamic evolution of the Palaeotethys Ocean (Majidi, 1975; Debon et al., 1987; Erkiil et al., 2008; Hennig et al., 2009). In the Talesh Mountain at the western continuation of the Alborz range, the Lisar granite occurs with tectonic contacts with Upper Cretaceous sandy limestone, which is covered by Paleogene polygenetic conglomerate. Based on petrography studies the main minerals are abundant coarse-gained K-feldspar, quartz, plagioclase, biotite and amphibole. This proposes A-type for the Lisar granite. Based on whole rock geochemistry, the Lisar granite has derived from a high K magma and is A-type in nature, belonging to  $A_2$  subgroup. The samples are characterized by negative Eu anomaly and a decrease from LREE to HREE contents. More likely the original magma forming the Lisar granite generated from partial melting of a lower continental crustal source with possible contribution from the mantle materials. Considering the already published age of Late Jurassic for the Lisar granite by Madanipour et al. (2015) using U/Pb method on zircon, this granite represents Cimmerian post-collision magmatism in north Iran following closure of Palaeotethys Ocean and subsequent collision.

## Acknowledgements

We would like to thank kind people of Lavandaville village for their hospitality during our field works and our stay in north Iran. Mrs. Nassrin R. Saadat form ZPS Ltd. Iran is acknowledged for her helps with analyses arrangement. Generous helps from Cahit Dönmez and Taner Ünlü during preparation of the manuscript are highly appreciated. We are grateful to Dr. Mehmet Arslan and an anonymous reviewer for their perceptive reviews and detailed comments.

## References

- Alavi, M. 1991. Sedimentary and Structural characteristics of the Paleo-Tethys remnants in northeastern Iran. Geological Society of America Bulletin 103, 983-992.
- Allen, M.B., Ghassemi, M.R., Shahrabi, M., Qorashi, M. 2003. Accommodation of late Cenozoic shortening in the Alborz range, northern Iran. Journal of Structural Geology 25, 659-672.

- Annells, R.N., Arthurton, R.S., Bazley, R.A., Davies, R.G. 1975. Explanatory text of the Qazvin and Rasht quadrangles map: Tehran, Geological Survey of Iran, 94 p.
- Annells, R.N., Arthurton, R.S., Bazley, R.A., Davies, R.G., Hamed, M.A.R., Rahimzadeh, F. 1977. Geological map of Iran, Shakran sheet 6162: Geological Survey of Iran, scale 1:100 000.
- Asadian, O. 1999. Geological map of Khalkhal, 1:100000. Geological Survey of Iran.
- Axen, G. J., Patrick, S.L., Marty, G., Stockli, D., F., Hassanzadeh, J. 2001. Exhumation of the west-central Alborz Mountains, Iran, Caspian subsidence, and collision-related tectonics. *Geology* 29.6, 559-562.
- Berberian, F., Berberian, M. 1981. Tectono-plutonic episodes in Iran. In: H. Gupta and F. Delany (Editors), *Zagros- Hindu Kush-Himalaya Geodynamic Evolution*. American Geophysical Union, *Geodynamic Series* 3, 5-32.
- Bonin, B. 2007. A-type granites and related rocks: evolution of a concept, problems and prospects. *Lithos* 97,1-29.
- Boulin, J. 1981. Afghanistan structure. Greater India concept and eastern Tethys evolution. *Tectonophysics* 72, 261-287.
- Clark, G.C., Davies, R.G., Hamzpour, G., Jones, C.R. 1975. Explanatory text of Bandar-e-Anzali quadrangle map, 1:250,000. Geological Survey of Iran.
- Clemens, J. D., Hollaway, J. R., White, A. J. R. 1986. Origin of an A-type granite: experimental constraints. *American Mineralogist* 71, 317-324.
- Collins, W.J., Beams, S.D., White, A.J.R., Chappell, B.W. 1982. Nature and origin of A-type granites with particular reference to southeastern Australia. *Contributions to Mineralogy and Petrology* 80, 189-200.
- Creaser, R.A., Price, R.C., Wormald, R. J. 1991. A-type granites revisited: Assessment of a residual-source model. *Geology* 19, 163-166.
- Debon, F., Afzali, H., LeFort, P., Sonet, J., Zimmermann, J.L. 1987. Plutonic rocks and associations in Afghanistan: typology, age and geodynamic setting. *Memoire Science de la Terre*, Nancy 49, 132 pp.
- Delaloy, M., Jenny, J., Stampfli, G. 1981. K-Ar dating in the eastern Elburz (Iran). *Tectonophysics* 79, 27-36.
- De La Roche, H., Leterrier J., GrandIauale, P., Marcher, M. 1980. A classification of volcanic and plutonic rocks using  $R_1$ -  $R_2$  diagrams and major element analysis. *Chemical Geology* 183-210.
- Ding, X., Lundstrom, C., Huang, F., Li, J., Zhang, Z.M., Sun, X.M., Liang, J.L., Sun, W.D. 2009. Natural and experimental constraints on formation of the continental crust based on niobium-tantalum fractionation. *International Geology Review* 51, 473-501.
- Eby, G. N. 1990. The A-Type granitoids: A Review for their occurrence and characteristics and speculations on their petrogenesis. *Lithos* 26, 115-134.
- Erkül, A., Sözbilir, R., Erkül, F., Helvacı, C., Ersoy, Y., Sümer, Ö. 2008. Geochemistry of I-type granitoids in the Karaburun Peninsula, West Turkey: Evidence for Triassic continental arc magmatism following closure of the Palaeotethys. *Island Arc* 17, 394-418.
- Foley, S., Tiepolo, M., Vannucci, R. 2002. Growth of early continental crust controlled by melting of amphibolite in subduction zones. *Nature*, 417, 837-840.
- Frost, B. R. , Arculus, R. J. , Barnes, C. G. , Collins, W. J., Ellis, D. J., Frost, C. D. 2001. A geochemical classification of granitic rock suites. *Journal of Petrology* 42, 2033 - 48.
- Gamkrelidze, I.P., Shengelia, D.M. 2007. Pre-Alpine geodynamics of the Caucasus, suprasubduction regional metamorphism and granitoid magmatism. *Bulletin of the Georgian national academy of sciences* 175.
- Ghavidel-Syooki, M. 2007. Palynostratigraphy and Palaeogeography of the Gorgan schists in southern Gorgan city (southeastern Caspian Sea), eastern Alborz range, northern Iran. *CIMP Lisbon Abstracts* 63-64.
- Green, T.H. 1995. Significance of Nb/Ta as an indicator of geochemical processes in the crust-mantle system. *Chemical Geology* 120, 347-359.
- Guest, B., Axen, G.J., Lam, P.S., Hassanzadeh, J. 2006. Late Cenozoic shortening in the west-central Alborz Mountains, northern Iran, by combined conjugate strike slip and thin-skinned deformation. *Geosphere* 2/1, 35-52.
- Harris, N.B.W., Marzouki, F.M.H., Ali, S. 1986. The Jabel Sayid Complex, Arabian Shield: geochemical constraints on the origin of peralkaline and related granites. *Journal of the Geological Society of London* 143, 287- 295.
- Hastie, A. R., Kerr, A. C., Pearce, J. A., Mitchell, S. F. 2007. Classification of Altered Volcanic Island Arc Rocks using Immobile Trace Elements: Development of the Th-Co Discrimination Diagram. *Journal of Petrology* 48, 2341-2357.

- Hennig, D., Lehmann, B., Frei, D., Belyatsky, B., Zhao, X.F., Cabral, A.R., Zeng, P.S., Zhou, M.F., Schmidt, K. 2009. Early Permian seafloor to continental arc magmatism in the eastern Paleo-Tethys: U-Pb age and Nd-Sr isotope data from the southern Lancangjiang zone, Yunnan, China. *Lithos* 113, 408-422.
- Huang, X.L., Xu, Y.G., Li, X.H., Li, W.X., Lan, J.B., Zhang, H.H., Liu, Y.S., Wang, Y.B., Li, H.Y., Luo, Z.Y., Yang, Q.J. 2008. Petrogenesis and tectonic implications of Neoproterozoic, highly fractionated A-type granites from Mianning, South China. *Precambrian Research* 165(3), 190-204.
- Jackson, J., Priestley, K., Allen, M., Berberian, M. 2002. Active tectonics of the South Caspian Basin. *Geophysical Journal International* 148, 214-245.
- Jassim, S. Z., Goff, J. C. 2006. *Geology of Iraq*. Dolin, Prague and Moravian Museum Brno. 338p.
- Jurvanen, T., Elkund, O., Väisänen, M. 2005. Generation of A-type granitic melts during the late Svecofennian metamorphism in southern Finland. *GFF* 127, 139-147.
- Katzir, Y., Eyal, M., Litvinovsky, B. A., Jahn, B. M., Zandvilevich, A. N., Valley, J. W., Beerli, Y., Pelly, I., Shimshilashvili, E. 2007. Petrogenesis of A-type granites and origin of vertical zoning in the Katharina pluton, Gebel Mussa (Mt. Moses) area, Sinai, Egypt. *Lithos*, 95(3), 208-228.
- Kaur, P., Chaudhri, N., Paczek, I., Kroner, A., Hofmann, A. W. 2007. Geochemistry, zircon ages and whole rock Nd isotopic systematics for the Palaeoproterozoic A-type granitoids in the northern part of the Delhi belt, Rajasthan, NW India: implications for late Palaeoproterozoic crustal evolution of the Aravalli craton. *Geological Magazine* 144(2), 361-378.
- Landenberger, B., Collins, W.J. 1996. Derivation of A-type Granites from a Dehydrated Charnokitic Lower Crust: Evidence from the Chaelundi Complex, Eastern Australia. *Journal of Petrology* 37, 145-170.
- Madanipour, S., Ehlers, T. A., Yassaghi, A., Enkelmann, E., Siebel, W. 2015. Time-temperature U-Th-Pb-He modelling of the Lisar Granite in the Talesh Mountains, Evidence for Late Cenozoic exhumation pattern at NW Iranian Plateau. The first meeting of Tectonic and Structural Geology Association of Iran, Tehran.
- Majidi, B. 1987. The geochemistry of ultrabasic and basic lava flows occurrences in northeastern Iran, In Geodynamic project in Iran. Geological Survey of Iran, Report No. 51,463-477.
- Majidi, B. 1991. Étude structurale de la région de Mashhad (Iran). Les problèmes des métamorphites, serpentinites et granitoïdes hercyniens. Thèse de Docteur Ingénieur, Université Scientifique et Médicale de Grenoble. 277 p.
- Maniar, P.D., Piccolli, P.M. 1989. Tectonic discrimination of granitoids. *Geological Society of America Bulletin* 101, 635-643.
- Manning, C.E., Bohlen, S.R. 1991. The reaction titanite + kyanite = anorthite + rutile and titanite-rutile barometry in eclogites. *Contributions to Mineralogy and Petrology* 109, 1-9.
- McDonough, W.F. 1991. Partial melting of subducted oceanic-crust and isolation of its residual eclogitic Lithology. *Philosophical Transactions of the Royal Society of London Series a-Mathematical Physical and Engineering Sciences* 335, 407-418.
- Mirnejad, H., Lalonde, A. E., Obeid, M., Hassanzadeh, J. 2013. Geochemistry and petrogenesis of Mashhad granitoids: An insight into the geodynamic history of the Paleo-Tethys in northeast of Iran. *Lithos* 170-171, 105-116.
- Moix, P., Beccalotto, L., Kozur, H.W., Hochard, C., Rosset, F., Stampfli, G.M. 2008. A new classification of the Turkish terranes and sutures and its implication for the paleotectonic history of the region. *Tectonophysics* 451, 7-39.
- Muttoni, G., Mattel, M., Balini, M., Zanchi, A., Gaetani, M., Berra, F. 2009. The drift history of Iran from the Ordovician to the Triassic. *The Geological Society, London, Special Publications* 312, 7-29.
- Omran, H., Moazzen, M., Oberhansli, R., Tsujimori, T., Bosuquet, R., Moayyed, M. 2013. Metamorphic history of glaucophane - paragonite-zoisite eclogites from the Shanderman area, northern Iran. *Journal of Metamorphic Geology* 31, 791-812.
- Pearce, J.A. 1996. Sources and settings of granitic rocks. *Episodes* 19, 120-125.
- Peccerillo, A., Barberio, M.R., Yirgu, G., Ayalew, D., Barbieri, M., Wu, T.W. 2003. Relationships between mafic and peralkaline silicic magmatism in continental rift settings: a petrological, geochemical and isotopic study of the Gedesma Volcano, Central Ethiopian Rift. *Journal of Petrology* 44 (11), 2003-2032.
- Rezaeian, M., Carter, A., Hovius, N., Allen, M. B. 2012. Cenozoic exhumation history of the Alborz Mountains, Iran: New constraints from low-temperature chronometry. *Tectonics*, 31(2).
- Ritz, J.F., Nazari, H., Ghassemi, A., Salavati, R., Shafei, A., Soleymani, S., Vernant, P. 2006. Active transtension

- inside central Alborz: A new insight into northern Iran–southern Caspian geodynamics. *Geology* 34/6, 477–480.
- Ruban, D.A., AL-Husseini, M.I., Iwasaki, Y. 2007. Review of Middle East Paleozoic plate tectonics. *GeoArabia* 12(3), 35-56.
- Rudnick, R.L., Barth, M., Horn, I., McDonough, W.F. 2000. Rutile-bearing refractory eclogites: Missing link between continents and depleted mantle. *Science*, 287, 278–281.
- Şengör, A.M.C. 1979. Mid-Mesozoic closure of Permo-Triassic Tethys and its implications. *Nature* 279, 590-593.
- Şengör, A.M.C. 1990. A new model for the late Palaeozoic–Mesozoic tectonic evolution of Iran and implications for Oman. In: Robertson, A. H., Searle, M. P. & Ries, A. C. (eds) *The Geology and Tectonics of the Oman Region*. Geological Society, London, Special Publications 49, 797–831.
- Shafaii Moghadam, H., Li, X.-H. Ling, X.-X. Stern, R. J., Khedr, M. Z. Massimo Chiaradia, M., Ghasem Ghorbani, G., Arai, S., Tamura, A. 2015. Devonian to Permian evolution of the Paleo-Tethys Ocean: New evidence from U–Pb zircon dating and Sr–Nd–Pb isotopes of the Darrehanjir–Mashhad “ophiolites”, NE Iran. *Gondwana Research* 28, 781–799
- Shellnut, J. G., Zhou, M.F., Zellmer, G.F. 2009. The role of Fe-Ti oxide crystallization in the formation of A-type granitoids with implications for the Daly gap: an example from the Permian Baima igneous complex, SW China. *Chemical Geology* 259, 204-217.
- Shkodzinskiy, V.S. 1985. *Magma Phase Evolution and Petrogenesis*. Moscow: Nauka, 232 pp. [In Russian].
- Stampfli G., Marcoux J., B., Baud, A. 1993. Tethyan margins in space and time: In: Channell, J.E.T., Winterer, E. L., Jansa, L.F. (Eds). *Palaeogeography, Palaeoclimatology and Palaeoecology* 87, 373-409.
- Stampfli, G.M., Kozur, H.W. 2006. Europe from the Variscan to the Alpine cycles. In: Gee, D.G., Stephenson, R.A. (Eds.), *European lithosphere dynamics*. Memoir of the Geological Society London, 57-82.
- Stöcklin, J. 1974. Possible ancient continental margins in Iran. In *The geology of continental margins* (pp. 873-887). Springer Berlin Heidelberg.
- Streckeisen, A. 1976. To each plutonic rocks its proper name. *Earth Science Reviews* 12, 1-33.
- Sun, S.S., McDonough, W.F. 1989. Chemical and isotopic systematic of oceanic basalts; implications for mantle composition and processes. In: Saunders, A.D., Norry, M.J. (eds.) *Magmatism in the ocean basins*. Geological Society of London 42, 313-345.
- Sylvester, P.J. 1989. Post-collisional alkaline granites. *Journal of Geology* 97, 261–280.
- Taylor, R.P., Strong, D.F., Fryer, B.J. 1981. Volatile control of contrasting trace element distributions in peralkaline granitic and volcanic rocks. *Contributions to Mineralogy and Petrology* 77, 267–271.
- Watson, E.B., Harrison T.M. 1984. Accessory minerals and the geochemical evolution of crustal magmatic systems: a summary and prospectus of experimental approaches. *Physics of Earth and Planetary Interiors* 35, 19–30.
- Whalen, J.B., Currie, K.L., Chappell, B.W. 1987. A-type granites: geochemical characteristics, discrimination and petrogenesis. *Contributions to Mineralogy and Petrology* 95, 407-419
- Zhanchetta, S., Zanchi, A., Villa, I., Poli, S., Muttoni, G. 2009. The Shanderman eclogites: a late carboniferous high-pressure event in the NW Talesh Mountains (NW Iran). *Geological Society London, Special publications*, 57-78.
- Zanchi, A., Zanchetta, S., Berra, F., Mattei, M., Garzanti, E., Molyneux, S., Nawab, A., Sabouri, J. 2009. The Eo-Cimmerian (Late-Triassic) orogeny in North Iran. In: Brunet, M.-F., Wilmsen, M., Granath, J. W. (eds) *South Caspian to Central Iran Basins*. Geological Society of London Special Publications 312, 31–55.
- Zhang, C.-Z., Li B., Cai, J.-X.a, Tang X.-C., Wei, Q.-G., Zhang, Y.-X. 2008. A-type granite and adakitic magmatism association in Songpan-Garze fold belt, eastern Tibetan Plateau: Implication for lithospheric delamination: Comment. *Lithos* 103, 562–564.





# Bulletin of the Mineral Research and Exploration

<http://bulletin.mta.gov.tr>



## GEOCHEMICAL CHARACTERISTICS AND RARE-EARTH ELEMENT DISTRIBUTIONS OF KOZBUDAKLAR W-SKARN DEPOSIT (BURSA, WESTERN ANATOLIA)

Ayşe ORHAN<sup>a\*</sup> and Halim MUTLU<sup>b</sup>

<sup>a</sup>Nevşehir Hacı Bektaş Veli University, Department of Geological Engineering, Nevşehir. [orcid.org/0000-0001-8103-5376](https://orcid.org/0000-0001-8103-5376)

<sup>b</sup>Ankara University, Department of Geological Engineering, Gölbaşı, Ankara. [orcid.org/0000-0002-4100-1363](https://orcid.org/0000-0002-4100-1363)

Research Article

### Keywords:

Scheelite Mineralization,  
Rare-Earth Elements,  
Kozbudaklar, Bursa,  
Western Anatolia.

### ABSTRACT

The Kozbudaklar W-skarn deposit occurs along the contact between Eocene Topuk granitoid and Triassic İnönü marble in Tavşanlı Zone. In the study area, the endoskarn is represented by plagioclase-pyroxene and exoskarn zone which is characterized by pyroxene, pyroxene-garnet, garnet and garnet-pyroxene skarn facies. According to major oxide element contents, exoskarn is of calcic character. In pyroxene and pyroxene-garnet skarn facies, tungsten and molybdenum abundances vary between 434-5507 ppm (mean 2330 ppm) and 8 - 90 ppm (mean 40 ppm). In the garnet and garnet-pyroxene skarns, concentrations of these elements are 271 - 7616 ppm (mean 2486 ppm) and 7 - 493 ppm (mean 107 ppm), respectively, and molybdenum concentration is increased. ΣREE contents of the Topuk granitoid, endoskarn, exoskarn and İnönü marble are in the range of 75.8 to 158.9 ppm (mean 106.2 ppm), 75.8 to 171.5 ppm (mean 114.6 ppm), 3.5 to 290.8 ppm (mean 48.7 ppm) and 2.3 to 15.3 ppm (mean 6.1 ppm), respectively. Although ΣREE concentrations of skarn zones are higher than those of Topuk granitoid and İnönü marble, ΣREE concentrations of tungsten-rich samples are significantly depleted. In areas of scheelite mineralization, REE trends and Eu anomalies display two different patterns. REE trends, HREE enrichments and negative Eu anomalies of pyroxene and pyroxene-garnet skarn facies exhibit similarities with Topuk granitoid. In these skarn facies, tungsten-rich samples are represented by a Ce depletion and low Eu/Eu\* (Eu/Eu\* = 0.56-0.88). Garnet and garnet-pyroxene skarn facies are characteristic with a convex LRRE pattern, maximum Pr and Nd concentrations and positive Eu anomalies. Ce-enrichment and high Eu/Eu\* ratios (Eu/Eu\* = 1.45 - 4.18) are observed in tungsten-rich samples. Considering the molybdenum enrichments and REE pattern, scheelite mineralization in the Kozbudaklar W-skarn deposit can be said to have developed at two different high temperature phases. In the first-phase mineralization was formed by early magmatic fluids under moderate oxidant conditions whilst the second-phase scheelite mineralization was formed under increasing oxidant conditions.

Received Date: 24.11.2016

Accepted Date: 08.02.2017

## 1. Introduction

Rare earth elements (REE) which are widely used for petrological classification of magmatic rocks have been recently commonly applied to assessment of several parameters including the degree of fluid-rock interaction, the source of fluids, pH variations, various agents in fluids (e.g. Cl, SO<sub>4</sub>, CO<sub>3</sub>), reducing mechanisms and temperature (Michard, 1989; Bau, 1991; Vander Auwera and Andre, 1991; Lottermoser, 1992; Whitney and Olmsted, 1998; Bi et al., 2004; Oyman et al., 2013; Song et al., 2014). Results of such studies showed that changes in oxidation conditions, pH and temperature exert a primary control on REE

distributions and particularly Eu and Ce concentrations. Fluid-rock interaction at low temperature may disturb REE pattern of whole rock whilst interaction at high-temperature has rather a limited effect on REE distribution. It was shown that pH decrease in fluids (acidic conditions) increases REE concentrations (Lottermoser, 1992) and fluid-rock interaction under high temperature and changes in oxidation conditions raise the Eu/Eu\* ratio (Bau, 1991; Whitney and Olmsted, 1998; Bi et al., 2004; Oyman et al., 2013; Song et al., 2014). It is also reported that depletion of REEs in the source rock or fluid-rock interaction triggered by fractionation of magmatic rocks have a limited effect on REE patterns (Bau, 1991).

\* Corresponding author: Ayşe ORHAN, [ayse.orhan@nevsehir.edu.tr](mailto:ayse.orhan@nevsehir.edu.tr)

<http://dx.doi.org/10.19111/bulletinofmre.305992>

Studies on W-skarn systems indicated that magma chemistry, host rock composition, skarn formation depth, reducing conditions and change in temperature are important parameters (Sato, 1980; Kwak and Tan, 1981; Newberry, 1982; Brown et al., 1985; Gerstner et al., 1989; Fonteilles et al., 1989; Zaw and Singoyi, 2000; Timon Sanchez et al., 2009; Orhan, 2017). It was stated that W-skarn deposits, which are classified as “reducing” and “oxidizing” types with respect to pressure and oxidation conditions, generally favour high-temperature systems (Einaudi et al., 1981; Meinert et al., 2005). According to these authors, reducing W-skarn systems of economic importance are represented by ferrous (e.g. hedenbergite, grossular) minerals at early (prograde) stage whilst oxidizing type skarn systems are enriched in ferric minerals (e.g. diopside, andradite). It was asserted that scheelite grade in both skarn systems attains an economic size with increasing degree of fluid-rock interaction and hydrous mineral abundance at the late (retrograde) stage (Brown et al., 1985; Zaw and Singoyi, 2000).

In this study, based on major oxide, trace and rare earth element characteristics of Kozbudaklar W-skarn deposit (Keles, Bursa) (Figure 1), the source of metasomatic mineralizing fluids, fluid-rock interaction, oxidation conditions and temperature variations were investigated. Previous studies were carried out to examine general geological features (Lisenbee, 1972; Okay, 1985; 2011; Orhan et al., 2015) and the ore potential of the region (Romberg, 1938; MTA, 1965; Pehlivan, 1987) and investigate the petrogenetic properties of Topuk granitoid (Harris et al., 1994; Delaloye and Bingöl, 2000; Okay and Satır, 2006; Altunkaynak, 2007; Orhan et al., 2014a). Romberg (1938) is the first to mention the occurrence of skarn minerals (e.g. pyroxene, garnet, epidote and vesuvianite) and scheelite, pyrrhotite, molybdenite and magnetite mineralizations around the Kozbudaklar village. Reserve and grade of scheelite deposit are estimated 238.000 tons and 0.31%  $WO_3$  (MTA, 1965). In a recent study by Orhan (2017), P-T conditions and composition of ore-forming fluids have been discussed. Orhan (2017) described at least four stages in the evolution of Kozbudaklar scheelite skarn deposit and proposed that scheelite mineralization occurred along the contact of Topuk pluton (in the proximal zone) in the prograde stage (I and II) rather than retrograde stage.

In the present study, based on previously described skarn facies (Orhan, 2017), the character of exoskarn

in the Kozbudaklar scheelite skarn deposit (calcitic or dolomitic) was determined using major oxide and trace element contents from various skarn facies. Comparing REE trends of Topuk granitoid and İnönü marble, the source of metasomatic fluids, the degree of fluid-rock interaction, oxidation conditions and temperature changes were also discussed.

## 2. Analytical Methods

Major oxide, trace and rare earth element analyses of samples from İnönü marble and skarn facies were carried out ACME (Canada) laboratories. The locations of samples are shown in Figures 1 and 2. Before the analysis, about 100 g from each sample was cleaned. Major oxides and some trace elements (Ba, Ni, Sr, Sc, Y and Zr) were analyzed with ICP-ES whilst rare earth elements were determined by ICP-MS method. During the analyses CANMET SY-4 and STD SO-17 standards were used and accuracy of major oxide and trace element analyses are 0.001–0.04% and 0.01–0.5 ppm, respectively.

## 3. General Geology

The İzmir-Ankara Suture Zone which defines the closure of Neotethys Ocean divides the northwest Anatolia into two parts – Sakarya Continent at north and Anatolide-Tauride Platform at south (Okay et al., 1998). The Topuk granitoid is located in the Tavşanlı Zone at north of Anatolide-Tauride Block in northwest Anatolia (Figure 1). In the Tavşanlı Zone four tectono-stratigraphic units have been described (Okay, 2011). These units from bottom to the top are the Orhaneli group consisting of terrestrial rocks, ophiolitic mélange and/or ophiolites, Eocene sedimentary rocks and Eocene granitoids. In the study area, Paleozoic-Mesozoic Kocasu formation of Orhaneli group, Triassic İnönü marble, Upper Cretaceous Orhaneli Ophiolite and Eocene Topuk granitoid are exposed (Figure 1).

The Kocasu formation at the base of Orhaneli group is composed of quartz-mica schist, quartz-calc schist and chlorite schist and distributed along southern and northern parts of Tavşanlı Zone (Okay and Kelley, 1994; Okay, 2004; Orhan et al., 2015). The mineral associations of quartz + phengite + jadeite + chloritoid + lawsonite + glaucophane and muscovite + biotite + chlorite + quartz + albite in the Kocasu formation indicate P-T conditions of  $20\pm 2$  kbar and  $430\pm 30^\circ\text{C}$  implying a blueschist metamorphic facies (Harris et al., 1994; Okay, 2011).  $^{40}\text{Ar}/^{39}\text{Ar}$  dating

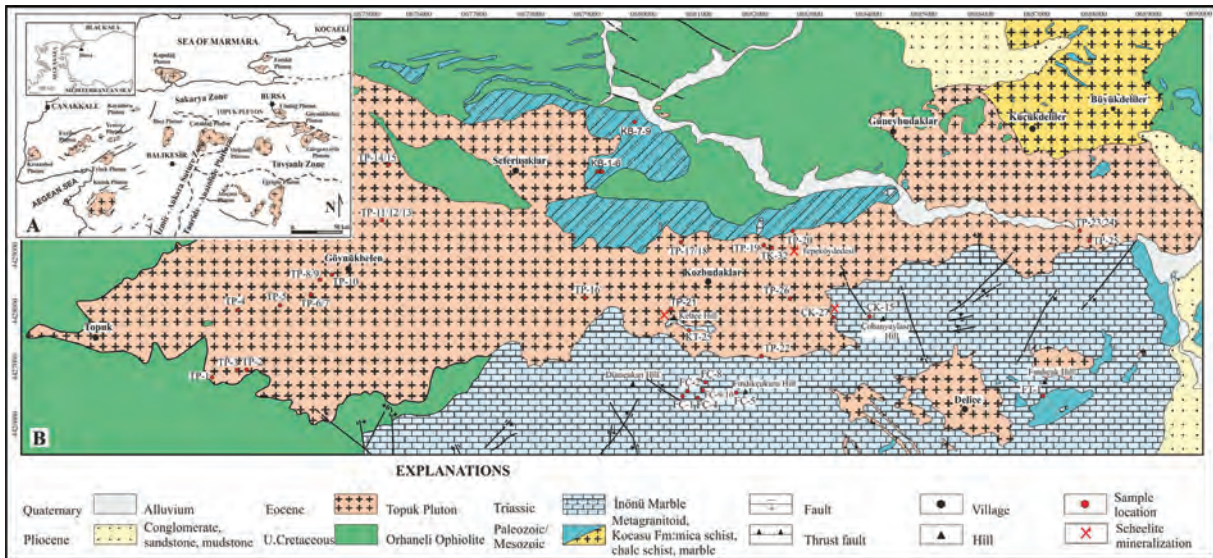


Figure 1- a) Tertiary plutonic rocks of Northwest Anatolia (simplified from MTA, 2002) and b) Geological and sample location map of the study area (MTA, 1973).

from phengite and glaucophane minerals yields that metamorphism was continued in the time interval of 108 to 88 Ma (Harris et al., 1994). The İnönü marble consisting of pure calcite crystals gradually changes to the schists of Kocasu formation. The calcitic marble is white colored, distinctly laminated and grain size is increased towards the skarn zone and pluton contact.

The Orhaneli ophiolite which is a relict mass of the Neotethys Ocean at northwest Anatolia has been thrust onto the Paleozoic-Mesozoic metamorphic rocks (Lisenbee, 1972; Örgün, 1993). The unit is composed chiefly of peridotites and partly of gabbro and pyroxenite dykes (Örgün, 1993; Emre, 1996; Okay, 2011). Paleontological descriptions on radiolarites within ophiolitic mélangé at northern part of Tavşanlı Zone yield Triassic-Cretaceous age for the unit (Tekin et al., 2002).

The Topuk granitoid, which is one of the intrusions formed subsequent to closure of Neotethys Ocean in the late Cretaceous (Şengör and Yılmaz, 1981) and collision between Anatolide-Tauride and Sakarya Continent, comprises an area of about 55 km<sup>2</sup> (Figure 1). The E-W trending and ellipsoidal-shaped granitoid was intruded the Paleozoic-Mesozoic metamorphics, Triassic marble and Upper Cretaceous ophiolitic rocks. The mineral assemblage of andalusite + cordierite + biotite + muscovite + K-feldspar + plagioclase at the contact of plutonic and metamorphic rocks implies that metamorphism took place at pressure of 2±1 kbar and temperature of 575±50°C (Okay and Satır, 2006).

At the contact between pluton and Triassic marble around the Kozbudaklar village, skarn zone has been developed as irregular roof pendants.

The Topuk granitoid is recognized in gray to light gray color and exhibits moderate-coarse equigranular texture. The host rock of pluton is granodiorite which contains spherical/ellipsoidal mafic mineral enclaves (MME) of monzodiorite/monzogabbro composition. The granitoid is often cut by porphyric granodiorite, granitic aplite and quartz veins at marginal facies and contain xenolith fragments (Orhan et al., 2014a; 2015). Alteration is quite common at the contacts of granitoid with other units. Particularly towards the skarn contacts, grain size of granitoid is reduced, feldspar content is increased and it is repeatedly cut by quartz veins. According to results of geochemical and isotopic analyses, the Topuk granitoid is a product of arc magmatism formed in an active continental margin and mantle and subduction-related melts greatly contributed to the magma development (Harris et al., 1994; Altunkaynak, 2007; Orhan et al., 2014a). K-Ar ages on various mineral separates from the pluton are reported 43.0±2.7 Ma for biotite, 49.8±2.7 Ma for orthoclase (Bingöl et al., 1982) and 47.8±4 Ma for hornblende (Lisenbee, 1972).

#### 4. Mineralogical Characteristics of Kozbudaklar Skarn Deposit

Detailed morphologic and mineralogic observations of skarn zones and micro probe analysis

on calc-silica and ore minerals (e.g. garnet, pyroxene, scheelite and plagioclase) at Kozbudaklar have been reported by Orhan (2017). Scheelite in the skarn zone is recognized at northeast (Tepeköydedesi), southeast (Çobanyaylası) and southwest (Kepçe Hill) parts of the Kozbudaklar village (Figure 2). According to Orhan et al. (2014b) and Orhan and Mutlu (2015), both endo and exoskarn zones have been developed with respect to type of rock replaced.

The endoskarn zone at the pluton contact is widely exposed at northeast of the area. The zone with a width varying from 75 to 165 m is composed chiefly of clinopyroxene ( $Hd_{95-96}$ ) and plagioclase ( $An_{55-64}$ ) (Table 1). Based on mineral abundances this zone has been described as plagioclase-pyroxene (Plg-Pyx) skarn. The exoskarn zone was developed as monomineralic zones, lenses and irregular bands at the contact of pluton and/or endoskarn (in proximal zone) and within the marble (in distal zone). The contacts of

exoskarn zone with pluton, endoskarn zone and marble are quite sharp. The exoskarn zone has a limited distribution at northeast and its width varies from 2 to 112 m at northeast and from 125 to 150 m at south. Considering mineral abundances, textural properties and mineral compositions, four different skarn facies have been recognized in the exoskarn zone (Table 1). All the skarn zones are composed mainly of garnet and/or clinopyroxene but textural characteristics of these minerals show differences. Pyx (pyroxene) skarn is observed only at Tepeköydedesi location whilst Pyx-Gar (pyroxene-garnet) skarn is exposed at Tepeköydedesi, Çobanyaylası and Kepçe Hill locations. Pyx skarn has been developed at endoskarn contact (in proximal zone). Pyx-Gar skarn is found in Pyx skarn (in proximal zone) at the Tepeköydedesi location and along marble contact (in distal zone) at Çobanyaylası and Kepçe Hill locations. Pyroxene and garnet are accompanied by scheelite in the proximal zone and by wollastonite in the distal zone. Garnets

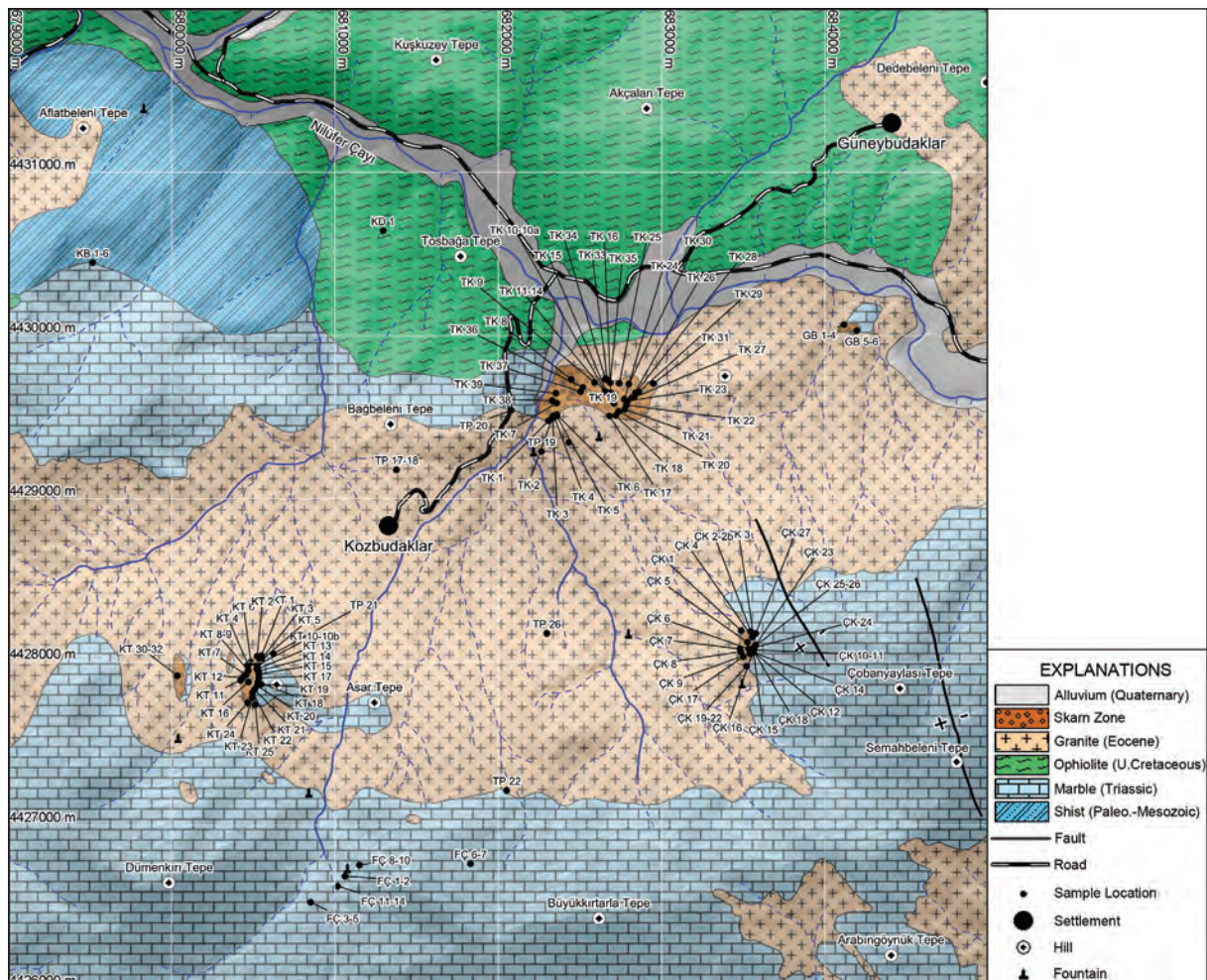


Figure 2- Skarn zone and sample location map of Kozbudaklar region.

Table 1- Characteristics properties of skarn zones and sample numbers of skarn facies from the Kozbudaklar W-skarn deposit (after Orhan, 2017).

Rock type	Sample no	Skarn facies	Mineral assemblages	Characteristic properties
Endo-skarn	TK-1-6, 8, 9, 15, 16, 18, 19, 21, 29, 37, 39; KT-9, 11, 13, 15, 17, 18, 20, 23; GB-2, 4	Plg-Pyx skarn	Plg (Lab) + Pyx (Hd) + Q ± Sph ± Ap ± Bi ± Amp ± Ort ± Cc ± Prt ± Cpr ± Pr ± Mt ± Src	Coarse-to fine-grained, granular texture, occurs at the contact of the Topuk Pluton and composed of labradorite plagioclase (An <sub>55-64</sub> ) and hedenbergitic (Hd <sub>95-96</sub> ) clinopyroxene.
Exoskarn	TK-10/10a, TK-11, 13, 14, 22, 23, 26-28, 30, 33, 35	Pyx skarn	Pyx (Hd) ± Q ± Cc ± Sph ± Sch ± Prt ± Pr ± Mrc ± Lm	Occurs at the endoskarn contact, it has granoblastic texture and is composed dominantly (>95 %) clinopyroxene (Hd <sub>93-94</sub> ). Mo-content low scheelite is formed with hedenbergite and gives blue reflection color under ultraviolet light. Interstitial quartz and calcite are observed.
	TK-17, 20, 31, 38; KT-3 21, 22, 24, 25; ÇK-23, 25, 26; GB-3, 6, 7	Pyx-Gar skarn	Pyx (Hd-Di) + Gar (Grs) ± Wo ± Q ± Cc ± Sph ± Sch ± Chl	Develops as lenses within pyroxene zone and at the marble contact (distal zone). In proximal zone, garnet (Grs <sub>48-94</sub> ) and clinopyroxene (Hd <sub>61-73</sub> ) are accompanied by scheelite (Pov <sub>1,4</sub> ). In distal zone, wollastonite is observed with garnet (Grs <sub>65-95</sub> ) and clinopyroxene (Hd <sub>17-22</sub> ). Calcite and chlorite are the main alteration products and interstitial quartz and calcite are observed.
	ÇK-2/2b, 5, 7, 9, 17, 19-22; KT-5-8, 12, 14, 16, 31	Gar skarn	Gar (And) ± Pyx (Di) ± Ve ± Plg (An) ± Q ± Cc ± Sch ± Pr ± Cpr ± Mgt ± Chl ± Hm ± Cov	Composed of zoned garnet in proximal zone. Garnet composition varies from grossular to andradite (Grs <sub>24-92</sub> ). Zoned garnet is replaced by vesuvianite and scheelite occurs in garnet rims. Mo-content in scheelite is high (Pov <sub>7-32</sub> ) and gives yellow reflection color under ultraviolet light. Minor magnetite and sulfide mineralization are developed with secondary quartz, calcite and chlorite over the garnet. Skarn facies is cut by quartz and calcite veins.
	KT-10/10b, 19; ÇK-3, 4, 6, 8, 12, 16, 18, 25, 26	Gar-Pyx skarn	Gar (And) + Pyx (Di) ± Q ± Cc ± Ve ± Ep ± Plg ± Sch ± Pr ± Mgt ± Ap ± Chl	Zoned garnet is replaced by clinopyroxene, plagioclase (An <sub>91-97</sub> ) inclusions are observed. Garnets represent composition between grossular and andradite (Grs <sub>30-90</sub> ). Clinopyroxene is dominantly in diopside (Hd <sub>16-48</sub> ) composition. Calcite and chlorite are the main alteration products. Pores and fractures of garnet are filled with quartz and calcite crystals.

Amp: amphibole; An: anorthite; And: andradite; Ap: apatite; Bio: biotite; Cc: calcite; Chl: chlorite; Cov: covellite; Cpr: chalcopyrite; Di: diopside; Ep: epidote; Gar: garnet; Hd: hedenbergite; Hm: hematite; Mgt: magnetite; Mrc: marcasite; Lab: labradorite; Lm: limonite; Ort: orthoclase; Pr: pyrite; Pyx: pyroxene; Prt: pyrrhotite; Q: quartz; Scp: scapolite; Sph: sphene; Src: sericite; Sch: scheelite; Ve: vesuvianite; Wo: wollastonite.

formed as replacement product of clinopyroxenes are mostly anhedral (Orhan, 2017). Clinopyroxenes in the proximal zone have hedenbergite (Hd<sub>94-61</sub>) composition and those in distal zone have diopside composition (Hd<sub>17-22</sub>). Garnets have composition varying from grossular to andradite (Grs<sub>48-95</sub>) and Mo content of scheelites is relatively low (Pov<sub>1,4-6</sub>) (Table 1). Gar (garnet) and Gar-Pyx (garnet –pyroxene) skarn which are represented by zoned garnets are formed at pluton contact (in proximal zone) at Çobanyaylası and Kepçe Hill locations. Zoned garnets show composition of grossular – andradite (Grs<sub>24-92</sub>) from core to the rim (Table 1). Clinopyroxenes have replaced the zoned garnets (Orhan, 2017) and have composition mostly of diopside (Hd<sub>16-48</sub>) (Table 1). Scheelites are formed at bands of zoned garnets or as monomineralic

occurrences between garnets and clinopyroxenes (Orhan, 2017). Mo content of scheelites in this zone is quite high (Pov<sub>7-32</sub>) (Table 1).

According to Orhan (2017), hydrous products of retrograde stage such as epidote are rarely occurred. Orhan (2017) also stated that scheelite mineralization was developed in the prograde (proximal zone) at different phases (stage I and II) under varying oxidation conditions. During retrograde (stage III) stage, main alteration minerals of calcite, chlorite and quartz and trace amount of magnetite and sulfur minerals were formed. In the last stage (stage IV) of Kozbudaklar skarn deposit, skarn facies in the proximal zone are interrupted by barren quartz and calcite veins.

## 5. Geochemical Characteristics of Kozbudaklar Skarn Deposit

Mineral associations (described with mineralogical and petrographic analyses) and corresponding sample names of skarn facies in the Kozbudaklar skarn deposit are shown in table 1. Results of major oxide and trace element analyses for representative samples from skarn facies, Topuk Granodiorite and İnönü marble are given in table 2. Chemical analysis of Topuk Granodiorite (host rock of Kozbudaklar skarn deposit) is taken from Orhan et al. (2014a).

### 5.1. Major Element Geochemistry

The exoskarn zone is classified based on compositions of carbonate rock (magnesian or calcic composition) and skarn minerals (Burt, 1977; Einaudi et al., 1981). According to Orhan (2017), exoskarn zone and carbonate host rock in the region are of calcic character which is clearly visible from ACF triangular  $[(Al_2O_3+Fe_2O_3)-(Na_2O+K_2O) - (CaO-3.3P_2O_5) - (MgO+MnO+FeO)]$  diagram (Figure 3) (Barton et al., 1991). In the diagram, exoskarn zone rocks (except for samples TK-22 and KT-3) are plotted in the field of calcium-silicate minerals (anorthite, garnet, vesuvianite, diopside and wollastonite/calcite). Samples of Pyx (TK-22) and Pyx-Gar skarn (KT-3) with high  $Al_2O_3$  content are sampled from plutonic rock and locations close to the plagioclase-pyroxene skarn contact.

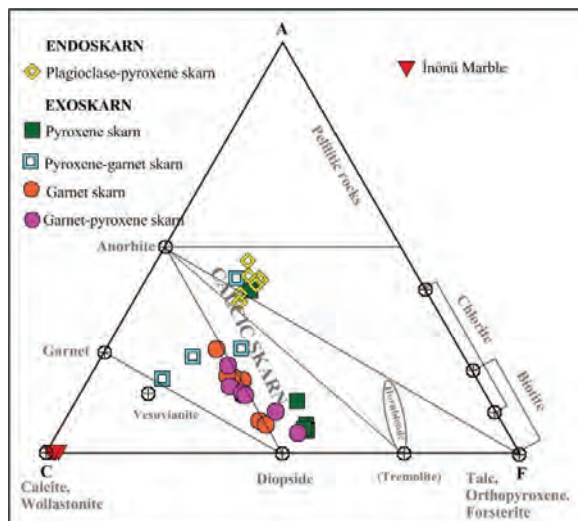


Figure 3- Positions of skarn zone samples in the AFC  $[(Al_2O_3+Fe_2O_3)-(Na_2O+K_2O) - (CaO-3.3P_2O_5) - (MgO+MnO+FeO)]$  ternary diagram (Barton et al., 1991).

### 5.2. Geochemistry of Ore Elements

Mineral content of skarn deposits is quite variable. Geochemical studies on these deposits indicate the development of metal separation zones from proximal to distal zone and metal contents attain a significant economic size at the distal zone (Meinert et al., 2005). Metal contents of the Kozbudaklar skarn deposit are high particularly in the proximal zone. In addition to W, Cu concentration is partly high for two samples (208.1 and 247.8 ppm) in Plg-Pyx skarn (in endoskarn zone) at the Tepeköydedesi location (Table 2). W and Mo concentrations are increased in the exoskarn zone at Tepeköydedesi, Çobanyaylası and Kepçe Hill locations. W and Mo contents in Pyx and Pyx-Gar skarn are 433.7 to 5507 ppm (ave. 2330 ppm) and 7.8 to 90.2 ppm (ave. 40.28 ppm), respectively. Concentrations of these elements in the Gar and Gar-Pyx skarn (where zoned garnets are occurred) are higher ranging from 270.8 to 7615.5 ppm (2485.8 ppm) and from 6.7 to 492.5 ppm (ave. 106.6 ppm), respectively.

### 5.3. Rare Earth Element Geochemistry

$\Sigma$ REE contents of Plg-Pyx and Pyx-Gar skarns at Kozbudaklar (except for samples with >400 ppm W) are recognized to be partly higher than those of granodiorite and metamorphic rocks (Tables 3).  $\Sigma$ REE contents are decreased from endoskarn zone (Plg-Pyx skarn) at the granitoid contact to the exoskarn zone.  $\Sigma$ REE contents of Topuk granodiorite, endoskarn, ekzoskarn zones and İnönü marble are 75.8 to 158.9 ppm (ave. 106.2 ppm), 75.8 to 171.5 ppm (ave. 114.6 ppm), 3.5 to 290.8 ppm (ave. 48.72 ppm) and 2.3 to 15.3 ppm (ave. 6.1 ppm) (Tables 2 - 3).

$\Sigma$ REE contents of Topuk granodiorite are higher with respect to chondrite and light rare earth elements (LREE: 15 to 110-fold) are much more enriched than those of heavy rare earth elements (HREE; 10 to 20-fold) (Figure 4 - 8).  $(La/Yb)_n$   $[(La/Yb)_n=(La/0.237)/(Yb/0.17)]$  (Sun and McDonough, 1989) ratio of samples is from 3.17 to 11.34 (ave. 6.35), LREE/HREE ratio ranges from 5.9 to 15.6 (ave. 9.1) and  $Eu/Eu^*$   $[Eu/Eu^*=(Eu/(Sm+Gd)*0.5)]$  ratio (Sun and McDonough, 1989) is in the range of 0.67 to 0.83 (ave. 0.76) (Tables 2 - 3). LREEs of Topuk granodiorite are greater than HREEs and show a slight convex pattern with a negative Eu anomaly.

The degree of enrichment of REEs for the İnönü marble is lower than that of chondrite. LREEs are

Table 2- Representative major oxide and trace element compositions of Topuk granodiorite, skarn facies and Inönü marble.

Sample no	TP-3	TP-10	TP-12	TP-18	TP-23	TK-1	TK-15	TK-13	KT-23	TK-17	TK-31	KT-3	KT-24	TK-10	TK-11	TK-13	TK-14	TK-22	
Rock type	TOPUK PLUTON										EXOSKARN ZONE								
Skarn facies	Plagioclase-pyroxene skarn										Pyroxene-garnet skarn								
Major oxide (%)	ENDOSKARN ZONE										PYROXENE SKARN								
SiO <sub>2</sub>	61.21	65.42	57.93	63.80	69.00	50.77	45.92	50.38	47.75	48.93	45.30	48.89	41.01	48.44	53.95	55.68	48.94	47.91	
TiO <sub>2</sub>	0.32	0.36	0.54	0.44	0.25	0.60	0.26	0.69	0.54	0.02	0.48	0.75	0.68	0.04	0.02	0.01	0.09	0.55	
Al <sub>2</sub> O <sub>3</sub>	15.34	16.37	18.18	16.62	15.35	19.37	20.84	18.03	17.84	0.61	12.74	20.17	12.13	1.32	0.31	0.24	5.27	17.79	
Fe <sub>2</sub> O <sub>3</sub>	4.10	4.64	7.39	5.04	3.08	7.07	10.07	7.56	8.43	24.55	11.74	6.66	8.61	25.72	23.66	22.80	21.02	10.22	
MnO	0.09	0.14	6.65	0.12	0.08	0.31					0.67	0.45	0.51	1.49	1.60	1.53	1.32	0.37	
MgO	1.25	1.37	0.22	1.62	1.06	2.86	1.48	2.61	2.75	3.07	3.12	2.19	2.40	1.82	1.34	1.27	2.37	1.50	
CaO	8.58	5.15	2.76	4.85	3.97	14.08	15.62	18.40	20.31	22.23	23.58	18.20	31.74	21.60	19.62	18.96	19.92	18.24	
Na <sub>2</sub> O	3.17	3.38	7.03	3.49	3.14	2.81	1.66	1.15	0.92	0.07	0.43	1.26	0.01	0.22	0.07	0.06	0.73	0.03	
K <sub>2</sub> O	1.67	1.79	3.43	2.52	3.22	0.14	0.98	0.05	0.07	<0.01	0.60	0.05	<0.01	0.18	<0.01	0.01	0.51	0.02	
P <sub>2</sub> O <sub>5</sub>	0.12	0.14	1.38	0.13	0.08	0.16	0.10	0.14	0.23	0.04	0.13	0.17	0.06	0.06	0.04	0.05	0.10	0.19	
Cr <sub>2</sub> O <sub>3</sub>	0.03	0.04	0.13	0.05	0.06	0.029	0.022	0.031	0.026	0.007	0.034	0.030	0.050	0.007	0.016	0.021	0.006	0.031	
A.Z.	4.00	1.00	0.04	1.10	0.50	1.7	2.4	0.3	0.5	1.2	0.9	1.0	2.6	1.0	1.1	1.4	0.4	3.0	
Total	99.88	99.80	0.80	99.78	99.80	99.85	99.84	99.82	99.87	99.85	99.77	99.80	99.85	99.92	99.54	99.20	99.87	99.84	
Trace elements (ppm)																			
W	<0.5	<0.5	<0.5	<0.5	<0.5	1.1	0.9	18.1	0.6	433.7	30.7	14.7	46.3	3.7	2944.5	5507.3	11.0	48.2	
Mo	0.20	<0.1	0.20	<0.1	0.60	1.0	46.2	1.0	0.6	7.8	1.4	0.7	5.0	1.9	55.3	90.2	0.6	1.0	
Cu	12.60	9.00	181.80	7.70	7.80	247.8	208.1	9.6	13.3	2.5	0.9	11.0	5.7	21.1	6.1	4.4	70.1	0.8	
Pb	1.00	2.00	2.00	2.70	5.80	2.3	5.7	2.1	1.7	0.7	1.9	2.1	1.7	1.8	0.8	1.2	1.8	1.4	
Zn	23.00	47.00	48.00	45.00	22.00	10	21	15	27	23	18	23	176	27	18	27	16	17	
Au (ppb)	<0.5	<0.5	1.00	<0.5	<0.5	<0.5	0.6	<0.5	<0.5	1.0	3.8	<0.5	1.6	<0.5	0.8	<0.5	2.6	3.7	
Rare earth elements (ppm)																			
La	20.00	16.70	16.60	39.20	14.50	11.0	40.4	31.3	22.0	0.9	74.0	36.7	14.6	2.7	0.4	0.7	11.4	17.4	
Ce	36.60	33.40	35.90	69.90	27.20	26.9	66.5	67.0	44.9	0.6	143.2	81.8	41.0	5.3	0.7	0.5	20.6	41.1	
Pr	4.21	4.13	5.05	7.11	3.47	3.67	7.70	8.46	5.28	0.16	13.62	9.11	5.65	0.60	0.14	0.18	2.05	4.97	
Nd	16.90	16.60	20.50	24.70	14.90	14.8	29.1	34.5	17.6	1.1	39.9	36.3	24.9	2.4	0.8	0.6	8.0	18.4	
Sm	20.00	3.58	4.69	3.86	2.86	3.49	3.84	6.99	2.95	0.16	5.22	7.10	5.53	0.34	0.15	0.22	1.06	4.41	
Eu	0.81	0.92	1.13	0.85	0.81	0.58	0.54	1.06	0.71	0.04	1.34	1.05	1.17	0.06	0.05	0.05	0.15	0.91	
Gd	2.76	3.52	4.5	3.75	3.06	3.68	3.32	6.33	2.60	0.16	4.42	6.43	5.03	0.46	0.20	0.34	1.05	4.71	
Tb	0.44	0.53	0.78	0.55	0.47	0.59	0.41	0.89	0.38	0.03	0.59	0.89	0.68	0.05	0.03	0.04	0.14	0.68	
Dy	2.78	3.24	5.20	3.20	3.29	3.89	2.70	5.82	2.50	0.22	3.51	5.52	4.06	0.44	0.22	0.18	0.92	4.60	

Table 2- continued

Sample no	TP-3	TP-10	TP-12	TP-18	TP-23	TK-1	TK-15	KT-13	KT-23	TK-17	TK-31	KT-3	KT-24	TK-10	TK-11	TK-13	TK-14	TK-22		
Rock type	TOPIK PLUTON				ENDOSKARN ZONE				Pyroxene-garnet skarn				EXOSKARN ZONE				Pyroxene skarn			
Skarn facies					Plagioclase-pyroxene skarn															
Rare earth elements (ppm)																				
Ho	0.51	0.72	1.03	0.69	0.60	0.82	0.58	1.17	0.46	0.03	0.62	1.06	0.80	0.12	0.06	0.06	0.19	0.94		
Er	1.70	2.30	3.23	1.93	1.89	2.56	1.70	3.40	1.46	0.11	1.85	3.10	2.36	0.43	0.21	0.21	0.57	2.67		
Tm	0.27	0.38	0.50	0.32	0.31	0.39	0.26	0.52	0.20	0.03	0.27	0.49	0.32	0.10	0.04	0.04	0.11	0.41		
Yb	1.79	2.57	3.76	2.48	2.07	3.01	1.90	3.50	1.48	0.32	1.94	3.10	2.31	0.87	0.47	0.29	0.83	2.86		
Lu	0.31	0.40	0.58	0.38	0.33	0.44	0.35	0.57	0.18	0.06	0.30	0.47	0.33	0.15	0.10	0.05	0.19	0.49		
ΣREE	92.15	88.59	103.90	158.92	75.76	75.82	159.30	171.51	102.7	3.92	290.78	193.12	108.74	14.02	3.57	3.46	47.26	104.5		
ΣLREE	84.35	78.85	88.82	149.37	66.80	64.12	151.40	155.64	96.04	3.12	281.70	178.49	97.88	11.86	2.44	2.59	44.31	91.90		
ΣHREE	7.80	10.14	15.08	9.55	8.96	11.70	7.90	15.87	6.66	0.80	9.08	14.63	10.86	2.16	1.13	0.87	2.95	12.65		
LREE/HREE	10.8	7.8	5.9	15.6	7.5	5.5	19.2	9.8	14.4	3.9	31.0	12.2	9.0	5.49	2.2	3.0	15.0	7.26		
(La/Yb) <sub>n</sub>	8.01	4.66	3.17	11.34	5.02	2.62	15.25	6.41	10.66	2.02	27.36	8.49	4.53	2.23	0.61	1.73	9.85	4.36		
Eu/Eu*	0.83	0.78	0.71	0.67	0.83	0.49	0.45	0.48	0.77	0.76	0.83	0.47	0.67	0.46	0.88	0.56	0.43	0.61		
Sample no	ÇK-2	ÇK-7	ÇK-9	ÇK-21	KT-12	KT-16	ÇK-4	ÇK-6	ÇK-12	ÇK-16	ÇK-26	KT-10b	KT-19	TK-24	KT-4	ÇK-14	ÇK-22	KB-7		
Rock type	EXOSKARN ZONE												İNGÖNÜ MARBLE							
Skarn facies	Garnet skarn				Garnet-pyroxene skarn															
Major oxide (%)																				
SiO <sub>2</sub>	36.38	36.26	38.59	36.63	60.98	41.18	37.65	38.54	38.68	38.30	37.43	76.79	69.70	0.53	0.16	0.23	0.10	0.37		
TiO <sub>2</sub>	<0.01	<0.01	0.21	0.01	0.15	0.07	0.01	0.01	0.19	0.22	<0.01	0.02	<0.01	<0.01	<0.01	<0.01	<0.01	<0.01		
Al <sub>2</sub> O <sub>3</sub>	2.22	9.23	13.33	1.46	5.48	8.82	7.79	11.02	6.28	6.70	6.36	1.29	0.31	0.07	0.05	<0.01	0.03	0.10		
Fe <sub>2</sub> O <sub>3</sub>	25.71	14.85	11.57	27.04	11.95	18.03	15.80	13.11	18.28	18.96	19.94	7.91	11.61	0.16	0.05	0.06	0.08	0.05		
MnO	1.00	1.80	2.38	1.03	0.94	0.79	1.88	2.70	1.62	1.57	1.51	0.59	1.68	0.02	<0.01	0.01	<0.01	<0.01		
MgO	0.70	1.09	0.64	0.49	0.33	0.33	1.49	1.54	2.00	1.38	1.04	1.21	2.32	0.81	0.56	1.43	1.00	0.83		
CaO	30.92	29.67	29.46	30.08	18.27	29.42	30.43	29.56	29.33	30.17	30.59	9.74	12.74	55.35	55.77	55.07	55.43	55.29		
Na <sub>2</sub> O	<0.01	<0.01	0.02	<0.01	0.08	<0.01	<0.01	0.02	0.02	0.01	<0.01	0.03	0.07	<0.01	<0.01	<0.01	<0.01	<0.01		
K <sub>2</sub> O	<0.01	<0.01	0.01	<0.01	0.10	0.03	<0.01	<0.01	<0.01	<0.01	<0.01	<0.01	<0.01	0.02	<0.01	<0.01	<0.01	0.03		
P <sub>2</sub> O <sub>5</sub>	0.03	0.03	0.02	0.02	0.04	0.02	0.04	0.05	0.05	0.04	0.04	0.06	0.05	<0.01	0.02	<0.01	<0.01	<0.01		
Cr <sub>2</sub> O <sub>3</sub>	0.034	0.029	0.035	0.031	0.032	0.034	0.030	0.056	0.024	0.028	0.024	0.063	0.051	<0.002	<0.002	<0.002	<0.002	0.002		
A.Z.	2.8	6.5	3.7	3.0	1.6	1.2	4.3	3.3	3.4	2.5	2.8	1.4	0.4	43.0	43.4	43.2	43.3	43.3		
Total	99.84	99.49	99.92	99.80	99.93	99.93	99.40	99.91	99.89	99.89	99.74	99.10	98.91	99.96	99.97	99.96	99.96	99.97		

Table 2- continued

Sample no	ÇK-2	ÇK-7	ÇK-9	ÇK-21	KT-12	KT-16	ÇK-4	ÇK-6	ÇK-12	ÇK-16	ÇK-26	KT-10b	KT-19	TK-24	KT-4	ÇK-14	ÇK-22	KB-7	
Rock type	İNÖNÜ MARBLE																		
Skarn facies	Garnet-pyroxene skarn																		
Trace elements (ppm)	Garnet skarn																		
	EXOSKARN ZONE																		
W	808.2	3411.5	86.3	1163.6	293.5	8.7	3853.9	38.6	107.9	270.8	1320.1	6013.4	7615.5	1.0	<0.5	<0.5	0.5	<0.5	
Mo	40.1	82.5	2.7	17.8	6.7	0.7	155.9	0.6	10.4	20.7	99.3	492.6	44.0	<0.1	<0.1	<0.1	<0.1	0.1	
Cu	1.4	1.0	1.2	0.8	2.6	15.0	1.4	1.2	1.1	1.0	0.8	2.9	1.6	5.5	1.9	1.4	2.6	0.9	
Pb	0.7	1.8	0.6	0.6	0.6	1.3	0.7	0.7	0.6	0.5	0.5	0.9	0.8	1.2	0.3	0.3	0.4	0.9	
Zn	11	32	43	17	17	38	32	26	36	32	8	19	29	1	2	2	2	1	
Au (ppb)	0.8	<0.5	<0.5	<0.5	0.6	1.8	0.6	<0.5	<0.5	<0.5	2.2	2.1	3.7	<0.5	<0.5	<0.5	<0.5	<0.5	
Rare earth elements (ppm)																			
La	1.6	0.3	0.8	1.8	1.9	1.0	0.9	0.6	2.1	2.4	1.0	0.8	0.9	4.4	1.8	1.4	0.7	0.8	
Ce	5.1	1.8	2.0	3.7	3.1	7.9	3.6	2.5	9.7	12.0	5.9	2.7	1.8	2.2	0.7	0.5	0.7	1.0	
Pr	0.79	0.54	0.45	0.38	0.69	2.25	0.91	0.82	1.67	2.08	0.97	0.40	0.21	0.87	0.24	0.20	0.11	0.16	
Nd	2.9	4.0	4.6	1.1	4.8	15.2	5.0	5.8	7.9	10.5	2.9	1.7	0.9	4.0	0.8	0.8	0.3	1.0	
Sm	0.27	0.58	1.76	0.20	1.49	2.92	0.37	0.72	1.78	2.27	0.22	0.28	<0.05	0.66	0.11	0.06	<0.05	0.11	
Eu	0.42	0.70	0.83	0.20	0.70	1.61	0.45	1.00	0.56	0.69	0.20	0.12	0.02	0.16	0.03	0.04	<0.02	0.04	
Gd	0.35	0.43	2.63	0.22	1.54	2.27	0.36	0.38	1.19	1.61	0.25	0.21	0.05	0.99	0.34	0.29	0.11	0.16	
Tb	0.04	0.03	0.36	0.02	0.17	0.27	0.05	0.04	0.13	0.15	0.03	0.03	<0.01	0.13	0.04	0.04	0.02	0.02	
Dy	0.28	0.19	2.65	0.18	1.17	1.70	0.38	0.37	0.52	0.77	0.27	0.18	<0.05	0.72	0.32	0.23	0.11	0.19	
Ho	0.06	0.05	0.66	0.04	0.17	0.34	0.07	0.05	0.10	0.11	0.04	0.03	<0.02	0.18	0.08	0.04	<0.02	0.04	
Er	0.11	0.11	2.04	0.11	0.44	1.11	0.12	0.19	0.27	0.24	0.14	0.07	<0.03	0.46	0.21	0.18	0.13	0.14	
Tm	0.03	0.02	0.29	0.01	0.08	0.17	0.02	0.03	0.04	0.05	0.02	0.01	<0.01	0.08	0.03	0.02	0.02	0.01	
Yb	0.21	0.18	1.76	0.07	0.49	1.06	0.17	0.14	0.20	0.33	0.12	0.09	<0.05	0.41	0.21	0.15	0.07	0.11	
Lu	0.03	0.03	0.27	0.01	0.06	0.15	0.03	0.01	0.04	0.05	0.02	0.02	<0.01	0.05	0.03	0.03	0.01	0.01	
ΣREE	12.19	8.96	21.10	8.04	16.80	37.95	12.43	12.65	26.20	33.25	12.08	6.64	3.81	15.31	4.94	3.98	2.28	3.79	
ΣLREE	11.43	8.35	13.07	7.60	14.22	33.15	11.59	11.82	24.90	31.55	11.44	6.21	3.81	13.28	4.02	3.29	1.92	3.27	
ΣHREE	0.76	0.61	8.03	0.44	2.58	4.80	0.84	0.83	1.30	1.70	0.64	0.43	-	2.03	0.92	0.69	0.36	0.52	
LREE/HREE	15.04	13.69	1.63	17.27	5.51	6.91	13.80	14.24	19.15	18.56	17.88	14.44	-	6.54	4.37	4.77	5.33	6.29	
(La/Yb)n	5.47	1.20	0.33	18.44	2.78	0.68	3.80	3.07	7.53	5.22	5.98	6.38	-	7.70	6.15	6.69	7.17	5.22	
Eu/Eu*	4.18	4.10	1.18	2.90	1.40	1.84	3.72	5.26	1.11	1.05	2.60	1.45	-	0.60	0.44	0.76	-	0.92	

Table 3-  $\Sigma$ REE concentrations and LREE/HREE, (La/Yb)<sub>n</sub>, Eu/Eu\* ratios of Topuk granodiorite, skarn facies and İnönü marble and scheelite-containing samples.

ROCKS	$\Sigma$ REE(ppm)	$\Sigma$ LREE(ppm)	$\Sigma$ HREE(ppm)	LREE/HREE	(La/Yb) <sub>n</sub>	Eu/Eu*
<i>TOPUK PLUTON</i>	75.8-158.9 (mean 106.2)	66.8-149.4 (mean 95.4)	7.8-15.1 (mean 10.7)	5.9-15.6 (mean 9.1)	3.17-11.34 (mean 6.35)	0.67-0.83 (mean 0.76)
<i>ENDOSKARN ZONE</i>						
Plg-Pyx skarn	75.8-171.5 (mean 114.6)	64.1-155.6 (mean 103.7)	6.7-15.9 (mean 10.9)	5.5-19.2 (mean 10.4)	2.62-15.25 (mean 10.17)	0.45-0.84 (mean 0.77)
<i>EXOSKARN ZONE</i>						
Pyx-Gar skarn	108.7-290.8 (mean 183.0)	97.9-281.7 (mean 171.9)	9.1-14.6 (mean 11.1)	9.0-31.0 (mean 16.3)	4.53-27.36 (mean 12.63)	0.47-0.83 (mean 0.63)
<i>Scheelite-containing samples</i>	3.9	3.1	0.8	3.9	2.02	0.76
Pyx skarn	14.0-104.6 (mean 55.3)	11.9-91.9 (mean 49.4)	2.2-12.7 (mean 5.9)	5.5-15.0 (mean 9.3)	2.23-9.85 (mean 5.48)	0.43-0.61 (mean 0.50)
<i>Scheelite-containing samples</i>	3.5-3.6 (mean 3.5)	2.4-2.6 (mean 2.5)	0.87-1.13 (mean 1.00)	2.2-2.9 (mean 2.6)	0.61-1.73 (mean 1.17)	0.56-0.88 (mean 0.72)
Gar skarn	16.8-38.0 (mean 25.3)	13.1-33.2 (mean 20.2)	2.6-8.0 (mean 5.1)	1.6-6.9 (mean 4.7)	0.33-2.78 (mean 1.26)	1.18-1.84 (mean 1.47)
<i>Scheelite-containing samples</i>	8.0-12.2 (mean 9.7)	7.6-11.4 (mean 9.1)	0.4-0.8 (mean 0.6)	13.7-17.3 (mean 15.3)	1.20-18.44 (mean 8.37)	2.90-4.18 (mean 3.73)
Gar-Pyx skarn	12.7-33.3 (mean 24.0)	11.8-31.6 (mean 22.8)	0.8-1.7 (mean 1.3)	14.2-19.6 (mean 17.3)	3.07-7.53 (mean 5.27)	1.05-5.26 (mean 2.47)
<i>Scheelite-containing samples</i>	3.8-12.4 (mean 8.7)	3.8-11.6 (mean 8.3)	0.4-0.8 (mean 0.5)	13.8-17.9 (mean 11.5)	3.80-6.38 (mean 4.04)	1.45-3.72 (mean 1.94)
<i>İNÖNÜ MARBLE</i>	2.3-15.3 (mean 6.1)	1.9-12.3 (mean 5.2)	0.4-2.0 (mean 0.9)	4.4-6.5 (mean 5.5)	5.22-7.70 (mean 6.57)	0.44-0.92 (mean 0.55)

enriched 0.3 to 15-fold whilst HREEs are enriched only 0.3 to 2-fold (Figure 4-8). Regarding marble, (La/Yb)<sub>n</sub> ratio is in the range of 5.22 to 7.70 (ave. 6.57), LREE/HREE ratio is between 4.4 and 6.5 (ave. 5.5 ppm) and (Eu/Eu\*)<sub>n</sub> ratio (except for sample ÇK-22) varies from 0.44 to 0.92 (Tables 2 - 3). Eu (<0.02 ppm) and Sm (<0.05 ppm) concentrations of sample ÇK-22 are quite low. According to these results, LREE and HREE contents of marbles show flat patterns with variable Eu anomaly. REE trends of marbles display a significant negative Ce anomaly indicating deposition in marine environment (Murray et al., 1990).

Regarding Plg-Pyx skarn samples collected from granitoid contact, LREEs and HREEs have been enriched 10 to 115-fold and 10 to 15-fold with respect to chondrite (Figure 4). LREE enrichment is slightly higher than granodiorite. For the endoskarn zone (La/Yb)<sub>n</sub> ratio is in the range of 2.62 to 15.25 (ave. 10.17), LREE/HREE ratio is between 5.5 and 19.2 (ave. 10.4) and (Eu/Eu\*)<sub>n</sub> ratio varies from 0.45 to 0.84 (ave. 0.77) (Tables 2 - 3). According to these results, like the Topuk granodiorite, the endoskarn zone is enriched by LREE and depleted in Eu.

Regarding Pyx-Gar skarn samples with low tungsten content, LREEs and HREEs have been enriched 10 to 200-fold and 15 to 20-fold with respect to chondrite (Figure 5). In one sample with relatively high tungsten concentration (TK-17) REEs are quite low; LREEs and HREEs have been enriched 0.5 to 3-fold and 0.5 to 2-fold. LREEs of samples with low tungsten content from Pyx-Gar skarn are much enriched than Topuk granodiorite. (La/Yb)<sub>n</sub>, LREE/HREE and (Eu/Eu\*)<sub>n</sub> ratios of these samples are 4.53 to 27.36 (ave. 12.63), 9.0 to 31.0 (ave. 16.3) and 0.47 to 0.83 (ave. 0.63), respectively (Tables 2 - 3). These samples are represented by REE patterns similar to Topuk granodiorite – enriched LREE and depleted Eu trends (Figure 5). For the sample with relatively high tungsten content, (La/Yb)<sub>n</sub>, LREE/HREE and (Eu/Eu\*)<sub>n</sub> ratios are found 2.02, 3.9 and 0.76. This sample shows depletion for Ce (consistent with marbles) and Eu and a flat pattern for LREE-HREE (consistent with Topuk granodiorite). Different from granodiorite and carbonate rocks, the same sample displays a relative enrichment for Tm, Yb and Lu.

$\Sigma$ REE contents of samples from the Pyx skarn facies (except for sample TK-22) are slightly depleted

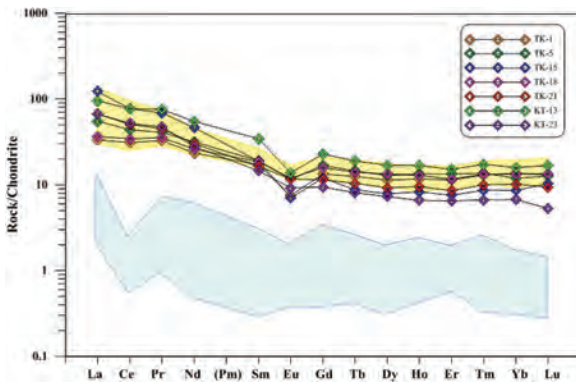


Figure 4- Rare earth element diagram for plagioclase-pyroxene skarn (endoskarn zone), Topuk pluton and İnönü marble (chondrite normalized values are from Nakamura, 1974) (yellow and blue shaded areas belong to Topuk pluton and İnönü marble).

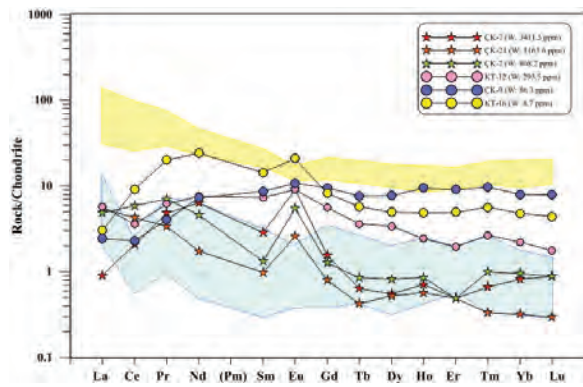


Figure 7- Rare earth element diagram for garnet skarn (exoskarn zone), Topuk pluton and İnönü marble (chondrite normalized values are from Nakamura, 1974) (yellow and blue shaded areas belong to Topuk pluton and İnönü marble).

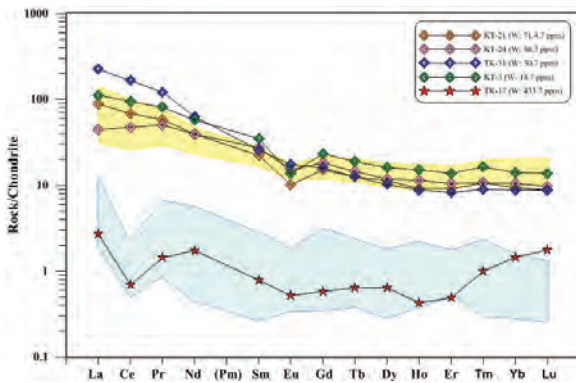


Figure 5- Rare earth element diagram for pyroxene-garnet skarn (exoskarn zone), Topuk pluton and İnönü marble (chondrite normalized values are from Nakamura, 1974) (yellow and blue shaded areas belong to Topuk pluton and İnönü marble).

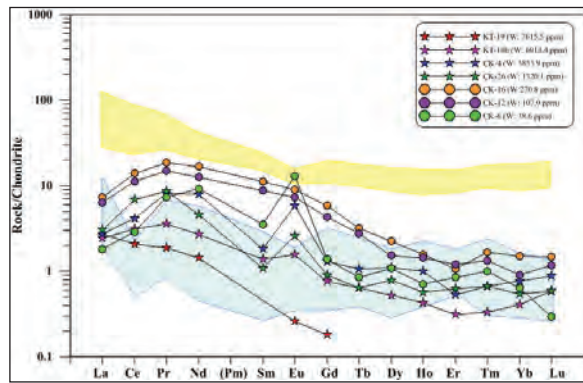


Figure 8- Rare earth element diagram for garnet-pyroxene skarn (exoskarn zone), Topuk pluton and İnönü marble (chondrite normalized values are from Nakamura, 1974) (yellow and blue shaded areas belong to Topuk pluton and İnönü marble).

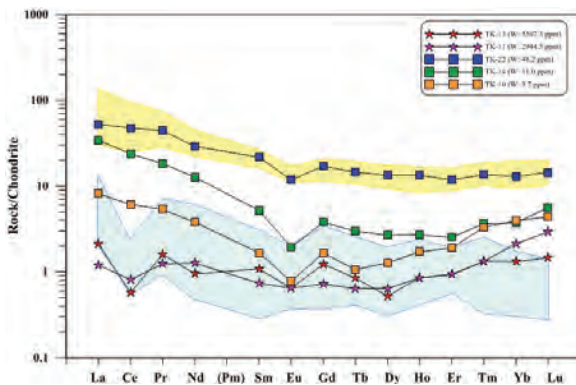


Figure 6- Rare earth element diagram for pyroxene skarn (exoskarn zone), Topuk pluton and İnönü marble (chondrite normalized values are from Nakamura, 1974) (yellow and blue shaded areas belong to Topuk pluton and İnönü marble).

with respect to Topuk granodiorite (Tables 2 - 3; Figure 6). However, their Tm, Yb and Lu concentrations are partly higher than those of granodiorite and carbonate rocks. Samples with low tungsten content (TK-10, TK-14 and TK-22) are represented by (La/Yb)<sub>n</sub>, LREE/HREE and (Eu/Eu\*)<sub>n</sub> ratios of 2.23 to 9.85 (ave. 5.48), 5.5 to 15.0 (ave. 9.3) and 0.43 to 0.61 (ave. 0.50) and resemble Topuk granodiorite with their enriched LREE pattern and negative Eu anomaly. With increasing W content, ΣREE and Ce concentrations are significantly decreased (Figure 6). Samples with low W content are similar to İnönü marble with their low ΣREE content, negative Ce anomaly and flat-like pattern of LREE and HREEs and their negative Eu trend is consistent with granodioritic rocks (Figure 6). For these samples (La/Yb)<sub>n</sub> is 0.61 to 1.73 (ave. 1.17), LREE/HREE is 2.2 to 2.9 (ave. 2.6) and (Eu/Eu\*)<sub>n</sub> is 0.56 to 0.88 (ave. 0.72) (Tables 2 - 3).

In Gar and Gar-Pyx skarn where zoned garnets are formed  $\Sigma$ REE contents are significantly lower than those of Topuk granodiorite (Tables 2 - 3; Figures 7 - 8). Samples with dominant andradite composition that formed via fluid infiltration are characteristic with convex LREE pattern, high Pr and Nd concentrations and positive Eu anomaly (Whitney and Olmsted, 1998).  $\Sigma$ REE contents of W-enriched samples from Gar skarn (8.0 to 12.2 ppm, ave. 9.7 ppm) are lower than those of W-poor samples (16.8 to 38.0 ppm, ave. 25.3 ppm) (Tables 2 - 3). Both type samples display positive Eu anomaly (Figure 7). Samples with low W content are represented by convex LREE trend and enriched HREE patterns. For these samples, (La/Yb)<sub>n</sub> is 0.33 to 2.78 (ave. 1.26), LREE/HREE ratio is 1.6 to 6.9 (ave. 4.7) and (Eu/Eu\*)<sub>n</sub> ratio is 1.18 to 1.84 (ave. 1.47). For W-enriched samples, (La/Yb)<sub>n</sub> is 1.20 to 18.44 (ave. 8.37), LREE/HREE ratio is 13.7 to 17.7 (ave. 15.3) and (Eu/Eu\*)<sub>n</sub> ratio is 2.90 to 4.18 (ave. 3.73). These samples with partly enriched LREE contents resemble the Topuk granodiorite and with HREE trends resemble the İnönü marble (Table 3; Figure 7).

$\Sigma$ REE contents of Gar-Pyx skarn samples are lower than Topuk granodiorite (3.8 to 33.3 ppm, ave. 15.29 ppm) (Tables 2 - 3; Figure 8). With increasing W concentration  $\Sigma$ REE content is definitively decreased. Sample KT-19 with W concentration (7615.5 ppm) higher than other samples have quite low Eu and HREE contents (Tables 2 - 3; Figure 8). For other samples, (La/Yb)<sub>n</sub> is 3.07 to 7.53, LREE/HREE ratio is 14.2 to 19.6 and (Eu/Eu\*)<sub>n</sub> is 1.05 to 5.26. Samples are characterized by convex LREE pattern, positive Ce, Pr, Nd and Eu anomalies and HREE trends similar to carbonate rocks.

## 6. Discussion and Results

Like other worldwide W-skarn deposits (Einaudi et al., 1981) the Kozbudaklar exoskarn zone is of calcic character with respect to major oxide content. This is consistent with mineralogical observations reported by Orhan (2017). The scheelite mineralization at Kozbudaklar occurs only in proximal zone of exoskarn zone. W and Mo concentrations are increased from Pyx and Pyx-Gar skarn (W: 433.7 to 5507 ppm, ave. 2330 ppm; Mo: 7.8 to 90.2 ppm, ave. 40.28 ppm) to Gar and Gar-Pyx skarn (W: 270.8 to 7615.5 ppm, ave. 2485.8 ppm; Mo: 6.7 to 492.5 ppm, ave. 106.6 ppm). Petrographic and mineral chemistry studies led Orhan (2017) to suggest that Pyx and Pyx-Gar skarn

were formed at the first phase of prograde stage and WO<sub>3</sub> and MoO<sub>3</sub> contents of scheelite in these skarn zones were found 76.95 to 78.3% and 0.35 to 1.42%, respectively. Scheelites in zoned garnets (Gar and Gar-Pyx skarn) which represent the second phase of prograde stage WO<sub>3</sub> MoO<sub>3</sub> in the range of 72.13 to 73.5% and 1.75 to 10.27% indicating a slight increase for Mo concentration.

Studies carried out on W-skarn deposits showed that due to circulation of hydrous fluids scheelite is sweep out towards the marble contact and scheelite grade is increased in the distal zone with the increase of hydrous mineral content and Ca ion activity (Kwak and Tan, 1981; Newberry, 1982; Zaw and Singoyi, 2000). By the mobilizing of Mo-enriched scheelites with meteoric water flux, pure scheelite and molybdenite are redeposited in association with hydrous minerals and quartz veins (Newberry, 1982). At Kozbudaklar skarn deposit, increase in Mo concentration cannot be attributed to molybdenite deposition indeed it is sourced from scheelite composition. According to Kwak and Tan (1981), scheelite forming in zoned garnet bands is not dissolved in some cases and therefore does not attain an economic size during the retrograde stage. At Kozbudaklar, increase in W and Mo contents indicates that oxidation conditions were changed during the fractionation of pluton (Newberry, 1998) which prevented scheelite to reach at a mineable grade.

The Topuk granodiorite hosting the scheelite mineralization is represented by an enriched LREE pattern and slight negative Eu anomaly (Eu/Eu\* = 0.67 to 0.83). The İnönü marble, however, shows more flat LREE trend and negative Ce and variable Eu anomalies.

The Kozbudaklar deposit shows two different REE patterns through the skarn formation process. In addition to diverse rare earth element trends representing two different stages,  $\Sigma$ REE concentrations and Eu/Eu\* ratios are also variable (Table 3). At Kozbudaklar, during the first phase of prograde stage (Plg-Pyx, Pyx-Gar and Pyx skarn), REE contents and Eu/Eu\* (0.43 to 0.84) of samples with low tungsten concentration are quite consistent with Topuk granodiorite (Figures 4-5-6; Table 3). In the first stage when high-temperature early magmatic fluids were mobilized,  $\Sigma$ REE concentrations are found to be partly higher than granodiorite. In this facies where LREEs are enriched, LREE/HREE and (La/Yb)

n ratios are 5.5 to 31.0 and 2.23 to 27.36, respectively. In the second phase of prograde stage  $\Sigma$ LREE tend to be decreased (Table 3; Figure 9). Gar and Gar-Pyx skarn facies are characterized by positive Pr and Nd patterns, high  $Eu/Eu^*$  (1.05 to 5.26) and low  $(La/Yb)_n$  ratios (0.33 to 7.53). In the progressive phase of prograde stage, LREE concentrations of the host rock were significantly depleted (by the fractionation of Topuk granitoid). High  $Eu/Eu^*$  anomaly implies mobilization of high-temperature fluids and changes in oxidation conditions in the second stage (Bau, 1991; Whitney and Olmsted, 1998; Bi et al., 2004; Oyman et al., 2013).

Samples with high scheelite contents also exhibit two different REE patterns. Scheelite-enriched samples show variable Ce and Eu anomalies. Mo-poor scheelites that formed in the first phase of prograde stage display flat-like LREE pattern and negative Ce anomaly resembling the İnönü marble and their  $Eu/Eu^*$  values (0.56 to 0.88) are similar to Topuk granodiorite (Figures 5-6; Table 3). LREE/HREE (2.2 to 3.9) and  $(La/Yb)_n$  (0.61 to 2.02) ratios are considerably low. Mo-enriched scheelites of the second stage are represented by HREE trend conformable with the marbles and positive Ce and Eu anomalies (Figures 7 - 8; Table 3). Their LREE/HREE and  $(La/Yb)_n$  ratios are 13.7 to 17.9 and 1.20 to 18.44, respectively. LREE/HREE ratios of Mo-enriched scheelites are greater than those of Mo-poor scheelites. However, it is clear that as the W concentration of samples is increased  $\Sigma$ REE concentrations are decreased (Figure

10). It was also observed in Moroccan tungsten skarn deposits where W concentrations are increased with decreasing  $\Sigma$ REE concentrations (Giuliani et al., 1987). Giuliani et al. (1987) found that  $(La/Yb)_n$  and  $Eu/Eu^*$  of tungsten are extremely low when W concentrations (>1000 ppm) attain an economical potential and concluded that scheelite was not affected by the metamorphism and fluid-rock interaction under hydrothermal alteration conditions, in other words it behaved immobile. Considering low  $Eu/Eu^*$  ratios, they proposed reducing conditions for the scheelite formation and crystal formation was completed long before the interaction process.

It can be said that scheelite mineralization with low  $\Sigma$ REE contents that represents different stages of the Kozbudaklar skarn deposit was not affected by metamorphism and fluid-rock interaction under hydrothermal conditions. However, with increasing W concentration  $Eu/Eu^*$  ratios are found to increased (Figure 11a). Likewise Mo concentrations of the same samples are also increased (Figure 11b). Since Eu can replace Ca in scheelite, using positive or negative Eu anomalies redox conditions of ore-forming fluids may be estimated (Ghaderi et al., 1999). Negative Eu ( $Eu/Eu^*=0.56$  to 0.88) anomaly recorded at Kozbudaklar may indicate partly reducing conditions for the formation of first-stage scheelites (Giuliani et al., 1987). However, increasing Mo concentration of scheelites (ave. 40.28 ppm  $\rightarrow$  ave. 106.6 ppm) might show oxidized conditions for scheelite-mineralizing fluids (Ghaderi et al., 1999). Song et

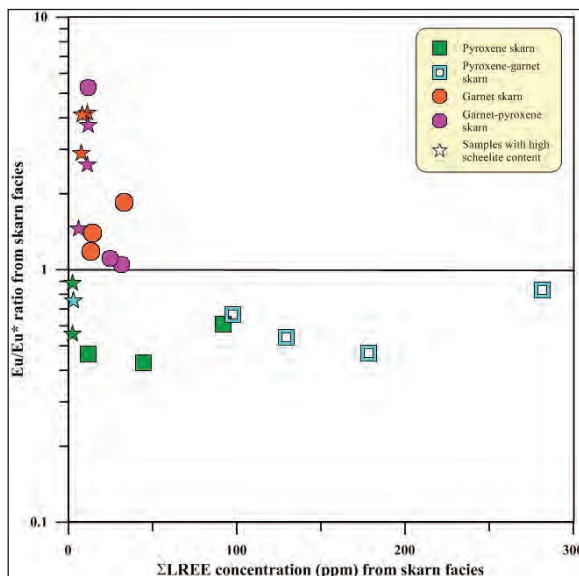


Figure 9-  $Eu/Eu^*$  ratios and  $\Sigma$ LREE concentrations of skarn zone samples.

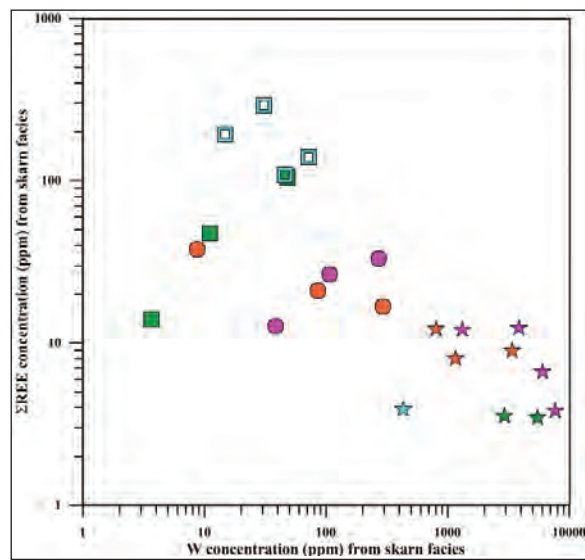


Figure 10-  $\Sigma$ REE and W concentrations of exoskarn zone samples (symbols as in figure 9).

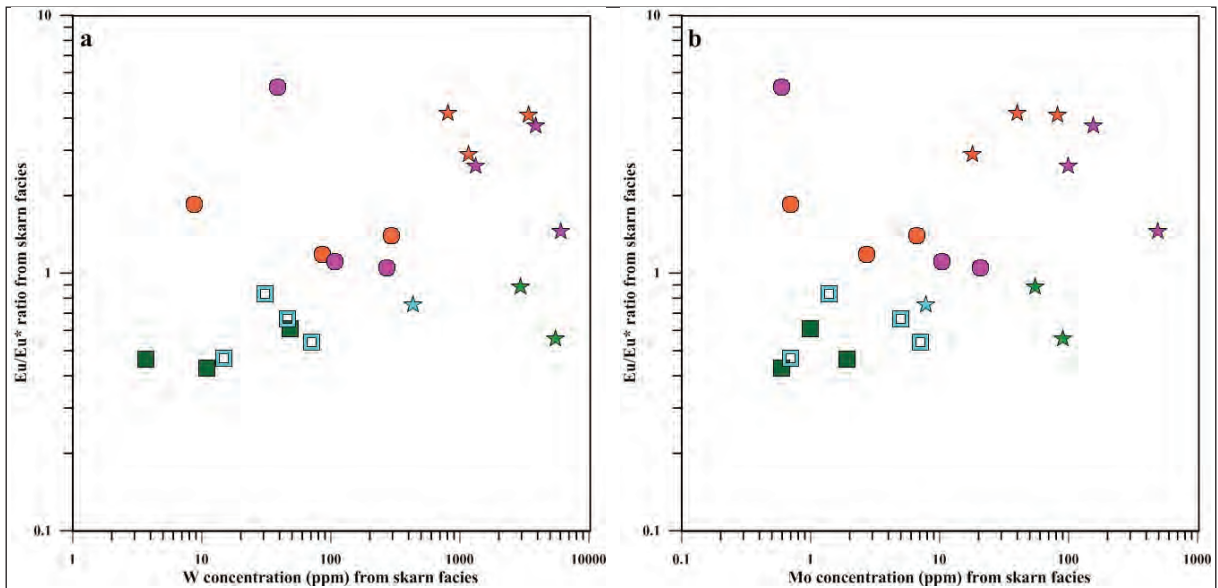


Figure 11- a) W and b) Mo concentrations and Eu/Eu\* ratios of exoskarn zone samples (symbols as in figure 9).

al. (2014) also pointed out that Mo concentration increases and maximum Eu anomaly exists under oxidizing conditions. However, it has been shown that under reducing conditions Mo content of scheelite is lowered which gives rise to formation of molybdenite. Orhan (2017) defined different reducing conditions for scheelites which deposited at different phases in the Kozbudaklar skarn deposit. The presence of calc-silicate minerals (due to their ferrous composition) (e.g. garnet, pyroxene) recognized in association with the first-phase scheelites led to Orhan (2017) to suggest that scheelite was deposited under moderately reducing/moderately oxidizing conditions whilst Mo-enriched scheelites were crystallized under much oxidizing conditions after the boiling. Decreases in  $\Sigma$ LREE and increases in W and Mo contents and Eu/Eu\* ratios support that second-phase scheelite mineralization took place during the fractionation of granitoid at much oxidizing conditions.

### Acknowledgement

This study was supported by the Scientific and Technological Research Council of Turkey under grand no YDABAG-111Y289. Authors thank to Dr. Mehmet Demirbilek and Dr. Ahmet Orhan for their help during field works. We are grateful for constructive review by Dr. Özcan Dumanlılar and two anonymous reviewers, which improved the manuscript.

### References

- Altunkaynak, Ş. 2007. Collision-driven slab break off magmatism in Northwestern Anatolia, Turkey. *Journal of Geology* 115, 63-82.
- Barton, M.D., Ilchik, R.P., Marikos, M.A. 1991. Metasomatizm. *Reviews in Mineralogy and Geochemistry* 26, 321-349.
- Bau, M. 1991. Rare-earth element mobility during hydrothermal and metamorphic fluid-rock interaction and the significance of the oxidation state of europium. *Chemical Geology* 93, 219-230.
- Bi, X., Hu, R., Cornell, D.H. 2004. The alkaline porphyry associated Yaoan gold deposit, Yunan, China: Rare earth element and stable isotope evidence for magmatic-hydrothermal ore formation. *Mineralium Deposita* 39, 21-20.
- Bingöl, E., Delaloye, M., Ataman, G. 1982. Granitic intrusion in Western Anatolia: a contribution to the geodynamic study of this area. *Ecloga Geologica Helvetica* 75 (2), 437-446.
- Brown, P.E., Bowman, J.R., Kelly, W. C. 1985. Petrologic and stable isotope constraints on source and evolution of skarn-forming fluids at Pine Creek, California. *Economic Geology* 80, 72-95.
- Burt, M.D. 1977. Mineralogy and petrology of skarn deposits. *Societa Italiana di Mineralogia e Petrologia* 33(2), 859-873.

- Delaloye, M., Bingöl, E. 2000. Granitoids from Western and Northwestern Anatolia: Geochemistry and modeling of geodynamic evolution. *International Geological Review* 42, 241-268.
- Einaudi, M.T., Meinert, L.D., Newberry, R.J. 1981. Skarn Deposits. *Economic Geology* 75, 317-391.
- Emre, H. 1996. Orhaneli Ofiyolitinin jeolojisi ve petrolojisi. Doktora Tezi, İstanbul Üniversitesi Fen Bilimleri Enstitüsü, İstanbul, 165 s. (unpublished).
- Fonteilles, M., Soler, P., Demange, M., Derre, C., Krier-Schellen, A.D., Verkaeren, J., Guy, B., Zahm, A. 1989. The scheelite skarn deposit of Salau (Ariege, French Pyrenees). *Economic Geology* 84, 1172-1209.
- Gerstner, M.R., Bowman, J.R., Parteris, J.D. 1989. Skarn formation at the Macmillan Pass Tungsten Deposit (Mactung), Yukon and Northwest Territories. I. P-T-X-V characterization of the methane-bearing skarn forming fluids. *The Canadian Mineralogist* 27, 545-563.
- Ghaderi, M., Palin, M.J., Sylvester, P.J., Campbell, I.H. 1999. Rare earth element systematics in scheelites from hydrothermal gold deposits in the Kalgoorlie-Norseman Region, Western Australia. *Economic Geology* 94, 423-437.
- Giuliani, G., Cheilletz, A., Mechiche, M. 1987. Behavior of REE during thermal metamorphism and hydrothermal infiltration associated with skarn and vein-type tungsten ore bodies in Central Morocco. *Chemical Geology* 64, 279-294.
- Harris, N.B.W., Kelley, S., Aral, I.O. 1994. Post-collision magmatism and tectonics in northwest Anatolia. *Contributions to Mineralogy and Petrology* 117, 241-252.
- Kwak, T.A.P., Tan, T.H. 1981. The geochemistry of zoning in skarn minerals at the King Island (Dolphin) mine. *Economic Geology* 76, 468-497.
- Lisenbee, A.A. 1972. Structural setting of the Orhaneli Ultramafic Massif near Bursa. Ph.D Thesis, University of State, Pennsylvania, USA, 170 pp. (unpublished).
- Lottermoser, B.G. 1992. Rare earth elements and hydrothermal ore formation processes. *Ore Geology Reviews* 7, 25-41.
- Meinert, L.D., Dipple, G.M., Nicolescu, S. 2005. World Skarn Deposits. Society of Economic Geologist, Inc. *Economic Geology* 100<sup>TH</sup> Anniversary volume, 299-336.
- Michard, A. 1989. Rare earth element systematics in hydrothermal fluids. *Geochimica et Cosmochimica Acta* 53, 745-750.
- MTA. 1965. Türkiye Volfram ve Molibden Yatakları, Maden Tetkik ve Arama Genel Müdürlüğü Rapor No: 128, Ankara (unpublished).
- MTA. 1973. 1/25.000 ölçekli jeoloji haritası, H22d4, H22d3, İ21b2, İ22a1, İ22a2 Paftaları. Maden Tetkik ve Arama Genel Müdürlüğü, Ankara.
- MTA. 2002. 1/500.000 ölçekli Türkiye Jeoloji Haritası, İstanbul ve İzmir Paftaları. Maden Tetkik ve Arama Genel Müdürlüğü, Ankara.
- Murray, R.W., Buchholz, T., Brink, M.R., Jones, D.L., Gerlach, D.C., Russ, G.P. 1990. Rare Earth Elements as Indicators of Different Marine Depositional Environments in Chert and Shale. *Geology* 18, 268-272.
- Nakamura, N. 1974. Determination of REE, Ba, Mg, Na and K in carbonaceous and ordinary chondrites. *Geochimica et Cosmochimica Acta* 38, 757-775.
- Newberry, R.J. 1982. Tungsten-bearing skarns of the Sierra Nevada. I, the Pine Creek mine, California. *Economic Geology* 77, 823-844.
- Newberry, R.J. 1998. W-and Sn-Skarn deposits, Lentz, D.R. (Ed.). Mineralized intrusion-related skarn systems. Mineralogical Association of Canada Short Course Series 26, 289-335.
- Okay, A.I. 1985. Kuzeybatı Anadolu'da yer alan metamorfik kuşaklar. *Ketin Sempozyumu Türkiye Jeoloji Kurultayı yayınları*, 83-93.
- Okay, A.I. 2004. Tectonics and high pressure metamorphism in northwest Turkey, Field trip guide book-P01. 32<sup>TH</sup> International Geological Congress, APAT, Italy, 56 pp.
- Okay, A.I. 2011. Tavşanlı Zonu: Anatolid-Torid Bloku'nun dalma-batmaya uğramış kuzey ucu. *Maden Tetkik ve Arama Dergisi* 142, 195-226.
- Okay, A.I., Kelley, S.P. 1994. Tectonic setting, petrology and geochronology of jadeite + glaucophane and chloritoid + glaucophane schists from northwest Turkey. *Journal of Metamorphic Geology* 12, 455-466.
- Okay, A.I., Harris, N.B.W., Kelley, S.P., 1998. Exhumation of blueschists along a Tethyan suture in northwest Turkey. *Tectonophysics* 285, 275-299.
- Okay, A.I., Satır, M. 2006, Geochronology of Eocene plutonism and metamorphism in northwest Turkey: evidence for a possible magmatic arc. *Geodinamica Acta* 19, 251-266.
- Orhan, A. 2017. Evolution of the Mo-rich scheelite skarn mineralization at Kozbudaklar, Western Anatolia, Turkey: Evidence from mineral chemistry and fluid inclusion. *Ore Geology Reviews* 80, 141-165.

- Orhan, A., Demirbilek, M., Mutlu, H. 2014a. Mineral and whole-rock chemistry of the Topuk Granitoid (Bursa, Western Anatolia, Turkey). EGU General Assembly, Geophysical Research Abstracts, v.16.
- Orhan, A., Mutlu, H., Demirbilek, M. 2014b. Kozbudaklar (Bursa, Batı Anadolu) Şeelit Skarn Yatağının Mineralojik ve Jeokimyasal Karakteristikleri. 67. Türkiye Jeoloji Kurultayı, 14-18 Nisan, Ankara, 516-517.
- Orhan, A., Mutlu, H. 2015. Topuk Plütunu ile İlişkili Şeelit Skarn Yatağının (Bursa, Batı Anadolu) Evrimi ve Hidrotermal Akışkanların Kökeni. 68. Türkiye Jeoloji Kurultayı, 6-10 Nisan, Ankara, 336-339.
- Orhan, A., Mutlu, H., Demirbilek, M. 2015. Topuk Plütunu ile ilişkili skarn yataklarının (Bursa, Batı Anadolu) mineralojik, jeokimyasal ve kökenselel incelenmesi. Türkiye Bilimsel ve Teknolojik Araştırma Kurumu Proje No: 111Y289, 212 s. (unpublished).
- Oyman, T., Özgenç, İ., Tokcaer, M., Akbulut, M. 2013. Petrology, geochemistry and evolution of the iron skarns along the northern contact of the Eğrigöz Plutonic complex, Western Anatolia, Turkey. Turkish Journal of Earth Science 22, 61-97.
- Örgün, Y. 1993. Topuk-Göynükbelen (Orhaneli-Bursa) Yöresi Nikel Oluşumlarının Kökenselel İncelenmesi. Doktora Tezi, İTÜ Fen Bilimleri Enstitüsü, İstanbul, 216 s. (unpublished).
- Pehlivan, A.N. 1987. Kuzeybatı Anadolu wolfram ağırlıklı polimetal arama projesi (Kavap Rapor No:1) Bursa-İnegöl-Keles-Orhaneli çevresinin genel jeokimya raporu. Maden Tetkik ve Arama Genel Müdürlüğü Rapor No: 8179, Ankara (unpublished).
- Romberg, H. 1938. Bursa Vilayetinde Sebihtepe'de, Karaisalak, Kuzbudak ve Keles'de Tetkik Olunan Yataklar Hakkında Rapor. Maden Tetkik ve Arama Genel Müdürlüğü Rapor No: 722, Ankara (unpublished).
- Sato, K. 1980. Tungsten Skarn Deposit of the Fujigatani Mine, Southwest Japan. Economic Geology 75, 1066-1082.
- Song, G., Qin, K., Li, G., Evans, N.J., Chen, L. 2014. Scheelite elemental and isotopic signatures: Implication for the genesis of skarn-type W-Mo deposits in the Chizhou Area, Anhui Province, Eastern China. American Mineralogist 99, 303-317.
- Sun, S.S., McDonough, W.F. 1989. Chemical and isotopic systematics of oceanic basalts: implications for mantle composition and processes. Saunders, A.D., Norry, M.J. (Eds.). Magmatism in ocean basins. Geological Society London. Special Publications 42, 313-345.
- Şengör, A.M.C., Yılmaz, Y. 1981. Tethyan Evolution of Turkey: A Plate Tectonic Approach. Tectonophysics 75, 181-241.
- Tekin, U.K., Göncüoğlu, M.C., Turhan, N. 2002. First evidence of Late Carnian radiolarians from the İzmir-Ankara suture complex, central Sakarya, Turkey: Implications of the opening age of the İzmir-Ankara branch of Neo-Tethys. Geobis 35, 127-135.
- Timon Sanchez, S.M, Moro Benito, M.C., Cembranos Perez, M.,L. 2009. Mineralogical and physiochemical evolution of the Los Santos scheelite skarn, Salamanca, NW Spain. Economic Geology 104, 961-995.
- Vander Auwera, J.V., Andre, L. 1991. Trace elements (REE) and isotopes (O, C, Sr) to characterize the metasomatic fluid sources: evidence from the skarn deposit (Fe, W, Cu) of Traversella (Ivrea, Italy). Contributions to Mineralogy and Petrology 106, 325-339.
- Whitney, P.R., Olmsted, J.F. 1998. Rare earth element metasomatism in hydrothermal system: The Willsboro-Lewis wollastonite ores, New York, USA. Geochimica et Cosmochimica Acta 62, 17, 2965-2977.
- Zaw, K., Singoyi, B. 2000. Formation of magnetite-scheelite skarn mineralization at Kara, Northwestern Tasmania: evidence from mineral chemistry and stable isotopes. Economic Geology 95, 1215-1230.



# Bulletin of the Mineral Research and Exploration

<http://bulletin.mta.gov.tr>



## GEOLOGY AND GEOCHEMISTRY OF NODULAR-PHOSPHATE AND FAULT-CONTROLLED HYDROTHERMAL-PHOSPHATE MINERALIZATIONS IN ARIKLI AND NUSRATLI VILLAGES (AYVACIK-ÇANAKKALE, NW TURKEY)

Abdulkali GÜNAYDIN<sup>a\*</sup>

<sup>a</sup>General Directorate of Mineral Reserach and Exploration, Middle Anatolia II.District Office, Konya. [orcid.org/0000-0002-4933-3936](https://orcid.org/0000-0002-4933-3936)

Research Article

### Keywords:

Arlıklı volcanites, phosphate, uranium, nodular phosphate, flourapatite.

### ABSTRACT

Uranium bearing phosphate mineralizations in the tuffs (ignimbrites) of Middle Miocene Arıklı volcanites in the vicinity of Arıklı and Nusratlı villages, Çanakkale have been known since 1977. In the study area, two types of phosphate mineralizations are present in different parts. First type and important one is in the tectonic zones in tuffs and along the contact between tuffs and Çetmi ophiolite and along the contacts of the units of the Küçükkuyu Formation in the Muharrem Tepe, Feyzullah Tepe, Örencik Tepe, Gedikharman Tepe in north and northwest of Arıklı village. Second type is the vein type mineralizations in the tuffs in Çarşılı Tepe, east of Nusratlı village. Both types of mineralizations are hydrothermal origin. Additionally, walnut-sized syngenetic phosphate nodules are also observed in the tuffs in Çarşılı Tepe. XRD and geochemical analysis of samples obtained from mineralizations indicated that the major phosphate bearing mineral is chlorapatite and they have P<sub>2</sub>O<sub>5</sub> contents ranging from 4.5 to 32.4%. The economic potential of the mineralization is not significant due to limited lateral and vertical continuity of the phosphate mineralization. So, in the study area, economically important phosphate deposit is not expected.

Received Date: 23.02.2016

Accepted Date: 28.07.2016

## 1. Introduction

Phosphate is an essential nutrient for livings but mostly used in fertilizer industry. In the earth's crust phosphates form hundreds of compounds but most important mineral is apatite. Phosphorus is the main element in apatite. Phosphorus is widespread in the earth's crust at an average concentration of about 0.081%.

Although, Turkey is an agricultural and industrial country, Turkey does not have enough phosphate potential to use in the agricultural industry. Turkey has to import phosphate to be able to meet the phosphate need of the agricultural industry. That is to say Turkey has to spend large sums of foreign currency to import phosphate. It is important that exploration potential of present phosphate deposits must be studied and efforts must be directed towards exploring new economic phosphate deposits (Önem, 2000).

The subject of phosphate mineralizations in this

study is located along Ayvacık town and Nusratlı village, in Çanakkale in the Biga Peninsula to the north of Edremit Bay. It is in the Ayvalık İ 17 d4 1/25000 scale map sheet.

Economic geology studies in the area were first conducted for uranium (Akgünlü and Sağlam, 1983). Çelik et al. (1999) and Günaydın and Çolak (2009) carried out studies on phosphate minerals, as uranium is intimately associated with phosphate minerals. Regional geological studies of the area were carried out by Oktay et al. (2003), Atabey et al. (2004), Duru et al. (2007). Günaydın (2013) conducted geological studies on alkali tuffs.

During this study all known phosphate occurrences have been re-viewed in order to find new phosphate deposits. To be able to detect phosphate presence in the rocks, scintillometer surveys and ammonium molybdate test have been applied. The scintillometer used was EDA 500. It measures CPS unit radioactivity

\* Corresponding author: Abdulkali GÜNAYDIN, [bakigunaydin@gmail.com](mailto:bakigunaydin@gmail.com)  
<http://dx.doi.org/10.19111/bulletinofmre.314197>

dispersed in the air. Measured radioactive CPS values have been relatively evaluated. To carry out test with ammonium molybdate, first the rocks were crushed then nitric acid ( $\text{HNO}_3$ ) was poured on to the powdered rock, then few drops of ammonium molybdate solution was put onto the sample. As a result of chemical reaction between nitric acid and ammonium molybdate, if the colour goes to canary yellow, it indicates the presence of phosphate in the rock. All former trenches were cleaned and new trenches were opened when necessary. In order to determine the relationship between the rock units and their relation with phosphate mineralizations, 1/5000 scaled detailed geological map covering all phosphate mineralizations have been prepared. 74 samples for chemical analyses, 4 samples for geochemical studies, 19 samples for petrography and 30 samples for XRD studies were collected from the tuffs from the trenches. Analyses of the samples were carried out in the MTA laboratories (Tables 1, 2, 3, 4).

The General Directorate of MTA, in collaboration with Turkish Armed Forces General Staff, carried out exploratory drilling surveys for uranium in the study area and totally 56 drill holes were drilled; 43 drill holes during 1968-1969 and 13 drill holes during 1981-1983. Although these studies have been mentioned in the previous reports, details of drilling surveys and the locations of the drill holes could not be found.

## 2. Geology

### 2.1. Regional Geology

In the Gelibolu Peninsula there are four NE-SW trending pre-Tertiary tectonic zones. These zones from northwest to southeast are Gelibolu, Ezine, Ayvacık-Karabiga and Sakarya zones. Gelibolu zone is an ophiolitic melange, in the form of an accretionary prism, consisting Cretaceous/Palaeocene pelagic limestone, radiolarian chert, serpentinites, gabbro, blue schist units. This zone is called Çetmi ophiolitic melange in the Gelibolu Peninsula, forms the basal part of the Eocene, starting with the sedimentary succession. In the south eastern part of the Gelibolu zone, the Ezine zone with continental origin rock unit is present. In the western part of the Ezine zone, Permo-Carboniferous sedimentary succession with greenschist metamorphism, is overlain by an ophiolite unit which was obducted in Permo-Triassic is located. In the eastern part, high grade metamorphic rocks of sedimentary origin are present. Ayvacık-Karabiga zone, located to the southeast of the Ezine zone, also

consists of the rock units of the Çetmi ophiolitic melange. Eclogite and upper Triassic limestone blocks in the ophiolitic melange are typical for the Ayvacık-Karabiga zone (Okay et al., 1990).

Sakarya zone consists mainly of Kazdağ group metamorphics, Karakaya complex units tectonically overlying Kazdağ metamorphics and the sediments of post-Triassic overlying it. In the Biga Peninsula, Karakaya complex consists of 4 tectono-stratigraphic units of similar age but each representing different sedimentary environment. They are Nilüfer Unit, Hodul Unit, Orhanlar greywacke and Çal Unit (Okay et al., 1990).

Sakarya zone starts with Paleozoic Kazdağ metamorphics at the base. Late Paleozoic Kalabak Unit and Middle Triassic Karakaya Group rocks have tectonic contacts with the Kazdağ metamorphics. Jurassic-Cretaceous carbonate rocks overlay all these units (Duru et al., 2012) (Figure 1).

In the Biga Peninsula, Upper Cretaceous-Oligocene sediments have been largely eroded as a result of a regional uplift which took place during Late Oligocene. As a result of extensive calc-alkaline magmatism during Early/Middle Miocene, numerous granodioritic plutons were emplaced and large areas were covered with andesitic and dacitic volcanic rocks (Okay et al., 1990).

Tertiary units covering large areas in the study area begin with Early Eocene Beyçayır volcanic rocks consisting andesitic lavas and pyroclastic rocks (Dönmez et al., 2005). Soğucak formation is represented by Middle Eocene fine grained pebble stones, shallow water-reef limestones, transitional with basalts, basaltic andesites and lavas. In Early Eocene, the area started becoming deeper and turbidites of Ceylan formation and Dedeadağ volcanic rocks of same age have developed. Late Eocene sandstones, mudstones and reef limestones of the Beybaşı formation overlay Ceylan and Dedeadağ formations. Basaltic lavas and pyroclastic rocks of Erdağ volcanites lie on the Beybaşı formation. Oligocene-Early Miocene age Hallaçlar formation including basaltic, andesitic, dacitic lavas and pyroclastites cover extensive areas. Rock units of the Hallaçlar formation have been subjected to intense alterations as a result of Oligocene granodioritic intrusives. Numerous lake basins were developed during Early Miocene time and conglomerates, sandstones, mudstones and shales of the Küçükuyu formation were deposited in these basins. Along with the Küçükuyu formation

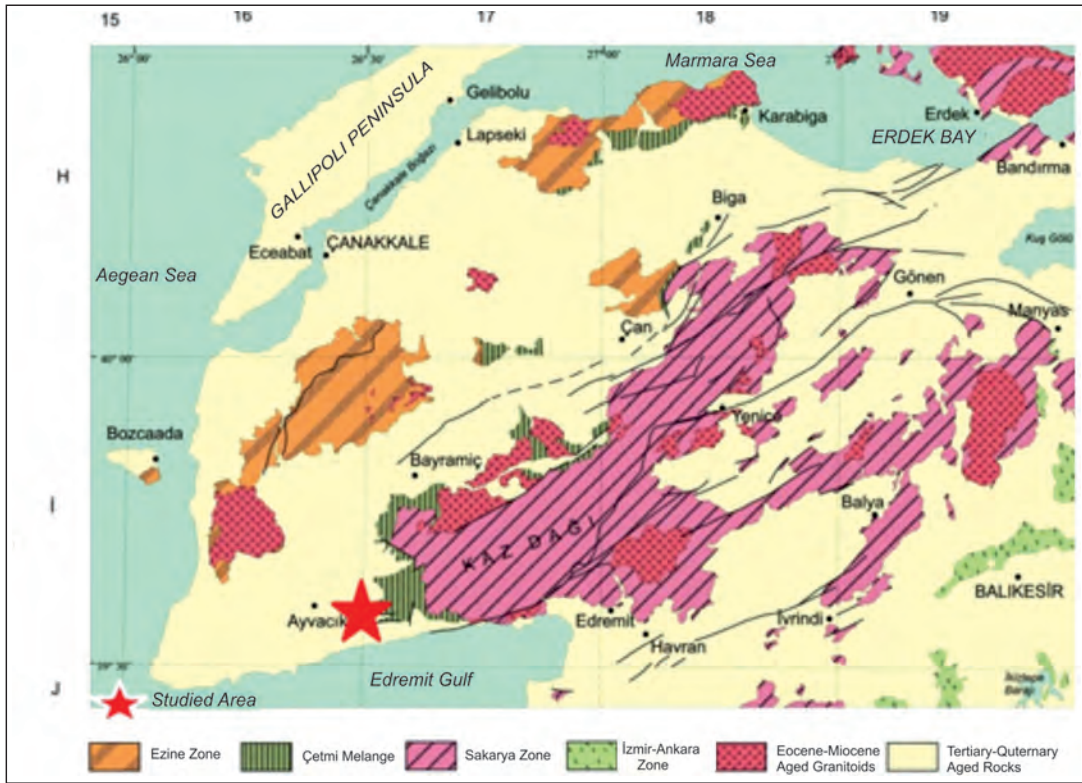


Figure 1- Tectonic zone map of the region (Duru et al., 2012)

extensive andesitic, basaltic and dacitic-rhyolitic lavas, pyroclastics and ignimbrites filled up these basins. All these units have been overlain with a discordance by shallow water sandstones, mudstones, shales, marls and limestones of the Çanakkale formation (Atabey et al., 2004; Dönmez et al., 2005) (Figure 2).

Late Miocene Taştepe alkali basalts in the study area represent the last volcanic activity. All these units have been overlain with a discordance by Pliocene stream-lake sediments of pebble stones, sandstones and shales of the Bayramiç formation (Dönmez et al., 2005), (Figure 2).

## 2.2. Geology of the Study Area

Geology of the study area and its surroundings is from Duru et al. (2007), (Figure 3).

### 2.2.1. Çetmi Melange

Units of the Çetmi melange are the oldest units in the study area. Çetmi melange was defined as 'Çetmi ophiolitic melange' by Siyako et al. (1989) and Okay et al. (1990). Duru et al. (2007) defined it as 'Çetmi melange'. The 'Çetmi melange' consists mainly of spilitic basic volcanic and pyroclastic rocks, limestone

blocks, shales and greywackes. Limestones are cream coloured, fine grained, thin to thick beds, in places with micritic cherts and biomicrites. These limestones are locally recrystallized. Some serpentinites, radiolarian cherts and garnet-bearing mica schists and meta-basic rocks subjected to eclogite facies metamorphism are present locally (Figure 3).

### 2.2.2. Küçükkuyu Formation

It was first defined and named by Saka (1979), it overlays discordantly Hasanoba volcanic rocks. It crops out in the south of Nusratlı village and in the Zindan Tepe and in the south of Andikini tepe in the Arıklı village.

Küçükkuyu formation starts with a basal conglomerate and has sandstone, mudstone, marl, mudstone and shales.

Sandstones are medium size thick beds; in places 1-2 m thick beds are also present. They have greyish, yellowish coloured are loosely cemented. Shales are brownish and greyish coloured and in general laminated.

In some places, coal interbeds with a thickness of 1-5 cm and bituminous shale are observed in the formation.

UPPER SYSTEM	SYSTEM	CYCLE	FORMATION	MEMBER	SYMBOL	ROCK TYPE	EXPLANATION
C E N O Z O I C	QUATERNARY	Pliocene	Bayramiç		Qal	Alluvial	
					Tp1b	Conglomerate, sandstone, mudstone	
	Pliocene		Gülpınar		Tgü	Fossiliferous - clayey limestone	
					Tmt	Basalt and basaltic pyroclastics	
	Eocene		Çamakkale	Taştepe basalt	Tmçt	Limestone, marl	
					Tmçt	(Tidal environment carbonates)	
					Tmçt	Mudstone, marl, siltstone, sandstone	
					Tmçg	(Tidal level and channel deposits)	
					Tms	Conglomerate, sandstone, mudstone	
					Tmi		
	Middle Miocene		Soma		Tmsö	Conglomerate, sandstone, limestone, mudstone, marl and tuff	
					Tmsö	(Lake shoreline, beach, levee mouth bar type delta, stream deposits)	
					Tmç	Sandstone, limestone, mudstone, bituminous shale, coal, volcaniclastic rocks	
					Tmç	Vitric-crystal-lithic tuff, Andesitic, rhyolitic-dacitic lavas and pyroclastics	
	Lower Miocene		Küçükkuyu		Tmk	Conglomerate, sandstone, limestone, bituminous shale mudstone and tuff (deep lake turbidites deposits)	
					Tmk		
	Oligocene		Biga Peninsula Granitoides	Hallaçlar	Tobg	Andesitic, basaltic-rhyolitic-dacitic lavas and pyroclastics	
					Tobg		
					Tos	Granitoidic rocks	
					Toy		
					Toa		
	Eocene		Ceylan Dedeoğlu Volcanics	Erdag Volcanics	Teer	Basalt lavas and basaltic pyroclastics	
					Tebe	Sandstone, claystone, reef limestone	
					Ted	Green colored tuff	
					Tedka		
					Tedk	Marine ignimbrite, andesite, dacite	
					Tedh		
Tec					Sandstone-claystone alternation (deep sea turbidite deposits)		
Tes					Reef limestone		
Teş					Basalt lavas and pyroclastics, volcaniclastic and basaltic dykes		
Tef					Conglomerate, sandstone, mudstone (Gilbert and levee type bar delta deposits)		
Eocene		Beyçayırı Volcanics		Teb	Andesitic lavas and pyroclastics		
				Teb			
				Tee	Andesitic lavas and pyroclastics		
Eocene		Edineik Volcanics		Tee	Andesitic lavas and pyroclastics		
				Tee			
MESOZOIC PALEOZOIC			Basement rocks			Pre Tertiary aged basement rocks	

Figure 2- Generalized columnar section of the Biga Peninsula (Atabey et al., 2004; Dönmez et al., 2005)

Spores in the units indicate Early Miocene age (İnci, 1984). The succession with sandstones, mudstones, limestones, shale intercalations have developed in a quiet, low energy environment. Some parts of the unit have been folded as a result of Miocene and post-Miocene tectonics. All these units appear to have sedimented in a lake basin.

### 2.2.3. Arıklı Volcanites

Arıklı volcanites which were previously named as Arıklı ignimbrite by Dönmez et al. (2005) are represented by andesite-dacite lavas and tuffs. In the study area tuffs of the Arıklı volcanites crop out. In this study, tuffs have been grouped as vitric tuff,





Figure 5- Field view of vitric tuffs.



Figure 6- Field view of crystal tuffs.



Figure 7- View of a hand specimen of lithic tuff.

part of the Köy Tepe. As a result of surface stripping they display exfoliation.

### 3. Petrography of the Tuffs in the Study Area

Crystal tuffs composed of angular-semi angular quartz, subhedral plagioclases with polysynthetic twinning's, subhedral alkali feldspars, subhedral biotite and rock fragments of basalt, andesite with minor limestone. They have been cemented by carbonated volcanic glass. Because of intensive alterations, vitric tuffs and lithic tuffs have lost their original

ductile texture. Limonite colouring, silicification and argillization are the alteration types present.

Vitric tuffs have feldspar and sanidine minerals and in chemical analyses they have  $K_2O$  contents over 5.0% (Günaydın, 2013).

### 4. Geochemical Characteristics of the Tuffs in the Study Area

Tuffs cropped out around Feyzullah Tepe and Kayabaşı Tepe are generally yellowish-brown and greyish-white in colours. They are welded as a result of silicification, and yellowish brown coloured parts of tuffs have gained ductile texture due to limonitization. The unit in places has rock fragments (enclaves).  $SiO_2$  content of the samples from Arıklı volcanites range from 55 to 70%. According to the  $SiO_2$  content, the rocks are 'intermediate-acid' in composition (Le Bas and Streckeisen, 1991), (Table 1-2).

The ratios of relatively immobile and/or immobile elements such as Zr, Y, La and Yb, are preferably used to classify the studied rocks since the volcanites in the studied area have experienced alterations. According to the  $Zr/TiO_2 * 0.0001$  versus  $Nb/Y$  plot of Winchester and Floyd (1976), the studied rocks are rhyolite, rhyodacite in composition (Figure 8). Zr versus Y and La versus Y diagrams of Winchester and Floyd (1976) demonstrate that they have generally calc-alkaline characteristics (Figure 9a, b).

### 5. Mineralizations

#### 5.1. Ore Minerals and Paragenesis

From the previous work it is well known that in the study area, phosphate and uranium have mineralized

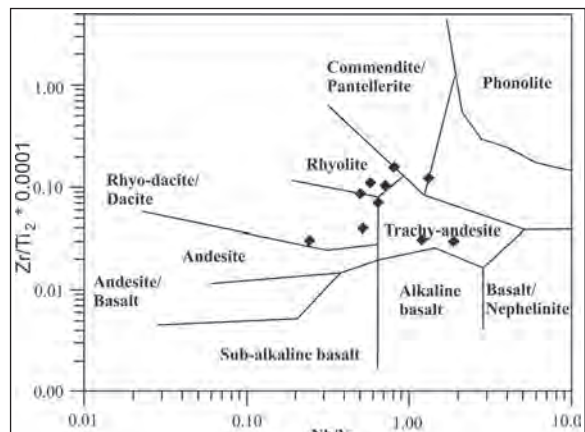


Figure 8-  $Nb/Y - Zr/TiO_2 * 0.0001$  diagram of the volcanic rocks from the Arıklı area (Winchester and Floyd, 1976).

Table 1- Major oxide (%) analysis of tuff samples from Arıklı volcanites (LOI: Loss On Ignitation).

Sample No	Na <sub>2</sub> O	MgO	Al <sub>2</sub> O <sub>3</sub>	SiO <sub>2</sub>	P <sub>2</sub> O <sub>5</sub>	K <sub>2</sub> O	CaO	TiO <sub>2</sub>	MnO	Fe <sub>2</sub> O <sub>3</sub>	LOI
06-ÇKF-02B	4.0	1.5	17.6	58.1	<b>0.2</b>	4.6	3.9	0.7	<0.1	5.9	1.66
06-ÇKF-06C	0.6	0.3	16.6	63.1	<b>0.1</b>	12.5	0.3	0.5	<0.1	3.2	1.55
06-ÇKF-08	0.5	8.5	10.6	44.5	<b>0.1</b>	4.1	10.5	0.4	0.1	3.9	17.54
06-ÇKF-9B	0.5	0.4	15.8	57.2	<b>3.0</b>	12.9	4.6	0.7	0.1	3.4	1.18
06-ÇKF-10B	<0.1	42.1	0.7	3.9	< <b>0.1</b>	<0.1	3.6	<0.1	<0.1	0.2	49.36
06-ÇKF-16	0.6	8.9	10.3	41.3	<b>0.1</b>	5.0	11.5	0.5	0.2	5.4	17.08
06-ÇKF-17	0.5	9.5	10.6	42.0	<b>0.1</b>	5.1	10.0	0.4	0.1	3.9	17.40
06-ÇKF-31A	2.5	0.9	15.2	65.7	<b>0.1</b>	7.8	0.5	0.4	0.1	2.6	3.99
06-ÇKF-31B	3.1	2.3	12.8	54.2	<b>0.1</b>	5.5	0.7	0.3	0.3	11.4	9.38
06-ÇKF-34	0.1	1.5	13.9	53.6	<b>0.1</b>	12.9	5.9	0.5	0.1	3.0	7.42
06-ÇKF-35	0.1	12	4.2	14.1	<b>0.5</b>	2.9	27.7	0.2	0.4	4.6	33.43
06-ÇKF-37	<0.1	13.8	3.8	11.5	<b>0.2</b>	2.2	26.5	0.2	0.2	3.7	37.67
06-ÇKF-39	3.8	2.7	14.2	63.6	<b>0.1</b>	6.4	1.2	0.4	0.1	2.3	4.60
06-ÇKF-40	2.3	5.3	5.6	24.2	< <b>0.1</b>	1.0	27.5	0.1	1.1	2.1	29.96
06-ÇKF-41	5.6	2.7	12.3	68.5	< <b>0.1</b>	1.8	0.5	0.2	<0.1	2.8	5.73
06-ÇKF-42A	5.9	5.7	12.8	53.6	<b>0.1</b>	1.7	1.1	0.2	<0.1	5.2	11.78
06-ÇKF-42B	3.3	3.7	14.5	55.8	<b>0.1</b>	6.5	3.4	0.5	0.1	3.2	7.21
06-ÇKF-43	0.2	1.2	13.8	69.4	<b>0.1</b>	9.5	0.4	0.4	0.1	2.4	2.44
06-ÇKF-44	<0.1	41.6	0.9	4.7	< <b>0.1</b>	0.1	2.9	<0.1	<0.1	0.3	49.49
06-ÇKF-45A	<0.1	13.9	8.1	37.6	<b>0.1</b>	5.4	7.1	0.2	0.1	2.0	23.67
06-ÇKF-45B	0.3	10.0	7.0	22.9	<b>0.2</b>	2.9	20.3	0.3	0.1	4.8	29.33
06-ÇKF-46B	3.1	0.6	14.0	63.7	<b>0.1</b>	5.7	2.6	0.6	0.1	7.7	2.41
06-ÇKF-47B	0.5	0.6	18.2	63.0	<b>0.3</b>	13.6	0.2	0.5	<0.5	2.4	0.71

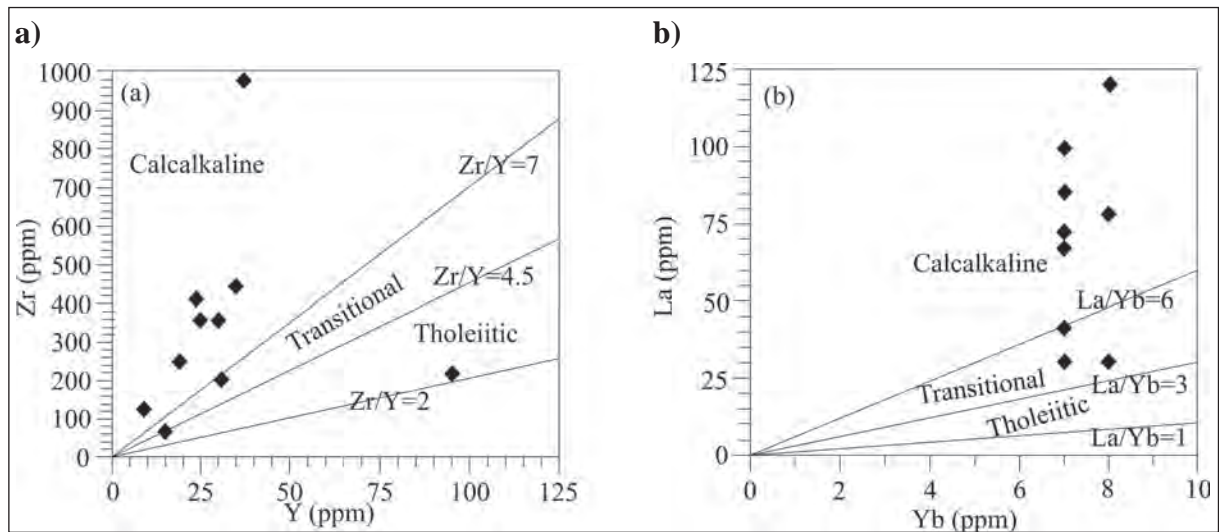


Figure 9- a) Zr-Y and b) La-Yb classification diagrams of the tuffs from Arıklı area (Winchester and Floyd, 1976).

together (Akgünlü and Sağlam, 1983). Uranium minerals cannot be seen with naked eye. Presence of uranium has been detected by using scintillometer and conducting chemical analyses. These tests showed that uranium minerals are bayleyite and ningyoite in

compositions and they appear to have developed as secondary uranium minerals.

Phosphate minerals cannot also be seen with naked eye. They can be detected by applying ammonium

Table 2- Major oxide, Cl, SO<sub>3</sub> analysis of tuff samples of Arıklı volcanites.

Sample No	Na <sub>2</sub> O	MgO	Al <sub>2</sub> O <sub>3</sub>	SiO <sub>2</sub>	P <sub>2</sub> O <sub>5</sub>	K <sub>2</sub> O	CaO	TiO <sub>2</sub>	MnO	Fe <sub>2</sub> O <sub>3</sub>	Cl	SO <sub>3</sub>
06-ÇKF-45C	<0.1	13.6	7.3	34.1	<b>0.1</b>	6.4	11.5	0.2	<0.1	2.2	0.03	0.177
06-ÇKF-49	0.1	18.5	1.2	4.7	<b>0.1</b>	1.1	28.4	0.1	0.1	1.2	0.09	0.050
06-ÇKF-50	0.1	18.5	0.5	6.4	<b>0.1</b>	0.2	29.8	0.5	<0.1	0.2	0.07	0.030
06-ÇKF-51B	0.2	1.6	10.8	63.5	<b>1.0</b>	5.9	3.7	0.5	0.2	6.6	0.08	0.142
06-ÇKF-52	0.5	0.2	17.4	61.9	<b>0.1</b>	13.9	0.2	0.6	<0.1	3.1	0.05	0.020
06-ÇKF-53	0.6	0.4	9.0	44.4	<b>12.6</b>	6.5	16.5	0.3	0.1	4.7	0.10	0.512
06-ÇKF-54A	0.5	0.6	13.4	47.7	<b>6.6</b>	10.1	8.3	0.5	0.2	6.5	0.09	0.097
06-ÇKF-54B	0.2	0.3	12.4	67.2	<b>0.5</b>	8.3	0.8	0.6	0.2	6.5	0.09	0.097
06-ÇKF-55	0.2	0.3	12.7	57.8	<b>4.5</b>	8.1	4.2	0.5	0.3	7.5	0.06	0.120
06-ÇKF-56	0.3	0.2	13.7	63.4	<b>1.7</b>	11.5	2.6	0.7	0.2	3.8	0.10	0.115
06-ÇKF-57A	0.2	0.4	11.6	70.5	<b>0.2</b>	7.4	0.3	0.8	0.1	5.6	0.04	0.037
06-ÇKF-57B	0.2	0.3	11.2	70.3	<b>0.5</b>	6.0	0.7	0.5	0.1	6.8	0.04	0.022
06-ÇKF-58	0.3	0.3	14.0	53.2	<b>4.5</b>	11.9	5.6	0.5	0.1	5.2	0.04	0.200
06-ÇKF-59A	0.3	10.2	1.2	6.2	<b>7.5</b>	0.2	29.5	0.1	0.5	10.2	1.24	0.187
06-ÇKF-59B	0.1	4.2	2.2	34.5	<b>13.0</b>	0.3	23.3	0.1	0.3	9.2	0.01	0.225
06-ÇKF-59C	0.3	5.7	1.3	40.9	<b>4.8</b>	0.3	20.4	0.1	0.3	4.6	0.26	0.137
06-ÇKF-60	0.1	1.2	2.5	13.3	<b>21.9</b>	0.4	29.1	0.1	0.2	17.6	0.07	0.710
06-ÇKF-61	0.1	3.4	3.1	67.9	<b>3.4</b>	0.5	9.6	0.1	0.1	3.7	0.13	0.102
06-ÇKF-62	<0.1	1.0	6.4	27.8	<b>16.6</b>	1.6	5.8	0.3	<0.1	22.1	0.01	4.597
06-ÇKF-63	0.1	0.4	3.9	85.7	<b>2.3</b>	0.8	2.4	0.2	<0.1	2.2	0.05	0.087
06-ÇKF-64A	0.3	<0.1	13.8	47.8	<b>7.1</b>	10.4	9.2	0.6	0.3	5.9	0.08	0.255
06-ÇKF-64B	0.2	2.0	3.2	11.2	<b>24.0</b>	2.4	40.8	0.1	0.6	3.2	0.01	0.292
06-ÇKF-64C	0.3	<0.1	2.7	9.3	<b>32.4</b>	1.8	42.5	0.1	0.1	2.4	0.07	0.200
06-ÇKF-64D	0.4	0.3	15.8	57.4	<b>1.8</b>	13.1	2.6	0.7	0.1	3.7	0.05	0.207
06-ÇKF-65	0.4	0.3	14.2	54.1	<b>3.5</b>	12.8	4.6	0.6	0.1	4.9	0.16	0.285
06-ÇKF-66	0.1	18.6	1.8	8.6	<b>0.4</b>	1.2	25.6	0.1	<0.1	1.1	0.05	0.060
06-ÇKF-67	0.4	7.7	13.3	45.1	<b>0.2</b>	6.6	6.3	0.7	0.1	4.8	0.05	0.270
06-ÇKF-68	0.5	15.2	9.7	38.6	<b>0.1</b>	2.8	5.7	0.5	0.1	3.0	0.04	0.115
06-ÇKF-69	0.2	1.8	14.6	51.2	<b>0.2</b>	7.4	3.3	1.0	0.2	11.7	0.06	0.165
06-ÇKF-70	0.2	3.1	0.9	46.9	<b>6.8</b>	0.1	21.1	<0.1	0.2	5.1	0.21	0.162
06-ÇKF-71	0.2	0.5	11.6	48.6	<b>0.5</b>	7.4	0.5	0.7	<0.1	11.5	0.01	7.177
06-ÇKF-73.A	4.4	0.2	8.2	32.7	<b>16.8</b>	2.2	22.5	0.2	0.4	2.0	0.01	1.052
06-ÇKF-74.A	4.1	1.3	14.1	65.3	<b>0.1</b>	5.7	0.6	0.4	<0.1	3.0	0.12	0.222
06-ÇKF-74.B	3.4	1.7	13.7	66.6	<b>0.1</b>	6.1	0.6	0.4	<0.1	2.5	0.16	0.195
06-ÇKF-75	1.9	0.1	4.1	20.8	<b>0.3</b>	1.6	36.5	0.1	0.7	1.5	0.06	0.292
06-ÇKF-76	3.1	0.3	5.1	18.9	<b>19.5</b>	1.0	35.8	0.1	0.7	1.5	0.06	0.292
06-ÇKF-77.A	5.9	0.9	14.6	58.8	<b>0.3</b>	2.9	0.9	0.4	2.5	3.4	0.06	0.085
06-ÇKF-78.A	0.3	0.3	14.6	65.8	<b>0.1</b>	12.2	1.0	0.3	0.1	2.4	0.60	0.095
06-ÇKF-79.A	<0.1	0.4	10.1	50.1	<b>0.3</b>	9.5	0.5	0.4	0.3	22.4	0.04	0.075
06-ÇKF-79.B	0.1	0.4	15.0	67.8	<b>0.1</b>	12.4	0.3	0.3	<0.1	2.3	0.05	0.082
06-ÇKF-80	1.3	4.3	12.1	59.5	<b>0.1</b>	3.3	3.3	0.8	0.1	6.6	0.05	0.042
06-ÇKF-81.A	0.5	7.4	9.9	42.8	<b>0.5</b>	5.1	10.5	0.6	0.1	4.5	0.06	0.080
06-ÇKF-81.B	1.5	5.8	10.8	36.9	<b>0.2</b>	5.5	13.1	0.5	0.2	5.9	0.05	0.070
06-ÇKF-81.C	1.00	5.6	8.6	53.3	<b>0.1</b>	2.2	9.2	0.5	0.1	5.8	0.03	0.200
06-ÇKF-82B	0.1	0.4	12.8	68.2	<b>0.2</b>	6.5	0.3	0.8	0.1	6.9	<0.01	0.020
06-ÇKF-83A	<0.1	0.2	10.2	83.7	<b>0.1</b>	0.7	0.2	0.1	<0.1	1.1	<0.01	0.235
06-ÇKF-84A	0.1	0.1	3.1	93.2	<b>&lt;0.1</b>	0.4	0.3	0.1	0.1	1.1	0.11	0.282
06-ÇKF-85A	0.9	6.5	10.8	53.1	<b>0.3</b>	5.2	6.9	0.4	<0.1	4.4	0.07	0.070
06-ÇKF-85B	0.5	3.6	13.9	54.7	<b>0.1</b>	7.5	5.1	0.4	0.1	4.3	0.09	0.120
06-ÇKF-86B	0.6	1.8	13.8	66.1	<b>0.1</b>	3.6	2.8	0.3	<0.1	1.8	<0.01	0.030

molybdate test (the color of phosphate-bearing rocks is converted to canary yellow by ammonium molybdate test) and also by conducting chemical analyses and mineralogical studies. Quartz, pyrite, magnetite, calcite and magnesite are macroscopically detected minerals in the rocks.

The samples 06-ÇKF-10 B, 06-ÇKF-37 and 06-ÇKF-44 have been collected from the magnesite veins and the samples 06-ÇKF-54B, 06-ÇKF-58 and 06-ÇKF-51B from the barite veins. They are all from the mineralizations in the fault and fracture zones. Barite and magnesite mineralizations are in the same fault and fracture zones along with the phosphate mineralizations. Presence of these mineralization demonstrate that phosphate mineralizations also have hydrothermal origin.

Detailed XRD mineralogical studies showed that phosphate minerals have fluorapatite-chlorapatite compositions. These minerals are generally associated with feldspars and quartz and rarely with analcime, barite and dolomite. In the Arıklı volcanites, chemical analyses of the samples collected from the fault, fracture and altered zones showed that phosphate minerals mainly have fluorapatite composition with minor amounts of chlorapatite. It is clearly shown from the Table 3 and 4 that fluor contents of phosphate minerals are quite high, indicating the phosphate minerals are fluorapatite in composition.

Field studies and mineralogical-petrographical studies showed that apart from nodular type phosphate mineralizations, all other phosphate mineralizations have developed along the tectonic zones and ore minerals are uranium-bearing fluorapatite. Presence of minerals like barite, magnesite and the lack of phosphate minerals in the rocks outside the tectonic zones reveal an hydrothermal origin for the mineralization. Nodular type phosphate mineralization has syn-sedimentary origin. On the other hand, when geochemical analyses of the rocks have been considered in samples having high  $P_2O_5$  contents also have high U values, indicating phosphate and uranium mineralized together (Tables 1, 2, 3, 4).

## 5.2. Mineralization Outcrops and Their Characteristics

Hydrothermal mineralizations in the study area are related to Late Miocene or Post-Miocene volcanic activities. Hydrothermal solutions generated from dacites which developed at the late stage of volcanic

Table 3- F, La, Th, U and Ba analysis of the tuff samples from Arıklı volcanites (in ppm).

Sample No	F	La	Th	U	Ba
06-ÇKF-45C	<1500	<40	<15	<15	226
06-ÇKF-49	<1500	<40	19	17	<100
06-ÇKF-50	<1500	<40	<15	<15	<100
06-ÇKF-51B	<1500	<40	27	115	938
06-ÇKF-52	<1500	56	58	25	657
06-ÇKF-53	15698	<40	112	>700	342
06-ÇKF-54A	4215	<40	169	>700	526
06-ÇKF-54B	<1500	<40	39	88	1098
06-ÇKF-55	1990	<40	33	581	402
06-ÇKF-56	1648	47	73	292	400
06-ÇKF-57A	<1500	57	33	37	305
06-ÇKF-57B	<1500	<40	41	105	321
06-ÇKF-58	6398	48	31	355	1343
06-ÇKF-59A	3289	<40	35	416	<100
06-ÇKF-59B	9891	<40	46	544	<100
06-ÇKF-59C	2360	<40	<15	254	<100
06-ÇKF-60	33863	<40	<15	>700	915
06-ÇKF-61	4033	<40	<15	149	119
06-ÇKF-62	15166	80	48	527	730
06-ÇKF-63	<1500	<40	<15	97	248
06-ÇKF-64A	9074	65	86	382	1414
06-ÇKF-64B	23400	<40	116	>700	663
06-ÇKF-64C	>40000	<40	136	>700	1158
06-ÇKF-64D	2491	98	77	126	1715
06-ÇKF-65	3573	62	156	321	1064
06-ÇKF-66	<1500	<40	>1000	289	393
06-ÇKF-67	<1500	<40	22	<15	>2500
06-ÇKF-68	<1500	43	43	<15	1717
06-ÇKF-69	3065	<40	<15	<15	351
06-ÇKF-70	7582	<40	<15	201	<100
06-ÇKF-71	<1500	<40	<15	21	1096
06-ÇKF-73A	12399	141	480	>700	2500
06-ÇKF-74A	<1500	139	68	<15	710
06-ÇKF-74B	<1500	108	152	<15	899
06-ÇKF-75	3259	<40	39	18	379
06-ÇKF-76	18395	72	264	>700	461
06-ÇKF-77A	<1500	159	133	25	1549
06-ÇKF-78A	<1500	96	65	<15	345
06-ÇKF-79A	<1500	65	37	21	608
06-ÇKF-79B	<1500	106	87	<15	891
06-ÇKF-80	<1500	52	25	<15	664
06-ÇKF-81A	<1500	<40	<15	<15	226
06-ÇKF-81B	<1500	<40	16	<15	223
06-ÇKF-81C	<1500	46	<15	<15	271
06-ÇKF-82B	<1500	79	25	20	315
06-ÇKF-83A	<1500	<40	<15	<15	>2500
06-ÇKF-84A	<1500	<40	<15	<15	379
06-ÇKF-85A	<1500	<40	16	<15	606
06-ÇKF-85B	<1803	48	38	<15	965
06-ÇKF-86B	<1500	88	69	22	1084

Table 4- Some trace element analyses of tuffs of the Arıklı volcanites (in ppm).

Sample No	F	Sc	V	Cr	Co	Ni	Cu	Zn	Rb	Sr
<b>06-CKF-2B</b>	<1500	<20	94	<60	<50	85	<30	65	195	843
<b>06-CKF-6C</b>	<1500	<20	75	<60	<50	45	<30	36	277	54
<b>06-CKF-08</b>	1539	<20	74	246	<50	238	<30	42	117	829
<b>06-CKF-17</b>	<1500	<20	90	71	<50	124	36	64	163	802

activities penetrated into the weak zones like faults, fractures, discordant planes causing mineralizations. On the other hand, in different parts of the study area, nodular phosphates developed through syn-sedimentary process with tuffs.

Mineralization outcrops are present in and around İmamoluk Çeşme, Feyzullah Tepe, Örencik Tepe, Çiçekharmanı Tepe and Çarşılı Tepe areas (Figure 4).

Although nodular phosphates and vein type mineralizations are mainly located in the vitric tuffs but mineralizations in the weak zones like in faults and fractures also appear both in vitric and lithic tuffs.

#### 5.2.1. İmamoluk Çeşme Phosphate Mineralizations

About 150 m northwest of the İmamoluk Çeşme, in the Çetmi Ophiolitic melange, a fault zone with N25°E, 65°SW attitude hosts a 200 m long mineralization zone. Hydrothermal solutions caused silicifications in the rocks and phosphate mineralizations developed in and along the weak fractured parts. Mineralization in the zone has dirty yellow colour and is subjected to limonitization and some argillization. Zeolite and some clay minerals identified by XRD analysis are common alteration minerals.

Samples were collected from the altered parts in the silicified zone (06-ÇKF-70) and from the basic rocks (06-ÇKF-69 and 71) of the ophiolitic melange in which the fault zone developed. Analyses of these samples showed that the  $P_2O_5$  contents of the basic rocks and altered rocks are 0.2-05% and 6.8 %, respectively (Table 3). These values indicate that phosphate mineralization were emplaced by hydrothermal solutions following the faulting.

A shaft was sunk and an addit was driven (Figure 10) and 3 trenches were opened around İmamoluk Çeşme (Figure 11). Samples were collected from these locations and they have been analysed and the  $P_2O_5$  contents of these samples obtained from mineralized zones range between 3.4 and 21.9% (Table 1, 2). The



Figure 10- View of the phosphate bearing zone in a trench.



Figure 11- View of the phosphate bearing zone in a shaft + addit.

average  $P_2O_5$  value of the samples 06-ÇKF-59A, 59B, 59C is 10.5%. XRD analysis indicated that phosphate mineral is chlorapatite. In the trenches in an order from 1<sup>st</sup> to 4<sup>th</sup> trench, radiation values were measured by scintillometer at 10 sec and Tc1 mode showed 6135, 3492, 6665 and 5965 cps values. Uranium contents of the samples from these trenches are 554, 149, 527 and >700 ppm.

### 5.2.2. Feyzullah Tepe Phosphate Mineralizations

The mineralizations in the Feyzullah Tepe are located in the east-west trending fault zone. The fault runs along the contact between lake sediments of the Küçükkuyu formation and andesitic vitric tuffs. Phosphate and uranium mineralizations were formed by hydrothermal solutions following the fault development. During uranium exploration along the fault zone, trenches were opened (Figure 12). Mineralizations occurred in the lake sediments and andesitic vitric tuffs have dirty yellow colour.

Analyses of the samples of the tuffs from the trenches (06- ÇKF-51, 5, 53, 54A, 54B, 55, 56, 57A, 57B; 06-ÇKF-51B, 57A, 57B) have 1.7-12.6%  $P_2O_5$ , 5.9-13.9%  $K_2O$  and 9.0-17.4%  $Al_2O_3$  values (Table 1, 2). All these values are from the samples along the fault zone.  $K_2O$  and  $Al_2O_3$  values are related to the kaolinization of the feldspar minerals. Hydrothermal solutions causing uranium and phosphate mineralizations also gave rise to weak kaolinization. Kaolinized tuffs (06-ÇKF-52) have 0.1%  $P_2O_5$  content. Kaolinized tuffs do not have economic importance. Surveying all these trenches by Eda 500 scintillometer at 10 sec, Tc1 mode, gave average 500 cps radioactivity value. On the other hand, uranium contents vary from 115 to >700 ppm.

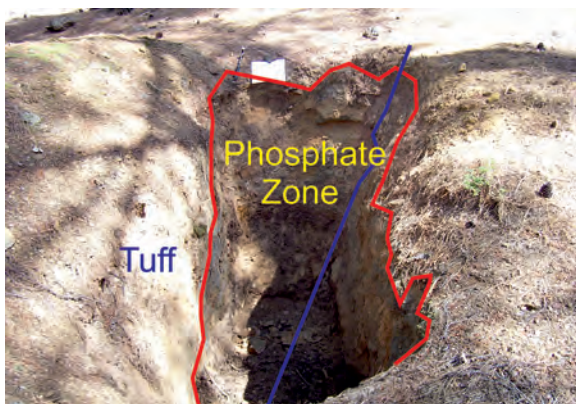


Figure 12- Phosphate bearing zone in a trench opened in Feyzullah Tepe.

### 5.2.3. Örencik Tepe Phosphate Mineralizations

In the Örencik Tepe, mineralizations are occurred in a NW-SE trending dip slip fault zone in the crystal tuffs. Tuffs in the mineralized zone have fractured and altered appearance with a colour of dirty yellow. Along the fault zone trenches were opened (Figure 13). In the mineralizations in Örencik Tepe hydrothermal barites (06-ÇKF-51B, 54B, 58) and magnesites (06-ÇKF-10B, 37, 44) are observed (Tables 1, 2, 3). Fine grained barites are disseminated in the rock, magnesites are in the form of brecciated pods (Figure 14). Analyses of the samples collected from the trenches (06-ÇKF-64A, 64B, 64C, 64D, 64E, 64F, 65, 66, 67, 68) showed 0.1-32.4%  $P_2O_5$ , 1.2-13.1  $K_2O$ , 0.3-18:6% Mgo and 15->700 ppm uranium, <100 - >2500 ppm Ba values (table 3). Th analyses of the sample 06-ÇKF-66 from the trench gave >1000 ppm value (Table 3). Scintillometer surveys conducted on all of the trenches at 10 sec Tc1 mode indicated 4800 cps radioactivity value.

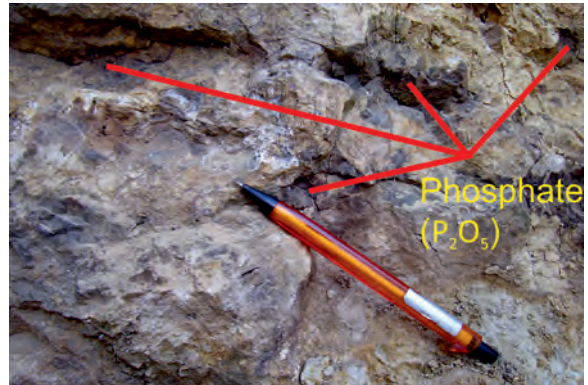


Figure 13- View of the phosphate bearing zone in a trench opened in the tuffs in the Örencik Tepe.



Figure 14- Hydrothermal magnesite mineralizations.

#### 5.2.4. Çarşılı Tepe Phosphate Mineralizations

Both vein and nodular types of phosphate mineralizations are present in the Çarşılı Tepe.

*Çarşılı Tepe vein type phosphate mineralizations:* They are vein like in the tuffs. They are like bundle of veins about 1 cm thick, have dried-rose colour. In places, veins appear not continuous but may appear again after short distance. Vein can be followed about 250 m along N75W direction. At the foot wall and hanging wall sides of the phosphate vein, 1-2 cm thick yellow colour traces of solutions can be observed (Figure 15). Walnut-sized phosphate nodules are observed around the vein but they have no connection with the vein itself. Detailed information on the nodules will be given in the next section.

XRD analysis of the sample (06-ÇKF-73A) collected from a phosphate vein showed the presence of analcime, chlorapatite, quartz, feldspar, calcite and



Figure 15- In the Çarşılı Tepe phosphate vein and solution stains in the tuff.

opal-ct minerals. The sample has 16.8%  $P_2O_5$ , 32.7%  $SiO_2$ , 22.5%  $CaO$ , 4.4%  $Na_2O$  and 2.2%  $K_2O$  contents (Table 2). On the other hand, analysis of the sample (06-ÇKF-74A) collected from the yellow coloured solution stained parts next to the vein has 0.1%  $P_2O_5$ , 65.3%  $SiO_2$ , 0.6%  $CaO$ , 4.1%  $Na_2O$ , 5.7%  $K_2O$  contents. Analysis of the sample (06-ÇKF-74B) from the host rock tuffs has 0.1%  $P_2O_5$ , 66.6%  $SiO_2$ , 0.6%  $CaO$ , 3.4%  $Na_2O$ , 6.1%  $K_2O$  contents (Table 2).

Low phosphate contents of the sample (06-ÇKF-74A) from the yellow coloured solution stained parts close to the vein and the sample from the host rock tuffs (06-ÇKF-74B) reveal that the host rock is not the source of phosphate. Data may indicate that vein type phosphates is epigenetic and related to the late stage hydrothermal activities.  $SiO_2$  contents of the host rock and mineralization are inversely proportional. The excess  $CaO$  content is due to the presence of apatite mineral. Relatively high  $Na_2O$  and  $K_2O$  values can be explained by the presence of alkali feldspar and sanidine in the samples (Günaydın, 2013), (Tables 1, 2).

*Çarşılı Tepe nodular phosphate mineralizations:* Walnut-sized spherical phosphate nodules display irregular distribution in the tuffs. When a nodule is cut, there is a calcite core encircled by numbers of 2-5 mm thick dried rose coloured concentric phosphate rings (Figures 16a, b). While some nodules have concentric rings of calcite and phosphate, some nodules are composed entirely of calcite. The distribution of nodules is irregular and do not have any connection with each other. Some nodules on the surface of the tuffs were removed in some places. In places, nodules have been altered by chemical and physical processes and they were argillitized and pulverized. Distribution

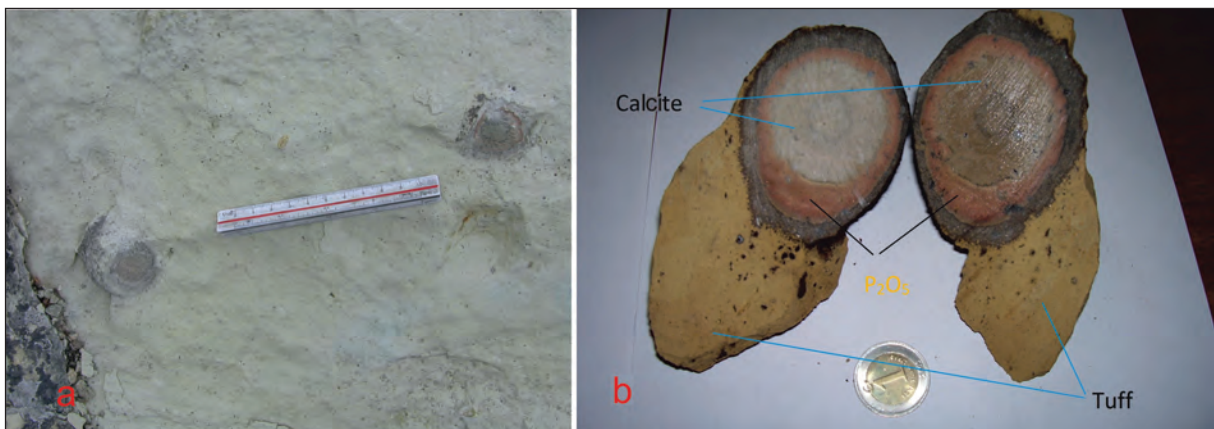


Figure 16- a: Phosphate bearing nodules, b: Sections of the nodules.

and the form of the nodules suggest that they were formed simultaneously with the host rock.

Chemical analysis of a sample (06-ÇKF-76) from a nodule with dried rose coloured rings has 19.5%  $P_2O_5$ , 18.9%  $SiO_2$ , 35.8%  $CaO$ , 3.1%  $Na_2O$ , 1.0%  $K_2O$  contents. Chemical analysis of an argillitized and pulverized nodule sample (06-ÇKF-77A) has 0.3%  $P_2O_5$ , 58.8%  $SiO_2$ , 0.9%  $CaO$ , 5.9%  $Na_2O$ , 2.9%  $K_2O$ , 14.6%  $Al_2O_3$ , 0.9%  $MgO$  contents. A sample (06-ÇKF-75) of a fresh surfaced nodule with light grey colour has following chemical analysis: 0.3%  $P_2O_5$ , 20.8%  $SiO_2$ , 36.5%  $CaO$ , 1.9%  $Na_2O$ , 1.8%  $K_2O$ , 20.3%  $Al_2O_3$ . On the other hand, the sample (06-ÇKF-74B) obtained from the host rock of the nodular phosphates has 0.1%  $P_2O_5$ , 66.6%  $SiO_2$ , 0.5%  $CaO$ , 3.4%  $Na_2O$ , 6.1%  $K_2O$ , 13.7%  $Al_2O_3$  contents (Table 2). These analyses show that phosphate mineralizations is occurred only in the nodules having dried rose coloured rings. The host rock tuffs of the nodules do not have phosphate mineralizations. Light grey coloured nodules with clean surfaces are composed of calcite crystals.

There are also nodules around the stone quarry in the Kestane Çukuru location in the Nusratlı village. A sample (06-ÇKF-78A) from these nodules has the following chemical analysis; 0.1%  $P_2O_5$ , 65.8%  $SiO_2$ , 0.9%  $CaO$ , 0.3%  $Na_2O$ , 12.2 %  $K_2O$ , 14.6%  $Al_2O_3$ . The sample (06-ÇKF-79A) obtained by grinding and subsequently mixing of various nodule samples from different locations has following analysis; 0.3%  $P_2O_5$ , 50.1%  $SiO_2$ , 0.5%  $CaO$ ,  $Na_2O < 0.1\%$ , 9.5%  $K_2O$ , 10.1%  $Al_2O_3$ . A nodule sample (06-ÇKF-79B) hosted in the tuffs of the stone quarry has the following analysis; 0.1%  $P_2O_5$ , 67.8%  $SiO_2$ , 0.3%  $CaO$ , 0.1%  $Na_2O$ , 12.4%  $K_2O$ , 15.0%  $Al_2O_3$  (Table 2). These analyses reveal that tuffs in the Kestane Çukuru area are alkaline in character and have K-feldspar and do not have phosphate mineralizations. A photograph of alkaline tuffs is given in figure 17.

$K_2O$  contents of the tuffs (06-ÇKF-74A, 78A, 79B) in the Çarşılı Tepe and Kestane Çukuru area vary between 7.0 and 12.4% (Table 2). XRD analysis of the tuffs demonstrated that they had feldspar, biotite, simectite, and calcite and/or sanidine mineral assemblage. High contents of  $K_2O$  in the rocks are related to the presence of feldspar and sanidine minerals in them.



Figure 17- Alkaline tuffs and  $K_2O$  rich nodules in the Kestane Çukuru area.

## 6. Ore Minerals and Paragenesis

Mineralogy of the phosphate nodules and relations of apatite with other minerals have been studied under the microscope (Figures 18, 19, 20, 21).

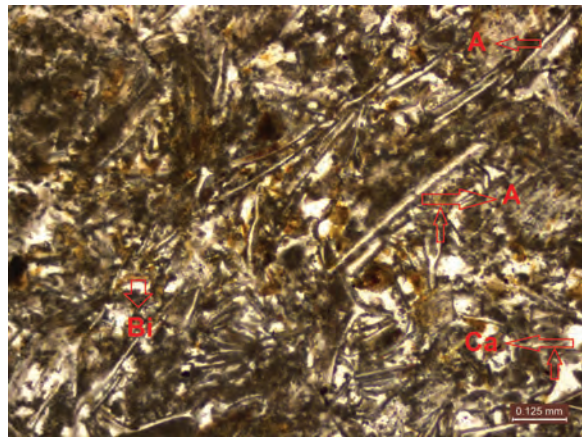


Figure 18- Thin section view of phosphate in the nodule (single nicol). A: apatite fibres, Bi: Biotite, Ca: Calcite.

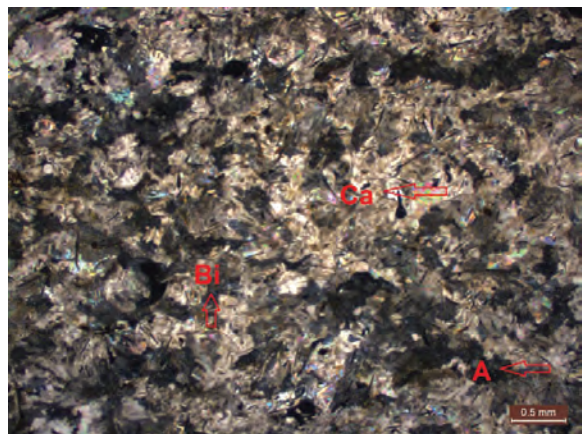


Figure 19- Thin section view of phosphate in the nodule (X nicols), A: Apatite fibres, Bi: Biotite, Ca: Calcite.

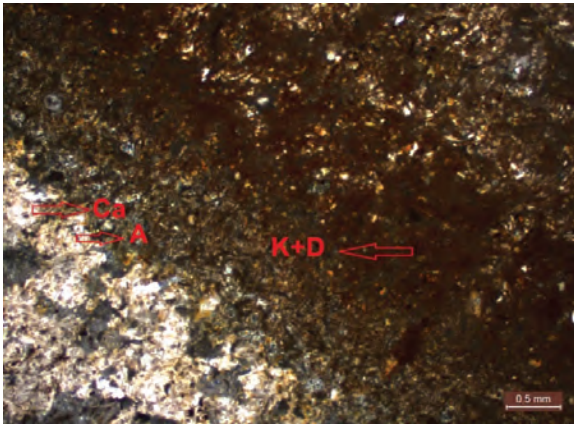


Figure 20- Thin section view of phosphate calcite boundary in the nodule under the microscope (X nicol). A: Apatite fibres, K + D: Clay and iron staining, CA: Calcite.

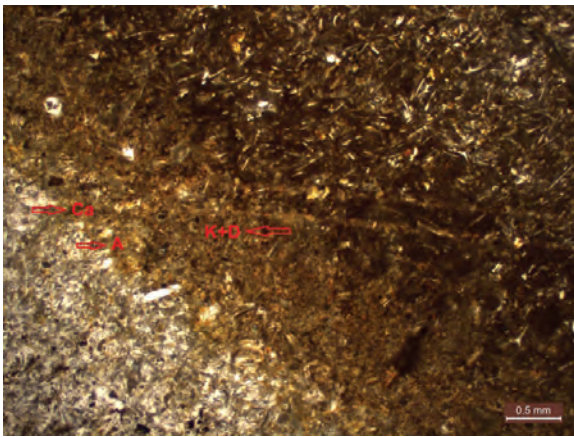


Figure 21- Thin section view of phosphate calcite boundary in the nodule under the microscope, (single nicol). A: Apatite fibres, K + D: Clay and iron staining CA: Calcite.

The ore having mesocrystalline-microcrystalline texture is composed mainly of carbonate and phosphate (apatite) minerals, biotite, and quartz. Mesocrystalline-microcrystalline carbonate minerals have uniform distribution. Prismatic and plate-like apatite crystals display uniform distribution. Biotites and quartz do not exhibit uniform distribution. Phosphate grains (apatite fibres) are observed within the carbonate cement. In thin sections under the microscope edge of the sample (pink part, phosphate rich) argillitization increases and staining is discernible (Figures 20 and 21) but phosphate content is still the same.

## 7. Origin of the Mineralization and Discussion

Phosphate nodules form in the restricted environments along the sediments-water interface if the pore water is rich in P and Ca but poor in Mg. Mild reducing environments may provide suitable

conditions for the development of phosphor minerals (Uzkut, 2006).

Vein type phosphate mineralizations in the İmamoluk Çeşme, Feyzullah Tepe, Örencik Tepe, Çiçekli Harman Tepe and Çarşılı Tepe were formed by hydrothermal solutions following sedimentation. In Çarşılı Tepe, hydrothermal solutions penetrated into the cracks, but in other areas into the cracks as well as into the contacts of the rock units, that is to say into the weak zones.

In the Çarşılı Tepe phosphate mineralizations are walnut-sized nodules floating like in the tuffs. Dissolving and transportation of phosphate in environments having low Eh and Ph conditions may be the source of phosphate nodules or during volcanic activity, huge amounts of phosphorus tuff material is transported into the lakes. During the process, pressurized phosphorus gas (P) in the tuffs combines with free oxygen in the lake forming apatite ( $P_2O_5$ ). On the other hand, another explanation is; in the high Ph (10-12) and Eh environments presence of phosphate in the lakes or in the lagoon's combines with calcite and aragonite to form phosphate nodules. Phosphate nodules are found only in the Çarşılı Tepe. Çarşılı Tepe area is a huge depression representing deepest part of the lake. This may explain why phosphate nodules are only found in this part in the region (Günaydın and Çolak 2009).

In Çarşılı Tepe nodular and vein type phosphate mineralizations are observed in the same area. Çelik et al. (1999) suggest that phosphate nodules are connected with each other with capillaries. But field observations and chemical analyses have not verified this statement. Because the  $P_2O_5$  contents of the samples (06-ÇKF-75,77A) from the tuffs between nodules and samples from the tuffs near the nodules is 0.3%. The samples from the tuffs hosting phosphate veins have also very low (0.1%)  $P_2O_5$  content (06-ÇKF-74A, 74B). This is why it is considered that hydrothermal solutions after the sedimentation caused the vein type mineralizations into the fractures and cracks of the rocks.

## 8. Conclusions

1- Phosphate and uranium in the field are found together. Mineralogical studies show that phosphate mineral is mainly chlorapatite but some fluorapatite is also present. Chemical analysis exhibit that Cl content is higher than Fl content. Therefore, it is more likely that phosphate mineral is flourapatite in composition

2- In the Çarşılı Tepe in the east of Nusratlı village a 1.0 cm thick mineralized phosphate zone along a line with some interruptions can be followed 250 m. This mineralized zone and phosphate mineralizations in the İmamoluk, Çeşme, Feyzullah Tepe, and Örencik Tepe in the north of Arıklı Village is considered to have resulted from hydrothermal solutions circulating in the structurally weak zones, like faults, discordance planes and lithological contacts.

3- Walnut-sized, dried rose coloured nodular phosphates in the Çarşılı Tepe in the Nusratlı village is considered to have formed by sedimentary processes in the vitric tuffs.

4-  $P_2O_5$  values in the sedimentary phosphates vary between 1.8-32.4%, but in the tuffs the values are rather low in the 0.01%  $P_2O_5$  range. This shows that phosphate mineralizations are not related with the tuffs.

5- In the Çiçekli Harman Tepe, hydrothermal magnesite breccias are found in a fracture zone. Although the magnesite breccias containing uranium according to scintillometer measurements have MgO contents ranging from 18.6 to 41.6%, they do not have any economic potential.

6- Chemical analyses of the host rock vitric tuffs of the nodular phosphate show following concentrations; 0.1%  $P_2O_5$ , 65.3%  $SiO_2$ , 0.1%  $CaO$ , 4.1%  $Na_2O$ , 12.4%  $K_2O$ , 13.7%  $Al_2O_3$ . High values of  $Na_2O$  and  $K_2O$  are related to feldspars and sanidines in the vitric tuffs.

7- Nodular phosphate is believed to have developed in lake or in lagoons. In favourable conditions increasing phosphate concentration in lakes/lagoons combines with calcite and turbulent water in the lake or laguna causes nodules to develop.

### Acknowledgements

This work was carried out within the Biga Peninsula phosphate exploration project of the Mineral Research and Exploration Department of MTA General Directorate. Geological Engineers Haşim Ağrılı, Turgut Çolak contributed to the field works. From time to time geological engineers Nafiz Demir and Ergun Çelik also took part in the field works. Their contributions are greatly acknowledged. My thanks are due to Geological Engineers S. Meltem Kadıncık, Semih Gürsu, Bülent Başara and Physics Engineer Yasemin Özdemir, Chemical Engineer Ayşe Özer who carried out the laboratory works.

### References

- Akgünlü, H., Sağlam, R. 1983. Çanakkale-Ayvacık-Arıklı Köyü Çevresindeki Uranyum Cevherleşmesi: Maden Tetkik ve Arama Genel Müdürlüğü Rapor. No: 542. Ankara (unpublished).
- Atabey, E., Ilgar, A., Sakitaş, A. 2004. Çanakkale Havzasının Orta Üst Miyosen Stratigrafisi, Çanakkale KB Türkiye: Maden Tetkik ve Arama Genel Müdürlüğü Derg. 128, 79-97, 2004.
- Çelik, E., Ayok, F., Demir, N. 1999. Ayvacık-Küçükkuyu (Çanakkale İli) Bölgesi Fosfat Cevherleşmesi Maden Jeolojisi Raporu: Maden Tetkik ve Arama Genel müdürlüğü-Balıkesir Bölge Müd. Arşivi Rap. No: 891. Ankara (unpublished).
- Dönmez, M., Akçay, A.E., Eyüpoğlu, M., Atıcı, Y. 2002-2003. Biga Yarımadası Tersiyer Volkanitleri, Maden Tetkik ve Arama Genel Müdürlüğü, Ara Rapor. Ankara (unpublished).
- Dönmez, M., Akçay A.E., Genç, Ş., Acar, Ş. 2005. Biga Yarımadasında Orta-Üst Eosen Volkanizması ve Denizel İgnimbiritler. Maden Tetkik ve Arama Genel Müdürlüğü dergisi Sayı 131, 49-62.
- Duru, M. 2009. Biga Yarımadasının Genel ve Ekonomik Jeolojisi. Maden Tetkik ve Arama Genel Müdürlüğü Rap. No 11101 Ankara (unpublished).
- Duru, M., Pehlivan, Ş., Ilgar, A., Dönmez, M., Akçay, A.E. 2007. 1/100.000 Ölçekli Türkiye Jeoloji haritaları Ayvalık 117 paftası, Maden Tetkik ve Arama Genel Müdürlüğü Yayın No: 98 Ankara.
- Duru, M., Pehlivan, Ş., Okay, A.İ., Şentürk, Y., Kar, H. 2012. Biga Yarımadası'nın Tersiyer Öncesi Jeolojisi, Maden Tetkik ve Arama Genel Müdürlüğü Özel yayın serisi No: 28 Ankara. Günaydın, A.B. 2013. Çanakkale-Ayvacık-Arıklı Köyü AR:201100370 No'lu (Alkali Tüf) Ruhsat Sahasının Maden Jeolojisi Raporu. Maden Tetkik ve Arama Genel Müdürlüğü, Ankara (unpublished).
- Günaydın, A.B., Çolak, T. 2009. Arıklı-Nusratlı KöyleriAyvacık-Çanakkale) Fosfat Sahası Maden Jeolojisi Raporu. Maden Tetkik ve Arama Genel Müdürlüğü. Derleme No: 11434 , Ankara (unpublished).
- İnci, U. 1984. Demirci ve Burhaniye bitümlü şeyllerinin stratigrafisi ve organik özellikleri. Türkiye Jeoloji Kurumu Bülteni 5, 27-40.
- Le Bas, M.J., Streckeisen, A.L. 1991. The IUGS Systematics of Igneous. Journal of Geological Society 143, S: 825-833.
- Okay, A.İ., Siyako, M., Bürkan, K.A. 1990. Biga Yarımadasının Jeolojisi ve Tek Evrimi. Türkiye Petrol Jeologları Derneği Bülteni, S: 83-121.

Önem, Y. 2000. Sanayi Madenleri,. Kozan Ofset Ankara.

Peccerillo A., Taylor, S.R. 1976. Geochemistry of Eocene calcalkaline volcanic rocks from the Kastamonu Area, Northern Turkey. Contributions to Mineralogy and Petrology 58, 63-81.

Saka, K. 1979. Edremit Körfezi ve civarı Neojeni'nin jeolojisi ve hidrokarbon olanakları: TPAO Arama Grubu Rap. No:1341, 17 s.

Siyako, M., Bürkan, K.A., Okay, A.İ. 1989. Biga ve Gelibolu Yarımadaalarının Tersiyer Jeolojisi ve

Hidrokarbon olanakları, TPJD Bülteni C 1/3 Aralık 1989, S183–199.

Uzkut, İ. 2006. Fosfat Yataklarının Oluşumu ve Araştırılması: [www.maden.org.tr](http://www.maden.org.tr)

Winchester, J.A., Floyd, P.A. 1976, Geochemical Magma Type Discrimination: Application To Altered And Metamorphosed Basic Igneous Rocks. Earth and Planetary Science Letters 28, 459-469.



# Bulletin of the Mineral Research and Exploration

<http://bulletin.mta.gov.tr>



## A COMPARATIVE ANALYSIS OF INDEX OVERLAY AND TOPSIS (BASED ON AHP WEIGHT) FOR IRON SKARN MINERAL PROSPECTIVITY MAPPING, A CASE STUDY IN SARVIAN AREA, MARKAZI PROVINCE, IRAN

Edris MANSOURİ<sup>a</sup>, Faranak FEİZİ<sup>b\*</sup>, Alireza Jafari RAD<sup>c</sup> and Mehran ARİAN<sup>d</sup>

<sup>a</sup>Department of Geology, Science and Research branch, Islamic Azad University, Tehran, Iran; Mailing address: Science and Research branch, Hesarak, Tehran, Iran, Postal code: 1477893855; orcid no: 0000-0001-7522-885X

<sup>b</sup>Mining Engineering Department, South Tehran Branch, Islamic Azad University, Tehran, Iran; Mailing address: Central Office of South Tehran Branch, Islamic Azad University, North Iranshahr Street, Karimkhan Zand Street, Tehran, Iran, Postal code: 4435/11365; orcid no:0000-0003-2863-4497

<sup>c</sup>Department of Geology, Science and Research branch, Islamic Azad University, Tehran, Iran; Mailing address: Science and Research branch, Hesarak, Tehran, Iran, Postal code: 1477893855; orcid no:0000-0002-4371-0841

<sup>d</sup>Department of Geology, Science and Research branch, Islamic Azad University, Tehran, Iran; Mailing address: Science and Research branch, Hesarak, Tehran, Iran, Postal code: 1477893855; orcid no0000-0002-4574-5116

Research Article

### Keywords:

TOPSIS, Index Overlay, AHP, Iron Skarn, Iran.

### ABSTRACT

The aim of this research is to compare index overlay and TOPSIS (based on AHP weight) for predictive Skarn potential map. In this paper, for Calcic Iron Skarn mineralization, criteria and subcriteria introduced and ranked for generating mineral prospectivity map. The values of final prospecting maps for Skarn deposit by index overlay and TOPSIS methods was specified by dividing the prospectivity values into 10 classes. For better comparison, values assign to classes base on their priority in mineral exploration. The comparative analyses of index overlay and TOPSIS integration methods, has been performed by selecting four GCPs for field checking. Field observation in GCP 1, 2 and 3, confirmed Iron mineralization in the contact of intrusive bodies with sedimentary units, where the contact metamorphism was obvious but there is no observable mineralization in GCP4. Although high magnetic is distinct in mentioned GCP. Based on the field checking in Sarvian area, the TOPSIS method has more accuracy compared to index overlay approach. Therefore, the TOPSIS method recommends for Calcic Iron Skarn Mineral Prospectivity Mapping in Sarvian and adjacent area.

Received Date: 07.10.2016

Accepted Date: 22.02.2017

## 1. Introduction

Discovering new mineral deposits and diagnosing prospective zones within the region of interest, is the ultimate purpose of mineral exploration. To achieve this goal, multiple datasets, or layers should be collected, analyzed and integrated for mineral prospectivity mapping (MPM) in the region of interest (Bonham-Carter, 1994; Carranza, 2008; Abedi et al., 2013; Najafi et al., 2014). There is obscure information on evaluating geo-evidential features as indicators for exploration of a desirable and appropriate deposit type, as a result of the complexity of geological scopes.

In mineral exploration, datasets are geo-datasets. Hence, MPM generates a predictive model for tracing prospective regions as a multiple criteria decision-

making (MCDM) function. In this manner producing evidential maps, combining evidential maps, and finally ranking promising target areas for further exploration have been performed. There are four types of methods to appropriate evidential weights and combine evidential maps for MPM. Evidential class weights can be assigned (1) based on the expert judgment of analyst through an approach called knowledge-driven MPM, for example, using index overlay and Boolean logic techniques (Bonham-Carter, 1994; Carranza and Hale, 2001; Rogge et al., 2006), (2) by using the locations of known mineral occurrences as training points through an approach called data-driven MPM (Bonham-Carter, 1994; Porwal et al., 2003), and (3) by using a hybrid of the two aforementioned approaches to MPM (Porwal et

\* Corresponding author: Faranak FEİZİ [faranakfeizi@gmail.com](mailto:faranakfeizi@gmail.com)  
<http://dx.doi.org/10.19111/bulletinmre.305201>

al., 2004, 2006) and (4) defining evidential weights without using expert judgments and without using location of known mineral deposits (Yousefi and Carranza, 2015). So, because the last method do not use location of known mineral deposits and expert judgments directly for weighting geological features, it is better to categorize it as an individual approach.

AHP has been used for weight calculating in mineral potential mapping as a result of the advantages for weight calculation procedures based on a pairwise comparison (Pazand et al., 2011). Among MCDM methods, the most popular ones are index overlay and technique for order preference by similarity to ideal solution (TOPSIS) (Dağdeviren et al., 2009; Noori et al., 2011). In the index overlay method each of the input maps is allocated a weight as well as all classes and spatial units existing in each factor map based on its relative importance in conjunction with expert opinion. In other words, the different classes on a single map have different weights (Pirmoradi et al. 2012). TOPSIS is based on the concept that the ideal alternative has the best level for all attributes, whereas the negative ideal is the one with all the worst attribute values (Önüt and Soner, 2008). The TOPSIS is a good

method for potential mapping but this method has been used rarely for mineral potential mapping. It seems, index overlay is preferred more than TOPSIS for mineral potential mapping. In this paper we investigate the result of calcic iron skarn potential mapping in Sarvian area generated by index overlay and TOPSIS methods (based on AHP weight). The Sarvian area has been studied before because of its mineral potential for iron mineralization. In this area, evidences of iron mineralization including magnetite and hematite have been reported (Feizi and Mansouri, 2013a). The goal in this paper is to iron skarn potential map by index overlay and TOPSIS methods (based on AHP weight). Furthermore, the output prospective maps are evaluated as to how well they have predicted the known Fe prospects and the results of two MCDM methods are compared with each other.

## 2. Materials and Methods

### 2.1. The Study Area and Geological Setting

The Sarvian area is located within the Orumieh-Dokhtar magmatic arc in Central of Iran (Figure 1); This magmatic arc is the most important for metals,

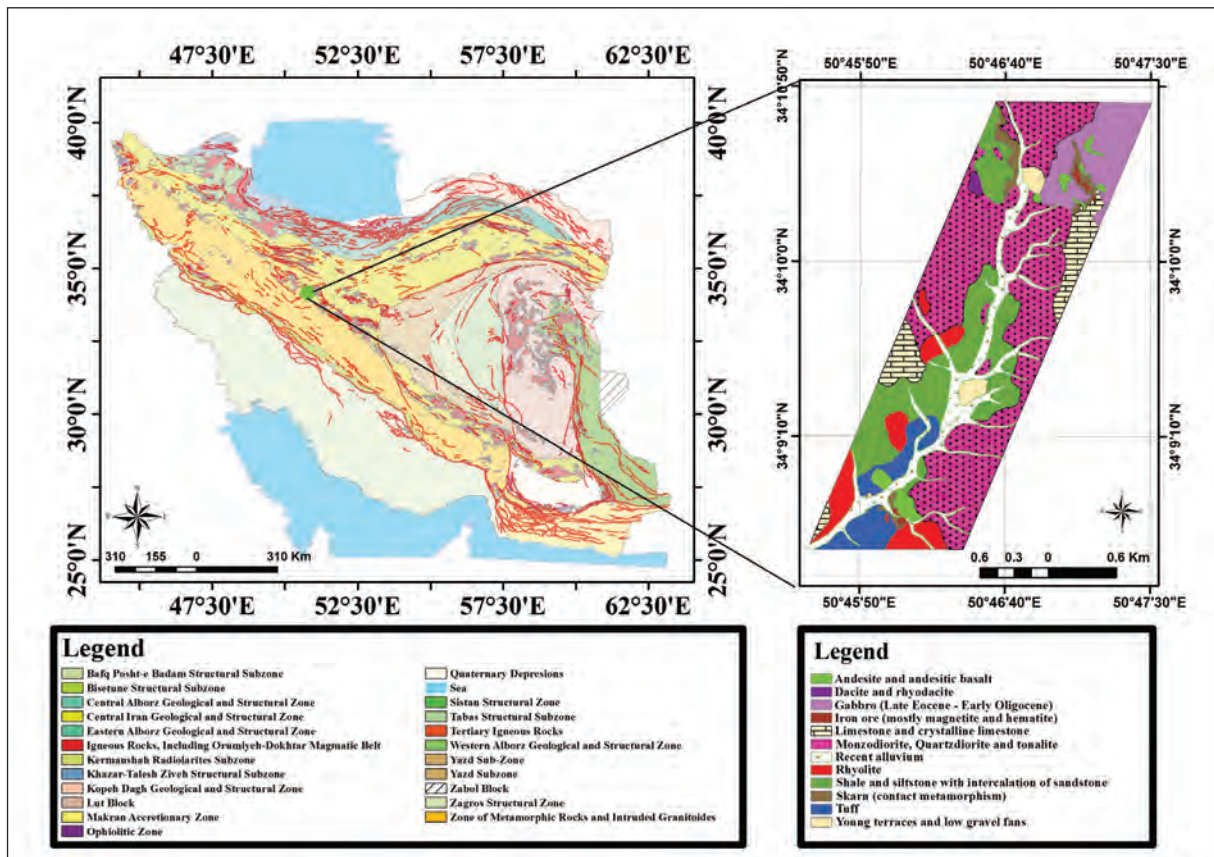


Figure 1- Physiographic-tectonic zoning map of Iran's sedimentary basins[modified from Sahandi et al. (2005)] and location of study area.

and hosts the majority of the larger metals deposits such as copper and iron (Hassan-Nezhad and Moore, 2006). The investigated area characterized by Eocene intrusive rocks and carbonates of Qom formation. Different types of metal ore deposits, such as iron, lead and zinc, copper and distributed manganese vein and also non-metal deposits (barite) have already been documented in near the study area.

The different alteration types have been recognized are phyllic zone (muscovite, illite and quartz), argillic zone (kaolinite and montmorillonite), propylitic zone (chlorite and epidote) and iron oxide (hematite, goethite and limonite) (Feizi and Mansouri, 2012; Feizi and Mansouri, 2013a).

In addition, evidences of iron mineralization include magnetite and hematite, have been reported (Feizi and Mansouri, 2013b). Based on the existing evidences, such as contact of intrusive bodies and carbonate rocks (Qom formation) in the studied area, calcic iron skarn mineralization is suggested.

2.2. AHP Method

AHP is a multi-criteria decision method that uses hierarchical structures to represent a problem and then develop priorities for alternatives based on the judgment of the user (Saaty, 1980). The AHP involves the three basic steps comprising construction of a hierarchy, priority setting, and logical consistency (Macharis et al., 2004; Najafi et al., 2014). These steps are described in the following.

(1) Construction of a hierarchy: In this step the complex problem is decomposed into a hierarchical structure with decision elements (objective, attributes i.e. criterion map layer and alternatives).

(2) Priority setting: The method of deriving evidential weights via the AHP involves pairwise comparisons of criteria according to their relative importance with respect to a proposition (Carranza, 2008; Nouri et al., 2013). The pairwise judgment starts from the second level and finishes in the lowest level, alternatives. The DM uses a standardized comparison scale of nine levels that is shown in table 1 (Saaty, 2005; Dağdeviren, 2008)

Table 1- Scales for pairwise comparison (Saaty, 1980).

Preferences expressed in numeric variables	Preferences expressed in linguistic variables
1	Equal importance
3	Moderate importance
5	Strong importance
7	Very strong importance
9	Extreme importance
2,4,6,8	Intermediate values between adjacent scale values

Let  $C = \{C_j | j = 1, 2, \dots, n\}$  be the set of criteria. The results of the pairwise comparison on  $n$  criteria can be summarized in an  $(n \times n)$  evaluation matrix  $A$  in which every element  $a_{ij}$  ( $i, j = 1, 2, \dots, n$ ) is the quotient of weights of the criteria as shown in Eq. (1) (Dağdeviren, 2008; Abedi et al., 2013).

$$A = \begin{bmatrix} a_{11} & a_{12} & \dots & a_{1n} \\ a_{21} & a_{22} & \dots & a_{2n} \\ \vdots & \vdots & \ddots & \vdots \\ a_{n1} & a_{n2} & \dots & a_{nn} \end{bmatrix}, a_{ii} = 1, a_{1/ji} = 1, a_{ji} \neq 0 \quad (1)$$

The mathematical process commences to normalize and find the relative weights for each matrix. The relative weights are given by the right eigenvector ( $w$ ) corresponding to the largest eigenvalue ( $\lambda_{max}$ ) as Eq. (2):

$$A_w = \lambda_{max} W \quad (2)$$

If the pairwise comparison are completely consistent, the matrix  $A$  has rank 1 and  $\lambda_{max} = n$ . In that case, weights can be obtained by normalizing any of the rows or columns of  $A$  matrix (Dağdeviren, 2008; Abedi et al., 2013).

(3) Logical consistency: The quality of the output of the AHP is strictly related to the consistency of the pairwise comparison judgments. The consistency is defined by the relation between the entries of  $A$  as follow Eq. (3):

$$a_{ij} \times a_{jk} = a_{ik} \quad (3)$$

When the pairwise comparison matrices are completely consistent, the priority (or weight) vector corresponds to the right eigenvector ( $w$ ). Therefore, the highest eigenvalue ( $\lambda_{max}$ ) is equal to  $n$ . In case the inconsistency of the pairwise comparison matrices is limited, slightly  $\lambda_{max}$  deviates from  $n$ . This deviation ( $\lambda_{max} - n$ ) is used as a measure for inconsistency. This measure that is divided by  $(n - 1)$  yields the average of

the other eigenvectors Eq. (4)(Macharis et al., 2004). The consistency index (CI) is:

$$CI = \frac{\lambda_{max} - n}{n - 1} \tag{4}$$

The final consistency ratio (CR), on the basis of which one can conclude whether the evaluations are sufficiently consistent, is calculated as the ratio of the CI and the random index (RI is given in table 2) and it corresponds to the degree of consistency that automatically arises when completing at random reciprocal matrices with the values on the 1–9 scale Eq. (5) (Macharis et al., 2004):

$$CR = \frac{CI}{RI} \tag{5}$$

The number 0.1 is the accepted upper limit for CR. If the final CR exceeds this value, the evaluation procedure has to be repeated to improve consistency. The measurement of consistency can be used to evaluate the consistency of DMs as well as the consistency of all the hierarchy (Dağdeviren, 2008).

Table 2- Some random inconsistency indices (RI) generated by Saaty (1977).

n	1	2	3	4	5	6	7	8	9	10
RI	0	0	0.58	0.9	1.12	1.24	1.32	1.41	1.45	1.49

### 2.3. Index Overlay Method

This method is known as a knowledge-based method. In the early steps of exploratory operations (especially in areas with minimum information) Knowledge-based methods are suggested. These methods are used in areas where there are no known resources or where resources are scarce (Green Fields) (Carranza, 2008; Yousefi and KmkarRouhani, 2010).

In this method each map consists of various classes to which different values have been assigned; these values are multiplied by the pertinent weight, and the average score of each item (polygon or pixel) is computed. Then, these scores are added to the maps and combined. Finally, they are normalized by the sum of the weights. This method follows the general form below Eq. (6) (Malczewski, 2006):

$$S = (\sum_i^n S_{ij} W_i) / (\sum_i^n W_i) \tag{6}$$

Where S denotes a weighted score for each condition  $W_i$  is the weight of  $i^{th}$  input map,  $S_{ij}$  show rating  $j^{th}$  class is the class of the  $i^{th}$  that are rated and weighted (Malczewski, 2006).

### 2.4. TOPSIS Method

The TOPSIS (technique for order preference by similarity to an ideal solution) method was first introduced by Hwang and Yoon (1981). The basic principle is that the best alternative should have the shortest distance from the ideal solution (also called the positive ideal solution) and the farthest distance from the negative ideal solution (also called the anti-ideal solution).

The TOPSIS procedure consists of the following steps (Dağdeviren et al., 2009):

(1) Create a decision matrix. This decision matrix can be established as follows Eq. (7):

$$D = \begin{matrix} & F_1 & F_2 & \dots & F_j & \dots & F_n \\ \begin{matrix} A_1 \\ A_2 \\ \vdots \\ A_j \\ \vdots \end{matrix} & \begin{bmatrix} f_{11} & f_{12} & \dots & f_{1j} & \dots & f_{1n} \\ f_{21} & f_{22} & \dots & f_{2j} & \dots & f_{2n} \\ \vdots & \vdots & \dots & \vdots & \dots & \vdots \\ f_{j1} & f_{j2} & \dots & f_{jj} & \dots & f_{jn} \\ \vdots & \vdots & \dots & \vdots & \dots & \vdots \\ f_{j1} & f_{j2} & \dots & f_{jj} & \dots & f_{jn} \end{bmatrix} \end{matrix} \tag{7}$$

(2) Calculate the normalized decision matrix. The normalized value is calculated as

$$r_{ij} = f_{ij} / \sqrt{\sum_{j=1}^n f_{ij}^2}, j = 1, \dots, J; i = 1, \dots, n \tag{8}$$

(3) Calculate the weighted normalized decision matrix. The weighted normalized value is calculated as

$$v_{ij} = w_j r_{ij}, j = 1, \dots, J; i = 1, \dots, n \tag{9}$$

Where  $w_j$  is the weight of the  $j^{th}$  attribute or criterion and  $\sum_{j=1}^n w_j = 1$ .

(4) Determine the ideal and negative-ideal solution.

$$A^+ = \{v_1^+, \dots, v_n^+\} = \{(max v_{ij} | i \in I'), (min v_{ij} | i \in I'')\}, \tag{10}$$

$$A^- = \{v_1^-, \dots, v_n^-\} = \{(min v_{ij} | i \in I'), (max v_{ij} | i \in I'')\} \tag{11}$$

Where  $v_{ij}^+$  is associated with benefit criteria, and  $v_{ij}^-$  is associated with cost criteria.

(5) The separation of each alternative from the positive-ideal solution ( $D_j^+$ ) is given as

$$D_j^+ = \sqrt{\sum_{i=1}^n (v_{ij} - v_i^+)^2} \quad j = 1, 2, \dots, J \tag{12}$$

Also, The separation of each alternative from the negative-ideal solution () is given as

$$D_j^- = \sqrt{\sum_{i=1}^n (v_{ij} - v_i^-)^2} \quad j = 1, 2, \dots, J \quad (13)$$

(6) Calculate the relative closeness to the ideal solution and rank the performance order.

$$CC_j^+ = \frac{D_j^-}{D_j^+ + D_j^-} \quad j = 1, 2, \dots, J; CC_j^+ \in [0, 1] \quad (14)$$

The larger the index value, the better the performance of the alternatives.

## 2.5. Calcic Iron Skarn (CIS) Deposits Model

The iron skarn deposits are significant and important for their high content of magnetite and minor amounts of Ni, Co, Cu and Au. Most of iron skarns are comprised of magnetite with only minor silicate gangue. The iron skarn deposits are very large (>500 million tons, with >300 million tons contained Fe) (Vidal et al., 1990). In oceanic island arcs, calcic iron skarns (CIS) are formed with iron-rich plutons intruded into volcanic wall rocks and limestone. Skarn minerals all are iron rich and generally include pyroxene and garnet, and small amount of actinolite, ilvaite and epidote (Purtov et al., 1989). Except CIS, magnesian iron skarns (MIS) that forms from iron-rich plutons intruded dolomitic wall, do not contain much iron. Russian deposits have more outcrops of CIS deposits against MIS (Sokolov and Grigorev, 1977).

## 2.6. Criteria Description and Application

In this paper, geological, geochemical and geophysical evidential data are selected considering the experiences reached from previous experiments of CIS deposit exploration in the study area (Feizi and Mansouri, 2012; Feizi and Mansouri, 2013b). The mentioned evidential layers (geological, geochemical and geophysical) are the most important layers for MPM which were utilized numerous (Abedi and Norouzi, 2012; Abedi et al., 2012a; Abedi et al., 2012b; Abedi et al., 2012c; Najafi et al., 2014). The main causes of using these layers are, availability and usefulness for MPM. For this based on the experiences, above description of deposit model of the deposit type mineralization, we used following evidential layers as the most principal regional scale criteria for prospecting CIS deposit in the study area; lithology of intrusive rocks as heat sources and host

rock lithology (based on 1:5000 geology map of the study area), ores and minerals (based on geological evidences), litho-geochemical anomalies (interpreted from analyses of rock samples taken from outcropping rocks that extended in the study area), and magnetic anomaly (based on ground magnetic data analyses).

For obtaining the evidential layers of intrusive rocks as heat sources and host rocks lithology, these layers, were generated from the 1:5000 geological map of the study area. In this paper tonalite, quartzdiorite, monzodiorite and gabbro were presented as heat sources lithology. In addition, skarn unit (contact metamorphism) and limestone and crystalline limestone of Qom formation were introduced as host rocks lithology.

Ores and minerals which are significant in CIS mineralization, were extracted by remote sensing and confirmed with check field and geological evidences. To separate ores and minerals; Spectral Angel Mapper (SAM) and Band Ratio techniques have been applied on ASTER data (Nouri et al., 2012; Feizi and Mansouri, 2012). Magnetite, pyrite, hematite, calcite, pyroxene and garnet were manifested as important ores and minerals in CIS deposit.

Also, litho-geochemical anomalies interpreted from the results of analyzing rock samples taken from outcropping rocks in the study area. In this area, the element content of Fe, Cu, Zn, Au and As in the samples were used as indicators for CIS deposits.

Ground geophysical magnetic data were used to define magnetic anomaly respectively with reduction-to-the-pole (RTP) technique (Mansouri et al. 2015). The RTP technique transforms total-magnetic-intensity (TMI) anomalies to anomalies that would be measured if the field were vertical (assuming there is only an inducing field). This RTP transformation makes the shape of magnetic anomalies more closely related to the spatial location of the source structure.

After that, for informing the classes relative importance, they must be specified with weights (Bonham-Carter, 1994; Carranza, 2008). Hence, the classes of processed maps were determined with scores within [1, 10] range (Table 3) (Porwal et al., 2004; Porwal et al., 2006). The generated weighted evidence layers were utilized for MPM of CIS deposit in the Sarvian prospecting area, have been demonstrated in figure 2. Furthermore, all pixel values of all evidential layers were normalized

Table 3- Summary of evidence maps, classes and their corresponding weights for skarn mineralization.

Data	Evidential layer	Class	Class score
Geological data	Heat source	Tonalite- Quartzdiorite	10
	Host rock	Skarn	10
		Limestone and crystalline limestone	9
	Ores and minerals	Magnetite	10
		Pyrite	8
		Hematite	8
		Garnet	6
		Pyroxene	4
		Calcite	2
Geochemical data	Lithogeochemical sample	Rock sample anomaly, Fe	10
		Rock sample anomaly, Cu	6
		Rock sample anomaly, Zn	4
		Rock sample anomaly, Au	2
		Rock sample anomaly, As	2
Geophysical data	Ground magnetic	Magnetic anomaly	10

between ranges of 0 to 1 with the same pixel or cell size.

### 2.7. Application of the AHP Method to CIS Deposit Potential Mapping

CIS potential mapping using AHP method consists of the following steps (Pazand et al., 2011):

1. The hierarchical structure which is used to generate MPM in this study is illustrated in figure 3.

2. A pairwise comparison method (Saaty, 1980) was used for computing relative importance weights for criteria. Each layer was compared in pairwise comparisons related to each of the elements at the level directly above.

3. Analyzing the relationship of each index caused establishing the level of the structure.

4. All of the weights determined by the pairwise comparison matrix (PCM).

Criteria and sub criteria were ranked by using table 1. A group of specialists in the study of skarn deposits determined and decided the relative importance of each factor for mineralization, then all the opinions have been analysed, and finally, the rank of relative importance have been gained for each factors as shown in table 1. The tree diagram with three main criteria (geological, geochemical and geophysical data layers) and five sub criteria (heat source, host rock, ores

and indications, geochemical anomaly, geophysical anomaly), was used for determination of each factor weight (Figure. 3). It should be noted also all pixels in final prospecting map are alternatives. By normalizing the weight of each factor,  $W_i$  is calculated.  $W_i$  is criteria weight. It is mentioned that the CR values of all the comparisons were lower than 0.1. The CR with range lower than 0.1 shows that the use of the weights was appropriate (Saaty, 1977).

Based on the results of pairwise comparison matrix (PCM), weights of sub criterias for geological data, including heat source, host rock, ores and minerals were calculated (Table 4). It is apparent that other weights of sub criterias (including geochemical anomaly and geophysical anomaly) were placed equivalent to 1, because with one sub criteria the PCM cannot be formed. With the results of tables 3 and 4, the main criteria including geological, geochemical and geophysical data, were used to calculate the final matrix. In this way the criteria importance coefficients were calculated. The PCM of table 5 was created based on expert opinion with accepted CR. For instance, the procedure of obtaining normalized weights from evaluation matrix with respect to geological data alternatives is illustrated. For this goal, firstly the total rows of each criterion was calculated. This number is then divided by the total of the row criteria sum. For example (based on table 5) the total row of geological data was  $(1+5+3) = 9$ . Also this number was 1.45 and 5.33 for geochemical data and geophysical

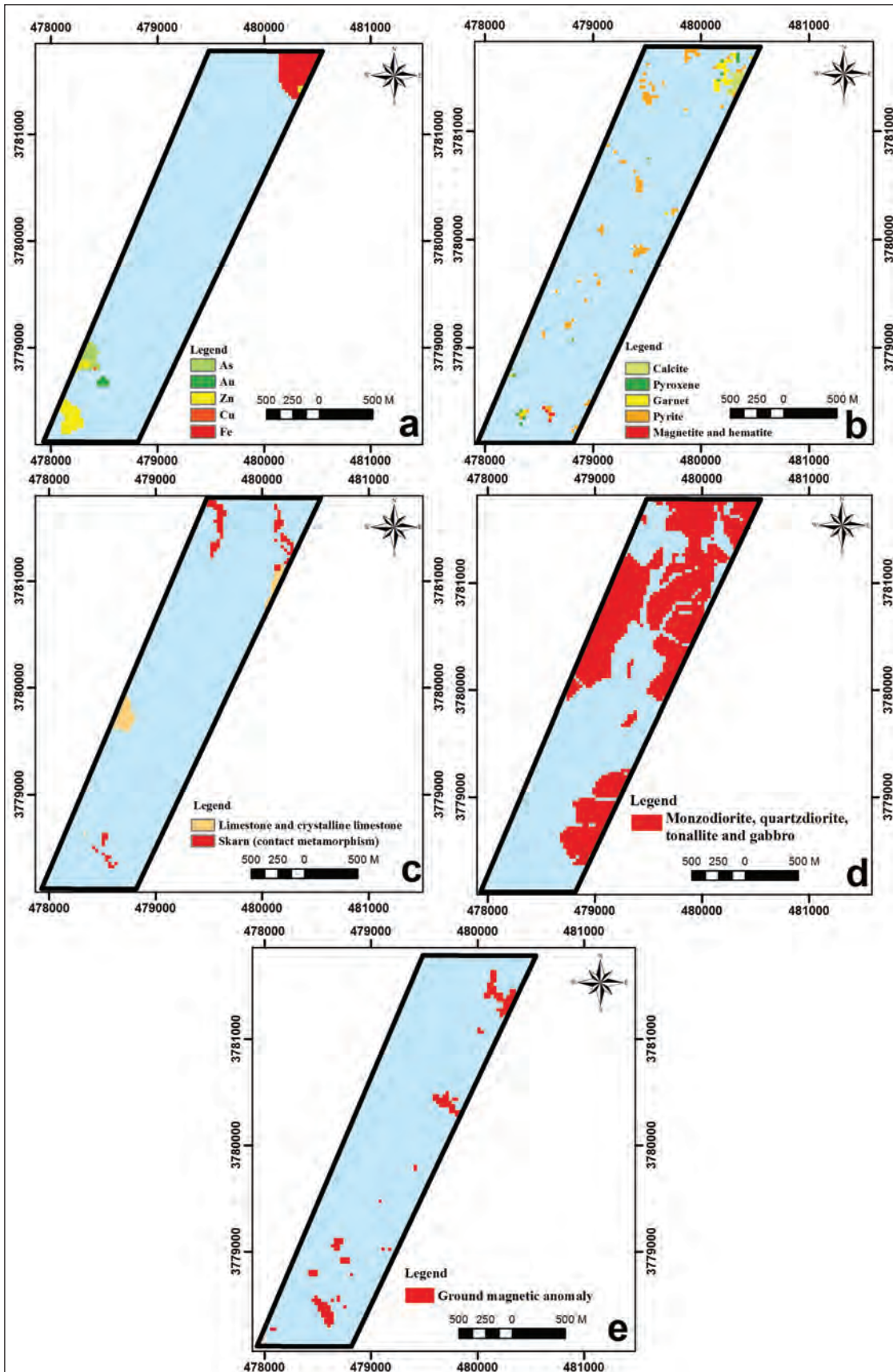


Figure 2- Derived geo-evidential layers for skarn mineralization used in index overlay and TOPSIS prospectivity mapping.

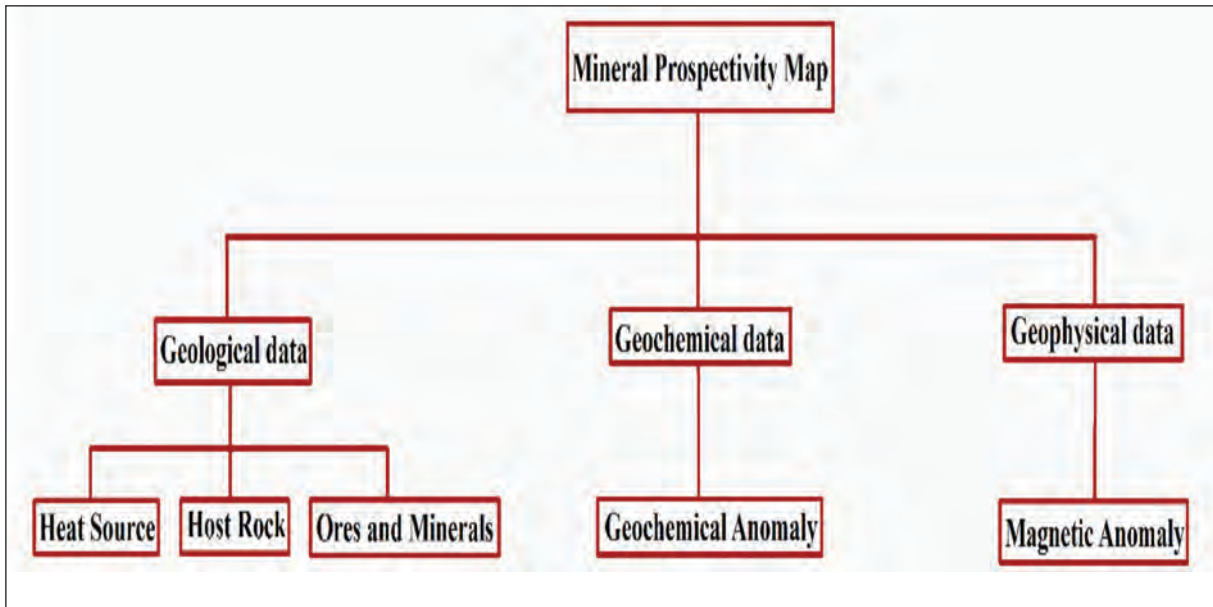


Figure 3- Hierarchy used for prospectivity mapping.

data respectively. Then, the total of the row criteria sum was (9+1.45+5.33=15.78). Finally, for weight calculating of each criterion, the total rows of each criterion was divided by the total of the row criteria sum. For example the weight of geological data was (9/15.78= 0.57) (Table 5). Also this number was 0.090 and 0.338 for geochemical data and geophysical data respectively (Table 5).

In table 5, the consistency ratio is CR=0.0726 which is suitable (CR<1). Geological data in table 5 is the most important factor (W=0.570). The next most important factor is geophysical data (W=0.338), followed by geochemical data (W=0.090).

Table 4- Weights of sub criteria for geological data.

CR=0.0405	Heat source	Ores and Minerals	Host rock	W
Heat source	1.000	3.000	5.000	0.370
Ores and Minerals	0.333	1.000	3.000	0.137
Host rock	0.200	0.333	1.000	0.493

Table 5- Weights of main criteria.

CR=0.0726	Geological data	Geochemical data	Geophysical data	W
Geological data	1.000	5.000	3.000	0.570
Geochemical data	0.2	1.000	0.25	0.090
Geophysical data	0.33	4.00	1.000	0.338

### 2.8. Application of the Index Overlay Method to CIS Deposit Potential Mapping

Based on the calculated weights by AHP method, index overlay method is used in this study via Eq. 15.

$$Result = \sum_{j=1}^n \sum_{i=1}^m W_j W_i \tag{15}$$

Where  $W_j$  is the importance weight of the  $j$ th criteria, and  $W_i$  is the preferred weight of the  $i$ th alternatives. In this method every layer, according to the values of their units, is given various classes. Additionally, every layer has an especial weight based on studies and expert opinion. After processing, the potential target map of iron is prepared using the Index Overlay method (Figure 4).

### 2.9. Application of the TOPSIS Method to CIS Deposit Potential Mapping

Application of the TOPSIS procedure for mineral potential mapping was proposed by Pazand et al. (2012). As it was explained each of the evidence maps has been converted to raster with specific cell size. So the final matrix should be with 10913 row ( $A_j$ ) cells and 5 columns ( $F_n$ ) (heat source, ores and minerals, host rocks, litho-geochemical anomaly, ground magnetic anomaly) was formed as explained in formula. 6. Hence, there are 5 evidential maps (each map include 10913 cells with unique values). Also each cell has unique geographical coordinates. First of all we convert each cell to a unique value with a

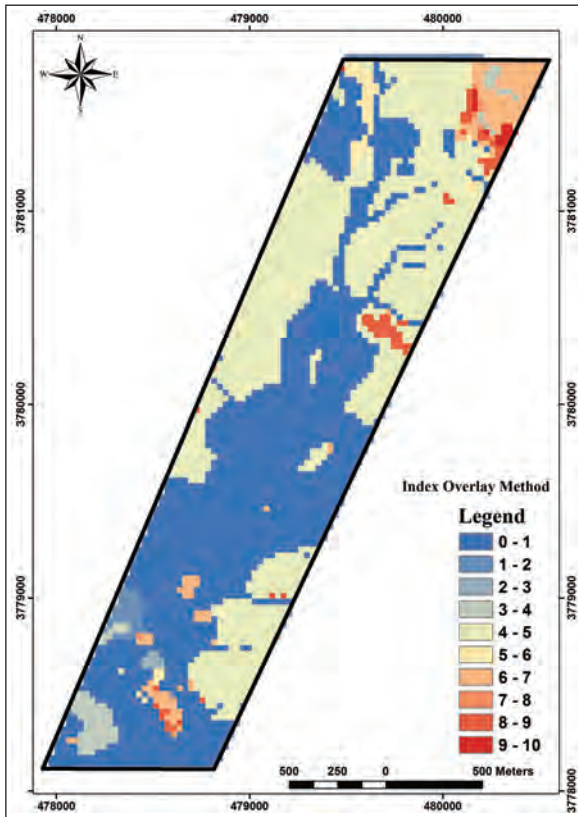


Figure 4- The final prospectivity map for Skarn deposit by index overlay method.

unique geographical coordinates. In this way the final matrix is generated.

For running the TOPSIS procedure, ranks of relative importance for each criterion should be determined. In this research, we used the same criteria weights (in AHP method) which is evaluated in table 6. It is obvious that calculating the final weight is created by, multiplying the weight of each criterion to alternatives. For example this number was calculated for Heat source by multiplying 0.570 (Geological data weight which was calculated in table 5) to 0.370 (Heat source initial weight which was calculated in table 4). So, the final weight was 0.078, 0.281, 0.092 and 0.338 for Ores and minerals, Host rocks, Lithogeochemical anomaly and Ground magnetic anomaly respectively (Table 6). After that the TOPSIS procedure runs in Matlab software. Hence, values of the alternatives has been determined. Thus, for each alternative (each cell), there is a unique value which is the result of TOPSIS method for each cell.

Table 6- Weight of each criterion and alternative to evaluate Skarnprospectivity map.

Criterion	Weight	Alternative	Weight	Final Weight
Geological data	0.570	Heat source	0.370	0.211
		Ores and minerals	0.137	0.078
		Host rocks	0.493	0.281
Geochemical data	0.092	Lithogeochemical anomaly	1	0.092
Geophysical data	0.338	Ground magnetic anomaly	1	0.338

At last, the final prospectivity map for CIS deposit is plotted by specific grid cell size. In this way the mapping of potential for CIS deposit mineralization in the Sarvian area, was prepared by Matlab and plot by ArcGIS software (Figure 5).

### 3. Discussion

The legend of final prospecting maps for Skarn deposit by index overlay and TOPSIS methods (based on AHP weight) was specified by dividing the prospectivity values into 10 classes for better comparison (Figure 4 and Figure 5). It is obvious that

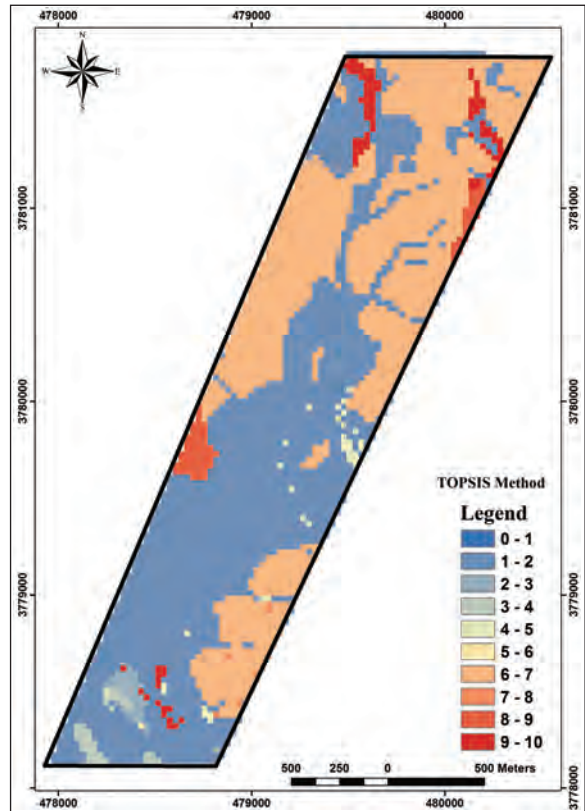


Figure 5- The final prospectivity map for Skarn deposit by TOPSIS method.

each class has a priority for exploration. For instance, for Index Overlay and TOPSIS final prospectivity maps, the first class (range of 0 – 1) has the lowest exploratory priority and the last class (range of 9 – 10) has the highest (Table 7). It is obvious that there are some differences between the results of each method. The comparative analyses of index overlay and TOPSIS integration models, has been performed by selecting four Ground Control Points (GCPs) for check field (Figure 6). Based on table 7 classification, the class number of GCPs in the study area, are specified in table 8.

Table 7- Classification of data values in final prospectivity maps.

Class number	The exploratory priority
1	The lowest
2	Intermediate exploratory priority between the lowest and highest precedence
3	
4	
5	
6	
7	
8	The highest
9	
10	

Table 8- The class numbers of GCPs in the Sarvian area.

GCP	Class number	
	Index Overlay	TOPSIS
1	10	10
2	5	10
3	6	10
4	9	6

In GCP1, four geological units were observed. The first unit contains shale and siltstone with intercalation of sandstone (with geological age of jurassic). In this unit, contact of intrusive bodies with shale and siltstone, caused contact metamorphism and hornfels creation; the second unit is Oligo-Miocene limestone; the third unit contains semi-basic intrusive rocks, such as diorite, monzonite and andesitic dykes; and the fourth geological unit contains skarn units and iron ore mineralization. The collision between intrusive rocks and limestone units causes the iron skarn mineralization, which is obvious in Figure 7a and 7b shows a polished section from GCP1 which contains magnetite and ilmenite. The magnetite is the most abundant ore of this unit (almost 90% of the rock volume). Also secondary replacement of hematite and ilmenite are obvious in mentioned polished section. Figure 7c shows a thin section

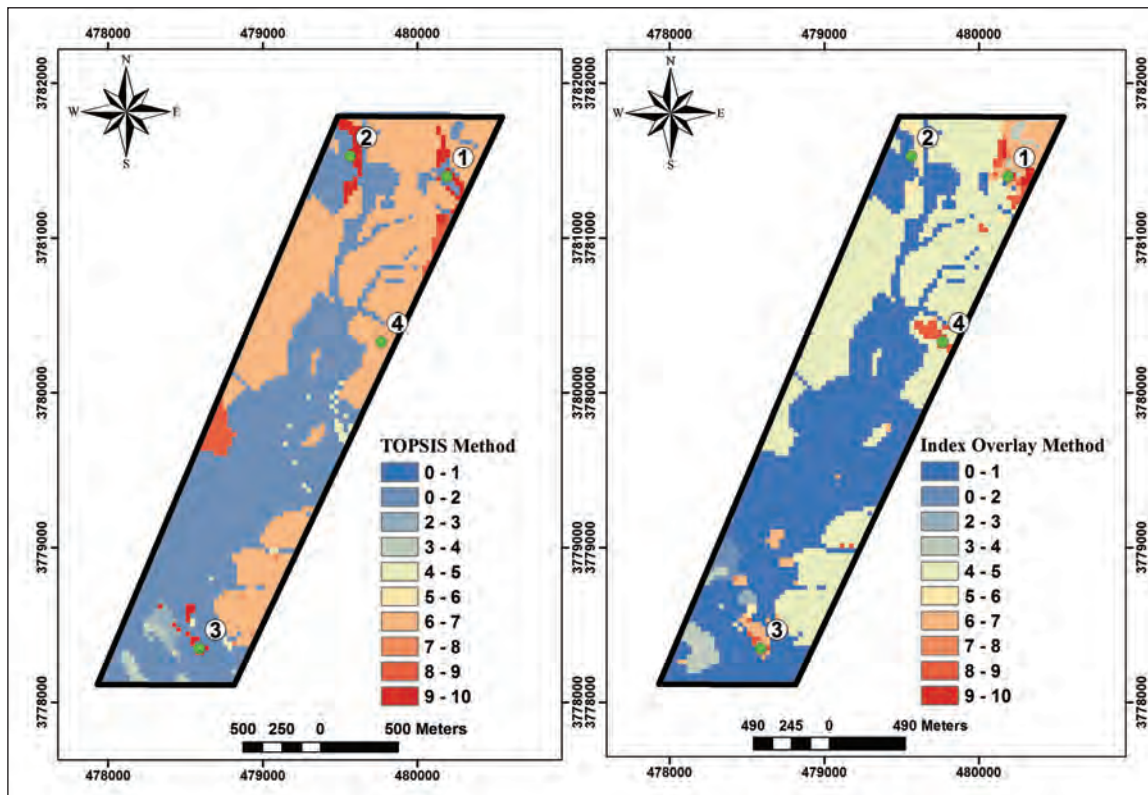


Figure 6- The comparative analyses of index overlay and TOPSIS integration models, with four GCPs for check field.

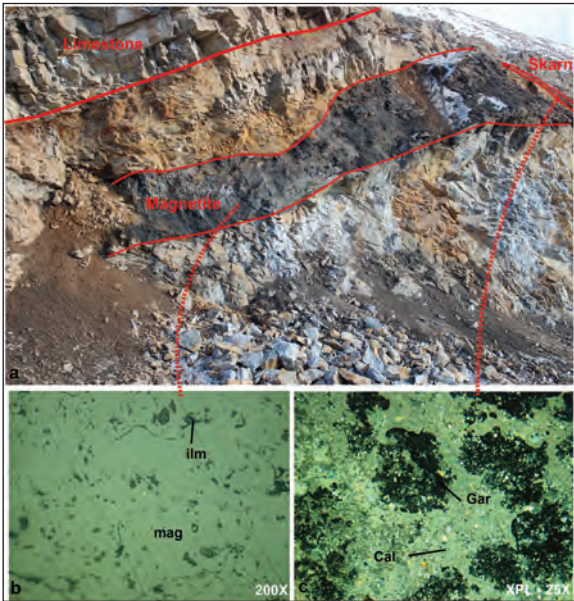


Figure 7- GCP1. a) Contains magnetite, intrusive rocks, limestone and skarn unit (contact metamorphism). b) Magnetite and ilmenite is obvious in prepared polished section from ore body. c) Thin section with granoblastic texture, contains calcite, garnet, tremolite, wollastonite and idocrase from skarn unit.

with granoblastic texture, contains calcite, garnet, tremolite, wollastonite and idocrase. This section prepared from host rock of magnetite mineralization. Thus, the skarn mineralization was observed in GCP1. In GCP1, the value of index overlay and TOPSIS prospectivity maps are the same and have the highest priority (class10) (Table 8).

In GCP2, contact of intrusive bodies with sedimentary units, caused contact metamorphism and hornfels creation. The most important skarn mineralization in GCP2 is magnetite. Also garnet has outcrop near iron mineralization. The hematite is obvious in mentioned GCP as a secondary mineral. In Figure 8a, contact of intrusive bodies with limestone causes iron skarn mineralization obviously. Figure 8b shows a thin section, mainly contains wollastonite, garnet, calcite and chlorite. Diopside and garnet are the most abundant minerals in mentioned section. In GCP2, the value of index overlay prospectivity is five and TOPSIS is ten (Table 8). So, according to the observed iron mineralization in GCP2, high accuracy of TOPSIS method in comparison with the index overlay was revealed.

In GCP3, magnetite is the most important skarn mineralization (Figure 9). The pyrite is obvious in iron



Figure 8- GCP2. a) Contact of intrusive rocks with limestone causes iron skarn mineralization. b) Thin section contains diopside, wollastonite, garnet, calcite and chlorite.



Figure 9- GCP3. a) Magnetite ore body. b) The pyrite mineralization in magnetite.

mineralization in figure 9. The skarn unit is the host rock of iron mineralization and the intrusive rocks haven't any outcrop in mentioned GCP. According to the ground geophysical studies, it seems the intrusive bodies are in the further depth. In GCP3, the value of index overlay prospectivity is six and TOPSIS is ten (Table 8). Thus, based on the observed iron mineralization in GCP3, high accuracy of TOPSIS method in comparison with the index overlay was confirmed.

In GCP4, the outcrop of limestone without any mineralization is obvious in figure 10. In GCP4, the value of index overlay prospectivity is nine and TOPSIS is six (Table 8). In the other words, index overlay method predicts higher exploratory priority against TOPSIS approach for GCP4, wrongly. Thus in GCP4, high accuracy of TOPSIS method in comparison with the index overlay was approved again.

#### 4. Conclusion

Exploration strategies for non-renewable resources have been changing rapidly along with the accelerating innovations in computer hardware and information-processing technology. The aim of this research is to compare index overlay and TOPSIS (based on AHP weight) model for predictive skarn potential map. In this paper, for Calcic Iron Skarn mineralization, criteria and subcriteria introduced and ranked for generating mineral prospectivity map. Each class had a priority for exploration. It was obvious that there are some differences between the results of each method. The comparative analyses of index overlay and TOPSIS



Figure 10- GCP4. The outcrop of limestone without any mineralization.

(based on AHP weight) integration models, has been performed by selecting four GCPs for check field.

In GCP 1, 2 and 3, contact of intrusive bodies with sedimentary units, caused contact metamorphism and iron ore mineralization but in In GCP4, The outcrop of limestone without any mineralization was obvious in surface, although high magnetic anomaly (based on ground magnetic data analyses) is distinct. The field study in Sarvian area shows that, separation anomaly has done better and more accurate in TOPSIS method against index overlay approaches. Thus, for reconnaissance of Calcic Iron Skarn in Sarvian area and near prospecting area the TOPSIS method is introduced in comparison with index overlay method.

#### Acknowledgement

The authors would like to thank Amir Abbas Karbalaee Ramezanali for his helpful suggestions for improving this paper.

#### References

- Abedi, M., Norouzi, G. H., 2012. Integration of various geophysical data with geological and geochemical data to determine additional drilling for copper exploration. *Journal of Applied Geophysics*, 83, 35-45.
- Abedi, M., Norouzi, G. H., Bahroudi, A. 2012a. Support vector machine for multi-classification of mineral prospectivity areas. *Computers & Geosciences*, 46, 272-283.
- Abedi, M., Torabi, S. A., Norouzi, G. H., Hamzeh, M., Elyasi, G. R. 2012b. PROMETHEE II: a knowledge-driven method for copper exploration. *Computers & Geosciences*, 46, 255-263.
- Abedi, M., Torabi, S. A., Norouzi, G. H., Hamzeh, M. 2012c. ELECTRE III: A knowledge-driven method for integration of geophysical data with geological and geochemical data in mineral prospectivity mapping. *Journal of applied geophysics*, 87, 9-18.
- Abedi, M., Torabi, S. A., Norouzi, G. H. 2013. Application of fuzzy AHP method to integrate geophysical data in a prospect scale, a case study: Seridune copper deposit. *Bollettino di Geofisica Teorica ed Applicata*, 54, 145-164.
- Bonham-Carter, G.F. 1994. *Geographic Information Systems for geoscientists-modeling with GIS*. Pergamon Press, Oxford, UK, 398.
- Carranza, E. J. M. 2008. *Geochemical anomaly and mineral prospectivity mapping in GIS*, Handbook of

- Exploration Environmental Geochemistry. Elsevier, Amsterdam, Netherlands, 368.
- Carranza, E.J.M., Hale, M. 2001. Geologically constrained fuzzy mapping of gold mineralization potential, Baguio district, Philippines. *Natural Resources Research*, 10, 125–136.
- Dağdeviren, M. 2008. Decision making in equipment selection: an integrated approach with AHP and PROMETHEE. *Journal of Intelligent Manufacturing*, 19, 397-406.
- Dağdeviren, M., Yavuz, S., Kılınç, N. 2009. Weapon selection using the AHP and TOPSIS methods under fuzzy environment. *Expert Systems with Applications*, 36, 8143-8151.
- Feizi, F., Mansouri, E. 2012. Identification of Alteration Zones with Using ASTER Data in A Part of Qom Province, Central Iran, *Journal of Basic and Applied Scientific Research*, 2,73-84.
- Feizi, F., Mansouri, E. 2013a. Separation of Alteration Zones on ASTER Data and Integration with Drainage Geochemical Maps in Soltanieh, Northern Iran, *Open Journal of Geology*, 3, 134-142.
- Feizi, F., Mansouri, E. 2013b. Introducing the Iron Potential Zones Using Remote Sensing Studies in South of Qom Province, Iran. *Open Journal of Geology*, 3, 278-286.
- Hassan-Nezhad, A.A., Moore, F. 2006. A stable isotope and fluid inclusion study of the Qaleh-Zari Cu–Au–Ag deposit, Khorasan Province, Iran. *Journal of Asian Earth Sciences*. 27, 805–818.
- Hwang, C.L., Yoon, K. 1981. *Multiple Attribute Decision Making-Methods and Applications: A State of the Art Survey*. Springer, New York.
- Macharis, C., Springael, J., De Brucker, K., Verbeke, A. 2004. PROMETHEE and AHP: The design of operational synergies in multicriteria analysis: Strengthening PROMETHEE with ideas of AHP. *European Journal of Operational Research*, 153, 307-317.
- Malczewski, J. 2006. Ordered weighted averaging with fuzzy quantifiers: GIS-based multicriteria evaluation for land-use suitability analysis, *International Journal of Applied Earth Observation and Geo information*, 8, 270-277.
- Mansouri, E., Feizi, F., Karbalaeei Ramezanali, A. A. 2015. Identification of magnetic anomalies based on ground magnetic data analysis using multifractal modelling: A case study in Qoja-Kandi, East Azerbaijan Province, Iran. *Nonlinear Processes in Geophysics*, 22, 579-587.
- Najafi, A., Karimpour, M. H., Ghaderi, M. 2014. Application of fuzzy AHP method to IOCG prospectivity mapping: A case study in Taherabad prospecting area, eastern Iran. *International Journal of Applied Earth Observation and Geoinformation*, 33, 142-154.
- Noori, R., Feizi, F., Jafari, M. R. 2011. Determination of Cu and Mo Potential Targets in the Khatunabad Based on Analytical Hierarchy Process, West of Mianeh, Iran. *World Academy of Science, Engineering and Technology*, 78, 828-831.
- Nouri, R., Jafari, M. R., Arain, M., Feizi, F. 2012. Hydrothermal Alteration Zones Identification Based on Remote Sensing Data in the Mahin Area, West of Qazvin Province, Iran. In *Proceedings of World Academy of Science, Engineering and Technology* 67, World Academy of Science, Engineering and Technology.
- Novri, R., Afzal, P., Arian, M., Jafari, M., Feizi, F. 2013. Reconnaissance of Copper and Gold Mineralization Using Analytical Hierarchy Process (AHP) in the Rudbar 1: 100,000 Map Sheet, Northwest Iran. *Journal of Mining and Metallurgy A: Mining*, 49, 9-19.
- Önüt, S., Soner, S. 2008. Transshipment site selection using the AHP and TOPSIS approaches under fuzzy environment. *Waste Management*, 28, 1552-1559.
- Pazand, K., Hezarkhani, A., Ataei, M., Ghanbari, Y. 2011. Combining AHP with GIS for predictive Cu porphyry potential mapping: a case study in Ahar Area (NW, Iran). *Natural resources research*, 20, 251-262.
- Pazand, K., Hezarkhani, A., Ataei, M. 2012. Using TOPSIS approaches for predictive porphyry Cu potential mapping: A case study in Ahar-Arasbaran area (NW, Iran). *Computers & Geosciences*, 49, 62-71.
- Pirmoradi, A., Vaezi, H., Baktash, P., Amiri, A. 2012. Role of SDI in index overlay Modeling and fuzzy logic in GIS to predict Malaria outbreak. Canada, *Proceedings of Global Geospatial Conference 2012 Québec City*, 14-17.
- Porwal, A., Carranza, E.J.M., Hale, M. 2003. Artificial neural networks for mineral-potential mapping: a case study from Aravalli Province, Western India. *Natural resources research*, 12, 156–171.
- Porwal, A., Carranza, E.J.M., Hale, M. 2004. A hybrid neuro-fuzzy model for mineral potential mapping. *Mathematical Geology*, 36, 803-826.
- Porwal, A., Carranza, E.J.M, Hale, M. 2006. A hybrid fuzzy weights-of-evidence model for mineral potential mapping. *Natural Resources Research*, 15, 1–14.

- Purtov, V.K., Kholodnov, V.V., Anfilogov, V.N., Nechkin, G.S. 1989. The role of chlorine in the formation of magnetite skarns: *International Geology Review*, 31, 63-71.
- Rogge, D.M., Halden, N.M., Beaumont-Smith, C. 2006. Application of data integration for shear-hosted Au potential modelling: Lynn Lake greenstone belt, northwestern Manitoba, Canada. *GIS for the Earth Sciences*, 44, 191–210.
- Saaty, T.L. 1977. A scaling method for priorities in hierarchical structures. *Journal of mathematical psychology*, 15, 234-281.
- Saaty, T.L. 1980. *The analytic hierarchy process: planning, priority setting, resources allocation*. New York: McGraw, pp, 281.
- Saaty, T.L., 2005. The analytic hierarchy and analytic network processes for the measurement of intangible criteria and for decision-making." *Multiple criteria decision analysis: state of the art surveys*. Springer New York, 345–408.
- Sahandi, M.R., Delavar, S.T., Sadeghi, M., Jafari, A., Moosavi, A. 2005. *Geological Map of Iran (1:1.000.000)*. Geological Survey of Iran. <<http://www.ngdir.ir>>.
- Sokolov, G.A., Grigorev, V.M. 1977. Deposits of iron, in smirnov, V.I., ed., *Ore deposits of the USSR*: Pittman, London, 1, 7-13.
- Vidal, C., Injoque-Espinoza, J., Sidder, G.B., Mukasa, S.B. 1990. Amphibolitic Cu-Fe skarn deposits in the central coast of Peru. *Economic Geology*, 85, 1447-1461.
- Yousefi, M., Kamkar Rouhani, A. 2010. *Principle of Mineral Potential Modeling Techniques (In Geographical Information System)*: Amirkabir University of Technology Press, Tehran.
- Yousefi, M., Carranza, E. J. M. 2015. Prediction-area (P-A) plot and C-A fractal analysis to classify and evaluate evidential maps for mineral prospectivity modeling. *Computers & Geosciences*, 79, 69-81.



# Bulletin of the Mineral Research and Exploration

<http://bulletin.mta.gov.tr>



## Pb – Zn - Cd ACCUMULATOR PLANTS GROWN AROUND THE GÖRGÜ Pb – Zn MINE, YEŞİLYURT-MALATYA, TURKEY

Güllü KIRAT<sup>a\*</sup>

<sup>a</sup>Bozok University, Faculty of Engineering and Architecture, Department of Geological Engineering, Yozgat. [orcid.org/0000-0002-1167-0574](http://orcid.org/0000-0002-1167-0574).

Research Article

### Keywords:

Accumulator, Indicator plant, Transition Factor, Hyperaccumulator plant, Enrichment Coefficients.

### ABSTRACT

A study was carried out to identify Cd, Pb and Zn concentrations which exist in the roots and stems of *Astragalus pycnocephalus* Fischer and *Verbascum euphraticum* L. plants which grow in the Görgü Pb-Zn mining area. A total of 60 samples were collected, 30 samples from plants and 30 samples from the soils where the plants grow. When the analytical results gained are statistically examined, according to correlation coefficients graphic between the soil and plant, finding positive correlation between (*A. Pycnocephalus*) soil-root (Cd,  $r = 0.77$ ), soil-stem (Cd,  $r = 0.86$ ) and soil-stem (Pb,  $r = 0.77$ ) could mean that these could be indicator plants and can be used for remediation of the soils polluted by Cd and Pb metals. It is observed that the metallic concentration times values of the plants in this study taken from polluted areas compared to the plants taken from unpolluted areas, are quite high in total 44 samples. Transition factor is  $>1$  in some sample locations and range between 0.13 and 2.07. Enrichment coefficients is  $>1$  for the location of V11 (Cd, root/soil). *A. Pycnocephalus* and *V. Euphraticum*, in some locations, according to transition factor, enrichment coefficients, times values and element concentrations could be identified as accumulator/hyperaccumulator for Cd, Pb and Zn elements..

Received Date: 18.05.2016

Accepted Date: 04.08.2016

## 1. Introduction

Mining industry has a destructive effect on the contamination of the environment because of the heavy metals (Navarro et al., 2008; Zhuang, 2009). Besides these mining works, industrial emissions, the use of fertilizers and pesticides increase the amount of heavy metals in the environment (Alloway, 1994; Yoon et al., 2006). Agricultural lands which are on the mining and its neighbouring area has the disadvantage of the accumulation of heavy metals in the soil in great amount which cause the increase of the content of heavy metals in food products and this increase affects the public health in dramatic way (Adriano, 2001; Pruvot et al., 2006). That's why, the heavy metals which exist in mineralization areas can be avoided thanks to growing the plants which are capable of collecting heavy metals in their structure (Wong, 2003; Yanqun et al., 2005). Also, techniques such as ditch opening, chemical stabilization, soil washing

and burying are used to remove the heavy metals from the soil but these techniques are expensive, so they are not practical (Mehes-Smith et al., 2013). Remedial techniques carried out in a specific area are cheaper and more appropriate than a regional research field (Mitch, 2002; Pulford ve Watson, 2003). Generally, the use of plants in the improvement of the environment is an old and cheap method and that gives no damage to the environment.

Baker and Walker (1990) studied the plants in three groups: the ones which do not take metals into their structure directly, the ones which take them directly and the ones which take them into their structure in excessive amounts (accumulator and hyperaccumulator). The plants which can take the metals in their structure are grown in such areas to remove heavy metallic contamination. They are also used to find mine deposits containing the metal.

\* Corresponding author: Güllü KIRAT, [gullu.kirat@bozok.edu.tr](mailto:gullu.kirat@bozok.edu.tr) / [gul.kirat@hotmail.com](mailto:gul.kirat@hotmail.com)  
<http://dx.doi.org/10.19111/bulletinofmre.306195>

There are many plant species discovered in Anatolia and the world for this purpose (Brook et al., 1995; Özdemir, 2003; 2005; 2009. Dunn, 2007). The metallic constructions are low in the plants which take place in non-metal containing group as metals are not carried from the roots to the branches but the metallic construction is high in the roots (Mehes-Smith et al., 2013). Heavy metal constructions accumulate in the tissues by moving from the plant roots to the top in a metal accumulator/hyperaccumulator (Salt et al., 1998; Kachout et al., 2009). Like accumulators, metal indicators accumulate the metals in the top tissues of the plants as well (Mganga et al., 2011; Mehes-Smith et al., 2013). While some species of plants only accumulate specific metals, some other plants accumulate many other metals in their structure (Mganga et al., 2011). Some kinds of plants die or undergo a physiological and morphological change as they continuously accumulate metals in their structure. These plants are biologically and ecologically important because they can be used as a contamination indicator. Also, they can absorb contaminants as accumulators (Mganga et al., 2011; Mehes-Smith et al., 2013).

The purpose of this study can be listed as below:

1. Identification of Cd, Pb ve Zn constructions in the *V. Euphraticum* and *A. Pycnocephalus* plant samples,
2. The comparison of element constructions in the plants with those of the soil in which they grow and their statistical examine
3. Identification of the accumulator/hyperaccumulator and indicator plants.

## 2. Geology of the Region and Mineralization

The study area is situated between the villages of Görgü and Seyitusagi in the city of Yesilyurt, Malatya (Figure 1). There are basically old Malatya metamorphics and Permo-Carbonifer which is formed from limestone and marbles in the region (Önal et al., 1990; Cengiz et al., 1991). They are found as comprised of schists. Malatya metamorphic rocks are overlain by volcano- sedimentary unit cut with andesitic volcanic rocks. Volcanits which exist in the study area near the business expose in a narrow area (Sağiroğlu, 1988). The third unit in the study area consists of alluvial deposits and soil cover. The mineralization exists in the fault zones which cut Malatya metamorphites (Figure 2).

According to Sağiroğlu (1988), Malatya metamorphites almost form from limestones in the study area. They observed as light grey limestones, mixed series, dark grey limestones and limestones breccia from the bottom to the top (Figure 2).

Volcanic rocks can be separated from alteration zones and manganese denticritics and the units in the region as they are in the yellowish cream colour. Fault zones are exposed along these rocks (Sağiroğlu, 1988) (Figure 2).

In the northern part of the study area is a unit consisting of an alluvium and soil cover, which includes a wide area and slope rubble in places (Figure 2).

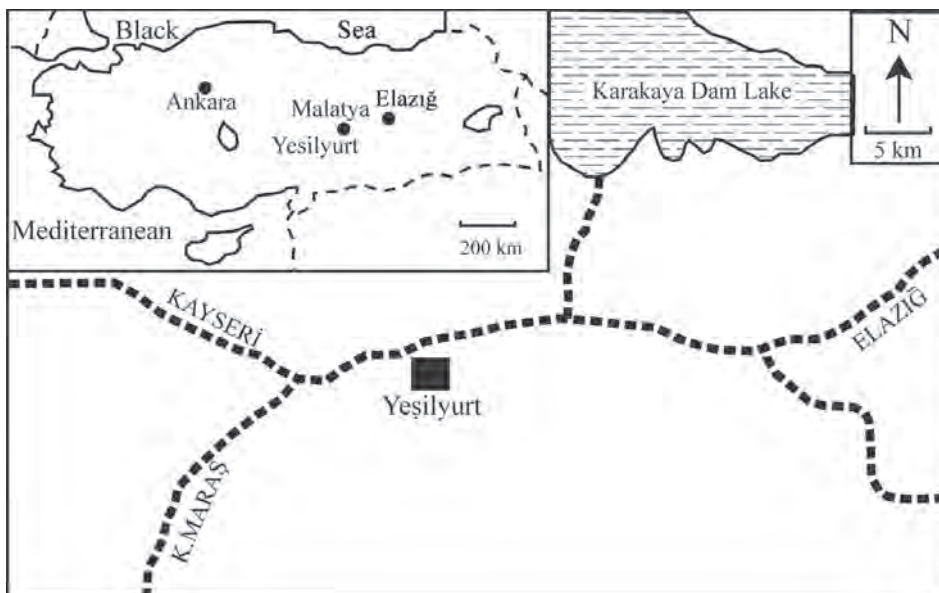


Figure 1- Location map of the study area.

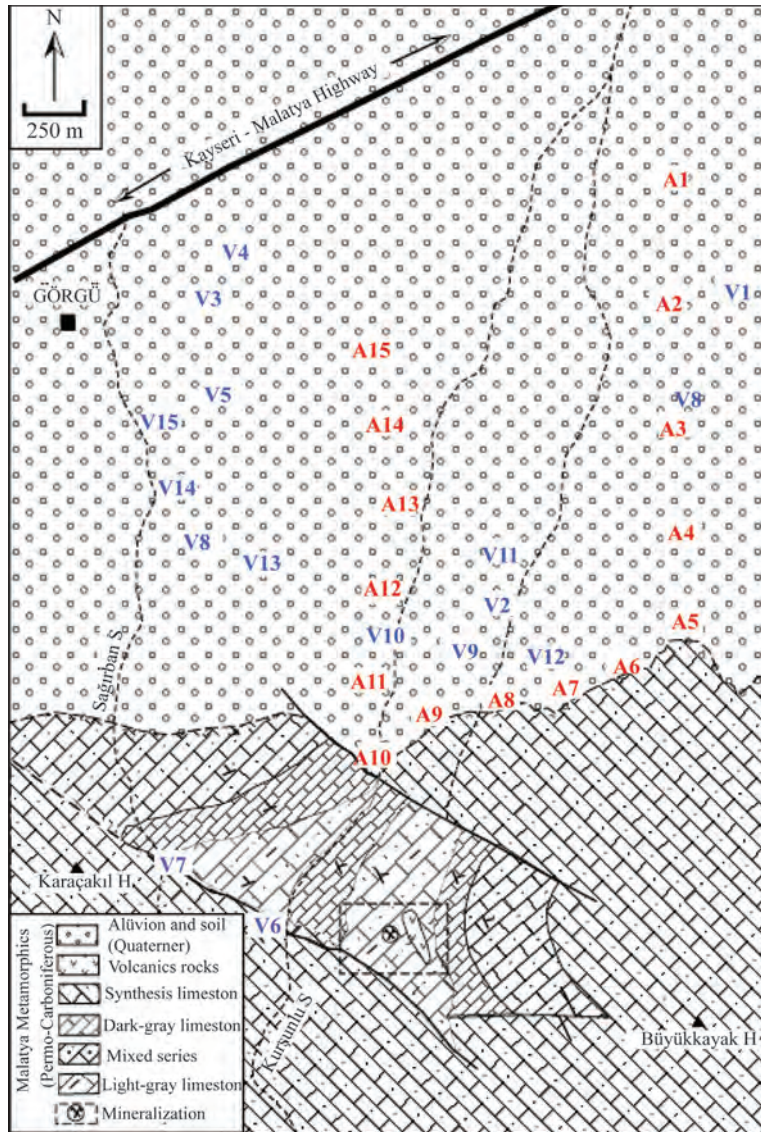


Figure 2- Distribution map of the geology of the study area (after Sağroğlu, 1988), A. *pycnocephalus* plant samples (sample number is given in red color) and V. *euphraticum* plant samples (sample number is given in blue color).

There are two fault zones in the north-west direction and parallel to each other in the study area. No mineralization or alteration have been found in these two fault zones (Sağroğlu, 1988).

This mineralization which is thought to have relation with dacitic-andesitic volcanism exists between volcano-sedimenter rocks and limestones contact and also in the units of both (Özen, 1991). Volcano-sedimenter rocks which are in grey, greenish grey, grayish blue and greenish brown colours have a structure which is rather weathered, cracked and with cavities. Also, sericitization and claying are seen locally in these rocks. The mineralogical composition

of the host rock is formed from plagioclase, tremolite-actinolite, calcite, chlorite, titanite, apatite and opaque minerals (Güdücü, 1994).

The Görgü Pb-Zn mineralization forms from two different mineralizations which are classified as carbonated and sulfidic ones (Pratt, 1990). Carbonated ore (e.g.,  $ZnCO_3$ ,  $PbCO_3$ ) exists around the cracks which start from the surface to the deeper parts where there is meteoric waters. This mineralization is in the yellow, brown-yellow colours and in the form of limonite rich Zn-carbonate. Ore minerals are simitsonite, limonite, zincite, hydrozincite, anglezite-serousite. The sulfidic ore (e.g.,  $ZnS$ ,  $PbS$ ) continues

vertically at a depth of 30-40 m. It is usually dark gray and exists scattered in limestones (Sağiroğlu, 1988). Ore minerals are galena, sphalerite, pyrite and marcasite (Sağiroğlu, 1988; Güdücü, 1994).

### 3. Material and Method

In the PhD study performed by Kırat (2009), two separate analyzes were carried out for *A. pycnocephalus* and *V. euphraticum* plants. Within the scope of this study, 30 specimens were taken from these two plants and the soil in which these plants were grown. Cd, Pb and Zn elemental analyses of the taken samples were carried out at ICP-MS (Inductively Coupled Plasma - Mass Spectrophotometer) and Yozgat-Bozok University, Science and Technology Application and Research Center (BILTEM).

ICP-MS device has the calibrations to carry out qualitative, quantitative and isotope ratio measurements. The Li, Be, and B measurements allow the passage of low-mass ions through the cell in the KED (Kinetic Energy Discrimination) mode in He. The quadrupole scan rate is 90.000 amu/s for each element. The system has a frequency of 2.0 MHz quadrupole for better peak resolution in complex samples and the linear dynamic range for the MS-detector in the system is 1-109 cps. Detection limits of analyzed soil and plant samples are Cd: 0.01 mg/kg, Pb: 0.01 mg/kg, Zn: 0.1 mg/kg.

#### 3.1. Plant Analysis

In the study area, a total of 30 samples (Figure 3) were taken sybranchatically from the roots and branches of *A. pycnocephalus* and *V. euphraticum* plant samples (Figure 2). The roots and branches of the samples were separated and passed through the

tap water first and pure water respectively. The plant samples which were dried at room temperature were then dehumidified by being kept waiting for 24 hours at 80-90°C in the oven.

4-5 g of dried plant samples were taken from each organ separately and placed in an ash oven. The samples which were placed in this oven were ashed at a temperature of 50°C for the beginning and burned to 550°C with an increase in temperature of 50°C per hour. Previous researchers have determined this temperature range to be between 475 - 550°C (Reichman et al., 2001).

#### 3.2. Soil Analysis

A total of 30 soil samples were taken from the soil on which the plant specimens were grown (Figure 2). Soil specimens were taken at the depth of approximately 15-20 cm in the location where it was taken care not to have any metallic contamination and where the plant samples were taken, with the help of plastic shovels and by removing the plant roots. The collected soil samples were bagged, numbered and brought to the laboratory by passing through a 2 mm spaced plastic sieve. These samples were dried at room temperature for about two weeks.

To measure the pH values of soil samples, test tubes were prepared by mixing 10 ml of pure water (1: 2.5) with 4 g of soil sample. These prepared tubes were occasional mixed within 20-25 minutes and then their pH values were measured by pH meter (Table 1 and table 4).

A mixture was prepared from ash-derived plant sample, one gram of the soil on which the plants were grown and adding to 2 ml of concentrated HNO<sub>3</sub> by



Figure 3- A view of (a) *A. pycnocephalus* and (b) *V. euphraticum* plants growing around the study area.

taking into account the sample preparation methods recommended by Hajara et al. (2014). The resulting mixture was dried by evaporating on a heating plate. The dried mixture was again mixed with HCl-HNO<sub>3</sub>-H<sub>2</sub>O (from each acid 6 ml of a 1: 1: 1 mixture solution in each case). And the resulting mixture was completed with pure water to 25 ml.

#### 4. Results and Discussion

##### 4.1. Concentrations of Cd, Pb and Zn in Soil

The chemical analysis results for the Cd, Pb and Zn elements in the soil were evaluated statistically (values of > 10000 mg/kg were not used in statistical evaluation) (Table 1-6). A positive correlation was observed between the Pb element ( $r = 0.2$ ) and pH of the soil where *A. pycnocephalus* plant was grown, while there was a negative correlation between Cd element ( $r = -0.47$ ) and Zn element ( $r = -0.24$ ) (Table 1-3). A negative correlation was observed between the Cd element ( $r = -0.22$ ) and the Pb element ( $r = -0.2$ ), while a positive correlation was found between the

pH of the soil of the *V. euphraticum* plant and the Zn element ( $r = 0.2$ ) (Table 4-6).

Cd is among the trace elements associated with phosphorites. Concentrations were found at 20 mg/kg in the phosphites (Il'in and Kiperman, 2001), at 0.15 mg/kg in granite, at 1.5 mg/kg in shales, at 6.5 mg/kg in black shales and at 2100-2600 mg/kg in sfaleritte (Olade, 1987). The existence of Cd in the soil depends on some properties such as organic matter, pH, grain size and cation exchange capacity. The mean Cd concentration in uncontaminated mine fields on Earth soil is 0.3 mg (Reimann and Caritat, 1998). According to a survey of Soil and Herbage contamination (Environment Agency, 2007), the contamination mean is 0.39 mg/kg in the soil of the UK (Health Protection Agency, 2009). The concentration of Cd in the soil was determined as 0.1-0.5 mg/kg by Rose et al. (1979) and 0.03 - 0.32 mg/kg in World Health Organization (Nazir et al., 2015).

The concentration of Cd in the soil where *A. pycnocephalus* plant grows ranges from 42.2-110.2

Table 1- Cd element distributions in *A. pycnocephalus* plant and statistical evaluations of distributions.

Sample	Cd (mg/kg)				Enrichment Coefficient		Transition Factor	Times
	pH	Soil	Root	Branch	R/S	B/S	B/R	B/Cd
A1	5.2	86.2	6.7	8.6	0.08	0.10	1.28	8.6
A2	5.3	93.6	7.8	10.2	0.08	0.11	1.31	10.2
A3	5.1	87.3	8.3	9.3	0.10	0.11	1.12	9.3
A4	4.9	75.7	7.4	6.7	0.10	0.09	0.91	6.7
A5	4.7	56.2	8.1	6.4	0.14	0.11	0.79	6.4
A6	5.4	61.3	6.3	7.1	0.10	0.12	1.13	7.1
A7	5.7	42.2	7.2	8.8	0.17	0.21	1.22	8.8
A8	6.9	45.7	4.9	3.5	0.11	0.08	0.71	3.5
A9	4.6	101.1	21.5	16.2	0.21	0.16	0.75	16.2
A10	5.1	98.7	14.7	23.3	0.15	0.24	1.59	23.3
A11	6.3	87.9	9.6	11.4	0.11	0.13	1.19	11.4
A12	7.01	65.6	5.1	6.3	0.08	0.10	1.24	6.3
A13	4.4	110.2	23.8	25.8	0.22	0.23	1.08	25.8
A14	4.6	85.6	7.5	10.1	0.09	0.12	1.35	10.1
A15	5.0	79.4	5.5	8.2	0.07	0.10	1.49	8.2
Minimum		42.2	4.9	3.5				
Maksimum		110.2	23.8	25.8				
Arithmetic mean		78.4	9.6	10.8				
Median		85.6	7.5	8.8				
Standard deviation		20.3	5.8	6.3				

R/S: Root/Soil, B/S: Branch/Soil, B/R: Branch/Root, B/Cd: Branch/Cd

Table 2- Pb element distributions in *A. pycnocephalus* plant and the statistical evaluations of distributions.

Pb (mg/kg)				Enrichment Coefficient		Transition Factor	Times
Sample	Soil	Root	Branch	R/S	B/S	B/R	B/Pb
A1	5639	450.7	789	0.08	0.14	1.75	157.8
A2	2198	124.4	83	0.06	0.04	0.67	16.6
A3	>10000	832.7	454	<0.08	<0.05	0.55	90.8
A4	>10000	1053.3	651	<0.11	<0.07	0.62	130.2
A5	5935	628	342	0.11	0.06	0.54	68.4
A6	3138	753.3	96	0.24	0.03	0.13	19.2
A7	>10000	762.3	378	<0.08	<0.04	0.50	75.6
A8	>10000	1420	298	<0.14	<0.03	0.21	59.6
A9	5572	324.3	94	0.06	0.02	0.29	18.8
A10	>10000	926.7	181	<0.09	<0.02	0.20	36.2
A11	>10000	1094	269	<0.11	<0.03	0.25	53.8
A12	>10000	1367	447	<0.14	<0.04	0.33	89.4
A13	>10000	1467	284	<0.15	<0.03	0.19	56.8
A14	3160	438.1	287	0.14	0.09	0.66	57.4
A15	>10000	1527.1	211	<0.15	<0.02	0.14	42.2
Minimum	2198	124.4	83				
Maksimum	>10000	1527.1	789				
Aritmetik Ortalama	4273.7	877.9	324.3				
Median	4366	832.7	287				
Standard deviation	1621.6	441.2	200.2				

R/S: Root/Soil, B/S: Branch/Soil, B/R: Branch/Root, B/Pb: Branch/Pb

Table 3 – Zn element distributions in *A. pycnocephalus* plant and the statistical evaluations of distributions.

Zn (mg/kg)				Enrichment Coefficient		Transition Factor	Times
Sample	Soil	Root	Branch	R/S	B/S	B/R	B/Zn
A1	>10000	981	1798	<0.10	<0.18	1.83	17.98
A2	9883	974	748	0.10	0.08	0.77	7.48
A3	8244	385	287	0.05	0.03	0.75	2.87
A4	>10000	899	478	<0.09	<0.05	0.53	4.78
A5	>10000	1034	736	<0.10	<0.07	0.71	7.36
A6	6088	321	179	0.05	0.03	0.56	1.79
A7	7244	1530	362	0.21	0.05	0.24	3.62
A8	>10000	787	515	<0.08	<0.05	0.65	5.15
A9	>10000	917	1491	<0.09	<0.15	1.63	14.91
A10	>10000	1083	1254	<0.11	<0.13	1.16	12.54
A11	>10000	1347	1208	<0.13	<0.12	0.90	12.08
A12	>10000	727	1236	<0.07	<0.12	1.70	12.36
A13	>10000	1380	1687	<0.14	<0.17	1.22	16.87
A14	>10000	755	1377	<0.08	<0.14	1.82	13.77
A15	7988	723	986	0.09	0.12	1.36	9.86
Minimum	6088	321	179				
Maksimum	>10000	1530	1798				
Aritmetik Ortalama	7889.4	922.9	956.1				
Median	7988	917	986				
Standard deviation	1393.9	335.8	524.9				

R/S: Root/Soil, B/S: Branch/Soil, B/R: Branch/Root, B/Zn: Branch/Zn

Table 4 - Cd elemental distributions in *V. euphraticum* plant and statistical evaluations of distributions.

Sample	Cd (mg/kg)				Enrichment Coefficient		Transition Factor	Times
	pH	Soil	Root	Branch	R/S	B/S	B/R	B/Cd
V1	4.9	119	7.53	7.8	0.06	0.07	1.04	7.8
V2	5.1	37.8	12.1	6.4	0.32	0.17	0.53	6.4
V3	4.7	438	15.3	4.4	0.03	0.01	0.29	4.4
V4	5.9	140	15.7	8.2	0.11	0.06	0.52	8.2
V5	4.5	225	8.1	6.7	0.04	0.03	0.83	6.7
V6	5.1	173	23.3	5.1	0.13	0.03	0.22	5.1
V7	5.7	115	54.4	7.2	0.47	0.06	0.13	7.2
V8	5.9	544	19.1	34.3	0.04	0.06	1.80	34.3
V9	4.5	21.6	4.3	6.5	0.20	0.30	1.51	6.5
V10	5.3	87	10.4	5.4	0.12	0.06	0.52	5.4
V11	5.8	4.1	10.1	1.9	2.46	0.46	0.19	1.9
V12	5.9	96	9.3	14	0.10	0.15	1.51	14
V13	6.4	22	8.7	3.5	0.40	0.16	0.40	3.5
V14	6.6	19	2.4	2.7	0.13	0.14	1.13	2.7
V15	4.7	34.9	6.5	5.8	0.19	0.17	0.89	5.8
Minimum		4.1	2.4	1.9				
Maksimum		544	54.4	34.3				
Arithmetic mean		138.4	13.8	8.0				
Median		96	10.1	6.4				
Standard deviation		157.8	12.5	7.8				

R/S: Root/Soil, B/S: Branch/Soil, B/R: Branch/Root, B/Cd: Branch/Cd

Table 5 - Pb elemental distributions in *V. euphraticum* plant and statistical evaluations of distributions.

Sample	Pb (mg/kg)			Enrichment Coefficient		Transition Factor	Times
	Soil	Root	Branch	R/S	B/S	B/R	B/Pb
V1	>10000	243	462	<0.02	<0.05	1.90	92.4
V2	>10000	762.5	434	<0.08	<0.04	0.57	86.8
V3	>10000	283	128	<0.03	<0.01	0.45	25.6
V4	>10000	756.6	131	<0.08	<0.01	0.17	26.2
V5	>10000	134.2	84	<0.01	<0.01	0.63	16.8
V6	7767	154.1	58	0.02	0.01	0.38	11.6
V7	>10000	640	243	<0.06	<0.02	0.38	48.6
V8	8906	340.7	89	0.04	0.01	0.26	17.8
V9	>10000	250.1	109	<0.03	<0.01	0.44	21.8
V10	7483	278	52	0.04	0.01	0.19	10.4
V11	6918	343.3	278	0.05	0.04	0.81	55.6
V12	>10000	443	282	<0.04	<0.03	0.64	56.4
V13	>10000	691	337	<0.07	<0.03	0.49	67.4
V14	9984	357	124	0.04	0.01	0.35	24.8
V15	9831	235	245	0.02	0.02	1.04	49
Minimum	6918	134.2	52				
Maksimum	>10000	762.5	462				
Arithmetic mean	8481.5	394.1	203.7				
Median	8336.5	340.7	131				
Standard deviation	1281.5	214.6	133.8				

R/S: Root/Soil, B/S: Branch/Soil, B/R: Branch/Root, B/Pb: Branch/Pb

Table 6 - Zn elemental distributions in the *V. euphraticum* plant and statistical evaluations of the distributions.

Sample	Zn (mg/kg)			Enrichment Coefficient		Transition Factor	Times
	Soil	Root	Branch	R/S	B/S	B/R	B/Zn
V1	>10000	289	598	<0.03	<0.06	2.07	5.98
V2	7998	743	708	0.09	0.09	0.95	7.08
V3	>10000	732	744	<0.07	<0.07	1.02	7.44
V4	>10000	444	532	<0.04	<0.05	1.20	5.32
V5	>10000	1145	860	<0.11	<0.09	0.75	8.6
V6	>10000	1043	431	<0.10	<0.04	0.41	4.31
V7	7512	967	789	0.13	0.11	0.82	7.89
V8	>10000	630	455	<0.06	<0.05	0.72	4.55
V9	5020	703	239	0.14	0.05	0.34	2.39
V10	>10000	765	233	<0.08	<0.02	0.30	2.33
V11	8903	631	211	0.07	0.02	0.33	2.11
V12	6269	157	264	0.03	0.04	1.68	2.64
V13	>10000	509	700	<0.05	<0.07	1.38	7
V14	>10000	2436	349	<0.24	<0.03	0.14	3.49
V15	9986	1874	367	0.19	0.04	0.20	3.67
Minimum	5020	157	211				
Maksimum	>10000	2436	860				
Aritmetik Ortalama	7614.7	871.2	498.7				
Median	7755	732	455				
Standard deviation	1787.9	592.9	222.4				

R/S: Root/Soil, B/S: Branch/Soil, B/R: Branch/Root, B/Zn: Branch/Zn

mg/kg (mean 78.4 mg/kg) while the concentration of Cd in the soil where *V. Euphraticum* plant grows ranges from 4.1-544 mg/kg (mean 138.4 mg/kg) (Table 1-6).

Pb is an element which has a low mobility in the soil. However, this mobility changes depending on the Fe-Mn oxides and the amount of insoluble organic matter. When Pb coexists with soluble organic complexes or anionic complexes, its mobility increases. Pb is associated with clay minerals, Mn oxides, Fe-Al hydroxide and organic materials in the soil. It is associated with CaCO<sub>3</sub> or phosphate concentrations in some soils (Kabata-Pendias and Pendias, 2001). According to the world mean, Pb is 44.0 mg/kg in uncontaminated soil (Kabata-Pendias and Pendias, 2001), it is 18.8 mg/kg in the soil of rural areas (Al Obaidy and Al Mashhadi, 2013), Rose et al. (1979) found a mean value of 17 mg/kg in uncontaminated soil. The value determined by WHO (Nazir et al., 2015) is between 0.061 mg/kg and 0.46 mg/kg and the mean value in the soil in the surface is 32 mg/kg (Kabata-Pendias and Pendias, 2001; Wuana

et al., 2011). Pb is 2198 - > 10000 mg/kg in the soil of *A. pycnocephalus* plant in the study area and it is in the range of 6918 - > 10000 mg/kg in the soil where *V. euphraticum* plant grows. It is significantly higher than the above mentioned values (Table 1-6).

The Zn element is found in the soil together with zinc sulphides, Fe-Mn oxides, mafic minerals (hornblende and biotite) and chalcophile elements (Cu and Pb) (Rose et al., 1979). In the soil, the total Zn concentration is 10 - 300 mg/kg and in rural areas it is 16.15 mg/kg (Alloway, 1995). According to Kabata-Pendias and Pendias (2001) it is 100 mg/kg in uncontaminated soil. The mean value is 36 mg/kg in the soil according to Rose et al. (1979) and it is in the range of 0.033-0.349 mg/kg according to World Health Organization and (Nazir et al., 2015). Zn concentration in the study area is in the range of 6088 - > 10000 mg/kg (*A. pycnocephalus*) and 5020 - > 10000 mg/kg (*V. euphraticum*), it is higher than the values indicated by some of the above researchers (Table 1-6).

The results obtained in this study conducted in and around Görgü village, and table 1 - table 6 show that the results obtained from Kırat (2009) are almost the same; it is 82.2 mg/kg in Cd, it is 5649 mg/kg in Pb, it is > 10000 mg/kg in Zn (*A. pycnocephalus*) and it is 109 mg/kg Cd.; it is > 10000 mg/kg in Pb and Zn (*V. euphraticum*).

#### 4.2. Cd, Pb and Zn Element Concentrations in the Plants

In plants grown in soil contaminated with heavy metals, higher concentrations of heavy metals are observed compared to plants growing in soil not affected by contamination (Guttormsen et al., 1995; Dowdy and Larson, 1995; Naser et al., 2012; Vural, 2014).

Generally, the Cd concentration specified by WHO for plants is 0.02 mg/kg, the Pb concentration is 2 mg/kg and the Zn concentration is 50 mg/kg (Nazir et al., 2015; Shah et al., 2011). According to Rose et al. (1979), the Cd concentration is 4.3 mg/kg, the Pb concentration is 30 mg/kg and the Zn concentration is 570 mg/kg on average.

The lowest concentration of Cd in the branch of *A. pycnocephalus* plant is 3.5 mg/kg in the A8 location, the highest concentration is 25.8 mg/kg in the A13 location and the mean is 10.8 mg/kg. The lowest concentration of Cd in the branch of *V. Euphraticum* is 1.9 mg/kg in the V11 location, the highest concentration is 34.3 mg/kg in the V8 location and the mean is 8.0 mg/kg.

In the root of *A. pycnocephalus* plant, the lowest concentration of Cd is 4.9 mg/kg, the highest concentration is 23.8 mg/kg and the mean is 9.6 mg/kg. The lowest concentration of Cd in the root of the *V. Euphraticum* plant is 2.4 mg/kg and the highest concentration is 54.4 mg/kg the mean is 13.8 mg/kg at 2.4 mg/kg. The element concentrations and mean values in the study area were found to be higher than the indicated values (Table 1-6).

It is determined that the results obtained in this study conducted in Görgü village and its surroundings and given in table 1, table 6 are similar to Kırat (2009)'s values obtained at same region from where Cd is 5.03 mg/kg, Pb is 445.7 mg/kg, Zn is 881 mg/kg (at the root of the *A. pycnocephalus*), and Cd is 6.53 mg/kg, Pb is 343 mg/kg and Zn is 409 mg/kg (at the root of *V. euphraticum*).

Sperman correlation coefficients (> 10000 mg/kg values are not taken into account) between *A. pycnocephalus* and *V. euphraticum* plants and Cd, Pb and Zn elements in the soil where this plant grows were calculated and given in figure 4 - 5 and Schroll (1975) evaluated the correlation between soil and plant samples at 95% and 99% confidence level (Özdemir and Demir, 2010). It was found from *A. pycnocephalus* plant that  $r = 0.77$  ( $n = 15$ ,  $p < 0.01$ , 99%) for Cd values of soil and root,  $r = 0.86$  ( $n = 15$ ,  $p < 0.01$ , 99%) for Cd values of soil and branch;  $r = 0.77$  ( $n = 6$ ,  $p < 0.01$ , 99%) for Pb values of soil and branch,  $r = 0.4$  ( $n = 6$ ) for Pb values of soil and root;  $r = 0.5$  ( $n = 5$ ,  $p < 0.05$ , 95%) for Zn values of soil and root,  $r = 0.3$  ( $n = 5$ ) for Zn values of soil-root. For *V. euphraticum* plant,  $r$  is 0.58 ( $n = 15$ ,  $p < 0.05$ , 95%) for Cd values of soil-root,  $r = 0.55$  ( $n = 15$ ,  $p < 0.05$ , 95%) for Cd values of soil and branch;  $r = 0.14$  ( $n = 6$ ) for Pb values of soil and root,  $r = 0.1$  ( $n = 6$ ) for Pb values of soil and branch;  $r = 0.5$  ( $n = 6$ ,  $p < 0.05$ , 95%) for

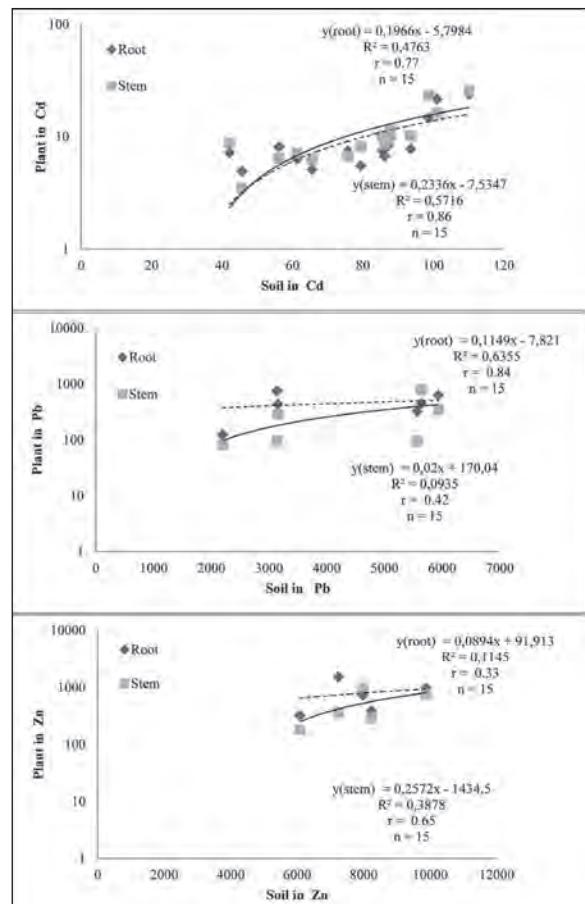


Figure 4- Correlation and distribution relation between the presence of Cd, Pb and Zn element rates in the soil and the rates in the root and branch of the plant in *A. pycnocephalus* plant samples.

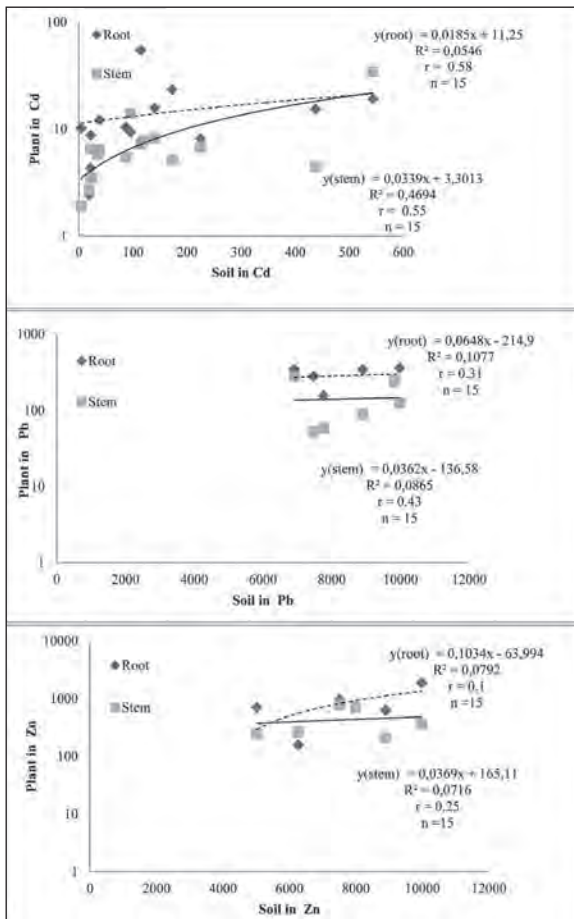


Figure 5- Correlation and distribution relation between the presence rates of Cd, Pb and Zn elements in the soil and their presence in the root and branch of the plant in *V. euphraticum* plant samples.

Zn values of soil and root, and  $r = 0.1$  ( $n = 6$ ) for Zn values of soil and branch.

*A. pycnocephalus* plant root for Pb; its roots and branches for Zn; The root and branch of *V. euphraticum* plant was seen not to be statistically significant ( $p < 0.05$ , 95% confidence level) for Cd, Pb and Zn. In the biogeochemical prospect, the root and branches of *A. pycnocephalus* plant for Cd, its branches for Pb can be suggested to identify indicator plants ( $p < 0.01$ , 99% confidence level) and they can be used to improve contaminated areas. It can be said that this plant species may be accumulator plant due to the excessive amounts of Cd and Pb values in the soil and excessive amounts of Cd and Pb the *A. pycnocephalus* plant can absorb.

There are 4 rules to define the hyperaccumulator: 1) branches of the plant /root of the plant  $> 1$  (transition factor  $> 1$ ) (Xiaohai et al., 2008); 2) plant / soil  $> 1$

(coefficient of enrichment  $> 1$ ) (Rotkittikhun et al., 2006; Harrison and Chirgawi, 1989); 3) the branches of the plant/the ratio of the metal (Cd: 1 mg/kg, Pb: 5 mg/kg, Zn: 100 mg/kg) ranged from 10 to 500 times (time value) (Fifield and Haines, 2000; Allen, 1989; Shen and Liu, 1998; Yanqun et al., 2005); and 4) the concentration of element in the plant (Cd  $> 100$  mg/kg, Pb  $> 1000$  mg/kg, and Zn  $> 10000$  mg/kg) (Mganga et al., 2011, Ernst, 2006, Brooks, 1998, Mehes-Smith et al., 2013).

The transition factor ranged from 0.13 (A6 and V7) to -2.07 (V1) for all samples taken. Transition factor for *A. pycnocephalus* plant is in 11 locations for Cd (A1-A3, A6, A7, A10-A15) for Pb, in 1 location (A1) for Zn in 7 locations (A1, A9, A10, A12-A15), and for *V. euphraticum* plant in 5 locations for Cd (V1, V8, V9, V12, V14) for Pb in 2 locations (V1, V15) and transition factor in 5 locations for Zn (V1, V3, V4, V12, V13) is greater than 1 (Table 1-6). In the study area, that the transition factor is  $> 1$  indicates that the metals are transported from the root to the branches.

The enrichment coefficient is mainly dependent on the soluble fraction of the metal and the organic material in the soil (Xiaohai et al., 2008). This coefficient is an important factor when considering the potential for improvement in plants. The enrichment coefficient is less than 1, either because the metal concentration in the soil is increased or the metal concentration in the plant is low (Zhao et al., 2003). In the study area, the enrichment coefficient of the *V. euphraticum* plant is 2.46 in the V11 location. In general, the enrichment coefficient at all locations where *A. pycnocephalus* and *V. euphraticum* plants are taken is less than 1 (Table 1-6).

The Cd values of *A. pycnocephalus* plant in A2, A9-A11, A13-A14, (Zn) A1, A9-A14 locations and Cd values of *V. euphraticum* plant in V8 location are between 10-500 times. In both plant species, Pb is between 10 and 500 times in all locations. The Pb values are higher than 1000 mg/kg for the root of *A. pycnocephalus* plant in the A4, A8, A11-13, and A15 locations (Table 1-6).

Times values range from 1.79-157.8 in all collected samples. Time values of *A. pycnocephalus* plant is greater than 10 in 6 locations for Cd, for Pb in all locations and 7 locations for Zn. Time values in *V. euphraticum* plant is greater than 10 for Cd in 1 location and for Pb in all locations while they are less than 10 for all Zn values (Table 1-6).

When plant specimens in the study area were compared with plants grown in the soil not affected by contamination (Cd: 1 mg/kg, Shen and Liu, 1998); *A. pycnocephalus* plant at A2, A9, A10, A11, A13, A14 locations and *V. euphraticum* plant at V8 location are between 10.2-25.8 times. Samples taken from all locations (A1-A15 and V1-V15) contain 10.4-157.8 times Pb compared to the ones which were not affected by contamination (Pb: 5 mg/kg; Shen and Liu, 1998). In the A1, A9-A14 locations, the time values of Zn in *A. pycnocephalus* plant are found between 12.08-17.98, whereas all time values in *V. euphraticum* plant are <10 (Zn: 100 mg/kg; Shen and Liu, 1998) (Table 1-6).

## 5. Conclusions

The following results were obtained by statistically evaluating the results of the analyzes to better determine the elemental distributions of Cd, Pb and Zn in the soil and their distributions in the *A. pycnocephalus* and *V. Euphraticum* plants in the study area:

1. The elemental values of Cd, Pb and Zn change depending on the pH values.

2. It has been determined that the concentrations of Cd, Pb and Zn obtained from the soil in the study area are higher than the values given in the literature.

3. Medium and low positive correlations were observed between soil-root and soil-branch for Cd, Pb and Zn in *A. pycnocephalus* and *V. euphraticum* plants. It was seen that for Cd the root and branches of *A. pycnocephalus* plant, its root for Pb, its branches for Zn; for Cd the root and branches of *V. euphraticum* plant can be used to determine indicator plants and to improve the environmental contamination.

4. Concentration values of Cd, Pb and Zn in *A. pycnocephalus* and *V. euphraticum* plants were observed to have higher metal concentrations than those planted in soil not affected by contamination. Transition factor for Cd in *A. pycnocephalus* plant is A1-A3, A6, A7, A10-A15, for Pb is A1 for Zn is A1, A9, A10, A12-A15 and for Cd in *V. euphraticum* plant is V1, V8, V9, V12, V14, for Pb is V1, V15 and for Zn is V1, V3, V4, V12, V13 which are greater than 1 at the specified locations. At the V11 location (Cd, Root/Soil), the enrichment coefficient of the *V. euphraticum* plant is > 1. Times values in the *A. pycnocephalus* plant for Cd are A2, A9-A11, A13, A14, for Pb they are A1-A15 and for Zn they are at A1, A9-A14; in *V.*

*euphraticum* plant for Cd it is V8 for Pb they are V1 and V15. As it is seen in these locations they range from 10 to 500. According to the analysis results obtained, plant samples of *A. pycnocephalus* and *V. euphraticum* can be described as an accumulator / hyperaccumulator for Cd, Pb and Zn.

## Acknowledgement

This work was carried out at Bozok University, Science and Technology Application and Research Center (BILTEM). The author thanks BILTEM for contribution.

## References

- Adriano, D.C. 2001. Trace elements in terrestrial environments: biogeochemistry, bioavailability and risks of metals. 2nd edition. Springer-Verlag.
- Al Obaidy, A.H.M.J., Al Mashhadi, A.A.M. 2013. Heavy Metal Contaminations in Urban Soil within Baghdad City, Iraq. Journal of Environmental Protection 4, 72-82.
- Allen, S.E. 1989. Chemical Analysis of Ecological Materials. 2nd edition, Blackwell Scientific Publications Oxford.
- Alloway, B.J. 1994. Toxic metals in soil-plant systems. Chichester, UK: John Wiley and Sons.
- Alloway, B.J. 1995. "Heavy Metals in Soils," Blackie Academic and Professional, London.
- Baker, A.J.M., Walker, P.L. 1990. Ecophysiology of metal uptake by tolerant plants: Heavy metal uptake by tolerant plants. In: Shaw, A.J. (Editors). Evolutionary Aspects. CRC, Boca Raton.
- Brooks, R.R. 1998. Plant that accumulate heavy metals. CAB International, Wallingford.
- Brooks, R.R., Dunn, C.E., Hall, G.E.M. 1995. Biological sybranch in mineral exploration and processing. Elles Horwood Limited, 538 p.
- Cengiz, R., Yılmaz, H., Türkyılmaz, B. 1991. Intermediate report of licensees of ÖIR: 671 and ÖIR: 1714 belonging to Çinkur near the Malatya – Yesilyurt – Cafana (Görgü). General Directorate of Mineral Research and Exploration. Ankara.
- Dowdy, R.H., Larson, W.E. 1995. The availability of sludge-borne metals to various vegetables. Journal of Environmental Quality 4, 278-282.
- Dunn, C.E. 2007. Biogeochemistry in Mineral Exploration. Handbook of Exploration and Environmental Geochemistry, 9, Elsevier,

- The Netherlands Environment Agency (EA), 2007. UK Soil and Herbage Pollutant Survey, Report Number 7. EA. Bristol, UK.
- Environment Agency, 2007. Flood estimation guidelines, Version 2. Environment Agency.
- Ernst, W.H.O. 2006. Evolution of metal tolerance in higher plants. *Forest Snow and Landscape Research* , 80, 251-274.
- Fifield, F.W., Haines, P.J. 2000. *Environmental Analytical Chemistry*. 2nd Edition, Blackwell Science Ltd., Oxford.
- Guttormsen, G., Singh, B.R., Jeng, A.S. 1995. Cadmium concentrations in vegetable crops grown in a sandy soil as affected by Cd levels in fertiliser and soil pH. *Fert. Res.* 41, 27–32.
- Güdücü, A. 1994. Series of geological maps of Turkey with 1:100 000 scale openings quality, Malatya L40 sheet. Firat University, Institute of Science, Master's degree seminar (unpublished).
- Hajara, E.W.I., Sulaimanb, A.Z.B., Sakinah, A.M.M. 2014. Assessment of Heavy Metals Tolerance in Leaves, Dals and Flowers of *Stevia rebaudiana* Plant. *Procedia Environmental Sciences* 20, 386 – 393, 2014.
- Harrison, R.M., Chirgawi, M.B. 1989. The Assessment of air and soil as contributors of some trace metals to vegetable plants I. Use of a filtered air growth cabinet. *Sci. Total Environ.* 83: 13-34
- Health Protection Agency (HPA), 2009. Contaminated Land Information Sheet. Cadmium. (Prepared by Bull, S. and Johnson, C.), HPA. Version 2. Chilton, UK.
- Il'in, A.V., Kiperman, Y.A. 2001. Geochemistry of Cadmium in Mesozoic Phosphorites of the East European Platform. *Lithology and Mineral Resources* 36/ 6, 576–581.
- Kabata-Pendias, A., Pendias, H. 2001. "Trace Element in Soils and Plants," CRC Press, London.
- Kachout, S.S., Ben Mansoura, A., Leclerc, J.C., Mechergui, R., Rejeb, M.N., Ouerghi, Z. 2009. Effects of heavy metals on antioxidant activities of *Atriplex hortensis* and *A. rosea*. *J. Food Agric. Environ.* 7, 938-945.
- Kirat, G. 2009. Reflections of Pb - Zn deposits and their surrounding metals. Firat University, Institute of Science, PHD Thesis. 210 p.
- Mehes-Smith, M., Nkongolo, K., Cholewa, E. 2013. Coping mechanisms of plants to metal contaminated soil. In Silvern, S. and S. Young, editors. *Environmental change and sustainability*. InTech.
- Mganga, N., Manoko, M.L.K., Rulangaranga, Z.K. 2011. Classification of plants according to their heavy metal content around north mara gold mine, Tanzania: Implication for phytoremediation. *Tanzania Journal of Science* 37, 109-119.
- Mitch, M.L. 2002. Phytoextraction of toxic metals: a review of biological mechanism. *J. Environ. Qual.* 31:109– 20.
- Naser, H.M., Mahmud, N.U., Sultana, S., Gomes, R., Rahman, M. 2012. Trace Elements Content In *VegeÇizelges Grown In Industrially Polluted And Non-Polluted Areas*. *Bangladesh J. Agril. Res.* 37/3, 515-527.
- Navarro, M.C., Perez-Sirvent, C., Martinez-Sanchez, M.J., Vidal, J., Tovar, P.J., Bech, J. 2008. Abandoned mine sites as a source of contamination by heavy metals: a case study in a semi-arid zone. *J. Geoche. Explor.* 96, 183–193.
- Nazır, R., Khan, M., Masab, M., Rehman, H.U., Rauf, N.U., Shahab, S., Ameer, N., Sajed, M., Ullah, M., Rafeeq, M., Shaheen, Z. 2015. Accumulation of Heavy Metals (Ni, Cu, Cd, Cr, Pb, Zn, Fe) in the soil, water and plants and analysis of physico-chemical parameters of soil and water Collected from Tanda Dam kohat. *J. Pharm. Sci. and Res.* 7/3, 89-97
- Olade, M.A. 1987. Dispersion of Cadmium, Lead, and Zinc in soils and sediments of a humid tropical ecosystem in Nigeria. In *Lead, Mercury, Cadmium and Arsenic in the Environment* (eds. T.C. Hutchinson and K.M. Meema). Wiley, New York, Scope, 31, 303–312.
- Önal, M., Tuzcu, N., Helvacı, C. 1990. Geological setting, mineralogy an origin of the Cafana (Malatya) Zn-Pb sulfide and carbonate deposit, E Anatolia, Turkey, in: *Int. Earth Sci. Congress on Aegean Regions, Proceedings*, ed: M. Y. Savaşçın and A. H. Eronat, Izmir, D. E. University, 1, 52-58.
- Özdemir, Z. 2003. Biogeochemical studies at the Musalı and Silifke-Anamur area in Mersin, Turkey. *Geochemistry International* 41/11, 1137-1142.
- Özdemir, Z. 2005. *Pinus brutia* as a biogeochemical medium to detect iron and inc in soil analysis, chromite deposits of the area Mersin, Turkey. *Chemie Der Erde-Geochemistry* 65, 79-88.
- Özdemir, Z. 2009. Can mines be found with plants? What is biogeochemical (plant geochemistry) prospecting? *Mining and Earth Sciences Journal* 1/3, 14-19.
- Özdemir, Z., Demir, E. 2010. Nickel Accumulating species of *Alyssum murale* Waldst.&Kit from Fındıklıpınarı-

- Erdemli/Mersin area. Geological Engineering 34/1, 57-70.
- Özen, N. 1991. Searches lead - zinc of the ÖİR:671 ve ÖİR:1714 licenses province belonging to Çinkur near Malatya – Yesilyurt – Cafana (Görgü), Geophysics - Induced Polarization (IP). Science of the Total Environment 407, 1551 – 1561.
- Pratt, A.D. 1990. The Geology, geochemistry and mineralogy of the sedimentary Cafana Zn-Fe-Pb-Ba deposits, SE Turkey. PHD Thesis, 2, 116 p., Copenhagen, Denmark.
- Pulford, I.D., Watson, C. 2003. Phytoremediation of heavy metal-contaminated land by tree—a view. Environ. Int. 29, 529–40.
- Pruvot, C., Douay, F., Herve, F., Waterlot, C. 2006. Heavy metals in soil, crops and grass as a source of human exposure in the former mining areas. Journal of Soils Sediments 6, 215–20.
- Reichman, S.M., Asher, C.J., Mulligan, D.R., Menzies, N.W. 2001. Seedling responses of three Australian tree species to toxic concentrations of zinc in solution culture. Plant and Soil 235, 151-158.
- Reimann, C., de Caritat, P. 1998. Chemical elements in the environment— factsheets for the geochemist and environmental scientist. Berlin, Germany7 Springer-Verlag; 1998. ISBN 3-540-63670-6.
- Rose, A.W., Hawkes, H.E., Webb, J.S. 1979. Geochemistry in Mineral Exploration, second ed., Academic Press, Newyork 657p.
- Rotkittikhun, R., Kruatrachue, M., Chaiyarat, R., Ngernsansaruay, C., Pokethitiyook, P., Pajitpraporn, A., Baker, A.J.M. 2006. Uptake and accumulation of lead by plants from the Bo Ngam lead mine area in Thailand. Environmental Pollution 144, 681-688.
- Sağıroğlu, A. 1988. Cafana (Görgü) Malatya carbonated Pb - Zn deposits. Cumhuriyet Univ. Engineering Faculty Journal, Serie A- Earth Sciences C. 5/1, 3-13.
- Salt, D.E, Smith, R.D., Raskin, I. 1998. Phytoremediation. Annu. Rev. Plant Physiol. Plant Mol. Biol. 49, 643-668.
- Schroll, E. (ed), 1975. Analytische Geochemie. Enke verl., Bd. I. Stuttgart, 292 p.
- Shah, A., Niaz, A., Ullah, N., Rehman, A., Akhlaq, M., Zakir, M., Khan, M.S. 2013. “Comparative Study of Heavy Metals in Soil and Selected Medicinal Plants”, Journal of Chemistry, 1-5.
- Shen, Z.G., Liu, Y.L. 1998. Progress in the study on the plants that hyperaccumulate heavy metal. Plant Physiol Commun. 34, 133-9.
- Xiaohai, L., Yuntao, G., Khan, S., Gang, D., Aikui, C., Li, L., Lei, Z., Zhonghan, L., Xuecan, W. 2008. Accumulation of Pb, Cu, and Zn in native plants growing on contaminated sites and their potential accumulation capacity in Heqing, Yunan. Journal of Environmental Sciences 20, 1469–1474.
- Vural, A. 2014. Trace / heavy metal distribution in soil and acacia tree shoots, Gümüşhane - Turkey. General Directorate of Mineral Research and Exploration Ankara 148, 85-106.
- Wong, M.H. 2003. Ecological restoration of mine degraded soils, with emphasis on metal contaminated soils. Chemosphere 50, 775–80.
- Wuana, R., Raymond, A., Okieimen, F.E. 2011. Heavy metals in contaminated soils: A review of sources, chemistry, risks and best available strategies for remediation. ISRN Ecology 402647, 20.
- Yanqun, Z., Yuan, L., Jianjun, C., Li, Q., Schwartz, C. 2005. Hyperaccumulation of Pb, Zn and Cd in herbaceous grown on lead – zinc mining area in Yunan, China. Environment International 31, 755-762.
- Yoon, J., Cao, X, Zhou, Q., Ma, L.Q. 2006. Accumulation of Pb, Cu, and Zn in native plants growing on a contaminated Florida site. Science of the Total Environment 368, 456-464.
- Zhao, F.J., Lombi, E., McGrath, S.P. 2003. Assessing the potential for zinc and cadmium phytoremediation with the hyperaccumulator *Thlaspi caerulescens*. Plant Soil 249, 37-43.
- Zhuang, P., McBride, M.B., Xia, H., Li, N., Li, Z. 2009. Health risk from heavy metals via consumption of food crops in the vicinity of Dabaoshan mine, South China. Sci Total Environ. 407(5):1551-61.





# Bulletin of the Mineral Research and Exploration

<http://bulletin.mta.gov.tr>



## GEOGRAPHICAL INFORMATION SYSTEMS BASED USING LOGISTIC REGRESSION LANDSLIDE SUSCEPTIBILITY ASSESSMENT OF THE ÇUBUK-KALECİK (ANKARA) BETWEEN ŞABANÖZÜ (ÇANKIRI) REGION

Hasan ELMACI<sup>a\*</sup>, Senem TEKİN<sup>b</sup> and Nail ÜNSAL<sup>c</sup>

<sup>a</sup>General Directorate of Mineral Research and Exploration, Dept. of Geological Researches, 06800, Çankaya, Ankara, Turkey [orcid.org/0000-0002-5076-1153](http://orcid.org/0000-0002-5076-1153)

<sup>b</sup>Çukurova University, Dept. of Geol. Eng., 01330, Balçalı, Adana, Turkey [orcid.org/0000-0001-7734-9700](http://orcid.org/0000-0001-7734-9700)

<sup>c</sup>Gazi University, Dept. of Civil Eng., Tandoğan, Ankara, Turkey [orcid.org/0000-0003-4381-6088](http://orcid.org/0000-0003-4381-6088)

### Keywords:

Çankırı, Geographic Information System (GIS), Landslide Susceptibility, Logistic regression.

### ABSTRACT

Landslides occur frequently in particular is in certain parts in our country as well as in the world, is caused from time to time to return to natural disasters and significant social and economic losses. In this study, landslide susceptibility analysis Çubuk-Kalecik (Ankara) between Şabanözü (Çankırı) were performed totally 2360 km<sup>2</sup> area. According to the inventory map that represents about 5,16 % of the spatial distribution of landslide at study area, landslide movement is generally seen as the type of the existing rotational slip. According to the Turkish Landslide Inventory database prepared by MTA, 876 landslides covering 122 km<sup>2</sup> were identified in the study area. A total of twelve independent variables for the landslide conditioning factors were used in the susceptibility assessments, being as lithological maps, landform classification, digital elevation model, slope, profile, plan, and tangent curvatures, roughness index, slope / aspect ratio, stream power index, topographic position index. Landslide susceptibility assessment was carried out using multivariate logistic regression method, one of statistical methods. The mapping unit 25 \*25 m pixels are used for statistical assessment. The obtained probability values of landslide susceptibility maps are very low and very high was evaluated in five grades in the range. Performance evaluation of susceptibility maps were performed with using receiver operating characteristic (ROC) and prediction success rate curves. The area under the ROC curves were found to be in 0,794. Susceptibility map, high and very susceptible regions correspond to 27 % of the study area. 78 % of the landslides are in medium, high and very susceptible regions. The accomplished landslide susceptibility map with relatively high performance could be used during the medium scale planning strategies.

Received Date: 05.08.2016

Accepted Date: 28.09.2017

## 1. Introduction

When damages originating from natural disasters in our country are taken into consideration, it is seen that the losses are consisted by earthquakes (61%) and landslides (20%) (Ergünay, 1999).

Landslides develop by geological, morphological and physical factors and by human effects. Landslide inventory maps generated are maps showing the types and spatial distribution of available landslides, and they form the basis of mitigation studies in planned areas.

In order that environmental factors causing the spatial distribution and formation of landslides should be understood, the digital landslide database was formed by MTA General Directorate (Çan and Duman, 2008; Duman et al.; 2011, Çan et al.; 2013). In the assessment of regional scale landslide database, it is essential to evaluate environmental variables controlling and forming the landslides in a good way. In this manner, the landslide inventory maps form the most basic need for landslide susceptibility and probable risk assessments.

In this study, landslide susceptibility assesment was conducted between Çubuk-Kalecik (Ankara) and

\* Corresponding author: Hasan ELMACI [hasan.elmaci@mta.gov.tr](mailto:hasan.elmaci@mta.gov.tr)

<http://dx.doi.org/10.19111/bulletinofmre.306692>

Şabanözü (Çankırı) which covers an area of 2360 km<sup>2</sup> (Figure 1). According to the landslide inventory map of Turkey, there are 876 landslides in the study area and cover an area of 122 km<sup>2</sup> (Duman et al., 2011). 68 landslide events affecting settlements between 1950 and 2008 have been reported in the region; A total of 834 effective transplants were carried out (Gökçe et al., 2008).

In this study, the lithological map, land-use classification, digital elevation model, hill slope, profile, plan and tangential slope curvatures, roughness index, stream power index and topographic wetness index were used and thus, the landslide susceptibility assessment was carried out using multivariate logistic regression method which is regarded as one of the statistical methods. As mapping unit 25 x 25 m pixels were used for the statistical assessment. The performance evaluation of the susceptibility maps were performed by using the receiver operating characteristic (ROC) (Metz, 1978; Metz, 2006) and prediction success rate curves which tests the accuracy of the results (Chung and Fabbri, 2003, Heckmann et al; 2014).

## 2. Geology and Seismicity of The Study Area

There are seen basement units belonging to three different environments in the study area (Figure 2). The area is represented by rocks of Sakarya Zone and İzmir-Ankara-Erzincan Suture Zone and by Neogene basin deposits overlying the basement units. In the study area, Triassic-Jurassic-Cretaceous rocks of the Sakarya Zone, Mesozoic Eldivan ophiolitic complex, Late Cretaceous Dereköy ophiolitic mélangé, which are tectono-stratigraphically associated with each other, and the rock assemblages of the İzmir-Ankara-Erzincan suture zone deposited between Late Cretaceous-Paleocene (Dönmez and Akçay, 2010). It was seen that the rocks of the Sakarya continent had been tectonically settled on rocks of the İzmir-Ankara-Erzincan suture zone, and the Neogene cover rocks had unconformably been deposited over units belonging to both zones. This sedimentary deposit is composed of volcanic and sedimentary rocks. The cover rocks has the characteristics of being the foreland basin deposits that have been opened on basement rocks (Dönmez and Akçay, 2010). These cover rocks are Late Paleocene-Early Eocene Sarıkoz volcanic, Middle Eocene Kurtsevrisi, Hüseyingazıdağ, Sele, Ömercik, Susuz and Yukarıemir volcanics, Miocene Kumartaş,

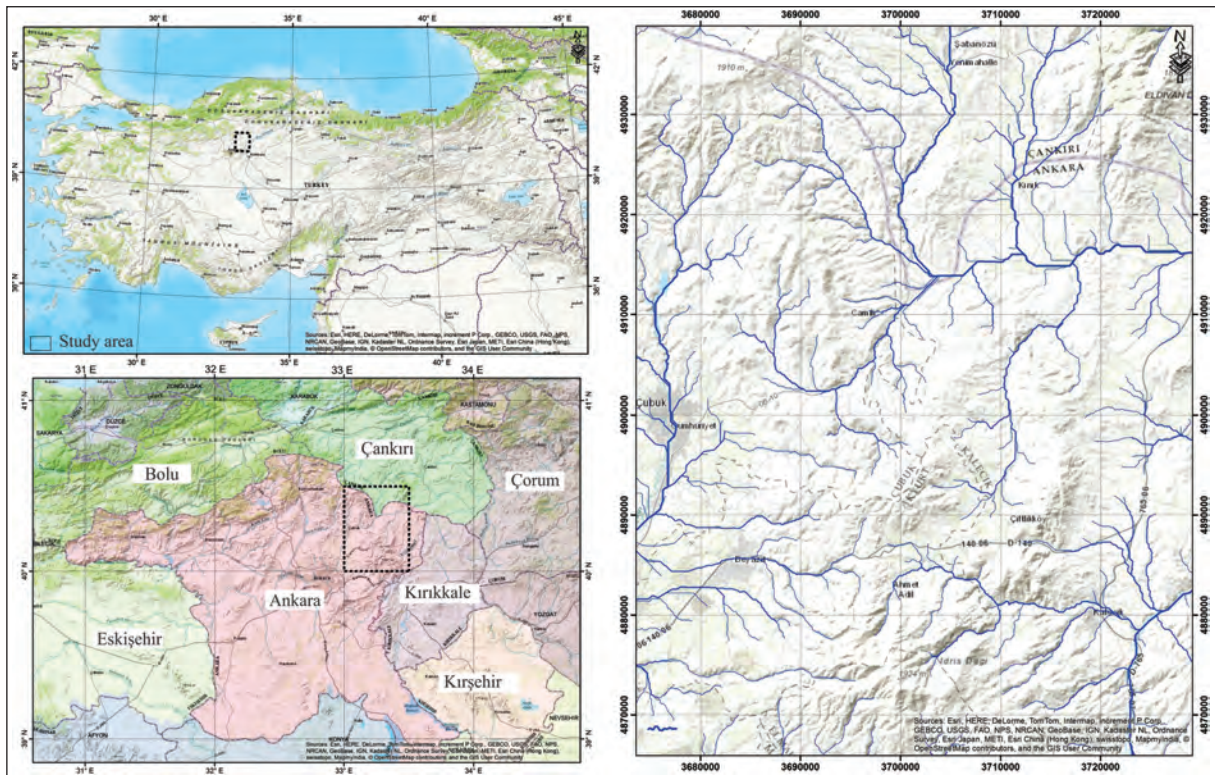


Figure 1- The location map of the study area.

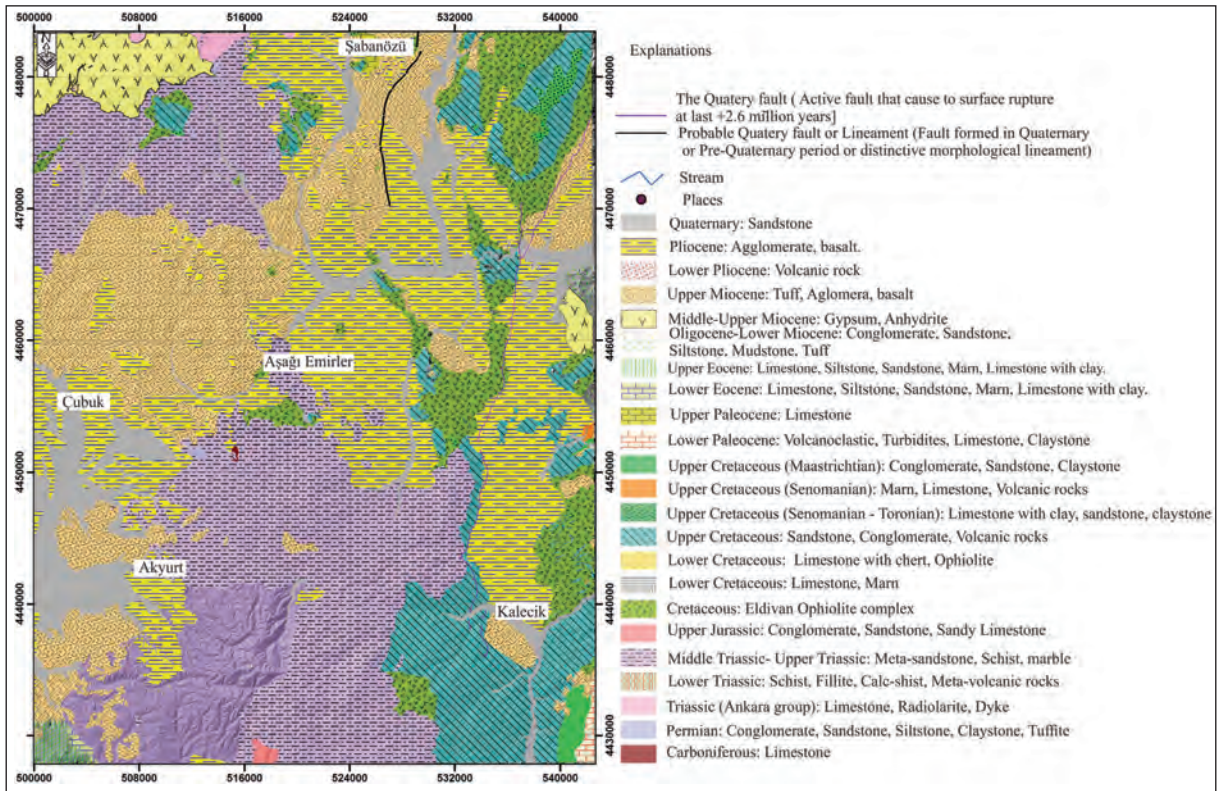


Figure 2- Geological map of the study area (Çankırı H30 sheet, 1/100000 in scale, MTA).

Hançili, Karakoca formations and Miocene Kalecik and Aydos volcanics. Pliocene Bozkır and Gölbaşı formations and Quaternary alluvial basin deposits cover all these units with an unconformity (Dönmez and Akçay, 2010).

According to the Active Fault Map of Turkey, the most of the Çankırı Fault, which moves with 34 km long inverse fault mechanism and regarded as one of the active faults, are located in the study area (Emre et al., 2013). In the region, there are 8 records of earthquake with  $M_w \geq 4$  present in instrumental period (1900-2010) (Figure 3) (Kadirioğlu et al., 2016).

### 3. Landslide Conditioning Factors

The 10 meters interval contour lines obtained from the General Command of Mapping were converted into raster format after establishing the triangulated irregular network (TIN) in GIS environment. Then the digital elevation model in 25 x 25 m resolution was produced. When looking at the elevation values of the study area, the north of Hacılar village and south of Eskiköy village reach the maximum height of 1990 meters and there occurs an elevation difference of 1405 meters (Figure 4).

In order to establish the morphological structure of the study area, the land classification was performed according to Weiss (2001) using the topographical position index. The land use classification of the study area was evaluated in 10 different classes as; open slopes, canyon, mid-slope drainage, mid-slope ridges, plain, U type valleys, local ridges, summits, upper-slope drainage and upper slopes (Figure 5a). According to the map of slope gradient (Figure 5b), the slope angles increase from south to north. Slopes with the highest angles are located in northern parts. The slopes in these areas occasionally have a degree of  $89^\circ$  (Figure 5c). Slope inclinations; concave and convex slope shapes are quite significant in controlling the hydrologic flow situation. The slope gradients are divided into three categories as; sectional (Figure 5c), planar (Figure 5d) and tangential (Figure 5e) based on the direction in which they are assessed (Wilson and Gallant, 2000). The roughness index was obtained by the multiplication of the square root of the height value in each cells and height differences among neighboring cells using 5x5 pixel windows (Riley et al., 1990). The roughness index values (Figure 5f) reach high values on rugged areas and along ridges. In slope/aspect map (Figure 5g) obtained by the rationing of slope gradient and slope aspect maps, the higher

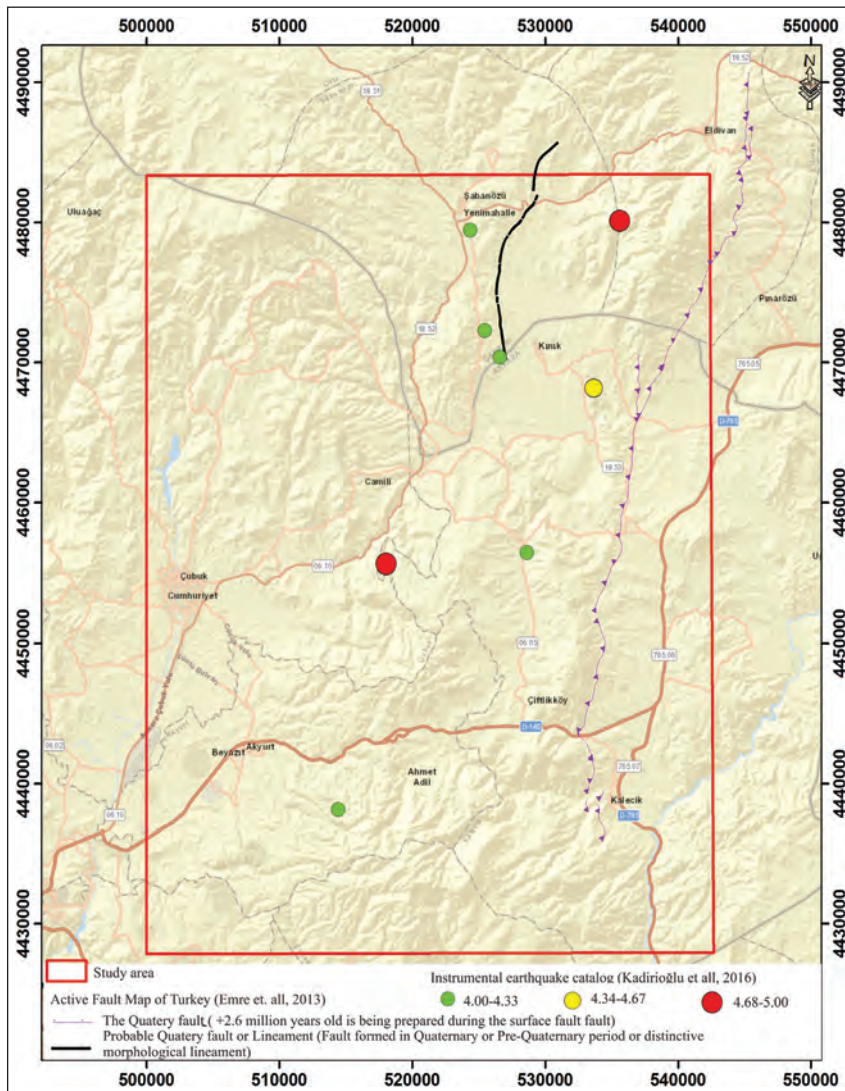


Figure 3- The Çankırı Fault located in the study area (Emre et al., 2013) and the records of instrumental earthquake (Kadıroğlu et al., 2016).

values show the inner sides of slopes; however, the lower values are seen on flat areas. The stream power index (SPI) is used for the determination of stream erosion that occurs in the valley. In the calculation of this parameter, it is suggested that the flow should be proportional with map unit areas (Moore et al., 1991). The stream power index is one of the major factors that control the erosional processes and it was used in the study as this is one of the parameters affecting the formation of landslide (Figure 5g). The topographical wetness index (TWI) dimensions the water saturation of the studied region in regional scale. The highest TWI values for the study area generally show high values inside the rivers.

#### 4. Landslide Inventory

The available landslide inventory maps produced do not reflect the landslide activities that have developed later than this time. They only show large scale previous or recent landslides that have preserved their morphological characteristics on the date of map generation. In this study, 1/25000 scale digital landslide inventory map, which had been produced by MTA, was used (Duman et al., 2009). In the study area, there are total of 876 landslips. The landslides, which cover an area of 122 km<sup>2</sup>, consists of 5.16 % of the investigation area (Figure 6a). 68 landslide events (Figure 6b) have been reported according to landslide records held between 1950-2008 (Gökçe et al., 2008).

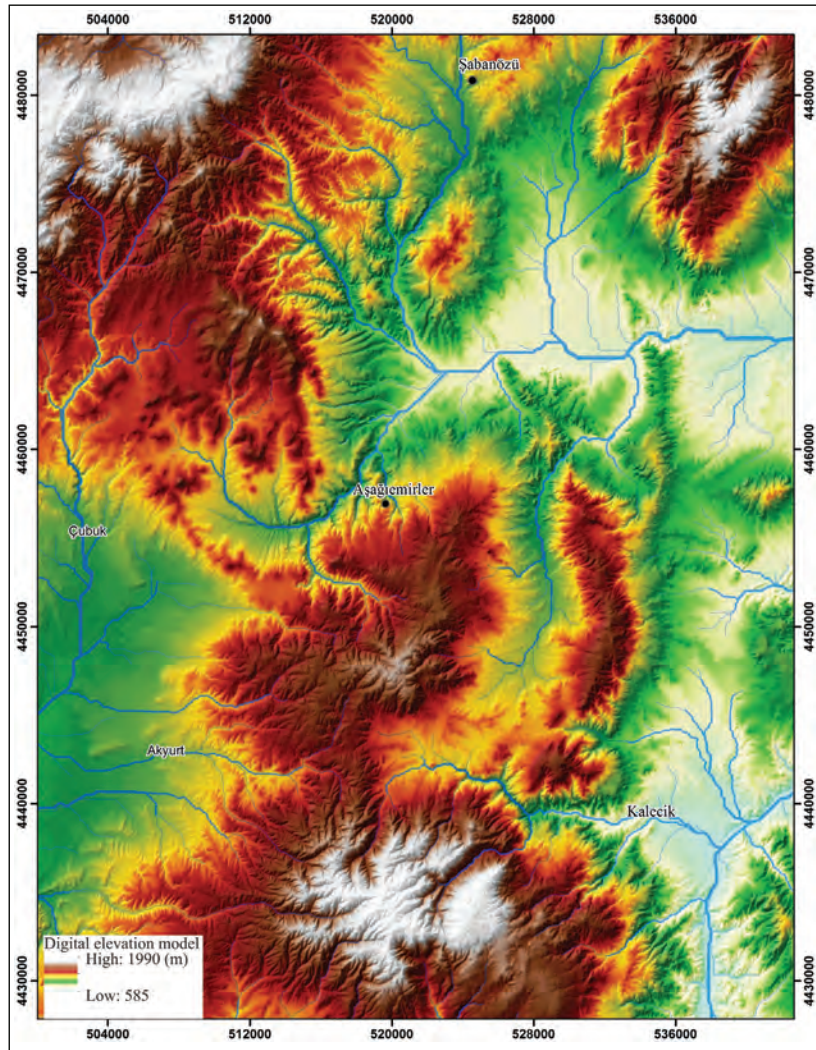


Figure 4- Digital elevation model (DEM) of the study area.

Located within the borders of Ankara; 293 in Elmadağ county Yeşildere village on September 22, 1969, 117 in Kozayağı village in Akyurt district, 274 in 1962 and 742 in July 6, 1965 in Kalecik county Gökdere village. In the section of the study area within the Çankırı province borders, on April 17, 1963, in Şabanözü district, Ödek village, 40 units of 92 effective transfers were realized (Table 1). The available landslides are lithologically observed in Miocene-Pliocene undifferentiated continental clastics, Paleocene-Pliocene undifferentiated volcanics, Eocene volcanic and sedimentary rocks, Late Cretaceous-Eocene clastic and mudstone, marl, conglomerate, silica-clastic, calci-turbiditic, carbonated mudstone, delta and fluvial clastics intercalated with carbonated volcanics, and Silurian-Permo-Triassic clastic and carbonated units (Figure 7).

## 5. Landslide Susceptibility Assessment

Landslide susceptibility assessments, which present approaches in which regions the landslides might occur, are prepared considering available landslide inventory maps of the region and landslide preparatory environmental factors. There are several approaches regarding landslide susceptibility assessments. Generally; the preparation of landslide susceptibility maps is divided into two categories as; qualitative and quantitative approaches. In this study, the GIS based landslide susceptibility map was produced by using logistic regression method, which is one of the multivariate statistical method, rather than quantitative method. The logistic regression method is used in determining the cause-effect relationship of both dependent and independent variables in which the expected values of dependent variables with

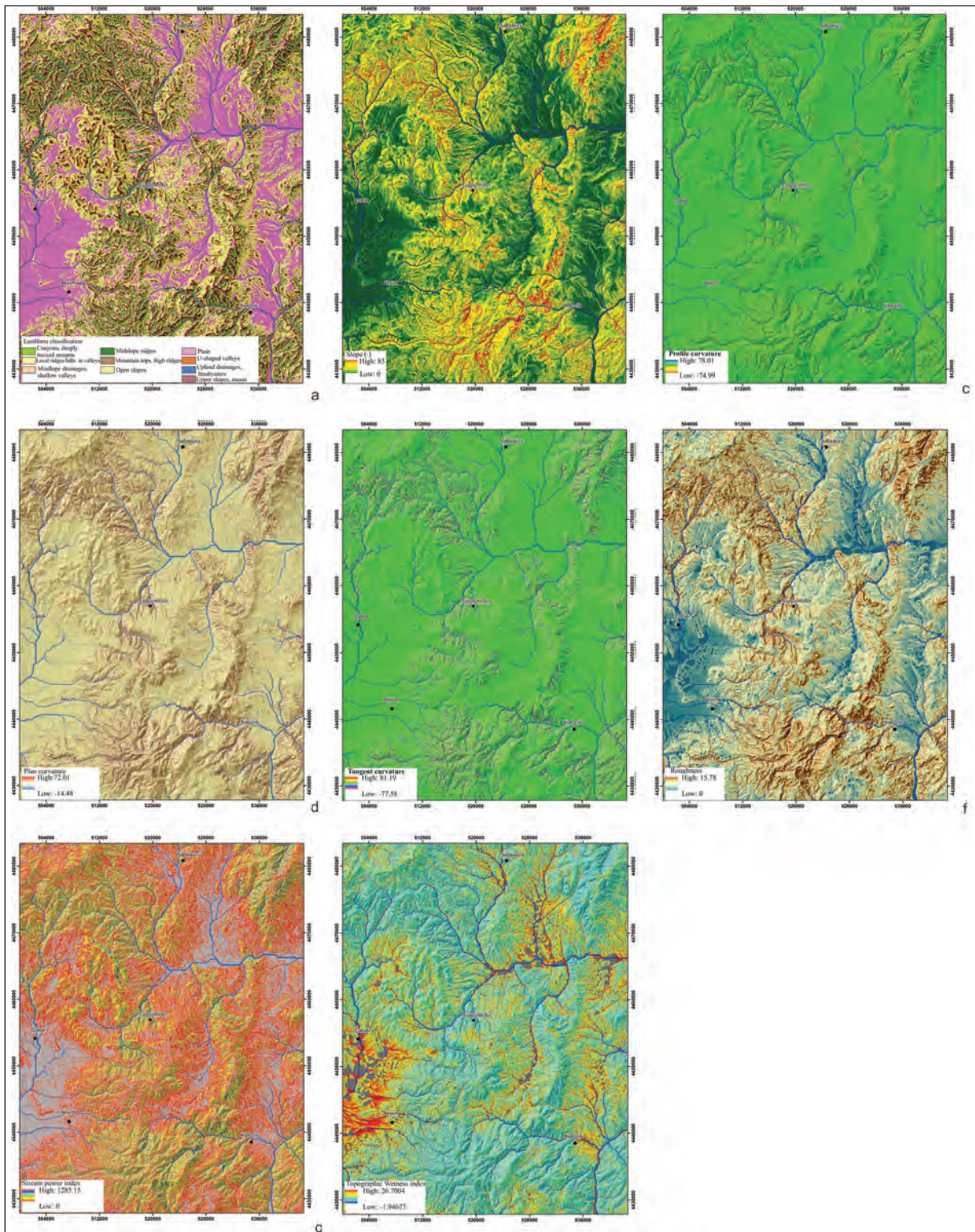


Figure 5- Land use (a), Slope (b), Curvature (c), Plan curvature (d), Tangential curvature (e), roughness index (f), stream power index (g) and topographic wetness index (h).

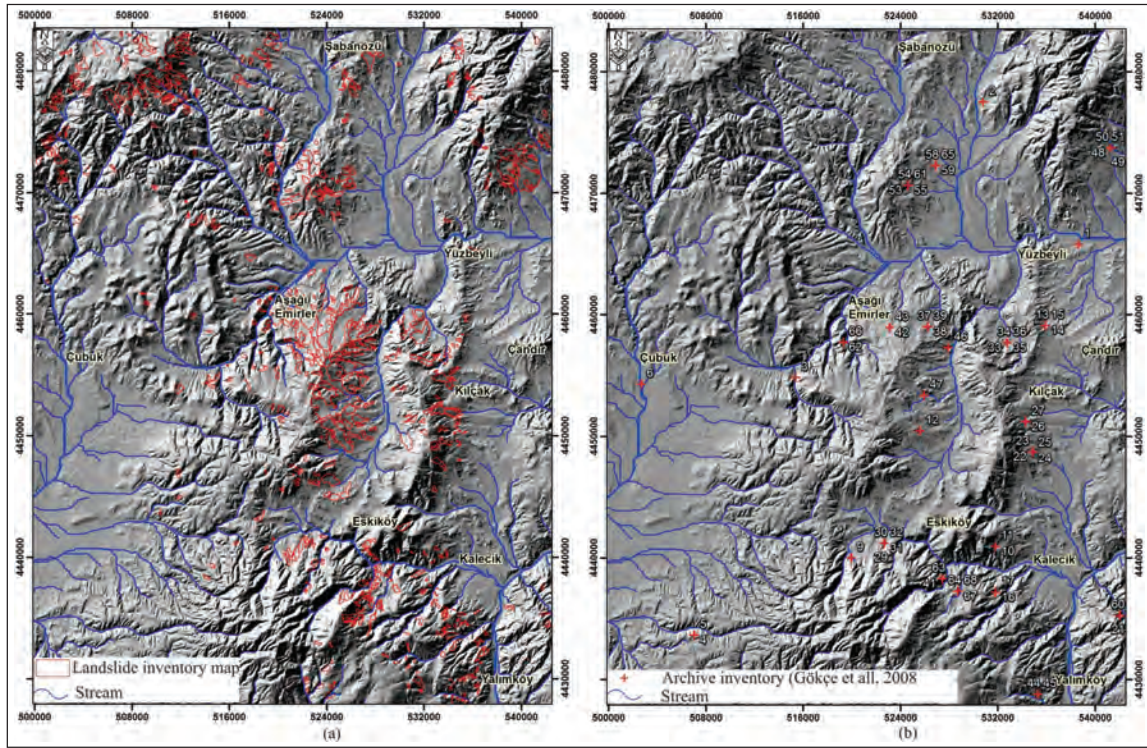


Figure 6- Landslide historical inventory (Duman et al., 2009) and archive (Gökçe et al., 2008) inventory maps.

Table 1- Landslide events reported in the study area (Gökçe et al., 2008).

City	Town	Village	Landslide	Rock fall	Water flooding	Date of report	Effective transport	ID
Ankara	Elmadağ	Yeşildere	+	+	+	6.21.1958		7
Ankara	Akyurt	Kozayağı	+			4.27.1962	117	28
Ankara	Çubuk	Akbayır	+			12.18.1963		3
Çankırı	Eldivan	Hisarcikkayı	+			7.18.1963		48
Çankırı	Şabanözü	Gündoğmuş	+			5.16.1963	7	52
Ankara	Kalecik	Çukur	+			12.27.1963	7	17
Çankırı	Şabanözü	Ödek	+			4.17.1963	4	56
Ankara	Kalecik	Kılçak	+			4.1.1964	9	26
Çankırı	Şabanözü	Ödek	+			5.22.1964		57
Ankara	Akyurt	Ahmetadil	+			7.7.1965	9	9
Ankara	Kalecik	Gökdere	+			7.6.1965	95	2
Ankara	Kalecik	Akbork	+			5.12.1966		1
Ankara	Kalecik	Kuyucak	+			5.6.1966	5	38
Ankara	Kalecik	Tavşancık	+			5.9.1966	15	42
Ankara	Kalecik	Keklicecek	+			7.13.1968		22
Ankara	Akyurt	Doğanoluk	+			8.22.1969		4
Ankara	Elmadağ	Yeşildere	+	+	+	9.22.1969	293	8
Ankara	Kalecik	Altıntaş	+			6.12.1969	21	34
Ankara	Kalecik	Kuyucak	+		+	3.24.1969		39
Ankara	Kalecik	Yalınkoy	+			12.3.1969		44
Çankırı	Eldivan	Hisarcikkayı	+			5.8.1969	13	49
Ankara	Kalecik	Keklicecek	+			11/21/197		23
Çankırı	Şabanözü	Gündoğmuş	+			1/6/197	11	53
Çankırı	Şabanözü	Ödek	+			1/6/197	12	58
Ankara	Kalecik	Altıntaş	+			2.16.1974		35
Çankırı	Şabanözü	Ödek	+			1.24.1974	9	59
Ankara	Kalecik	Çaykaya	+			11.28.1975		13
Ankara	Akyurt	Doğanoluk	+			3.1.1976		5
Ankara	Kalecik	Çukur	+			12.23.1976		16
Ankara	Kalecik	Gökdere	+			1/25/198		21
Ankara	Kalecik	Akcataş	+			5.13.1981		12
Ankara	Kalecik	Çaykaya	+			3.2.1981	11	14
Ankara	Kalecik	Keklicecek	+			9.6.1981	9	24
Ankara	Kalecik	Şeyhmahmut	+	+		5.13.1981	1	4
Ankara	Kalecik	Çaykaya	+			12.3.1982		15
Ankara	Kalecik	Gökdere	+			12.29.1982		19
Ankara	Akyurt	Kozayağı	+			12.3.1982	14	29
Ankara	Kalecik	Altıntaş	+		+	12.31.1982		36
Ankara	Kalecik	Kuyucak	+		+	12.3.1982		37
Ankara	Kalecik	Yalınkoy	+			12.3.1982		45
Ankara	Kalecik	Keklicecek	+			3.28.1983		25
Çankırı	Eldivan	Hisarcikkayı	+			5.24.1983		5
Çankırı	Şabanözü	Gündoğmuş	+			5.27.1983		54
Ankara	Kalecik	Altıntaş	+			12.24.1984		33
Çankırı	Şabanözü	Gündoğmuş	+			6.28.1984		55
Ankara	Kalecik	Şeyhmahmut	+			6.15.1984		63
Ankara	Kalecik	Gökdere	+			9.5.1985		18
Ankara	Kalecik	Şeyhmahmut	+			7.9.1985		41
Ankara	Kalecik	Tavşancık	+			3.12.1985	17	43
Ankara	Kalecik	Yeşilöz	+			3.18.1985		46
Ankara	Kalecik	Kılçak	+			12.7.1987		27
Ankara	Akyurt	Kozayağı	+			12.14.1987	2	3
Ankara	Kalecik	yılanlı	+			12.29.1987	12	47
Ankara	Akyurt	Kozayağı	+			7.6.1989	14	31
Ankara	Kalecik	Akbork	+		+	2/26/199		11
Ankara	Kalecik	Gökdere	+			6/27/199		6
Ankara	Çubuk	Çubuk	+			8.9.1991		6
Ankara	Akyurt	Kozayağı	+			12.28.1991	1	32
Ankara	Çubuk	Aşağiemirler	+			4.19.1994		62
Çankırı	Eldivan	Hisarcikkayı	+			3.3.1997		51
Çankırı	Şabanözü	Gündoğmuş	+			8.21.1998		61
Ankara	Kalecik	Satılarkoy	+			11.26.2002		1
Çankırı	Şabanözü	Karakocaş	+			3.3.2002		2
Ankara	Kalecik	Göl	+			12.16.2004		64
Ankara	Çubuk	Aşağiemirler	+			12.2.2007		66
Ankara	Kalecik	Göl	+			2.29.2008		67
Ankara	Kalecik	Göl	+			5.7.2008		68
Çankırı	Şabanözü	Ödek	+			1.9.2008		65

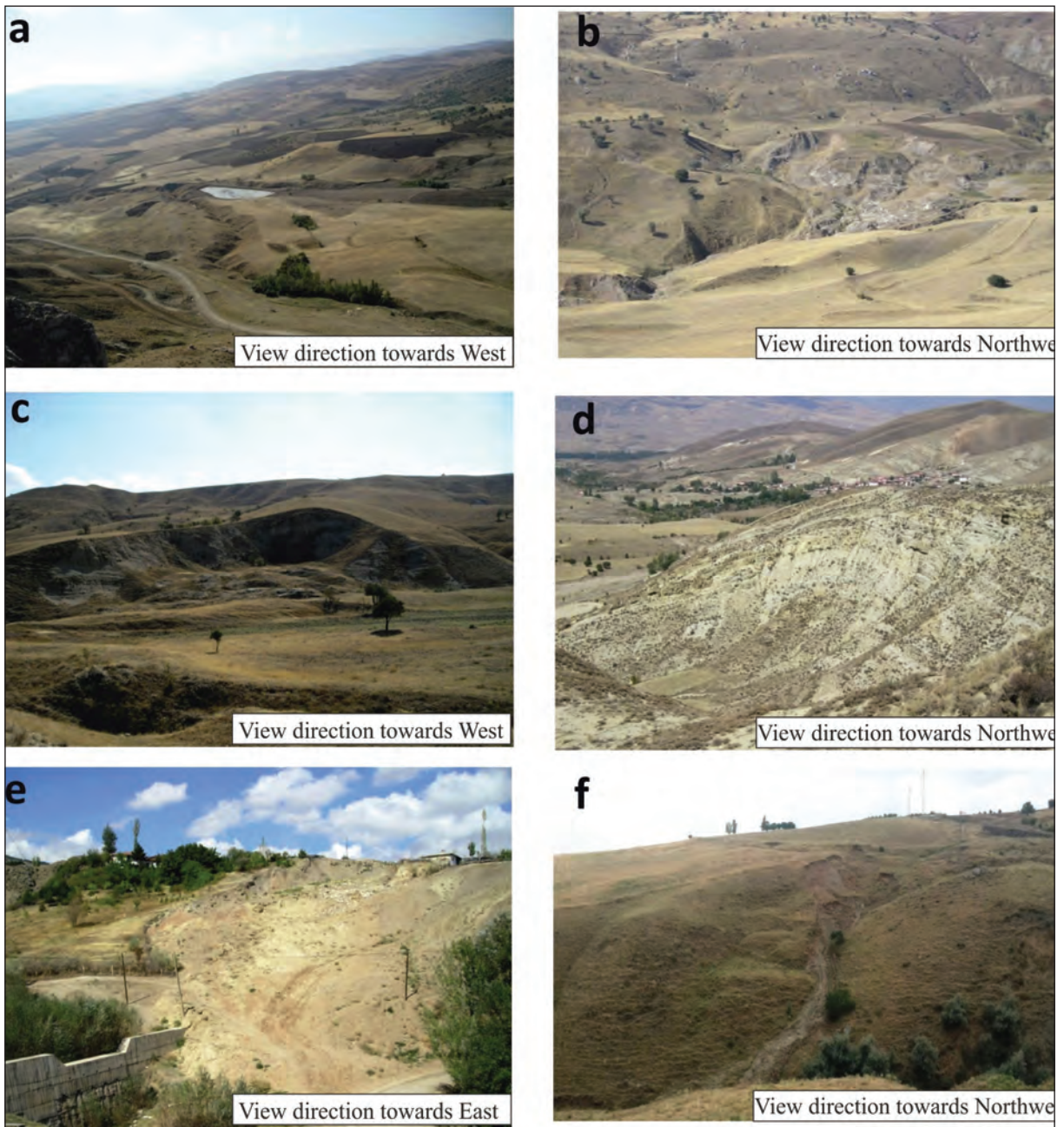


Figure 7- Examples of active landslides observed in the study area: a) the south of the Keklicek village, b) the northwest of the Altuntaş village, c) the west of the Kızılkaya village, d) the northwest of the Karatepe village, e) the Kılçak village, f) the west of the Yeşilöz village.

respect to independent variables are obtained as the probability in cases when the dependent variable is observed as binary.

X values denote for independent variables (landslide preparatory factors) and  $\beta$  values indicate the regression coefficients of dependent variables. As the Z value shows a variation between  $-\infty$  and  $+\infty$  in Equation 1, the logistic transformation was applied to convert into linear state.

$$Z = b_0 + b_1 X_1 + b_2 X_2 + b_3 X_3 + \dots + b_n X_n \quad \text{Equation 1}$$

As the Z value, which is calculated by the Equation 1, shows a variation between  $-\infty$  and  $+\infty$  the logistic transformation was applied in order to make the probability calculation (Equation 2). In order to reveal the relationship between the available landslide inventory and independent variables used in the study the probability values were used. In this equation, P presents the probability of occurrence of an event.

Calculated P values show the probability of occurrence of landslides that might occur in the region.

$$P = 1 / (1 + e^{-z}) \quad \text{Equation 2}$$

When the P probability value approaches to zero, the state of probability is  $-\infty$ , however; it becomes  $+\infty$  when it approaches to 1 in this transformation (Hosmer et al., 2013).

The ratio of binary (1, 0) dependent variables to each other in data sets, which will be used in the logistic regression method, are effective on the results of general accuracy classification. In this case, the logical regression model yields favorable results for the class with high values (Hosmer et al., 2013). Therefore; the modelling is generally made by selecting dependent variables belonging to both classes in equal numbers in logistic regression method (Ayalew and Yamagishi 2005; Duman et al., 2006; Heckmann et al., 2014; Hosmer et al., 2013; Süzen and Doyuran 2004; Yesilnacar and Topal 2005; Nefeslioglu et al., 2008, Tekin 2014, Tekin and Çan 2016). The data set for analysis was formed by combining pixels as much as the pixels that corresponds to the inventory map (180.812 pixels) from the non-sliding regions (3.594.338 pixels) by random selection, so the landslide susceptibility map was produced. The regression error matrix of the landslide susceptibility map is given in table 2 and the general accuracy value was obtained as 76,9 %.

Table 2- Error Matrix.

Observed Landslide		Expected Landslide		Accuracy
		0	1	
	0	37870	10784	77.8
	1	11712	36942	75.9
General %				76.9

In the logistic regression analysis performed, the land classification and lithology map were assessed as categorical data in analyses. However; other variables were evaluated as continuous data. The results of the analysis carried out are seen in table 3. The positive and negative values in B values are the landslide preparatory and preventive factors, respectively.

As a result of the analyzes made, the probability values of the landslide susceptibility map of the study

area were evaluated at 5 class between very low and very high considering equal intervals (Figure 8a). According to the susceptibility map; 31.42 % of the study area is very low, 22.84 % is low, 18.18 % is medium, 15.26 % is high and 12.28% is in very high regions. 8.54% of the existing landslides are very low, 13.36% is low, 18.30 % is moderate, 26.20 % is high and 33.57 % is in very high sensitive class range (Figure 8b). Logistic regression analysis results were evaluated with the Receiver Operating Characteristic Curve (ROC), which gave the correctness statistic, and the under-curve (AUC) was found to be 0.794 (Figure 8c).

## 6. Results

Landslide susceptibility assessments form a basis for the landslide risk maps produced in order to prevent damages that will result from the landslide. These are also based on the mapping of landslides that have developed in the studied region until today and well detection of factors causing the formation or triggering of these landslides. With this study, the landslide susceptibility assessment of the region that lies among Çubuk and Kalecik towns of Ankara and Şabanözü town of Çankırı was performed by logistic regression method, which is one of the multivariate statistical analyses, rather than quantitative methods. As mapping unit; pixels in 25x25 m resolution were preferred. In assessing the landslide susceptibility, lithological map, landform classification, digital elevation model, slope, profile, plan and tangential slope curvatures, roughness index, stream power index and topographic wetness index were used as landslide conditioning factors. The performance evaluations of the susceptibility maps were performed using Receiver operating characteristic (ROC) and success-prediction curves. The area under the ROC curves was obtained as 0.794. High and very sensitive regions in the susceptibility map almost correspond to 27 % of the study area; 78% of landslides are present in medium, high and very sensitive areas.

It is considered that the determination of environmental variables that control landslides and areas in which landslides could spatially occur will contribute a lot in the mitigation of damages resulting from landslides in risk and hazard studies that will be carried out in the region.

Table 3- Results of the landslide susceptibility map analysis.

Variable	(B)	Standard error	Wald	Exp(B)
Digital elevation model	.0018	.000	4495.492	1.002
Topographic wetness index	-.0140	.006	4.943	.986
Stream power index	.274	.013	445.740	1.317
Profile curvature	-.278	.030	85.860	.757
Plan curvature	-.111	.021	29.391	.894
Slope	-.058	.008	58.528	.944
Open slope	-.0722	.027	7.095	.930
Canyon	.159	.028	33.224	1.173
Upper slope drainage	.381	.124	9.526	1.464
Plain	.921	.022	1677.995	2.513
Upper slopes	.483	.017	811.919	1.621
U-type valleys	-1.102	.026	1754.652	.332
Local ridges	-.656	.030	472.251	.518
Mid-slope drainage	-1.678	.034	2376.680	.187
Roughness	1.656	.050	1117.859	5.239
Oligocene-Lower Miocene: conglomerate, sandstone, siltstone	2.269	.031	5453.729	9.677
Paleocene-Pliocene undifferentiated volcanics	.544	.031	307.001	1.723
Upper Cretaceous: limestone, sandstone, pebblestone, volcanics	1.819	.038	2312.234	6.171
Lower Paleocene: volcanics	1.657	.033	2543.396	5.247
Lower Paleocene: limestone	1.583	.034	2229.537	4.871
Carboniferous: limestone	1.888	.036	2731.964	6.609
Silurian-Permo-Triassic clastic and carbonated	1.010	.036	786.147	2.748
Miocene-Pliocene undifferentiated continental clastic	.460	.034	188.562	1.586
Middle Miocene-Upper Miocene: gypsum	-.419	.055	58.751	.658
Eocene volcanic and sedimentary rocks	-2.151	.060	1302.877	.116
Late Cretaceous-Eocene clastic and carbonates	2.092	.038	3093.636	8.109
Oligocene-Lower Miocene: conglomerate, sandstone, siltstone	1.735	.038	2073.487	5.674
Paleocene-Pliocene undifferentiated volcanics	1.953	.040	2361.721	7.056
Upper Cretaceous: limestone, sandstone, conglomerate, volcanics	.593	.053	126.727	1.810
Lower Paleocene: volcanics	1.445	.056	675.230	4.242
Lower Paleocene: limestone	1.870	.051	1366.873	6.492
Carboniferous: limestone	-.602	.080	56.671	.548
Constant	13.374	.774	298.629	643628.055

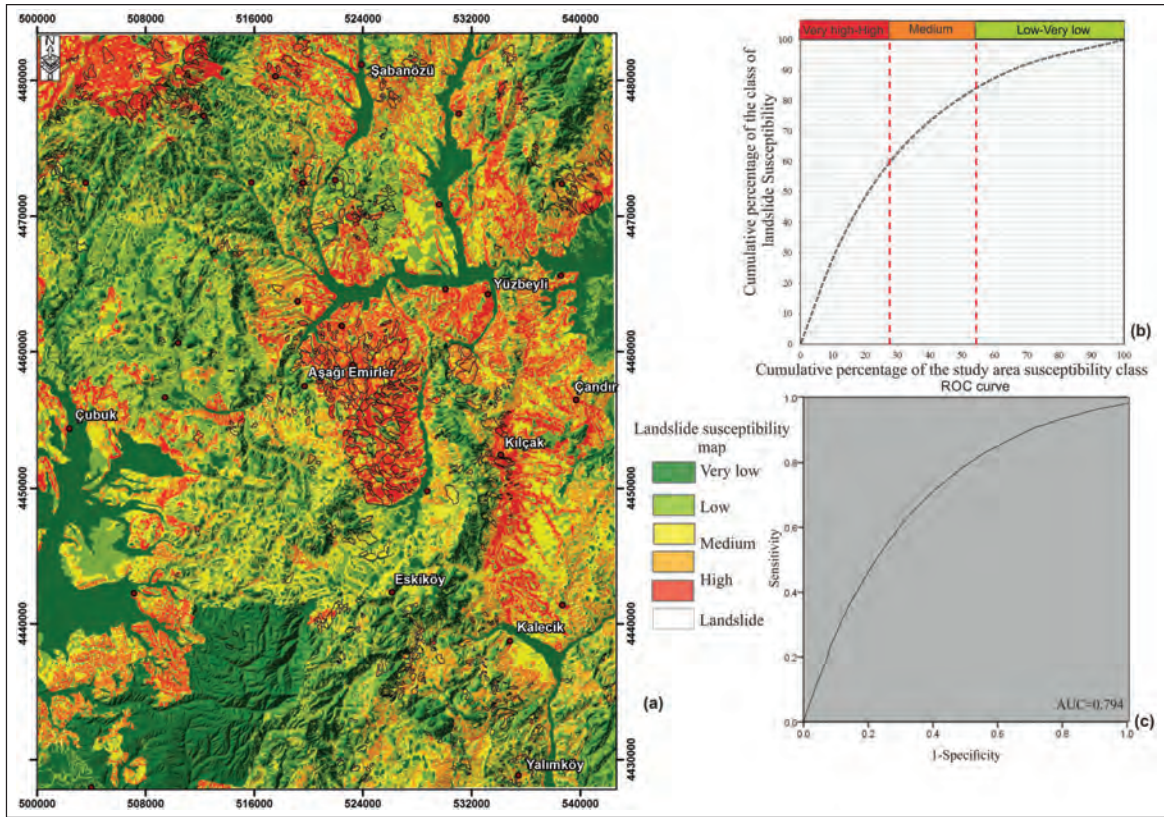


Figure 8- Landslide susceptibility map (a), prediction-success rate (b), ROC curve (c).

## Acknowledgement

The authors would like to thank to the Civil Engineering Department of the Gazi University for their helps provided during the preparation of this article, which was produced from the Master Thesis, to Assoc. Prof. Tolga Çan, Geological Engineering department of the Çukurova University, to the General Directorate of Mineral Research and Exploration (MTA), which gave support at all stages of this study and to referees who criticized the article.

## References

- Ayalew, L., Yamagishi, H. 2005. The application of GIS-based logistic regression for landslide susceptibility mapping in the Kakuda-Yahiko Mountains, Central Japan. *Geomorphology* 65: 15-31.
- Çan, T., Duman, T.Y. 2008. General evaluation of historical landslide inventory of Turkey. *Proceedings in Symposium of Paleoenvironmental Reconstruction and Material Circulation by Water System*. Abstracts book, pp.6-8. Hakozaki Campus Kyushu Univ., Fukuoka Japan.
- Çan, T., Duman T.Y., Olgun, Ş., Çörekçioğlu, Ş., Karakaya-Gülmez, F., Elmacı, H., Hamzaçebi, S., Emre, Ö. 2013. Türkiye Heyelan Veri Tabanı, TMMOB Coğrafi Bilgi Sistemleri Kongresi 2013, Ankara, Türkiye.
- Çan, T., Duman, T.Y., Olgun, Ş., Çörekçioğlu, Ş., Karakaya-Gülmez, F., Elmacı, H., Olgun, Ş., Hamzaçebi, S. Emre, Ö. 2013. Türkiye Heyelan Veri Tabanı. TMMOB Coğrafi Bilgi Sistemleri Kongresi 2013, 11-13 November 2013, Proceedings, Interactive CD, No: 217, 6 p., Ankara.
- Chung, C. F., Fabbri A. G., 2003. Validation of Spatial Prediction Models for Landslide Hazard Mapping. *Natural Hazards* 30: 451-472.
- Dönmez, M., Akçay, A.E. 2010. Türkiye Jeoloji Haritaları, 1:100.000 Ölçekli Çankırı-H30 Paftası ve Açıklaması, MTA Jeoloji Etütleri Dairesi, No: 138, Ankara.
- Duman, T.Y., Çan, T., Gökçeoğlu, C., Nefeslioğlu, H. A., Sönmez, H., 2006a. Application of logistic regression for landslide susceptibility zoning of Çekmece Area, Istanbul, Turkey. *Environmental Geology*, 51, 241-256.

- Duman, T.Y., Can, T., Gökçeoğlu, C., Nefeslioğlu, H.A., Sönmez, H. 2006b. Application of logistic regression for landslide susceptibility zoning of Çekmece Area, Istanbul, Turkey. *Environ Geol* 51(2): 241-256.
- Duman, T.Y., Olgun, Ş., Çan, T., Nefeslioğlu, H.A., Hamzaçebi, S., Durmaz, S., Elmacı, H., Çörekçioğlu, Ş. 2009. "Türkiye Heyelan Envanteri Haritası-1/500.000 ölçekli Sinop Paftası," Maden Tetkik Arama Özel Yayınlar Serisi-14, 27 s. Ankara.
- Duman, T.Y., Çan, T., Emre, Ö. 2011. Türkiye Heyelan Envanteri Haritası - 1/1.500.000 Ölçekli, Maden Tetkik ve Arama Genel Müdürlüğü Özel Yayınlar Serisi-27, Ankara, 23.
- Emre, Ö., Duman, T.Y., Özalp, S., Elmacı, H., Olgun, Ş., Şaroğlu, F. 2013. 1/1.250.000 Ölçekli Türkiye Diri Fay Haritası, Maden Tetkik ve Arama Genel Müdürlüğü, Özel Yayınlar Serisi, Ankara, Türkiye.
- Ergünay, O. 1999. A Perspective of Disaster in Turkey: Issues and Prospects, Urban Settlements and Natural Disasters, Proceedings of UIA Region II Workshop, Chamber of Architects of Turkey.
- Gökçe, O., Özden, Ş., Demir, A. 2008. Türkiye'de Afetlerin Mekansal ve İstatistiksel Dağılımı Afet Bilgi Envanteri, p 117, T.C. Bayındırlık ve İskan Bakanlığı Afet İşleri Genel Müdürlüğü Afet Etüt ve Hasar Tespit Daire Başkanlığı. Ankara.
- Heckmann, T., Gegg, K., Gegg, A., Becht, M. 2014. Sample size matters: investigating the effect of sample size on a logistic regression susceptibility model for debris flows. *Nat Hazard Earth Sys* 14:259-278.
- Hosmer, D., Stanley Lemeshow, S., Sturdivant, R. 2013. Applied Logistic Regression. John Wiley & Sons, Inc.
- Kadirioğlu, FT., Kartal, RF., Kılıç, T., Kalafat, D., Duman, TY., Eroğlu Azak, T., Özalp, S., Emre, Ö. 2016. An Improved Earthquake Catalogue (M ≥ 4.0) for Turkey and Its Near Vicinity (1900-2012). *Bulletin of Earthquake Engineering*, Published online 19 December 2016 DOI 10.1007/s10518-016-0064-8.
- Metz, C.E. 1978. Basic principles of ROC analysis. *Semin Nucl Med.* 8, 283-298.
- Metz, C.E. 2006. Receiver operating characteristic analysis: a tool for the quantitative evaluation of observer performance and imaging systems. *J Am Coll Radiol.* 3,413-422.
- Nefeslioğlu, H.A., Duman, T.Y., Durmaz, S. 2008. Landslide susceptibility mapping for a part of tectonic Kelkit Valley (Eastern Black Sea region of Turkey). *Geomorphology* 94(3-4): 401-418.
- Riley, S. J., DeGloria, S. D., Elliot, R. 1999. A terrain ruggedness index that quantifies topographic heterogeneity. *Intermountain Journal of Sciences*, 5(1-4).
- Süzen, M. L., Doyuran, V. 2004. Data driven bivariate landslide susceptibility assessment using geographical information systems: a method and application to Asarsuyu catchment, Turkey. *Engineering Geology*, 71, 303-321.
- Tekin, S. 2014. Kadirli-Aslantaş (Osmaniye) Dolaylarının Cbs Tabanlı Heyelan Duyarlılık Değerlendirilmesi. Çukurova Üniversitesi Fen Bilimleri Enstitüsü, 93., Adana.
- Tekin, S., Çan, T. 2016. Heyelanlı Örneklem Seçimindeki Farklı Yaklaşımların Heyelan Duyarlılık Haritalarının Başarı Tahmin Davranışları Üzerine Etkisi, 413-423 S. VI. Uzaktan Algılama ve Coğrafi Bilgi Sistemleri Sempozyumu, Adana, Türkiye.
- Weiss, A. 2001. Topographic Position and Landforms Analysis, Poster presentation, ESRI User Conference, San Diego, CA.
- Wilson, J. P., Gallant, J. C. 2000. Terrain analysis: principles and applications. John Wiley and Sons: New York.
- Yeşilnacar, E., Topal, T. 2005, Landslide susceptibility mapping: A comparison of logistic regression and neural networks methods in a medium scale study, Hendek region (Turkey). *Eng Geol* 79:251-266.



# Bulletin of the Mineral Research and Exploration

<http://bulletin.mta.gov.tr>



## 29 NOVEMBER 1795 KAHRAMANMARAŞ EARTHQUAKE, SOUTHERN TURKEY

Mahmut PALUTOĞLU<sup>a</sup> and Ahmet ŞAŞMAZ<sup>b</sup>

<sup>a</sup> Fırat University, Department of Geological Engineering, 23119, Elazığ, Turkey. [orcid.org/0000-0002-1109-9152](https://orcid.org/0000-0002-1109-9152)

<sup>b</sup> Fırat University, Department of Geological Engineering, 23119, Elazığ, Turkey. [orcid.org/0000-0003-1154-732X](https://orcid.org/0000-0003-1154-732X)

Research Article

### Keywords:

Kahramanmaraş,  
Manuscript, Intensity,  
Historical Earthquake, East  
Anatolian Fault Zone.

### ABSTRACT

Major tectonics on the Kahramanmaraş region are the northern strand of EAFZ (Sürgü fault zone, Çardak segment, Savrun segment and Toprakkale segment) and the southern strand of EAFZ (Gölbaşı segment, Amanos segment), Engizek Fault Zone, Kahramanmaraş Fault Zone and The Narlı segment of DSFZ. An earthquake, occurred in Kahramanmaraş, 1795, is mentioned a manuscript named Divan-ı Hasmi which is found at Koyunoğlu Library in Konya. According to manuscript the Mercalli Intensity of the earthquake has calculated as eight and the magnitude is seven. The calculations made have strengthened the possibility of earthquake occurrence on the Gölbaşı segment of EAFZ.

Received Date: 02.06.2016

Accepted Date: 22.02.2017

## 1. Introduction

Kahramanmaraş city, which has an area of 14.346 km<sup>2</sup> and the population of 1.089.038 according to 2014 data, is the 11<sup>th</sup> biggest in population and the 18<sup>th</sup> largest city of Turkey ([www.kahramanmaras.gov.tr](http://www.kahramanmaras.gov.tr)). The northern parts of the city is rather mountainous. The landforms in Kahramanmaraş city where three different geographical regions approach to each other (the Mediterranean, the East Anatolian and the Southeast Anatolian regions) are generally formed by mountains which are the extensions of the Southeast Taurides and depression zones among them.

The manuscript, which has remained until today and is the subject of the study, was found among rare manuscripts in the library of the Konya Metropolitan Municipality. The manuscript takes place between the 138b and 143a foils of the Divan-ı Hasmi. In the Ottoman work of arts during that period, many manuscripts in different subjects were combined between the two covers, and the works called as “Divan” were formed. The name of the manuscript collected and written by Hafız Ahmet Nuri bin Hafız Halil is “Tarih-i Zelzele-i Mara’aş”. In the manuscript, the earthquake, which happened in 17 Cemaziye’l-Evvel 1210 according to the Islamic calendar, is

mentioned and the information on the earthquake given by different people takes place. The information regarding the earthquake has drawn attention of Daş (2005) who studied in the Koyunoğlu Library. The transcription of the manuscript was made by the investigator and given to the author.

## 2. Regional Tectonic Setting

The Neotectonic period in Turkey began by the depletion of the E-W extending southern branch of the Neotethy’s Ocean in north of the African-Arabian plates along the Bitlis-Zagros Suture belt at the easternmost part and continent to continent collision between the Arabian and Anatolian plates at the end of Middle Miocene (11 million years ago) (Koçyiğit, 1984; Şengör and Yılmaz, 1981; Bozkurt, 2001). Following this collision, the East Anatolia was compressed and thickened. This thickening reached a level which cannot be compensated by the continental crust. This movement was then compensated by the formations of NAFZ and EAFZ, and it is the beginning of Neotectonic period in Turkey (Koçyiğit, 1984). This westward movement of Anatolia developed along the right lateral NAFZ and the left lateral EAFZ (Figure 1). As a result of the collision between the Eurasian and Arabian plates the Zagros Suture Belt was formed.

\* Corresponding author: Mahmut PALUTOĞLU, [mpalutoglu@firat.edu.tr](mailto:mpalutoglu@firat.edu.tr)  
<http://dx.doi.org/10.19111/bulletinofmre.314211>

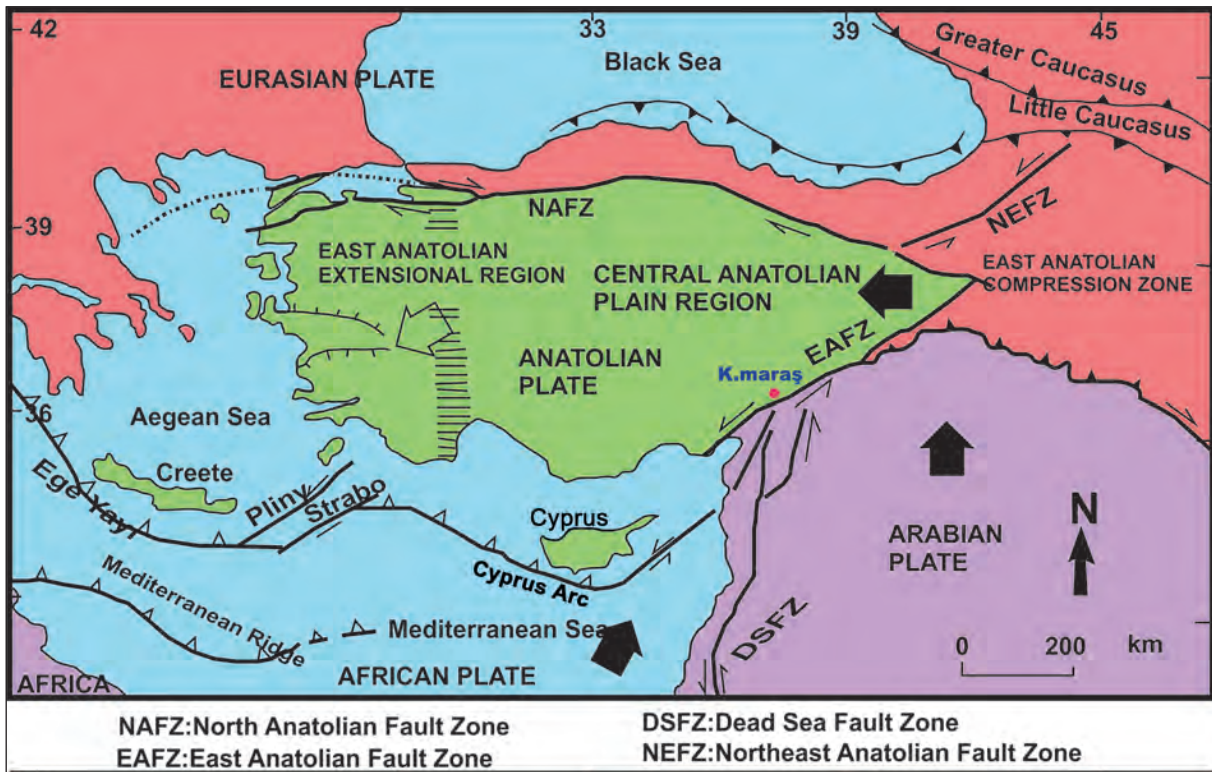


Figure 1- The tectonic setting of Turkey (modified from Bozkurt, 2001).

However, as a result of the subduction of the African plate beneath the Anatolian Block in west the Hellenic and Cyprus Arcs were formed (McKenzie, 1970 and 1972; Şengör and Yılmaz, 1981; Dewey et al., 1986).

The boundary between the Eurasian plate and the Anatolian block was distinguished by NAFZ; however, the boundary between the Arabian and African plates was detected by the DSFZ. The movement between Africa and Anatolia is compensated by Hellenic and Cyprus arcs. The convergence between Anatolia and Arabia is compensated by the left lateral strike slip movement that forms along the EAFZ (McKenzie, 1972; Harch et al., 1981; Şengör and Yılmaz, 1981; Şengör et al., 1985; Parlak, 2004).

There is a close relationship among the geographical, morphological and tectonic characteristics. Kahramanmaraş takes place on the suture belt where the Arabian and Anatolian plates collide; therefore, it has a very complicated geodynamic evolution. There are observed many rock assemblages and traces of deformation which formed in different environments within period ranging from Paleozoic to recent.

Kahramanmaraş and its surround is located in tectonically very complicated active region. It is stated that the junction point of faults, which form the tectonic framework in this region, is the region between Kahramanmaraş and Gölbaşı (Figure 2) (McKenzie, 1972; Dewey et al., 1973; Jackson and McKenzie, 1984; Şengör et al., 1985; Gülen et al., 1987; Karig and Kozlu, 1990; Kempler and Grafunkel, 1991; Chorowicz et al., 1994). This region, which is named as the Maraş triple junction, covers the northwestern corner of the Arabian plate and the Eurasian and African plates which synchronously deformed, and it consists of all characteristics that can be seen in a continental collision zone (Gülen et al., 1987; Westaway, 2003).

The continuation of the EAFZ after Kahramanmaraş is in debate. Some investigators emphasize that the fault zone after Kahramanmaraş continues towards Antakya and combines with the DSFZ (Allen, 1969; Arpat and Şaroğlu, 1975; Rotstein, 1984; Kelling et al., 1987; Şaroğlu et al., 1992b; Kiratzi, 1993; Rojay et al., 2000; Sezgin et al., 2002). However, the other investigators claim that the fault zone extends to Yumurtalık fault and Cyprus in southwest direction after Kahramanmaraş (McKenzie, 1972; Dewey et al., 1973; Jackson and McKenzie, 1984; Gülen et al., 1987;

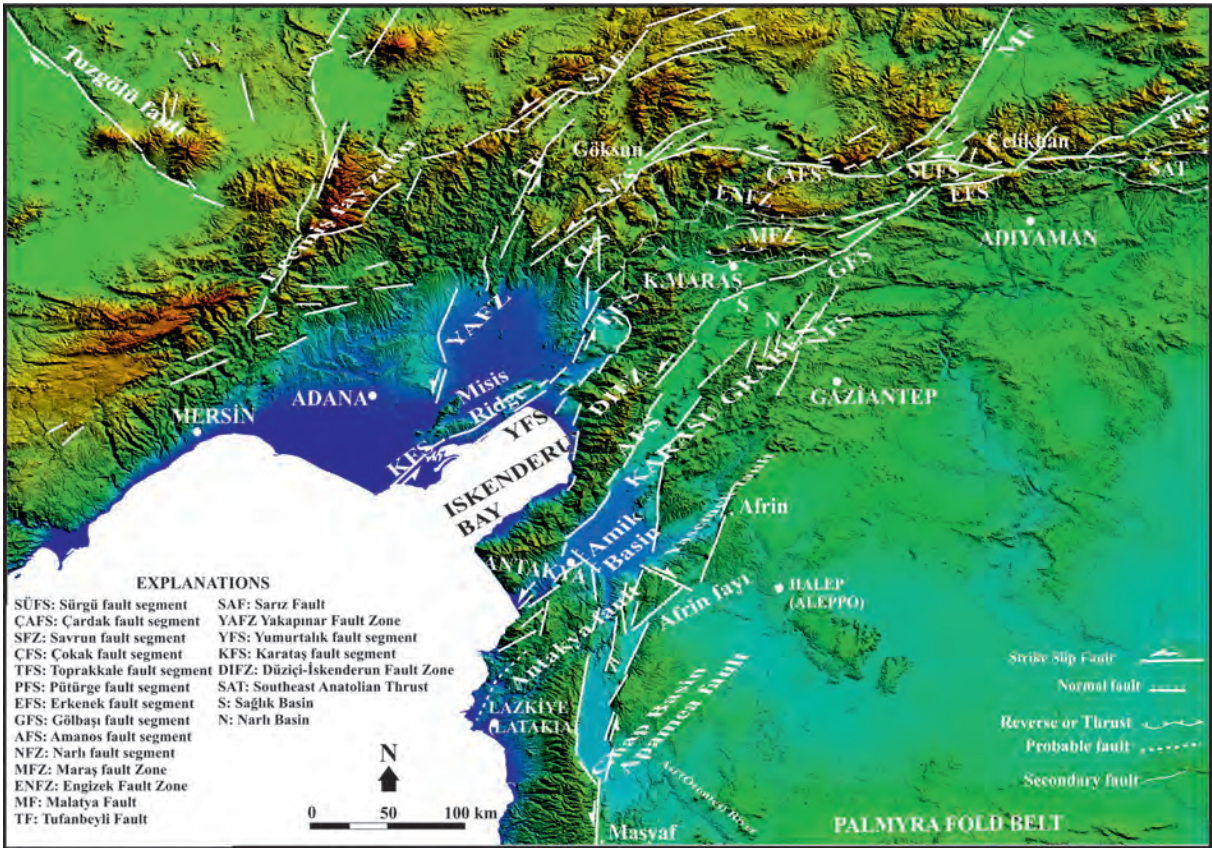


Figure 2- The tectonic map of Kahramanmaraş and its surround (modified from Emre and Duman, 2013).

Barka and Kadinsky-Cade, 1988; Karig and Kozlu, 1990; Kempler and Garfunkel, 1991; Westaway and Arger, 1996). Another group of researchers consider that the fault zone ends around Türkoğlu (Lovelock, 1984; Chorowicz et al., 1994). The EAFZ crosses the Aksu river in east of the Northern Amanos mountains and form the northern branch of the DSFZ. Some researchers state that there is such a fault, but it is not the segment of the EAFZ. They say that this section is the plate boundary between Anatolia and Africa (Muehlberger and Gordon, 1987).

Important tectonic structures located in Kahramanmaraş and its surround are the northern branch (Allen, 1969; Arpat and Şaroğlu, 1975; Herece, 2008; Duman and Emre, 2013; Robertson et al., 2013) (Sürgü segment, Çardak segment, Savrun segment, Çokak segment and Toprakkale segment) and the southern branch of the EAFZ (Gölbaşı segment and Amanos segment), the Engizek fault zone, Kahramanmaraş fault zone and Narlı segment of the DSFZ (Figure 2). It is also known that there have been numerous earthquakes in the region in the historical period along the faults and associated

segments (Ergin, 1966; Soysal et al., 1981; Özmen, 1999).

The E-W extending fault, which separates from the Gölbaşı segment of the EAFZ, is named as the Sürgün fault (Ergin, 1966; Soysal et al., 1981; Özmen, 1999) and it is 75 km away from the city center. The Sürgün fault begins at the south of Çelikhhan town and ends in the vicinity of Nurhak town. It is formed from three segments with lengths of 28, 25, and 11 km's and has a total length of 64 km (Duman and Emre, 2013; Emre et al., 2013; Menekşe, 2016). The fault, which extends in E-W direction, is named as the Çardak fault (Duman and Emre, 2013; Emre et al., 2013). It is formed by two segments with lengths of 34 and 50 km's (Duman and Emre, 2013; Emre et al., 2013; Menekşe, 2016) and approximately 55 km's away from the Kahramanmaraş city center. The Savrun fault (Kozlu, 1987; Perinçek and Kozlu, 1984; Robertson et al., 2004) begins at Göksun and ends around Sumbas. It is in NE-SW direction and has a total length of 63 km's (Duman and Emre, 2013; Emre et al., 2013; Menekşe, 2016). It is 63 km's away from the city center. The Çokak fault has a strike of N15E and a length of 25

km's. It is 53 km's away from Kahramanmaraş. The Toprakkale fault has a strike of N30-35E and a length of 52 km's (Duman and Emre, 2013). It has 90 km's distance from the city center.

The Gölbaşı segment is 90 km's long and formed by N55E extending many parallel faults (Figure 3). The segment becomes apparent at a point in near northeast of Harmanlı located in the Gölbaşı town of Adıyaman. The fault extends to Gölbaşı town as one branch, but it is divided into many branches in the vicinity of Gölbaşı (Çıplak, 2004). The approximate direction of the fault in this region is N60E. While the main branch runs towards Gölbaşı town starting from the west of Harmanlı, the Azaplı fault zone in north is observed which is formed by fault segments in similar directions (İmamoğlu, 1993).

The fault zone loses its appearance because of swampy areas and alluvial around Gölbaşı Lake. It again becomes distinctive in southwest of Gölbaşı town. The direction of the EAFZ is N50E here. The EAFZ is divided into branches starting from the south

of the Azaplı Lake and extends towards the southern part of the İnekli Lake. The EAFZ continues along the Kısıklı Dere Valley in northeast of Sakarkaya with a strike of N55E. The EAFZ, which runs along the Koca Dere Valley, passes through the northern part of Tetirlik village and reaches Kartal village. It jumps to the left in east of Kartal village and forms a small sag pond then extends southward. The fault zone, which continues from the south of Kartal village to the southwest, passes through the Tevekkeli village and extends until the north of Türkoğlu town (Erkmen et al., 2009). The Gölbaşı segment is linear between Harmanlı-Sakarkaya, slightly concave between Sakarkaya-Elmalar towards north and convex between Elmalar-Türkoğlu towards south (Şaroğlu et al., 1987).

The Amanos segment of the EAFZ is composed of three sections as; Nurdağı, Hassa and Kırıkhan. These sections are 40, 45 and 35 km's long respectively with the total length of 120 km's (Duman and Emre, 2013). The distance of the nearest section of the Nurdağı segment to the Kahramanmaraş city center is 35 km's.

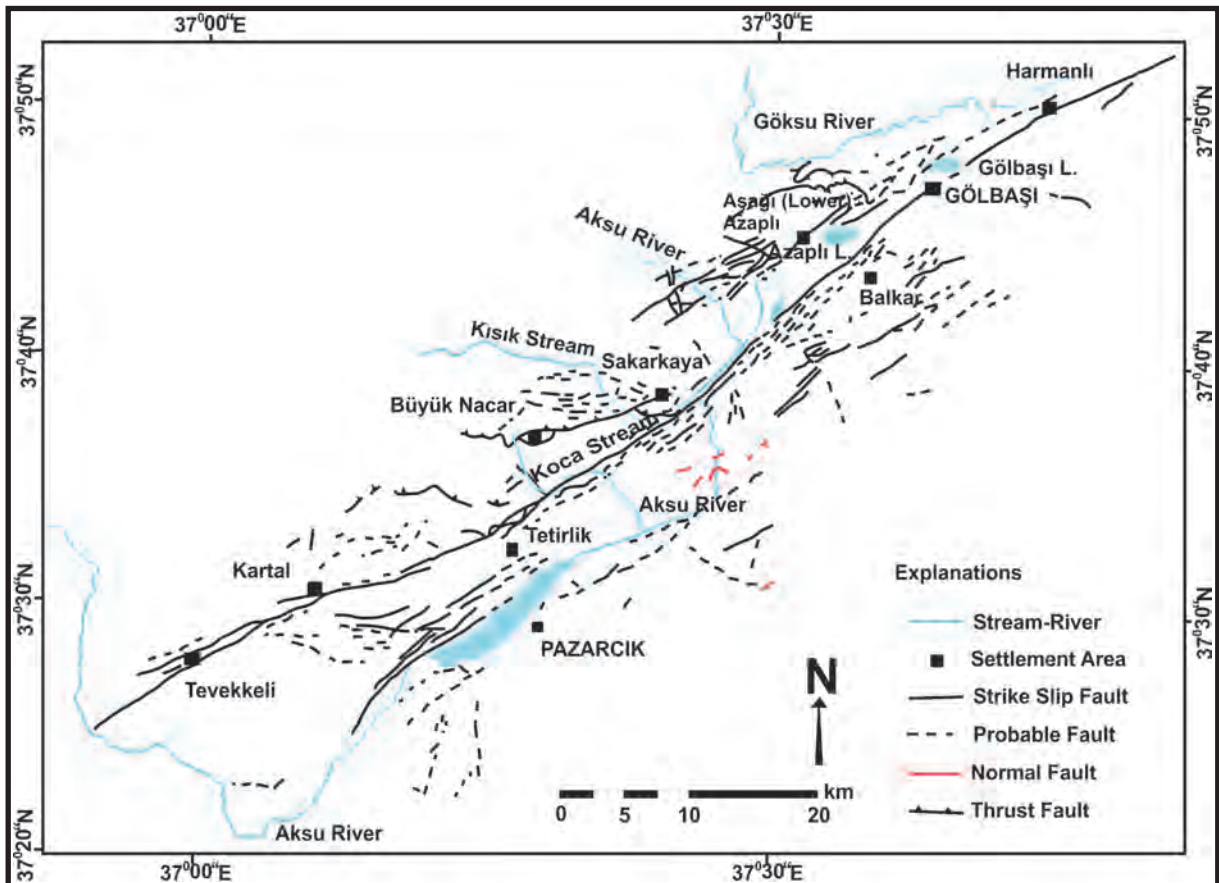


Figure 3- The tectonic map of Gölbaşı segment of the EAFZ (İmamoğlu, 1993; Erkman et al., 2009).

The Narlı segment of the DSFZ has a strike of N15-20E and is 35 km's long (Duman and Emre, 2013). It has a distance of 25 km's from the city center.

The Engizek thrust is formed by many large and small thrusts, and it is roughly in E-W direction. It begins at the northeast of Çağlayancerit town, passes through the northern part of the Menzelet Dam and extends until the west of Suçatı Dam (Emre et al., 2012a, b). It has an approximate length of 66 km's and is 30 km away from the city center.

The Kahramanmaraş fault zone is in E-W direction and begins from the vicinity of Sakarkaya in east of Kahramanmaraş. It passes through the southern part of Kahramanmaraş and extends until the Kılavuzlu Dam (Emre et al., 2012a, b). This thrust is 3 km's away from the city center.

### 3. The Evaluation of the Earthquake

Kahramanmaraş is one of the oldest cities of the Anatolia. In Kahramanmaraş; the Hittites, Assyrians, Macedonians and the Romans have reigned, respectively (Atalay, 1929). The oldest name of the Kahramanmaraş city is observed in the Assyrian written sources. According to these written sources the name of the city state was "Gurgum", and the capital city was "Markasi", the name of Kahramanmaraş in that period (Göl, 2006).

The city has taken the name of Mar'aş after the conquest of the Muslims. Mar'aş means the place of trembling in Arabic. This name was given as the area had turned into a swampy land because of rice cultivation and malaria has been extensively seen. When Maraş has been conquered by the Byzantines the name of the city has changed into "Marasaion". Then; the name of the city has changed into Maraş after the conquest of the Muslims. Although the name of the city has not been subjected to much changes, its location has continuously altered. The antic city, which had settled in southeast of the recent Kahramanmaraş, has been moved to the bank of Karasu in the Roman times. In the Middle age, first Reban then Altuntaş has become the city center. Due to the collapse of Altuntaş in an earthquake, the city center has moved to a place called "Kara Maraş" which is located in east of Kahramanmaraş in today. The Dulkadiroğulları have been the first to settle in today's city center (Göl, 2006).

Historical earthquakes that have occurred in the vicinity of Kahramanmaraş are given in different

earthquake catalogues. Soysal et al. (1981) suggest the following earthquakes and associated magnitudes for the historical earthquakes in and around the study area as; the İslâhiye earthquake with magnitude of VII in 131 B.C., the İslâhiye and Maraş earthquakes with magnitude of VIII in A.D. 128, the Ceyhan, Antakya and Maraş earthquakes with magnitude of IX in A.D. 1114, the Maraş, Urfa and Harran earthquakes with magnitude of VIII in 1114 and the Elbistan and Maraş earthquakes with magnitude of VIII in 1544. However, Özmen (1999) proposes the İslâhiye earthquake with magnitude of VII in 131 B.C., the İslâhiye and Maraş earthquakes with magnitude of VIII in A.D. 128, the Maraş, Urfa and Harran earthquakes with magnitude of VII in 1114 November 29<sup>th</sup>, the Ceyhan, Antakya and Maraş earthquakes with magnitude of IX in 1114 August 10<sup>th</sup>, the Elbistan and Maraş earthquakes with magnitude of VIII in 1544 January 22<sup>nd</sup> for the earthquakes in and around the study area. In addition to the historical earthquake catalogues given above there is not mentioned about any earthquakes in Ergin (1966) and Ambraseys (1971), which occurred in Kahramanmaraş in 1210 (according to Islamic calendar), the topic of the study.

#### 3.1. The Occurrence Date of Earthquake

The information below is given about the occurrence time, day and season of the earthquake in the manuscript (Figure 4) (Daş, 2005);

1<sup>st</sup> poetic; lines 7 and 8:

Ruz-i saat yedide, mah-ı Cemâziye'l-Ula (in November, at seven o'clock)

Maraş'ı yevm- sebte eyledi Allah lerzan (Allah flattened Maraş on Saturday)

2<sup>nd</sup> poetic; Lines 10 and 11:

On yedincisi Cemâziye'l-Evvel'inin yevm-i Sebt (On Saturday, November the 17th)

Rûz saat yedide oldı tezeliül âşikâr (It happened at 7 o'clock in the morning).

3<sup>rd</sup> poetic, lines 15 and 16:

Mâh-ı Cemâziye'l-Evvel'inin on yedincisi (on the 17th day of November)

Sa'at yedide yevm-i Sebtde kıldı herkesi (It hit everyone at seven o'clock on Saturday)

4<sup>th</sup> poetic, lines 19, 20, 21 and 22:



Figure 4- The identity of the manuscript (Daş, 2005).

Doğru çün Cemâziye'l-Evvel (In November)

On üçü kaldı hemân şöyle mesel, (Therefore, this parable remained)

Tut kulağına sözümü dinle işit, (Listen and hear my word carefully)

Öğle vakti idi çün yevm-i Sebt (It happened at noon of Saturday)

When the given information in poetical form are assessed, it is understood that the earthquake occurred in 1210 Cemaziye'l Evvel 17<sup>th</sup> (in Islamic calendar). The equivalents of the dates in Islamic calendar are given on table 1.

Table 1- The conversion of Islamic calendar into Gregorian calendar (<http://www.ttk.gov.tr>).

	Hijri	Gregorian	Rumi
Day	17	29	18
Month	Cemazeyilevvel	November	Teşrinisani
Year	1210	1795	1209
	Saturday	Sunday	

It is clearly seen that the season is winter and the earthquake occurred at seven o'clock on Saturday morning. On conversion process, the date is given

as Sunday. However, the Saturday is absolutely emphasized in the manuscript. The “Sunday” on table 1 originates from conversion.

Estimation of Parameters Related to the Earthquake

Magnitude and Intensity of the Earthquake

Details stated in the manuscript related to the intensity of the earthquake are as follows;

1<sup>st</sup> poetic; lines 25, 26, 27, 28, 29 and 30:

Oldu virane cami u mescid şimdi, (Mosques and prayer rooms are ruined now)

Kalmadı dense seza bunda, dekakin ile han (There are not any shops and inns)

Münhedim oldı heman nice minare, mekteb (Several minarets and schools were blown up)

Okunur mu ola minba'd, ezn u Kuran (Will Ezan (call for pray) be read from the minaret anymore?)

Ak minare hele, ser çekmiş idi eflake (Ak minare would magnificently rise up to the sky before)

Her gören derdi anın kametini, serv-i revan (But today it is like a ruined cypress)

1<sup>st</sup> poetic; lines 37 and 38:

Kal'a-i Maraş'ı ser-tabe kıldı harab, (Maraş castle is almost ruined)

Burcu baru komayup eyledi hâke yeksan (There is not any bastion in the castle and blown up)

2<sup>nd</sup> poetic; lines 14 and 15:

Nâ-bedîd oldu bir anda çok dekâkîn, buyût (Many shops were blown up)

Kal'madı Mar'aş'ta her giz câmi u mescîd u menâr (There is not any mosque and praying room in Maraş)

2<sup>nd</sup> poetic; lines 18, 19, 20 and 21:

Her kesin virâne oldu menzil ü kâşânesi (Houses of citizens' are ruined)

Kal'madı bir kimsede tamirine iktidâr (There is no possibility to repair these houses)

Kal'a-i Mar'aş'da hergiz burc u bâru kalmayup, (There is not any bastion in Maraş castle, it has been ruined, fell down)

Münhedim olddukda, oldu ehl-i kal'a hâksâr (Maraş castle has been ruined by Allah)

3<sup>rd</sup> poetic; lines 27, 28 and 29:

Ez cümle Ak Minâre ki, serv-i revân idi, (Everybody knew the magnificence of the Ak minare (like the cypress rising up to the sky)

Ecsâd-ı şehir-i Mar'aş'a rûh-i revân idi (Maraş was a magnificent city)

Virân kıldı dest-i kazâ vü kader anı, (But, today it is ruined)

3<sup>rd</sup> poetic; lines 35 and 36:

Oldı derûn-i kal'ada nice hâneler harâb, (Many houses in the castle are ruined)

Üçyüz denildü hâne-i virân ale'l-hesâb (It was stated that three hundred houses had been ruined)

4<sup>th</sup> poetic; lines 29 and 30:

Şiddeti üç dakika oldu ammâ (It took three minutes)

Şehri baştanbaşa kıldı yağma (The city has entirely been ruined)

4<sup>th</sup> poetic; lines 33-34:

Kal'asında dahi muhkem hâne (Even the house in the castle)

Kal'madı câna sezâ kâşâne (It is true to say that it is not available anymore)

4<sup>th</sup> poetic; lines 43-53:

Sorma ahvâl-ı perişân hisâr (If you ask about the castle; it is miserable)

Bir lağımla atılıp oldu ğubâr (It is as if it had been exploded by a tunnel and fallen down)

Kal'a-i biçâre başdan başa (The whole castle is entirely ruinous)

Bir yumurta gibi çaldı taş (It hit on the ground like hitting an egg on the ground)

Nice câmi ile minârelerin (Many mosques and minarets)

Sorma ahvâlin açar yaraların (Do not ask the general view and gash my wound)

Ağ Minâre idi makbul-i enâm (It was well known as the Ak minare)

Bir beyâz câmelü nâzik-endâm (It would rise up to the sky with a white figure)

Gör ne itdi ana da devrân (Watch! How it was pushed away)

Yıkılıp hâke ile oldu yeksân (Knocked down and ruined)

Telef etdi nice câmi-i şerîf (Many mosques were knocked down)

In the manuscript, it is stated that shops and houses in the city were knocked down and ruined. Besides; it is mentioned that almost all mosques and praying rooms were collapsed, and the Ak minaret, which is one of the oldest known mosques of Kahramanmaraş, crumbled like a cypress tree. It is also emphasized that bastions and towers in the Maraş castle were heavily damaged. In the manuscript, it is written that people were in panic and ran away to shelter.

As it is understood from the manuscript, the statement of "fall of chimneys, factory stacks, columns, monuments, walls" mentioned in the Modified Mercalli Intensity Scale (MMI), indicates the "VII" scale earthquake. Empirical formulas

giving the magnitude of earthquake from the detected intensity value are available. Using these formulas the magnitude of earthquake was estimated.

$$I=(1,129 \times M_b)+0,103 \text{ (Bayrak, 2005)}$$

where; I is the earthquake intensity and  $M_b$  is the body-wave magnitude.

$$8=(1,129 \times M_b)+0,103$$

Then,

$$M_b=7,0$$

#### With respect to the Length of the Fault

The magnitude of the earthquake, which the active strike slip fault could generate with respect to its length;

$$M_w=5,16+(1,12 \times \log(L)) \text{ (for strike slip faults)} \\ \text{(Wells and Coppersmith, 1994)}$$

$$M_w=5,00+(1,22 \times \log(L)) \text{ (for reverse faults)} \\ \text{(Wells and Coppersmith, 1994)}$$

where;  $M_w$  is the Moment magnitude and L is the fault length (km)

The maximum earthquake magnitudes of the active faults in Kahramanmaraş and its surround with respect to their lengths were estimated using the formula given above and on table 2.

Table 2- Faults and earthquake magnitudes which they could generate with respect to their lengths.

Name of fault	Length of fault (km)	Largest earthquake magnitudes which could be generated with respect to length ( $M_w$ )
Gölbaşı segment	90	7,3
Çardak fault	84	7,3
Sürgü fault	64	7,2
Savrun fault	63	7,2
Toprakkale fault	52	7,1
Amanos segment	40	7,0
Narlı segment	35	6,9
Çokak fault	25	6,7
Engizek fault	66	7,2
Kahramanmaraş Fault Zone	30	6,8

### 3.2. With Respect to the Fault Slip Rate

The slip rates in strike slip faults and the magnitude of earthquake which can cause this rate is as follows;

$$M_w=6,81+(0,78 \times \log(MD)) \text{ (Wells and Coppersmith, 1994)}$$

Here, MD (Maximum Displacement) (slip rate of the East Anatolian Fault Zone; 5 mm/yr (Arpat and Şaroğlu, 1975; Öncel, 2000)) is given in meters in different studies using seismological data as 4-6 mm/y by Kasapoğlu and Toksöz, 1983; and 6 mm/y by Kiratzi, 1983 and Öncel, 2000). Again; the annual displacement of the Çardak Fault is 2 mm (Menekşe, 2016). In and around Kahramanmaraş; the earthquakes with  $M=7,4$  in 1513 on Gölbaşı segment (Ambrseys, 1988) and  $M=6,8$  in 1544 on Çardak Fault (Kondorsskaya and Ulomow, 1999) take place in historical records before the earthquake mentioned in the manuscript (Demirtaş and Erkmen, 2000; Duman and Emre, 2013; Figure 5). The maximum slip rate on the EAFZ is accepted as 6 mm/y. Thus, it was calculated that there had been a strain accumulation of 169 cm in 282 years from 1513 to 1795 on the Gölbaşı segment and 50 cm strain accumulation from 1544 to 1795 on the Çardak Fault in this study.

The magnitude of the earthquake  $M_w$ , which will release this strain on the Gölbaşı segment, is;

$$M_w=6,81+(0,78 \times \log(1,69))=6,987 \approx 7,0$$

$$M_w=7,0$$

and the magnitude of the earthquake ( $M_w$ ) that will release this strain on the Çardak Fault is;

$$M_w=6,81+(0,78 \times \log(0,5))=6,575 \approx 6,6$$

$$M_w=6,6$$

### 3.3. Intensity of the Earthquake

Along active strike slip fault belts the earthquake intensity, which the magnitude of maximum earthquake could form, is as follows;

$$I=5,867+1,5 \times M_w-(2,1 \times \ln(R+25)) \text{ (Hu et al., 1996)}$$

where; I is the Intensity,  $M_w$  is the magnitude,  $R=(D^2+h^2)^{1/2}$  (D is the closest distance to fault of the

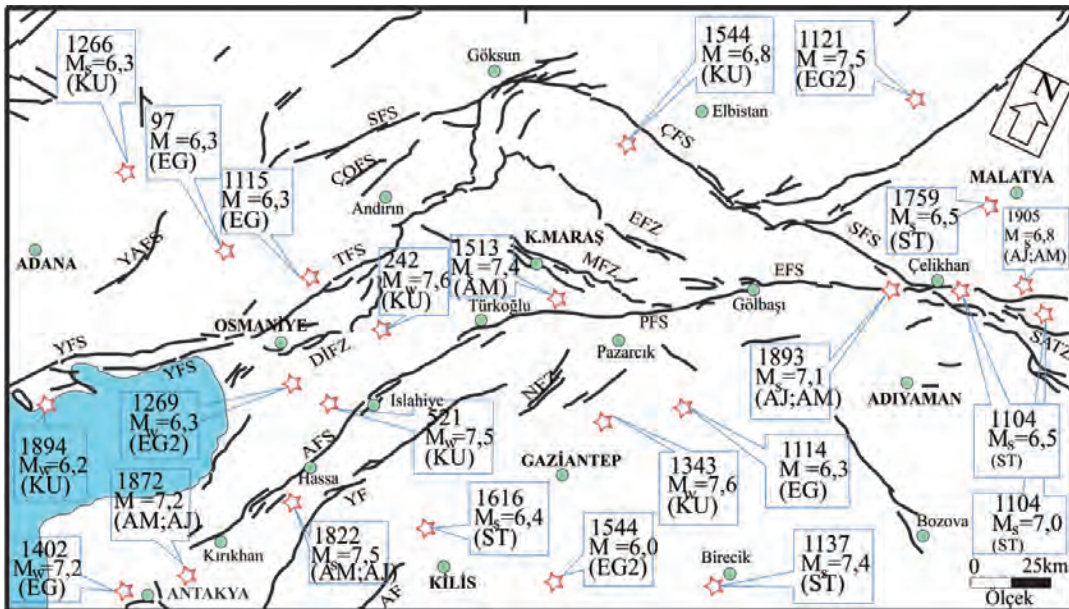


Figure 5- Historical earthquakes that occurred in Kahramanmaraş and its surround (modified from Ambraseys, 1988; Ambraseys and Jackson, 1998; Tan et al., 2008; Duman and Emre, 2013; abbreviations: ST, Shebalin and Tatevossian, 1997; KU, Kondorskaya and Ulomov, 1999; EG, Guidoboni et al., 1994; AM, Ambraseys, 1988; AJ, Ambraseys and Jackson, 1998).

study area (km) and  $h$  is the epicenter of earthquake ( $h=15$  km for the Anatolian peninsula).

### 3.4. Duration of Earthquake

If we again use some empirical equations to predict the duration of earthquake as given below;

$t=10^{(M-2.5)/(3.23)}$  (Watabe, 1977; Arıoğlu and Yılmaz, 2000).

Where;  $t$  is the time (sec) and  $M$  is the earthquake magnitude, then

$$t=10^{(7.0-2.5)/(3.23)}$$

$$t=24,8 \text{ sec}$$

$t=4+11(M-5)$  (Donovan, 1973; Arıoğlu and Yılmaz, 2000)

$$t=4+(11(7,0-5))$$

$$t=26 \text{ sec}$$

$$t \approx L/V \text{ (Arıoğlu and Yılmaz, 2000)}$$

$\log L = -3,55 + 0,74 \times M_w$  (Wells and Coppersmith, 1994)

$$\log L = -3,55 + (0,74 \times 7,0)$$

$$L = 89,12 \text{ km}$$

$V = 3,55$  km/sec (accepted as the rupture velocity of the fault (Arıoğlu and Yılmaz, 2000)).

$$t = 89,12 / 3,5$$

$$t \approx 25,4 \text{ sec}$$

Thus, the duration of earthquake is predicted as;  $(24,8 + 26 + 25,4) / 3 = 25,4$  sec.

### The Energy Generated by Earthquake

One of the magnitude parameters of earthquake is the “seismic energy”. Different formulas were given in order to predict the seismic energy of earthquake. We can calculate the seismic energy using those formulas.

The formula suggested by Gutenberg and Richter (1944), which is associated with energy-magnitude relationship, is as follows;

$$\log E = 2,4 \times M_b + 5,8 \text{ (Bayrak, 2005)}$$

where;  $E$  is the energy

Then,

$$\log E = (2,4 \times 7,0) + 5,8$$

$$E_b = 10^{22,6} \text{ erg}$$

#### Ground acceleration of the Earthquake

There are formulas, which give the ground acceleration with respect to intensity that the earthquake would generate. Using these formulas the ground acceleration can be predicted.

$$\log a = 0,30(I) + 0,014 \quad (\text{Trifunac and Brady, 1975; Trifunac 1976; Arıođlu and Yılmaz, 2000})$$

where; a is the horizontal ground acceleration

$$a = 259 \text{ cm/sec}^2$$

$$I = 3,66 + \log a - 1,6 \quad (\text{Wald et al., 1999; Arıođlu and Yılmaz, 2000})$$

$$a = 419 \text{ cm/sec}^2$$

$$\log a = (3/7)I - (9/10) \quad (\text{Hershberger, 1956; Arıođlu and Yılmaz, 2000})$$

$$a = 337 \text{ cm/sec}^2$$

$$\log a = 0,25I + 0,25 \quad (\text{Murpy, 1977; Arıođlu and Yılmaz, 2000})$$

$$a = 178 \text{ cm/sec}^2$$

If we take the arithmetical mean of all values, then the horizontal ground acceleration “a” is found as 298 cm/sec<sup>2</sup>.

#### Recurrence Interval of the Earthquake

The recurrence interval of the earthquake for Kahramanmaraş and its surround is found by the formula given below;

$$t \approx A_0 / \Delta \quad (\text{Arıođlu and Yılmaz, 2000})$$

where, A<sub>0</sub> is the mean offset of fault and Δ is the slip rate of fault in mm

$$\log(A_0) = -6,32 + 0,90 M_w \quad (\text{Wells and Coppersmith, 1994})$$

$$(A_0) = 10^{(-6,32 + (0,9 \times 7,0))}$$

$$(A_0) = 10^{(-0,02)}$$

$$(A_0) = 0,955 \text{ m} = 955 \text{ mm}$$

If the minimum and maximum slip rates of the EAFZ are taken as 4 and 6 mm's, respectively, then t<sub>min</sub> and t<sub>max</sub> values are found as;

$$t \approx 955/4 \quad t \approx 955/6$$

$$t_{\min} \approx 159 \text{ years} \quad t_{\max} \approx 239 \text{ years}$$

#### Seismic Moment

The seismic moment that forms during the fault rupture is calculated by the formula given below;

$$\log(M_0) = 1,33 \times M_s + 17,32 \quad (\text{Bayrak and Yılmaztürk, 1999})$$

where, M<sub>0</sub> is the seismic moment

So;

$$(M_0) = 10^{26,63} \text{ dyn.cm}$$

$$(M_w) = 2/3 \times (\log(M_0) - 10,7) \quad (\text{Arıođlu and Yılmaz, 2000})$$

$$M_w = 7,05 = 7,0$$

$$M_b \approx M_w = 7,0$$

#### Other Information related to the Earthquake

The information given below is for the aftershocks of the earthquake in the manuscript. According to this; it is understood that the aftershocks of the earthquake continued forty days and fire occurred because of friction at the time of earthquake.

*1<sup>st</sup> poetic, line 45:*

Ruz u Őeb oynadı kırk güne dek bu cirm-i zemin  
(The ground vibrated forty days after the earthquake)

*2<sup>nd</sup> poetic, line 17:*

Sahn-ı Mar'aş oynadı kırk güne dek yerde nâr  
(Maraş city vibrated forty days after the earthquake and fire occurred)

*3<sup>rd</sup> poetic, line 39:*

Kırk gün oynadı efendi bu cirm-i zemîn  
(The ground vibrated forty days)

Related to the events for earthquake it is stated that the water was cut off just before the earthquake.

3<sup>rd</sup> poetic, line 40:

Cûlar kesildi zelzele vaktinde bül-aceb (Waters were cut off before the earthquake)

### 3.4. The importance of the Earthquake

The earthquake stated in the manuscript is not mentioned in any of the historical earthquake catalogues as there is not any information; thus, it is not known by the investigators. Therefore; Kahramanmaraş and its surround is defined as the seismic gap and large earthquakes are predicted in this area in the near future (Table 3).

If it is accepted that this historical earthquake has not occurred, the maximum earthquake magnitude predicted for the study area can be calculated as explained below. If it is regarded that the slip rate of the EAFZ is 6 mm/y, and the latest and largest earthquake, which forms a surface rupture along the closest EAFZ segment to Kahramanmaraş is the 1513 earthquake (Demirtaş and Erkmén, 2000; Duman and Emre, 2013), then it was calculated that there had been a tension of 3,024 m along the EAFZ since 1513.

$$2017-1513= 504 \text{ years}$$

$$504 \times 6= 3024 \text{ mm} = 3,024 \text{ m.}$$

Thus; the magnitude of the earthquake  $M_w$ , which will release this tension, is calculated as;

$$M_w = 6,81 + (0,78 \times \log(3,024)) \quad (\text{Wells and Coppersmith, 1994})$$

$$M_w = 6,81 + (0,78 \times \log(3,024)) = 7,18 \approx 7,2$$

$$M_w = 7,2$$

Investigators, who calculated the magnitude values similar to that, expect devastating earthquakes in this section of the EAFZ.

The below calculation will be useful in order to better understand the situation.

According to the relationship of energy-magnitude by Gutenberg and Richter (1944),

$$\log E = 2,4 M_b + 5,8 \quad (\text{Bayrak, 2005})$$

if we take  $M_b$  as 7,0 then,

$$\log E = (2,4 \times 7,0) + 5,8$$

$$E_{7,0} = 10^{22,6} \text{ erg}$$

if we take  $M_b$  as 7,2 then,

$$\log E = (2,4 \times 7,2) + 5,8$$

$$E_{7,2} = 10^{25} \text{ erg}$$

If we rate these energies then we find;

$$10^{23,8} / 10^{22,6} = 10^{1,2} = 16$$

The strain energy that will be released by 16 earthquakes with magnitudes of 7 is equal to the amount of strain energy that will be released by one earthquake with magnitude of 7,2.

Table 3- The earthquake intensity predicted in the center of Kahramanmaraş when faults generate maximum earthquake.

Fault Name	Maximum earthquake magnitude ( $M_w$ ) which could generate with respect to length	Distance to Kahramanmaraş (km)	Intensity (I)
Gölbaşı segment	7,3	10	8,9
Çardak fault	7,3	55	7,6
Sürgü fault	7,2	75	7,0
Savrun fault	7,2	60	7,3
Toprakkale fault	7,1	90	6,5
Amanos segment	7,0	35	7,7
Narlı segment	6,9	25	7,8
Çokak fault	6,7	53	6,7
Engizek fault	7,2	30	8,1
Kahramanmaraş Fault Zone	6,8	3	8,3

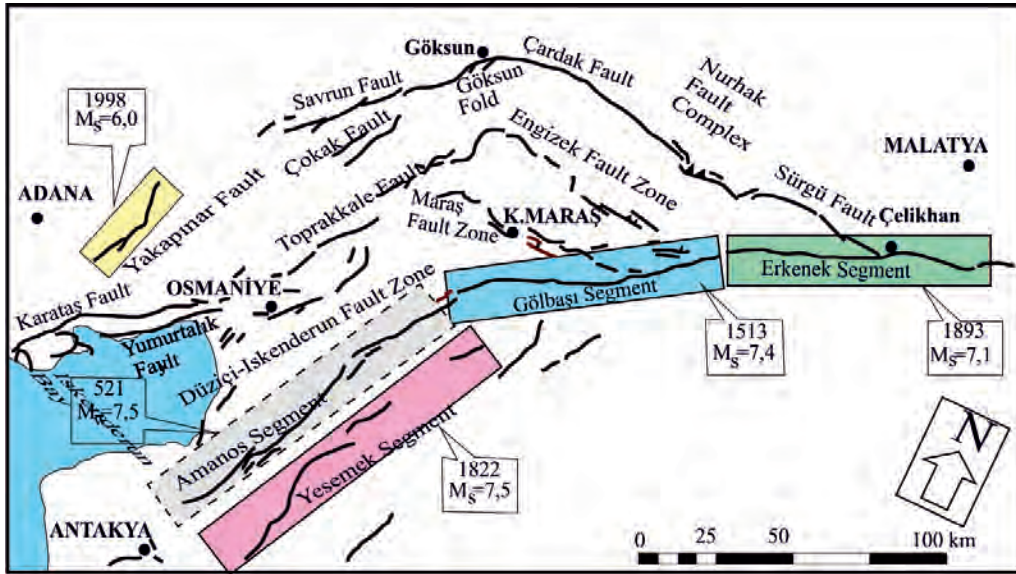


Figure 6- Surface ruptures formed by large earthquakes which formed in 19th and 20th centuries along the East Anatolian Fault System (modified from Arpat, 1971; Arpat and Şaroğlu, 1972; Seymen and Aydın, 1972; Ambraseys, 1988; Ambraseys and Jackson, 1998; Çetin et al., 2003; Herece, 2008; Karabacak et al., 2011; Duman and Emre, 2013).

#### 4. Discussion

Erkmen et al. (2009) detected the traces of at least 2 or 3 faults (ancient earthquake) as a result of paleoseismological studies carried out on the Gölbaşı segment. According to the correlations of Optically Simulated Luminescence (OSL) dating results and sedimentary accumulations, the dates of ancient earthquakes were obtained as in between 148 BC and AD 115; AD 458-589 and towards the end of 1000's or the beginning of 1100's. There was not encountered any traces of 1514 earthquake in excavated trenches. These information state that an earthquake with magnitude of 7,0-7,5 has happened between the years of 1000-1100, and for approximately 900 years there has not been any large earthquake which forms a surface rupture. It can also be said that the Gölbaşı-Türkoğlu fault segment is in a position to form a seismic gap which has a very high earthquake potential in near future.

Çetin et al. (2003) emphasize that the last earthquake, which has occurred on the segment and formed a surface rupture, has happened after 1890 (Figure 6). They also state that this earthquake can be associated with the 1874 ( $M_s=7,1$  (Ambraseys, 1988)) and 1875 ( $M_s=6,7$  (Ambraseys and Jackson, 1998)) earthquakes in the study they carried out on the Palu-Hazar segment of the EAFZ. Moreover; it is considered that another large earthquake has occurred

100-200 years later than AD 1420 and could be associated with the 1513 ( $M_s=7,4$  (Ambraseys, 1988)) earthquake. There have been two large earthquakes in AD 130 and AD 400-450 years. However, there has not been encountered any traces of the 995 and 1789 earthquakes which are associated with Karlıova-Bingöl segment. In the Palu-Hazar Lake segment the recurrence interval for the earthquake with  $M>7$  is expected to be  $100\pm35$  as the minimum and 360 years as the maximum (Çetin et al., 2003).

It can be asserted that large earthquakes in the Gölbaşı segment of the EAFZ have empirically occurred ( $M\geq7,0$ ) once in approximately 200 years. However, as a result of paleoseismological studies carried out in Gölbaşı town and its surround, which is located on the Gölbaşı segment, the recurrence interval of large earthquakes ( $M\geq7,0$ ) were found to be as 403 years as the maximum and  $253 \pm 30$  years as the minimum (Yüksel, 2009). When the average of these values are taken, a recurrence interval of  $328 \pm 30$  years can be suggested. The youngest paleoseismological information detected during excavations date back to  $371 \pm 30$  years and there is not encountered any younger earthquake data in the historical/instrumental period.

#### 5. Results

This earthquake, which is mentioned in the

historical manuscript, does not take place neither in domestic nor in international earthquake catalogues. It was assessed and introduced for the first time in the light of earth science data.

The earthquake stated in the manuscript exactly occurred in 1795 November the 29, on Saturday morning at 7 o'clock. The intensity of the earthquake was predicted as VIII based on the lines in historical poetics. The magnitude of the earthquake with respect to intensity was estimated as 7,0 using empirical formulas.

The lengths of active faults with the earthquake magnitudes ( $M_w$ ) that could be generated in Kahramanmaraş and its surround were calculated as follows; the Gölbaşı segment 90 km with  $M_w=7,3$ , the Çardak fault 84 km with  $M_w=7,3$ , the Sürgü fault 64 km with  $M_w=7,2$ , the Savrun fault 63 km with  $M_w=7,2$ , the Toprakkale fault 52 km with  $M_w=7,1$ , the Amanos segment 40 km with  $M_w=7,0$ , the Narlı segment 35 km with  $M_w=6,9$ , the Çökak fault 25 km with  $M_w=6,7$ , the Engizek fault 66 km with  $M_w=7,2$ , the Kahramanmaraş Fault Zone 30 km with  $M_w=6,8$ .

It was also calculated that an earthquake with  $M_w=9,0$  in the center of Kahramanmaraş might occur when an earthquake happens on the Gölbaşı segment with  $M_w=7,3$ . Besides; the occurrence of an earthquake on the Kahramanmaraş fault with  $M_w=6,8$  also creates an earthquake with  $M_w=8$  in the center of Kahramanmaraş.

There has been a strain accumulation of 169 cm on the Gölbaşı segment from 1513 to 1795. However, there has been a strain accumulation of 50 cm on the Çardak fault from 1544 to 1795. The earthquakes, which would release that much strain on the Gölbaşı segment and the Çardak Fault, were estimated to be  $M_w=7,0$  and  $M_w=6,6$ , respectively.

Using empirical equations, the earthquake duration was predicted as 25,4 sec. The seismic energy of the earthquake was found as  $E_b=1022,6$  erg. The horizontal ground acceleration that the earthquake could create was obtained as 298 cm/sec<sup>2</sup> using the related formulas.

The recurrence interval of the earthquake for Kahramanmaraş and its surround (if the lowest and highest slip rates of the EAFZ are taken as 4 and 6 mm, respectively) was calculated as  $t_{min} \approx 159$  years and  $t_{max} \approx 239$  years.

It is understood from the handwritten documents that there was a devastating earthquake in the vicinity of Kahramanmaraş in 1795. However, it is not clear by which fault the earthquake mentioned in the manuscript was generated. As a result of the estimations made the Gölbaşı segment, the Kahramanmaraş Fault Zone, the Engizek Fault and the Çardak Fault come to the forefront.

As a result; the presence of an earthquake, which had not previously taken place in historical earthquake catalogues and literature, were put forward. It is suggested that the slip rate and paleoseismological behaviors of the triggering fault, which generate this earthquake in terms of regional earthquake risk analyses, should be studied in detail.

## References

- Allen, C.R. 1969. Active Faulting in Northern Turkey. Contribution No: 1577, Division of Geological Sciences, California. Institute. Technology, 32 pp.
- Ambraseys, N.N. 1971. Value of historical records of earthquakes. Nature, Vol. 232, 375-379.
- Ambraseys, N. N. 1988. Temporary seismic quiescence: SE Turkey. Geophysical Journal, 96, 311-331.
- Ambraseys, N. N., Jackson, J. A. 1998. Faulting associated with historical and recent earthquakes in the Eastern Mediterranean region. Geophysical Journal International, 133, 390-406.
- Arioğlu, E., Yılmaz, A.O. 2000. Çözümlü Problemlerle Yeraltı Mühendislik Yapılarına Deprem Etkileri. TMMOB Maden Mühendisleri Odası İstanbul Şubesi Yayını, İstanbul.
- Arpat, A. E. 1971. 22 Mayıs, 1971 Bingöl Depremi Ön Rapor. Institute of Mineral Research and Exploration Report 4697.
- Arpat, A. E., Şaroğlu, F. 1972. Doğu Anadolu Fayı ile ilgili bazı gözlem ve düşünceler. Bulletin of the Mineral Research and Exploration, 73, 1-9.
- Arpat, A. E., Şaroğlu, F. 1975. Türkiye'deki bazı önemli genç tektonik olaylar. Türkiye Jeoloji Kurumu Bülteni, 18/1, 91-101.
- Atalay, B. 1929. Maraş Tarihi Coğrafyası. Matbaa-i Amire, 235s.
- Barka, A.A., Kadinsky-Cade K. 1988. Strike-slip fault geometry in Turkey and influence on earthquake activity, Tectonics. Vol.7, No 3, pp.663-684.
- Bayrak, Y. 2005. Global Sismisite. Karadeniz Teknik Üniversitesi Mühendislik-Mimarlık Fakültesi

- Yayını, Trabzon.
- Bayrak, Y., Yılmaztürk, A. 1999. Türkiye ve Civarında Sismik Moment ve Gerilim Dağılımı. Hacettepe Üniversitesi Yerbilimleri Uygulama ve Araştırma Merkezi Bülteni, 21, 1-15.
- Bozkurt, E. 2001. Neotectonics of Turkey-a synthesis. *Geodinamica Acta*, 14, 3-30.
- Chorowicz, J., Luxey, P., Lyberis, N., Carvalho, J., Parrot, J.F., Yürür, T., Gündoğdu, N. 1994. The Kahramanmaraş Triple Junction (southern Turkey) based on digital elevation model and satellite imagery interpretation. *Journal of Geophysical Research*, 99, 20225-20242.
- Çetin, H., Güneşli, H., Mayer, L. 2003. Paleoseismology of the Palu-Lake Hazar segment of the East Anatolian Fault Zone, Turkey. *Tectonophysics*, 374, 163-197.
- Çıplak, R. 2004. Erkenek-Gölbaşı (Adıyaman) Arasında Doğu Anadolu Fayının Özellikleri, Master Thesis, İstanbul Teknik Üniversitesi Avrasya Yer Bilimleri Enstitüsü 76s. İstanbul (unpublished).
- Daş, A. 2005. Hicri 1210 Maraş Depremi İlgili Manzum El Yazması Tarihler. I. Kahramanmaraş Sempozyumu 6-8 Mayıs 2004. Kahramanmaraş, Vol.1, page: 355-365.
- Demirtaş, R., Erkmen, C. 2000. Deprem ve Jeoloji. Jeoloji Mühendisleri Odası Yayınları, 52s.
- Dewey, J.F., Pitman, W.C., Ryan, W.B.F., Bonnin, J. 1973. Plate tectonics and the evolution of the Alpine system. *Geological Society of America Bulletin*, 84, 3137-3180.
- Dewey, J.F., Hempton, M.R., Kidd, W.S.F., Şaroğlu, F., Şengör, A.M.C. 1986. Shortening of continental lithosphere: the neotectonics of Eastern Anatolia-a young collision zone. In *Collision Tectonics*. Coward, M.P., A.C. Ries (eds.). *Geology Society of London, Special Publication*, 19, 3-36.
- Donovan, N.C. 1973. A Statistical evaluation of strong motion data including the February 9, 1971 San Fernando earthquake. *Proceedings 5th World Conferences Earthquake Engineering*, Rome, 1: 1252-1261.
- Duman, T.Y., Emre, Ö. 2013. The East Anatolian Fault: geometry, segmentation and jog characteristics. *Geological Society, London, Special Publications* published online February 19, 2013 as doi: 10.1144/SP372.14
- Emre, Ö., Duman, T.Y., Elmacı, H. 2012a. 1:250.000 Ölçekli Türkiye Diri Fay Haritası Serisi. Elbistan (NJ 37-5) Sheet. Seri No: 37, General Directorate of mineral and Exploration, Ankara.
- Emre, Ö., Duman, T.Y., Olgun, Ş., Elmacı, H., Özalp, S. 2012b. 1:250.000 Ölçekli Türkiye Diri Fay Haritası Serisi. Gaziantep (NJ 37-9) Sheet. Seri No: 38, General Directorate of mineral and Exploration, Ankara.
- Emre, Ö., Duman, T.Y., Özalp, S., Elmacı, H., Olgun, Ş., Şaroğlu, F. 2013. Açıklamalı Türkiye Diri Fay Haritası Ölçek: 1:1250 000, General Directorate of mineral and Exploration, Special Edition-30, Ankara.
- Ergin, K. 1966. Türkiye ve Civarının Deprem Kataloğu. İstanbul Teknik Üniversitesi Maden Fakültesi Arz Fiziği Enstitüsü Yayınları, 170 s.
- Erkmen, C., Eravcı, B., Özşaraç, V., Yaman, M., Tekin, B.M., Albayrak, H., Kuterdem, K., Aktan, T., Tepeuğur, E. 2009. Doğu Anadolu Fayı'nın Paleosismolojisi; Pilot Bölge Gölbaşı-Türkoğlu Arası. TUJJB Ulusal Deprem Programı Proje No: TUJJB-UDP-1-07, Ankara.
- Göl, E. 2006. Cumhuriyet Döneminde (1923-1950) Maraş'ın Sosyo-Ekonomik Yapısı ve Gelişimi, Master of Thesis, Kahramanmaraş Sütçü İmam Üniversitesi Sosyal Bilimler Enstitüsü Tarih Anabilim dalı, 78s. Kahramanmaraş (unpublished).
- Guidoboni, E., Comastri, A., Triana, G. 1994. Catalogue of Ancient Earthquakes in the Mediterranean Area up to the 10th Century. *Istituto Nazionale di Geofisica, Rome*.
- Gutenberg, R., Richter, C.F. 1944. Frequency of earthquakes in California. *Bulletin Seismological Society of America* 34, 185-188.
- Gülen, L., Barka, A., Toksöz, M.N. 1987. Kıtaların Çarpışması ile ilgili Kompleks Deformasyon, Maraş Üçlü Eklemleri ve Çevre Yapıları. *Yerbilimleri* 14, 319-336.
- Harch, W., Kupfer, T., Rust, B., Sagesser, R. 1981. Seismotectonic consideration on the nature of the Turkish-African plate boundary, *Geol. Rundsch.*, 70, 368-384.
- Herece, E. 2008. Doğu Anadolu Fayı (DAF) Atlası. General Directorate of Mineral Research and Exploration. Special Publications, Ankara, Serial Number, 13, 359.
- Hershberger, J. 1956. A comparison of earthquake accelerations with intensity ratings. *Bulletin Seismological Society of America* 46, 317-320.
- Hu, X.Y., Liu, S.C., Dong, W., 1996. *Earthquake Engineering*. E and FN Spon, an imprint of Chapman and Hall, London, 403 p.

<http://www.ttk.gov.tr> (2016, 6 May).

<http://www.kahramanmaras.gov.tr> (2016, 6 May).

İmamoğlu, M.Ş. 1993. Gölbaşı (Adıyaman)-Pazarcık-Narlı (Kahramanmaraş) Arasındaki Sahada Doğu Anadolu Fayı'nın Neotektonik incelemesi. PhD Thesis, A.Ü. Fen Bilimleri Enstitüsü, 138s. Ankara (unpublished).

Jackson, J.A., McKenzie, D. 1984. Active tectonic of the Alpine-Himalayan belt between western Turkey and Pakistan. *Geophysical Journal of the Royal Astronomical Society*, 77, 185-264.

Karabacak, V., Önder, Y., Altunel, E., Yalçın, C., Akyüz, H. S., Kıyak, N. G. 2011. Doğu Anadolu Fay Zonunun güney batı uzanımının paleosismolojisi ve ilk kayma hızı. *Proceeding of the Aktif Tektonik Araştırma Grubu 15. Çalıştay (ATAG-15)*, 19–22 October 2011, Çukurova University, Karataş, -Adana, 17.

Karig, D.E., Kozlu, H. 1990. Late Palaeogene-Neogene evolution of the triple junction region near Kahramanmaraş, south-central Turkey, *Journal of the Geological Society, London*, 147, 1023-1034.

Kasapoğlu, E., Toksöz, M.N. 1983. Tectonic consequences of the Arabian and Eurasian plates: finite element models. *Tectonophysics*, 100 71-96.

Kelling, G., Gökçen, S.L., Floyd, P.A., Gökçen, N. 1987. Neogene tectonics and plate convergence in the Eastern Mediterranean: new data from southern Turkey, *Geology*, 15, 425-429.

Kempler, D., Garfunkel, Z. 1991. Northeast Mediterranean triple junction from a plate kinematics point of view, *Bulletin of the Technical University of İstanbul, Special Issue*, 44, 425-454.

Kiratzı, A. 1993. A study on the active crustal deformation of the North and East Anatolian Fault Zones. *Tectonophysics*, 225, 191-203.

Koç, A., Kaymakçı, N. 2013. Kinematics of Sürgü Fault Zone (Malatya, Turkey): A remote sensing study. *Journal of Geodynamics*, 65, 292-307.

Koçyiğit, A. 1984. Güneybatı Türkiye ve yakın dolayında levha içi yeni tektonik gelişim. *Türkiye Jeoloji Kurumu Bülteni*, No: 27, 1-16.

Kondorskaya, N. V., Ulomov, V. I. 1999. Special catalogue of earthquakes of the Northern Eurasia (SECNE). <http://www.seismo.ethz.ch/static/gshap/neurasia/nordasiacat.txt>, 3 May, 2015.

Kozlu, H. 1987. Structural Development and Stratigraphy of Misis-Andırın Region. In *Proceedings of the Seventh Turkish Petroleum Congress of Turkey*, 6-10 April 1987, Ankara, 104–116.

Lovell, P.E.R. 1984. A review of the tectonics of the northern Middle East region. *Geological Magazine*, 121, 577-587.

McKenzie, D.P. 1970. Plate tectonics of the Mediterranean region, *Nature*, 220, 239-343.

McKenzie, D.P. 1972. Active tectonics of the Mediterranean region. *Geophysical Journal of the Royal Astronomical Society*, 30. 109-185.

Menekşe, A. 2016. Probabilistic Seismic Hazard Assessment for East Anatolian Fault Zone Using Planar Source Models. Master Thesis, the Graduate School of Natural and Applied Science of Middle East Technical University, 112 p, Ankara (unpublished).

Muehlberger, R.W., Gordon, M.B. 1987. Observations on the complexity of the East Anatolian Fault, Turkey. *Journal of Structural Geology*, 9, 899-903.

Murphy, J.R. 1977. Seismic source functions for underground and magnitude determinations nuclear detonations. *Bulletin .Seismological Society of America Vol. 67(1)*, pp1675-1692.

Öncel, A.O. 2000. Fraktal Analiz İle Türkiye'deki Doğrultu Atımlı Fayların Yapısal Ve Sismolojik Özelliklerinin Belirlenmesi. *Deprem Araştırma Bülteni*, sayı; 84, 5–109s.

Özmen, B. 1999. Türkiye ve Çevresinin Tarihsel Deprem Kataloğunun Bölgesel Düzenlenmesi. *Deprem Araştırma Bülteni*, sayı; 82, 5–83s.

Parlak, O. 2004. Çelikhan-Erkenek Arasında Doğu Anadolu Fayı'nın Özellikleri, Master of Thesis, Istanbul technical University, Avrasya Yer Bilimleri Enstitüsü 99s, İstanbul (unpublished).

Perinçek, D., Kozlu, H. 1984. Stratigraphy and Structural Relations of the Units in the Afşin - Elbistan -Doğanşehir Region (Eastern Taurus). O., Tekeli, M.C. Gönçüoğlu (eds.). *Geology of Taurus Belt, Mineral Research and Exploration Institute*, p.181-198.

Perinçek, D., Günay, Y., Kozlu, H. 1987. New Observations on Strike-Slip Faults in East and Southeast Anatolia. *Proceedings of the 7th Petroleum Congress of Turkey*, 6–10 April, 1987, Ankara, 89–103.

Robertson, A. H. F., Ünlügenç, Ü.Ç. İnan, N., Taşlı, K. 2004. The Misis-Andırın Complex: A Mid-Tertiary Melange related to late-Stage subduction of the southern Neotethys in S Turkey. *Journal of Asian Earth Sciences* 22, 413–53.

Robertson, A.H.F., Parlak, O., Ünlügenç, U.C. 2013. *Geological Development of Anatolia and*

- Easternmost Mediterranean Region. Robertson, A.H.F., Parlak, O., Ünlügenç, U.C. (eds). Geological Society, London, Special Publications, 372, 495-529. doi:10.1144/SP372.14.
- Rojay, B., Heimann, A., Toprak, V. 2000. Neotectonic and Volcanic Characteristics of the Karasu Fault Zone (Anatolia, Turkey): The Transition Zone between the Dead Sea Transform and the East Anatolian Fault Zone. *Geodinamica Acta*, 14, 197-212.
- Rotstein, Y. 1984. Counterclockwise rotation of the Anatolian block, *Tectonophysics*, 108, 71-91.
- Seymen, İ., Aydın, A. 1972. Bingöl deprem fayı ve bunun Kuzey Anadolu fay zonu ile ilişkisi. *Bulletin of the General Directorate of Mineral Research and Exploration*, 79, 1-8.
- Sezgin, N., Pınar, A., Utkucu, M. 2002. Maraş Üçlü Eklem Bölgesinde Etkin Olan Tektonik Rejim. *Istanbul University, Fac. Of Eng. Yerbilimleri Dergisi*, Cilt: 15(1), 43-55.
- Shebalin, N.V., Tatevossian, R.E. 1997. Catalogue of large historical earthquakes of the Caucasus. Giardini, D., Balassanian, S. (eds). *Historical and Prehistorical Earthquakes in the Caucasus*. NATO ASI Series Partnership Sub-series 2, Environment, Kluwer Academic Publishers, Dordrecht, The Netherlands, 28, 201-232.
- Soysal, H., Sipahioğlu, S., Kolçak, D., Altınok, Y. 1981. Türkiye ve Çevresinin Tarihsel Deprem Kataloğu. TÜBİTAK, Proje No: TBAG 341, İstanbul.
- Şaroğlu, F., Boray, A., Emre, M. 1987. Türkiye'nin Diri Fayları, General Directorate of mineral and Exploration Rapor No: 8643, 394s. Ankara (unpublished).
- Şaroğlu, F., Emre, E., Kuşçu, İ. 1992b. The East Anatolian fault zone of Turkey. *Annalae. Tectonicae*, 6, 99-125.
- Şengör, A.M.C., Yılmaz, Y. 1981. Tethyan evolution of Turkey: A plate tectonic approach. *Tectonophysics*, 75, p.181-241.
- Şengör, A.M.C., Görür, N., Şaroğlu, F. 1985. Strike slip faulting and related basin formation in zones of tectonic escape; Turkey as a case study. Biddle K.T., Christie-Blick N. (Eds.). *Strike-slip Deformation, Basin Formation and Sedimentation*. Society of Economic Paleontologists and Mineralogists, Special Publications, 37, 227-264.
- Tan, O., Tapırdamaz, M. C., Yörüük, A. 2008. The earthquake catalogues for Turkey. *Turkish Journal of Earth Sciences*, 17, 405-418.
- Trifunac, M.D. 1976. Preliminary analysis of the peaks of strong earthquake ground motion-dependence of peaks on earthquake magnitude, epicentral distance and recording site conditions. *Bulletin .Seismological Society of America* 66, 189-219.
- Trifunac, M.D., Brady A.G. 1975. On the correlation of seismic intensity scales with the peaks of recorded strong ground motion. *Bulletin .Seismological Society of America* vol. 65, No 1 pp 139-162
- Wald, D.J., Quitoriano, V., Heaton, T.H., Kanamori, H. 1999. Relationship between Peak Ground Acceleration, Peak Ground Velocity and Modified Mercalli Intensity in California. *Earthquake Spectra*, Volume 15, No: 3.
- Watabe, M. 1977. Digitized of strong-motion earthquake accelerograms in Romania. Romania Central Institute for Research, Design and Guidance in Building, March 4, 1977 Japan.
- Wells, D.L., Coppersmith, K.J. 1994. New Empirical Relationships among Magnitude, Rupture Length, Rupture Width, Rupture Area and Surface Displacement. *Bulletin .Seismological Society of America*, Vol: 84, No: 4, pp 974-1002.
- Westaway, R. 2003. Kinematics of the Middle East and Eastern Mediterranean Updated, *Turkish Journal of Earth Science* 12, 5-46.
- Westaway, R., Arger J. 1996. The Gölbaşı Basin, Southeastern Turkey: A Complex Discontinuity in a Major Strike-Slip Fault Zone. *Journal of the Geological Society* 153, 729-744.
- Westaway, R., Demir, T., Seyrek, A., Beck, A. 2006. Kinematics of Active Left lateral Faulting in SE Turkey from Offset Pleistocene River Gorges: Improved Constraint on the Rate and History of Relative Motion between the Turkish and Arabian Plates. *Journal of the Geological Society of London* 163, 149-164.
- Yüksel, Ö. 2009. Gölbaşı (Adıyaman) Dolayında Doğu Anadolu Fay Sistemi'nin Paleosismisitesi ve Zeminlerin Değerlendirilmesi. Master of Thesis, Çukurova University, Institute of Applied Science, 117s, Adana (unpublished).



# Bulletin of the Mineral Research and Exploration

<http://bulletin.mta.gov.tr>



## DETERMINATION OF HYDROLOGIC CHARACTERISTICS OF SİNOP DEMİRCİKÖY WATERSHED AND PRODUCTION OF MONTHLY SATURATION DEGREE MAPS

Mustafa Can CANOĞLU<sup>a\*</sup>

<sup>a</sup> Sinop University, Faculty of Engineering and Architecture, Environmental Engineering Department Osmaniye Village, Nasuhbaşoğlu District, 57000, Sinop/TURKEY. orcid :0000-0003-4028-0046

Research Article

### Keywords:

Sinop City, Demirciköy Watershed, GIS, SMDR model, Saturation degree.

### ABSTRACT

The aim of this study is to determine the hydrologic characteristics and to analyze the temporal saturation degree variations of Demirciköy Watershed which is located in Sinop City and subjected to rapidly increasing population. This study is important in terms of preventing the natural disasters such as flood, storm water, landslide and mitigation of damages within the frame of watershed planning concept. This study consists of field, office and laboratory stages. In context of field studies, representative soil samples are taken from study area. Within the scope of laboratory studies, soil hydrologic properties are characterized with the determination of soil texture of the soil samples handled from study area. The results of the laboratory tests are utilized as part of office studies with the use of the Soil Moisture Distribution and Routing (SMDR) model in Geographic Information Systems (GIS) environment considering the meteorological data such as precipitation, temperature and evapotranspiration. Spatial and temporal variation of saturation degree in Demirciköy Watershed is determined with SMDR model. The obtained monthly saturation degree maps show the variation of soil moisture in a year and allow determining the potential runoff generation zones. The results of the study show that soil moisture in South part of watershed is lower than in North part.

Received Date: 10.08.2016

Accepted Date: 07.11.2016

## 1. Introduction

In Turkey, cities are enlarging based on the rapidly increasing population and rural areas get involved in city boundaries. Population of Sinop city increased in a short span of time in connection with the touristic benefits, new constructed highways and continuously developing university. Under the circumstances, the needs of increasing urbanization should be satisfied. Watershed planning have a great importance on the prediction of natural disasters such as flood, landslide etc. as well as the water demand. For this reason, it is important to determine the hydrologic characteristics of Demirciköy Watershed, located in Sinop City which enlarge unrestrainedly trough the Southwest.

Geographical Information Systems (GIS) are utilized by many researchers in watershed planning and hydrogeological investigations in Turkey (Kurtuluş, 2012; Kurtuluş and Flipo, 2012; Kurtuluş

and Razack, 2010; Canoğlu, 2015). Furthermore, the SMDR model which is based on GIS is also used by several researchers in hydrological modelling of unsaturated zone (Easton et al., 2007; Alwis et al., 2007; Campos et al., 2008; Rao et al., 2009; Frey et al., 2009; Canoğlu, 2017).

Hydrologic conditions of Demirciköy Watershed which is located in southeast of Sinop city are modeled spatio-temporally by use of SMDR model and water content variations of vadose zone are determined. This study consists of office works, field works and laboratory works. Within office studies, literature review, the data collection about Demirciköy Watershed, thematic map production by GIS, processing SMDR model and evaluation of obtained results are performed. Field works include observations on landslides and soil sampling from 10 representative points (Figure 1). Basic soil mechanics tests are performed on the samples in context of

\* Corresponding author: Mustafa Can CANOĞLU, e-mail: mccanoglu@sinop.edu.tr  
<http://dx.doi.org/10.19111/bulletinofmre.336469>

laboratory works and the results of these tests are utilized as input data of SMDR model.

The monthly mean moisture content maps obtained from SMDR model provide the opportunity of determination of potential runoff productive areas in Demirciköy Watershed during a year. In this way, critical locations which can produce natural disasters such as landslide, flood etc. are determined by modeling and possible solutions are suggested.

### 1.1. General Characteristics of Study Area

Study area is located in north of Turkey, Karadeniz region. The climate is typical Karadeniz climate with hot-damp summers and cold-rainy winters (Atalay, 1997). Karadeniz region is the most rain receiving geographic region. Snowfall can be occurred rarely and severe between December and March. A number of landslide events have been recorded due to the severe and unstable rainfall and snowfall in Sinop city and it the surrounding area (Ertek et al., 1993; Işık et al., 2004; Özdemir, 2005, 2007; Canoğlu, 2017). The residential areas in Sinop city are shifted through the Demirciköy Watershed. Demirciköy Watershed delineation is determined by ArcGIS 10.0 software. It covers an area of 8,71 km<sup>2</sup> and is located 11,2 km southwest of Sinop City center (Figure 1).

## 2. Geological Setting of Study Area and Surrounding

Sinop tectonic basin represents sedimentary units which is subsided between Lias – Quaternary period (Gedik et al., 1984; Gedik and Korkmaz, 1984). Geological formations of the basin are generally discordant within each other.

Stratigraphy of Sinop starts with Boyabat metamorphites as substratum. Outcrops of metamorphic rock units are observed extensively in south and west zones of Boyabat – Durağan and Saraydüzü district. These units are formed by metamorphism of schist facies with high pressure and temperature in a large period of time (Çellek, 2013).

Jurassic aged Akgöl and Bürnük formations overlap Boyabat metamorphics. Akgöl formation is formed by sandstone, siltstone and shale intercalations and Bürnük formation is formed only by gravelstone. The limestone within the lower Cretaceous aged İnaltı formation overlaps Jurassic aged units discordantly. Çağlayan formation formed by the marl, shale, sandstone and limestone covers İnaltı formation concordantly. Paleocene aged Akveren formation which is formed by limestone, shale, marl and mudstone overlaps all these units discordantly. In this region Eocene aged limestone, sandstone, marl and gravelstone can be also observed. Miocene aged Sinop

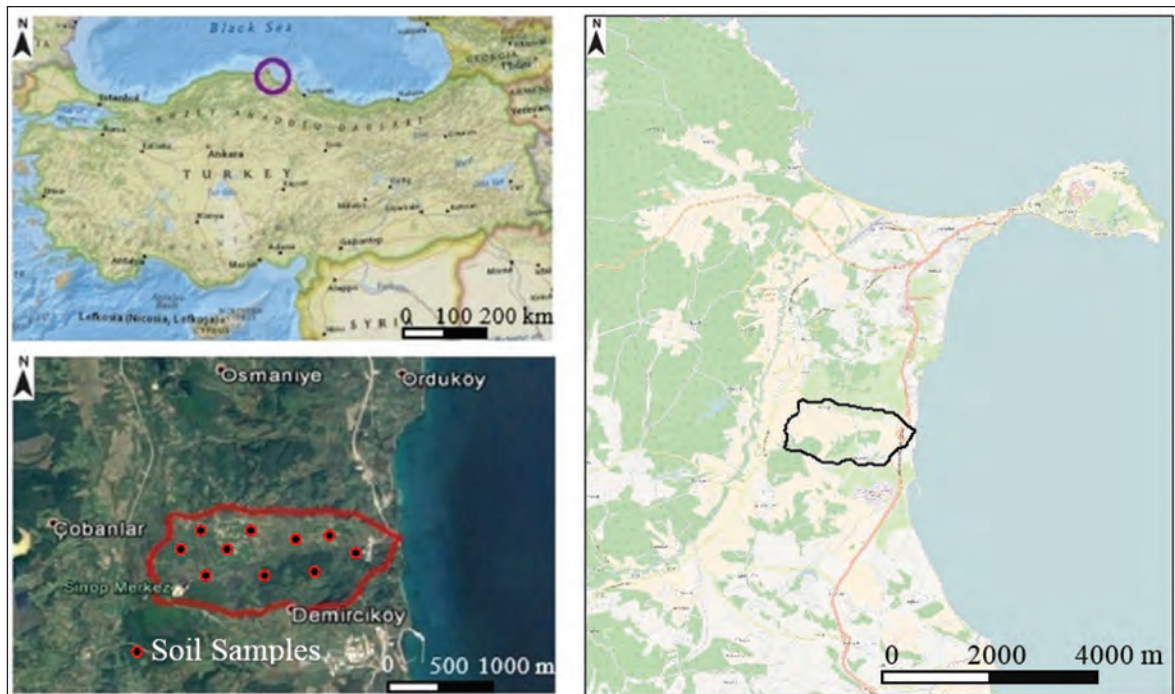


Figure 1- Location map of study area.

formation is formed by sandstone, limestone and marl and Plio-Quaternary aged Sarıkum formation is formed by sandstone, gravel and sand. Finally, alluvium covers all these units discordantly (modified from Çellek, 2013).

In Demirciköy watershed weathering products of Miocene aged Sinop formation formed by sandstone, limestone and marl units are observed (Figure 2). Sandstones and marls crop out in the watershed. Apart from these, 6 landslides are recorded within the weathered units of Sinop formation.

### 3. Material and Methods

The SMDR model (Soil and Water Lab., 2003) is employed in order to model the water flux of the vadose zone and to specify the potential runoff generating areas in Demirciköy Watershed. The SMDR model is created for the determination of spatio-temporal characteristics of variable source areas. This approach is developed for the soils which have vegetational

activities, gentle slope and high infiltration capacity. Different watersheds can be modeled by the modular structure of the model. According to Gerard-Marchant et al. (2006) no calibration need of the model and already present electronic input data are the important advantages.

#### 3.1 Structure of SMDR Model

The Soil Moisture Distribution and Routing (SMDR) model is based on a water balance and hydrologic model for soils within each pixel of watershed. In this model, when defining the soil hydrologic parameters, watershed is divided up to square cells (pixels) and geological, topographic and hydrologic parameters of each cell assumed as homogenous. In water mass balance calculation, water incomes to a cell are daily precipitation and lateral flow from upslope cell. As for water outputs, lateral outflow to downslope cells, percolation and evapotranspiration are considered (Figure 3).

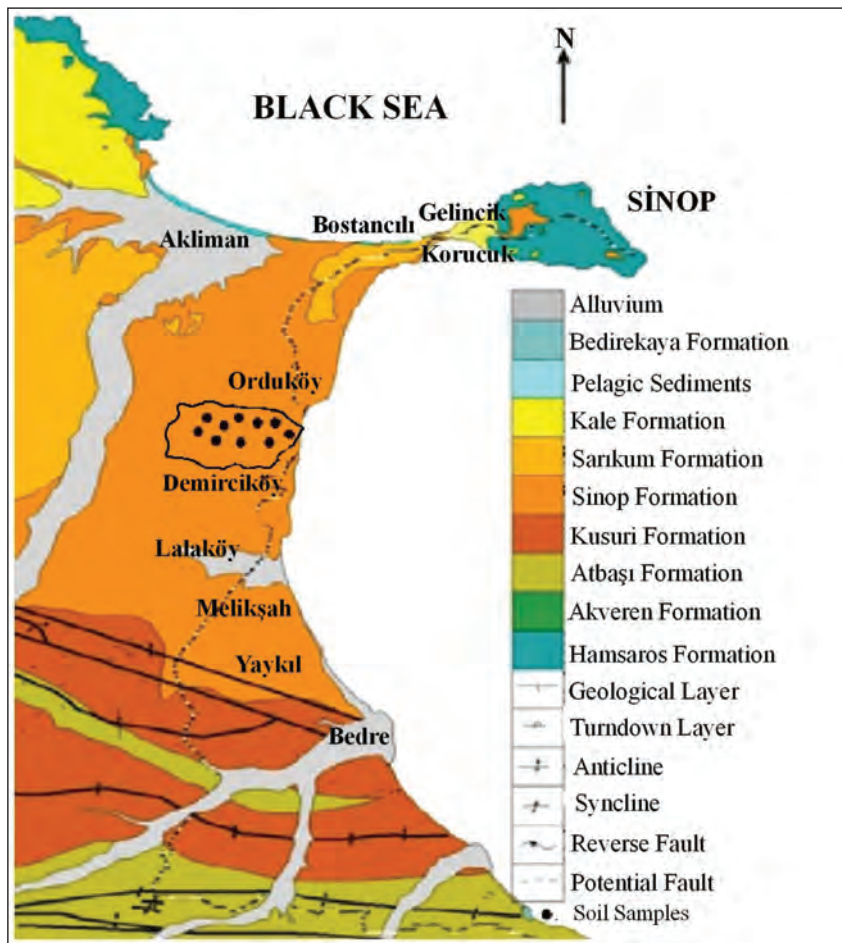


Figure 2- General geology map of the study area and its near environ (modified from Çellek, 2013).

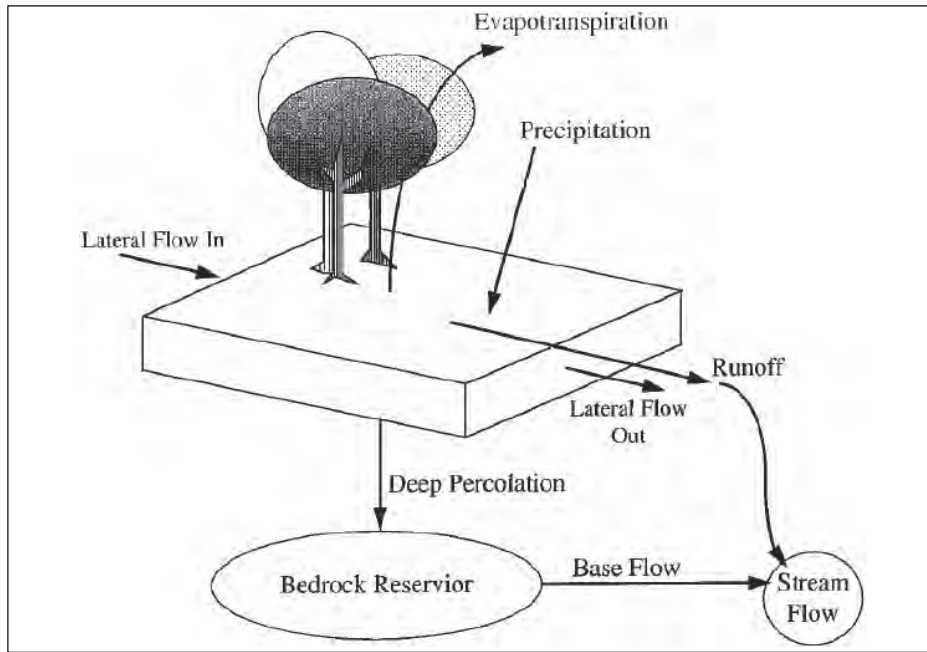


Figure 3- Hydrological processes of a cell used in SMDR model (Modified from Frankenberger et. al., 1999).

Water mass balance equation calculated for each cell from SMDR model is given below;

$$W^2 / \Theta(t) - \Theta(t - \Delta t) = |RF(t) + SM(t)| + Qi(t) - Qo(t) - ET(t) - P(t) - SE(t) \text{ (equation 1)}$$

In this equation,  $W$  is cell size of a square cell (m),  $\Theta$  is mean moisture content ( $\text{cm}^3.\text{cm}^{-3}$ ),  $\Delta t$  is time interval (day),  $RF$  is rainfall (volume),  $SM$  is snowmelt (volume),  $Qi$  is water income from upslope cell (volume),  $Qo$  is water output to downslope cell (volume),  $ET$  is evapotranspiration (volume),  $P$  is percolation (volume),  $SE$  is saturation excess runoff (volume). In equation 1 soil thickness is considered as 1m and unit of volume is  $\text{m}^3$ .

In SMDR model, the defined meteorological information is assumed as the same for each pixels. In the model, effect of the local elevation variations on daily mean temperature is corrected by adiabatic deviation ratio ( $6,5 \times 10^{-3}$ ) (Boll et al., 1988). If daily mean temperature is lower than 0 C, the model assumes that it snows and no snowmelt occurs until the daily mean temperature becomes more than  $0^\circ\text{C}$ . The snowmelt  $SM$  in SMDR model is calculated by the temperature index method proposed by US Army Corps of Engineers (1960).

The underground lateral flow is calculated by Darcy's law. Water output ( $Qo$ ) expressed with the

equation 2 is calculated with the assumption that the local slope is equal to hydraulic gradient. In other words, hydraulic gradient can be interpreted as the angle between the horizontal of each cell. This assumption is not completely correct with regard to Darcy's law but the SMDR model represents unsaturated soil conditions and Richard's equation is utilized in the model instead of Darcy equation. For this reason, using local slope in lieu of hydraulic gradient gives real-like results.

$$Q_o = -\kappa K(\theta) W \beta \Delta t \text{ (equation 2)}$$

In this equation  $K$  is the mean hydraulic conductivity of the cell ( $\text{m}.\text{day}^{-1}$ ).  $\kappa$  is a factor dependent of cell depth (it changes typically between 2 and 10) employed for the transmissivity correction for the macroporosity inflow (Boll et. al., 1998). Hydraulic conductivity of the unsaturated zone in the model is determined as follow:

$$\begin{aligned} \theta < \theta_f & \text{ for } K(\theta) = 0 \\ \theta_f \leq \theta < \theta_m & \text{ for } K(\theta) = K_s \exp \alpha \frac{(\theta - \theta_f)}{(\theta_m - \theta_f)} \\ \theta_m \leq \theta & \text{ for } K(\theta) = K_m + K_s \frac{(\theta - \theta_m)}{(\theta_m - \theta_m)} \end{aligned} \text{ (equation 3)}$$

In this equation,  $\theta_f$ ,  $\theta_m$ ,  $\theta_s$  are field capacity, macropore drainage limit and saturated moisture content respectively. In addition,  $K_s = K(\theta_s)$  and  $K_m = K(\theta_m)$  are hydraulic conductivity for saturated

conditions and for moisture content of macropore drainage limit. The parameter  $\alpha$  shown in the equation 3 is a universal constant specified as 13 for many soil types (Bresler et al., 1978; Steenhuis and van der Molen, 1986). Distribution of the lateral outflow from a cell is determined by  $D^\infty$  algorithm (Tarboton, 1997).

In SMDR model calculation of evapotranspiration is realized based on the method proposed by Thornthwaite and Mather (1957) in which the potential evapotranspiration, moisture content of soil and vegetation cover are considered. Percolation is expressed by the equation below:

$$P = \min[K(\theta); K_{sub}]W^2 \Delta t \quad (\text{equation 4})$$

In equation 4  $K_{sub}$  is the hydraulic conductivity of the unit under the cell ( $\text{m.day}^{-1}$ ).

In SMDR model, if the mean moisture content of a cell is lower than field capacity, percolation stops. The saturation excess water at the end of the time interval is added to runoff component.

### 3.2 Parametrization and Input Data of SMDR Model

The SMDR model utilizes two types input data, such as raster maps and tables. Raster maps are digital elevation model, watershed boundary map, soil type map, aspect map and vegetative characteristics map. And tables are soil characteristics table, vegetation characteristics table and meteorological data table.

Digital elevation map is obtained from digitizing of the E34-a1 named 1:25,000 scale topographic map (National Mapping Agency, 1993) (Figure 4a). Watershed boundary and aspect maps are reproduced from digital elevation model with the use of ArcGIS 10.0 (ESRI, 2010) (Figure 4b). In SMDR model, geological, topographic and hydrologic parameters are assumed homogenous for each cell, for this reason cell sizes are set to the minimum possible. All maps prepared as input data for SMDR model have 10m x 10m horizontal resolution. In addition, in some ancient cell based models it is revealed that, enlarging the cell size, decreases the resolution of the curvilinearity and soil moisture content and evapotranspiration rate cannot be correctly represented (Kuo et al., 1999).

Vegetative cover map and vegetation characteristics table are generated based on the information gathered from Sinop City Regional Directorate of Forestry. As for the soil characteristics table, the sieve analysis and hydrometer tests are performed on the soil samples handled from Demirciköy Watershed according to ASTM D-422-63 standards. Soil texture of the samples is specified based on the grain size distributions (Figure 5) and USDA (United States Department of Agriculture) soil texture classification system (Figure 6). Thereafter, soil characteristics table is generated as an input data of the SMDR model with the use of the soil hydrologic properties index table which base the soil texture proposed by Rawls and Brakensiek (1982, 1985) (Table 1). This soil characteristics table

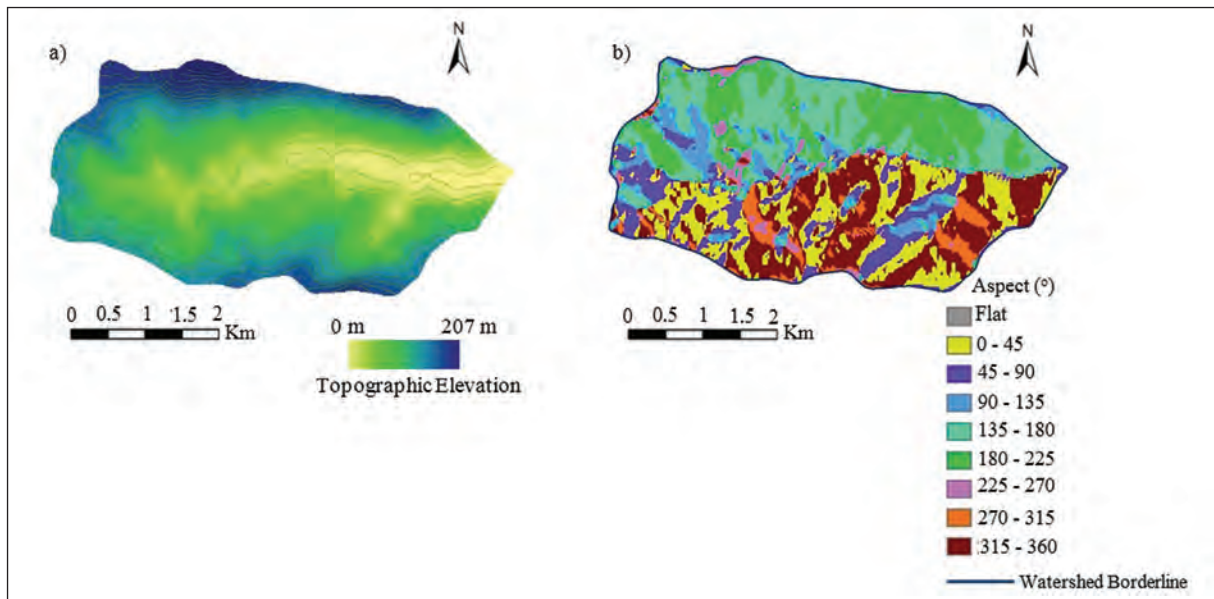


Figure 4- Digital elevation model map (a), aspect map and the watershed boundary (b).

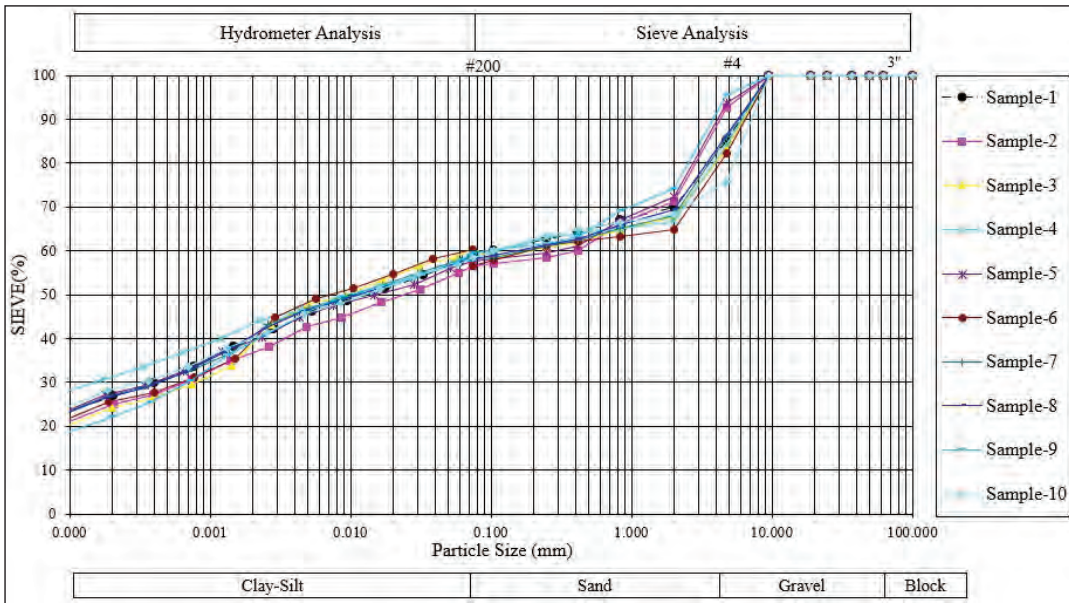


Figure 5- Grain size distributions of soil samples handled from study area.

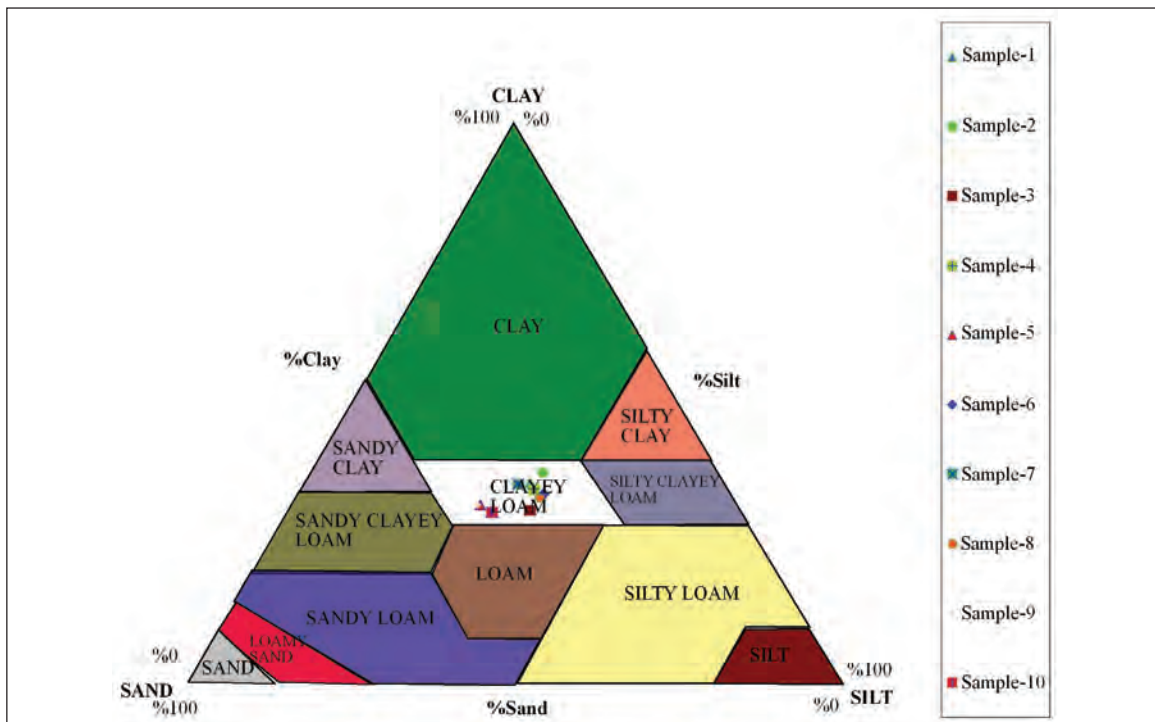


Figure 6- Textural classification of soil samples handled from the study area based on USDA soil texture classification system.

generating method is also proposed by Soil and Water Lab. (2003) in user manual of SMDR model.

As can be seen in figures 5 and 6, the soil material within Demirciköy Watershed is “clayey loam” according to USDA soil texture classification system and represented in only one textural class. Due to the domination of a monotype soil texture in

Demirciköy Watershed, soil characteristics map is homogenous and represents only one soil type. Soil hydrologic properties of clayey loam are given in soil hydrologic properties index table proposed by Rawls and Brakensiek (1982, 1985) (Table 1).

As for meteorological data are obtained from General Directorate of Meteorological Affairs Sinop

Table 1- Soil hydrologic properties index table based on soil texture

Textural Class	Porosity (cm <sup>3</sup> /cm <sup>3</sup> )	Residual water content (%)	Wilting point (%)	Field capacity (%)	Water content at saturation (%)	Maximum available water content (%)	K <sub>sat</sub> vertical (mm/d)
Clayey Loam	46,4	7,5	19,7	31,8	39	31,5	48

Station (MGM, 2010). These daily meteorological data are handled between the years 1975 – 2010 are monthly mean precipitation, daily temperature and monthly mean potential evapotranspiration and these data is prepared as an input data of SMDR model (Table 2). The SMDR model is run on a daily time step and the obtained daily saturation degree maps are transformed to monthly saturation degree maps by ArcGIS 10.0 software.

Table 2- Monthly meteorological data of Sinop city (1975-2010 General Directorate of Meteorological Affairs)

	Monthly Mean Precipitation (mm)	Monthly Mean Daily Temperature (C°)	Monthly Mean Potential Evapotranspiration (mm)
January	71,2	7	0
February	49,2	6	0
March	49,3	7	0
April	37,7	11	16
May	33,1	15	24
June	35,3	20	29
July	36,3	23	37
August	42,2	23	27
September	66,0	20	22
October	91,4	16	14
November	87,3	12	0
December	82,3	9	0
Yearly	681,3	14	169

#### 4. Results and Discussion

The Soil texture of each soil sample handled from the field is specified based on the sieve analysis. Hydrologic properties of soil sample are determined according to in soil hydrologic properties index table proposed by Rawls and Brakensiek (1982, 1985). Thereafter, water balance elements are modelled with the use of SMDR model considering the processes schematized in figure 3 and monthly saturation degree maps of Demirciköy Watershed are generated (Figure 7). In this way, the variations of saturation excess runoff generating areas are determined during a year.

Following results and conclusions can be deduced from this study:

- The soil structure is homogenous within the watershed and specified as clayey loam according to USDA soil texture classification system. In this context, there is no spatial variation of the soil hydrologic properties within the watershed.
- The saturation degree of north faced hillsides are fewer (Figure 7). This shows that the effect of solar radiation on evaporation is not very crucial and saturation degree is not decreased importantly by solar radiation. In addition, the expression such as the moisture in the air is splashed on north faced hillsides utilized generally for Blacksea Region does not reflect the reality. However, considering the low saturation degree in botanically active regions, the effect of evapotranspiration on the saturation degree can be remarked. Under these circumstances, it can be drawn that transpiration is more effective than evaporation in terms of saturation degree.
- The saturation degree in May and August are generally low within the watershed. Evapotranspiration effect in May and high daily mean temperatures for August can decrease the saturation degree. In addition, it is observed that saturation degree is locally low for March, October, November and December. However, for these months the saturation degree of some pixels decreases, in some of them increases and becomes nearly saturated.
- The saturation degree in June and September are higher than other months. It can be said that high precipitation and water income from the upslope pixels augment the moisture content. Besides, the saturation degree values in January, April and July are also high as a result of high precipitation during subjected months and relatively decreasing evapotranspiration.

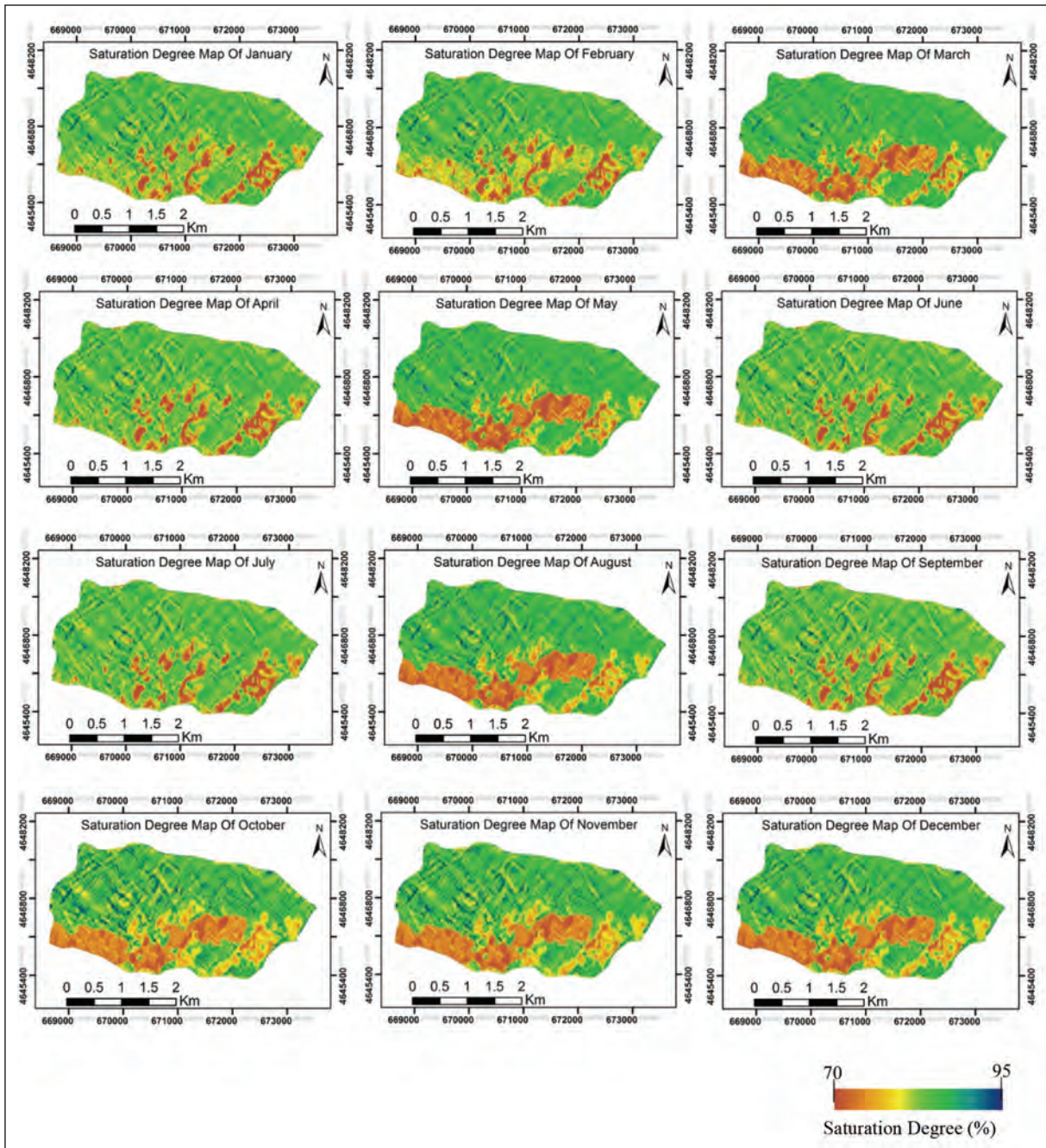


Figure 7- Monthly saturation degree variations of Demirciköy Watershed.

– The high potential of saturation excess runoff generation for south faced hillsides does not mean that these hillsides produce flood and overflows. The reason is that the floods and overflows cannot be explained by saturation excess runoff concept but the infiltration excess runoff mechanisms may sort out this situation. For the infiltration excess runoff initiation, rainfall intensity should be more than infiltration capacity of soil.

– There is no any pixel that reaches saturation and generates runoff in Demirciköy Watershed, modeled with the monthly mean meteorological data. Therewithal, it can be inferred that the pixels giving more than 90% moisture content have the potential of runoff generation with the increasing rainfall intensity especially for June which is higher saturation degree than other months (Figure 8). Additionally, some landslides are observed in the zones concentrated with

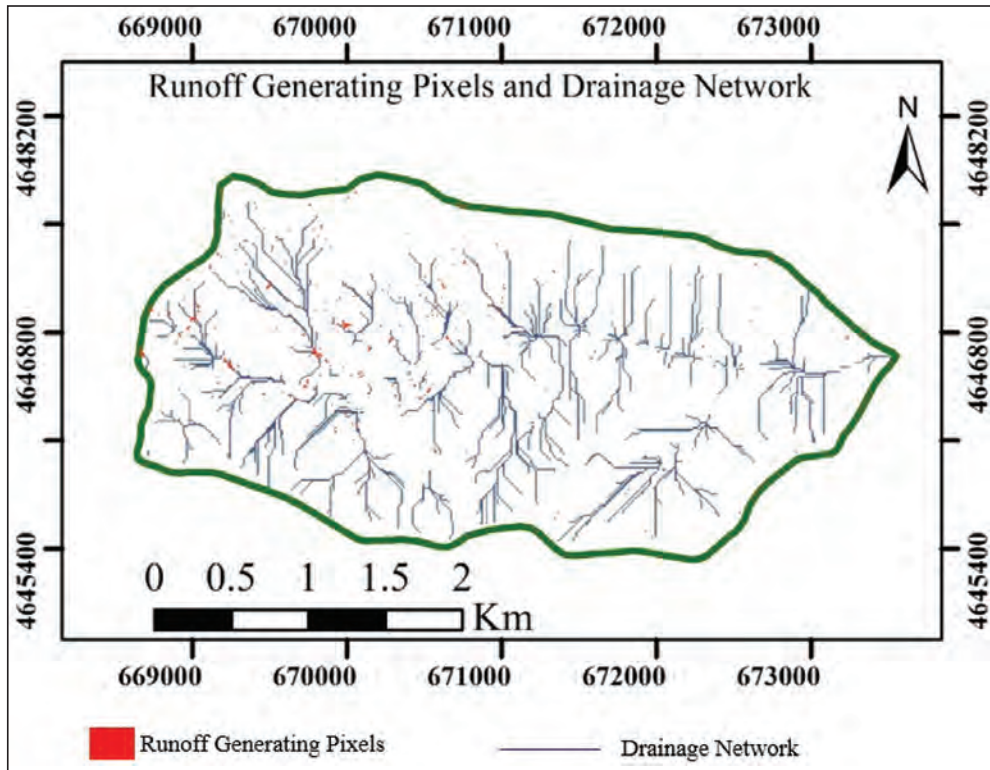


Figure 8- Potential runoff generating pixels map of June and Drainage network

these pixels. Comparison of the zones with a high degree of soil saturation with areas subject to landslide processes may be treated as the perspective of future research works.

- Finally, application of this method is simple and expeditious for the countries which have a soil characteristics database (such as SSURGO). However, application of this method in Turkey requires funding and takes time due to the absence of soil characteristics database.

### Acknowledgements

Author thanks to “SuYapı Engineering and Consulting Co.” family especially to direction for funding and their experience share in terms of scientific support. In addition, author thanks to Regional Directory of Forestry in Sinop and General Directorate of Meteorological Affairs for data share.

### References

- De Alwis, D. A., Easton, Z. M., Dahlke, H. E., Philpot, W. D., Steenhuis, T. S. 2007. Hydrology and Earth System Sciences Unsupervised classification of saturated areas using a time series of remotely sensed images. *Hydrology and Earth System Science*, 11,1609–1620.
- Atalay, İ., 1997. Türkiye Coğrafyası, Ege Üniversitesi Basımevi, ISBN 975-95527-5-2, Bornova, İzmir.
- Boll, J., Brooks, E.S., Campbell, C.R., Stockle, C.O., Young, S.K., Hammel, J.E., McDaniel, P.A. 1998. Progress toward development of a GIS based water quality management tool for small rural watersheds: modification and application of a distributed model. U.S. Army Corps of Engineers, 1960, Engineering and Design: Runoff from Snowmelt. EM 1110-2-1406.
- Bresler, E., Russo, D., and Miller, R. D. 1978. Rapid estimate of unsaturated hydraulic conductivity function, *Soil Science Society of America Journal*, 42, 170–177.
- Campos, I., Coterillo, I., Marco, J. 2008. Modelling of a watershed: A distributed parallel application in a Grid Framework, *Computing and Informatics*, 27, 285–296.
- Canoğlu, M.C. 2015. An Investigation On The Surface Water Effect In Landslide Susceptibility Mapping: An Example From Yenice (Karabük) Basin. PhD thesis, Hacettepe University.
- Canoğlu, M.C. 2017. Deterministic landslide susceptibility assessment with the use of a new index (Factor of Safety Index) under dynamic soil saturation: an example from Demirciköy Watershed, *Carpathian Journal of Earth and Environmental Sciences*, 12 (2), 423-436.

- Çellek, S. 2007. Gerze (Sinop) yöresindeki aktif heyelan alanlarının mühendislik jeolojisi açısından incelenmesi. Karadeniz Teknik Üniversitesi Fen Bilimleri Enstitüsü, Yüksek Lisans Tezi, 114s.
- Çellek, S. 2013. Sinop-Gerze yöresinin heyelan duyarlılık analizi. Karadeniz Teknik Üniversitesi Fen Bilimleri Enstitüsü, Doktora Tezi, 309s.
- Easton, Z. M., Gérard-Marchant, P., Walter, M. T., Petrovic, A. M., Steenhuis, T. S. 2007. Hydrologic assessment of an urban variable source watershed in the northeast United States, *Water Resources Research*, 43.
- Ertek, T. A., Turoğlu, H., Mater, B. 1993. Çiftlik Heyelanı (Sinop). *Türk Coğrafya Kurumu Dergisi*, 181-188.
- ESRI, Environmental Systems Research Institute, ArcGIS 10.0 software. 2010.
- Frankenberger, J., Brooks, E., Walter, M., Steenhuis, T. 1999. A GIS-based variable source area hydrology model, *Hydrological Processes*, 13, 805–822.
- Frey, M. P., Schneider, M. K., Dietzel, A., Reichert, P., Stamm, C. 2009. Predicting critical source areas for diffuse herbicide losses to surface waters: Role of connectivity and boundary conditions, *Journal of Hydrology*, 365, 23–26.
- Gedik, A., Korkmaz, S. 1984. Sinop Havzasının Jeolojisi ve Petrol Olanakları, TMMOB Jeoloji Mühendisleri Odası Yayınları, MTA Derleme No. 7575, *Jeoloji Mühendisliği Dergisi*, 19, 53-79.
- Gedik A., Ercan T., Korkmaz S. 1984. Orta Karadeniz (Samsun-Sinop) Havzasının Jeolojisi ve Volkanik Kayaçların Petrolojisi, *MTA Dergisi*, 99, 34-50.
- Gerard-Marchant, P., Hively, W. D., Steenhuis, T. S. 2006. Distributed hydrological modeling of total dissolved phosphorus transport in an agricultural landscape, part I: distributed runoff generation, *Hydrology and Earth System Science*, 10, 245–261.
- Harita Genel Komutanlığı. 1993. Sinop - E34-a1 pafta numaralı 1/25.000 ölçekli topoğrafik haritası.
- Işık, N. S., Doyuran, V., Ulusay, R. 2004. Assessment of coastal landslide subjected to building loads at Sinop, Black Sea region, Turkey, and stabilization measures. *Engineering Geology*, 75, 69-88.
- Kuo, W. L., Steenhuis, T., McCulloch, C., Mohler, C., Weinstein, D., DeGloria, S., Swaney, D. 1999. Effect of grid size on runoff and soil moisture for a variable-source-area hydrology model, *Water Resources Research*, 35, 3419–3428.
- Kurtuluş, B. 2012. High Resolution Numerical Modelling of SO<sub>2</sub> Emission: A Power Plant Case Study. *Building Simulation*, 5, 135-146.
- Kurtuluş, B., Razack, M. 2010. Modeling daily discharge of a large karstic aquifer using soft computing methods: Artificial neural network and neuro-fuzzy. *Journal of Hydrology*, 381, 1-2, 101-111.
- Kurtuluş, B., Flipo, N. 2012. Hydraulic head interpolation using ANFIS—model selection and sensitivity analysis. *Computers and Geosciences*, 38, 43–51.
- MGM. 2010. Meteoroloji İşleri Genel Müdürlüğü 1975-2010 yılları arası Sinop ili aylık meteoroloji verileri.
- Özdemir, N. 2005. Sinop ilinde etkili bir doğal afet türü heyelan. *D.Ü. Ziya Gökalp Eğitim Fakültesi Dergisi*, 5, 67-106.
- Rawls, W. J., Brakensiek, D. L., Saxton, K.E. 1982. Estimation of soil water properties. *Transactions of the American Society of Agricultural Engineers*, 25, 1316-1328.
- Rawls, W., Brakensiek, D. 1985. Prediction of soil water properties for hydrologic modeling. *Watershed Management in the Eighties*, 293–299.
- Rao, N.S., Easton, Z.M., Schneiderman, E. M., Zion, M.S., Lee, D. R., Steenhuis, T. S. 2009. Modeling watershed-scale effectiveness of agricultural best management practices to reduce phosphorus loading, *Journal of Environmental Management*, 90, 1385–1395.
- Soil and Water Laboratory. 2003. SMDR – The Soil Moisture Distribution and Routing model, version 2.0 – documentation, Department of Biological and Environmental Engineering, Cornell University, Ithaca, New York.
- Steenhuis, T., W. Van der Molen. 1986. The Thornthwaite-Mather method procedure as a simple engineering method to predict recharge, *Journal of Hydrology*, 84, 221–229.
- Tarboton, D. 1997. A new method for the determination of flow directions and upslope areas in grid digitale elevation models, *Water Resources Research*, 33, 309–319.
- Thornthwaite, C.W., Mather, J.R. 1957. Instructions and tables for computing potential evapotranspiration and the water balance. Publication in *Climatology*, 10, 185-311.
- US Army Corps of Engineers. 1960. Engineering and design: Runoff from snowmelt, Tech. Rep. EM 1110-2-1406, U.S. Army Corps of Engineers, Government Printing Office, Washington, D.C.
- USDA Soil Survey Staff. 1999. Natural Resources Conservation Services, A Basic System of Soil Classification for Making and Interpreting Soil Surveys, United States Department of Agriculture, second edition.



# Bulletin of the Mineral Research and Exploration

<http://bulletin.mta.gov.tr>



## APPLICATION OF TILT ANGLE METHOD TO THE BOUGUER GRAVITY DATA OF WESTERN ANATOLIA

Fikret DOĞRU<sup>a,b</sup>, Oya PAMUKÇU<sup>b\*</sup>, and İlkin ÖZSÖZ<sup>c</sup>

<sup>a</sup>Ataturk University, Oltu Earth Sciences Faculty, Department of Geophysics, Oltu, Erzurum [orcid.org/0000-0002-6973-1157](http://orcid.org/0000-0002-6973-1157)

<sup>b</sup>Dokuz Eylül University, Engineering Faculty, Geophysical Engineering, 35160, Buca, Izmir. [orcid.org/0000-0003-3564-1919](http://orcid.org/0000-0003-3564-1919)

<sup>c</sup>Dokuz Eylül University, Engineering Faculty, Geophysical Engineering, 35160, Buca, Izmir. [orcid.org/0000-0001-5907-4176](http://orcid.org/0000-0001-5907-4176)

Research Article

### Keywords:

Tilt angle, geological structural edges, Western Anatolia, Bouguer anomaly.

### ABSTRACT

In this study, tilt angle method was applied to Western Anatolia gravity data in order to estimate edges of the geological structures. Tilt angle was obtained in two different ways by using gravity and its vertical derivative. In potential field methods, tilt angle technique is expressed as the ratio of vertical derivative to horizontal derivatives of anomaly. In the tilt angle map, 0° contours defines structure edges, half of the distance between  $\pm 45^\circ$  defines depth of upper structure. In the field work of the study, gravity data, which was measured in Western Anatolia, was used to obtain regional anomaly maps and tilt angle and tilt angle of vertical directional derivative were applied to these maps. A significant difference was observed between western and eastern parts of the N-S striking line, throughout 28° longitude, from the results of tilt angle which was obtained by applying upward continuation method (50, 75 and 100 km) to the Bouguer anomaly. Same difference was determined from the results of vertical derivative of tilt angle which was obtained from upward continuation of Bouguer anomaly. Depth values were obtained from the results of tilt angle and vertical derivative of tilt angle methods between 7 and 43 km in study area. The obtained results were compared with geological structural boundary and possible depths of geological discontinuities were estimated. In addition, obtained results were investigated with seismic activity in the study area and compared with previous geological and geophysical studies.

Received Date: 21.06.2016

Accepted Date: 02.12.2016

## 1. Introduction

The general extent of fault-controlled Neogene basins occurring in Western Anatolia since Middle Miocene is NE-SW. The fillings which deposited during the Middle Miocene in these graben basins characterize generally fluvial, deltaic and lacustrine environments around Kütahya-Uşak in the north and the lacustrine environment around Aydın-Denizli-Muğla regions in the south (Kaya, 1979; Leflef, 1980; Yılmaz, 2000). In other words, during this period fluvial systems developed roughly from north to south in many places and the lakes were located in the south and occasionally moved north. These NE-SW-trending graben basins, which contain fillings with ages reaching up to Middle Miocene to Pliocene and which are significant especially in the north of

Gediz Graben, have no genetic relationships with E-W and NW-SE stretching grabens resulting from K-G expansion (Hakyemez et al., 1999).

Extensive surfacing of the Early Quaternary fluvial sediments on the main active fault base block, which is located on the active south side of the graben, north of the main detachment fault and forming the boundary between the Holocene sediments and the Pleistocene sediments, probably indicates that the supra-detachment fault system over the fault of Gediz River basin filling axis in the late Pleistocene- early Holocene (in other words Gediz river bed) advanced towards the basin and as a result migrated towards the north (Hakyemez et al., 1999). Figure 1 shows a geology map of the study area and a map related to the location of the grabens.

\* Corresponding author: Oya PAMUKÇU, [oya.pamukcu@deu.edu.tr](mailto:oya.pamukcu@deu.edu.tr)  
<http://dx.doi.org/10.19111/bulletinmre.305177>

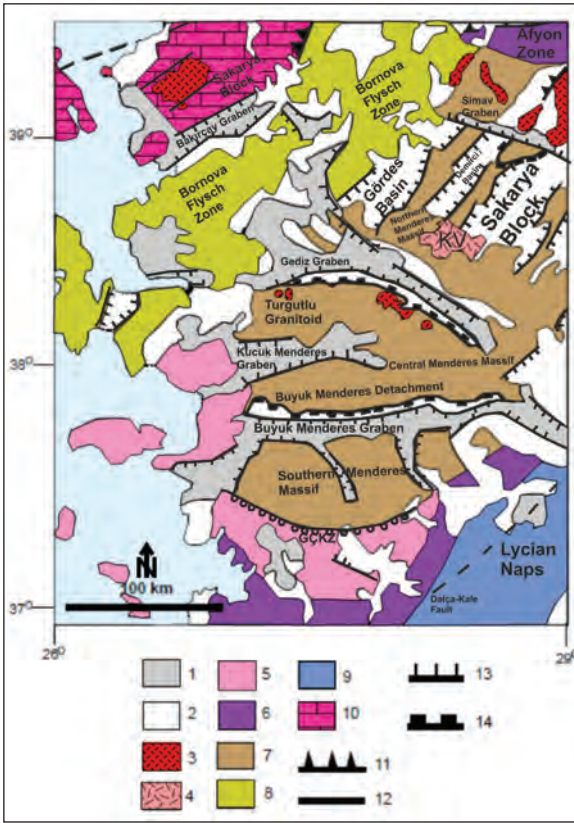


Figure 1- Geological map of Western Anatolia. Numbers are correspond to: 1: Alluvion, 2: Neogenevol-Volcano-Sedimentary Rocks, 3: Granite intrusions (Eocene-Miocene), 4: Alkaline Basalt Flow of Kula Volcanic Area (Upper Miocene-Quaternary), 5: Cycladic Complex (schist, marble, eclogite), 6: Afyon Zone metasedimanter and Pan-Afrikan basement rocks, 7: High-Grade Metamorphic Units of Menderes Core Complex (Precambrian-Senozoic), 8: Bornova Flysch and ophiolitic melange (Paleozoic-Paleocene), 9:Likya Naps and Tetis Ophiolits (Upper Cretaceous-Eocene), 10: Karakaya Complex (Permo-Trias) and Limestones (Jura-Upper Cretaceous), 11: Covergent boundary and major faults, 12: Continental minor strike slip faults, 13: Continental normal faults, 14: Detachment faults, KV: Kula Volcanites, GÇKZ: South Çine Shear Zone (It modified from Akay et al., 2013).

Determination of the boundaries of underground structures is very important in the modelling and mapping of geological structures. In geophysics, many methods are used to determine the boundaries of the anomaly-causing structure in potential methods. These methods are especially analytical signal (Roest et al., 1992), horizontal derivative, first and second vertical derivatives (Hood and Teskey, 1989; Roest et al., 1992), Euler deconvolution (Thompson, 1982; Blakely and Simpson, 1986, Pamukcu et al., 2007), Normalized Full Gradient (NFG) method (Pamukcu and Akcig, 2011), tilt angle map of vertical direction

derivative of gravity data (Oruç, 2011), which are used to reveal the boundaries of mass causing anomalies in gravity and magnetic methods. The arctangent of the ratio of the vertical derivative to the amplitude of total horizontal derivative gives the tilt angle. The comparison of tilt angle with horizontal derivative, second vertical derivative and analytical signal techniques was performed by Miller and Singh (1994). In this study, tilt angles of gravity anomaly and tilt angle values of the vertical derivative of anomaly were calculated and the results were interpreted. Tilt angle and tilt angle of the vertical derivative of anomaly methods were applied to the Bouguer gravity data of Western Anatolia and the geological structures in the area were examined.

During the field application phase of the study, tilt angle and tilt angle of vertical derivative methods were applied to the gravity data in the area where grabens in Western Anatolia are located. By using  $0^\circ$  and  $\pm 45^\circ$  contours in the tilt angle contour map, which was calculated at the end of the application, it is aimed to find possible geological structure boundaries and possible depths of the structures. Moreover, the anomalies created by the changes of the detected tilt values and the tectonic mechanisms defined in the study conducted by Gessner et al. (2013) have been compared. In Gessner et al. (2013) studies, it is seen that the region defined as Western Anatolia Transfer Zone (BATZ) is compatible with the findings obtained with the methods used in this study. In addition, the depth values found were compared with seismic activity and previous heat flux studies in the region and the results were found to be consistent.

## 2. Material and Method

The tilt angle in gravity is defined as the ratio of the vertical derivative of anomalies to the horizontal derivative. Mathematical expression of tilt angle;

$$\theta = \tan^{-1} \left( \frac{\frac{\partial^2 g_z}{\partial z^2}}{HGM} \right) \quad (1)$$

is defined as follows: Total horizontal component is defined as follows;

$$HGM = \left[ \left( \frac{\partial^2 g_z}{\partial x \partial z} \right)^2 + \left( \frac{\partial^2 g_z}{\partial y \partial z} \right)^2 \right]^{1/2} \quad (2)$$

In these equations, *HGM* shows total horizontal derivation;  $\theta$ , tilt angle;  $\frac{\partial^2 g_z}{\partial x \partial z}$ , the derivative of the Bouguer anomaly in the x direction;  $\frac{\partial^2 g_z}{\partial y \partial z}$ , the derivative of Bouguer anomaly in the y direction;  $\frac{\partial^2 g_z}{\partial z^2}$ , the derivative of Bouguer anomaly in the z direction.

The geometric meaning of the tilt angle is shown in figure 2.

An approach can be made about the depth of the source by the tilt angle contours. Tilt angle method's less sensitive to noise than other methods using higher order derivatives provides the commentator with a qualitative and quantitative perspective on the location and the depth, which is an important acquisition of the method (Akın et al., 2011).

$0^\circ$  value of the tilt angle gives the source limits. The half of the distance between the tilt angle contours ( $\pm 45^\circ$ ) gives the top depth of the structure (Salem et al., 2007; Oruç, 2011; Akın et al., 2011). The fact that the half-distance between the  $\pm 45^\circ$  contours in the gravity and magnetic tilt angle map does not show much change means that the structure depth does not show much change within itself.

### 3. Application

The study area is between  $36^\circ$  and  $40^\circ$  North latitudes,  $27^\circ$  and  $30^\circ$  East longitudes. The Bouguer gravity data collected by MTA (1979) in the studied area is overlaid on topographic data in figure 3. It is observed that the highest gravity value in the region is 90 mGal and the lowest value is -90 mGal. Figure 1 shows that the N-S stretch in the region is shown by normal faults. The grabens against N-S stretching are

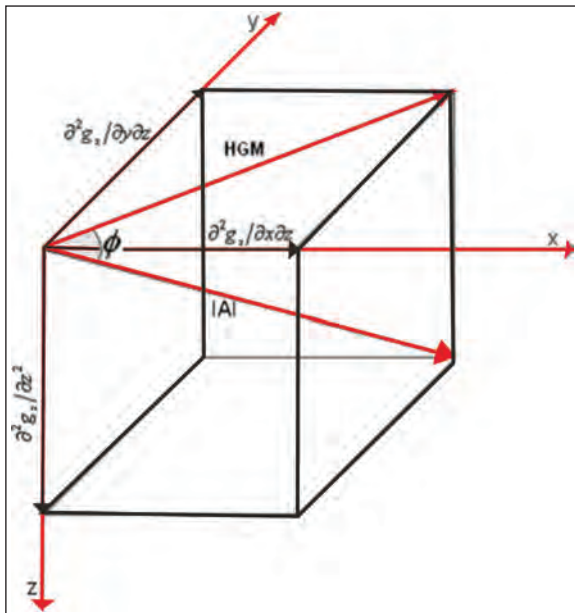


Figure 2- Geometrical representation of tilt angle for gravity method (It is modified from Oruç, 2011).

formed in E-W direction. Upwards analytical extension was applied on the Bouguer gravity anomaly of the study area and regional data were obtained (Figure 4).

The results of the tilt angle applied to figure 4 are shown in figure 5. Also, the results of the tilt angle applied after taking the vertical derivatives of figure 4 are shown in figure 6. It is observed that the results of the tilt angle method show the boundaries of the distinct geological structure in the region. The Menderes massif region in figure 1 corresponds to the low amplitude gravity anomaly seen in figure 4. The relative amplitude of anomaly rises towards the western Aegean Sea.

As mentioned earlier, half of the distance between the  $\pm 45^\circ$  contours provides information about the top depth of the structure. As a requirement of the method, the sections were selected in the places where the  $\pm 45^\circ$  contours were placed. In particular, to study the depth values in the north and south of the study area, the distances between the contours of  $\pm 45^\circ$  were determined by taking the slices using the maps in figures 5 and 6, and the obtained results are given in figures 7-8. The depths found as a result of the calculations made in the sections taken in figures 7-8, are given in table 1.

Gessner et al. (2013) suggested that a shear zone was formed as a result of the tectonic erosion formed in the Menderes Massif by the subduction zone defined in the Aegean region and Decomposition in the lithospheric mantle beneath the continent and they defined it as Western Anatolia Transfer Zone. The Western Anatolia Transfer Zone defines the lateral boundary between the Hellenide and Anatolide orogenies. The Anatolian Transfer Zone has a transtensional structure which is the result of the erosion of the Menderes Massif in Miocene with extensive lithospheric stress (Gessner et al., 2013). Figures 6c, 6d and 6e show an N-S stretch between  $27^\circ$  and  $28^\circ$  east longitudes. This structure is defined as Western Anatolia Transfer Zone (WATZ) by Gessner et al. (2013).

The tilt angle change maps are shown in in figures 6c, 6d, and 6e, which are determined in this study, and approximate boundaries of WATZ as defined by Gessner et al. (2013) are given in figure 9. According to Gessner et al. (2013), it is seen that the marked WATZ is compatible with the N-S striking structure between the  $27^\circ$  and  $28^\circ$  east longitudes in figures 9a, 9b and 9c.

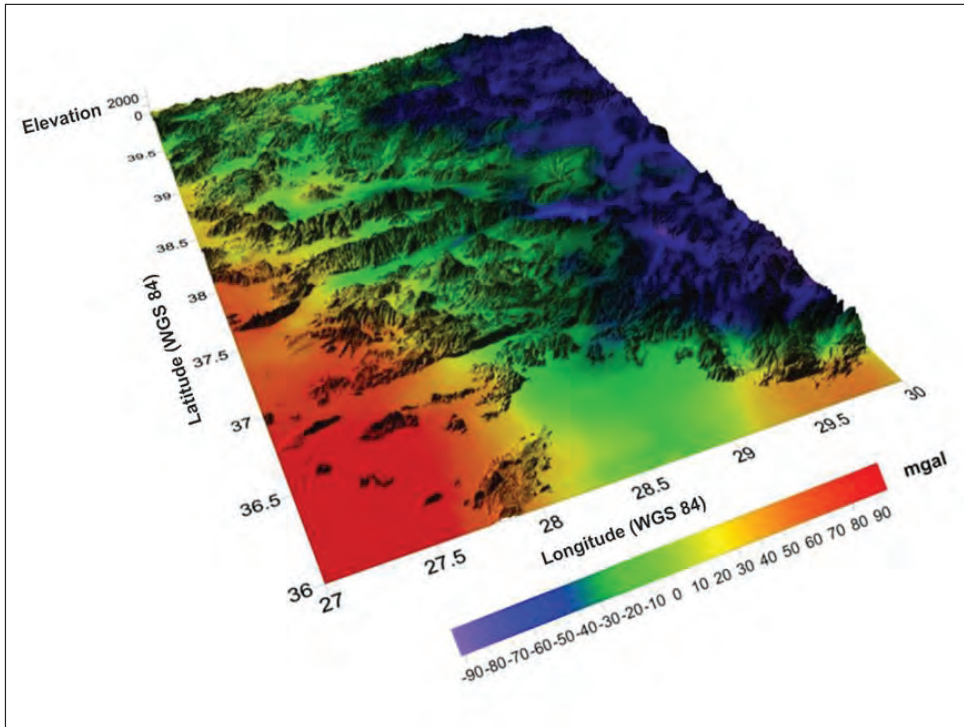


Figure 3- Bouguer gravity anomaly map illustrated on topography of study area.

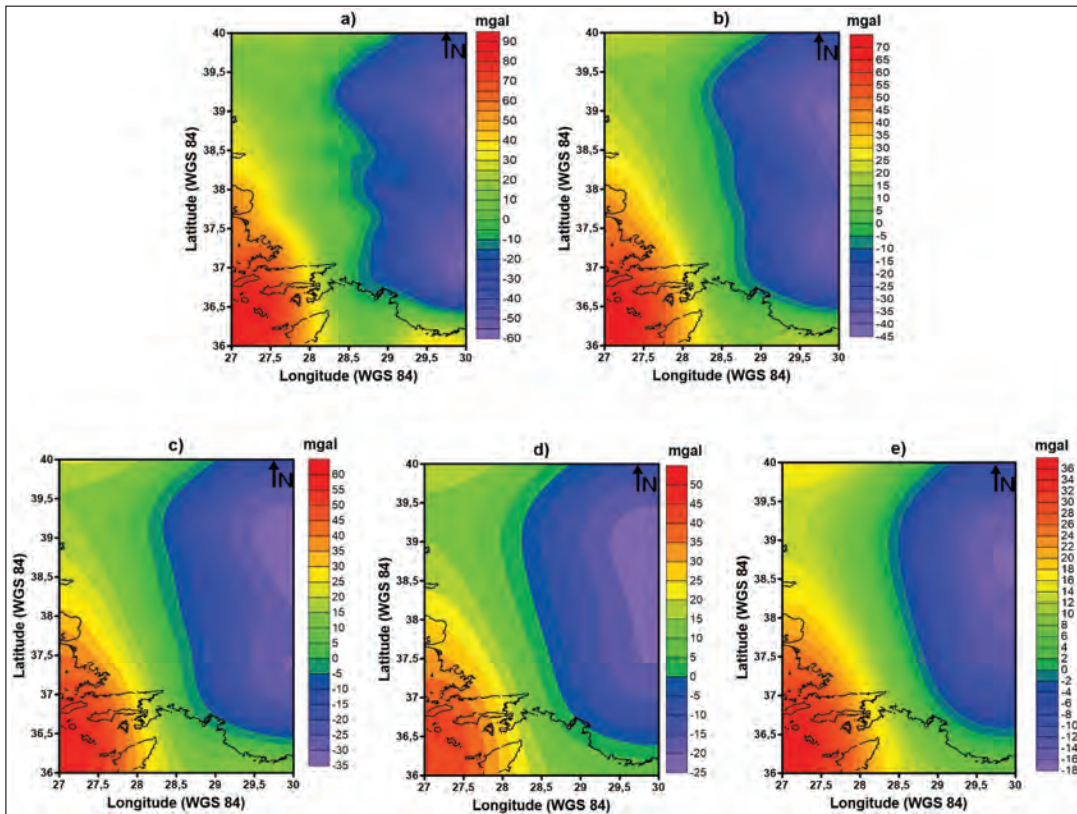


Figure 4- Regional data having different upward continuation values in study area: a) Continuation plane is 15 km, b) 35 km, c) 50 km, d) 75 km and e) 100 km (Black line illustrates coastal boundaries).

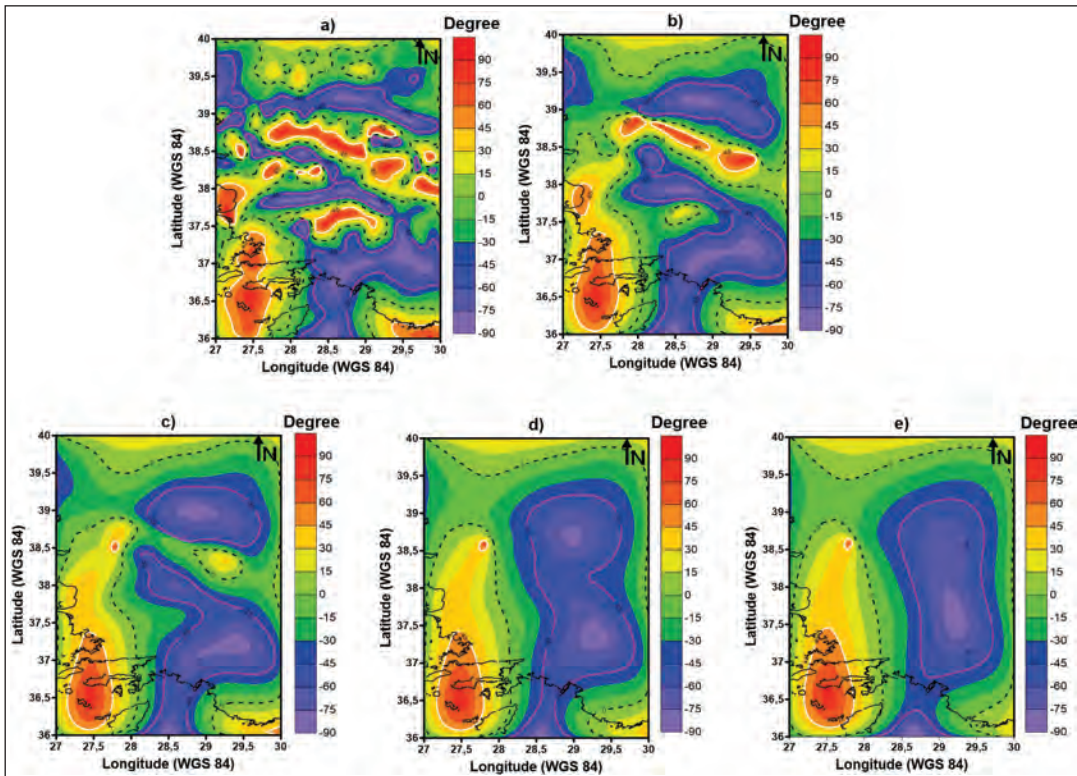


Figure 5- Tilt angle results of regional data having different upward continuation values: a) Continuation plane is 15 km, b) 35 km, c) 50 km, d) 75 km, e) 100 km (Contours are illustrated following, White +45°, Pink -45° and black dashed lines 0°).

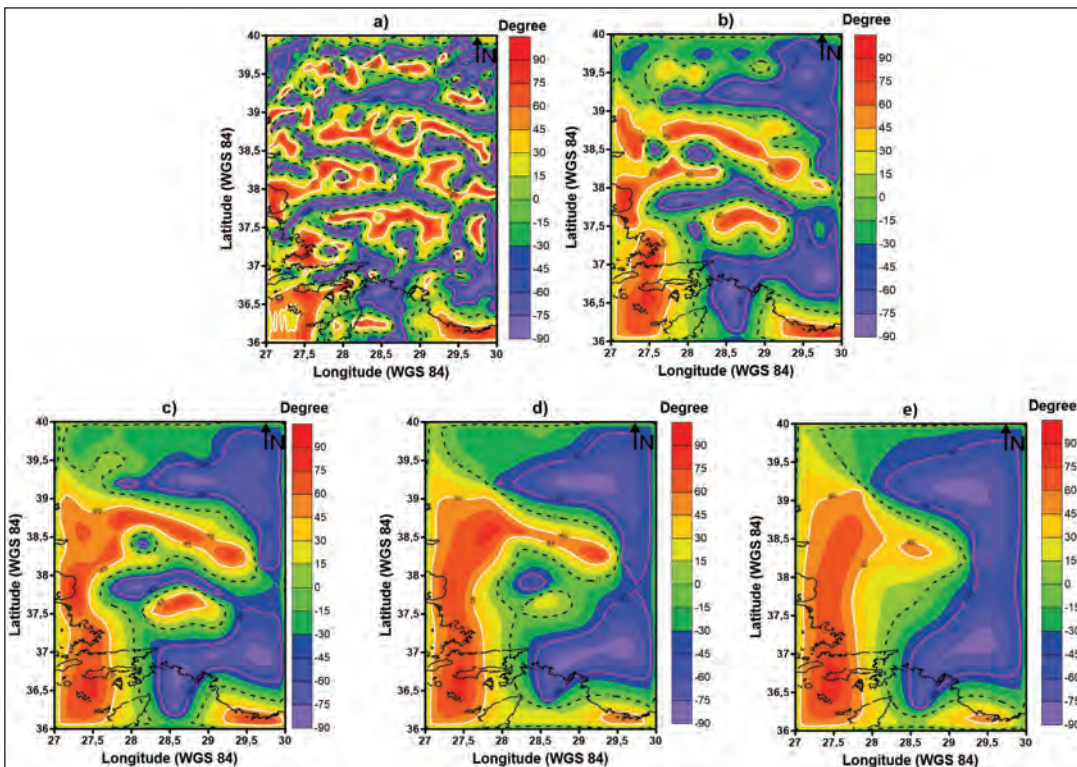


Figure 6- Tilt angle results of vertical derivative of regional data having different upward continuation values: a) Continuation plane is 15 km, b) 35 km, c) 50 km, d) 75 km, e) 100 km (Contours are illustrated following, White +45°, Pink -45° and black dashed lines 0°).

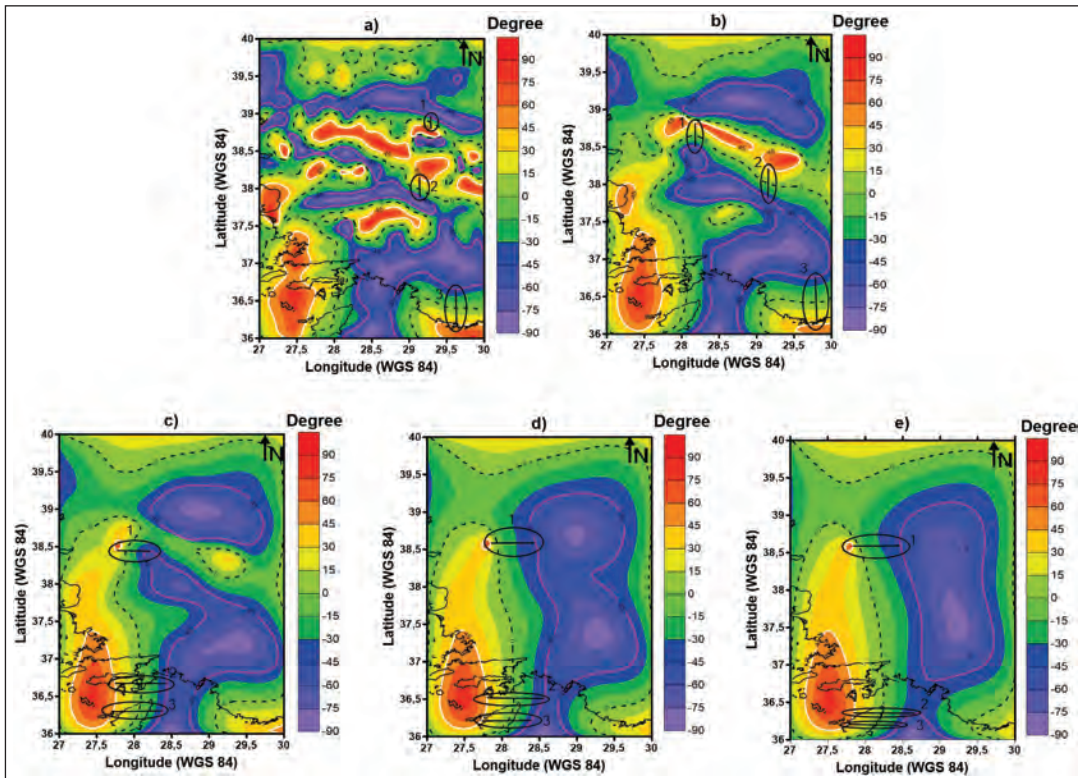


Figure 7- Sections are shown in ellipses which illustrate depth estimation of regional data having different upward continuation values using tilt angle method: a) Continuation plane is 15 km, b) 35 km, c) 50 km, d) 75 km, e) 100 km.

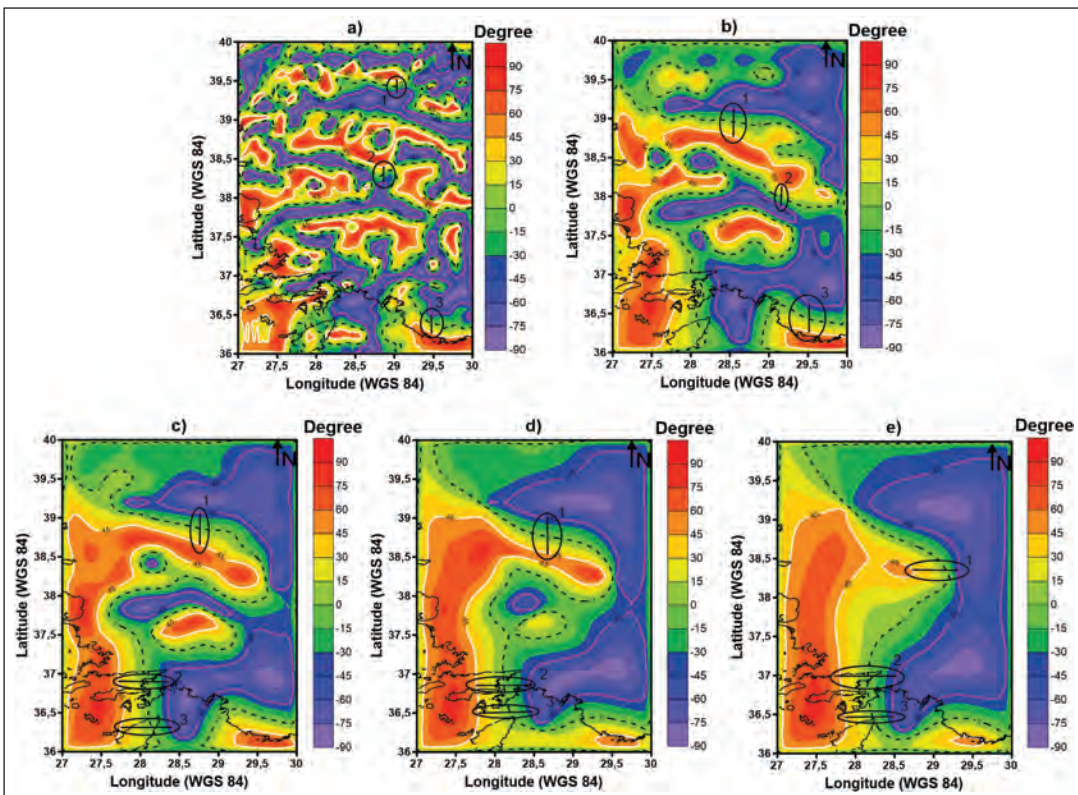


Figure 8- Sections are shown in ellipses which illustrate depth estimation of vertical derivative of regional data having different upward continuation values using tilt angle method: a) Continuation plane is 15 km, b) 35 km, c) 50 km, d) 75 km, e) 100 km.

Table 1- Top depths are obtained from tilt angle method and tilt angle of vertical derivative of anomaly.

Data	Depths are Obtained from Tilt Angle Method			Depths are Obtained from Tilt Angle of Vertical Derivative of Anomaly			Averages		
	Section 1 (km)	Section 2 (km)	Section 3 (km)	Section 1 (km)	Section 2 (km)	Section 3 (km)	Section 1 (km)	Section 2 (km)	Section 3 (km)
Continuation Plane 15 km	7.78	13.55	25.14	7.16	10.33	12.55	7.47	11.94	18.84
Continuation Plane 35 km	17.28	21.66	33.33	13.27	13.50	20	15.27	17.58	26.66
Continuation Plane 50 km	23.88	39.44	36.66	23.33	34.99	34.88	23.61	37.21	35.77
Continuation Plane 75 km	31.63	41.1	36.10	24.16	35.83	37.61	27.89	38.46	36.85
Continuation Plane 100 km	33.88	43.84	37.20	31.66	41.00	34.44	32.77	42.42	34.98

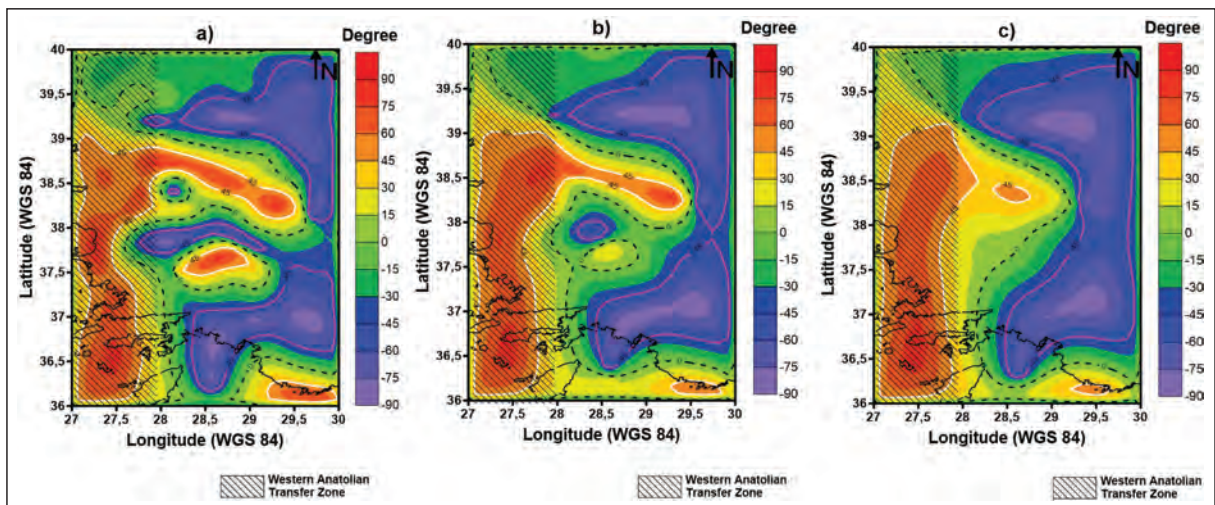


Figure 9- Boundary of Western Anatolian Transfer Zone. Western anatolian Transfer Zone illustrated on regional datas that are: a) Continuation plane is 50 km, b) 75 km, c) 100 km.

In order to approach the possible structure depth, the depths of the tilt angle data and averages of the depths were found at the tilt angle of the vertical derivative. As can be seen, the average of the sections 1, 2 and 3 from the data with the extension plane of 50 km gave similar depths. Also, the  $\pm 45^\circ$  contours of the data in which tilt angle is taken from the vertical derivative showed less variation than the  $\pm 45^\circ$  contours obtained from the tilt angle. The sections were first taken from the tilt map of the vertical derivative and then taken from the tilt angle map, corresponding to approximately the same latitude.

The average crustal thickness is 26 km deep in the eastern part of WATZ, according to tilt angle result, considering section 1 values of the results of the upward extension of 35, 50 and 75 km in table 1. At the same time, looking at the upwards extension values in this region, a sudden decrease in gravity value was

observed. According to Şalk et. al (2005) it is observed that the values of the heat flux obtained by using Curie depths calculated from magnetic data are increased. In addition, it is observed that there is a passive zone in terms of producing earthquakes here, considering the earthquakes with 3.5 or above magnitude were taken from the USGS earthquake catalogue. The heat fluxes obtained by using the magnitudes and depths of the earthquakes in the region and the Curie depths calculated from the magnetic data are associated with each other and they are shown in figure 10 (Şalk et al., 2005).

As can be seen from figure 10; in regional data, between  $28.5^\circ$  and  $29.5^\circ$  East longitudes and between  $38^\circ$  and  $39^\circ$  North latitudes, the number of earthquakes is small and they are in shallow depths. When we look at the heat flux maps obtained using the Curie depths calculated from magnetic data, there is a zone where

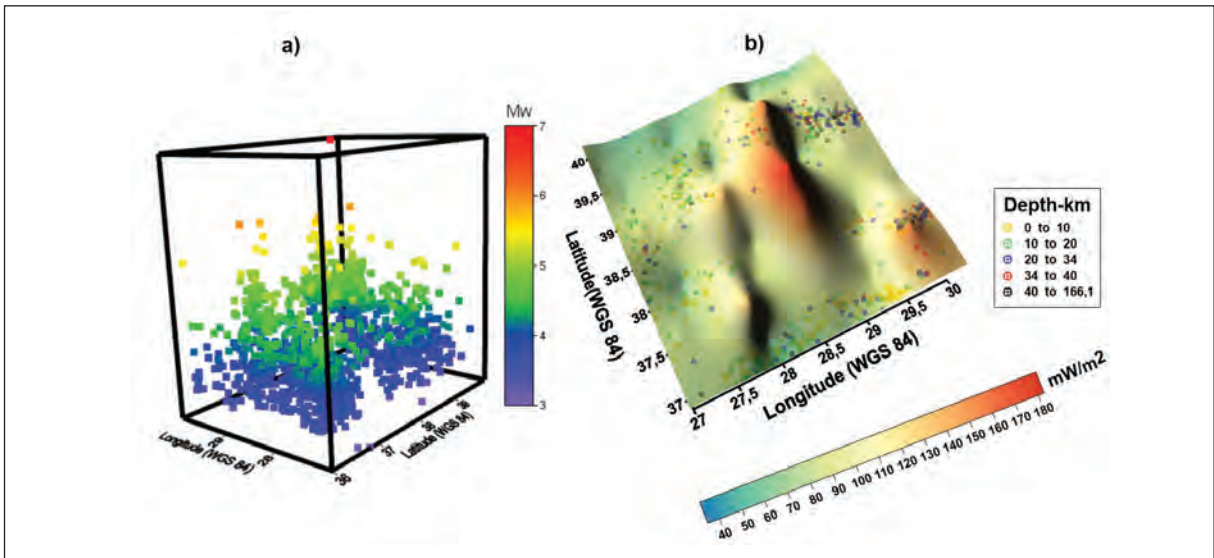


Figure 10- Examination of Earthquakes and heat flow maps that obtained from Curie depths in study area: a) Earthquakes in study area is showed latitude, longitude and magnitude, b) Examination of earthquake depths and heat flow map for study area. (Earthquake data is downloaded from USGS).

the heat flux is increased in the same region between 28.5° and 29.5° East longitudes, 38° and 39° North latitudes.

The earthquake depth relation graph is shown in figure 11. As a result of the earthquake analysis made in the study area, it is observed that the number of earthquakes decreased significantly between 34 and 200 km depths. Especially in isostatic studies, such environments are considered as the transition from a rigid environment to a ductile environment (Watts,

2001; Pamukcu and Yurdakul, 2008; Pamukcu and Akçığ, 2011). As can be understood from this chart, there is a decrease of about 50% in the number of earthquakes at 34 km. This decrease in the number of earthquakes corresponds to the area of the third section of the observed area, 35 km upwards extension and 50 km upwards extension (Table 1). When compared to the change of the heat flux values determined by Şalk et al (2005); regions with high heat flux were observed to be related to this field (Figure 10).

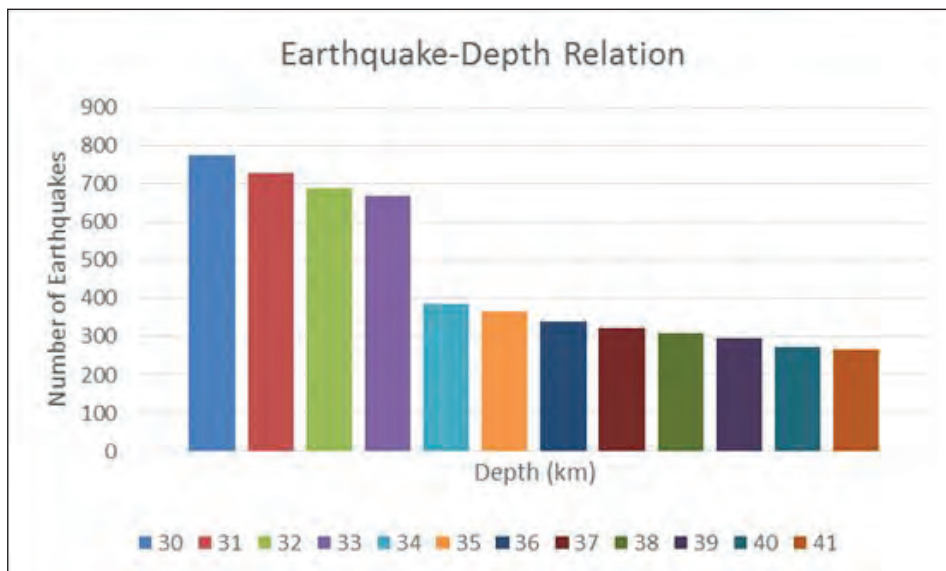


Figure 11- Relationship between number and depth of earthquakes. (<https://www.usgs.gov/>).

#### 4. Results

In this study, the results obtained by applying the tilt angle method to the land gravity data have been examined. In addition, tilt angle method was applied to the vertical derivatives of terrain data using the approach in Oruç's study (2011).

The upper depths found by using tilt angle for western Anatolia were compatible with the depths in the studies conducted by Çifçi et al. (2011), Pamukcu and Yurdakul (2008) using seismology, gravity and seismic data in the same region. The average depths obtained for the various upward extension planes in table 2 are compatible with depths of crustal corrugations determined by seismic reflection evaluation by Çifçi et al. (2011). Depths determined in applications after 50 km of extension plane and the upper depth of deep structure controlling the anomaly were determined to change in the north- east direction between 30 and 40 km in the Western Anatolia Region (Table 2). This result is consistent with the crustal thickness value determined by Zhu et al. (2006).

Depths and boundaries obtained from the tilt angle of the vertical derivative method in field study are quite compatible with boundaries of the lithospheric zone offered for the Western Anatolia Region by Gessner et al. (2013). This lithospheric zone, which is also observed by the tilt angle method, is thought to be caused by the progression of the hot material formed by subduction zone defined by Gessner et al. (2013) in the part where the number of earthquakes is small to the upper part of the lithosphere and making the environment ductile. A decrease in the number and depth of earthquakes is seen as a result of being ductile (Figure 11) and the heat flux values in the same region are observed to rise (Figure 10b). In this study, it was found that the upper depth of zone from tilt values changed between 18 and 38 km from table 1.

In this study, two approaches can be mentioned by looking at the  $0^\circ$  and  $\pm 45^\circ$  contours in the anomalies in figures 9a, 9b and 9c. In the first approach, there are two different geological structures extending from north to south. In the second approach, there is a single structure here, but the structure remaining in the east underwent deformation. The second approach was also mentioned in the study conducted by Gessner et al. (2013).

When the earthquake quantities and depths in the study area are analyzed together (Figure 11), it can

be said that there is a fragile environment up to 34 km in the region and after 34 km, the transition to the ductile environment begins. When the regional maps in figure 4 are examined, it can be observed that the Bouguer anomaly is low in the east of the study area and it is also observed that the values of the heat flux obtained by using Curie depths calculated from the magnetic data in the east of the field increase. These characteristics indicate a ductile environment, but the Bouguer anomaly is high at the west of the field (Figure 4) and the heat flux values obtained using Curie depths calculated from magnetic data are low (Figure 10b). As a result, the western part, which is determined from the tilt angle change and is defined as the Western Anatolian Transfer Zone by Gessner et al. (2013), may still be a rigid structure even at a depth of about 34 km.

#### Acknowledgement

We would like to thank Prof. Dr. Bülent Oruç, who shared his valuable opinions in the evaluation of the article and the two reviewers.

#### References

- Akay, T., Bilim F., Koşaroğlu, S. 2013. Menderes Masifi tektonik yapılarının (Batı Anadolu, Türkiye) Bouguer gravite analizi kullanılarak incelenmesi. Cumhuriyet Yerbilimleri Dergisi, 30, 2, 71-86.
- Akın, U., Şerifoğlu, B.I., Duru, M. 2011. Using the tilt angle in gravity and magnetic methods. Bulletin of the Mineral Research and Exploration, 143, 1-12.
- Blakely, R.J., Simpson, R.W. 1986. Approximating edges of source bodies from magnetic or gravity anomalies. Geophysics, 51(7), 1494-1498.
- Çifçi, G., Pamukcu, O., Çoruh, C., Çopur, S., Sözbilir, H. 2011. Shallow and deep structure of a supradetachment basin based on geological, conventional deep seismic reflection sections and gravity data in the Buyuk Menderes Graben, western Anatolia. Surveys in Geophysics, 32(3), 271-290.
- Gessner, K., Gallardo, L.A., Markwitz, V., Ring, U., Thomson, S.N. 2013. What caused the denudation of the Menderes Massif: Review of crustal evolution, lithosphere structure, and dynamic topography in southwest Turkey. Gondwana Research, 24(1), 243-274.
- Hakyemez, H.Y., Erkal, T., Gökteş, F. 1999. Late Quaternary evolution of the Gediz and Büyük menderes

- grabens, western Anatolia, Turkey. *Quaternary Science Reviews*, 18(4), 549-554.
- Hood, P.J., Teskey, D.J. 1989. Aeromagnetic gradiometer program of the geological survey of Canada. *Geophysics*, 54(8), 1012-1022.
- Kaya, O., 1979. Ortadoğu Ege çöküntüsünün (Neojen) stratigrafisi ve tektoniği. *Türkiye Jeoloji Kurumu Bült.*, 22, 35-58.
- Leflef, D., 1980. Muratdağı güneyi Neojen havzasının çökel ortamları ve paleocoğrafik evrimi. Maden Tetkik ve Arama Genel Müdürlüğü Raporu No: 6812, Ankara (unpublished).
- Maden Tetkik ve Arama Genel Müdürlüğü (MTA) 1979. Batı Anadolu Bouguer gravite haritası (unpublished).
- Miller, H.G., Singh, V. 1994. Potential field tilt—a new concept for location of potential field sources. *Journal of Applied Geophysics*, 32(2), 213-217.
- Oruç, B. 2011. Edge detection and depth estimation using a tilt angle map from gravity gradient data of the Kozaklı-Central Anatolia region, Turkey. *Pure and applied geophysics*, 168, 10, 1769-1780.
- Pamukcu, O. A., Akçığ, Z., Demirbaş, Ş., Zor, E. 2007. Investigation of crustal thickness in Eastern Anatolia using gravity, magnetic and topographic data. *Pure and Applied Geophysics*, 164, 11, 2345-2358.
- Pamukcu, O. A., Yurdakul, A. 2008. Isostatic compensation in western Anatolia with estimate of the effective elastic thickness. *Turkish Journal of Earth Sciences*, 17, 3, 545-557.
- Pamukcu, O. A., Akçığ, Z. 2011. Isostasy of the Eastern Anatolia (Turkey) and discontinuities of its crust. *Pure and applied geophysics*, 168, 5, 901-917.
- Roest, W.R., Verhoef, J., Pilkington, M. 1992. Magnetic interpretation using the 3-D analytic signal. *Geophysics* 57, 1, 116-125.
- Salem, A., Williams, S., Fairhead, D., Smith, R., Ravat, D. 2007. Interpretation of magnetic data using tilt-angle derivatives. *Geophysics*, 73, 1, L1-L10.
- Şalk, M., Pamukcu, O., Kaftan, I. 2005. Determination of the Curie point depth and heat flow from MAGSAT data of Western Anatolia. *Journal of the Balkan Geophysical Society*, 8, 4, 149-160.
- The United States Geological Survey (USGS) Earthquake hazards program, URL: <http://earthquake.usgs.gov/>.
- Thompson, D.T. 1982. EULDPH: A new technique for making computer-assisted depth estimates from magnetic data. *Geophysics*, 47, 1, 31-37.
- Watts, A. B. 2001. *Isostasy and Flexure of the Lithosphere*. Cambridge University Press.
- Yılmaz, Y. 2000. Ege Bölgesinin aktif tektoniği. Batı Anadolu'nun deprenselliği Sempozyumu (BADSEM 2000), 24-27 Mayıs 2000, İzmir, Bildiriler, 3-14.
- Zhu, L., Mitchell, B. J., Akyol, N., Cemen, I., Kekovali, K. 2006. Crustal thickness variations in the Aegean region and implications for the extension of continental crust. *Journal of Geophysical Research: Solid Earth*, 111(B1).



# Bulletin of the Mineral Research and Exploration

<http://bulletin.mta.gov.tr>



## ALTERATION ZONES ASSOCIATED WITH EOCENE MAGMATISM IN THE OLUR (ERZURUM) AREA, EASTERN PONTIDES AND THEIR SIGNIFICANCE

Güzide ÖNAL<sup>a\*</sup>, Mustafa AKYILDIZ<sup>b</sup>, İsmet CENGİZ<sup>c</sup>, Mehmet ASLAN<sup>d</sup> and Serkan ÖZKÜMÜŞ<sup>e</sup>

<sup>a</sup>Çağkurova University, Department of Geology Engineering 01330 Balcalı, Adana [orcid.org/0000-0001-9290-0371](https://orcid.org/0000-0001-9290-0371)

<sup>b</sup>Çağkurova University, Department of Geology Engineering si, Jeoloji Mühendisliği Bölümü, 01330 Balcalı, Adana [orcid.org/0000-0002-0371-8646](https://orcid.org/0000-0002-0371-8646)

<sup>c</sup>Demir Export A.Ş., Directorate of Mineral Research, 06440 Kızılay/Ankara [orcid.org/0000-0003-3851-0287](https://orcid.org/0000-0003-3851-0287)

<sup>d</sup>General Directorate of Mineral Research and Exploration, department of Mineral Research and Exploration, 06800 Çankaya/Ankara. [orcid.org/0000-0003-1518-2575](https://orcid.org/0000-0003-1518-2575)

<sup>e</sup>General Directorate of Mineral Research and Exploration, department of Mineral Research and Exploration 06800 Çankaya/Ankara

Research Article

### Keywords:

Eastern Pontides, Early Eocene, porphyry system, alteration, FT-IR, XRD.

### ABSTRACT

The Alpine Orogenic Belt with numerous porphyry Cu-Mo-Au mineralizations, starts from Eastern Europe continues through Turkey and the Caucasus and extends into Iran and Afghanistan. The study area of the Eastern Pontides is in this orogenic belt. Using field and laboratory studies an attempt has been made to establish the origin of Yeşilbağlar, Kaban and Köprübaşı alteration zones in the Olur area (Erzurum). In the study area Early Eocene Coşkunlar volcanics and sub volcanic rocks have contact with the Oltu çayı volcanics of Early-Middle Jurassic. Alteration in the study area effects these Oltuçayı and Kaban volcanics. In the study area mineralizations are present in the alteration zones. Disseminated, stockwork, vein/veinlet and fissure type mineralizations are present in the Coşkunlar dacite. Paragenesis in the alteration zones are pyrite, chalcocopyrite, sphalerite, galena, pyrrhotite, quartz, calcite and barite. FT-IR and XRD studies showed the presence of clay, sulphate, sulphur, carbonate, silicate and oxide minerals in the alteration zones. Field and petrographical studies showed that alteration types in the Yeşilbağlar, Kaban and Köprübaşı areas are, advanced argillic-argillic, pyrolytic and sericitic. They are similar to the alterations present in the upper part of the mineralizations in the porphyry systems of the Alpine Orogenic Belt. In the Eastern Pontides starting in Early Jurassic, continuation of subductions resulted in closure of the İzmir-Ankara-Erzincan ocean and in Early Eocene the Taurid platform collided with the Eurasian active continental margin. Data from the study area indicate the presence of alteration zones in the upper part of the buried porphyry system and the possibility of mineralized parts in the deeper parts of the system.

Received Date: 27.02.2017

Accepted Date: 11.04.2017

## 1. Introduction

The base metals and precious metals of the Eastern Pontides have for a long time drawn the attention of earth scientists (a) Geological evolution of the İzmir-Ankara-Erzincan suture zone in particular and its continuation to the East Minor Caucasus are especially important (Okay, 1984; Evans and Hall, 1990; Okay and Şahintürk, 1997; Yılmaz et al., 1997; Okay and Tüysüz, 1999; Yılmaz et al., 2000; Hakyemez and Konak, 2001; Konak et al., 2001; Topuz et al., 2004; Okay et al., 2006; Rice et al., 2006; Konak and Hakyemez, 2008a; Rice et al., 2009; Rolland et al., 2009a, b; Çelik

et al, 2011; Ustaömer and Robertson, 2010; Topuz et al., 2012; Ustaömer et al., 2012; Robertson et al., 2013), (b) Origin of Late Cretaceous massive sulphide deposits (Kraeff, 1963; Hirst and Eğin, 1979; Çağatay and Boyle, 1980; Akıncı, 1984), (c) Late Cretaceous-Eocene porphyry Cu deposits, (Çağatay and Çağatay, 1978; Aral and Erler, 1981; Er et al., 1995; Soylu, 1999; Singer et al., 2008; Yiğit, 2006, 2009; Oğuz, (d) Ophiolites and their emplacements along İzmir-Ankara-Erzincan suture zone (Rice et al., 2006, 2009; Özen et al., 2008; Çolakoğlu et al, 2009, Sarfakioğlu et al., 2009; Parlak et al., 2013; Topuz et al., 2013). and in the Minor Caucasus (Galoyan et al., 2007, 2009; Rolland et

\* Corresponding author: Güzide ÖNAL, e-posta: [guzideonal@gmail.com](mailto:guzideonal@gmail.com)

al., 2009b, 2010; Sosson et al., 2010), the formation and settlement of ophiolites is very important. The presence of metallogenic provinces along the Alpine Orogenic Belt has been described by scientists (Moore et al., 1980; Yiğit, 2006, 2009). The study area is located in the belt extending from the Macedonia-Balkans, Istranca belt in NW Turkey, then diving into the Black Sea, coming out near Sinop in Northern Turkey, it then continues along the coast of Northern Turkey to the Caucasus, into Iran and extending to the Himalayas. Along these belts porphyry copper and Kurokko type massive sulphide deposits are quite extensive.

The study area is located between Eastern Pontides and Torids in the northern part of the East Anatolia accretionary belt. The zone extends from the Balkans into Eastern Turkey along a West-East direction and then enters Iran. In this belt porphyry, copper and Krouko type massive sulphide deposits are quite extensive (Figure 1). The Alpine Orogenic Belt, in which the study area is located has Porphyry copper deposits in the active continental margins (Andes type) and porphyry deposits (Philippine type) forming

the inner ocean island arc. Porphyry copper deposits in Bor, in Maydenpek (Yugoslavia), in Medet (Bulgaria), (Sar Çeşme) Shar Cheshme (Iran) are Andes type deposits developed in the active continental margins (Waterman and Hamilton, 1975; Hezarkhani, 2006; Singer et al., 2008). In Turkey Dereköy (Kırklareli, Bakırçay (Amasya) and Ulutaş-İspir (Erzurum) porphyry copper deposits display similar features of the Andes type deposits (Çağatay and Çağatay 1978; Jankovic 1977; Taylor, 1981; Ohta et al., 1988; Er et al., 1995; Soylu, 1999; Popov et al., 2002; Singer et al., 2008; Yiğit, 2006, 2009). Part of the Alpine Orogenic Belt between Samsun and Georgia is named as 'Pontide Metallogenic Belt' and forms 'Philippine type porphyry belt' (Çağatay and Çağatay, 1978).

Yeşilbağlar, Kaban and Köprübaşı (Olur, Erzurum) alteration zones, subject of this study are considered to be in the 'Eastern Pontide Metallogenic Belt' and are located within the Oltu imbricated zone. Metamorphic and sedimentary units outcropping along this zone belong to the rocks of the Olur Group within the Olur-Tortum zone (Figure 2), (Konak et al., 2001). Alteration zones extend East-West direction in the Southern part

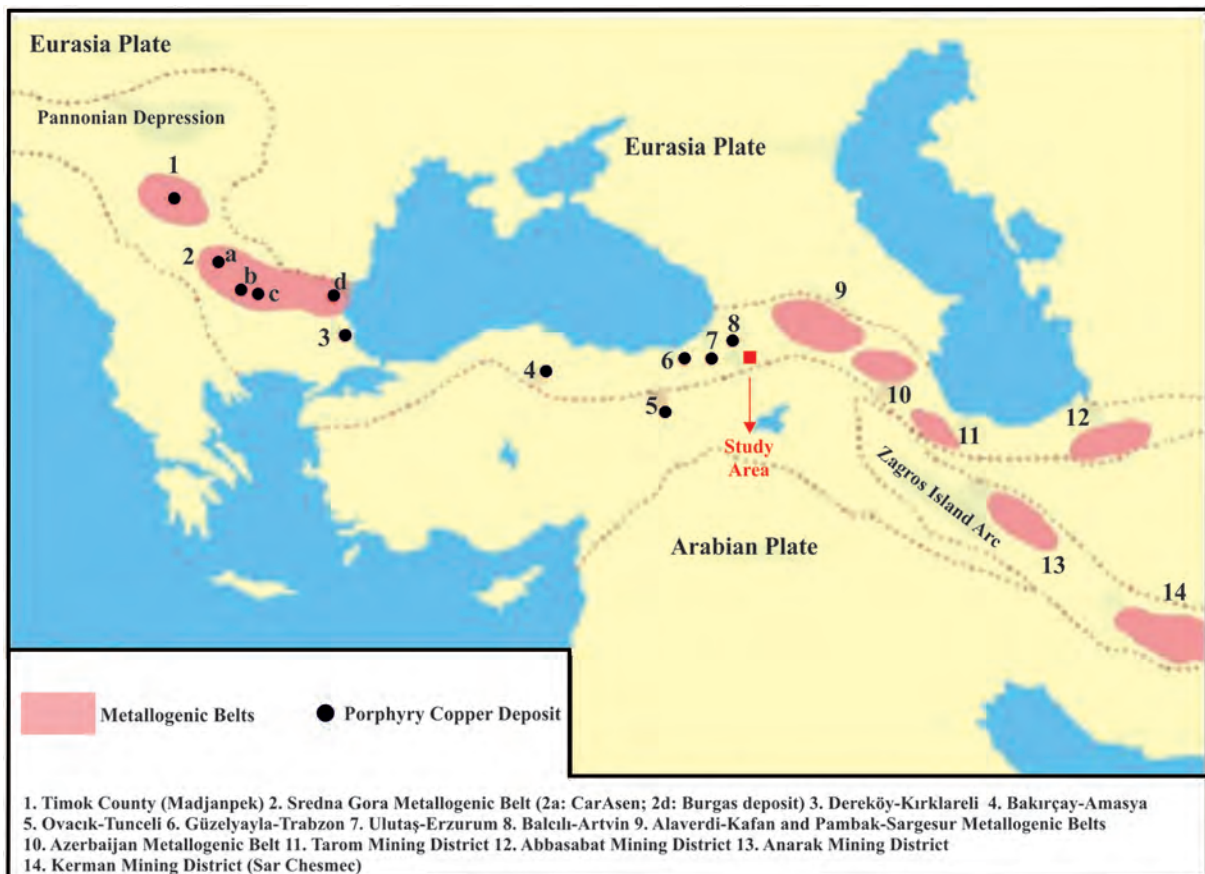


Figure 1- Porphyry-Cu occurrences along the Alpine orogenic belt and location of the study area (from Çağatay and Çağatay, 1978).

of Olur (Erzurum) (Figure 3). Yeşilbağlar alteration developed in Jurassic Oltuçayı volcanites and in the apophysis of the Early Eocene Coşkunlar dacites. Kaban and Köprübaşı alterations have developed in the Jurassic Kaban dacites and along the contact zone of the Cretaceous Soğukçam formation (Figure 3). All these alterations are believed to have generated from the quartz porphyries of the apophysis of the Early Eocene Coşkunlar dacites (Konak et al., 2001).

The aims of this study are (a) to prepare 1/5000 scale detailed geological map of the host rocks and

intrusive body in which mineralisations are associated and to gain more definite knowledge of the alteration zones, (b) to collect samples from the alteration zones and host rocks to study mineralogy and petrography of the units, (c) to conduct XRD (X-Ray Diffractometer) and FT-IR (Fourier Transform-Infrared Spectroscopy) studies to compute the mineralogy of the alteration zone, (d) to evaluate all of the findings together to be able to carry out regional scale correlations to find out the mineralogical deposit type to which the alteration zone is associated.

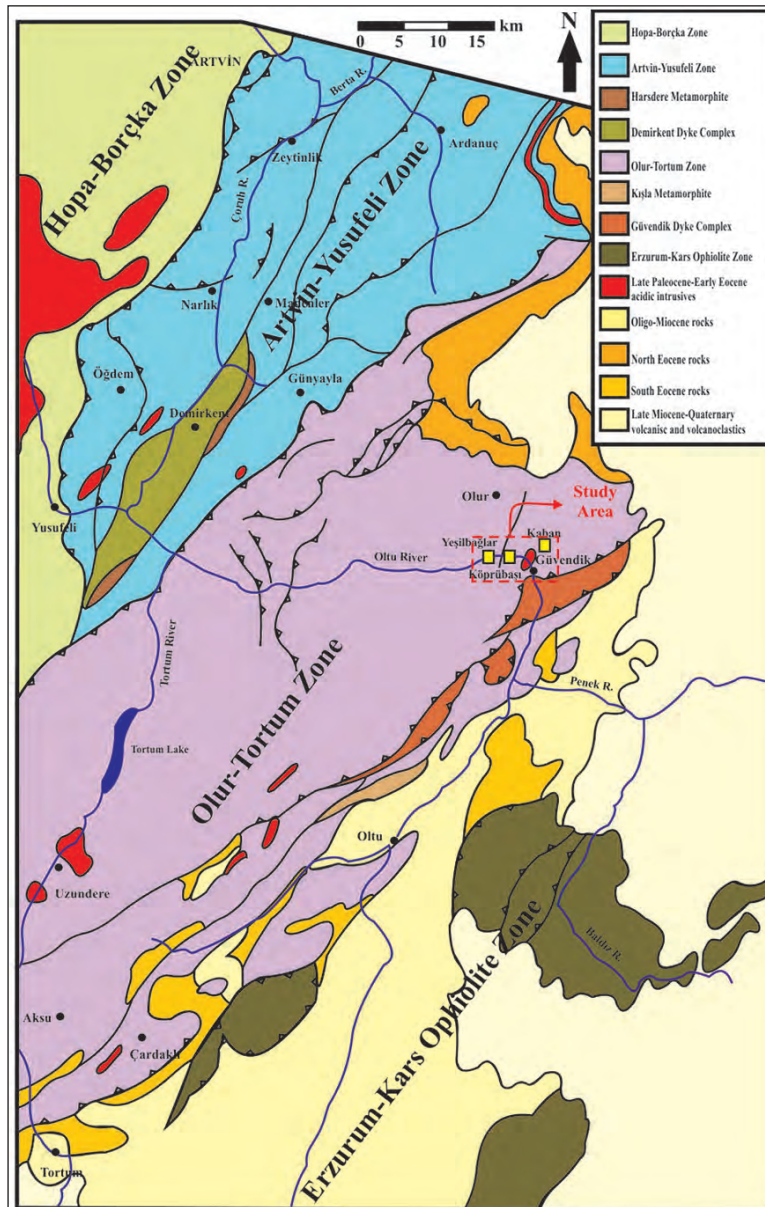


Figure 2- Simplified geological map of the tectonic units in the study area and surroundings (from Konak et al., 2001).

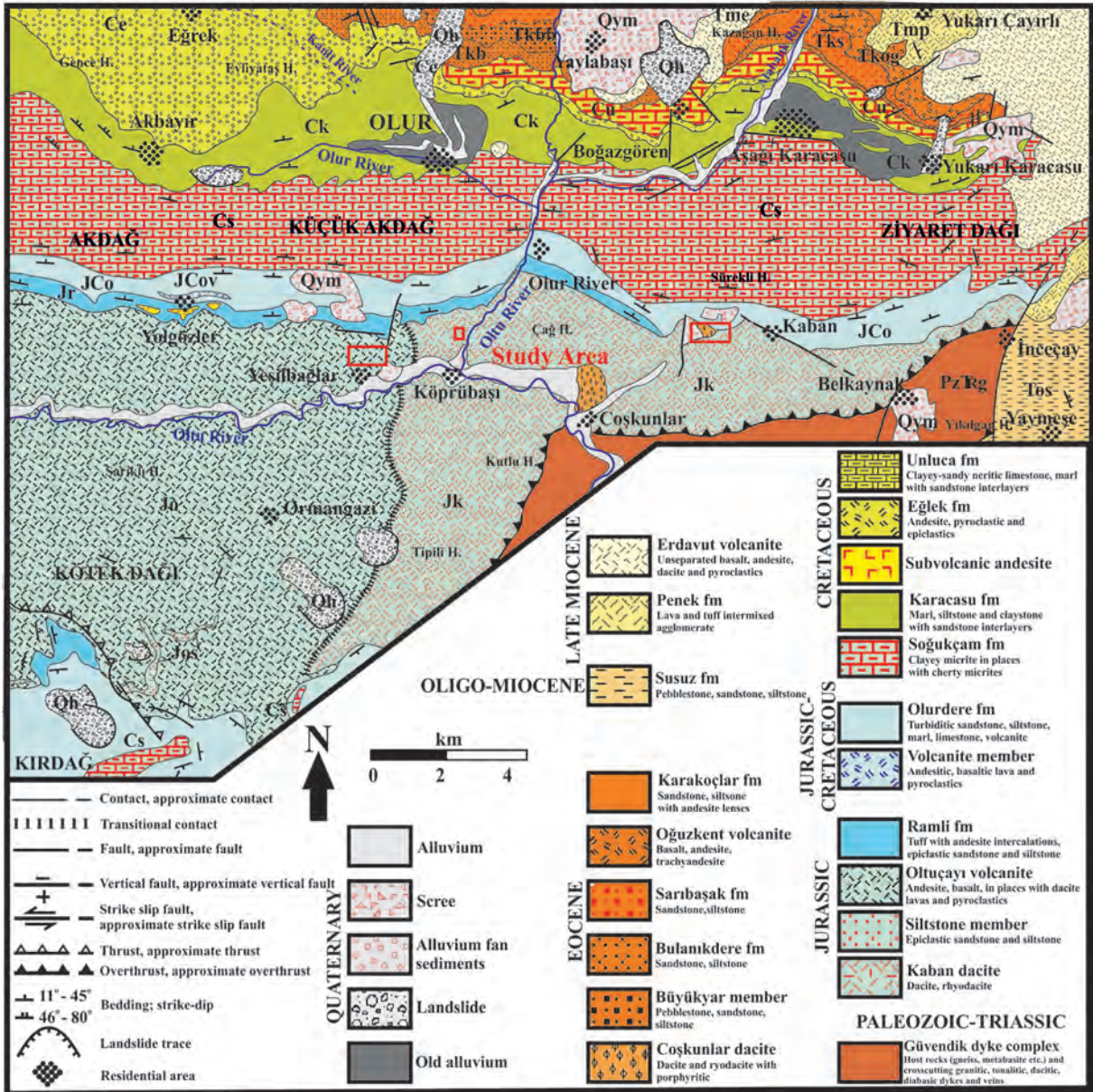


Figure 3- Geological map of the units in the study area and surroundings (Simplified from Konak ve Hakyemez, 2008a).

## 2. Regional Geology and Stratigraphy

The study area is located in the Sakarya zone (Okan and Tüysüz, 1999) of the eastern part of the Pontides (Ketin, 1966), forming the western extension of the Trans Caucasians and bound by the East Anatolia Accretionary Complex in the South (Şengör and Yılmaz, 1981). In the Eastern part of the Eastern Pontides, four different tectonic slices with NE-SW orientations, bound by tectonic zones have been identified (Konak and Hakyemez, 1996, 2001). These tectonic slices have been thrust in South-North direction. From north to south these

tectonic slices are (a) Hopa-Borçka zone, (b) Artvin-Yusufeli zone, (c) Olur-Tortum zone and (d) Erzurum-Kars ophiolite zone (Konak and Hakyemez, 1996, 2001; Konak et al., 2001), (Figure 2). Hopa-Borçka zone is the autochthon units of the Eastern Pontides. Autochthon units mainly have fragments of Permian granites, Early Jurassic-Palaeocene covering units and Middle Eocene volcanics, detritic units (Konak and Hakyemez 2001; Ustaömer and Robertson, 2010; Konak and Hakyemez, 2008a, 2008b). Artvin-Yusufeli zonu overlay autochthon units with a tectonic contact. On the other hand, the zone consisting Artvin-

Yusufeli zone, Paleozoic basal metamorphic units, Late Paleozoic-Middle Jurassic sheeted dyke complex and Jurassic sedimentary and volcanic units have been described as '*Basal Tectonic Slice Complex*' by Ustaömer and Robertson (2010). Further to the south Artvin-Yusufeli zone was overlain by Olur-Tortum zone with a tectonic contact. The zone in general has small outcrops of basal units, Middle Jurassic volcanics and Late Cretaceous-Early Senozoic volcanics and sedimentary units. This zone has been described as '*Upper Tectonic Slice Complex*' by Ustaömer and Robertson (2010). Structurally Erzurum-Kars Ophiolite Zone overlying at the top forms tectonic slice in the further south. This zone in general has rocks of ophiolite suite, high pressure-low temperature (HP/LT) metamorphics (blue schists) and Late Cretaceous-Palaeocene sedimentary rocks (Konak and Hakyemez, 2001; Ustaömer and Robertson, 2010). All these above mentioned tectonic-stratigraphic/magmatic units observed in the described tectonic zones in the further south, form haphazardly sliced thrust sheets along the southern part of the Tertiary volcano-sedimentary basin. This zone was named as Oltu Thrust Sheets Zone (OTSZ) by Konak et al., (2001).

In the area along the Oltu Thrust Sheets Zone, two different rock units of the Pre Jurassic basement form narrow tectonic slices. These tectonic units are mainly low grade metamorphics of the Kışla metamorphics and gneiss, amphibolite, metagabbro, metadiabase, metabasic like rocks heavily cut by metagranitic, pegmatitic, dioritic, tonalitic, dacitic and diabase dykes and veins of the Güvendik dyke complex. Relations of these rocks with each other are not clearly observed in the field (Konak et al., 2001) (Figure 3).

In the field Early-Middle Jurassic basic, intermediate and acidic lavas and pyroclastics overlay Güvendik dyke complex with a tectonic contact (Figure 3). Between Yeşilbağlar and Kötek Dağı (mountain) Oluçayı volcanites mainly consisting of andesites, basalts and in places dacitic lavas and pyroclastics have large areas of outcrops (Figure 4). In the upper levels of Oluçayı volcanites, lens shaped epiclastic-sandstone-siltstone interlayers are present. In the East of Yeşilbağlar, in the Körübaşı and Coşkunlar areas Kaban dacite has large areas of outcrops (Figure 4). Contact relation of Oluçayı volcanite with the Kaban dacite is considered to be transitional (Konak and Hakyemez, 2001; 2008a). Ramli formation of Dogger, mainly consisting andesitic lavas and fine grained sandstones in

places interlayered with silicified pyroclastics transitionally overlay Oluçayı volcanites (Konak et al., 2001). Ramli formation in the area extends about E-W direction in the Northern part of Kırdag and Yeşilbağlar and Yolgözler and Olurdere areas (Figure 3). Ramli formation with a possible unconformity is overlain by Oxfordian-Berriasian Olurdere formation (Yılmaz, 1985). The unit mainly consists of volcanic intermixed pebble stone, sandstone, siltstone and marl intercalations (Konak and Hakyemez, 2001, 2008a). Berriasian-Aptian (Early Cretaceous) Soğukçam formation (Altınlı, 1973) concordantly overlies Olurdere formation (Konak et al., 2001). It mainly consists of micrite and clayey micritic limestones and has chert bands and chert concretions in the upper levels. Soğukçam formation in the study area has outcrops along E-W direction to the North of Yolgözler, Yeşilbağlar, Olurdere and Kaban (Figure 3). Karacasu formation of Aptian-Santonian (Early-Late Cretaceous) concordantly overlay Soğukçam formation (Figure 4). The unit, mainly consists of marls intercalated with sandstones and siltstones and some clayey limestones (Konak et al., 2001). Andesitic pyroclastics and in places lens like sandstones are observed at the bottom of the Karacasu formation. In the Olur-Karacasu areas the unit has outcrops oriented along E-W direction (Figure 3). Turonian-Santonian Eğlek formation mainly consisting of andesites and agglomerates concordantly overlay Karacasu formation (Konak et al., 2001). The unit has outcrops in the northern part of the mapped area (Figure 3). Unluca formation mainly consisting of clayey-sandy limestones with sand intercalations and in the upper level marls with clayey limestone intercalations concordantly overlay Eğlek formation (Konak et al., 2001). The age of the unit is determined to be Late Santonian-Maastrichtian. In the area Alos formation concordantly overlays Unluca formation (Konak et al., 2001). The age of this unit is Early Paleocene and it is mainly made of platform carbonates (Figure 4). During Late Palaeocene the platform (Alos formation) became deeper by collapsing and in the deepening basin conditions Kaltarmak formation developed with siltstones and marls with turbiditic sandstones and calcic turbidite intercalations (Konak et al., 2001). Acidic Coşkunlar dacite dykes cut all units in the area. Units of the Coşkunlar dacite cutting all of the units in the area is in accord with the Eocene fold axis and with the tectonics like thrusts considered to be the products associated with the Early Eocene magmatic activity (Konak et al., 2001). In the area Coşkunlar Dacite intruded Lias-Dogger Kaban dacite

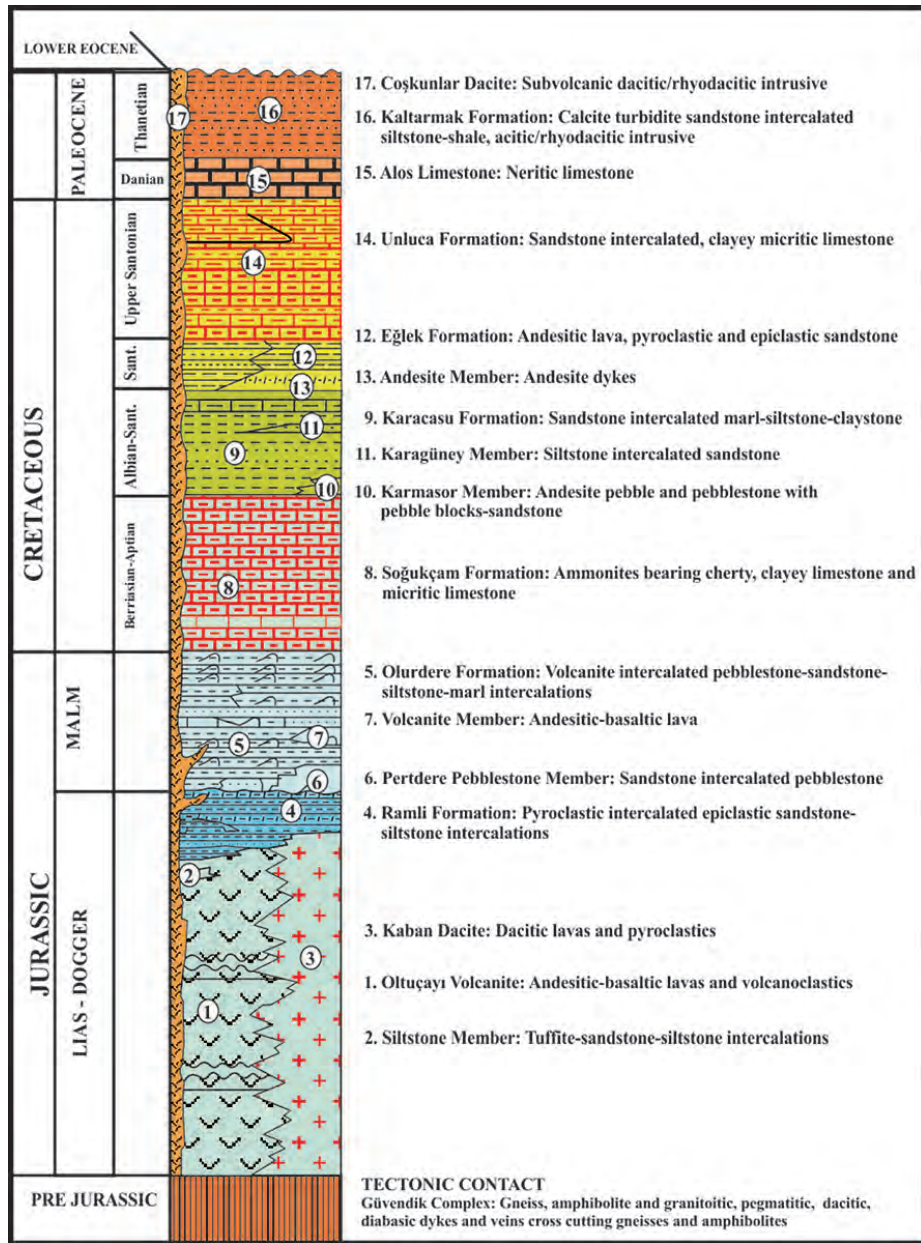


Figure 4- Stratigraphic columnar section of the units in the study area and surroundings (from Konak and Hakyemez, 2008a).

and Oltuçayı volcanites. Extensive hydrothermal alteration and associated mineralizations have large areas of outcrops along the contact zones (Figure 3).

### 3. Method

To enable our mineralogical, petrographic and geochemical studies to be carried out 94 samples were collected from the host rocks and alteration zones. For the mineralogical and petrographic studies, thin and polished sections of the samples were prepared in the thin section laboratory of the Geological Engineering

Department of Çukurova University. Mineral chemistry of the 6 mineralized samples collected from the Yeşilbağlar and Kaban alteration zones were examined in the Mineralogy and Petrology Institute of the Earth Sciences Faculty of Vienna University Austria. Studies were carried out by using CAMECA-SX100 electron microprobe. Standard 27x46 mm rectangular and 1 inch diameter circular samples were prepared. Using electromagnetic lenses, speeded electron rays were focused on to the samples surface producing characteristic X-rays, these energetic electrons were bombarded into a small volume space

(Typically 1-9 micron) of the specimen. As each element has certain X-ray distribution, characteristic X-rays were determined with their wave lengths and concentrations of all elements (except H, He and Li) have been determined. Diameter of the X-ray was set to be 1  $\mu\text{m}$  and analyses were carried out at 20 kV and 20 nA.

X-Ray diffractometer analyses have been carried out on the 8 pyrite samples from the alterations from the Coşkunlar dacite. For the mineralogical studies samples were prepared in the crushing-powdering and geochemistry laboratory of the Geological Engineering Department of the Çukurova University and analyses were carried out in the Mineralogy Department of the Geneva University in Switzerland.

92 samples were selected from the alteration zones and host rocks for FT-IR analyses and FT-IR KBr tablet technique has been used. Analyses were carried out in the Chemistry Laboratory of the Science-Arts Faculty of the Çukurova University. For the analyses 1 mg samples were mixed with 900 mgr KBr and the

mixture pelletized to 13 mm diameter pellets by using Graseby Specac compaction device. The reference pellet (KBr) and specimen pellets (1 mg specimen/900 mg KBr) were analysed by scanning them in the Perkin-Elmer 1600 FT-IR spectrometer.

#### 4. Petrographic Characters of the Magmatic Rocks Outcropping in the Study Area

Late-Middle Jurassic Oltuçayı volcanites, Kaban Dacite, and Late Eocene Coşkunlar Dacite cutting Early Cretaceous pelagic-semi pelagic limestones of Soğukçam formation are the magmatic rocks in the area (Figure 5). From the main trace elements content point of view of the Jurassic-Eocene volcanics, they have calcalkaline origin and they developed as a result of northward subduction of Neo Tethys (Önal, 2015). Petrographic characters of the magmatic rocks which caused the alteration zones are given below.

Late-Middle Jurassic Oltuçayı volcanics are noticeable in the field with their dark green-near black colours. The unit is mainly represented by basaltic-andesitic lavas (Figure 6a). Basaltic lavas have

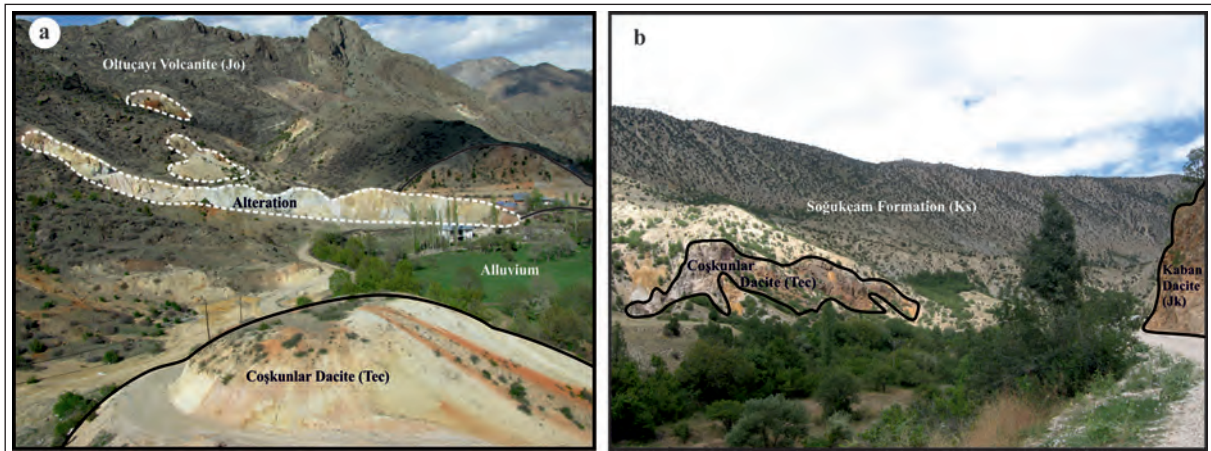


Figure 5- a) General view of the alterations and Coşkunlar Dacite cutting the Oltuçayı Volcanites (West of Yeşilbağlar village), b) Field view of the Coşkunlar Dacite, Soğukçam Formation and Kaban Dacite (West of Kaban village).



Figure 6- a) Field view of the volcanic rocks (basaltic andesite) (Oltuçayı Volcanites) in the study area, b and c) Plane polarized view of the thin sections from the Oltuçayı Volcanites (Pl: Plagioclase, Amp: Amphibole).

plagioclase and pyroxenes and display hyalopilitic porphyritic and microlithic porphyritic textures. Plagioclases are phenocrysts and microlites and have euhedral and subhedral forms. Calcites, sericites and albites developed as secondary minerals from the alteration of the plagioclases. Pyroxenes in general have anhedral, subhedral forms. Chlorites are anhedral and have irregularly filled interspaces of the plagioclases and pyroxenes. Calcites in general developed as a result of alteration of the plagioclases and in places through secondary processes filled the cracks and fissures (Figure 6b). Andesitic lavas mainly consist of plagioclases and amphiboles displaying porphyritic and microlithic textures. Plagioclases appear as large phenocrysts and microlites have euhedral and subhedral forms. Amphiboles in general are anhedral or subhedral and some green coloured amphiboles result of chloritization can be seen in the rocks. Amphiboles in places have an opaque rim (Figure 6c). Quartz and chlorite are the secondary minerals developed.

Early-Middle Jurassic Kaban dacite has beige, dirty yellow, light grey colours and has parallel or irregular columnar structures (Figure 7a). Dacitic lavas mainly have quartz, plagioclase and biotite and has porphyritic or micro granular porphyritic textures. In the rocks, euhedral in places corroded quartz

phenocrysts and micro granular quartz are in micro granular matrix. Quartz phenocrysts appear highly fractured (Figure 7b). Plagioclases phenocrysts and microlites have been altered to albite and sericite. Biotites are rather limited and have been extensively chloritized (Figure 7c).

Early Eocene Coşkunlar Dacite in the field has beige, dirty white colours and have been heavily altered (Figure 8a). Dacitic lavas mainly have quartz, plagioclase and some biotites and have porphyritic and micro granular porphyritic texture. Quartzs in general have euhedral form and in places have been corroded and phenocrystal and micro granular quartz are embedded in fine grained matrix. Plagioclases in the rocks are in the form of phenocrysts and microlites. Plagioclases have been subjected to alteration and have been albitized and partly sericitized. Biotites have been chloritized (Figure 8b). Pyrite is the opaque mineral in the rocks. Prehnite and sericitizations are also present in the rocks (Figure 8c).

In the field quartz porphyries are found to be associated with Coşkunlar Dacite and they are considered to be the subvolcanic equivalents of the dacites. Quartz porphyries are dykes and apophysis in the dacites. In the 1/5.000 scale geological map it was rather difficult to mark these quartz porphyry dykes

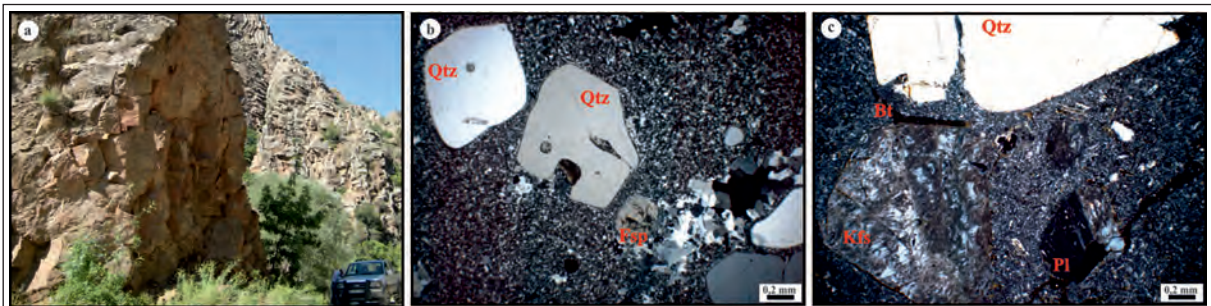


Figure 7- a) Field view of the dacitic rocks (Kaban Dacite), b and c) Thin section views of the Kaban Dacite (Qtz: Quartz, Fsp: Feldspar, Kfs: K-feldspar, Bt: Biotite).

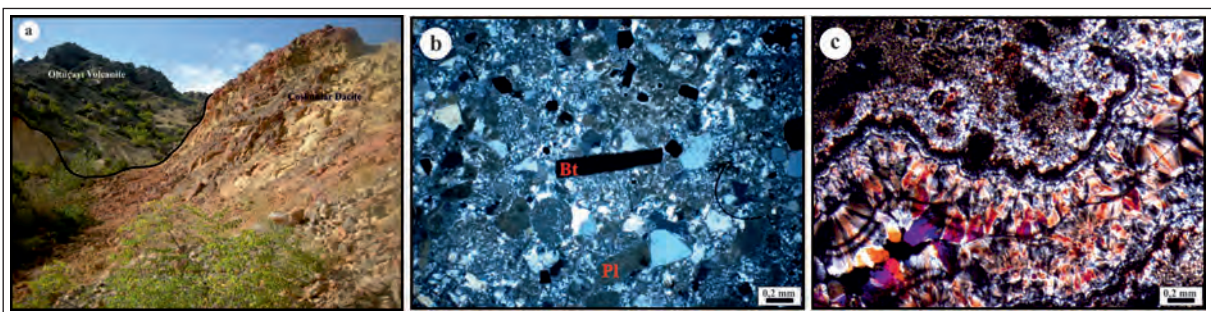


Figure 8- a) Field view of the Coşkunlar Dacite in the study area, b and c) Thin section view of prehnite and sericitization in the Coşkunlar Dacite (Pl: Plagioclase, Bt: Biotite).

and apophysis separately so they were marked together with dacites. Quartz porphyries in the field are noticeable with their beige, light yellow colours and quartz phenocrysts (Figure 9a). Primary mineralogy and texture of the rocks has been intensively effected by the alteration, porphyritic and micro granular texture traces are recognizable. Mineralogical studies indicate that apart from quartz all other minerals have been altered (Figure 9b). Plagioclases have been subjected to argillization and carbonatization, quartz has been corroded. Secondary quartz veins/veinlets are also present (Figure 9c).

From the intensity point of alteration and opaque mineral contents Kaban and Coşkunlar dacites are quite different from one another. Early Jurassic Kaban Dacite is characterized with less intense alteration and

with not having opaque minerals. On the other hand, Coşkunlar Dacite has been heavily altered and is rich in opaque minerals.

## 5. Economic Geology

Yeşilbağlar, Kaban and Köprübaşı alterations have East-West extensions in the South of Olur (Erzurum).

### 5.1. Yeşilbağlar Alterations and Mineralizations

Yeşilbağlar alterations are located approximately 10 km south of the Yeşilbağlar village. It is about 300 m wide and has 600 m extension along N10°-15°E direction (Figure 3). Basaltic Jurassic Oltuçayı volcanites and Early Eocene quartz porphyry apophysis of the Coşkunlar dacites cutting Oltuçayı volcanites have been altered (Figure 10). In the alteration zones

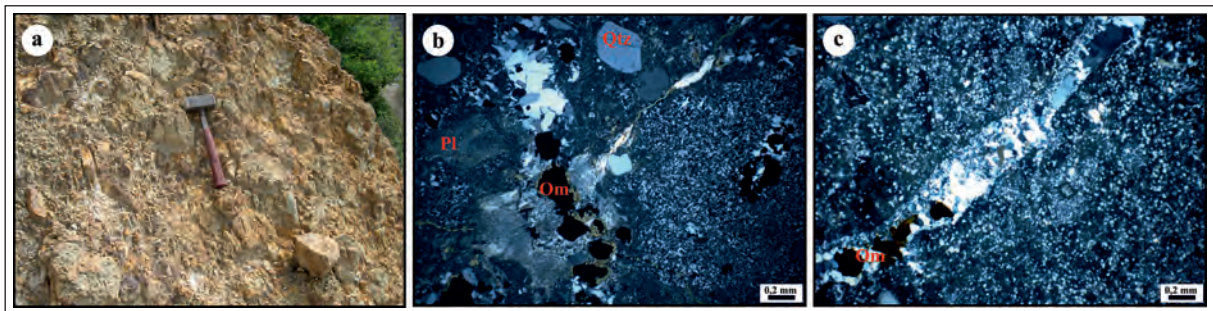


Figure 9- a) Field view of the quartz porphyries in the study area, b and c) Thin section views of the quartz porphyries (Qtz: Quartz, Pl: Plagioclase, Om: Opaque mineral).

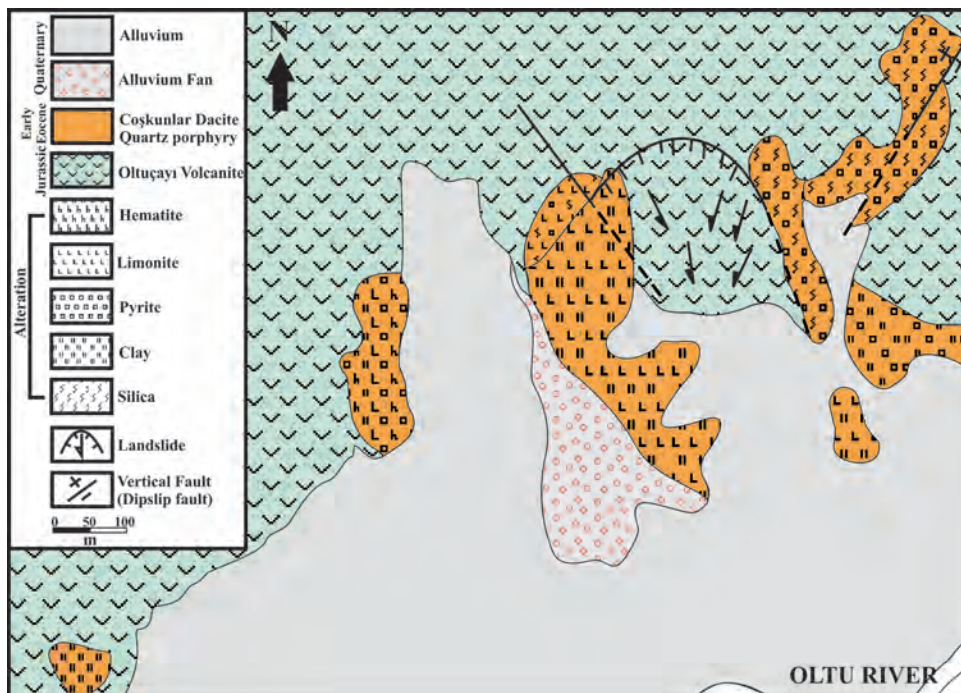


Figure 10- 1/5.000 scale geological map of the alteration zone in Yeşilbağlar (Olur-Erzurum) region (Önal, 2015).

silicifications, argillizations, sulphatizations are common, sericitization and chloritization are limited. Stockwork of limonite and hematite are commonly present. Brecciations and elementer sulphurs are also present in the alteration zones (Figures 11a-d). In the advanced argillic alterations in the leach zone of the dacites, hematitization is seen in the upper part, pyrites together with hematization and elementer sulphurs are in the lower part. In the oxidation zone hematitization (iron cap-gossan) along N30°W direction is about 20 m long and 2 m thick. In the alteration zone white coloured stockwork of quartz veins/veinlets in places are chalcedonic and are found together with pyrites. Gypsum is also commonly present. The size of the pyrites in the silicification zone is 1-2 cm (Figures 11e-h). In the parts where rocks are crowded with pyrite, hematitization and limonitization appear to have developed as alteration products from the alteration of iron rich minerals like amphiboles, biotites, hematites and limonitization are also present around the brecciations. In the study area along some fractures from the alteration of pyrites, limonitizations and hematitization have also been noticed to have developed.

### 5.2. Kaban Alteration and Mineralization

Kaban alteration zone is situated approximately 17km to the Southeast of Olur (Erzurum) and about 10km to the East of Yeşilbağlar alteration zone (Figure 3). Coşkunlar Dacite has intruded into the contact zone between Kaban Dacite belonging to the Olur Group and Soğukçam formation. The alteration zone developed in the Coşkunlar Dacite along this contact zone (Figure 12). Within the Coşkunlar Dacite the alteration zone is quite extensive and along E-W direction it is about 100 m wide, 300 m long (Figure 12). Kaban alteration is quite similar to the Yeşilbağlar alteration. In the alteration zone silicifications, argilization are extensive, chloritization and sericitization are also present. In the oxidation zone along with hematitization (iron cap-gossan) zones, sulphates (barite) and gypsums are also common (Figures 13a-d). In the Kaban alteration zone along with disseminated pyrites, malachites and azurites are also present in the fracture zones. Within the brecciated block there are remains of addit entrances belonging to the pre republic time copper mining (Figures 13e-h).

### 5.3. Köprübaşı Alteration and Mineralization

Köprübaşı alteration is situated between Yeşilbağlar and Kaban alteration zones 8 km to the south of Olur

(Erzurum). Alteration is in the Coşkunlar Dacite which has intruded along the contact between Kaban Dacite and Soğukçam formation. These alterations extend about 100 m in an E-W direction (Figure 3). In the Köprübaşı silicifications, limonitizations, hematitization are common but argilization is less than other alteration zones (Figure 14). In the field outcrop of Köprübaşı alteration zone is very small, so it was not marked on the 1/5.000 scale geological map. Samples could not be collected from the Köprübaşı alteration zone therefore the mineralogy and chemistry of this zone could not be studied in detail.

### 5.4. Mineralization Type

In the alteration zones of the study area, disseminated, stockwork, vein/veinlet and smear like different types of mineralizations are present. Disseminated type mineralizations are commonly present in the quartz porphyry apophysis of the Coşkunlar Dacite and in the host rocks. In these mineralizations pyrite was macroscopically observed (Figure 15a). Limonitization and hematitization are the stockwork type mineralizations in the alteration zones (Figures 15b, c). Vein-veinlet type mineralizations have developed in the grey and grey-white coloured quartz veins which include pyrites. In the Yeşilbağlar alteration zone pyrite bearing zones are mm-cm thick and are 1-2 m long. Veins and veinlets have cross cutting relations (Figures 15d, e). Smears of malachites and azurites are seen in the fracture zones in various directions and have irregular dispositions (Figure 15f).

## 6. Ore Mineralogy and Chemistry

Ore mineralogy and chemistry of the mineralizations in the Yeşilbağlar and Kaban alteration zones have been separately evaluated and mineral paragenesis have been described. In the alteration zones the ore minerals present are; pyrites, chalcopyrites, galena, sphalerites and pyrrhotites, gang minerals present are quartz, barites and calcites.

### 6.1. Yeşilbağlar Alteration

Macroscopic and microscopic mineralogical studies were carried out on the samples collected from the Yeşilbağlar alteration zone. Paragenesis of the minerals show that pyrite is the most abundant ore mineral. Chalcopyrite, sphalerite, galena, chalcocite, rutile are present in decreasing order. Hematite, limonite, malachite, azurite ore minerals are the

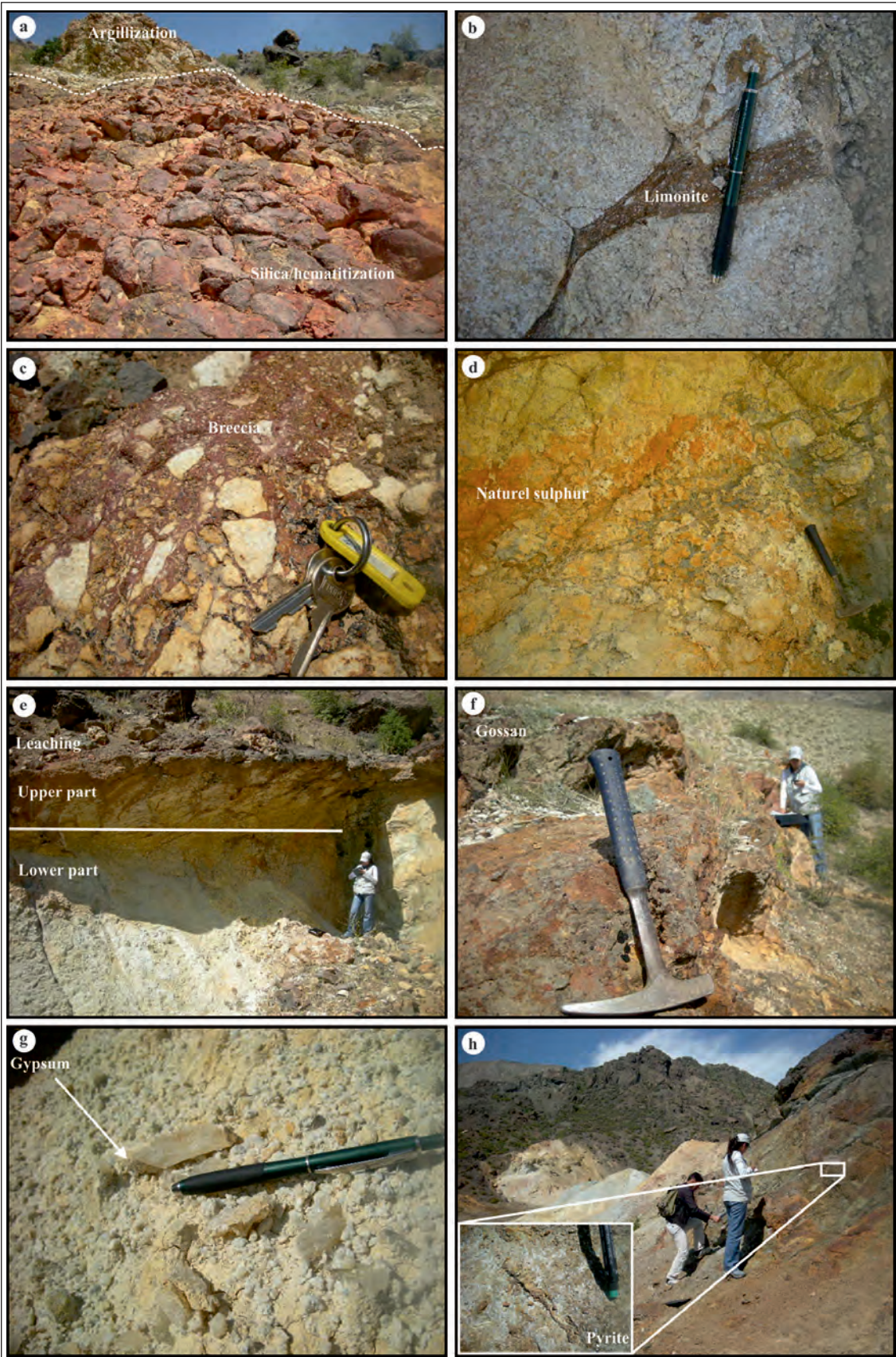


Figure 11- Field views from the Yeşilbağlar (Olur-Erzurum) alteration zone.

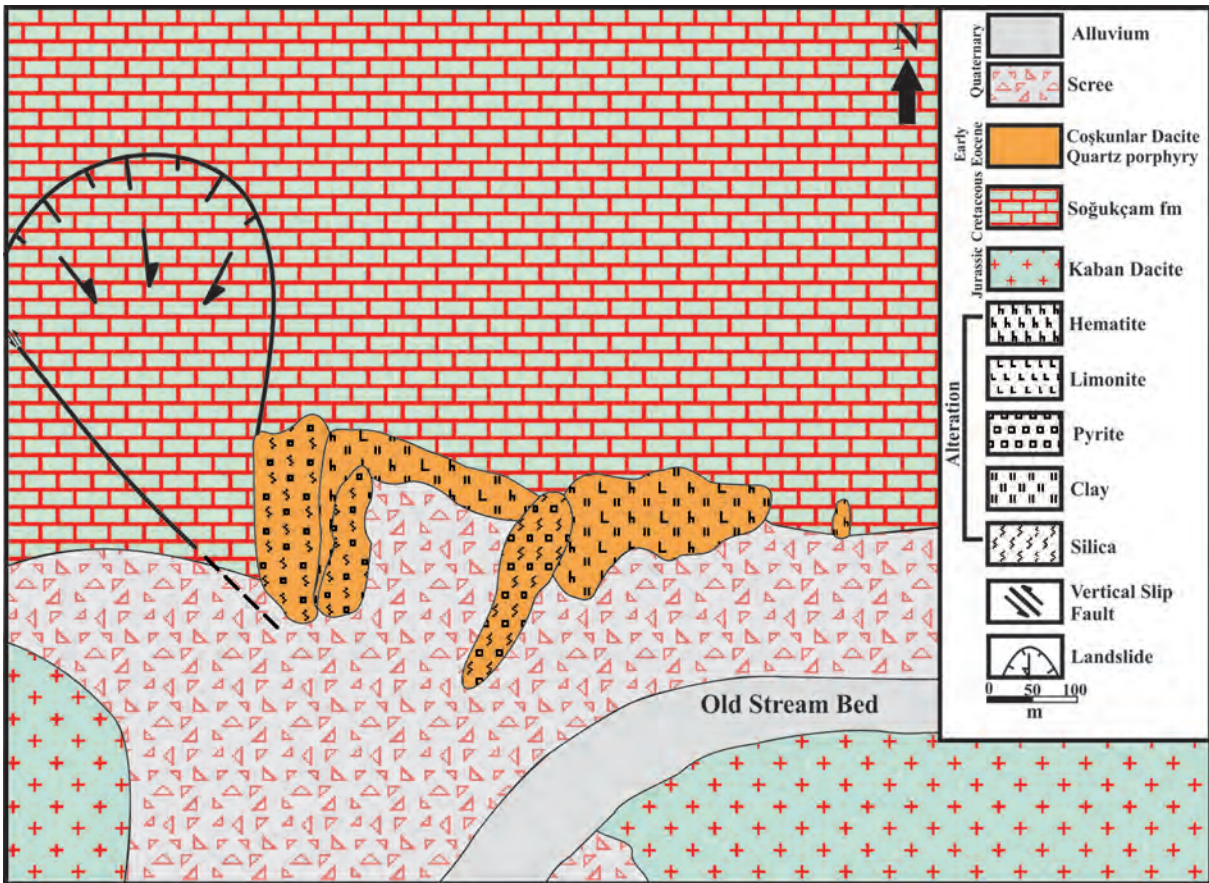


Figure 12- 1/5.000 scale geological map of the alteration zone in Kaban (Olur-Erzurum) region (Önal, 2015).

minerals present in the oxidation zone. Details of the mineralogy, texture and chemical compositions of the ore minerals are given below.

**Pyrite:** Pyrite is the most common ore mineral present in the alteration zone. Size of the pyrite crystals is up to 1 mm, idiomorph, pseudomorph crystals have skeleton textures (Figure 16a, b). In the ore samples chalcopyrites and sphalerites appear to have metasomatised pyrites (Figures 16c, d). This indicates that pyrites were formed earlier than chalcopyrites and sphalerites. Because of the deformations they became subjected to pyrites were fractured and broken and in some cases they were metasomatized by chalcocite. Secondary rutiles are also present (Figure 16e). Cataclastic textures observed in the pyrites indicate that deformations developed in rather low temperatures. As pyrites are harder, they were effected more than the other sulphide minerals present together with pyrite (Craig and Vaughan, 1981; McClay and Ellis, 1984; Craig and Vokes, 1993; Kuşçu and Erler, 1999, 2002) (Figure 16f). Temperature and pressure

conditions causing changes of textures to develop in pyrites give information on the deformation textures and tectonic past of the deposit (Craig et al., 1998; Lianxing and McClay, 1992). In the mineral deposit if changes of textures when pyrite are present in other ore minerals too and have been repeated several times over, this indicates continuous deformations in the process of their developments (Kuşçu and Erler, 2002; Demir, 2010). Pyrites have been analysed for S, Fe, Mn, Co, Ni, As, Pb, Ag, Cu, Ga, In, Sb, Zn and Cd (Table 1). S and Fe are the main content of pyrites. Range of contents of other elements are; Ni 0.01-1.08%, Zn 0.01-0.13%, Cd 0.01-0.21 %, Co 0.01-0.04%. Based on these analyses the chemical formulae of the pyrites have been calculated as  $Fe_{0.81-0.85}S_{1.6-1.7}$  ( $FeS_2$ ). Chemical compositions and textures of the pyrites reflect the process they were subjected to during and later stages of their developments. Some scientists use Co/Ni ratio of pyrites to understand development processes. Co/Ni ratio gives information on the primary development temperatures and also independent from this metamorphism temperature.

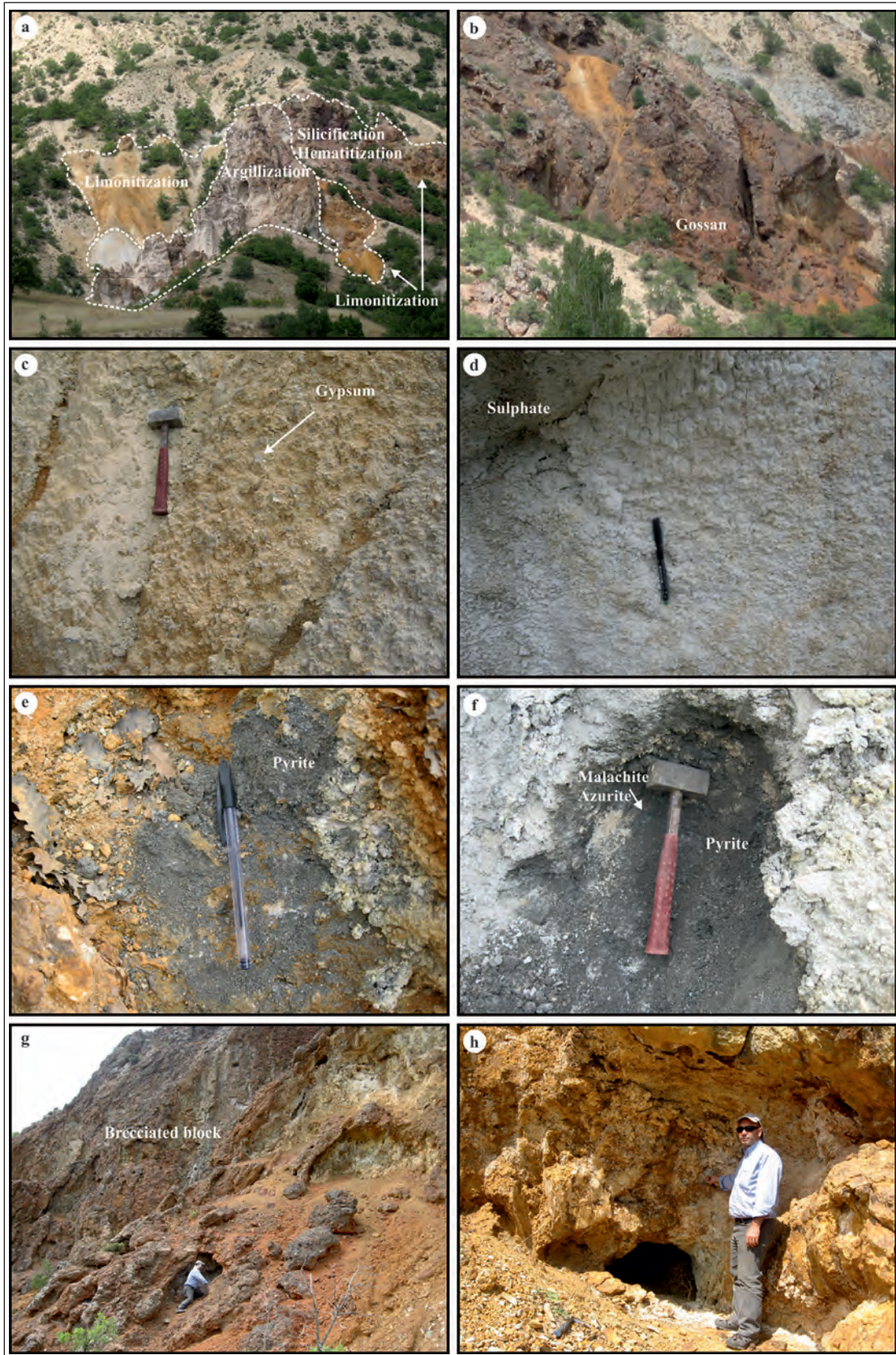


Figure 13- Field views from the Kaban (Olur-Erzurum) alteration zone.

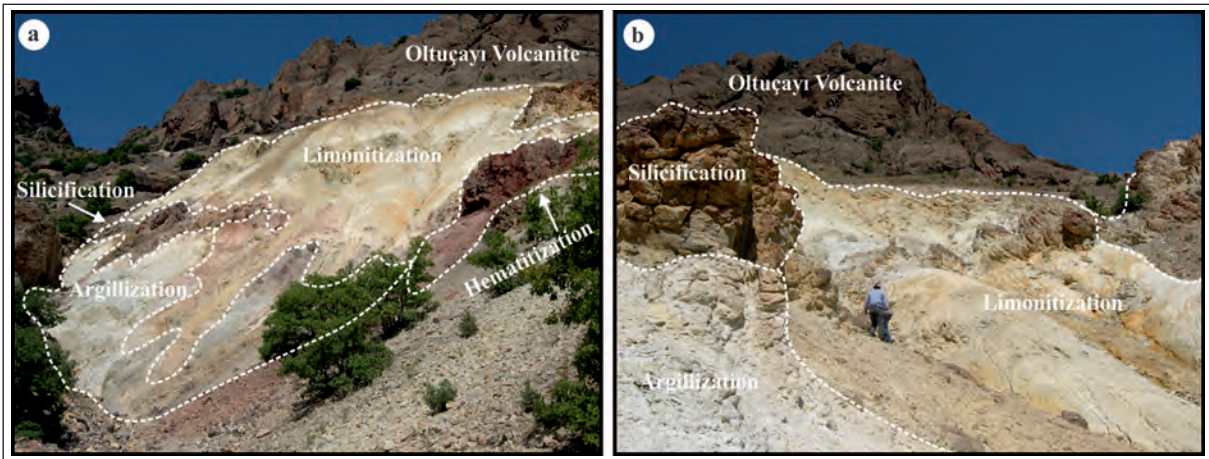


Figure 14- Field views from the Köprübaşı (Olur-Erzurum) alteration zone.

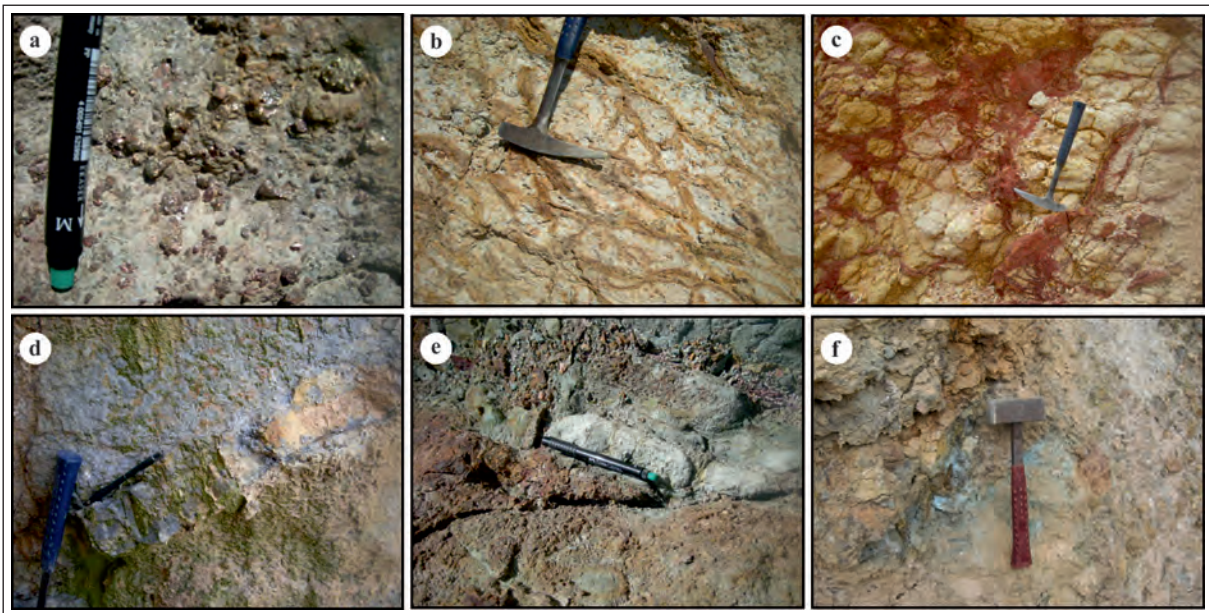


Figure 15- Types of mineralization observed in the study area.

If  $Co/Ni < 1$ , it indicates sedimentary origin,  $Co/Ni > 1$  indicates hydrothermal origin (Loftus-Hills and Solomon, 1967; Bralía et al., 1979; Roberts, 1982; Xuexin, 1984; Raymond, 1996; Kant et al., 2012). Analyses of the pyrites from the Yeşilbağlar alteration zone show  $Co/Ni > 1$  ( $Co/Ni$ : 1-2.83) indicating hydrothermal origin (Table 1).

**Chalcopyrite:** In the Yeşilbağlar alteration, after pyrite chalcopyrite is the most abundant primary Cu mineral. They are all pseudomorph crystals. Chalcopyrites developed after pyrites and have metasomatized pyrites (Figure 17a). Chemical analyses of chalcopyrites show that apart from main elements of S, Fe and Cu, Cd is also present. Analysed

all other elements are below detection limits (Table 1). Cd content of chalcopyrites is 0.02%. General chemical formulae of chalcopyrites have been calculated as  $Cu_{0.52}Fe_{0.55}S_{1.10}$  ( $CuFeS_2$ ) (Table 1).

**Sphalerite:** In the Yeşilbağlar alteration zone sphalerite is less abundant than pyrite and chalcopyrite. Under microscope sphaerite is in various shades of grey colour and has yellowish brown internal reflections (Figure 17b). Fe content of sphalerite is relatively low, this is in accordance with their light coloured internal reflections. Sphalerites have pseudomorphic crystal forms and have metasomatized pyrites (Figures 17c, d). Mineral chemical analyses of sphaerites are given in table 1. Chemical analyses of

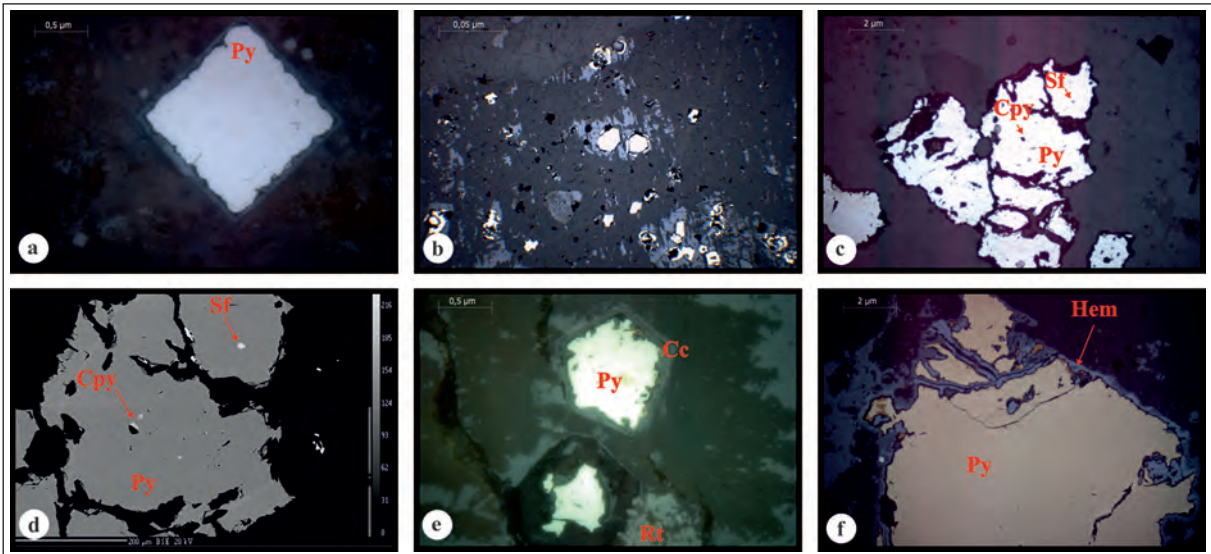


Figure 16- Polished thin section views of pyrites from the Yeşilbağlar alteration zone, d) Back-scattered electron (BSE) image (Py: Pyrite, Cpy: Chalcocopyrite, Sf: Sphalerite, Cc: Chalcocine, Ru: Rutile, Hem: Hematite).

sphaerites show that ranges are; Fe 1.91-12.76%, Cu 0.01-0.21%, Zn 50.76-64.68% and Cd 0.22-0.42%. General formulae of sphaerites have been calculated as  $Zn_{0.80-1.00}Fe_{0.0-0.2}S_{1.01-1.03} [(Zn, Fe)S]$  (Table 1). Sphalerite is an important mineral indicating origin and mineralizing conditions of the mineralizations (Craig and Vaughan, 1994; Cook, 1996; Holten et al, 2000; L'Heureux and Jamtveit, 2002; Palero and Martin-Izard, 2005). Variations in the chemical compositions reflects variations in developing conditions during crystallization process (Grammatikopoulos and Roth, 2002). Compositional changes in sphalerites are better represented from their primary compositions when

they were first formed then changes that developed at a later stage resulting from balancing conditions (Dibenedetto et al., 2005). Sphalerites in the Yeşilbağlar alteration zone do not show any compositional element zonings. This indicates that during crystallizations physicochemical conditions of the environment were stable (Demir, 2010). Studies on mineral chemistry of the sphalerites suggest that Cd contents and Zn/Cd ratios could be used to determine crystallization types of the mineralizations (Jonasson and Sangster, 1978; Xuexin, 1984; Brill, 1989; Xu, 1998; Gottesman and Kampe, 2007; Demir, 2010; Kant et al., 2012). In volcano sedimentary deposits Zn/Cd ratios show

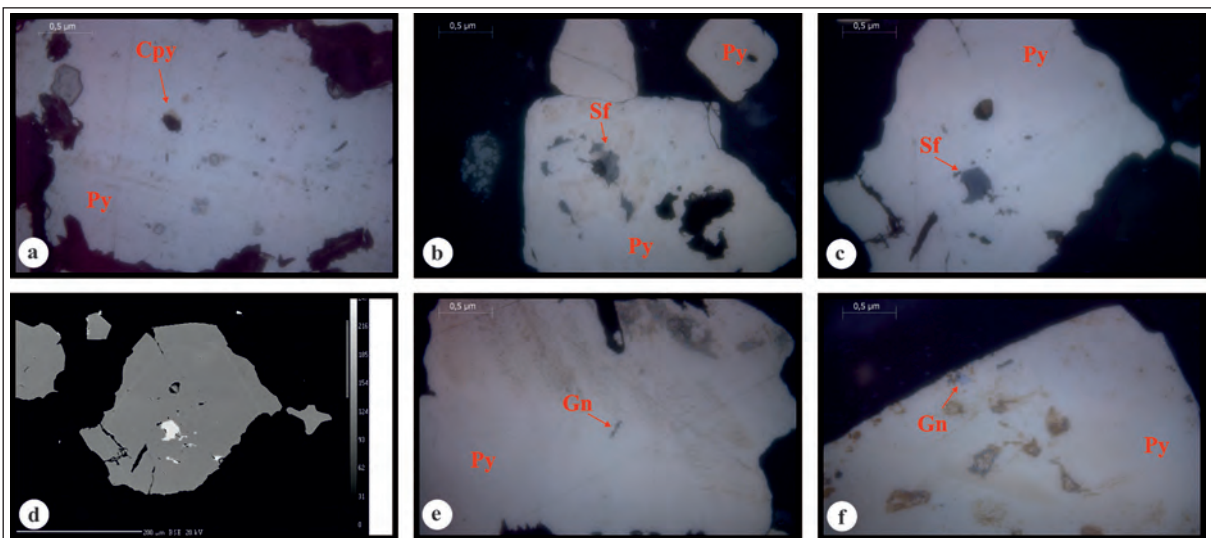


Figure 17- Polished thin section views of chalcopyrite, sphalerite and galenite from the Yeşilbağlar alteration zone, d) Back-scattered electron (BSE) image (Py: Pyrite, Cpy: Chalcocopyrite, Sf: Sphalerite, Gn: Galenite).

Table 1- Mineral chemistry analyses of the minerals of the alteration zones (weight %) (YB-Yeşilbağlar, K-Kaban alterations).

Sample	Mineral	S	Mn	Fe	Co	Ni	As	Pb	Ag	Zn	Cu	Ga	Cd	In	Sb	Total
YB34_C_pt52	Chalcopyrite	35.15		30.5							32.7		0.02			98.401
YB6_A_pt2	Pyrite	53.32		46.6						0.02	0.01		0.12			100.12
YB6_A_pt3	Pyrite	53.62	0.01	46.8					0.02				0.19	0.03		100.62
YB6_A_pt4	Pyrite	53.29		46.5		0.01			0.01		0.01		0.14		0.03	100.04
YB6_A_pt5	Pyrite	53.3		46.7		0.01			0.02	0.02		0.01	0.13		0.03	100.17
YB6_A_pt6	Pyrite	53.5		46.7							0.02		0.21			100.44
YB6_A_pt7	Pyrite	53.41		46.6		0.01			0.02	0.01			0.13			100.15
YB6_A_pt8	Pyrite	53.38		46.7								0.01	0.09		0.01	100.19
YB6_B_pt9	Pyrite	53.05		46.8			0.01				0.01	0.02	0.06			99.96
YB6_B_pt10	Pyrite	53.13	0.01	46.8	0.01				0.03	0.04	0.03	0.01	0.16	0.03		100.22
YB6_B_pt11	Pyrite	53.2		46.7					0.02				0.08	0.01	0.01	100.01
YB6_B_pt12	Pyrite	52.9		46.6	0.01		0.03					0.01	0.16	0.02		99.717
YB6_B_pt13	Pyrite	53.29	0.01	46.8		0.02	0						0.09	0.05		100.24
YB6_B_pt14	Pyrite	53.13	0.01	46.7			0.07			0.03		0.02	0.11		0.02	100.1
YB6_C_pt15	Pyrite	53.21		46.8	0.02		0.01		0.02	0.02			0.12			100.25
YB6_C_pt16	Pyrite	53.12		46.6					0.04	0.13	0.01	0.01	0.11	0.01		99.994
YB6_D_pt20	Pyrite	53.3		46.9	0.01				0.05		0.01		0.03		0.02	100.32
YB6_D_pt21	Pyrite	53.17		46.7			0.01		0.03		0.02		0.13			100.1
YB13_A_pt23	Pyrite	53.26	0.01	46.6		0.14	0.02		0.04		0.03	0.01	0.08	0.01	0.01	100.23
YB13_A_pt24	Pyrite	52.84	0.01	46.5		0.1	0.02			0.02	0.04		0.13	0.05	0.01	99.664
YB13_A_pt25	Pyrite	53.03	0.01	46.3	0.02	0.53					0.02		0.08	0.01		99.985
YB13_A_pt26	Pyrite	52.89	0.01	46.9		0.02				0.05	0.01		0.05	0.03	0.01	99.939
YB13_A_pt27	Pyrite	53.46		46.4		0.09				0.08		0.01	0.12		0.01	100.18
YB13_B_pt28	Pyrite	53.44	0.01	45.6		1.08			0.05				0.04			100.26
YB13_B_pt29	Pyrite	53.09		46.4		0.17					0.02		0.07			99.782
YB18_A_pt2	Pyrite	53.33		47.1		0.01	0.36	0.08	0.04		0.01				0.03	100.99
YB18_A_pt3	Pyrite	53.73		46.7			0.04	0.11					0.02			100.61
YB18_A_pt4	Pyrite	53.46		46.8			0.05	0.19	0.03		0.02					100.56
YB18_A_pt5	Pyrite	52.58		46.2		0.02	1.8	0.24			0.03		0.03		0.02	100.94
YB18_A_pt6	Pyrite	52.77		46.6		0.01	1.19	0.09	0.02		0.06				0.01	100.69
YB18_A_pt7	Pyrite	53.41		46.8				0.1							0.01	100.34
YB18_A_pt8	Pyrite	53.69		47.2		0.01	0.05	0.1		0.02	0.03		0.12			101.24
YB18_A_pt9	Pyrite	53.74		46.5			0.01	0.07		0.05	0.02				0.01	100.44
YB18_A_pt10	Pyrite	52.72		46.3		0.01	1.3	0.12	0.01	0.03	0.04					100.48
YB18_A_pt11	Pyrite	53.22		46.3			0.68	0.04		0.03						100.29
YB18_A_pt12	Pyrite	53.47		47		0.01	0.03	0.03	0.02	0.02						100.61
YB18_A_pt13	Pyrite	51.97		46.2			2.18	0.07					0.01		0.01	100.41
YB26_A_pt5	Pyrite	53.48		47.2		0.01	0.04	0.02					0.13			100.88
YB26_A_pt6	Pyrite	52.02		46.6			2.19	0.05	0.01		0.01		0.15			101.02
YB26_A_pt7	Pyrite	53.46		47.2			0.01	0.08	0.08		0.02		0.12			100.97
YB26_B_pt8	Pyrite	53.58		46.9	0.01		0.01	0.1	0.01				0.06		0.01	100.73
YB26_B_pt9	Pyrite	53.8		47.2			0.03	0.09		0.03	0.02					101.18
YB26_B_pt10	Pyrite	52.12		46.7			2.02	0.03	0.01		0.04		0.06			100.99
YB26_B_pt11	Pyrite	53.56		47.2	0.04		0.02	0.08		0.01	0.04		0.11			101.07
YB26_B_pt12	Pyrite	53.66		47.3		0.02	0.01	0.11		0.03	0.01		0.12			101.26
YB26_C_pt13	Pyrite	53.57		47.4		0.01	0.01	0.15					0.08			101.17
YB26_C_pt14	Pyrite	53.67		47.3			0.02	0.06	0.04				0.02			101.1
YB26_C_pt15	Pyrite	53.66		47				0.02	0.01				0.1		0.02	100.82
YB26_C_pt16	Pyrite	53.28		47.4			0.03	0.06	0.04	0.01	0.01		0.05		0.02	100.96
YB26_C_pt17	Pyrite	53.44		47.2			0.03	0.16	0.02				0.12			100.95

Table 1- (continued).

Sample	Mineral	S	Mn	Fe	Co	Ni	As	Pb	Ag	Zn	Cu	Ga	Cd	In	Sb	Total
YB26_C_pt18	Pyrite	53.72		47.4				0.09	0.01				0.08		0.02	101.31
YB26_C_pt19	Pyrite	53.66		47.4			0.01	0.06					0.04			101.14
YB26_C_pt20	Pyrite	53.62		47.6			0.02	0.09			0.03		0.05			101.45
YB34_A_pt30	Pyrite	53.07	0.01	46.6									0.09		0.03	99.84
YB34_A_pt32	Pyrite	52.96		46.7			0.01		0.01				0.07			99.71
YB34_B_pt33	Pyrite	52.82		46.5					0.03		0.03	0.01	0.07		0.01	99.494
YB34_B_pt36	Pyrite	52.85		46.5					0.01	0.02		0.01	0.06	0.03	0.01	99.454
YB34_B_pt37	Pyrite	52.9		46.8		0.01	0.06				0.01	0.02	0.05			99.837
YB34_B_pt38	Pyrite	52.76		46.9					0.01	0.02				0.04	0.02	99.74
YB34_C_pt39	Pyrite	53.13		46.8	0.01	0	0.01		0.04	0	0.01		0.05	0.08		100.09
YB34_C_pt40	Pyrite	53.02	0.01	46.6						0.01	0.01		0.02			99.626
YB34_C_pt41	Pyrite	51.83	0.01	45.3	0.02	0.01	2.09				0.02	0.01	0.06	0.06	0.04	99.468
YB34_C_pt42	Pyrite	52.92		46.7		0.02							0.04			99.691
YB34_C_pt43	Pyrite	53.26		46.6					0.04	0.07	0.02			0.02		100.02
YB34_C_pt45	Pyrite	52.89		46.6						0.03	0.02		0.06	0.06	0.03	99.661
YB34_C_pt46	Pyrite	53.1		46.6		0.01			0.03					0.01		99.708
YB34_C_pt41a	Pyrite	51.76	0.01	45.6			1.85			0.02	0.01	0.01			0.08	99.308
YB34_C_pt48	Pyrite	53.56		46.6		0.01			0.04	0.02			0.04	0.01		100.29
YB34_C_pt47	Pyrite	51.34	0.01	45.9		0.02	1.75			0.06			0.09		0.08	99.2
YB34_C_pt49	Pyrite	53.26		46.6							0.02				0.01	99.941
YB34_C_pt50	Pyrite	52.05		45.6			1.99		0.03	0.02			0.07		0.06	99.825
YB34_C_pt51	Pyrite	52.48		46.4			2				0.03		0.07		0.07	101.06
YB34_C_pt53	Pyrite	53.56		46.8			0.01			0.01	0.01		0.04	0.02		100.49
YB6_A_pt1	Galena	14.81		5.22				82.6			0.06	0.05		0.02		102.72
YB26_pt2	Galena	13.59		2.23				86	0.12	0.05	0.04			0.02		102.02
YB26_pt3	Galena	13.64		2.55				86.8	0.04	0.02				0.05		103.06
YB26_pt4	Galena	13.48		1.42				85.9	0.23	0.04				0.04		101.13
YB6_C_pt17	Sphalerite	32.68	0.04	4.54	0.01	0.01			0.01	62.3	0.01		0.22	0.01		99.825
YB6_C_pt18	Sphalerite	35.75	0.01	12.8						50.8	0.01		0.22	0.06		99.571
YB6_C_pt19	Sphalerite	32.45	0.03	3.26			0.14		0.03	63.1			0.31			99.304
YB6_D_pt22	Sphalerite	32.98	0.03	3.15			0.11			63	0.01		0.3		0.01	99.633
YB34_A_pt31	Sphalerite	32.42		2.5	0.01	0.01				64.3			0.42		0.02	99.674
YB34_B_pt34	Sphalerite	32.64	0.01	2.21						63.9	0.11		0.24			99.136
YB34_B_pt35	Sphalerite	32.38		1.91						64.7			0.28			99.257
YB34_C_pt44	Sphalerite	32.64		2.89	0.01				0.01	63.1	0.21	0.02	0.3	0.01	0.12	99.267
K27_B_pt33	Chalcopyrite	34.77		31			0.22		0.01		32.9					98.952
K27_A_pt26	Pyrite	53.3		47.1		0.01	0.06		0.03							100.48
K27_A_pt27	Pyrite	52.79		46.9			0.4				0.01					100.04
K27_A_pt30	Pyrite	52.39		47	0.01	0.01	0.12									99.547
K27_B_pt31	Pyrite	52.74		47		0	0.27									100.01
K27_B_pt32	Pyrite	53.14		47.2		0.01	0.05									100.37
K27_B_pt34	Pyrite	53.21		46.7		0.01	0.25		0.02							100.19
K27_A_pt28	Pyrrhotite	38.26		60.6		0.01	0				0.02					98.899
K27_A_pt29	Pyrrhotite	38.37		60.6			0.16									99.129
K27_B_pt35	Pyrrhotite	39.02		60.4		0.01	0.3									99.754

changes in 417-531 range, in magmatic hydrothermal deposits in 104-214 range and in stratiform deposits related with carbonates in 252-330 range (Jonasson and Sangster, 1978; Xuexin, 1984). Zn/Cd ratio of the sphalerites in the Yeşilbağlar alteration zone on average is 223.2, suggesting magmatic hydrothermal origin.

**Galena:** Galena in the Yeşilbağlar alteration zone have idiomorphic and pseudomorphic crystal forms, filling interspaces of other minerals present. In the polished sections idiomorphic galenas are white coloured and have characteristic triangular shapes (Figures 17e, f). In paragenesis galenas are after pyrite and have metasomathised pyrites. Metasomatism has obscured the contacts of galenas with other minerals and they appear irregular. Like pyrites, chalcopyrites and sphalerites, galenas have also been fractured. Fractures in galenas are along the cleavages, in other minerals they are rather irregular. Mineral chemistry analyses of the galenas from the alteration zone are given in table 1. Pb and S are the main elements of galena. Apart from these elements, samples were analysed for Fe, Ag, Zn and In. Analyses of these elements in galenas have given the following values: Fe 1.42-5.22%, Ag 0.02-0.23%, Zn 0.02-0.05%, In 0.02-0.05. From these values, general chemical formulae of galena has been calculated as  $Pb_{0.40-0.42}Fe_{0.03-0.09}S_{0.42-0.46} ([Pb, Fe]S)$  (Table 1).

## 6.2. Kaban Alteration

Based on the macroscopic and microscopic studies of the samples collected from the Kaban alteration zone. Paragenesis of the minerals in decreasing order are; pyrite-chalcopyrite-pyrrhotite. In the oxidation zone hematite, limonite, malachite and azurite are the minerals present. Details of the mineralogical and textural characteristics and chemical compositions of the minerals in paragenesis are given below.

**Pyrite:** As is the case in Yeşilbağlar alteration zone, pyrite is the most common mineral in the Kaban alteration zone. In general pyrites have idiomorphic pseudomorphic crystal forms and have cataclastic texture. Grain size varies from several microns to 5-6 mm. Polished section studies show that pyrites are highly fractured and have hematite rims developed along the margins (Figure 18a). In general pyrites developed ahead of chalcopyrites and are surrounded by gang minerals. From the alteration zone, in one sample chemical analyses have been carried out on 6 points. Chemical analyses of pyrites gave results S, Fe, Mn, Co, Ni, As, Pb, Ag, Cu, Ga, In, Sb, Zn and Cd concentrations. (Table 1). Fe and S are the main elements of pyrites. Ni and Co contents respectively are 0.00-0.01% and 0.01%. Based on these values general chemical formulae of pyrites has been calculated as  $Fe_{0.83-0.84}S_{1.6-1.7} (FeS_2)$ . Co and Ni concentrations of the pyrites from Kaban are rather low (Table 1). Co/Ni ratio of the pyrites is 1.4 (Co/Ni=1.4). As this ratio is greater than 1 (Co/Ni >= 1) alteration is considered to have hydrothermal origin.

**Chalcopyrite:** In the study area chalcopyrites are the second most abundant mineral after pyrites. They in general have irregular, pseudomorphic crystal forms and have metasomathized pyrites (Figure 18b). S, Fe and Cu are the main elements of chalcopyrite, apart from these elements As and Ag are also present. Other elements were under the detection limits (Table 1). Based on the chemical analyses chemical general formulae of the chalcopyrite has been calculated as  $Cu_{0.52}Fe_{0.56}S_{1.08} (CuFeS_2)$ .

**Pyrrhotite:** In the alteration zone it is not a commonly found mineral. They are generally found in pyrites developed as a result of metasomatism. Pyrites are cataclastic, coarse to fine grained and have developed ahead of pyrrhotites (Figure 18c). In some cases, in cataclastic pyrites, along fractures and cleavages pyrrhotites are seen as metasomatism



Figure 18- Polished thin section views of chalcopyrite, sphalerite and pyrotine from the Kaban alteration zone (Py: Pyrite, Cpy: Chalcopyrite, Po: Pyrotine, Hem: Hematite).

products. S and Fe are the main elements of pyrrhotite. Apart from these elements analyses show presence of Ni 0.01%, As 0.01-0.3% and Cu 0.02%. Other elements are below detection limits (Table 1). On the base of chemical analyses, chemical formulae of pyrrhotite has been calculated as  $Fe_{1.08-1.09}S_{1.19-1.22}$  (FeS).

6.3. FT-IR Fourier Transform-Infrared Spectroscopy Analyses

FT-IR analyses carried out on the specimens collected from the Yeşilbağlar alteration zone showed the presence of kaolinite, chlorite (clinochlore), quartz, illite-muscovite, gypsum, jarosite and barite minerals. Some of the findings are given in table 2. IR spectrums of typical mineral peaks of the minerals present in the samples from the Yeşilbağlar alteration are given in Figures 19a-e. In some of the analysed samples characteristic peaks indicating carbonate presence can also be seen (Figure 19a).

FT-IR analyses results of the samples from the Kaban alteration zone are similar to the Yeşilbağlar alteration. In the analysed samples presence of kaolinite, chlorite (clinochlore) quartz, gypsum and barite have been detected (Table 3). IR spectrums of typical mineral peaks of the minerals present in the Kaban alteration samples are given in figures 20f-h.

6.4. X-Ray Diffraction Analysis

XRD studies carried out on the samples from the Yeşilbağlar alteration zone showed, presence of

quartz, chlorite group minerals (clinochlore), sulphate minerals (gypsum, bassanite, barite), muscovite and pyrite (Figures 20a-f). In the analysed samples quartz and chlorite group minerals are the main minerals. In all of the analysed samples minor amounts of non-clayey minerals are also present. Among those jarosite  $[KFe_3(SO_4)_2(OH)_6]$  is an alteration product mineral. Oxidation of pyrites produces sulfuric acid. Sulphuric acid reacts with K-feldspars and illite, causing  $K^+$  extractions, and jarosite develops (Karakaya, 2006). Bassanite  $[CaSO_4 \cdot 1/2H_2O]$  is another mineral detected. It is a pseudomorph of gypsum. Clinochlore is a chlorite mineral containing Mg-Al (Karakaya, 2006). Results of XRD studies are in agreement with FT-IR analyses results.

Table 3- Wave lengths of some of the minerals in the Kaban alteration zone.

Mineral	Wave length of the mineral (cm <sup>-1</sup> )			
	K-1	K-16	K-18-A	K-27
Kaolinite		3695 3652 3620	3696	3693 3619
Chlorite	3635 3420			
Quartz	796 777	796 777		796 780
Gypsum and Barite			3546 3404 1142 1118 669 602	
Carbonate		1438		

Table 2- Identifying wave lengths of some of the minerals in the Yeşilbağlar alteration zone

Mineral	Wave length of the mineral (cm <sup>-1</sup> )							
	YB-3	YB-4	YB-13	YB-20	YB-26	YB-34	YB-41	YB-48
Kaolinite	3695	3695 3654 3620	3696	3697				
Chlorite		3695		3557 3433				
Clinochlore			3546 3420				3563 3445	
Illit/Muscovite	3620 3428 827 760			3619 3433	3630 3402			
Quartz	796 777	797 778	799 777	794 779		797 778	797 777	
Gypsum								3546 3405 1147 1120 669 602
Jarosite ve Barite						3387,1084 632		
Carbonate	1450	1452						

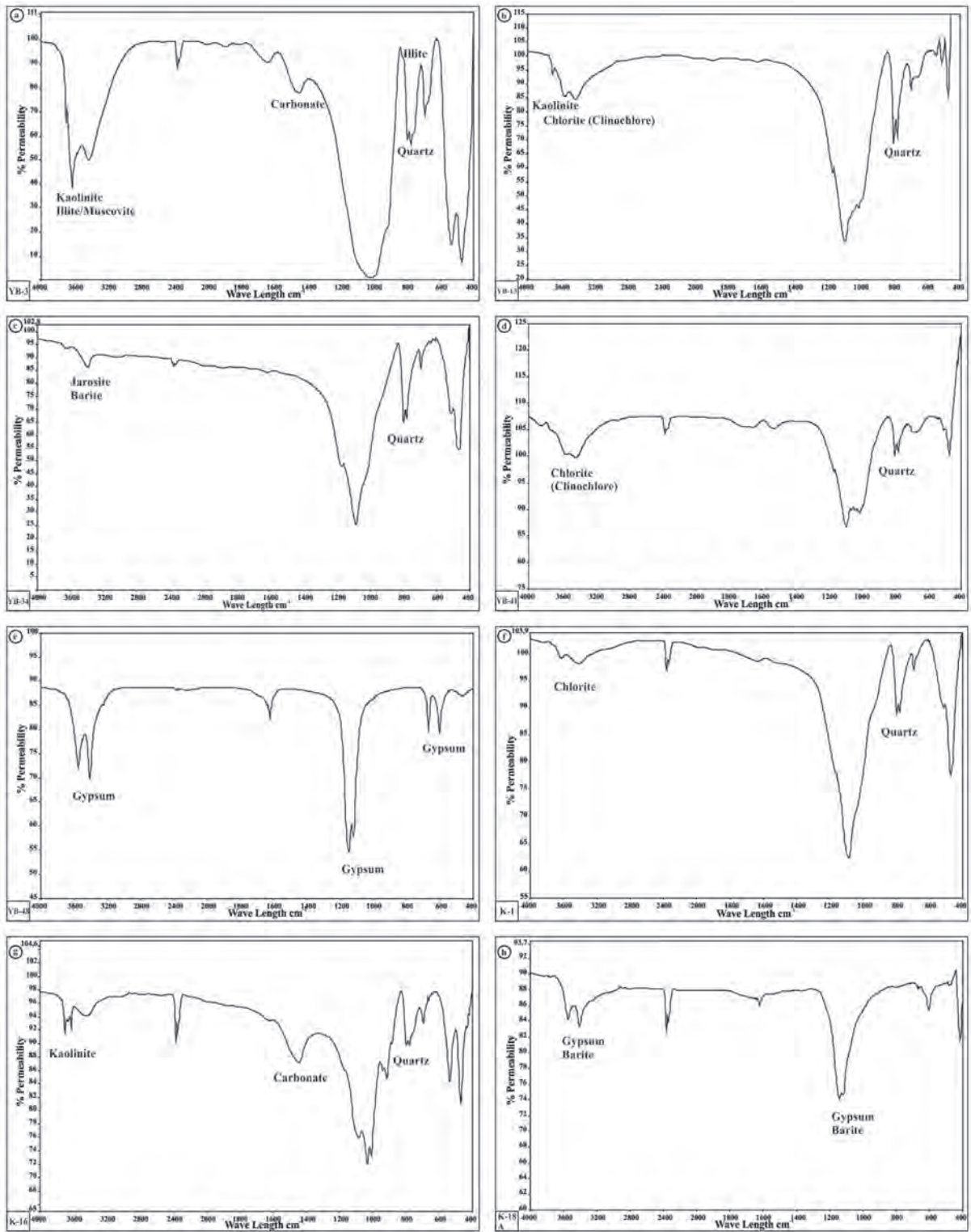


Figure 19- Spectrums of the FT-IR analyses, a-e) Samples from the Yeşilbağlar alteration zone, f-h) Samples from the Kaban alteration zone.

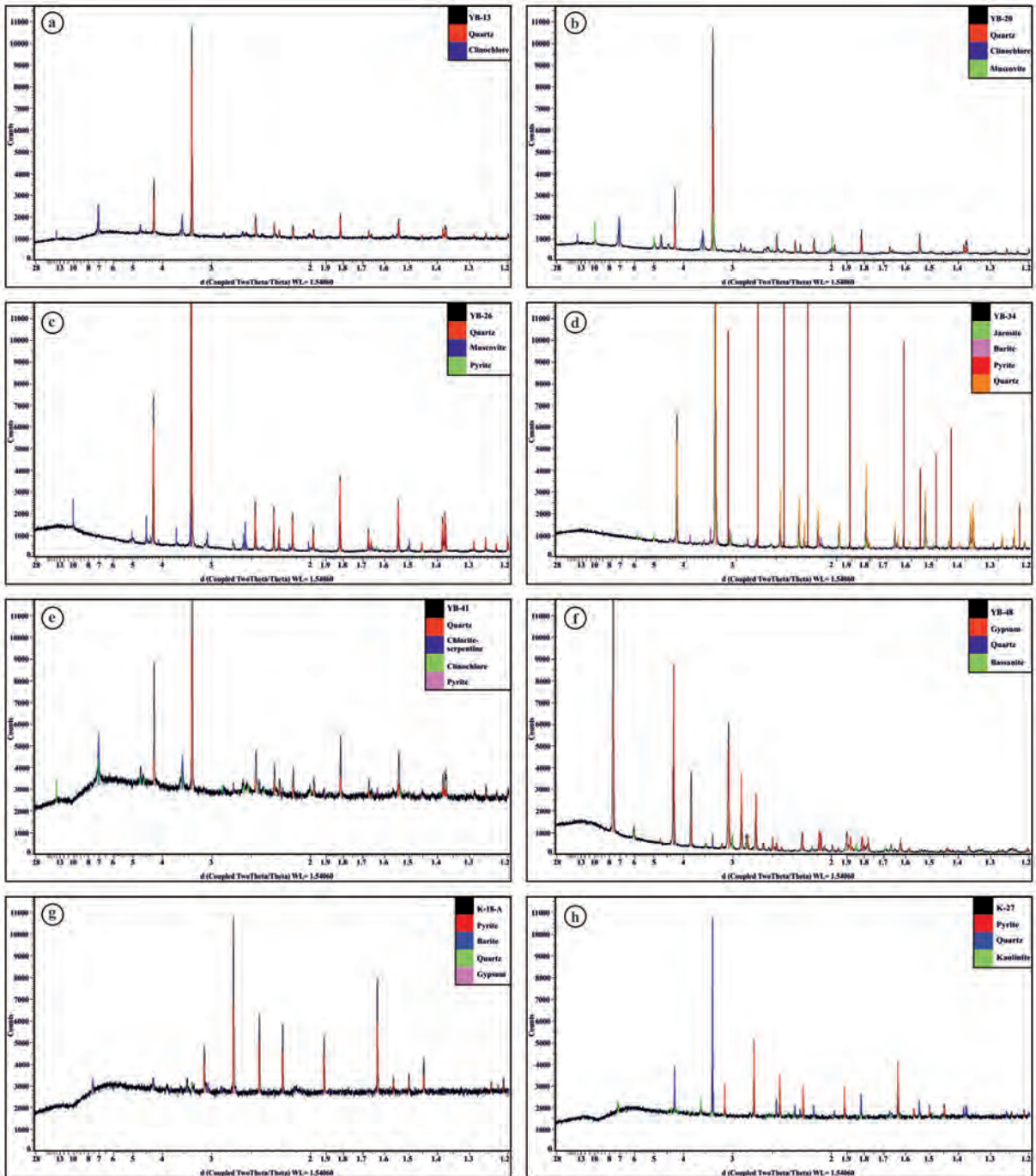


Figure 20- Diffractograms of the XRD analyses, a-f) Samples from the Yeşilbağlar alteration zone, g-h) Samples from the Kaban alteration zone.

XRD studies carried out on the samples from Kaban alteration zone showed the presence of quartz, sulphate (gypsum, barite), clay (kaolinite) and pyrite (Figures 20g, h). As in the Yeşilbağlar alteration, results of the XRD and FT-IR analyses of the samples from the Kaban alteration zone are in agreement with each other.

## 7. Alteration

The units present in the study area belong to the Olur Group defined within the Olur-Tortum zone (Konak and Hakyemez, 2001) Alteration associated units of Early-Middle Jurassic Oltuçayı volcanics and Kaban Dacite, Early Cretaceous pelagic-semi pelagic limestones all belong to the Soğukçam formation

and have been cut by Eocene Coşkunlar Dacite. Quartz porphyry apophysis of the Coşkunlar Dacite also cover large areas. All of the defined alteration zones with some interruptions have 11 km extensions along NE-SW direction. To study the characteristics of the alteration zones, samples were collected from Yeşilbağlar, Kaban and Köprübaşı alteration zones and petrographical, mineralogical, FT-IR and XRD studies were carried out on these samples.

The rocks in the study area have been extensively subjected to hydrothermal alterations. This caused difficulties in the identifications of the rocks. Petrographical studies showed that the rocks in the area are andesitic-basaltic-dacitic volcanics (Oltuçayı volcanite, Kaban and Coşkunlar dacite) and their subvolcanic equivalents (quartz porphyries). As a result of hydrothermal alterations their initial primary mineralogical contents have been changed to another new group of minerals. The original compositions and textures of the rocks have been partly or completely destroyed and with the hydrothermal alterations identification of the intrusion and the breccias has been problematical. Early Eocene Coşkunlar Dacite is the most differentiated mineralization containing the youngest intrusive rock. Yeşilbağlar, Kaban and Köprübaşı alteration textures are complicated, so

quartz porphyry intrusives and related brecciations have been considered to have been caused by solutions with different chemical compositions.

(a) Advanced Argillic-Argillic Zone: The advanced argillic zone covers large areas in the study area and they are seen along the contacts with breccias. The zone developed from the alteration of andesites, basalts and dacites and towards the upper parts it passes into a silicified zone. In topographically higher parts quartz content of the silicified zone is more than 80% with very small amount of clay. Original mineralogic composition and textures have been completely destroyed (Figure 21). In the field silicified structures stand out like notches and caps. The rocks in this zone are rather hard and have fractures and breaks on their outer faces. In the area starting in Early Eocene volcanic activities rose subsurface and silicified volcanics. In the field breccias in the silicified zones are grey, yellowish grey, brownish red and purple coloured. In the host rock, in most cases as a result of alteration quartz has been infiltrated by iron oxide. As a result of hematitization, rocks in this zone have brownish, purplish appearance. Petrographical studies showed that all of the plagioclases have been fully altered to clay minerals. FT-IR and XRD studies indicated that clay minerals are kaolinite, away from

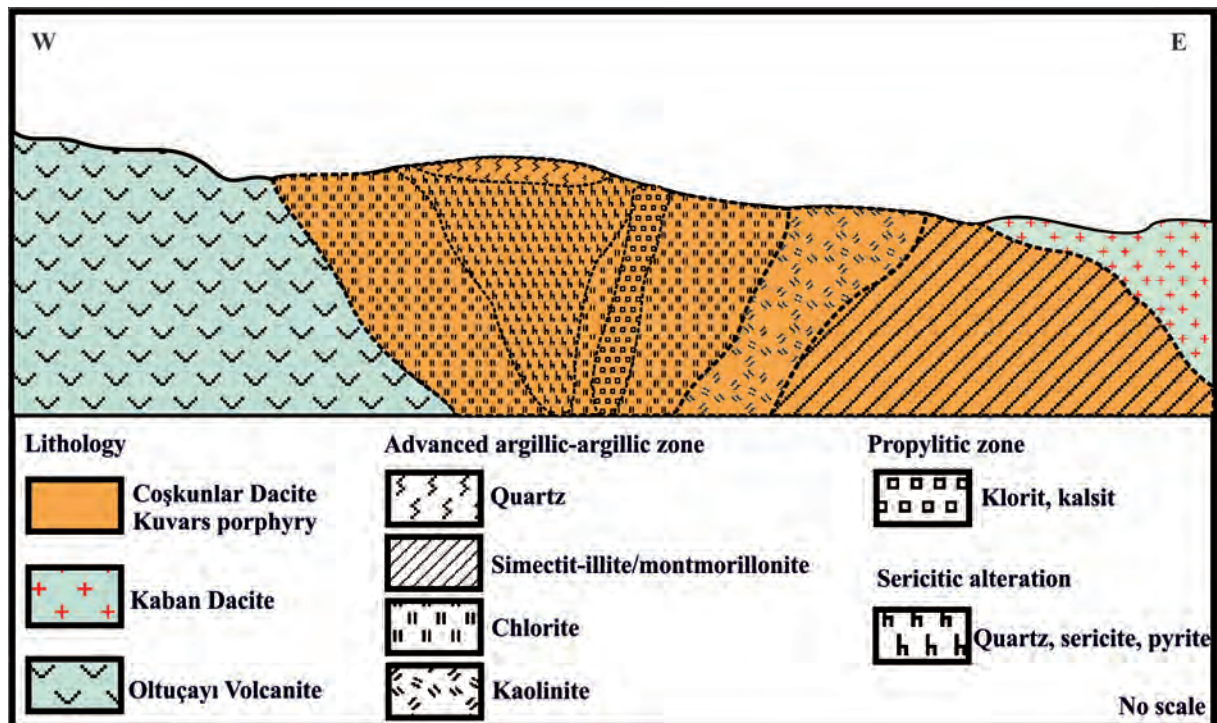


Figure 21- Schematic illustration of the alteration zone in Yeşilbağlar area.

the zone they are montmorillonite. Considering their topographical distributions limits of advanced argillic zone cannot be marked clearly but they have iron oxide smeared breccias at the top and have a clayey zone below it (Figure 21). The argillic zone in the field is marked with light yellow and white colours. Particularly in the heavily hematitized, limonitized parts plagioclases have mostly been altered to clay minerals. Along the fractures, along with hematitization and limonitization, limited carboations can also be observed. FT-IR and XRD studies carried out on the samples collected indicated developments of smectite±illite±muscovite±montmorillonite minerals. The presence of kaolinite mineral in the argillic and advanced argillic zone in the Yeşilbağlar and Kaban alteration zones indicates that clay minerals dominate these zones. Kaolinites dominate the mineralized zones; montmorillonites represent the zones away from the mineralizations. In the field sulphate mineralizations are the guides for argillic alteration zones. The alteration with these characteristics is quite similar to the argillic alteration described by Lowell and Guilbert (1970) with paragenesis of quartz, kaolinite, montmorillonite and a small amount of leucoxene.

(b) Pyrophyllitic Zone: It is overlain by the advanced argillic alteration zone and mostly observed as protected along the outer zones. It has been subjected to chlorite, carbonate alterations. It is observed in the rocks with basaltic, andesitic and dacitic compositions and has redish bordeaux colour. Towards outer zones where hematitization and limonitization have developed, it passes into advanced argillic zone. Particularly in the Yeşilbağlar alteration zone pyrophyllitic alteration zones have been cut by pyrite containing quartz veins and veinlets. Petrographic studies showed that plagioclases were carbonatized, and argillitized and were slightly sericitized. FR-IR and XRD studies showed that chlorite (clinocllore) and carbonate (calcite) minerals were also present (Figure 21). Alteration is similar to the pyrophyllitic alteration defined by Lowell and Guilbert (1970) with chlorite, calcite, epidote, adularia and albite paragenesis.

(c) Sericitic Alteration: It has been overlain by advanced argillic alteration and has almost been masked or wiped out. In the study area it has limited coverage and mainly has sericite and quartz and a small amount of carbonatization. FR-IR and XRD studies carried out on the samples collected along the

contact of host rock-with quartz porphyry showed the presence of quartz, sericites, and pyrites and in some samples chlorite, illite and rutile were also present. In the inner parts of the alteration zone sericites is dominant and illite is dominant at the outer parts. Sericization is mainly related to feldspar minerals. In this zone pyrite is mainly disseminated (Figure 21). This defined alteration is similar to the phyllic alteration defined by Lowell and Gilbert (1970).

Microscopical, FT-IR and XRD studies carried out on the samples collected from the alteration zones showed that the general mineral assemblance consists of quartz, smectite, illite, kaolinite, chlorite, clinocllore, carbonate (calcite), sulphate (gypsum, bassanite). From the points of primary texture and mineralogy, the rocks in the study area have been identified as andesite, basalt and dacite and main alterations are argillization, silicification, chloritization, sericitization. Zones with hematite, limonite and sulphae are common in the oxidation zone. With the increasing alteration clay minerals and quartz also increase. Copper carbonate (malachite-azurite) minerals are also present. By using analytical methods characteristics of the alterations have been defined. Eocene tectonic activities and later developing alterations have masked developments of the previous period consequently during the 1/5.000 scale geological mapping all these mentioned alteration zones could not be marked on the map.

## 8. Discussion and Results

### 8.1. Discussion

In this study area it was difficult to make separations on the base of distribution of alteration minerals. Alteration minerals in general show that advanced argillic alteration zones in the study area are quite extensive. Quartz, kaolinite, illite, montmorillonite and jarosite are the commonest alteration minerals. In places they are accompanied by chlorite, and sericite. Paragenesis of this group of minerals are considered to be the evidence of typical advanced argillic alteration. Jarosite and gypsum are also common in this zone. The presence of some alteration mineral relics eg sericite, chlorite and carbonate show that alterations in the field are overlying each other. In general, it is considered that solutions from the alteration zones at relatively shallow depths react with previously developed alterations at depths and replacing them causing alteration mineral types becoming younger towards the upper zones.

In the advanced argillic zones, the roots of the lithocaps have structural control. In the high temperature parts below the lithocaps, sericitic alteration passes into quartz-pyrophyllite. In the low temperature parts also below the lithocaps, quartz-kaolinite are dominant. More than mafic magmatic rocks, felsic magmatic rocks have been subjected to argillic alteration. In some locations advanced alterations below lithocaps characteristically display a typical patchy texture. These textures have been embedded into the silicified rocks and contain pyrophyllite and kaolinite.

In the porphyry Cu mineralizations, vertical distributions of the mineralization types depend on to the overlying and the interminglings. In high temperature intermingled systems in the porphyry stocks the advanced argillic lithocap may effect upper parts and in the root parts may effect downwards, down to 1 km depths. In this kind of situation argillic alteration overlying the potassic alteration may be 1-2 Ma younger than the potassic alteration (Sillitoe, 2010). In places where interminglings are limited, lithocap and stocks with potassic alterations may be separated with ~0.5-1 km from each other. The gap in between is filled with pyritic chlorite-sericitic alterations.

Copper deposits developed in the porphyry systems are low grade but with large reserves and have developed in the near surface intrusive rocks in the island arc environments and in the intrusive rocks of the calcalkaline magmatism near the continents. Most characteristic features of the porphyry systems are defined alteration and mineralized zones. These zones from outer towards inner part are prophyllitic, phyllic and potassic zones. The main mineralizations are along the zones between phyllic and potassic alteration zones (Lowell and Guilbert, 1970; Sillitoe, 1972, 1973; Lowell and Gilbert, 1974; Berger et al., 2008; Sillitoe, 2010). In the porphyry systems most of the ore mineralizations containing intrusives, have calc-alkaline character. In general, in the volcanic and pyroclastic rocks, particularly in andesitic, dacitic, rhyodacitic rocks and in their subvolcanic equivalents, veins, breccias and metasomatism of the sulphur bearing minerals are present (Sillitoe, 1972; Mitchell and Bell, 1973, Sillitoe, 1973; Aral and Erler, 1981; Ayhan, 1991, Sillitoe and Hedenquist, 2003; Berger et al., 2008; Sillitoe, 2010). The main mineralization body is found enclosed by a pyrite rich shell. In the porphyry systems the most important sulphur minerals

found are pyrite, chalcopyrite and molybdenite. They are present in the rocks as veins, veinlets and are in accord with the alteration zones (Lowell and Guilbert, 1970; Sillitoe, 1972, 1973; Lowell and Guilbert, 1974; Richards, 2003; Seedorff et al., 2005; Kesler and Wilkonson, 2006; Sillitoe, 2010; Oğuz, 2010).

Hydrothermal solutions described as solutions at 50°C-500°C temperature and have Na, K, Ca and Cl as main elements and Mg, B, S, Sr, Fe, CO<sub>2</sub>, H<sub>2</sub>S, NH<sub>4</sub>, Cu, Pb, Zn, Sn, Mo, Ag and Au as secondary elements (Skinner, 1979). Hydrothermal solutions could only have magmatic, metamorphic, sedimentary, meteoric or marine origin and could also be a mixture of these sources (Evans, 1987). In host rocks with high permeability, hot acidic hydrothermal solutions with low internal pressure, flow and carry their element contents through cavities and channels. In host rocks with low permeability, solutions move by filtering and in host rocks with very low permeability solutions move by absorption (Pirajno, 1992; Hedenquist et al., 2001; Einaudi et al., 2003; Sillitoe and Hedenquist, 2003; Pirajno, 2009; Sillitoe, 2010) (Figure 22). In the porphyry systems, minerals which have developed numbers of alteration types have been defined and sub groups like chloritization, hematitization, pyritization have been described (Meyer and Hemley, 1967; Lowell and Guilbert, 1970, 1974; Pirajno, 1992; Sillitoe, 1993; Pirajno, 2009; Sillitoe, 2010). The subvolcanic intrusive/breccia complex is closely related with time and place of the hydrothermal alteration and mineralization. Silica rich volatile phase is believed to be the mechanism which brought mineralization to the area (Giles, 1973; Pirajno 1992, 2009; Sillitoe, 2010).

The Alpine Orogenic Belt which starts in Turkey, passes through The Caucuses and Iran then extends into Afghanistan, hosts numerous porphyry Cu-Mo-Au deposits. With limited explorations carried out in Turkey some low grade porphyry systems like Bakırçay (Amasya), Güzelyayla (Trabzon), Ulutaş (Erzurum), Balcılı (Artvin), Gümüşhane (Artvin) have been discovered. The ages of the intrusive rocks causing the development of the porphyry systems are Late Cretaceous (80 Ma), Eocene (45 Ma) and Oligocene (25 Ma) (Giles, 1973; Moore et al., 1980; Yiğit, 2006, 2009). In the host rocks of the porphyry copper mineralizations in Eastern Pontides have tonalite, quartz-monzonite, granodiorite and granite mineralogies (Pejatovic, 1971; Çağatay and Çağatay, 1978; Yalçınalp, 1995; Soylu, 1999; Singer et al., 2008; Oğuz, 2010). Among these porphyry systems Ulutaş-

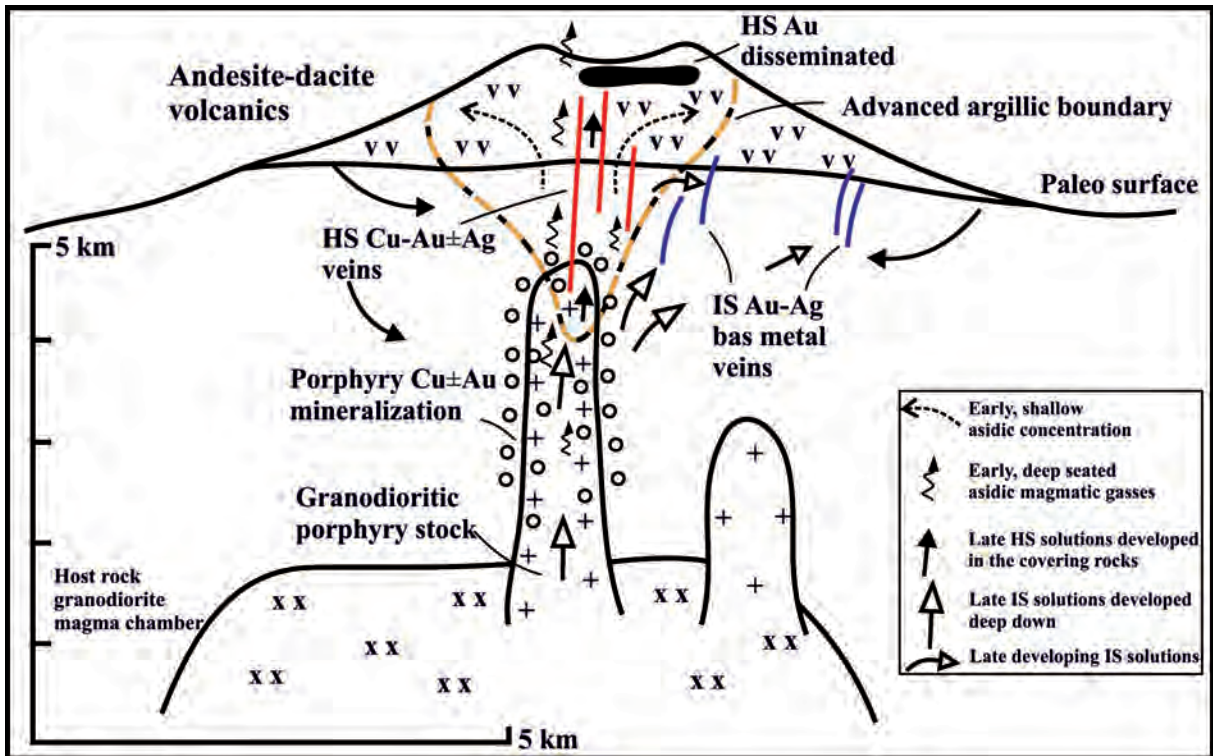


Figure 22- Schematic illustration of the hydrothermal alteration in porphyry system (Simplified from Hedenquist et al., 2001; Sillitoe and Hedenquist, 2003; Sillitoe, 2010).

İspir (Erzurum) porphyry Cu-Mo deposit is quite close to the study area. Developments of Yeşilbağlar, Kaban and Köprübaşı alteration zones may be explained by the presence of Ulutaş-İspir porphyry Cu-Mo deposit. In the Eastern Pontides presence of various porphyry systems in different areas and the data presented in this study support the view that Cu, Mo, As type deposits associated with porphyry systems along belt are all subduction related.

In the study area advanced argillic-argillic, pyrophyllitic and sericitic alterations are the alteration types present. Advanced argillic alteration zones are quite extensive. Because of this, it is considered to be similar to the island arc porphyry system (Pejatovic, 1971; Çağatay and Çağatay, 1978; Yalçınalp, 1995). Mineralizations generally are pyrite, less chalcopyrite, galena, sphalerite and pyrrhotite. The main copper mineralization representing middle-deep sections of the porphyry systems are not clearly seen in the field. In Eastern Pontides from Early Jurassic onwards İzmir-Ankara-Erzincan ocean started closing subduction related (Çelik et al., 2011; Topuz et al., 2012; Robertson et al., 2013). Collision between Taurus platform and Eurasia active continental margin took place in Early Eocene. Continent to-continent

collision causing crustal thickening, continents gaining heights and erosions being effective. All these processes are believed to have affected the mineralized zone in the study area. Data collected show that Yeşilbağlar, Kaban, Köprübaşı alteration zones in the Olur (Erzurum) area and associated mineralizations show similarities to the upper portion of the porphyry mineralizations in the Pontides as well as in the Alpine Orogenic Belt, meaning, this may be taken as a clue of possible buried porphyry mineralization in the study area. Not having drilling data in the study proved to be a handicap. In the Kaban area there are abandoned adit entrances for copper mining belonging to pre Republic time.

## 8.2. Results

(a) In the study area in Olur (Erzurum) Yeşilbağlar, Kaban, Köprübaşı, alteration zones are situated in the Eastern Pontides in the Alpine Orogenic Belt. These alteration zones have developed in the quartz porphyry apophysis of the Coşkunlar Dacite where Early Eocene Coşkunlar Dacite have intruded Early-Middle Jurassic Oltuçayı volcanics (basalt-andesite) and Kaban Dacite.

(b) Alteration in the study area has been defined as advanced argillic-argillic, propylitic and sericitic zones.

(c) A late stage advanced argillic zone covers large areas and early stage alterations have been wiped out or masked and mineralization types of the advanced argillic alterations like veins-veinlets, smear and limited stockwork-disseminated, are present.

(d) FT-IR analyses showed that kaolinite, chlorite (clinochlore), quartz, illite, muscovite, gypsum, jarosite and barite are the minerals in the alteration zones. XRD studies agreed with the FR-IR results.

(e) Mineralizations present in the Yeşilbağlar, Kaban and Köprübaşı alteration zones are quite similar to the porphyry system mineralizations present in the upper part of the porphyry systems in the Pontides as well as in the Alpine Orogenic Belt. Based on this similarity it is concluded that in the study area there may be some buried porphyry type mineralizations in the deeper part of the system.

#### Acknowledgments

This study has been supported by the Research Project Unit (Project No: MMF2010D5) of the Çukurova University, Adana. Our thanks are due to Prof. Dr. Osman Parlak, Prof. Dr. Ahmet Gökçe, Dr. Özcan Dumanlılar and an unnamed referee who have each critically read the manuscript and made constructive suggestions. We also thank Prof. Dr. Friedrich Koller from Vienna University, Austria for his contributions to the mineral chemistry studies and to Prof. Dr. Selahattin Serin and research scientists of the Chemistry Department of the Çukurova University who contributed to the FT-IR analyses. We also thank the Mineral Research and Exploration Department personnel and to the Oltu (Erzurum) field camp personnel of the MTA (Mineral Research and Exploration General Directorate, Ankara, Turkey) for their support during the field work.

#### References

Akıncı, Ö. T. 1984. The eastern Pontide volcanosedimentary belt and associated massive sulphide deposits. In: Dixon, J. E. and Robertson, A. H. F. (Eds.) The Geological Evolution of the Eastern Mediterranean. Geological Society, London, Special Publications, 17, 415-428.

- Altunlı, İ.E. 1973. Orta Sakarya'nın jeolojisi, Cumhuriyet'in 50. Yılı Yerbilimleri Kong. Tebliğleri. Maden Arama ve Tetkik yayını, s. 159-191.
- Aral, H., Erler, A. 1981. Porfiri Bakır Yatakları, ODTÜ Mühendislik Fakültesi Yayını, No: 67, Ankara.
- Ayhan, A. 1991. Maden Jeolojisi Arama ve Etüt Teknikleri. S.Ü. Mimarlık-Mühendislik Fakültesi, Konya, 328 s.
- Berger, B.R., Ayuso, R.A., Wynn, J.C., Seal, R.R. 2008. Preliminary Model of Porphyry Copper Deposits. U.S. Geological Survey, Open-File Report 2008-1321, 55 p.
- Bralia, A., Sabatini, G., Troja, F. 1979. A revaluation of the Co/Ni ratio in pyrite as geochemical tool in ore genesis problems. Mineral. Deposita, 14, 353-374.
- Brill, B.A. 1989. Deformation textures and recrystallisation microstructures in deformed ores from the CSA mine, Cobar, Australia. Journ. of Struct. Geol., 11, 591-601.
- Cook, N.J. 1996. Mineralogy of the sulphide deposits at sulitjelma, northern Norway. Ore Geol. Rev., 11, 303-338.
- Craig, J.R., Vaughan, D.J. 1981. Ore Microscopy and Ore Petrology. John Wiley and Sons, p. 406.
- Craig, J.R., Vokes, F.M. 1993. The metamorphism of pyrite and pyritic ores: an overview, Mineral. Mag., 57, 3-18.
- Craig, J.R., Vaughan D.J., 1994. Ore microscopy and ore petrography, 2nd. Edition.
- Craig, J.R., Vokes, F.M., N Solberg, N. 1998. Pyrite Physical and chemical textures. Mineralium Deposita, 34, p. 82-101.
- Çağatay, A., Çağatay, N. 1978. Porfiri Bakır Yatakları, Yeryuvarı ve İnsan, 3/1, 32-37.
- Çağatay, M. N., Boyle, D. R. 1980. Geology, geochemistry and hydrothermal alteration of the Madenköy massive-sulphide deposits, Eastern Black Sea region, Turkey. In: Ridge, J. D. (Ed.) International Association of the Genesis of Ore Deposits (IAGOD). 5th Symposium Proceedings, E. Schweizerbartsche Verlagsbuchhandlung, Stuttgart, 653-678.
- Çelik, Ö. F., Marzoli, A., Marschik, R., Chiaradia, M., Neubauer, N., Öz, İ. 2011. Early-Middle Jurassic intra-oceanic subduction in the İzmir-Ankara-Erzincan Ocean, Northern Turkey. Tectonophysics, 509, 120-134.

- Çolakoğlu, O. A., Özen, H., Türkel, A., Sayak, H., Dönmez, C., Odabaşı, İ. 2009. Tekman-Pasinler-Karayazi (Erzurum) yöreleri Cr-Ni prospeksiyon raporu. Maden Tetkik ve Arama Genel Müdürlüğü (MTA) Rapor No: 11117, Ankara (unpublished).
- Demir, Y. 2010. Kabadüz (Ordu, KD-Türkiye) Yöresi Pb-Zn-Cu Cevherlerinin Jeolojik, Mineralojik, Jeokimyasal ve Kökensel İncelenmesi, Doktora Tezi, Karadeniz Teknik Üniversitesi Fen Bilimleri Enstitüsü, Trabzon.
- Dibenedetto, F., Bernardini, G.P., Costagliola, P., Plant, D., Vaughan, D. 2005. Compositional zoning in sphalerite crystals. *Amer. Mineral.*, 90, 1384-1392.
- Einaudi, M.T., Hedenquist, J.W., Inan, E.E. 2003. Sulfidation state of fluids in active and extinct hydrothermal systems: Transitions from porphyry to epithermal environments. *Society of Economic Geologists Special Publication*, 10, 285-313.
- Er, M., Özdoğan, K., Tüysüz, N. 1995. Geology and mineralization of Güzelyayla porphyry Cu-Mo occurrence, Trabzon, NE Turkey, In: Erler, A., Ercan T., Bingol, E. and Orcen, S. (Eds.), *Proceedings of the International Symposium on the geology of the Black Sea Region*, Ankara, MTA and JMO, p. 226-231.
- Evans, A.M. 1987. *An Introduction to Ore Geology*, Blackwell Sci. Publ. (2ed.), 358 p.
- Evans, I., Hall, S. A. 1990. Palaeomagnetic constraints on the tectonic evolution of the Sakarya continent, northwestern Anatolia. *Tectonophysics*, 182, 357-372.
- Galoyan, G., Rolland, Y., Sosson, M., Corsini, M., Melkonyan, R. 2007. Evidence for superposed MORB, oceanic plateau and volcanic arc series in the Lesser Caucasus (Stepanavan, Armenia). *Comptes Rendus Geosciences*, 339, 482-492.
- Galoyan, G., Rolland, Y., Sosson, M., Corsini, M., Billo, S., Verati, C., Melkonyan, R. 2009. Geology, geochemistry and  $40\text{Ar}/39\text{Ar}$  dating of Sevan ophiolites (Lesser Caucasus, Armenia): evidence for Jurassic Back-arc opening and hot spot event between the South Armenian Block and Eurasia. *Journal of Asian Earth Sciences*, 34, 135-153.
- Giles, D.L. 1973, Geology and mineralization of the Ulutaş Copper-molybdenum prospect, UNDP Mineral Exploration in Two Areas, General Directorate of Mineral Research and Exploration (MTA), Report: 5237, 40 p., Ankara (unpublished).
- Gottesman, W., Kampe, A. 2007. Zn/Cd ratios in calcisilicate- hosted sphalerite ores at Tumurtijn-Ovoo, Mongolia. *Chemie Der Erde*, 67, 323-328.
- Grammatikopoulos, T.A., Roth, T. 2002. Mineralogical characterization and Hg deportment in field samples from the Polymetallic Eskay Creek Deposit, British Columbia, Canada. *Int. J. Surf. Min. Recl.*, 16, 180-195.
- Hakyemez, H. Y., Konak, N. 2001. Tectonic evolution and stratigraphy of Eocene basins in the easternmost part of the Pontides. In: *Proceedings of the 2nd International Symposium on the Petroleum Geology and Hydrocarbon Potential of the Black Sea Area*. Turkish Association of Petroleum Geologists, Special Publications, Ankara, 4, 19-25.
- Hedenquist, J.W., Claveria, R.J.R., Villafuerte, G.P. 2001. Types of sulfide-rich epithermal deposits, and their affiliation to porphyry systems: Lepanto-Victoria-Far Southeast deposits, Philippines. *Congreso Internacional de Prospectores y Exploradores*, 2<sup>nd</sup>, Lima, Instituto de Ingenieros de Minas del Perú, CD-ROM, 29 p.
- Hezarkhani, A. 2006. Hydrothermal evolution of the Sar-Cheshmeh porphyry Cu-Mo deposit, Iran, Evidence from fluid inclusions, *Journal of Asian Earth Sciences*, v. 28, p. 409-422.
- Hirst, D. M., Eğin, D. 1979. Localization of massive, polymetallic sulphide ores in the northern Harşit River area, Pontide Volcanic Belt, Northeastern Turkey. *Annales de la Societé Géologique de Belgique*, 102, 465-484.
- Holten, T., Jamtveita, B., Meakina, P. 2000. Noise and oscillatory zoning of minerals. *Geochim. Cosmochim. Acta*, 64-11, 1893-1904.
- Jankovic, S. 1977. Major Alpine ore deposits and metallogenic units in the northeastern Mediterranean and concepts of plate tectonics, Jankovic, S. (Eds.) *Metallogeny and Plate Tectonics in Northeastern Mediterranean*, Univ. Belgrade, p. 105-171.
- Jonasson, I.R., Sangster, D.F. 1978. Zn/Cd ratios for sphalerites from some Canadian sulfide ore samples. *Geol. Surv. Can.*, 78, 195-201.
- Kant, W., Warmada, I.W., Idrus, A., Setijadji, L.D., Watanabe, K. 2012. Ore Mineralogy and Mineral Chemistry of Pyrite, Galena, and Sphalerite at Soripesa Prospect Area, Sumbawa Island, Indonesia. *J. SE Asian Appl. Geol.*, 4 (1), 1-14.
- Karakaya, M.Ç. 2006. Kil Minerallerinin Özellikleri ve Tanımlama Yöntemleri, Ankara, 640 s.
- Kesler, S.E., Wilkonson, B.H. 2006. The role of exhumation in the temporal distribution of ore deposits. *Economic Geology*, 101, 1096-1117.

- Ketin, İ. 1966. Anadolu'nun Tektonik Birlikleri. Maden Tetkik ve Arama Genel Müdürlüğü Dergisi, Ankara, 66, 20-30.
- Konak, N., Hakyemez, H.Y. 1996. Tectonic units of the easternmost Pontides: stratigraphical and structural implications. In: Derman, A.S., Toksoy, F., Yılmaz, E. (Eds.), Proceedings of 2nd International Symposium on the Petroleum Geology and Hydrocarbon Potential of the Black Sea Area, İstanbul, Turkey, 32-33.
- Konak, N., Hakyemez, H.Y., 2001. Tectonic units of the easternmost part of the Pontides: Stratigraphical and structural implications. In: Derman, A.S., Toksoy, F., Yılmaz, E. (Eds.), Proceedings of the 2nd International Symposium on the Petroleum Geology and Hydrocarbon Potential of the Black Sea Area, Şile-Turkey, 22-24th September 1996, Turkish Association of Petroleum Geologist, Special Publication, Ankara, Turkey, 4, p. 93-103.
- Konak, N., Hakyemez, H. Y., Bilgiç, T., Bilgin, R., Hepşen, N. ve Ercan, T. 2001. Kuzeydoğu Pontidlerin (Olut-Olur-Şenkaya-Narman-Uzundere-Yusufeli) Jeolojisi. Maden Tetkik ve Arama Genel Müdürlüğü (MTA), Rapor No: 10489, Ankara(yayınlanmamış).
- Konak, N. ve Hakyemez, H. Y. 2008a. 1/100 000 ölçekli Türkiye jeoloji haritaları serisi, Kars-G48 paftası. Maden Tetkik ve Arama Genel Müdürlüğü, Jeoloji Etütleri Dairesi, 104, 69s.
- Konak, N. ve Hakyemez, H. Y. 2008b. 1/100 000 ölçekli Türkiye jeoloji haritaları serisi, Tortum-H47 paftası. Maden Tetkik ve Arama Genel Müdürlüğü, Jeoloji Etütleri Dairesi, 95, 46s.
- Kraeff, A. 1963. Geology and mineral deposits of the Hopa-Mugrul region. Bulletin of the Mineral Research and Exploration Institute of Turkey, 60, 44-59.
- Kuşçu, İ., Erler, A. 1999. Deformation of stibnites and pyrites in the Madsan antimony deposit (Niğde, Turkey): implications for pressure-temperature conditions of local deformation. Turkish Journal of Earth Sciences, 8, 57-66.
- Kuşçu, İ., Erler, A. 2002. Pyrite deformation textures in the deposits of the Küre mining district (Kastamonu, Turkey). Turkish Journal of Earth Sciences, 11, 205-215.
- L'Heureux, I., Jamtveit, B. 2002. A model for oscillatory zoning in solid solutions grown from aqueous solutions: applications to the (Ba, Sr)SO<sub>4</sub> system. Geochim. Cosmochim. Acta, 66, p. 417-429.
- Lianxing, G., McClay, K.R. 1992. Pyrite deformation in stratiform lead-zinc deposits of the Canadian Cordillera. Mineral. Deposita, 27, 169-181.
- Loftus-Hills, G., Solomon, M. 1967. Cobalt, nickel and selenium in sulphides as indicators of ore genesis. Mineral. Deposita, 2, 228-242.
- Lowell, J.D., Guilbert, J.M. 1970. Lateral and vertical alteration-mineralization zoning in porphyry ore deposits. Economic Geology, 65, 373-408.
- Lowell, J.D., Guilbert, J.M. 1974. Variations in Zoning Patterns in Porphyry Ore Deposits. CIM Bull., 61.
- McClay, K.R., Ellis, P.G. 1984. Deformation of pyrite, Economic Geology, 79, 400-403.
- Meyer, C., Hemley, J.J. 1967. Wall-rock alteration. In: Barnes, H.L. (Ed.), Geochemistry of hydrothermal ore deposits, 1<sup>st</sup> ed., New York, Holt, Rinehart Winston, 166-235.
- Mitchell, A.H., Bell, J.D. 1973. Island-arc evolution and related mineral deposits. Journ. Geol., 81, 381-405.
- Moore, W.J., McKee, E.H., Akinci, O.T. 1980. Chemistry and chronology of plutonic rocks in the Pontid mountains, northern Turkey. In: Jankovic, S., Sillitoe, R.H. (Eds.) European Copper Deposits: Belgrade, UNESCO-IGCP, 209-216.
- Oğuz, E. 2010. Ulutaş (İspir-Erzurum) Bakır-Molibden Porfiri Sisteminin Yeniden Değerlendirilmesi ve Altın Potansiyelinin Araştırılması. Yüksek Lisans Tezi, Hacettepe Üniversitesi Fen Bilimleri Enstitüsü, 110 s., Ankara.
- Ohta, E., Doğan, R., Batık, H., Abe, M. 1988. Geology and mineralization of Dereköy porphyry copper deposit, northern Thrace, Turkey, Bulletin of the Geological Survey of Japan, v. 39, p. 115-134.
- Okay, A. İ. 1984. The geology of the Ağvanis metamorphic rocks and neighbouring formations. Bulletin of the Mineral Research and Exploration Institute of Turkey, 99/100, 16-36.
- Okay, A.İ., Şahintürk, Ö. 1997. Geology of the Eastern Pontides. In: Robinson, A. G. (Ed.) Regional and Petroleum Geology of the Black Sea and Surrounding Region. American Association of Petroleum Geologists, Tulsa, OK, Memoirs, 68, 291-311.
- Okay, A. İ., Tüysüz, O. 1999. Tethyan sutures of northern Turkey. In: Durand, B., Jolivet, L., Horvath, F., Séranne, M. (Eds.) The Mediterranean Basins: Tertiary Extensions within the Alpine Orogen. Geological Society of London, Special Publications, 156, 474-515.
- Okay, A. İ., Tüysüz, O., Satır, M., Özkan-Altuner, S., Altuner, D., Sherlock, S., Eren, R. H. 2006. Cretaceous and Triassic subduction-accretion, high pressure-low temperature metamorphism, and continental

- growth in the Central Pontides, Turkey. Geological Society of America Bulletin, 118, 1247-1269.
- Önal, G. 2015. Yeşilbağlar-Kaban (Olur-Erzurum) Bölgesindeki Alterasyonların Mineralojik ve Jeokimyasal İncelenmesi. Doktora Tezi, Çukurova Üniversitesi Fen Bilimleri Enstitüsü, Adana, 182 s. Ankara (unpublished).
- Özen, H., Çolakoğlu, A. O., Sayak, H., Dönmez, C., Türkel, A. ve Odabaşı, İ. 2008. Erzincan-Tercan-Çayırılı yöresi ofiyolit jeolojisi ve krom-nikel prospeksiyon raporu. Maden Tetkik ve Arama Genel Müdürlüğü (MTA) Rapor No: 11055, Ankara (unpublished).
- Palero, F.J., Martin-Izard, A. 2005. Trace element contents in galena and sphalerite from ore deposits of the Alcudia Valley mineral field, Eastern Sierra Morena, Spain. Jour. of Geochem. Expl., 86, 1-25.
- Parlak, O., Çolakoğlu, A., Dönmez, C., Sayak, H., Türkel, A., Yıldırım, N., Odabaşı, İ. 2013. Geochemistry and Tectonic Significance of Ophiolites Along the İzmir-Ankara-Erzincan Suture Zone in northeastern Anatolia. In: Robertson, A.H.F., Parlak, O., Ünlügenç, U. C. (Eds.) Geological Development of Anatolia and the Easternmost Mediterranean Region. Geological Society of London, Special Publication, 372, 75-105.
- Pejatovic, S. 1971. Doğu Karadeniz-Küçük Kafkasya bölgesindeki metalojenik zonlar ve bunların metalojenik özellikleri. MTA Dergisi, 77, 1-14.
- Pirajno, F. 1992. Hydrothermal mineral deposits: Principles and fundamental Concepts for Exploration geologist. Springer-Verlag, Berlin, 709 p.
- Pirajno, F. 2009. Hydrothermal processes and mineral systems, Dordrecht; London. Springer, Geological Survey of Western Australia, 1250 p.
- Popov, P., Berza, T., Grubic, A., Ioane, D. 2002. Late Cretaceous Apuseni-Banat-Timok-Srednagorie (ABTS) magmatic and metallogenic belt in the Carpathian-Balkan orogen, Geologic Balcanica, v. 32, p. 145-163.
- Raymond, O.L. 1996. Pyrite composition and ore genesis in the Prince Lyell copper deposit, Mt Lyell mineral field, western Tasmania, Australia. Ore Geol. Rev., 10, 231-250.
- Rice, S. P., Robertson, A. H. F., Ustaömer, T. 2006. Late Cretaceous–Early Ceneozoic tectonic evolution of the Eurasian active margin in the Central and Eastern Pontides, northern Turkey. In: Robertson, A. H. F., Mountrakis, D. (Eds.) Tectonic Development of the Eastern Mediterranean Region. Geological Society, London, Special Publications, 260, 413-445.
- Rice, S. P., Robertson, A. H. F., Ustaömer, T., İnan, N., Tashlı, K. 2009. Late Cretaceous–Early Eocene tectonic development of the Tethyan suture zone in the Erzincan area, Eastern Pontides, Turkey. Geological Magazine, 146, 567-590.
- Richards, J.P. 2003. Tectono-magmatic precursors for porphyry Cu-(Mo-Au) deposit formation. Economic Geology, 98, 1515-1533.
- Roberts, F.I. 1982. Trace element chemistry of pyrite: A useful guide to the occurrence of sulfide base metal mineralization, Jour. of Geoch. Expl., 17, 49-62.
- Robertson, A. H. F., Parlak, O., Ustaömer, T., Tashlı, K., İnan, N., Dumitrica, P., Karaoğlu, F. 2013. Subduction, ophiolite genesis and collision history of Tethys adjacent to the Eurasian continental margin: new evidence from the Eastern Pontides, Turkey. Geodinamica Acta, 26 (3-4), 230-293.
- Rolland, Y., Billo, S., Corsini, M., Sasson, M., Galoyan, G. 2009a. Blueschists of the Amassia-Stepanavan suture zone (Armenia): linking Tethys subduction history from E-Turkey to W-Iran. International Journal of Earth Sciences, 98, 533-550.
- Rolland, Y., Galoyan, G., Bosch, D., Sosson, M., Corsini, M., Fornari, M., Vérati, C. 2009b. Jurassic Back-arc and hot-spot related series in the Armenian ophiolites – Implications for the obduction process. Lithos, 112, 163-187.
- Rolland, Y., Galoyan, G., Sosson, M., Melkonyan, R., Avagyan, A. 2010. The Armenian Ophiolite: insights for Jurassic back-arc formation, Lower Cretaceous hot spot magmatism and Upper Cretaceous obduction over the South Armenian Block. In: Sosson, M., Kaymakçı, N., Stephenson, R. A., Bergerat, F., Starostenko, V. (Eds.) Sedimentary Basin Tectonics from the Black Sea and Caucasus to the Arabian Platform. Geological Society, London, Special Publications, 340, 353-382.
- Sarıfakıoğlu, E., Özen, H., Winchester, J. A. 2009. Petrogenesis of Refahiye ophiolite and its tectonic significance for Neotethyan ophiolites along the İzmir-Ankara-Erzincan Suture zone. Turkish Journal of Earth Sciences, 18, 187-207.
- Seedorff, E., Dilles, J.H., Profett, J.M., Jr., Einaudi, M.T., Zucher, L., Stavast, W.J.A., Johnson, D.A., Barton, M.D. 2005. Porphyry deposits: Characteristics and origin of hypogene features. Economic Geology 100<sup>th</sup> Anniversary Volume, 251-298.
- Sillitoe, R.H. 1972. A plate tectonic model for the origin of porphyry copper deposits. Econ. Geol., 67, 184-197.

- Sillitoe, R.H. 1973. The Top and Bottoms of Porphyry Copper Deposits. *Econ. Geol.*, 65, 373-408.
- Sillitoe, R.H. 1993. Giant and bonanza gold deposits in the epithermal environment. In: Whiting B.H., Mason R., Hodgson C.J. (Eds.) *Giant ore deposits*, Soc. Econ. Geol. Spec. Publ., 2, 125-156.
- Sillitoe, R.H. 2010. Porphyry Copper System. *Society of Economic Geologists, Ins. Economic Geology*, 105, 3-41.
- Sillitoe, R.H., Hedenquist, J.W. 2003. Linkages between volcanotectonic settings, ore-fluid compositions, and epithermal precious-metal deposits. In: Simmons, S.F., Graham, I. (Eds.), *Volcanic, geothermal, and ore-forming fluids: rulers and witnesses of processes within the earth*. Society of Economic Geologists Special Publication, 10, 315-343.
- Singer, D.A., Berger, V.I., Moring, B.C. 2008. Porphyry copper deposits of the world: Database and grade and tonnage models, U.S. Geological Survey Open-File Report 2008-1155.
- Skinner, B.J. 1979. The many origins of hydrothermal mineral deposits. *Geochemistry of Hydrothermal Ore Deposits*, 2nd ed., H.L. Barnes (Ed.), John Wiley and Sons, New York.
- Sosson, M., Rolland, Y., Danelian, T., Muller, C., Melkonyan, R., Adamia, S., Galoyan, G. H. 2010. Subductions, obduction and collision in the Lesser Caucasus (Armenia, Azerbaijan, Georgia), new insights. In: M. Sosson, N. Kaymakci, R. Stephanson, F. Bergerat and V. Storatchenko (Eds.). *Sedimentary Basin Tectonics from the Black Sea and Caucasus to the Arabian Platform*. Geological Society, London, Special Publications, 340, 329-352.
- Soylu, M. 1999. Modeling of porphyry copper mineralization of the Eastern Pontides. Ph.D. thesis, Middle East Technical University, p. 127. Ankara (unpublished).
- Şengör, A.M.C., Yılmaz, Y. 1981. Tethyan Evolution of Turkey: A Plate Tectonic Approach. *Tectonophysics*, 75, 181-241.
- Taylor, R.P. 1981. Isotope geology of the Bakırçay porphyry copper prospect, northern Turkey, *Mineralium Deposita*, v. 16, p. 375-390.
- Topuz, G., Alther, R., Satır, M., Schwartz, W. H. 2004. Low-grade metamorphic rocks from the Pulur complex, NE Turkey: implications for the pre-Liassic evolution of the Eastern Pontides. *International Journal of Earth Sciences*, 93, 72-91.
- Topuz, G., Göçmengil, G., Rolland, Y., Çelik, Ö. F., Zack, T., Schmitt A. K. 2012. Jurassic accretionary complex and ophiolite from northeast Turkey: No evidence for the Cimmerian continental ribbon. *Geology*, 41, 255-258.
- Topuz, G., Çelik, Ö. F., Şengör, A. M. C., Altıntaş, İ. E., Zack, T., Rolland, Y., Barth, M. 2013. Jurassic ophiolite formation and emplacement as backstop to a subduction-accretion complex in northeast Turkey, the Refahiye ophiolite, and relation to the Balkan ophiolites. *American Journal of Science*, 313, 1054-1087.
- Ustaömer, T., Robertson, A. H. F. 2010. Late Paleozoic-Early Cenozoic tectonic development of the eastern Pontides (Artvin area), Turkey: stages of closure of Tethys along the southern margin of Eurasia. In: Sosson, M., Kaymakçı, N., Stephenson, R. A., Bergerat, F., Starostenko, V. (Eds.) *Sedimentary Basin Tectonics from the Black Sea and Caucasus to the Arabian Platform*. Geological Society, London, Special Publications, 340, 281-327.
- Ustaömer, T., Robertson, A. H. F., Ustaömer, P. A., Gerdes, A., Peytcheva, I. 2012. Constraints on Variscan and Cimmerian magmatism and metamorphism in the Pontides (Yusufeli-Artvin area), NE Turkey from U-Pb dating and granite geochemistry. In: Robertson, A. H. F., Parlak, O., Ünlügenç, U. C. (Eds.) *Geological Development of Anatolia and the Easternmost Mediterranean Region*. Geological Society, London, Special Publications, 372. First Published online November 1, 2012, <http://dx.doi.org/10.1144/SP372.13>.
- Waterman, G.C., Hamilton, R.L. 1975. The Sar Cheshmeh porphyry copper deposit, *Economic Geology*, v. 70, p. 568-576.
- Xu, G. 1998. Geochemistry of sulphide minerals at Dugald River, NW Queensland, with reference to ore genesis. *Mineral and Petrol.*, 63, 1-2, 119-139.
- Xuexin, S. 1984. Minor elements and ore genesis of the Fankou Lead-Zinc deposit, China. *Mineral. Deposita*, 19, 95-104.
- Yalçınalp, B. 1995. The geochemical characteristics of the granitoids bearing porphyry Cu-Mo mineralization in eastern Pontides. *Türkiye Jeoloji Bülteni*, 30/1, 25-32.
- Yılmaz, H. 1985. Olur (Erzurum) yöresinin jeolojisi. *Karadeniz Teknik Üniversitesi Yerbilimleri Dergisi*, 4, 1-2, 23-41.
- Yılmaz, Y., Tüysüz, O., Yiğitbaş, E., Genç, S. C., Şengör, A. M. C. 1997. Geology and tectonic evolution of the Pontides. In: Robinson, A. G. (Ed.) *Regional and Petroleum Geology of the Black Sea and*

- Surrounding Regions. American Association of Petroleum Geologists, Tulsa, OK, Memoirs, 68, 183-226.
- Yılmaz, A., Adamia, S., Chabukiani, A., Chkhotua, T., Erdoğan, K., Tuzcu, S., Karabıyıköğlü, M. F. 2000. Structural correlation of the southern Transcaucasus (Georgia)-eastern Pontides (Turkey). In: Bozkurt, E., Winchester, J. A., Piper, J. D. A. (Eds.) Tectonics and Magmatism in Turkey and the Surrounding Area. Geological Society of London, Special Publications, 173, 171-182.
- Yiğit, Ö. 2006. Gold in Turkey-a missing link in Tethyan metallogeny. *Ore Geology Reviews*, 28, 147-179.
- Yiğit, Ö. 2009. Mineral Deposits of Turkey in Relation to Tethyan Metallogeny: Implications for Future Mineral Exploration, Society of Economic Geologists, Inc. *Economic Geology*, v. 104, p. 19-51.





# Bulletin of the Mineral Research and Exploration

<http://bulletin.mta.gov.tr>



## WHEN DID THE PLATE TECTONICS BEGIN? THE INCEPTION OF PLATE TECTONICS BASED ON THE EXISTENCE OF KOMATIITES AND THEIR MgO VARIATIONS

Anıl ARDAHANLIOĞLU<sup>a\*</sup> and Efe DEMİRCİ<sup>b</sup>

<sup>a</sup>Ankara University, Dept. of Geological Eng., Tectonics Research Group, Gölbaşı, Ankara. [orcid.org/0000-0001-9309-3872](https://orcid.org/0000-0001-9309-3872)

<sup>b</sup>Ankara University, Dept. of Geological Eng., Tectonics Research Group, Gölbaşı, Ankara. [orcid.org/0000-0002-6290-1731](https://orcid.org/0000-0002-6290-1731)

Short Note

### Keywords:

Crust, Plate Tectonic, Continental Crust, Earth, Komatiite.

### ABSTRACT

The geoscientists have always wondered what evolutionary processes the Early Earth went through until it reached today. The beginning of the plate tectonics poses another matter of debate in these processes. Yet, the debates on when the plate tectonics began have not been resolved. In this sense, especially the lack of records regarding the period of time before the Cambrian Era is considered the biggest obstacle against resolution of these debates. The geoscientists have benefitted from various methods to come up with different proposals about the beginning of the plate tectonics. The most notable rock type among the ones produced by the mantle is the komatiites. While the oldest datable komatiite is 3.82 Ga; the youngest is 0.086 Ga. With the high content of magnesium they contain, their special texture and the geological setting, the komatiites are not similar to any other rock groups which can currently be examined. Though they were produced in different geological times, no up to date forms of these rocks have been observed. Given the formation conditions of komatiites, recorded time intervals and the content of magnesium they contain, they might indicate when the plate tectonics began.

Received Date: 03.03.2017

Accepted Date: 24.04.2017

## 1. Introduction

In order to understand the Earth's history it is of a great importance to know when and how the plate tectonics began. Korenaga (2013) summarized certain studies on the beginning of plate tectonics, proposing that the plate tectonics might have begun between Hadean (>4.2 Ga) and Mesoproterozoic (~1 Ga) (Figure 1). The differences observed in the suggested age ranges is due to the fact that each researcher use different probable evidences in order to make proposals about the beginning of plate tectonics. New studies conducted in this field lead to new probable evidence. Examining the studies which have been conducted until today, it is possible to say that to resolve the debates on the beginning of plate tectonics is not an easy task.

Gerya et al. (2015) showed that the plate tectonics involve the independent movement of lithospheric plates and therefore understanding how plate tectonics began requires an understanding of how the first subduction zone formed. Further, Gerya et al. (2015)

provided a detailed examination of various proposals about the beginning of plate tectonics and their relationship with the mantle plumes.

Examining the previous studies on the beginning of plate tectonics (Komiya et al., 1999; Stern, 2005; Brown, 2006; Cawood et al., 2006; Hopkins et al., 2008; Shirey et al., 2008; Condie and Kröner, 2008; Harrison, 2009; Korenaga, 2013; Blichert-Toft et al., 2015; Nutman et al., 2015; Stern et al., 2017) it can be seen that the majority of these works comply with the indicators of plate tectonics proposed by Condie and Kröner (2008). Within the scope of this paper, it is proposed that there might be a link between the age interval of komatiites (Condie et al. 2016) and the beginning of plate tectonics.

## 2. Komatiites, a Proposed Indicator of the Beginning of the Plate Tectonics

Komatiites were first recognised in the Barberton greenstone belt (South Africa) by Viljoen and Viljoen (1969). The simple definition of komatiite is an

\* Corresponding author: Anıl ARDAHANLIOĞLU, [a.ardahanli@gmail.com](mailto:a.ardahanli@gmail.com)  
<http://dx.doi.org/10.19111/bulletinofmre.314227>

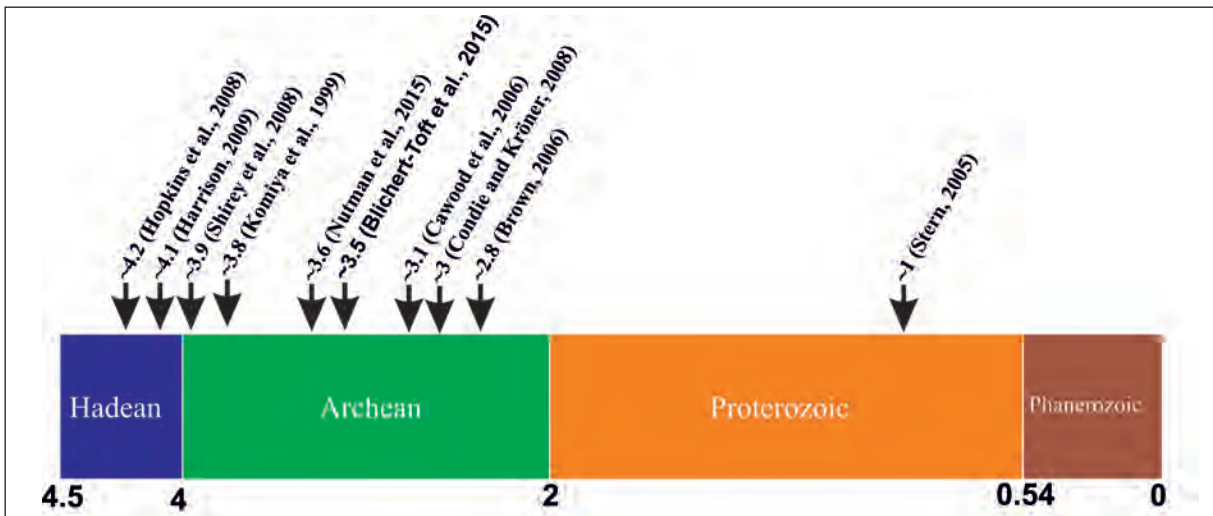


Figure 1- Proposals for the beginning age of plate tectonics (after Korenaga, 2013). The ages are billion years.

ultramafic volcanic rock (Arndt and Nisbet 1982). According to IUGS rock classification (Le Bas and Streckeisen, 1991; Le Maitre et al., 2002) komatiites contain more than 18 wt.% MgO and less than 1 wt.% TiO<sub>2</sub>. Though it is difficult to prove, komatiites crystallize from liquids that contained more than about 18 % MgO (Arndt and Lesher, 2004). Condie et al. (2016) limited the definition of Basalt to MgO of 7-17 wt.% and SiO<sub>2</sub> of 45-55 wt.%, whilst Komatiites are restricted to MgO of 17-35 wt.%. Thus, the MgO of wt.% value is a distinguishing feature for Komatiites (Le Bas and Streckeisen, 1991; Kerr and Arndt, 2001;

Le Maitre et al., 2002; Arndt and Lesher, 2004; Condie et al., 2016).

The oldest datable is 3.8 Ga (Nuvvuagittuq greenstone belt; Condie et al., 2016), with the youngest being 0.86 Ga (Gorgona Island, Colombia; Revillon et al., 2000; Kamenetsky et al., 2010). Komatiites are rarely found today. Condie et al. (2016) (Figure 2) summarized the previous studies on komatiites.

When the MgO of wt.% averages and age values of the komatiites are examined, it is seen that there is a

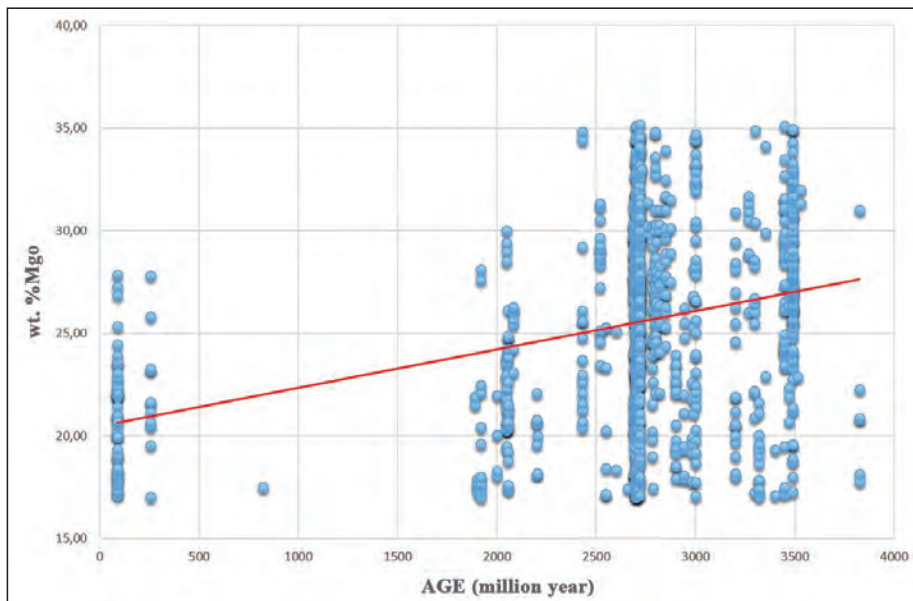


Figure 2- The graphic about age and w% MgO values given for komatiites. The red line represents the decreasing trend of w% MgO depending on age (after Condie et al., 2016).

significant decrease in these values from the oldest to the young ones (Figure 2).

Parman et al. (2001) describe in detail the geological settings of the chemical composition and formation mechanisms between basaltic komatiites and boninites. In addition, based upon their geochemical similarity, Parman et al. (2001) propose that the 3.5 Ga Barberton basaltic komatiites are the Archean equivalents of modern boninites, showing a possible relationship between basaltic komatiites and boninites. The Gorgona and Belingwe komatiites were formed by the melting of pyrolite; but it is not possible to explain some of the komatiitic geochemical features within the context of pyrolyte melting process (Walter, 1998). Parman et al. (2001) proposed that the relatively low pressures and temperatures required to produce Barberton komatiitic magmas by hydrous melting are consistent with formation in a subduction zone.

### 3. Relation Between Komatiites and Plate Tectonics

Given the proposed formation temperatures of komatiites by Parman et al. (2001), the Earth's primitive crust should be of a komatiitic character (Santosh et al., 2017). Therefore, the mantle forming the primitive crust must also be komatiitic. Next, the primitive crust and mantle could have formed the primitive continental nuclei by independent systems of plate tectonics (non-subduction systems), as proposed by Bédard (2006) and Zhang et al. (2013). Gerya et al. (2015) proposed that plume-induced subduction initiation started plate tectonic processes in the transition from stagnant lid convection. In this sense, the plumes formed in this period, when the first movements of the plate tectonics started should also be komatiitic (Figure 3).

According to IUGS rock classification (Le Bas and Streckeisen, 1991; Le Maitre et al., 2002), a significant decrease is observed in the amount of wt.% MgO (on average 10%) in the transition from komatiites (MgO > 18wt.%, TiO<sub>2</sub> <1%) to boninites (MgO > 8%, TiO<sub>2</sub> < 0.5%). It is also possible to see this theoretical case in the figure about komatiites (Figure 2). This significant decrease can be explained with the increase degree in partial melting processes and the formation of SiO<sub>2</sub>-rich melts as a result of subduction. Condie et al. (2016) examined the reason for the reduction in MgO of wt.% and observed that the primary komatiitic

mantle composition what is possible to remove the result that the komatiites having a lower wt.% MgO content are produced with developing subduction zones diluted over time (Figure 3). In this sense, the komatiites which have more SiO<sub>2</sub> and less MgO, must have turned into to juvenile basaltic komatiites and later boninites by increasing SiO<sub>2</sub> amounts over time.

Transition from komatiites to basaltic komatiites and boninites observed in relation to the beginning of plate tectonics is also supported by Parman et al. (2001).

According to the current data, examining all these proposals and considering the significant decrease in the wt.% MgO of komatiites, the starting age of the plate tectonics and subduction should be 3.8 Ga due.

### 4. Conclusions and Recommendations

No consensus has been reached in the literature on the formation of komatiites. There are studies to suggest that based on subductions (Parman et al., 2001, Parman et al., 2004) and based on mantle plumes (Arndt et al., 1998, 2008; Herzberg et al., 2007) of komatiites. Parman et al. (2001) suggested that the formation of Barberton komatiitic magmas in the subduction zones is consistent. Researchers who prefer based on mantle plumes, said that the temperature and depth conditions required for the formation of komatiites could not be met in subduction zones. However, according to Korenaga (2013) for Archean, considering the different ambient conditions of this period, the hotter Archean mantle may have provided the adequate temperature conditions for the komatiites to form in subduction zones.

The decrease in MgO wt.% in the komatiites (Figure 2) should be examined to identify if they can be count as a proxy of the beginning of the plate tectonics.

Plate tectonics, which are proposed to have started at least 3.8 Ga, should have continued by accelerating to evolve over time until 1.9 Ga. As of 1.9 Ga, the system, was accelerated by the development of all the force mechanisms that currently operate the plate movements, has stopped the production of komatiites.

While Archean komatiites formed at high temperature, Cretaceous komatiites were formed at lower temperatures (Walter, 1998). Due to changed ambient conditions (Korenaga, 2013) and significant

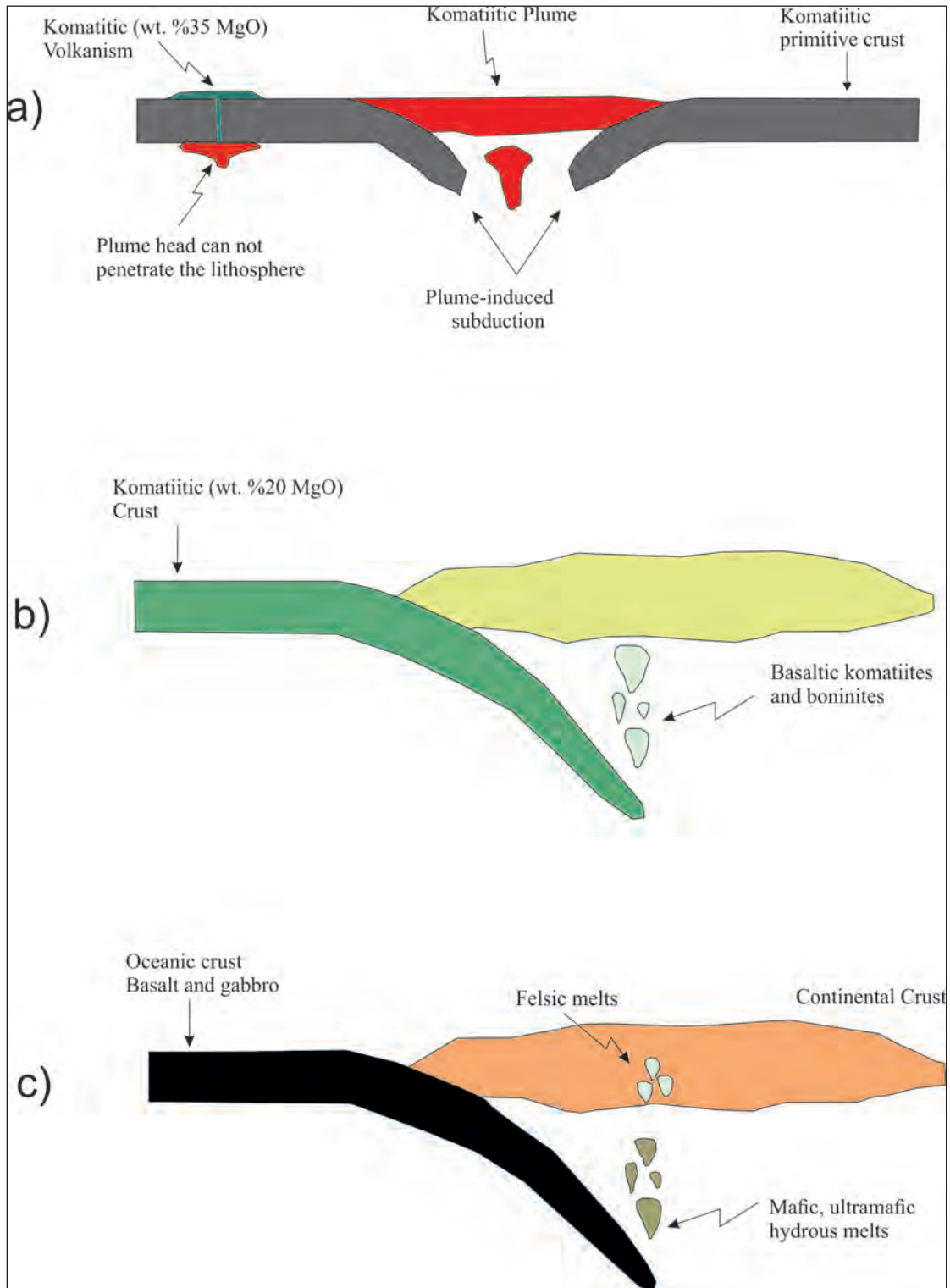


Figure 3- Schematic representation of the relationship between komatiites and plate tectonics (Unscaled). Respectively a-b-c are geologically ordered from older to younger. a) Gerya et al. (2015) initiates the first subduction events that result in the penetrate the lithosphere. b) Formation of solutions with less w% MgO content than the already existing komatiitic crust, which is partially melted by subduction events. c) Formation of felsic melts by partial melting from the currently observed oceanic crust. The proposed plate movements, which began about 3.8 billion years ago, have resulted in the production of mantle material with a lower w% MgO content, depending on the time. In other words, it reduces the content of w% MgO that the mantle composition possesses, thus laying the groundwork for diluting the mantle.

differences in MgO contents it would be more accurate to evaluate the role of komatiites formed in two different times in separate systems.

The details and the development of the working mechanisms of the first plate movements, which are considered to be slower than today (Bradley, 2008; Korenaga, 2013), are not fully known.

It should be investigated whether all of the mechanisms that currently operate the plate movements were present in the Paleoproterozoic.

While investigating the history of Earth (especially before 2 Ga) within the principle of actualism, considering the processes that occurred on Earth's crust which cannot be subjected to a present-day analogy, the idea of change should not be ignored.

### Acknowledgements

We would like to thank our valuable Professors Gürol Seyitoğlu and Korhan Esat for providing us full support and contribution to our work. We are also immensely grateful to Aral İ. Okay, Halim Mutlu and Ali Polat for their contribution to this paper with their valuable critics. The manuscript is benefited critical reviews of Timur Ustaömer, Franco Pirajno and other anonymous referee for which we are grateful.

### References

- Arndt, N. T., Nisbet, E. G. 1982. What is a komatiite?, in Komatiites, edited by N. T. Arndt and E. G. Nisbet, Allen and Unwin, Concord, Massachusetts 19–28
- Arndt, N., Ginibre, C., Chauvel, C., Albarède, F., Cheadle, M., Herzberg, C., Jenner, G., Lahaye, Y. 1998. Were komatiites wet? *Geology*, 26, 739–742.
- Arndt, N., Lesher, C.M. 2004. Komatiite. *Encyclopedia of Geology*. Elsevier, 260-268.
- Arndt, N., Lescher, C., Barnes, S. J. 2008. Komatiite. Cambridge University Press, Cambridge.
- Bédard, J.H. 2006. A catalytic delamination-driven model for coupled genesis of Archaean crust and sub-continental lithospheric mantle. *Geochimica et Cosmochimica Acta* 70, 1188–1214, doi:10.1016/j.gca.2005.11.008.
- Blichert-Toft, J., Arndt, N.T., Wilson, A., Coetsee, G. 2015. Hf and Nd isotope systematics of early Archean komatiites from surface sampling and ICDP drilling in the Barberton Greenstone Belt, South Africa. *American Mineralogist* 100, 2396–2411.
- Bradley D. C. 2008. Passive margins through earth history. *Earth-Science Reviews*. 91:1–26
- Cawood, P.A., Kröner A., Pisarevsky S. 2006. Precambrian plate tectonics: criteria and evidence. *Geological Society of America Today* 16, 4–11.
- Condie, K.C., Kröner A. 2008. When did plate tectonics begin? Evidence from the geologic record. See Condie & Pease 2008. *Geological Society of America Special Papers* 440, 281–94, doi: 10.1130/2008.2440(14)
- Condie, K.C., Aster, C.R., van Hunen, J. 2016. A great thermal divergence in the mantle beginning 2.5 Ga: Geochemical constraints from greenstone basalts and komatiites. *Geoscience Frontiers* 7, 4, 543-553, doi:10.1016/j.gsf.2016.01.006.
- Gerya, T. V., Stern, B., Baes, M., Sobolev, S. V., Whattam, S. A. 2015. Plate tectonics on the Earth triggered by plume-induced subduction initiation. *Nature* 527, 221-225, DOI: 10.1038/nature15752
- Harrison, T.M. 2009. The Hadean crust: Evidence from >4 Ga zircons. *Annual Reviews of Earth and Planetary Sciences*, 37, 479–505.
- Herzberg, C., Asimow, P., D., Arndt, N., Niu, Y., Lesher, C., M., Fitton, J., G., Cheadle, M., J., Saunders., A., D. 2007. Temperatures in ambient mantle and plumes: constraints from basalts, picrites, and komatiites. *Geochemistry, Geophysics, and Geosystems*, 8, 1–34.
- Hopkins M., Harrison T.M., Manning C.E. 2008. Low heat flow inferred from > 4Gyr zircons suggests Hadean plate boundary interactions. *Nature* 456, 493–96.
- Kerr, A. C., Arndt, N. T. 2001. A note on the IUGS reclassification of the high-Mg and picritic volcanic rocks. *Journal of Petrology* 42, 11, 2169-2171.
- Komiya T., Maruyama S., Masuda T., Nohda S., Hayashi M., Okamoto K., 1999. Plate tectonics at 3.8–3.7 Ga: field evidence from the Isua accretionary complex, southern West Greenland: *Journal of Geology* 107, 515–54.
- Korenaga, J. 2013. Initiation and evolution of plate tectonics on Earth. *Theories and Observations. Annual Review of Earth and Planetary Sciences* 41, 117–151.
- Le Bas, M.J., Streckeisen, A. L. 1991. The IUGS systematics of igneous rocks. *Journal of the Geological Society, London* 148,825-833.
- Le Maitre, R. W. 2002. *Igneous Rocks. A Classification And Glossary Of Terms. Recommendations Of*

The International Union Of Geological Sciences  
Subcommission On The Systematics Of Igneous  
Rocks, 2nd Ed. Xvi + 236 Pp. Cambridge

Tectonics Begin on Planet Earth?: Geological  
Society of America Special Paper 440, p. 1–29,  
doi: 10.1130/2008.2440(01))

- Nutman, A.P., Bennett, V.C., Friend, C.R.L. 2015. Proposal for a continent 'Itsaqia' amalgamated at 3.66 Ga and rifted apart from 3.53 Ga: Initiation of a Wilson Cycle near the start of the rock record. *American Journal of Science*, 315, 509–536.
- Parman, S. W., Grove, S. T., Dann, J. 2001. The production of Barberton komatiites in an Archean subduction zone. *Geophysical Research Letters* 28, 2513–2516.
- Parman, S. W., Grove, T. L., Dann, J. C., de Wit, M. J. 2004. A subduction origin for komatiites and cratonic lithospheric mantle. *South African Journal of Geology*, 107, 107–118.
- Santosh, M., Arai, T., Maruyama, S. 2017. Hadean Earth and primordial continents: the cradle of prebiotic life. *Geoscience Frontiers*, 8, 309–327.
- Shirey S.B., Kamber B.S., Whitehouse M.J., Mueller P.A., Basu A.R. 2008. A review of the isotopic and trace element evidence for mantle and crustal processes in the Hadean and Archean. implications for the onset of plate tectonic subduction. in *Condie, K.C., and Pease, V., eds., When Did Plate*

- Stern, R.J. 2005. Evidence from ophiolites, blueschists, and ultrahigh-pressure metamorphic terranes that the modern episode of subduction tectonics began in Neoproterozoic time. *Geology* 33, 557–60
- Stern, R. J., Leybourne, M. I., Tsujimori, T. 2017. Kimberlites and the start of plate tectonics. *Geology*. DOI: 10.1130/G38024.1
- Viljoen, M. J., Viljoen, R. P. 1969. The geology and geochemistry of Lower Ultramafic Unit of the Onverwacht Group and a proposed new class of igneous rocks. In: *Upper Mantle Project, Geological Society of South Africa Special Publication 2*, 55–85.
- Walter, J. M. 1998. Melting of Garnet Peridotite and the Origin of Komatiite and Depleted Lithosphere. *Journal of Petrology* 39, 1, 29–60.
- Zhang, C., Holtz, F., Koepke, J., Wolff, P. E., Ma, C., Bedard, J. 2013. Constraints from experimental melting of amphibolite on the depth of formation of garnet-rich restites, and implications for models of Early Archean crustal growth. *Precambrian Research* 231, 206–217.

## ACKNOWLEDGEMENT

We would like to thank to the honored reviewers whose names are written below by contributing to the Bulletin of the Mineral Research and Exploration during the article review process between the 14th of December.2016 and 12nd of December 2017 in the name of the Executive Publication Editorial.

Abbas MAGHSOUDÍ (Iran)	Gordon Robert J. COOPER (South Africa)	Okan TÜYSÜZ (Turkey)
Agah KÖKER (Turkey)	Gökhan KADINKIZ (Turkey)	Oktay ÇELMEN (Turkey)
Ahad NAZARPOUR (Iran)	Gönül ÇULHA (Turkey)	Orhan TATAR (Turkey)
Ahmad ARYAFAR (Iran)	Gülcan BOZKAYA(Turkey)	Osman CANDAN (Turkey)
Ahmet GÖKÇE (Turkey)	Güldemin DARBAŞ (Turkey)	Osman PARLAK (Turkey)
Ahmet ŞAŞMAZ (Turkey)	Güllü Deniz KÜLAHÇI (Turkey)	Oya CENGİZ (Turkey)
Alaaddin VURAL (Turkey)	Gültekin TARCAN (Turkey)	Ömer Işık ECE (Turkey)
Alastair H.F. ROBERTSON (England)	Gülten Abanoz YAYLALI (Turkey)	Önder KAYADİBİ (Turkey)
Aleksey BENDEREV (Bulgaria)	Gürol SEYİTOĞLU (Turkey)	Özcan DUMANLILAR (Turkey)
Alessandro Maria MICHETTI (Italy)	Hakan ERSOY (Turkey)	Özcan Yıldırım GÜLSOY (Turkey)
Ali AKSU (Canada)	Hakan GÜNEYLİ (Turkey)	Paul UMHOEFER (USA)
Ali BÜLBÜL (Turkey)	Hakan NEFESLİOĞLU (Turkey)	Peter BİRKLE (USA)
Ali Akbar DAYA (Iran)	Hasan HACIFAZLIOĞLU (Turkey)	Peyman AFZAL (Iran)
Ali AL JUBOURY (Iraq)	Hasan SÖZBİLİR (Turkey)	Prakash K SINGH (India)
Ali İhsan KARAYİĞİT (Turkey)	Hayrettin KORAL (Turkey)	Rens VERBURG (USA)
Alper KIYAK (Turkey)	Huriye DEMİRCAN (Turkey)	Ricardo ALONSO (Argentina)
Alvis L. LISENBEE (USA)	Hüseyin ÖZTÜRK (Turkey)	Robin W. RENAUT (Canada)
Amir Bijan YASREBİ (England)	İbrahim UYSAL (Turkey)	Sabah YILMAZ ŞAHİN(Turkey)
Ana PARRAS (Argentina)	Imre MAGYAR (Hungary)	Sacit ÖZER (Turkey)
Aral OKAY (Turkey)	İlkay KUŞÇU(Turkey)	Sait KIZGUT (Turkey)
Arie W. JANSSEN (Holland)	İrfan TEMİZEL (Turkey)	Selami TOPRAK (Turkey)
Axel K. SCHMITT (Germany)	James ROSS (Avustralya)	Selahattin KADİR (Turkey)
Aynur BÜYÜKUTKU(Turkey)	Kadir DİRİK (Turkey)	Selim ÖZALP (Turkey)
Ayşe ERDEM (Turkey)	Kamil KAYABALI (Turkey)	Serdar YILMAZ (Turkey)
Azad SAĞLAM SELÇUK(Turkey)	Kimon CHRİSTANİS (Greece)	Serkan ÜNER (Turkey)
Bahattin GÜLLÜ (Turkey)	Klaus GESSNER (Avustralya)	Sevcan KÜRÜM (Turkey)
Bakhtiar Mohamad AMEEN (Iraq)	Korhan ÇAKIR (Turkey)	Sezai KIRIKOĞLU (Turkey)
Behzad Vaziri HASSAS (USA)	Kurtuluş GÜNAY (Turkey)	Solmaz BABAKAN (Iran)
Bele SIRELDA (Arnavutluk)	Kürşat Kadir ERİŞ (Turkey)	Ş. Can GENÇ (Turkey)
Bruno LEMİÈRE (Fransa)	Levent GÜLEN (Turkey)	Şenel ÖZDAMAR (Turkey)
Bülent ÇİFT (Turkey)	Levent SELÇUK (Turkey)	Tamer RIZAOĞLU (Turkey)
Bülent KAYPAK (Turkey)	Leyla KALENDER (Turkey)	Tamer TOPAL (Turkey)
Can AYDAY (Turkey)	Luca TOFFOLO (Italy)	Thanh NGUYEN TIEN (Vietnam)
Carlos ALVES (Portugal)	Makarand Ganesh KALE (India)	Thomas DENK (Sweden)
Carlos M. DA SILVA (Portugal)	Marek WIDERA (Poland)	Timur USTAÖMER (Turkey)

Cemal TUNOĞLU (Turkey)	Maria BONI (Italy)	Tiziano BOSCHETTÍ (Italy)
Cihat ALÇİÇEK(Turkey)	Mehdi ESHAGH (Sweden)	Todor TODOROV (Bulgaria)
Coşkun SARI(Turkey)	Mehmet ARSLAN (Turkey)	Tolga ÇAN (Turkey)
Christopher SORLIEN (USA)	Mehmet ÇELİK (Turkey)	Tolga GÖNENÇ (Turkey)
Dave LENTZ (Canada)	Mehmet EKMEKÇİ(Turkey)	Tolga OYMAN (Turkey)
David BANKS (England)	Mehmet Ali ÖZDEMİR (Turkey)	Torsten UTESCHER (Germany)
Emin CANDANSAYAR (Turkey)	Mehmet Feyzi TANER (Turkey)	Tugce BASER (Canada)
Emin ÇİFTÇİ (Turkey)	Mehmet Sabri ÇELİK (Turkey)	Ümit ŞAFAK (Turkey)
Emin ULUGERGERLİ (Turkey)	Mine ÖZER (Turkey)	Ünal DİKMEN (Turkey)
Emre ÖZGÜR (Turkey)	Mohammad Ali RAJABZADEH (Iran)	Üner ÇAKIR (Turkey)
Erdinç YİĞİTBAŞ (Turkey)	Mohammad Reza HOSSEINZADEH (Iran)	Victor PUCHKOV (Russia)
Erdal ŞEN(Turkey)	Mohssen MOAZZEN (Iran)	Volkan KARABACAK (Turkey)
Erhan TERCAN (Turkey)	Mustafa AFŞİN (Turkey)	Vural OYAN (Turkey)
Ertan PEKŞEN (Turkey)	Murat GÜL (Turkey)	Wencheng XIA (China)
Esra YILDIRIM (Turkey)	Mustafa AKGÜN (Turkey)	Xavier EMERY (Chile)
Fahri ESENLİ (Turkey)	Mustafa KUŞÇU (Turkey)	Yahya ÇİFTÇİ (Turkey)
Faruk AYDIN (Turkey)	Mustafa Yavuz ÇELİK (Turkey)	Yalçın ERSOY (Turkey)
Faruk OCAKOĞLU (Turkey)	Najla AYADI (Tunusia)	Yeşim BÜYÜKMERİÇ (Turkey)
Fatma ARSLAN (Turkey)	Namık ÇAĞATAY (Turkiye)	Yong Sik GİHM (Korea)
Fatih KARAOĞLAN (Turkey)	Neşet ACARKAN (Turkey)	Yue LİU (China)
Fırat ATALAY (Turkey)	Nicoletta MANCIN (Italy)	Yusuf Kağan KADIOĞLU (Turkey)
Franco PİRANJO (Avustralya)	Nima NEZAFATİ (Iran)	Zana KARIMI (USA)
Fuat ERKÜL (Turkey)	Nizamettin KAZANCI (Turkey)	Zeynep ÖNER BARAN (USA)
Funda AKGÜN (Turkey)	Nurdane İLBEYLİ (Turkey)	Zihni Mümtaz HİSARLI (Turkey)
Ghasem NABATIAN (Iran)	Nurullah HANİLÇİ (Turkey)	Zülfü GÜROCAK (Turkey)
Ghebrebrhan OGUBAZGHI (Eritrea)		

# **PUBLICATION RULES FOR THE BULLETIN OF THE GENERAL DIRECTORATE OF MINERAL RESEARCH AND EXPLORATION**

## **1. Aims of Publication**

- To contribute to the providing of scientific communication on geosciences in Turkey and international community.
- To announce and share researches in all fields of geoscientific studies in Turkey with geoscientists worldwide.
- To announce scientific researches and practices on geoscientific surveys carried out by the General Directorate of Mineral Research and Exploration (MTA) to the public.
- To use the journal as an effective media for international publication exchange by keeping the journal in high quality, scope and format.
- To contribute to the development of Turkish language as a scientific language.

## **2. Scope**

At least one of the following qualifications is required for publishing the papers in the *Bulletin of Mineral Research and Exploration*.

### **2.1. Research Articles and Review Articles**

#### **2.1.1. Original Scientific Researches**

- These articles cover and contribute to the main subjects of the earth sciences, the original scientific researches and its results related to all aspects of disciplines in geoscience like exploration and evaluation of the underground sources and environmental problems, and
- The studies, which apply new aspects and methods for the solution of problems about the earth sciences and researches, which apply new aspects and methods for the solution of the problems, in the engineering sciences carried out in MTA.

#### **2.1.2. Review articles**

- These papers include comprehensive scholarly review articles that summarize and critically assess previous geoscientific researches with a new perspective and reveal a new approach.

## **2.2. Discussion/Reply**

- This type of article is intended for the discussion of papers that have already been published in the latest issue of the *Bulletin*. The discussion/reply type articles, which criticize all or a part of a recently published article, are published in the following first issue if it is submitted within six months after the publication of the *Bulletin*.
- The discussions are sent to the corresponding author of the original paper to get their reply before publication. The discussions about the paper with two or more authors are sent only to the corresponding author.
- If the review article is not published within the prescribed period then it is published alone. Later sent replies are not published. Re-criticising of the replies is not allowed.
- The authors should obey the rules of scientific ethics and discussions in their discussion/reply papers. The papers in this category should not exceed four printed pages of the journal including figures and tables etc. The format of the papers should be compatible with the "Spelling Rules" of the *Bulletin*.

## **2.3. Short Notes**

- The short notes part of the *Bulletin* covers short, brief and concisely written research reports for papers including the data obtained from ongoing and/or completed scientific researches and practices related to geoscience and new and/or preliminary factual findings from Turkey and worldwide.
- The short notes will follow a streamlined schedule and will normally be published in the following first or second issue shortly after submission of the paper to the *Bulletin*.
- This type of articles should not exceed four printed pages of the journal including figures, tables and an abstract.

## **3. Submission and Reviewing of Manuscripts**

Manuscript to be submitted for publishing in the Journal must be written clearly and concisely in Turkish and/or English and prepared in the *Bulletin of Mineral Research and Exploration* style guidelines. All submissions should be made online at the <http://dergi.mta.gov.tr> website.

- The manuscript submitted for reviews must not have been published partially or completely previously in another journal.
- The rejected manuscripts are not returned back to author(s) whereas a letter of statement indicating the reason of rejection is sent to the corresponding author.
- Submitted manuscripts must follow the *Bulletin* style and format guidelines. Otherwise, the manuscript which does not follow the journals' style and format guidelines, is given back to corresponding author without any reviewing.
- Every manuscript which passes initial Editorial treatise is reviewed by at least two independent reviewers selected by the Editors. Reviewers' reports are carefully considered by the Editors and associated editors.
- The manuscript that need to be corrected with the advices of reviewer(s) is sent back to corresponding author(s) to assess and make the required corrections suggested by reviewer(s) and editors. The authors should prepare a letter of well-reasoned statement explaining which corrections are considered or not.
- If there are any suggestions given by editors and referees that are not accepted and corrected by the author, then it should be sent to the Editor's Office with corrected copies of the report explaining the reason for not accepting these suggestions and corrections.
- Figures and tabless should be 1/3 of the main text.
- To be published in the *Bulletin of Mineral Research and Exploration*, the printed length of the manuscript should not exceed 30 printed pages of the journal including an abstract, figures and tables. The publication of longer manuscripts will be evaluated by Editorial Board if it can be published or not.
- The authors must do the reviewer's corrections and proposals in 60 days and must upload to the system.
- At the printing stage after the last control, the first print of the manuscript are sent to the author/authors in pdf version and asked from the author/authors to make the press control.

#### 4. Publication Language and Periods

- *The Bulletin of Mineral Research and Exploration* is published at least twice a year and each issue is published both in Turkish and English. Thus, the manuscripts are accepted in Turkish or English. The spelling and punctuation guidelines of Turkish Language Institution are preferred for the Turkish issue. However, the technical terms related to geology are used in accordance with the decision of the Editorial Board.

#### 5. Spelling Draft

- Manuscripts should be written in word format in A4 (29.7 x 21 cm) size and double-spaced with font size Times New Roman 10-point, margins of 25 mm at the sides, top and bottom of each page.
- The formulas requiring the use of special characters and symbols must be submitted by the symbols part of the Microsoft Office Word Program on computer.
- Initial letters of the words in sub-titles must be capital. The first degree titles in the manuscript must be numbered and left-aligned, 10 point bold Times New Roman must be used. The second degree titles must be numbered and left-aligned, they must be written with 10 point normal Times New Roman. The third degree titles must be numbered and left-aligned, they must be written with 10 point italic Times New Roman. The fourth degree titles must be left-aligned without having any number; 10 point italic Times New Roman must be used. The text must continue placing a colon after the title without paragraph returns (See: Sample article: <http://bulletin.mta.gov.tr>).
- One line spacing must be left after paragraphs with-in text.
- Paragraphs must begin with 0.5 mm indent.
- The manuscript must include the below sections respectively;
  - o Title Page
  - o The Name and Surname of the author and \* sign (Adress, e-mail adres must be given at the bottom of the page)
  - o Abstract
  - o Key Words

- o Introduction
- o Body
- o Discussion
- o Conclusion
- o Acknowledgements
- o References

### 5.1. Title of the Article

- The title must be short, specific and informative and written with capital letters font size Times New Roman 10-point bold. The title mustn't contain the subjects insufficiently processed in the article.

### 5.2. The Name of the Author, Address and E-Mail Address

- The name and surname of the author/authors must be written without affiliations. Name must be written in small letters, the surname must be written in capital letters.
- At the affiliation (work adres) written after the name and the surname of the author/authors only the name of the company must be written, the author's job mustn't be written.
- Information about the addresses must be given at the next line as 10-point and italic.
- At the articles with two or more than two authors, the numbers must be written above the surnames of the authors, the informations about their addresses must be given at the next line by leaving one space line. Also, at this part the corresponding author must be indicated by the (\*) symbol and the telephone, FAX and e-mail address of the corresponding author must be given.
- Abbreviations must not be made while writing the name of the uthor and the affiliation adres. Adresses must be given in Turkish in the Turkish version, in English in the English version.
- At the end of the article the name of the corresponding author and contact informations must be added.

### 5.3. Abstract

- The abstract must be understandable before having a look at the text.

- The abstract should state briefly the overall purpose of the research, the aim of the article, its contributions to the known theories, new data, principle results and major conclusions.
- The abstract must contain short and brief sentences.
- Addressing other sections and illustrations of the text or other writings must be avoided.
- The information, which have not been mentioned in the text, must not be in the abstract.
- The article must be written as one paragraph, preferably. Please provide an abstract which doesn't exceed 200 words.
- The abstract must be written with 10-point, normal Times New Roman in single-spaced lines.
- "Abstract" must not be given for the writings that will be located in "Short Notes" section.
- The English abstract must be under the title of "Abstract".

### 5.4. Key Words

Immediately after the abstract, please provide up to 5 key words and with each words seperated by comma. These key words will be used for indexing purposes.

### 5.5. Introduction

- The introduction section should state the objectives of the work, research methods, location of the study area and provide an adequate and brief background by avoiding a detailed literature survey.
- Non-standard or uncommon classifications or abbreviations should be avoided. But if essential, then they must be defined at their first mention and used consistently thereafter. Seperate paragraphs could be organized for each of the subjects at the introduction part. If it is necessary, the subtitle can be given for each of them (for example method, material, terminology etc.).
- When pre-information is needed for facilitating the understanding of the text, this section can also be used (for example, statistical data, bringing out the formulas, experiment or application methods, and others).

## 5.6. Body

- In this chapter, there must be data, findings and opinions that are intended to convey to the reader about the subject. The body section forms the main part of the article.
- The data used in other sections such as “Abstract”, “Discussions”, and “Results” are caused by this section.
- While processing the subject, the care must be taken not to go beyond the objective highlighted in the “Introduction” section. The knowledge, which do not contribute to the realization of the purpose of the article or are useless for conclusion, must not be included.
- All data used and the opinions put forward in this section must prove the findings obtained from the studies or they must be based on a reference by citation.
- The guidance and methods to be followed in processing subjects vary according to the characteristics of the subjects mentioned. Various topic titles can be used in this section as many as necessary.

## 5.7. Discussions

- Discussion of the data and findings that are objectively transferred in the Main Text section of the article should be done in this section. This must be written as a separate section from the results section.

## 5.8. Conclusions

- The main conclusion of the study provided by data and findings of the research should be stated concisely and concretely in this section.
- The subjects that are not mentioned sufficiently and/or unprocessed in the body section must not be included in this section.
- The conclusions can be given in the form of substances in order to emphasize the results of the research and to make the expression understandable.

## 5.9. Acknowledgements

In this section, the significant contributions made in the realization of investigation that form the topic of the paper is specified. While specifying contributions, the attitude diverted the original purpose of

this section away is not recommended. Acknowledgements must be made according to the following examples.

- This study was carried out within scope of .....project.
- I/we would like to thank to ..... for contributing to the development of this article with his/her critiques.
- Academic and/or authoritorial affiliations are written for the contributions made because of requirement of ordinary task.

### *For example:*

- o “Prof. Dr. İ. Enver Altınlı has led the studies”.
- o “The opinions and warnings of Dr. Tandoğan Engin are considered in determining the chemistry of chrome minerals.”
- The contributions made out of the requirement of ordinary task:

### *For example:*

- o “I would like to thank to Professor Dr. Melih Tokay who gives the opportunity to benefit from unpublished field notes”; “I would like to thank to the preliminary-Plan Chief Engineer Ethem Göğer, State Hydraulic Work, 5<sup>th</sup> Zone”. Academic and /or task-occupational titles are indicated for such contributions.
- The contributions, which are made because of requirement of ordinary task but do not necessitate responsibility of the contributor mustn’t be specified.

### *For example:*

- o Sentences such as “I would like to thank to our General Manager, Head of Department or Mr. /Mrs. President .....who has provided me the opportunity to research” must not be used.

## 5.10. References

- All references cited in the text should be given in the reference list.
- The authors must be careful about the accuracy of the references. Publication names must be written in full.

- Reference list must be written in Times New Roman, 9-point type face.
- The reference list must be alphabetized by the last names of the first author of each work.
- If an author's more than one work is mentioned, then ranking must be made with respect to the publication year from old to new.
- In the case that an author's more than one work in the same year is cited, the lower-case alphabet letters must be used right after publication year (for example; Saklar, 2011a, b).
- If the same author has a publication with more than one co-author, firstly the ones having single author are ranked in chronological order, then the ones having multiple authors are ranked in chronological order.
- In the following examples, the information related to works cited is regulated in accordance with different document/work types, considering punctuation marks as well.
- If the document is located in a periodical publication (if it is an article), then the information about the document must be given in the following order: surnames of the author/authors, initial letters of author's/authors' first names. Year of publication. Name of the document. Name of the publication where the document is published, volume and/ or the issue number, numbers of the first and last pages of the document.

***For example:***

- o Pamir, H.N. 1953. Türkiye'de kurulacak bir hidrojeoloji enstitüsü hakkında rapor. Türkiye Jeoloji Bülteni 4, 1, 63-68.
- o Barnes, F., Kaya, O. 1963. İstanbul bölgesinde bulunan Karbonifer'in genel stratigrafisi. Maden Tetkik ve Arama Dergisi 61, 1-9.
- o Robertson, A.H.F. 2002. Overview of the genesis and emplacement of Mesozoic ophiolites in the Eastern Mediterranean Tethyan region. Lithos 65, 1-67.
- If more than one document by the same authors is cited, first the documents having single name must be placed in chronological order, second the documents having two names must be listed in accordance with the chronological order and second author's surname, and finally the documents having multiple names must be listed in accordance with chronological order and third author's surname.

accordance with the chronological order and second author's surname, and finally the documents having multiple names must be listed in accordance with chronological order and third author's surname.

- If the document is a book, then; the surname of the author/authors, initial letters of the author's/authors' first names. Year of publication. Name of the book (initial letters are capital). Name of the organization, which has published the book, name of the publication where the document is published, volume and/ or the issue number, total pages of the book.

***For example***

- o Meric, E. 1983. Foraminiferler. Maden Tetkik ve Arama Genel Müdürlüğü Eğitim Serisi 23, 280 s.
- o Einsele, G. 1992. Sedimentary Basins. Springer-Verlag, 628 p.
- If the document is published in a book containing the writings of various authors, the usual sequence is followed for the documents in a periodic publication. Then the editor's surname and initial letters of their name/names are written. "Ed.", which is an abbreviation of the editor word, is written in parentheses. Name of the book containing the document (initial letters are capital). Name of the organization which has published the book. Place of publication, volume number (issue number, if any) of the publication where the document is published, numbers of the first and last page of the document.

***For example:***

- o Göncüoğlu, M.C., Turhan, N., Şentürk, K., Özcan, A., Uysal, Ş., Yalınz, K. 2000. A geotransverse across northwestern Turkey. Bozkurt, E., Winchester, J.A., Piper, J.D.A. (Ed.). Tectonics and Magmatism in Turkey and the Surrounding Area. Geological Society of London Special Publication 173, 139-162.
- o Anderson, L. 1967. Latest information from seismic observations. Gaskell, T.F. (Ed.). The Earth's Mantle. Academic Press. London, 335-420.
- If the name of a book, where various authors' writings have been collected, is specified, those must be indicated respectively: book's editor/editors'

surname/surnames and initial letters of their name/names. “Ed.”, which is an abbreviation of the editor word, must be written in parentheses. Year of Publication. Name of the book (initial letters are capital). Name of the organization which has published the book, total pages of the book.

**For example:**

- o Gaskel, T.F. (Ed.) 1967. The Earth’s Mantle. Academic Press, 520 p.
- If the document is an abstract published in a Proceedings Book of a scientific activity such as conference/symposium/workshop ...etc., the information about the document must be given in the following order: surnames of the author/authors, initial letters of author’s/authors’ first names. Year of publication. Title of the abstract. Name, date and place of the meeting where the Proceedings Book is published, numbers of the first and last pages of the abstract in the Proceedings Book.

**For example:**

- o Yılmaz, Y. 2001. Some striking features of the Anatolian geology. 4. International Turkish Geology Symposiums 24-28 September 2001, London, 13-14.
- o Öztunalı, Ö., Yenyol, M. 1980. Yunak (Konya) yöresi kayaçlarının petrojenezi. Türkiye Jeoloji Kurumu 34. Bilim Teknik Kurultayı, 1980, Ankara, 36
- If the document is one of the unpublished documents as a report, lecture notes, and so on, the information about the document must be given by writing the word “unpublished” in parentheses at the end of information about the document after it is specified in accordance with usual order which is implemented for a document included in a periodic publication.

**For example:**

- o Özdemir, C. Biçen, C. 1971. Erzincan İli, İliç ilçesi ve civarı demir etütleri raporu. *General Directorate of Mineral Research and Exploration Report No: 4461*, 21 p. Ankara (unpublished).
- o Akyol, E. 1978. Palinoloji ders notları. EÜ Fen Fakültesi Yerbilimleri Bölümü, 45 p., İzmir (unpublished).

- The followings must be specified for the notes of unpublished courses, seminars, and so on: name of the document and course organizer. Place of the meeting, name of the book, corresponding page numbers must be given.

**For example:**

- o Walker, G. R. Mutti, E. 1973. Turbidite facies and facies associations. Pacific Section Society for Sedimentary Geology Short Course. Anaheim. Turbidities and Deep Water Sedimentation, 119-157.
- If the document is a thesis, the followings are written: surname of the author, initial letter of the author’s first name. Year of Publication. Name of the thesis. Thesis type, the university where it is given, the total number of pages, the city and “unpublished” word in parentheses.

**For example:**

- o Seymen, İ. 1982. Kaman dolayında Kırşehir Masifi’nin jeolojisi. Doçentlik Tezi, İTÜ Maden Fakültesi, 145 s. İstanbul (unpublished).
- Anonymous works must be regulated according to the publishing organization.

**For example:**

- o MTA. 1964. 1/500.000 ölçekli Türkiye Jeoloji Haritası, İstanbul Paftası. Maden Tetkik ve Arama Genel Müdürlüğü, Ankara.
- The date after the name of the author is not given for on-printing documents; “in press” and / or “on review” words in parenthesis must be written. The name of the article and the source of publication must be specified, volume and page number must not be given.

**For example:**

- o Ishihara, S. The granitoid and mineralization. Economic Geology 75<sup>th</sup> Anniversary (in press).
- Organization name, web address, date of access on web address must be indicated for the information downloaded from the internet. Turkish sources must be given directly in Turkish and they must be written in Turkish characters.

**For example:**

- o ERD (Earthquake Research Department of Turkey). <http://www.afad.gov.tr>. March 3, 2013.

- While specifying work cited, the original language must be used; translation of the title of the article must not be done.

## 6. Illustrations

- All drawings, photographs, plates and tables of the article are called as “illustration”.
- The illustrations must be used when the use of them is inevitable or when they facilitate the understanding of the subject.
- While selecting and arranging the illustrations’ form and dimensions, the page size and layout of the *Bulletin* must be considered. The unnecessary loss of space must be prevented as much as possible.
- The pictures must have high quality, high resolution suitable for printing.
- The number of illustrations must be proportional to the size of the text.
- All illustrations must be sent as in separate files independent from the text.
- While describing illustrations in the text, the abbreviations must be avoided and descriptions must be numbered in the order they are mentioned in the text.
- Photographs and plates must be given as computer files containing EPS, TIFF, or JPEG files in 600 dpi and higher resolutions (1200 dpi is preferable) so that all details can be seen in the stage of examination of writing.

### 6.1. Figures

- Drawings and photos (except for the plates in the text) will be evaluated together as “Figure” and they must be numbered in the order they are mentioned in the text.
- The figures published in the *Bulletin of Mineral Research and Exploration* must be prepared in computer considering the dimensions of single-column width 7.4 m or double-column width 15.8 cm. Figure area together with the writing at the bottom should not exceed 15.8x21in maximum.
- Unnecessasry details must not be given in figures or care must be taken not to use much space for information transfer.

- Figures must be arranged in such a way to be printed in black/white or colored.
- The figure explanations being justified in two margins must be as follows:

Figure 1. Sandıklı İlçesinin (Afyon); a) güneybatısının jeolojik haritası, b) İnceleme alanının genel dikme kesiti (Seymen 1981), c) Türkiye’nin önemli neotektonik yapıları (Koçyiğit 1994’den değiştirilerek).

Figure 1.a) Sandıklı ilçesinin güneybatısının jeolojik haritası, b) İnceleme alanının genel dikme kesiti (Seymen 1981), c) Türkiye’nin önemli neotektonik yapıları (Koçyiğit 1994’den değiştirilerek).

- Drawings must be made by well-known computer programs painstakingly, neatly and cleanly.
- Using fine lines, which can disappear when figures shrinks, must be avoided. Symbols or letters used in all drawings must be in Times New Roman and not less than 2 mm in size when shrink.
- All standardized icons used in the drawings must be explained preferably in the drawing or with figure caption if they are too long.
- Linear scale must be used for all drawings. Author’s name, figure description, figure number must not be included into the drawing.
- Photos must be in quality and quantity that will reflect the objectives of the subject.

### 6.2. Plates

- Plates must be used when needed a combination of more than one photo and the publication on a special quality paper.
- Plate sizes must be equal to the size of available magazine page space.
- Figure numbers and linear scale must be written under each of the shapes located on the Plate.
- The original plates must be added to the final copy, which will be submitted, if the article is accepted.
- Figures and plates must be independently numbered. Figures must be numbered in Latin numerals and plates with Roman numerals (e.g., Figure1, Plate I).

- There must be no description text on Figures.

### 6.3. Tables

- All tables must be prepared preferably in word format in Times New Roman fonts.
- Tables together with table top writing must not exceed 15x8 cm in size.
- The table explanations being justified in two margins must be as follows:

Table 1- Hydrogeochemical analysis results of geothermal waters in the study area.

### 7. Nomenclature and Abbreviations

- Non-standard and uncommon nomenclature abbreviations should be avoided in the text. But if essential, then they must be described as below. In cases where unusual nomenclatures and unstandardized abbreviations are considered to be compulsory, the way followed and method must be described.
- Full stop must not be placed between the initials of words for standardized abbreviations (MER, SHW, etc.).
- Geographical directions must be abbreviated in English language as follows: N, S, E, W, NE ...etc.
- The first time used abbreviations in the text are presented in parenthesis, the parenthesis is not used for subsequent uses.
- The metric system must be used as units of measurement.

Super family: Alveolinacea Ehrenberg, 1939

Family: Borelidae Schmarada, 1871

Type genus: *Borelis* de Montfort, 1808

Type species: *Borelis melenoides* de Montfort, 1808;

*Nautilus melo* Fitchel and Moll, 1789

*Borelis vonderschmitti* (Schweighauser, 1951) (Plate, Figure, Figure in Body Text)

1951 *Neoalveolina vonderschmitti* Schweighauser, page 468, figure 1-4

1974 *Borelis vonderschmitti* (Schweighauser), Hottinger, page, 67, plate 98, figure 1.7

- Figure, plate and table names in the article must not be abbreviated. For example, “as shown in the generalized stratigraphic cross-section of the region (Figure 1.....)”

### 7.1. Stratigraphic Terminology

Stratigraphic classifications and nomenclatures must be appropriate with the rules of International Commission on Stratigraphy and/or Turkish Stratigraphic Committee. The formation names, which have been accepted by International Commission on Stratigraphy and/or Turkey Stratigraphy Committee, should be used in the manuscript.

### 7.2. Paleontologic Terminology

Fossil names in phrases must be stated according to the following examples:

- o For the use of authentic fossil names;

e.g. Limestone with *Nummulites*

- o When the authentic fossil name is not used;

e.g. nummulitic Limestone

- o Other examples of use;

e.g. The type and species of *Alveolina/ Alveolina* type and species

- Taxonomic ranks must be made according to the following examples:

*Not reference, Not stated in the Reference section*

*Schweighauser, 1951 not reference*

*Cited Schweighauser (1951), stated in the Reference section.*

*Cited Hottinger (1974), stated in the Reference section.*

- The names of the fossils should be stated according to the rules given below:

- o For the first use of the fossil names, the type, species and the author names must be fully indicated;

*Alveolina aragoensis* Hottinger

*Alveolina* cf. *aragoensis* Hottinger

*Alveolina* aff. *aragoensis* Hottinger

- o When a species is mentioned for the second time in the text;

*A.aragoensis*

*A.cf.aragoensis*

*A.aff.aragoensis*

- o It is accepted as citation if stated as *Alveolina aragoensis* Hottinger (1966).

- The statement of plates and figures (especially for the articles of paleontology):

- o for the statement of species mentioned in the body text;

*Borelis vonderschmitti* (Schweighauser, 1951).

(plate, figure, figure in the body text).

- o When cited for other articles;

1951 *Neoalveolina vonderschmitti* Schweighauser, page 468, figure 1-4, figure in body text

1974 *Borelis vonderschmitti* (Schweighauser), Hottinger, page 67, plate 98, figure 1-7

- For the citation in the text

(Schweighauser, 1951, page, plate, figure, figure in the body text)

(Hottinger, 1974, page, plate, figure 67, plate 98, figure 1-7, figure in the body text.)

## 8. Citations

All citations in the body text must be indicated by the last name of the author(s) and the year of publication, respectively. The citations in the text must be given in following formats:

- For publications written by single author;
  - It is known that fold axes of Devonian and Carboniferous aged units around Istanbul is in NS direction (Ketin, 1953, 1956; Altınlı, 1999).

- Altınlı (1972, 1976) defined the general characteristics of Bilecik sandstone in detail.

- For publications written by two authors;

- The upper parts of the unit contain Ilerdian fossils (Sirel and Gündüz, 1976; Keskin and Turhan, 1987, 1989).

- For publications written by three or more authors;

According to Caner et al. (1975) the Alicı formation reflects the fluvial conditions.

The unit disappears by wedging out in the East direction (Tokay et al., 1984).

- If reference is not directly obtained but can be found in another reference, the cross-reference should be given as follows:

- It is known that Lebling has mentioned the existence of Lias around Çakraz (Lebling, 1932: from Charles, 1933).

## 9. Reprints

The author(s) will receive (2) two hard copies of the related issues.

## 10. Copyright and Conditions of Publication

- It is necessary that the work submitted for the publication must be original and has not been previously unpublished in whole or partially.
- It is necessary that the authors who send their publications to the *Bulletin of Mineral Research and Exploration* hereby accept the conditions of publication of the Bulletin in advance.
- All copyrights of the accepted manuscripts belong to MTA. The author or corresponding author on behalf of all authors (for papers with multiple authors) must sign and give the agreement under the terms indicated by the Regulations of Executive Publication Committee. Upon acceptance of an article, MTA can pay royalty to the authors upon their request according to the terms under the “Regulations of Executive Publication Committee” and the “Regulations of Royalty Payment of Public Office and Institutions”

All the information and forms about the *Bulletin of Mineral Research and Explorations* can be obtained from <http://dergi.mta.gov.tr>